

AD-A198 195

(4)
DASIAC-TN-87-35-V2

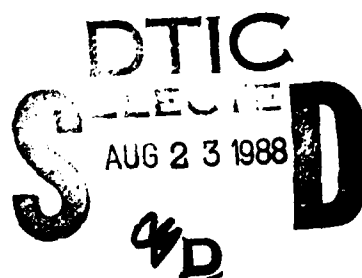
**TECHNICAL PAPERS PRESENTED AT THE DEFENSE
NUCLEAR AGENCY GLOBAL EFFECTS
REVIEW—7 - 9 APRIL 1987**

Volume II

**Kaman Sciences Corporation
Alexandria Office
Huntington Building, Suite 500
2560 Huntington Avenue
Alexandria, VA 22303-1410**

19 May 1987

Technical Report



CONTRACT No. DNA 001-82-C-0274

**Approved for public release;
distribution is unlimited.**

**THIS WORK WAS SPONSORED BY THE DEFENSE NUCLEAR AGENCY
UNDER RDT&E RMSS CODE B331086466 P99QMXDC00003 H2590D.**

**Prepared for
Director
DEFENSE NUCLEAR AGENCY
Washington, DC 20305-1000**

88 8 23 031

DISTRIBUTION LIST UPDATE

This mailer is provided to enable DNA to maintain current distribution lists for reports. We would appreciate your providing the requested information.

- ☐ Add the individual listed to your distribution list.
- ☐ Delete the cited organization/individual.
- ☐ Change of address.

NAME: _____

ORGANIZATION: _____

OLD ADDRESS

CURRENT ADDRESS

TELEPHONE NUMBER: () _____

SUBJECT AREA(s) OF INTEREST:

DNA OR OTHER GOVERNMENT CONTRACT NUMBER: _____

CERTIFICATION OF NEED-TO-KNOW BY GOVERNMENT SPONSOR (if other than DNA):

SPONSORING ORGANIZATION: _____

CONTRACTING OFFICER OR REPRESENTATIVE: _____

SIGNATURE: _____

CUT HERE AND RETURN



Director
Defense Nuclear Agency
ATTN: TITL
Washington, DC 20305-1000

Director
Defense Nuclear Agency
ATTN: TITL
Washington, DC 20305-1000

UNCLASSIFIED

SECURITY CLASSIFICATION OF THIS PAGE

ADAM98195

REPORT DOCUMENTATION PAGE				
1a. REPORT SECURITY CLASSIFICATION UNCLASSIFIED		1b. RESTRICTIVE MARKINGS		
2a. SECURITY CLASSIFICATION AUTHORITY N/A since Unclassified		3. DISTRIBUTION / AVAILABILITY OF REPORT Approved for public release; distribution is unlimited.		
2b. DECLASSIFICATION / DOWNGRADING SCHEDULE N/A since Unclassified				
4. PERFORMING ORGANIZATION REPORT NUMBER(S)		5. MONITORING ORGANIZATION REPORT NUMBER(S) DASIAC-TN-87-35-V2		
6a. NAME OF PERFORMING ORGANIZATION Kaman Sciences Corporation Alexandria Office	6b. OFFICE SYMBOL (If applicable)	7a. NAME OF MONITORING ORGANIZATION Director Defense Nuclear Agency		
6c. ADDRESS (City, State, and ZIP Code) Huntington Building, Suite 500 2560 Huntington Avenue Alexandria, VA 22303-1410		7b. ADDRESS (City, State, and ZIP Code) Washington, DC 20305-1000		
8a. NAME OF FUNDING / SPONSORING ORGANIZATION	8b. OFFICE SYMBOL (If applicable) RARP/Auton	9. PROCUREMENT INSTRUMENT IDENTIFICATION NUMBER DNA 001-82-C-0274		
8c. ADDRESS (City, State, and ZIP Code)		10. SOURCE OF FUNDING NUMBERS		
		PROGRAM ELEMENT NO 62715H	PROJECT NO P99QMXD	TASK NO C
11. TITLE (Include Security Classification) TECHNICAL PAPERS PRESENTED AT THE DEFENSE NUCLEAR AGENCY GLOBAL EFFECTS REVIEW—7 - 9 April 1987, Volume II				
12. PERSONAL AUTHOR(S) Various; Alderson, D. (Compiler)				
13a. TYPE OF REPORT Technical	13b. TIME COVERED FROM 870407 TO 870409	14. DATE OF REPORT (Year, Month, Day) 870519	15. PAGE COUNT 386	
16. SUPPLEMENTARY NOTATION This work was sponsored by the Defense Nuclear Agency under RDT&E RMSS Code B331086466 P99QMXDC00003 H2590D.				
17. COSATI CODES			18. SUBJECT TERMS (Continue on reverse if necessary and identify by block number) Nuclear War Global Climate Effects	
FIELD	GROUP	SUB-GROUP		
04	01			
15	06			
19. ABSTRACT (Continue on reverse if necessary and identify by block number) This document contains technical papers presented at the Defense Nuclear Agency Review of Global Effects held at Mission Research Corporation, Santa Barbara, CA 7-9 April 1987.				
20. DISTRIBUTION / AVAILABILITY OF ABSTRACT <input type="checkbox"/> UNCLASSIFIED/UNLIMITED <input checked="" type="checkbox"/> SAME AS RPT. <input type="checkbox"/> DTIC USERS		21. ABSTRACT SECURITY CLASSIFICATION UNCLASSIFIED		
22a. NAME OF RESPONSIBLE INDIVIDUAL Sandra E. Young		22b. TELEPHONE (Include Area Code) (202) 325-7042	22c. OFFICE SYMBOL DNA/CSTI	

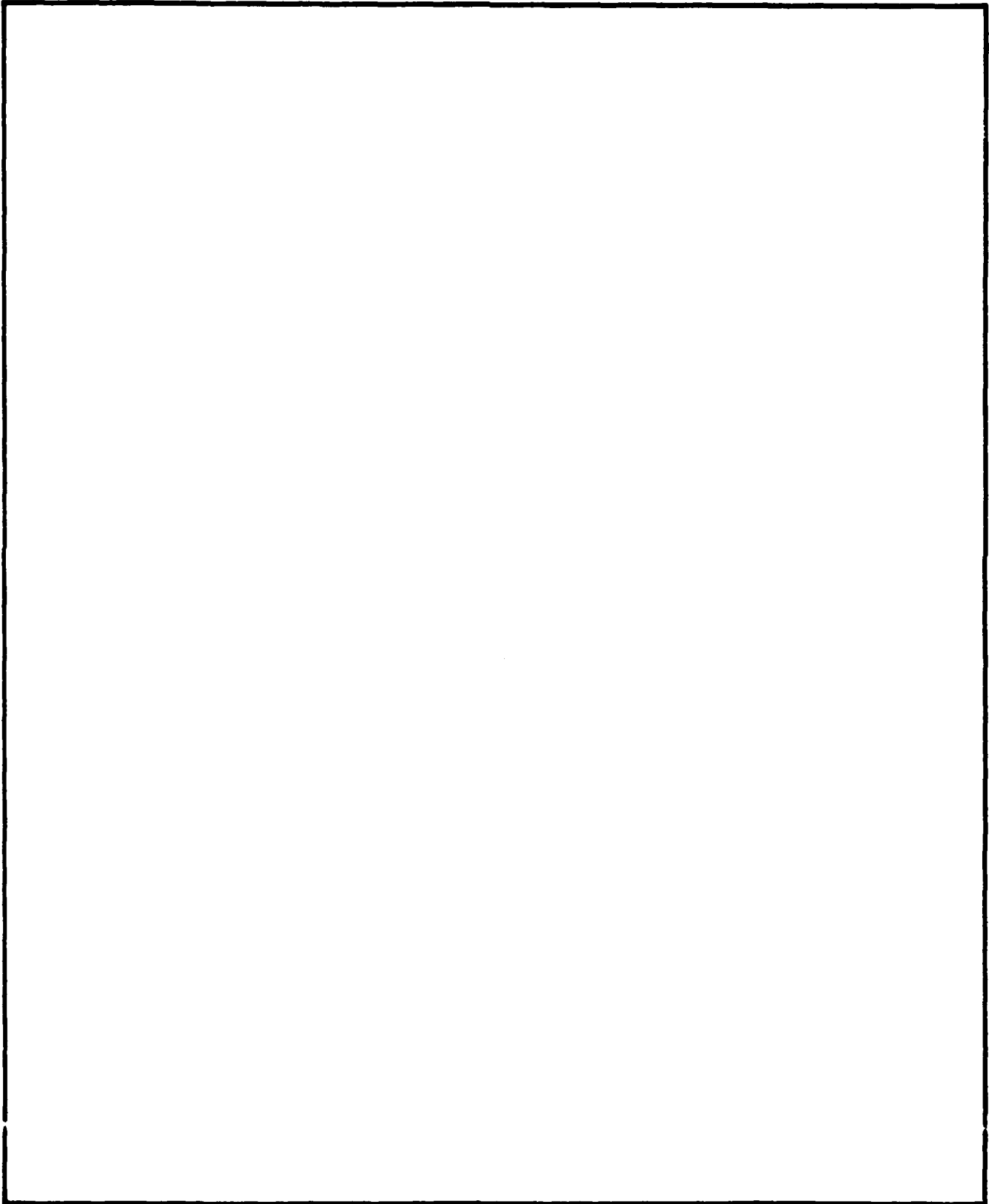
DD FORM 1473, 84 MAR

83 APR edition may be used until exhausted.

All other editions are obsolete.

SECURITY CLASSIFICATION OF THIS PAGE

UNCLASSIFIED
SECURITY CLASSIFICATION OF THIS PAGE



SUMMARY

NUCLEAR WINTER: WHERE DO WE STAND?

R. P. Turco

Four years of research on nuclear winter has greatly improved our understanding of this complex phenomenon. Studies have confirmed the possibility of significant temperature decreases and other severe environmental perturbations following a nuclear war, with potentially critical implications for human survival. Nevertheless, important uncertainties remain to be resolved. The major issues and their present research status are reviewed.

o Fuel Inventories: Fuel burdens in rural and urban settings appear to be known to within a factor of 2, and are lower than earlier estimates by a factor of 2 or so;

o Fuel Impaction: The quantities of fuels affected by nuclear explosions are sensitive to the scenario adopted; although definitive targeting analyses are forthcoming, issues of targeting policy may never be fully resolved and must necessarily remain uncertain; ignition and burning of rubblized fuels, while likely after a nuclear attack, may be of lower intensity; it is presently understood that a major nuclear attack against identified military/industrial targets would cause extensive collateral damage in urban areas;

o Smoke Emission Factor: Burning petroleum, plastics and related materials can emit 5% or more of their mass as soot; recent experiments reveal that the combustion of wood under restricted ventilation can convert up to 2% to soot; such emission factors imply blacker smoke than has been presumed in most existing studies; soot emission factors for large scale nuclear-induced oil refinery and urban fires are still uncertain, but have more likely been underestimated than overestimated;

o Plume Heights: Simulations and observations indicate initial smoke injection as high as 15 kilometers; soot generated under intense flaming conditions is likely to be injected into the middle and upper troposphere, while smoke produced by lower intensity combustion would be deposited in the middle and lower troposphere;

o Prompt Scavenging: The immediate rainout of the sooty component of smoke emissions is probably less than 50%, because of its poor nucleation properties relative to other materials, and because of the likely overseeding and reduced precipitation efficiencies of smoke clouds; actual scavenging processes remain to be tested in full-scale field tests;

o Mesoscale Dispersion: Observations of large smoke plumes caused by fire complexes suggest rapid regional dispersion; the role of water vapor in modifying soot properties and initiating precipitation requires investigation; smoke aging by coagulation and chemical reaction must also be carefully defined in this regime;

o Acute Climate Change: The extent of land surface cooling for a specific smoke injection can presently be estimated to within a factor of 2; the primary unknowns concern the surface boundary layer response to a sudden loss of solar energy, including the formation of fogs and inversion layers; critical changes in precipitation rates may also occur, but are currently less well understood;

o Long-term Climate Change: Preliminary investigations show important couplings between smoke injections, oceanic responses, ice formation and other processes that drive persistent climate fluctuations over periods of years; residual stabilized smoke layers could greatly enhance these effects; uncertainty about the long-term chemical interaction between soot and ozone must be resolved;

o Other Environmental Effects: Substantial ozone layer depletions are expected following a nuclear war due to smoke-induced perturbations in atmospheric temperatures, composition and circulation, but the effect has not been quantified; radiological impacts would be severe over large areas because of local fallout, although global health effects need to be more clearly defined; release of chemical toxins leading to hazardous local pollution of air, soil and water must be quantified;

o Biological Impacts: The human consequences of nuclear war as described in the SCOPE Report must be extended and refined; an organized research program should be developed in the U.S. to place the biological conclusions on a firmer analytical foundation.

PREFACE

The Defense Nuclear Agency has collected and printed the attached papers from the April 7-9 1987 Global Effects review as a service to the community. The Defense Nuclear Agency takes this opportunity to express its gratitude to the numerous participants in the Global Effects review.

The technical papers enclosed include all those which were received by DNA prior to the closing date of 15 May 1987. Where papers are missing their place is occupied by the abstract received prior to the meeting.

The inclusion of a paper in this proceedings does not necessarily imply endorsement of the results of the research reported or conclusions which might be drawn from that research. It is the opinion of the Defense Nuclear Agency that, while good progress is being made in improving our understanding of Global Effects, the results to date are tentative and preliminary and should not be used for planning beyond the planning of future research.

Approved For	
NTIS ORDA	<input checked="" type="checkbox"/>
DTIC TAB	<input type="checkbox"/>
Unannounced	<input type="checkbox"/>
Justification	
By	
Distribution	
Availability Codes	
Dist	Avail and/or Special
A-1	



TABLE OF CONTENTS

	Page
SUMMARY	iii
PREFACE	v
SECTION 1 <u>Mesoscale</u>	1
1. Atmospheric Heating With Mixed Soot and Water Clouds - Lauer, McCartor	2
2. Simulation of Costal Flow Fields when the Incident Solar Radiation Is Obscured - Molenkamp	13
3. Mesoscale Aspects of the Climatic Effects of a Large Nuclear War - Giorgi	28
4. A Case Study of A Forest Fire Smoke Plume - Westphal, Toon	38
5. Microphysical and Radiative Simulations of Optically Thick Smoke Clouds on the Continental Scale - Toon, Wesphal, Santhanam	50
6. Surface Temperature Effects of Forest Fire Smoke Plumes - Robock	69
7. Radioactivity; A Survey - Shapiro and Harvey	88
8. Symptomatology of Acute Radiation Effects in Humans After Exposure to Doses of 50 to 3000 Rads (cGy) - Anno, Baum, Young, Withers	123
SECTION 2 <u>Global Climate Simulations</u>	183
9. A Comparison of Eulerian and Lagrangian Methods for Tracer Transport in a GCM - Malone, Glatzmaier, Langley	184
10. Improvements in the Los Alamos Global Climate Model and Their Effects on Nuclear Winter Simulations - Glatzmaier, Malone and Langley	198
11. A Theory of Radiative-Dynamical Instability - Ghan	210
12. Unstable Radiative-Dynamical Interactions - Ghan	225
13. Chronic Effects of Large Atmospheric Smoke Injections: Interactions with the Ocean Mixed Layer, Sea, Ice, and Ground Hydrology - Ghan, MacCracken, Walton	229
14. The Climatic Response to Large Atmospheric Smoke Injections - MacCracken, Ghan, Walton	260

15.	Protracted Climatic Effects of Massive Smoke Injection Into the Atmosphere - Covey	299
16.	Effects of Vertical Injection Profile and Infrared Opacity in GCM Simulations of Nuclear War Smoke - Schneider	307
17.	Analysis of Surface Temperature Variability and Extremes in GCM Simulations of Large Smoke Injections - Thompson	308
SECTION 3	<u>Lodi Canyon Experiment</u>	332
18.	Emission Factor Measurements for Lodi Test Fires Using Surface Based Emissions Sampling Equipment - Ward, Hardy	333
19.	Absorption Measurements from Preliminary Site Burns in Lodi Canyon - Patterson	334
20.	Vertical Plume Velocities in a Controlled Burn - Hallett	335
21.	Anomolous Production of Sulfur and Nitrogen Species in the Lodi Fire - Hegg, Radke, Hobbs, Brock, Riggan	340
22.	Plume Characterization Studies on the Lodi Canyon Prescribed Burn - Einfield, Zak, Mokler and Morrison	341
23.	Measurements of Cloud Active Aerosol in Large Scale Fires - Hudson	356
24.	Optical Depth Measurements of Forest Fire Smokes: Two Case Studies - Pueschel, Russel, Ackerman, Allen and Colburn	369

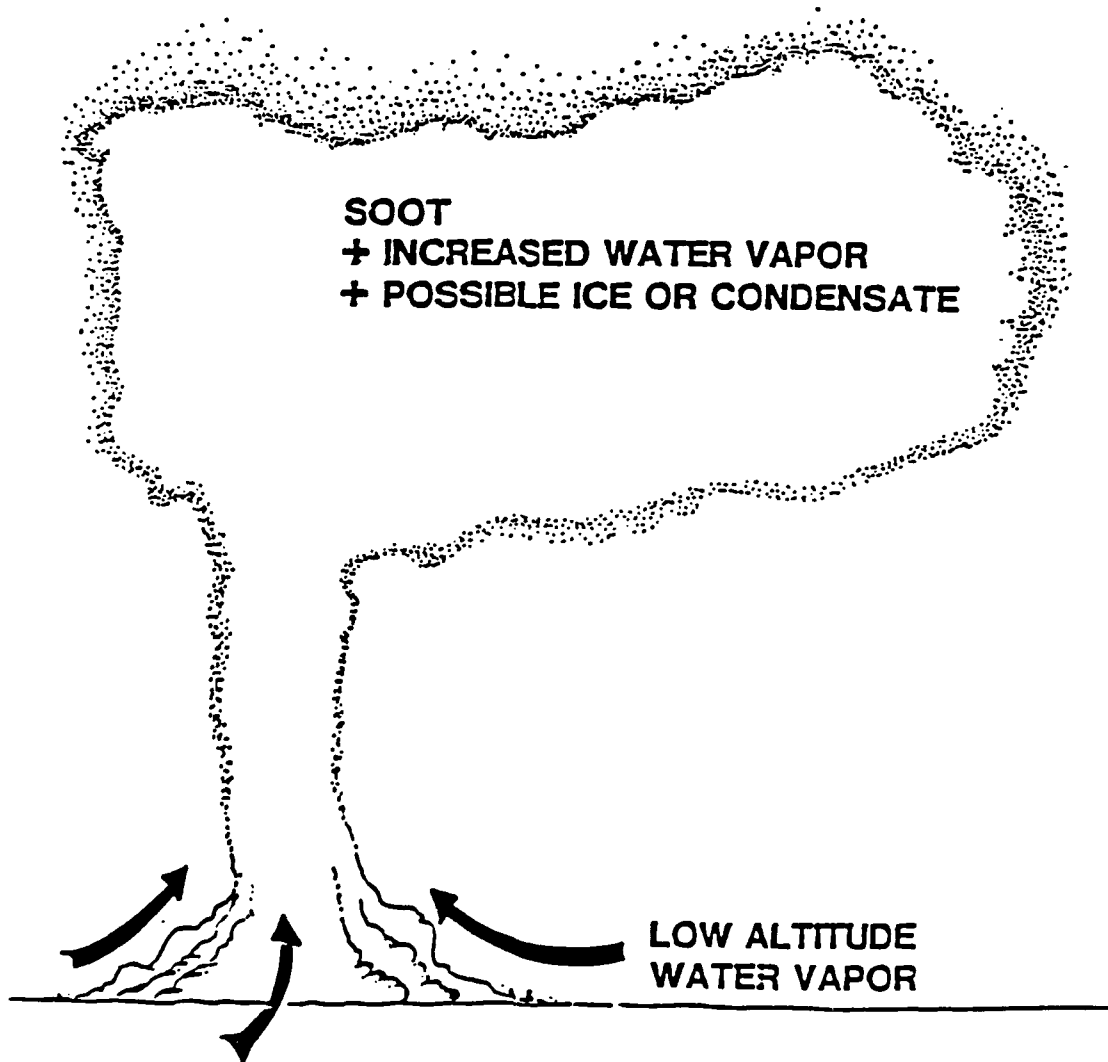
SECTION 1

MESOSCALE

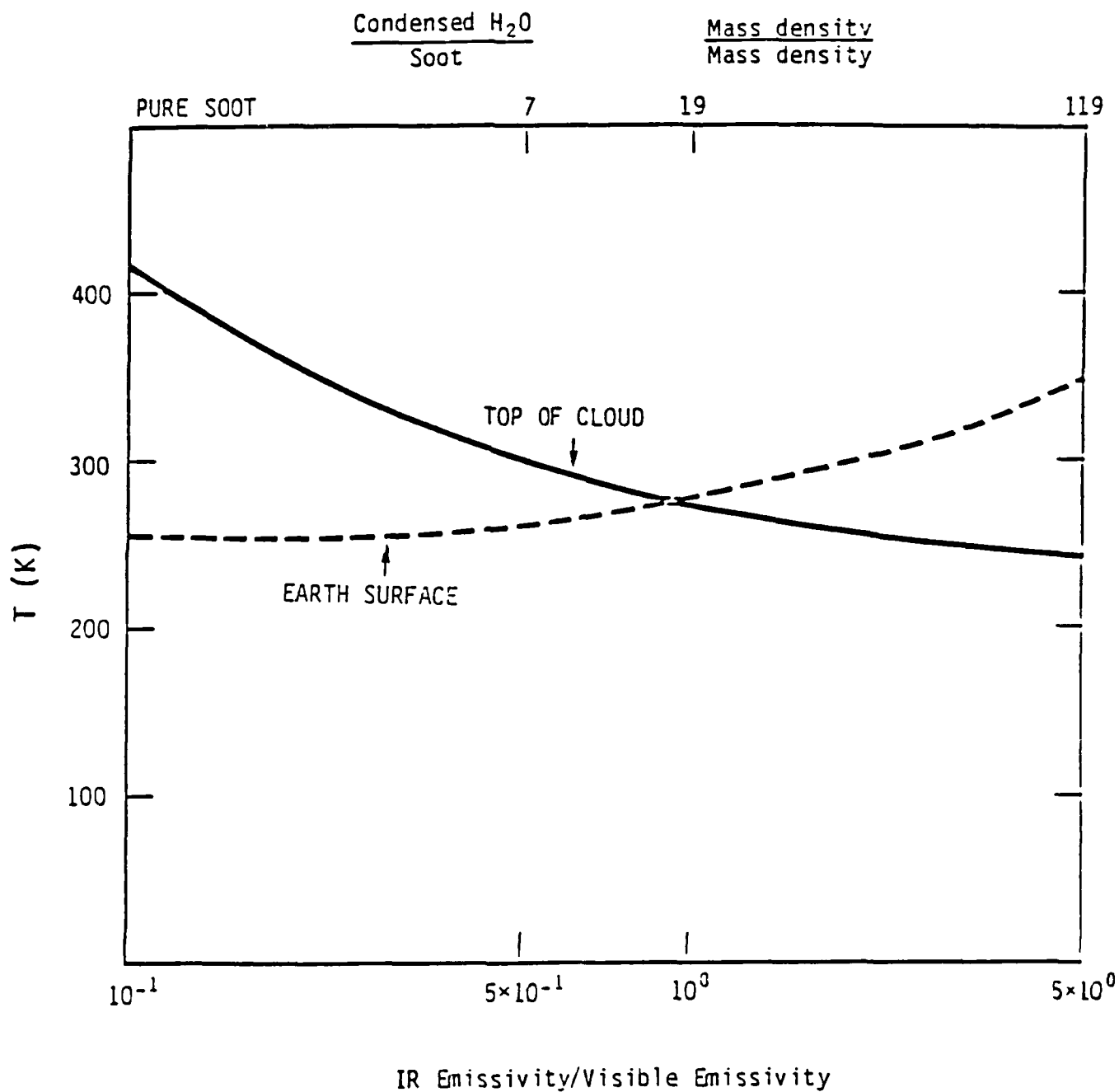
ATMOSPHERIC HEATING WITH MIXED SOOT AND WATER CLOUDS

Carl J. Lauer
Gary D. McCartor

Mission Research Corporation
Santa Barbara, California



ANALYTIC EQUILIBRIUM PREDICTIONS



CURRENT CALCULATIONS

1-D RADIATIVE CONVECTIVE
HEAT TRANSFER SIMULATION

RADIATIVE TRANSPORT

2 STREAMS
1 GROUP VISIBLE, 4 GROUPS INFRARED

CONVECTION

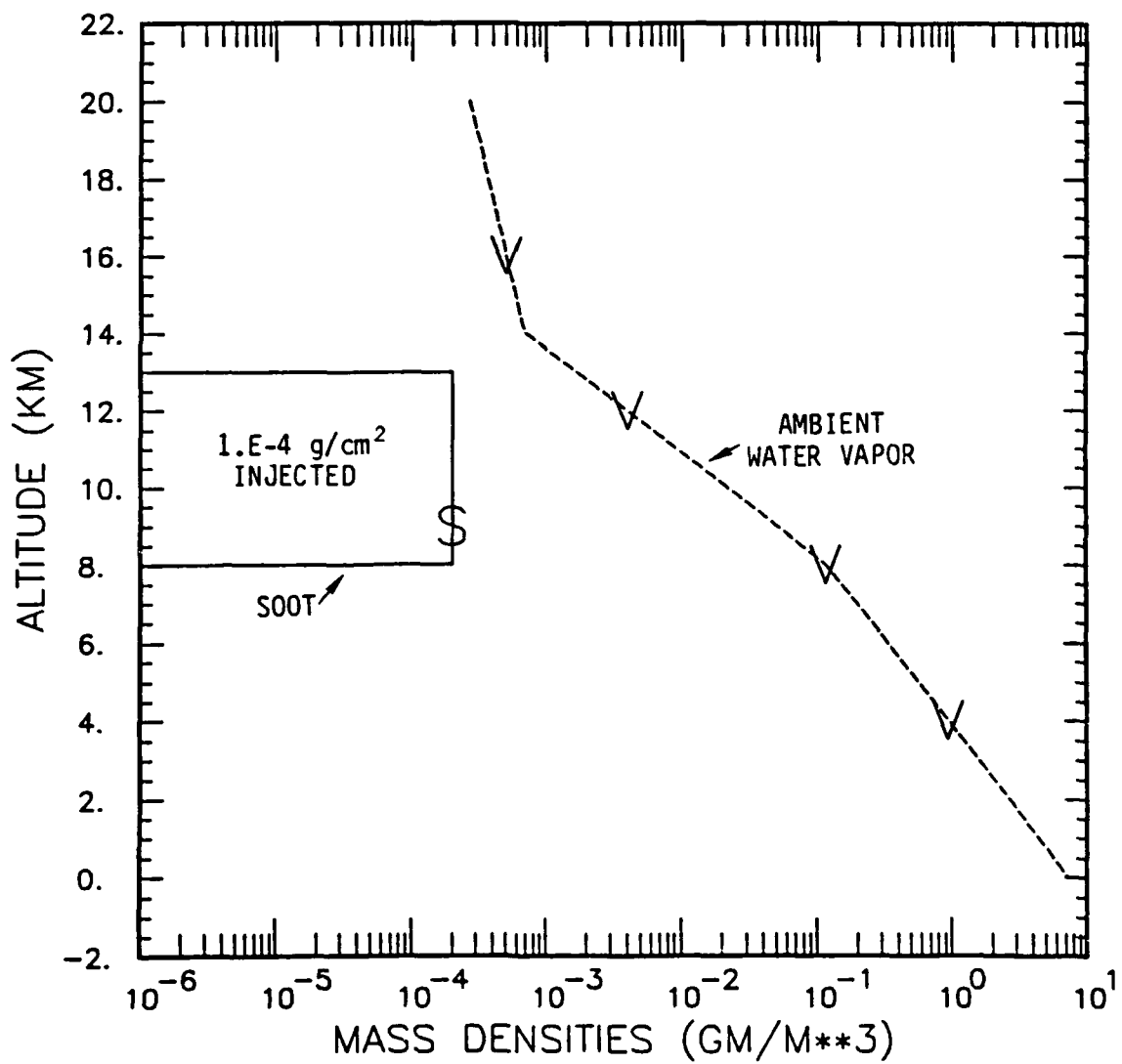
- 6.5°K/KILOMETER LAPSE RATE IS MAINTAINED
BY EXCHANGING MASS BETWEEN LAYERS

WATER LATENT HEATS FUSION, EVAPORATION

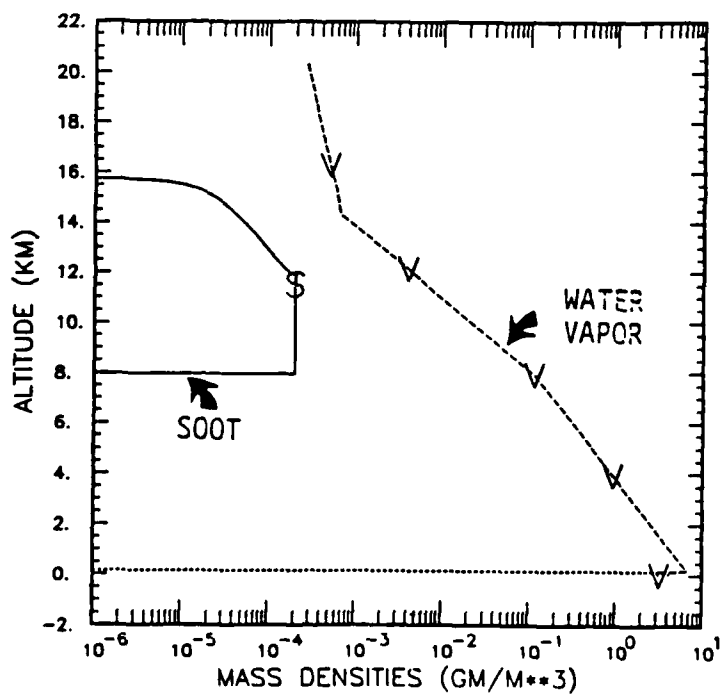
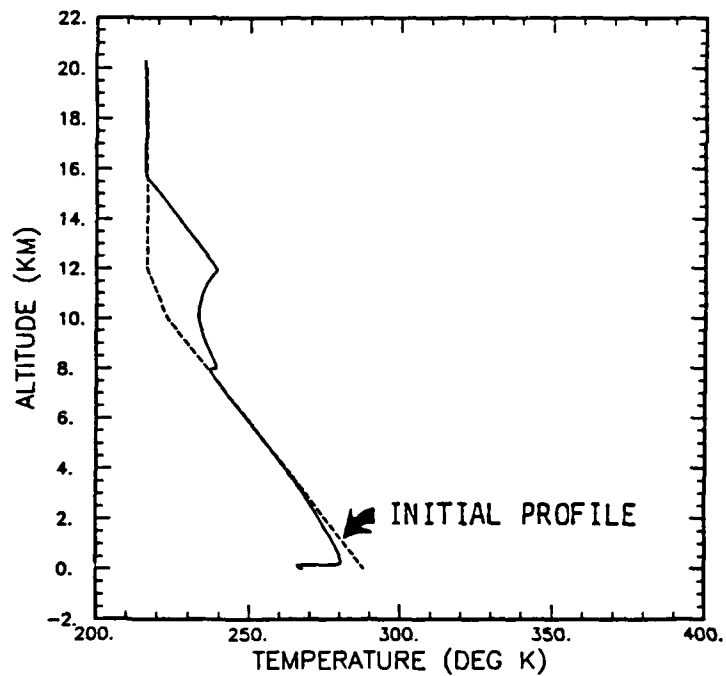
BLACK BODY (ZERO HEAT CAPACITY) OR
CONSTANT TEMPERATURE EARTH SURFACE

SOOT CLOUD 1-D SIMULATION

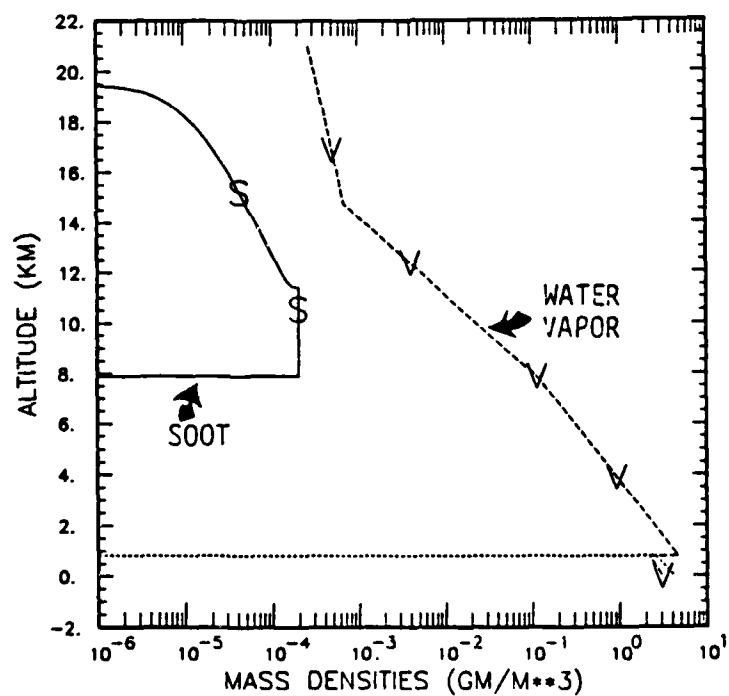
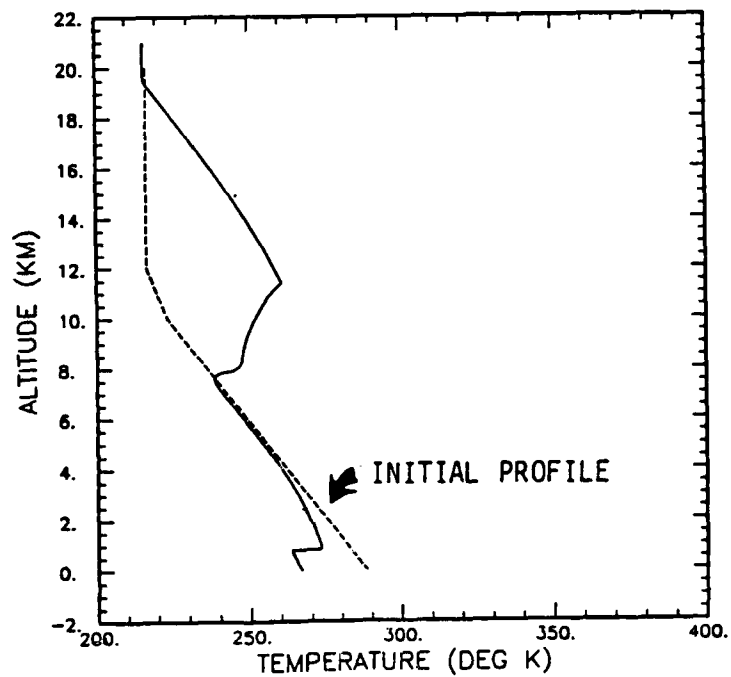
INITIAL CONDITIONS



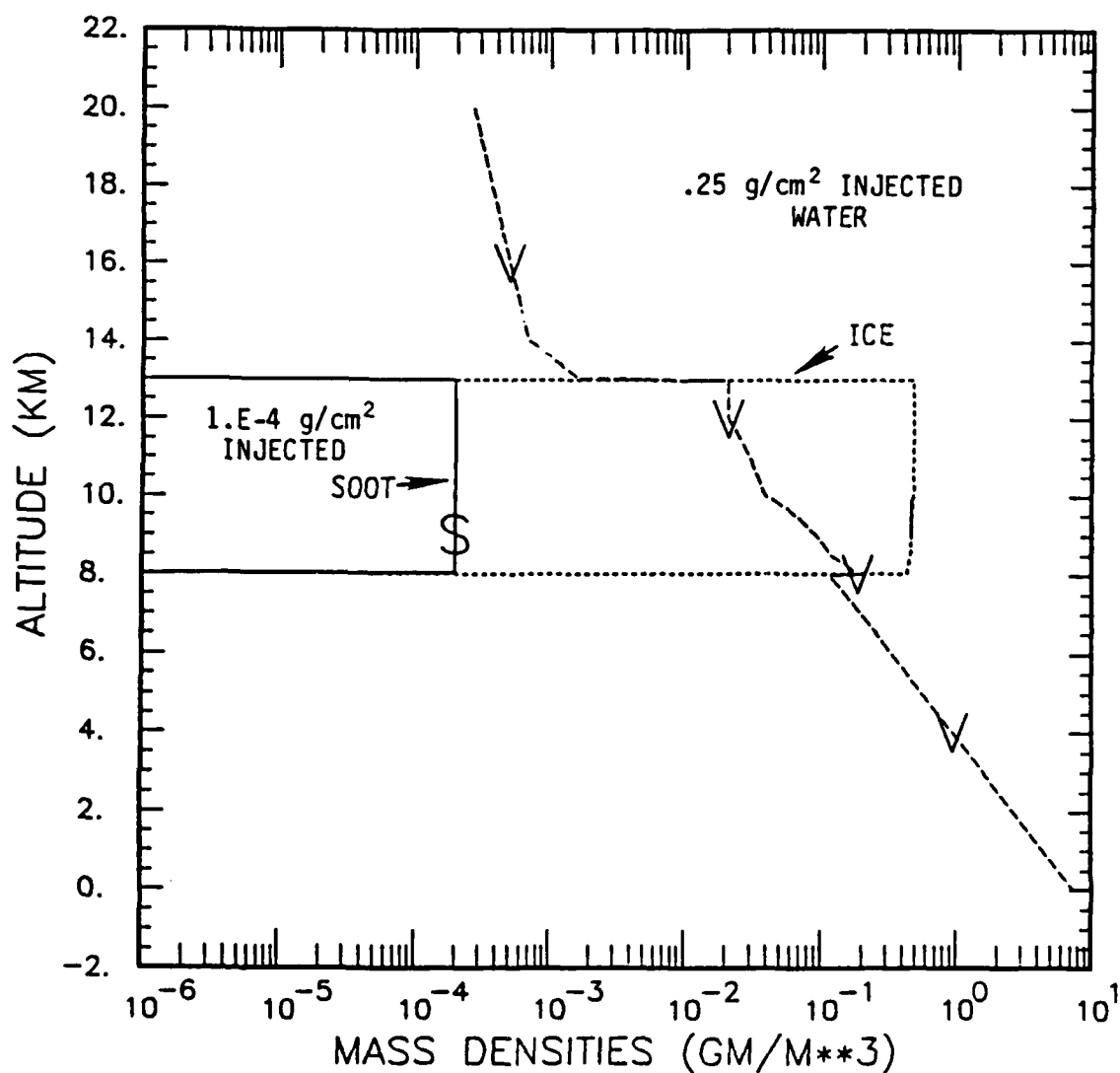
SOOT CLOUD AT 1.2 DAYS



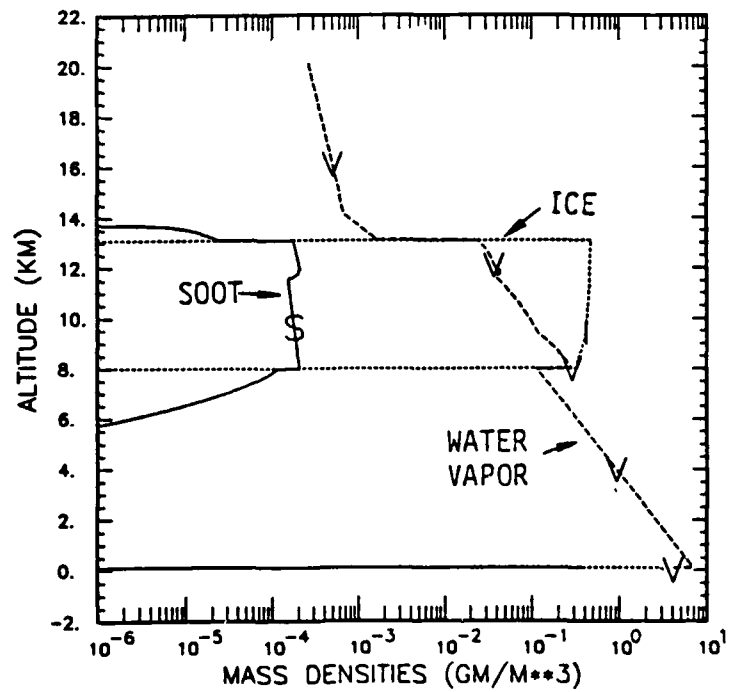
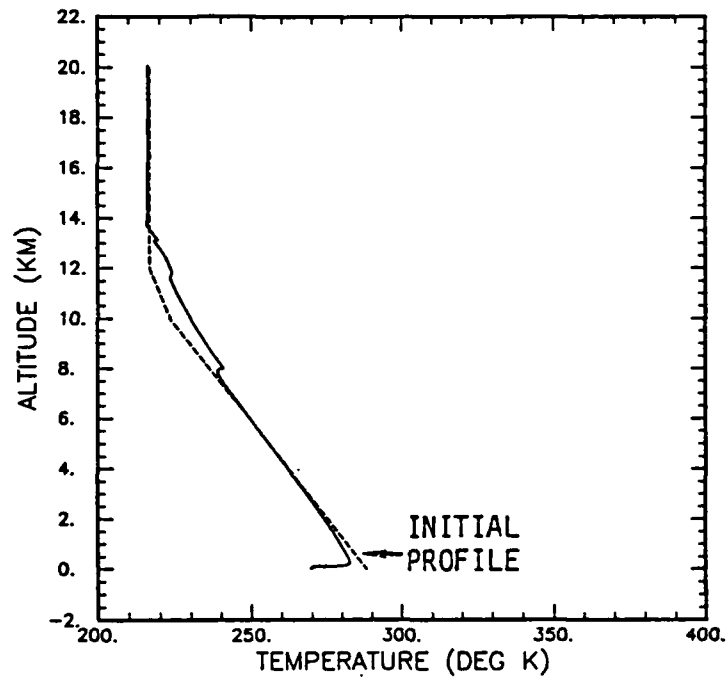
SOOT CLOUD AT 3.5 DAYS



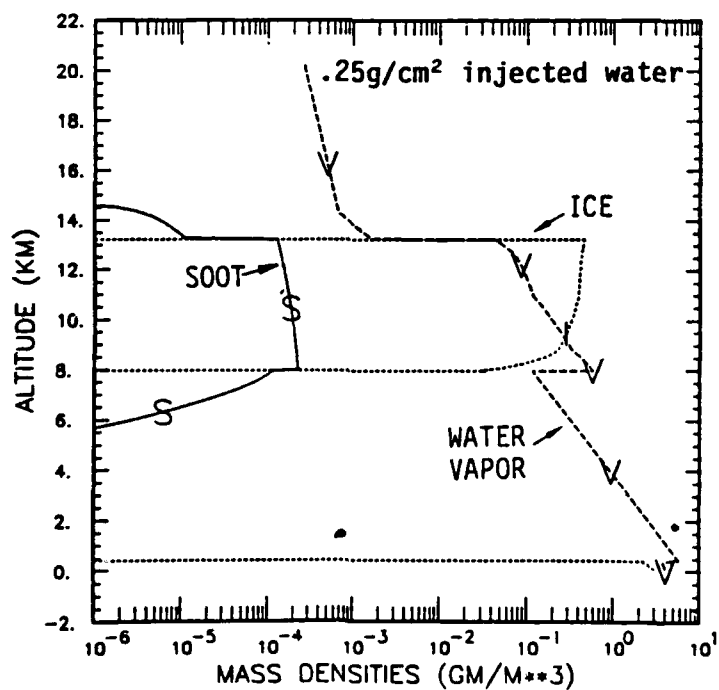
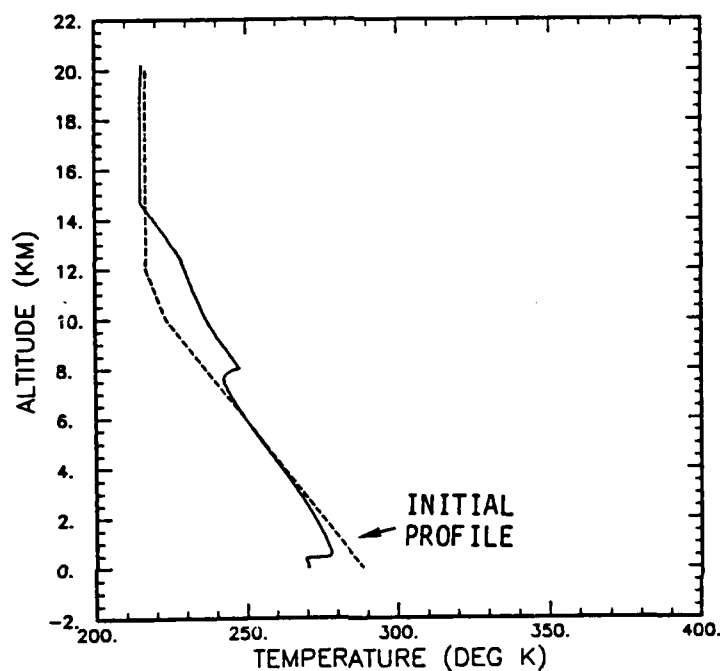
SOOTY WATER CLOUD 1-D SIMULATION INITIAL CONDITIONS



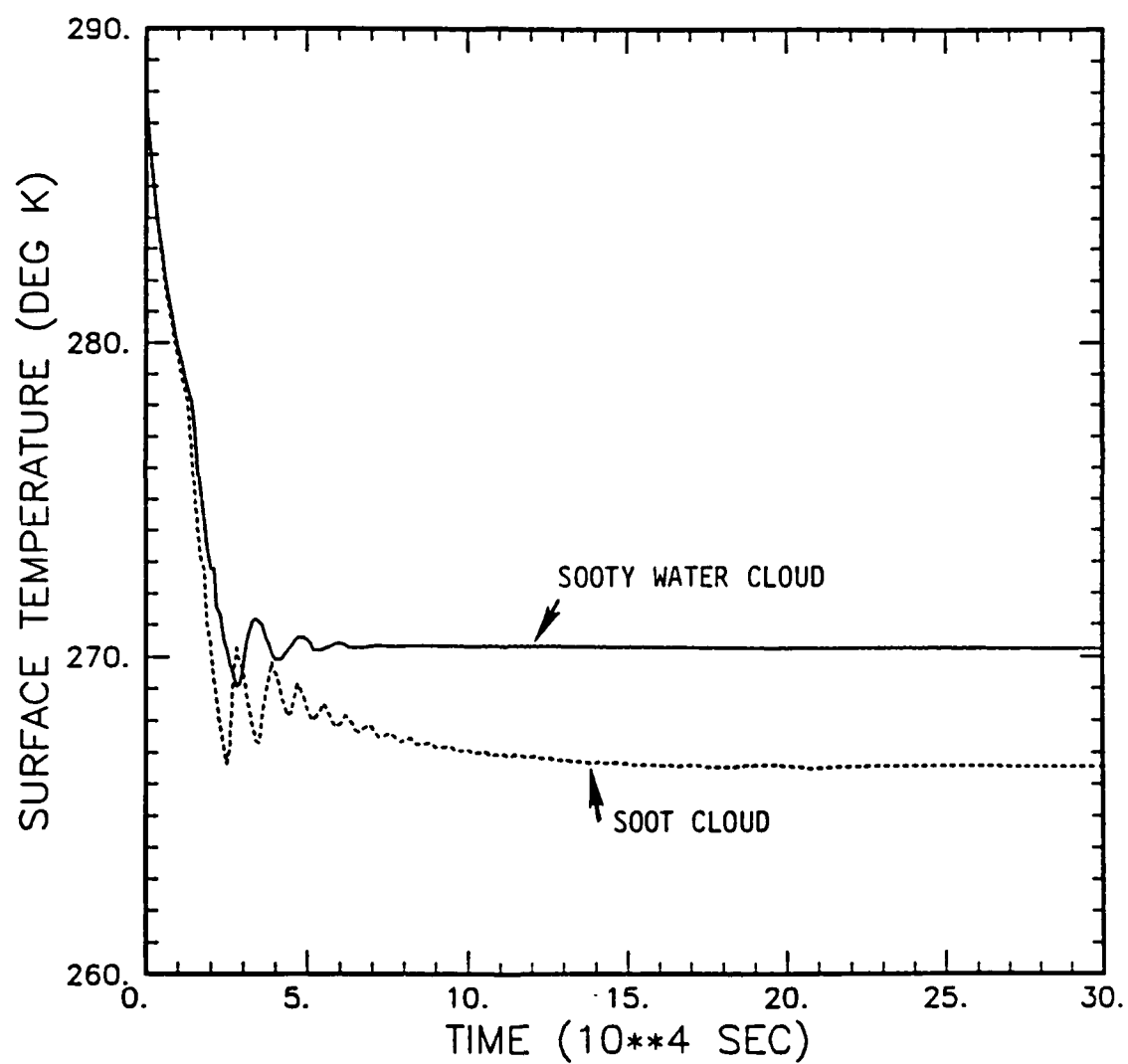
SOOTY WATER CLOUD AT 1.2 DAYS



SOOTY WATER CLOUD AT 3.5 DAYS



TEMPERATURE HISTORIES



CONCLUSIONS

EFFECTS OF CONDENSED WATER ON ATMOSPHERIC
HEATING BY SOOT CLOUDS WHICH HAVE BEEN
SUPPORTED BY NUMERICAL CALCULATIONS

WARMER EARTH SURFACE TEMPERATURES

COOLER CLOUD TEMPERATURES

REDUCTION IN CLOUD RISE
(THIS MAY OCCUR TO A LESSER EXTENT
FROM WATER VAPOR)

ON-GOING WORK WILL EXAMINE THESE EFFECTS OVER
THE RANGE OF CLOUD DENSITIES OF INTEREST

Simulation of Coastal Flow Fields
when the Incident Solar Radiation
Is Obscured

by

Charles R. Molenkamp

Lawrence Livermore National Laboratory



SIMULATION OF COASTAL FLOW FIELDS
WHEN THE INCIDENT SOLAR RADIATION IS OBSCURED*

Charles R. Molenkamp

Lawrence Livermore National Laboratory
Livermore, CA 94550

ABSTRACT

In the aftermath of a large scale nuclear exchange, smoke from many intense fires would be injected into the upper troposphere and stratosphere in such amounts that very little incident solar radiation would reach the ground. It has been suggested that, in coastal regions, the air over land would cool much more rapidly than that over the ocean. In response to this thermal gradient, a super land breeze would form, lifting the moist air over the ocean and producing a zone of anomalous persistent precipitation.

Using an enhanced version of the Colorado State University Mesoscale Model, the development of coastal flow fields are being simulated during periods of extended obscuration of solar energy by completing one normal diurnal cycle starting at dawn and then extending the simulation for an additional 24-48 hours with no incident solar radiation. For these simulations two changes have been made to the model. First, a cloud module has been added that allows for the formation of a cloud or fog whenever the atmosphere is saturated. Second, the longwave cooling module has been rewritten to improve its accuracy and allow for the effects of clouds.

For a typical west coast situation, with a moderate westerly mean flow, the surface layer over land cools a few degrees during the night to a temperature where saturation occurs and a thin ground fog forms. This fog protects the ground surface from further rapid cooling and grows in height as a reasonably well-mixed layer forms over land with a cloud layer at the top. Over the ocean, moisture is vertically mixed upward into layers that are cooling radiatively so a similar cloud forms. With clouds over both land and sea there are only small thermal gradients so the hypothesized precipitation zones do not occur.

Simulations for a typical east coast situation are currently underway.

*This work was performed under the auspices of the U.S. Department of Energy by the Lawrence Livermore National Laboratory under Contract W-7405-Eng-48.

Basic Question:

If solar radiation were blocked from the ground by a layer of smoke, would the flow fields at the continental coastlines be modified to increase the likelihood of precipitation and scavenging?

Preliminary Answer:

The formation of fog or cloud over both land and sea prevents the development of large thermal gradients and significant induced flows.

Approach:

Numerical Simulation Using the Colorado State University Mesoscale Model (Pielke, et. al.)

- **Hydrostatic incompressible flow**
- **Surface flux, planetary boundary, and synoptic layers**
- **Vertical diffusion in the planetary boundary layer
depends on atmospheric stability**
- **Solar and infrared heating/cooling of surface and
atmosphere**
- **Surface heat budget (land and sea surfaces)**

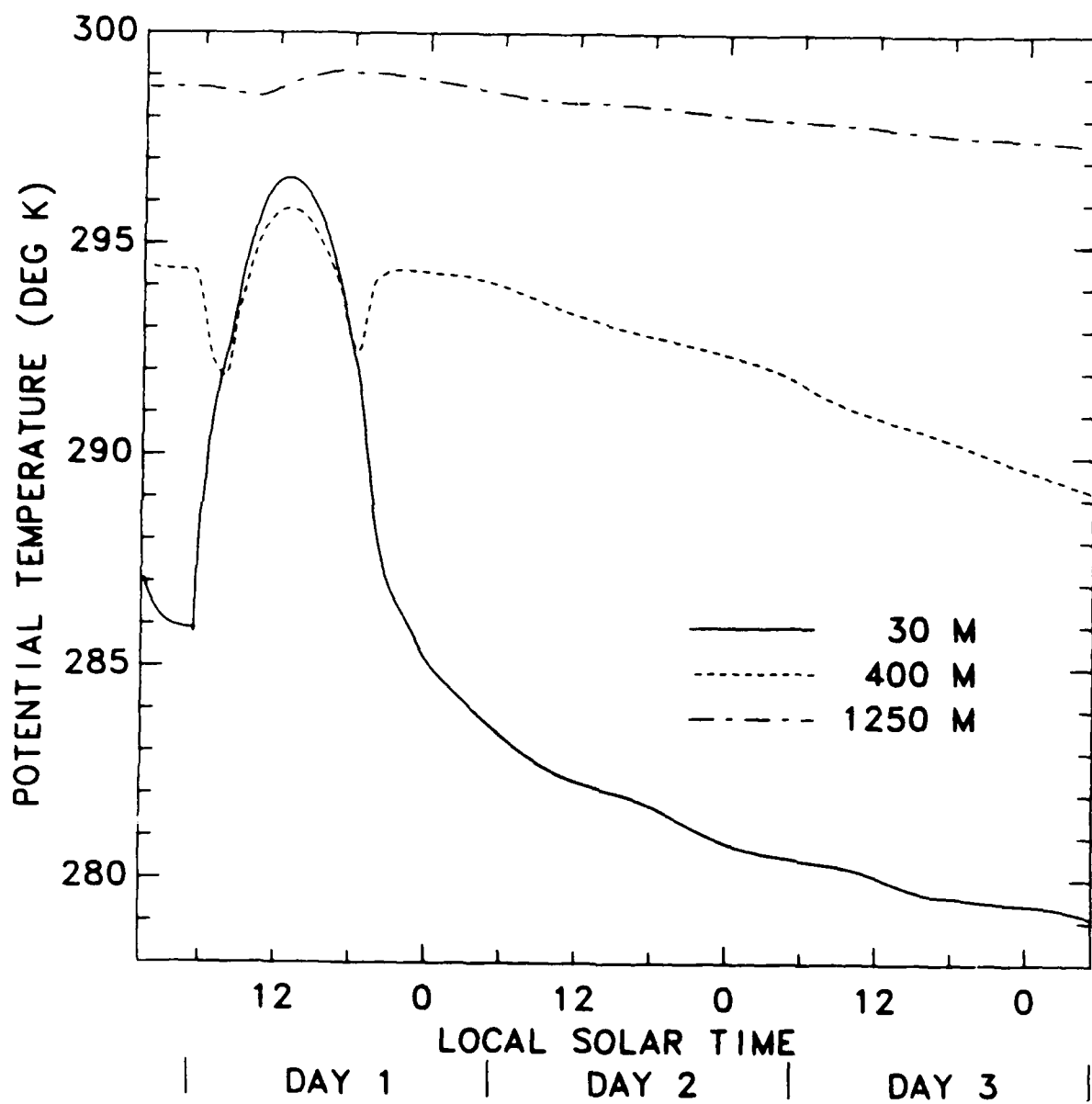
Procedure:

Run CSU Model (2D)

- 4 hour initialization
- 24 hour diurnal cycle starting at dawn (05:18)
- 24 hours with no solar input

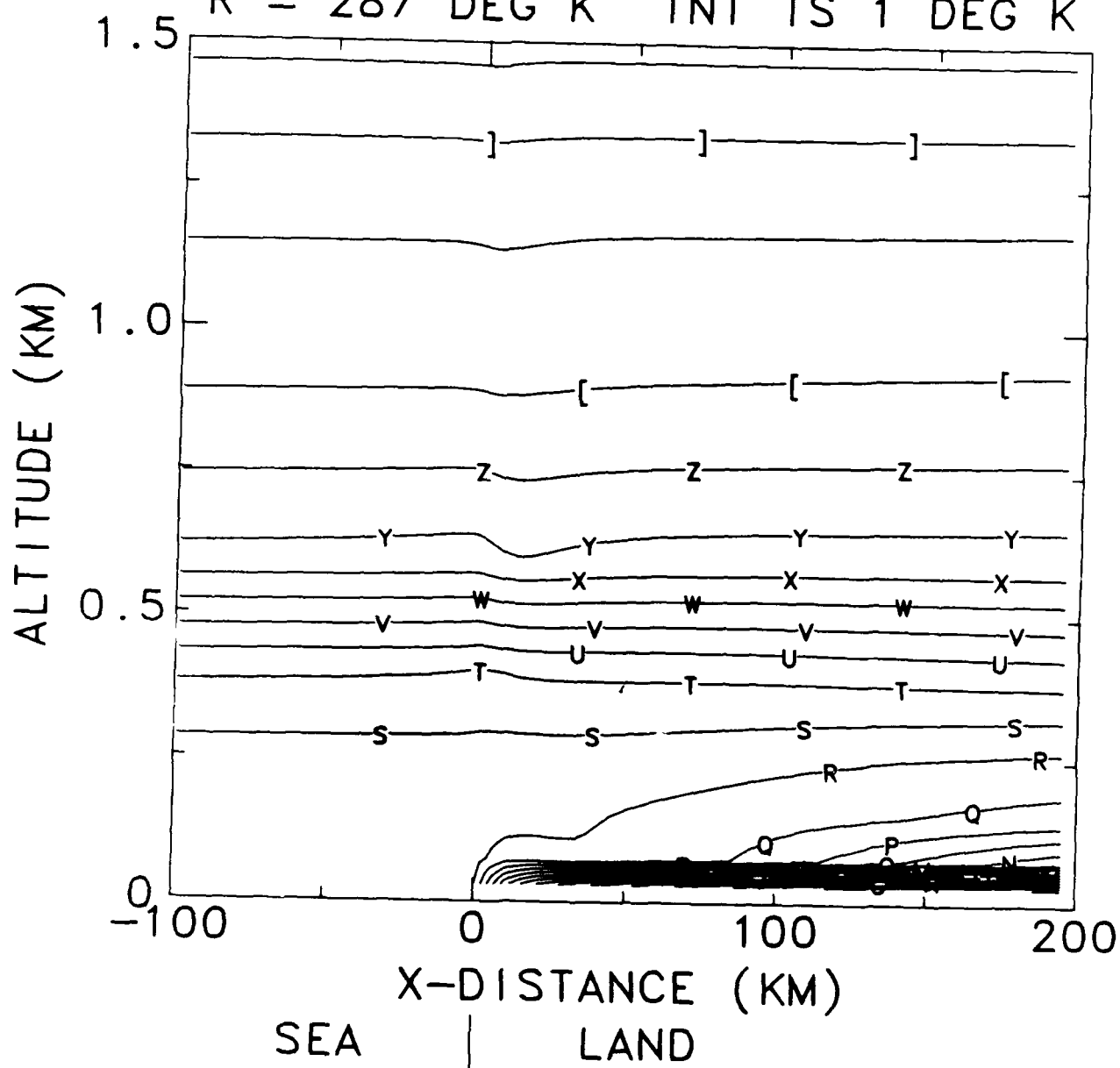
Initial Conditions

- Sounding for the Oregon Coast on 23 Aug 72
- 5 m/sec onshore synoptic flow from West
- Sea surface temperature is 289K



WCSLK8
+27 KM

POTENTIAL TEMP DAY 4 05:18LST
R = 287 DEG K INT IS 1 DEG K



WC5LK8
76HRS

MODIFICATIONS TO THE CSU MESOSCALE MODEL

- **CLOUDS**

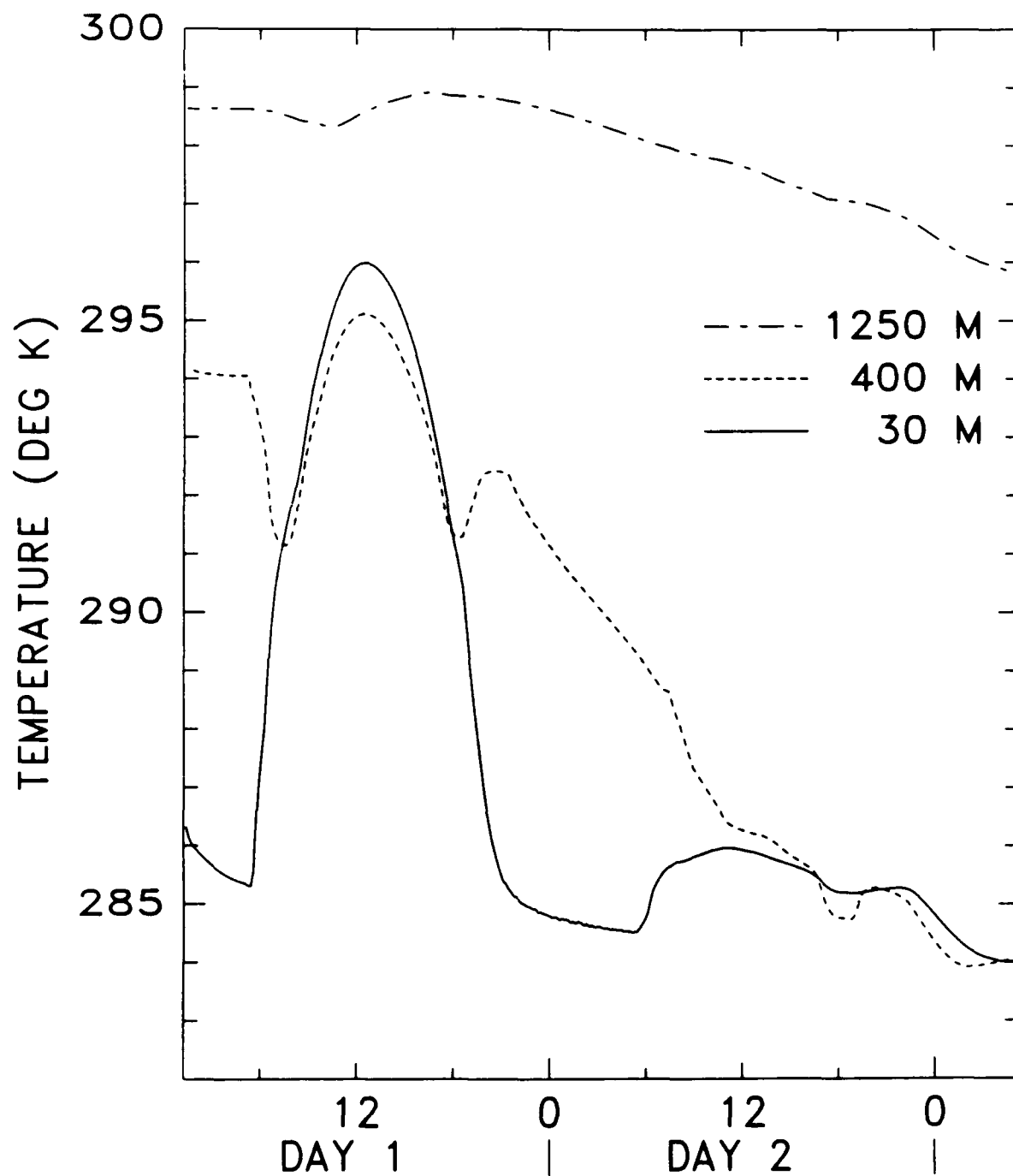
- Original water vapor equation retained but represents vapor plus liquid
- New liquid water variable is the excess water over saturation
- Condensational heating and evaporative cooling change the atmospheric temperature (iterative)

- **RADIATION (long wave)**

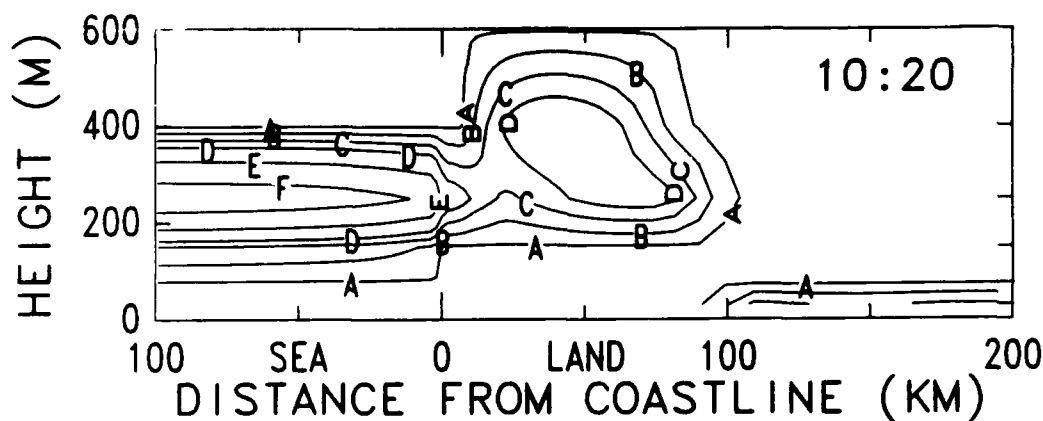
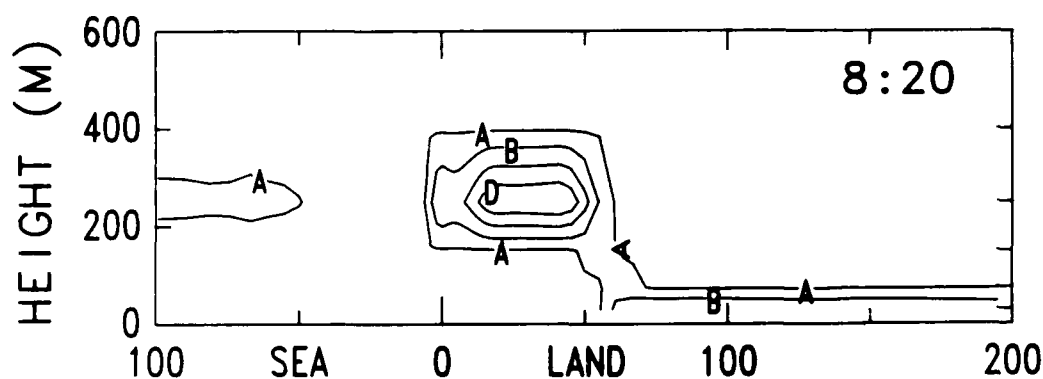
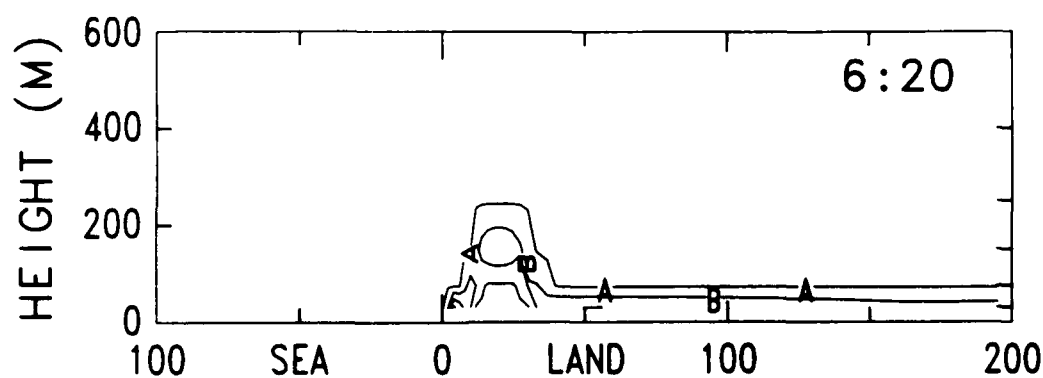
MODIFICATIONS TO THE CSU MESOSCALE MODEL

- **CLOUDS**
- **RADIATION (long wave)**
 - New model for clear air long wave radiation
 - + incorporates temperature variation with height
 - + emissivities taken from Liou & Ou (3 water vapor, 1 carbon dioxide, and 1 overlap band)
 - Clouds treated as gray bodies with emissivities given by Stephens
 - Clouds act as boundaries for the clear air flux calculations

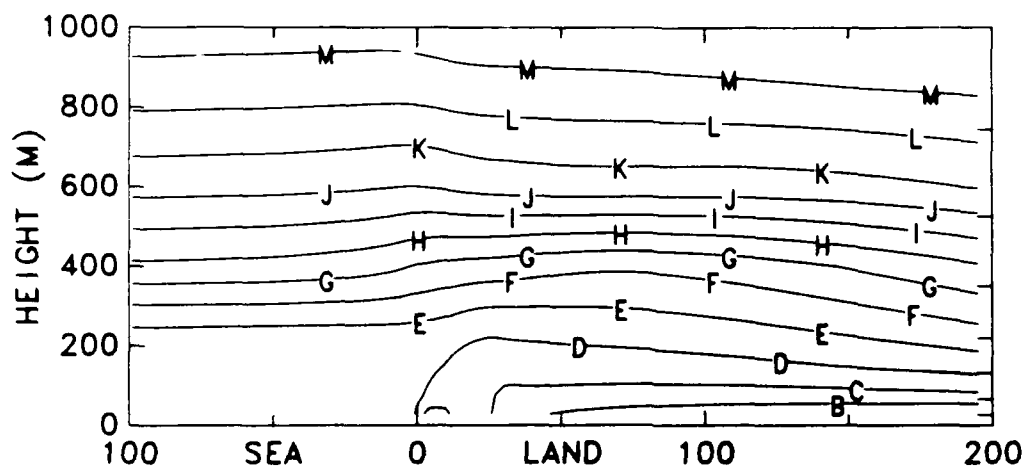
POTENTIAL TEMPERATURE
AT A POINT 27KM INLAND



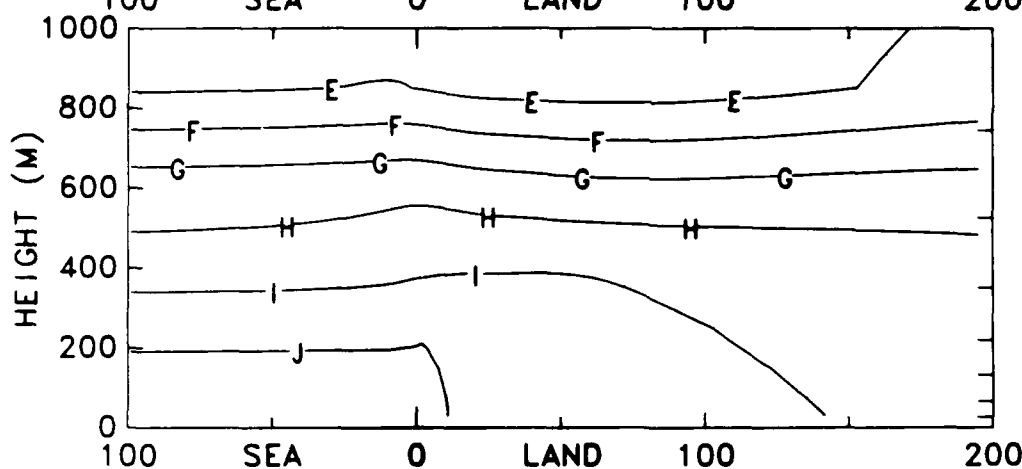
FORMATION OF CLOUD FROM 6:20 TO 10:20 ON DAY 2



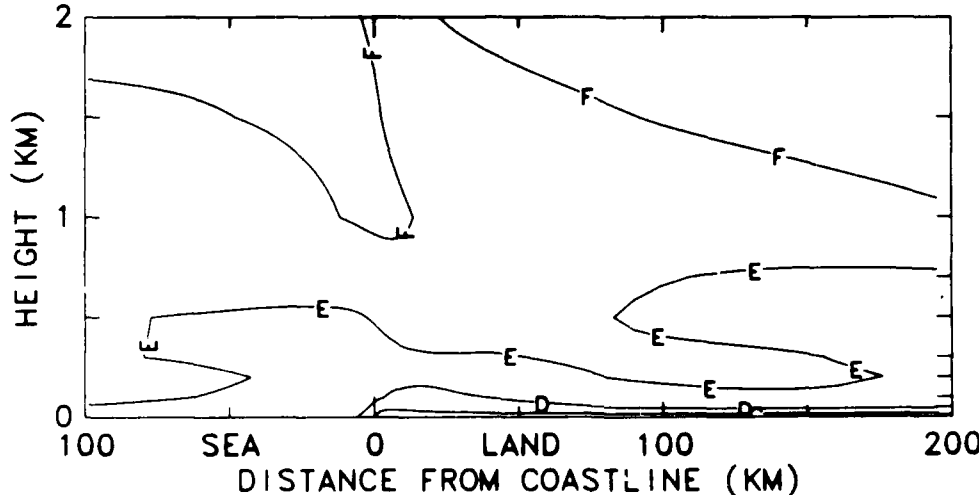
POT TEMP, WATER CONTENT AND WIND SPEED AT 6:20 ON DAY 2



B = 285
D = 287
F = 289
H = 291
J = 293
L = 295

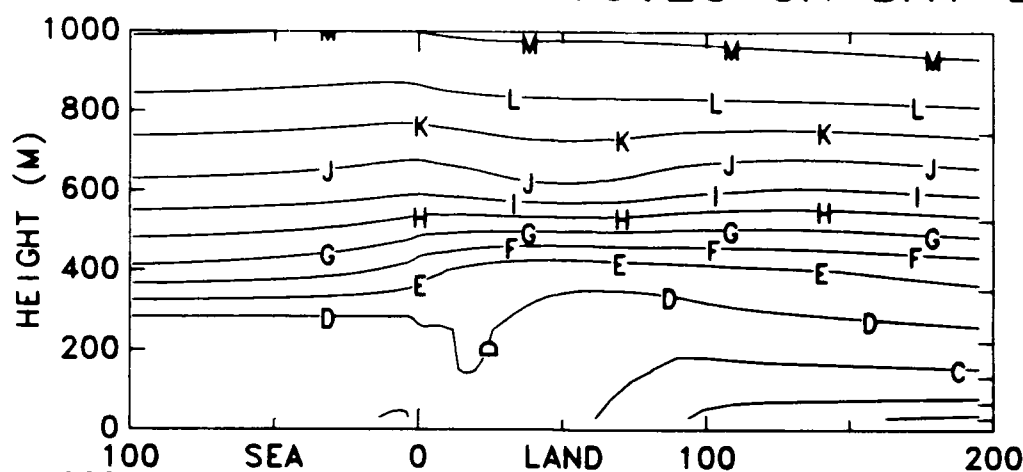


E = .005
F = .006
G = .007
H = .008
I = .009
J = .010

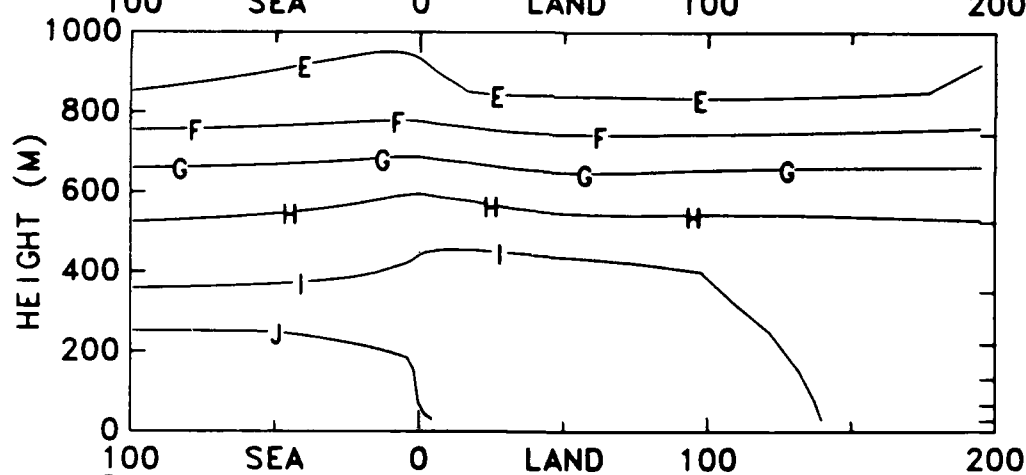


C = 2 M/S
D = 3 M/S
E = 4 M/S

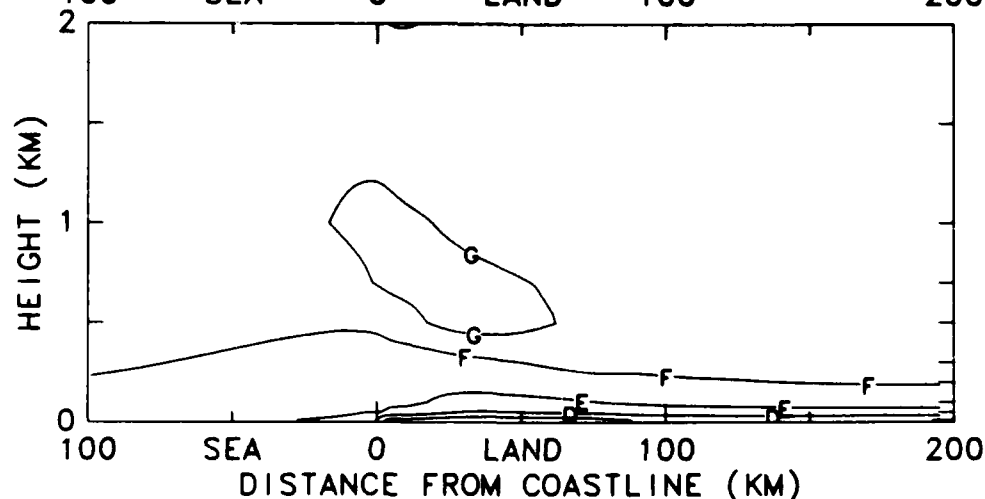
POT TEMP, WATER CONTENT AND WIND SPEED AT 10:20 ON DAY 2



A = 284
C = 286
E = 288
G = 290
I = 292
K = 294
M = 296

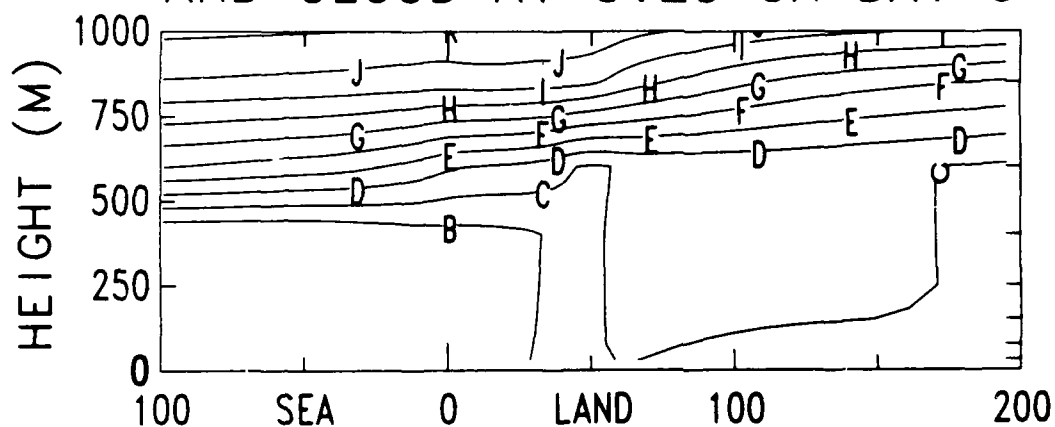


E = .005
F = .006
G = .007
H = .008
I = .009
J = .010

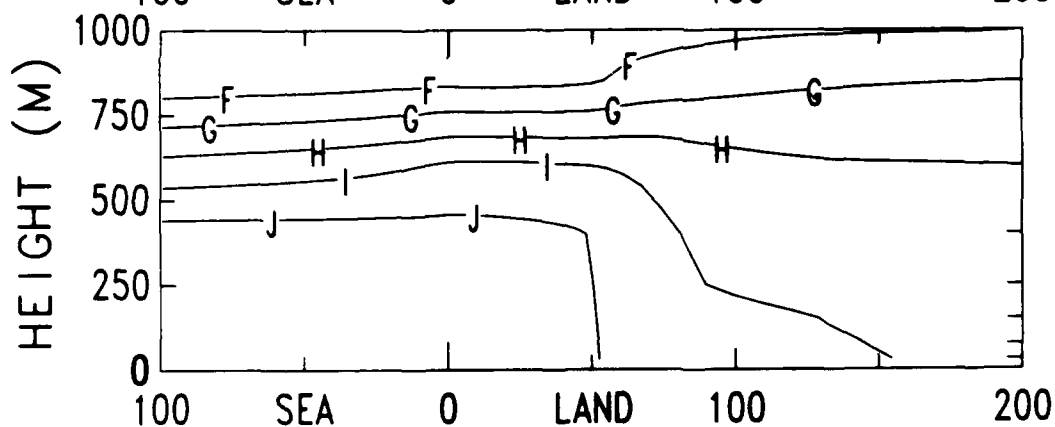


C = 2 M/S
D = 3 M/S
E = 4 M/S
F = 5 M/S
G = 6 M/S

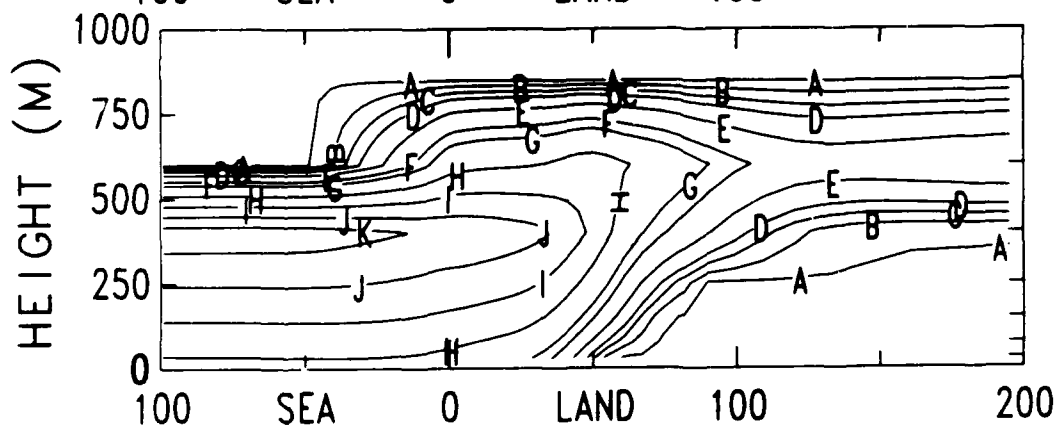
POT TEMP, WATER CONTENT AND CLOUD AT 3:20 ON DAY 3



B = 285
C = 286
D = 287
E = 288
F = 289
G = 290



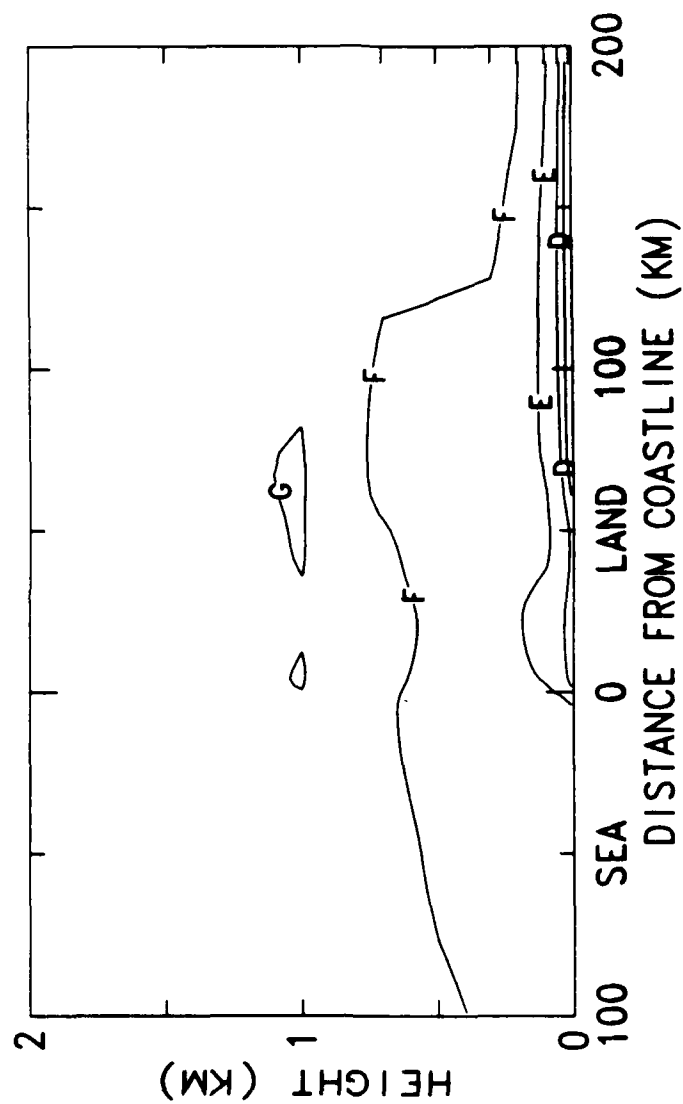
F = .006
G = .007
H = .008
I = .009
J = .010



K = .003
J = .0025
I = .002
H = .0015
G = .001
F = .0008
E = .0005

DISTANCE FROM COASTLINE (KM)

ACROSS COAST WIND SPEED AT 3:20 ON DAY 3



Mesoscale Aspects of the Climatic Effects of a Large Nuclear War

Filippo Giorgi

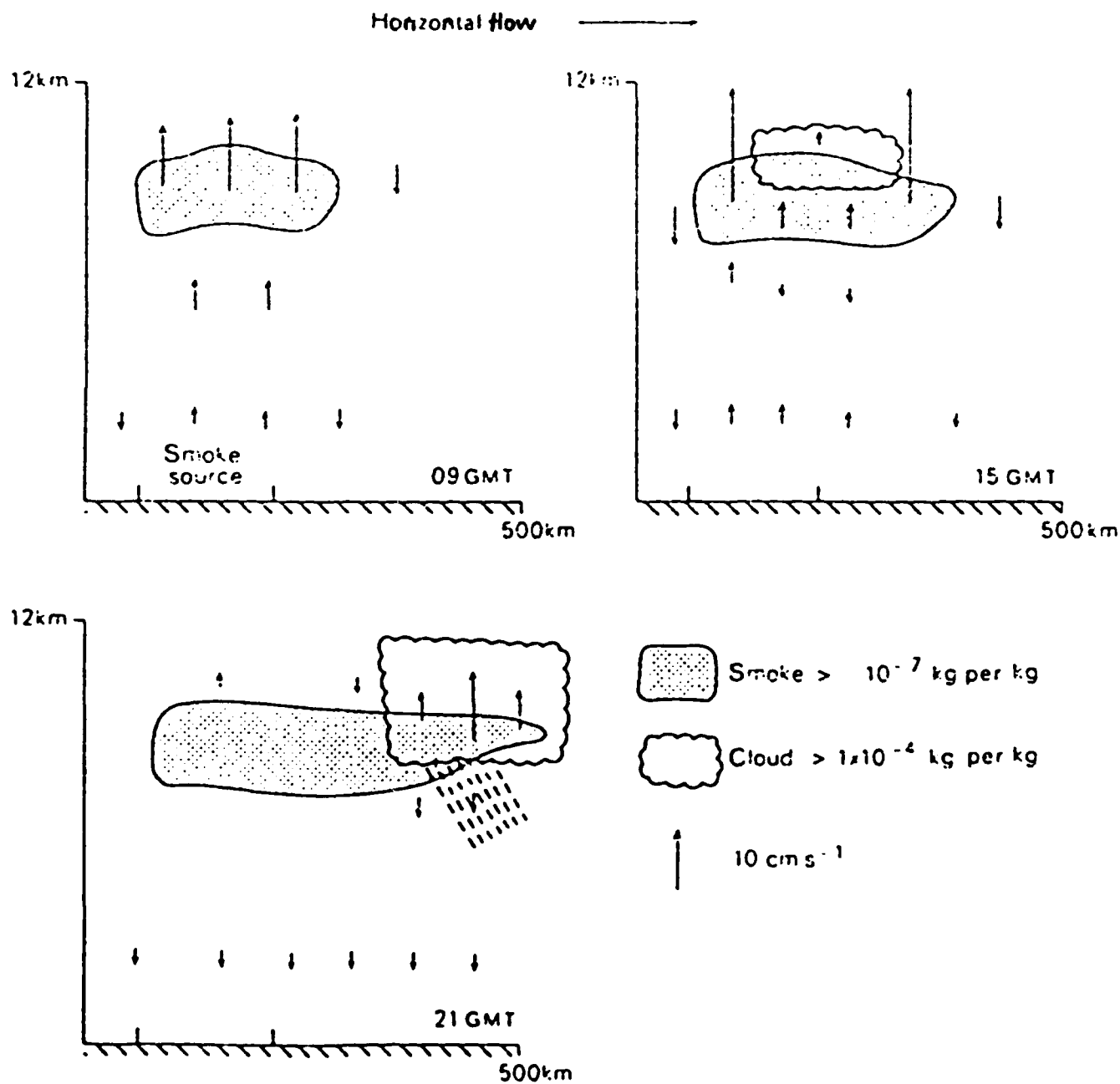
*National Center for Atmospheric Research
P.O. Box 3000, Boulder, Colorado 80307*

Most assessments of the climatic consequences of a major nuclear conflict have been made using 1-dimensional (1D) radiative-convective models or 3-dimensional general circulation models (GCM). In these studies, initial distributions of nuclear smoke and dust uniform over large scale domains were employed. The assumption was that the thousands of smoke and dust plumes generated in the aftermath of the conflict would rapidly merge, due to the atmospheric winds, to form a widespread cloud. A few preliminary studies, however, have indicated that atmospheric perturbations can be induced by the nuclear aerosols on the mesoscale (10-1000 km), which can strongly affect the aerosol distribution and properties. This, in turn, will influence both local or regional "acute" effects (by perturbing the local meteorology) and long term "chronic" effects (by modifying the amount and properties of the injected material). In this study it is proposed to employ a mesoscale model to investigate behaviour, interactions, and meteorological effects of the aerosol plumes in the first several days (5-10) after the conflict. Results will be compared with GCM predictions of acute climatic effects, and the implications on the initial smoke distribution and properties to be used in GCM studies will be analyzed. An augmented, 2D version of the Penn State/NCAR mesoscale model will be initially used. A number of physics parameterizations will be added to the current version of the model. These include a detailed description of surface physics and radiative transfer, an improved description of the atmospheric water cycle, and aerosol transport, microphysics, and interactive radiative effects. The sensitivity of the results to model resolution and physical domain, physics parameterizations, and aerosol injection scenarios will be examined. Depending on the indications of these 2D simulations the possibility of performing 3D simulations will be considered.

MESOSCALE ASPECTS OF THE CLIMATIC EFFECTS OF A LARGE NUCLEAR WAR

MAIN OBJECTIVES

- Study of regional, "acute", climatic effects of massive aerosol injections from a large nuclear war (5–10 days after the conflict)
 - Prediction of atmospheric perturbations on the mesoscale (10–1000 km), and related perturbations of surface climatic variables (e.g., surface temperature)
 - Comparison with general circulation model (GCM) predictions
- Study of the effect of aerosol-induced mesoscale atmospheric perturbations on the aerosol properties and distribution; implications for injection scenarios used in global scale studies.



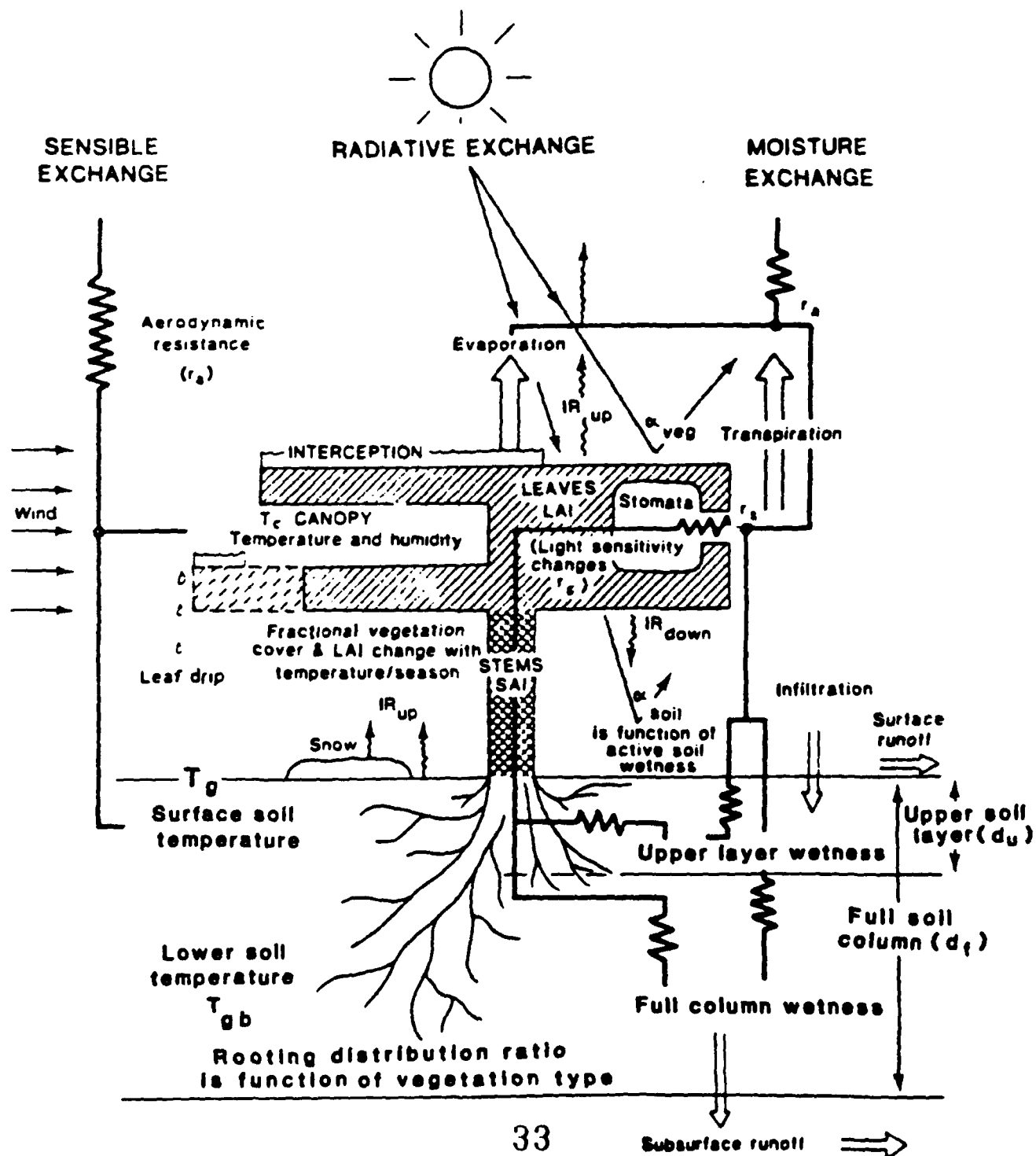
MODELING APPROACH

- Penn State/NCAR mesoscale model, version MM4
(2D version for now)
 - Primitive equations
 - σ vertical coordinate
 - Hydrostatic
 - Compressible
- Physics included in the current version of the model
 - Moisture
 - * Cumulus parameterization (Anthes, 1977)
 - * Explicit liquid water scheme (Hsie et al., 1984)
 - Boundary layer
 - * Bulk PBL (Deardorff, 1972)
 - * High resolution PBL (Zhang and Anthes, 1982)
 - Radiative transfer (simple parameterization)
 - Ground temperature calculated via an energy balance equation (Blackadar, 1979)
 - Horizontal and vertical sub-grid scale eddy diffusion

- Model enhancements planned for this study
 - Improve surface physics description
 - Improve radiative transfer calculations
 - Include simple ice physics parameterization
 - Include aerosol transport, microphysics, and interactive radiative effects

SURFACE PHYSICS MODEL ENHANCEMENTS

- Apply to MM4 the surface physics package developed by R. Dickinson and collaborators

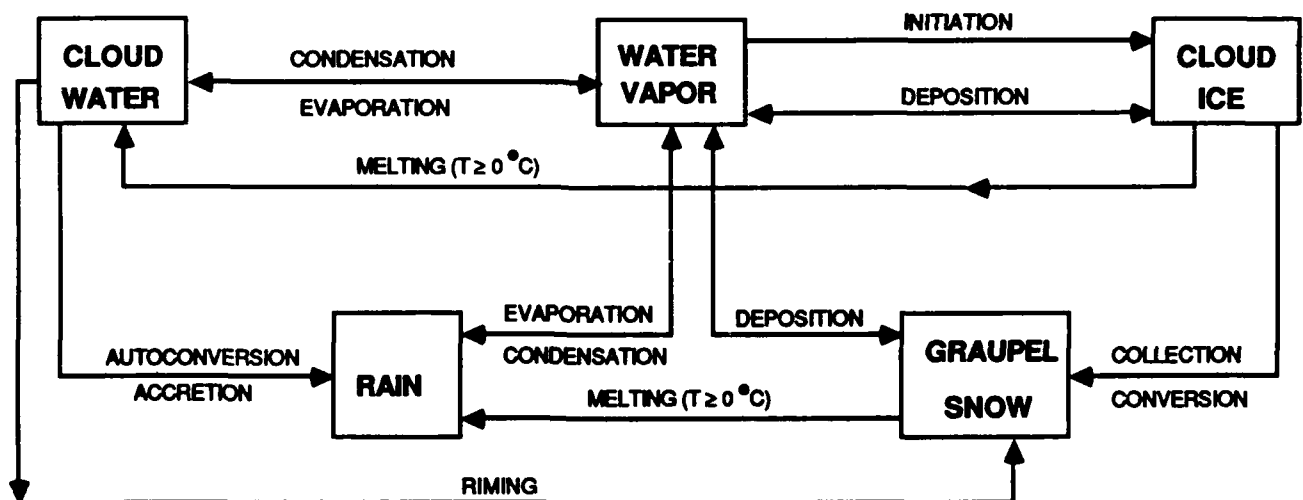


RADIATIVE TRANSFER MODEL ENHANCEMENTS

- Apply to MM4 the radiative transfer package of the Community Climate Model (version CCM1). This package includes:
 - Clear sky
 - * Longwave → H_2O , CO_2 , O_3
 - * Shortwave → Rayleigh scattering, absorption by O_3 , H_2O , CO_2 , O_2
 - Cloud–radiation interactions
 - * Longwave → Clouds are assumed to be black for $\sigma \geq 0.5$, for $\sigma \leq 0.5$ clouds are assumed to be black only if the cloud water content exceeds 10 g/m^2
 - * Solar → Cloud albedo depends on zenith angle and cloud type. Accounts for multiple reflection between different cloud layers and between clouds and surface. Gaseous absorption within clouds included.

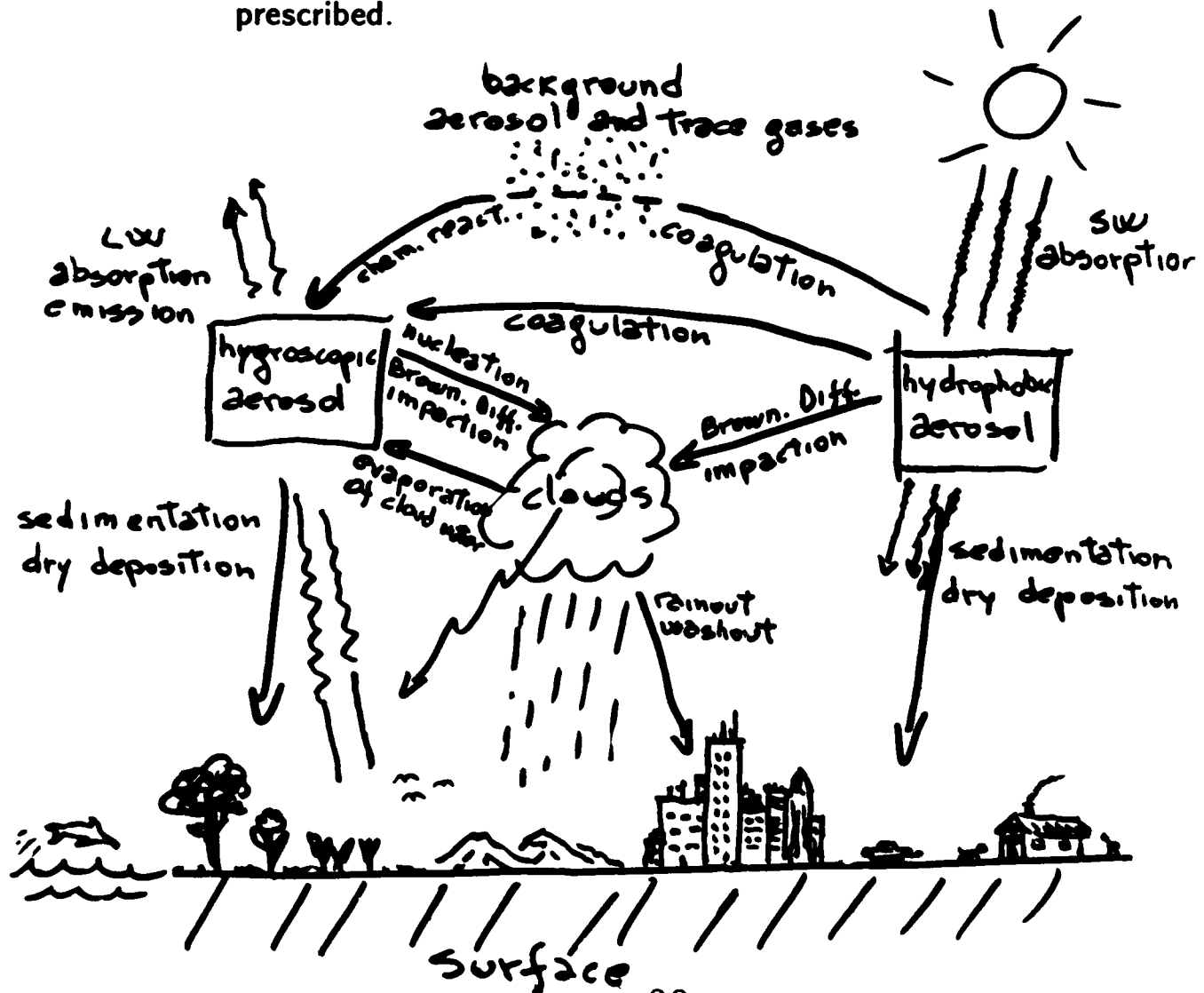
MOISTURE PHYSICS MODEL ENHANCEMENTS

- A prognostic equation for cloud ice is added to those for cloud water and rain water present in the current explicit liquid water scheme (after Rutledge and Hobbs, 1983, 1984)



AEROSOL PHYSICS

- Prognostic equations are solved for the hygroscopic (includes also large wettable particles and IN) and hydrophobic fractions of a given nuclear aerosol (smoke, dust). The equations include transport and several microphysical processes. For both aerosol fractions the size distribution is prescribed.



EXPERIMENTS PLANNED

- Test the new physics parameterizations; use as a “control case” the sea-breeze simulations of Yan and Anthes (1987)
- Sensitivity to injection scenarios; use results from plume dynamics simulations
 - Plume distribution
 - Injection height
 - Properties of injected aerosol
 - Aerosol loading
- Sensitivity to model physics options
 - Surface physics options
 - Radiation transfer options
 - Moisture physics options
- Sensitivity to model domain and resolution
 - Surface characteristics
 - Seasonal effects
 - Initial conditions
 - Boundary conditions

**A CASE STUDY OF A
FOREST FIRE SMOKE PLUME**

Douglas L. Westphal

Pennsylvania State University

Owen B. Toon

NASA Ames Research Center

PROJECT SUMMARY

- **Goals**

- Understand the regional-scale interactions between large soot clouds and atmospheric circulations
- Determine the impact of soot clouds on local climate

- **Method**

- Study natural analogs to nuclear winter
- Develop numerical models; verify their accuracy by modeling the natural analogs
- Use the models to study possible nuclear winter scenarios

FORT NELSON FIRE CHRONOLOGY

- June 19 – Fire started by lightning
400 ha (100 ha = 1 km²).
- June 24 – 20,000 ha
- July 15 – 78,000 ha
- July 26 – 87,000 ha
- July 28 – 88,000 ha
- July 29 – 160,000 ha (40 km x 40 km)
Fire doubled in size in 24 hrs.
16 km run in 4 hours.
Convective column was observed.
(~ 0.07 to 0.4 Tg soot produced)

FORT NELSON FIRE DATA SUMMARY

- **Fire Data**

- Fire spread maps, fuel loading (Lawson, Canadian Forest Service)
- Lodi Canyon fire and Fresno area fire (Peuschel et al.)
- Landsat and AVHRR satellite imagery

- **Meteorological Data**

- Surface observations
- Upper air (NMC analyses and Navy data archives)
- MOS analyses (Robock, U. of Mary.)

- **Aerosol Data**

- Aircraft pilot reports
- Surface radiometric measurements (Ryznar, U. of Mich.)
- Satellite data (Fraser and Ferrare, Goddard)
- Nephelometer measurements (Eloranta, U. of Wisc.)

CONCLUSIONS

- Significant dataset is available
 - Source term information
 - Soot cloud optical properties
 - Observations of perturbations due to smoke cloud
- Transport modified by small-scale wave
- Model shows skill at forecasting small-scale waves
- Ready to carry out interactive calculations

FIGURE CAPTIONS

- Fig. 1 Outline of the area where surface meteorological stations reported "visibility reduced by smoke" during the period 4 am (PST) 29 July to 4 am 30 July, 1982.
- Fig. 2 Contours of the analyzed (\sim observed) height (gpm) of the 500 mb surface at 4 pm (PST) 31 July, 1982.
- Fig. 2 Contours of the analyzed (\sim observed) height (gpm) of the 500 mb surface at 4 pm (PST) 2 August, 1982.
- Fig. 4 Contours of the predicted height (gpm) of the 500 mb surface at 4 pm (PST) 2 August, 1982. Compare with Fig. 3.
- Fig. 5 Contours of the analyzed (\sim observed) surface temperature ($^{\circ}\text{C}$) at 4 pm (PST) 2 August, 1982.
- Fig. 6 Contours of the predicted surface temperature ($^{\circ}\text{C}$) at 4 pm (PST) 2 August, 1982. Compare with Fig. 5.

Fig. 1 Area of "Visibility reduced by smoke"
4 am (PST) 29 July to 4 am 30 July, 1982

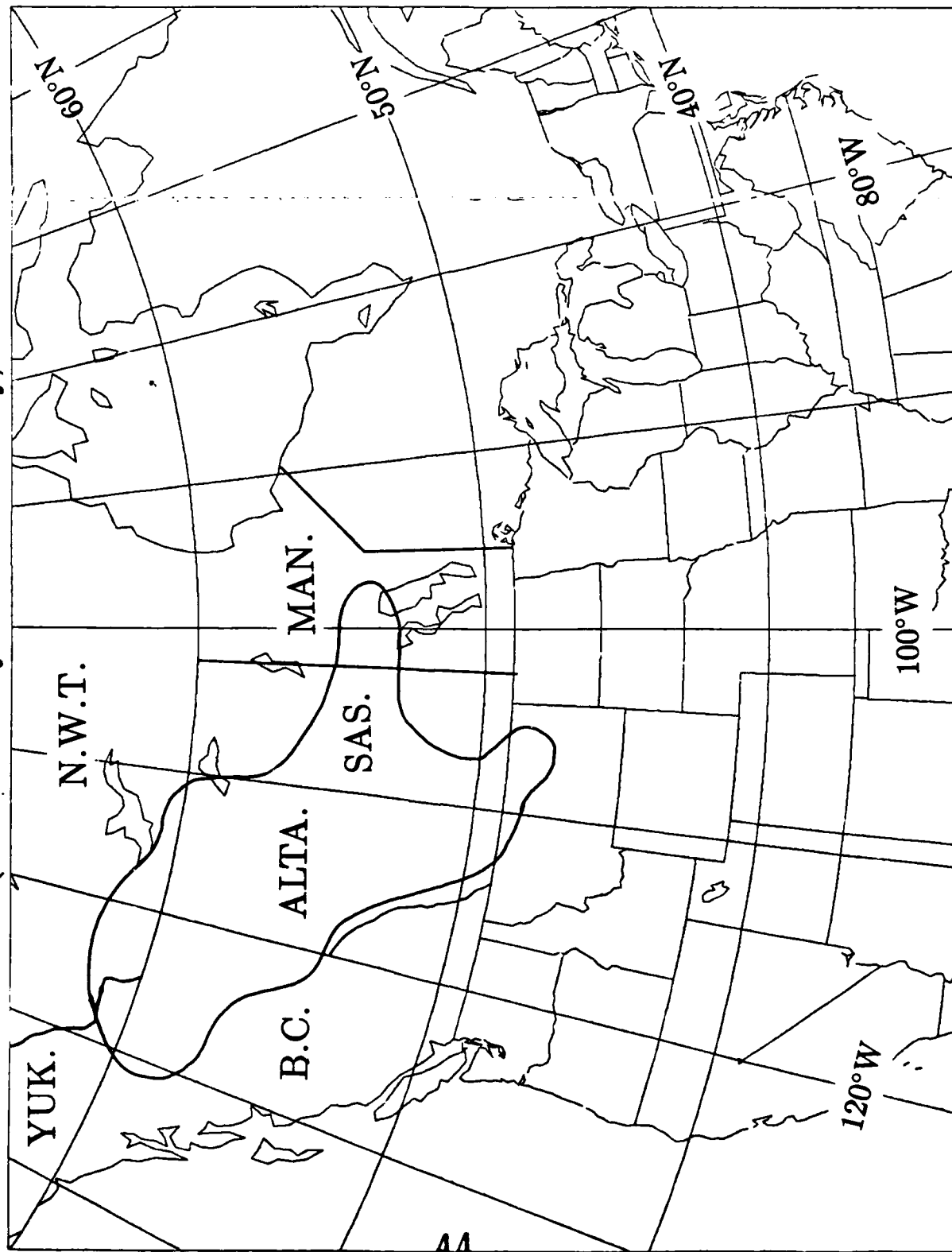


Fig. 2 Observed 500 mb height (gpm) at 4 pm (PST) 31 July, 1982

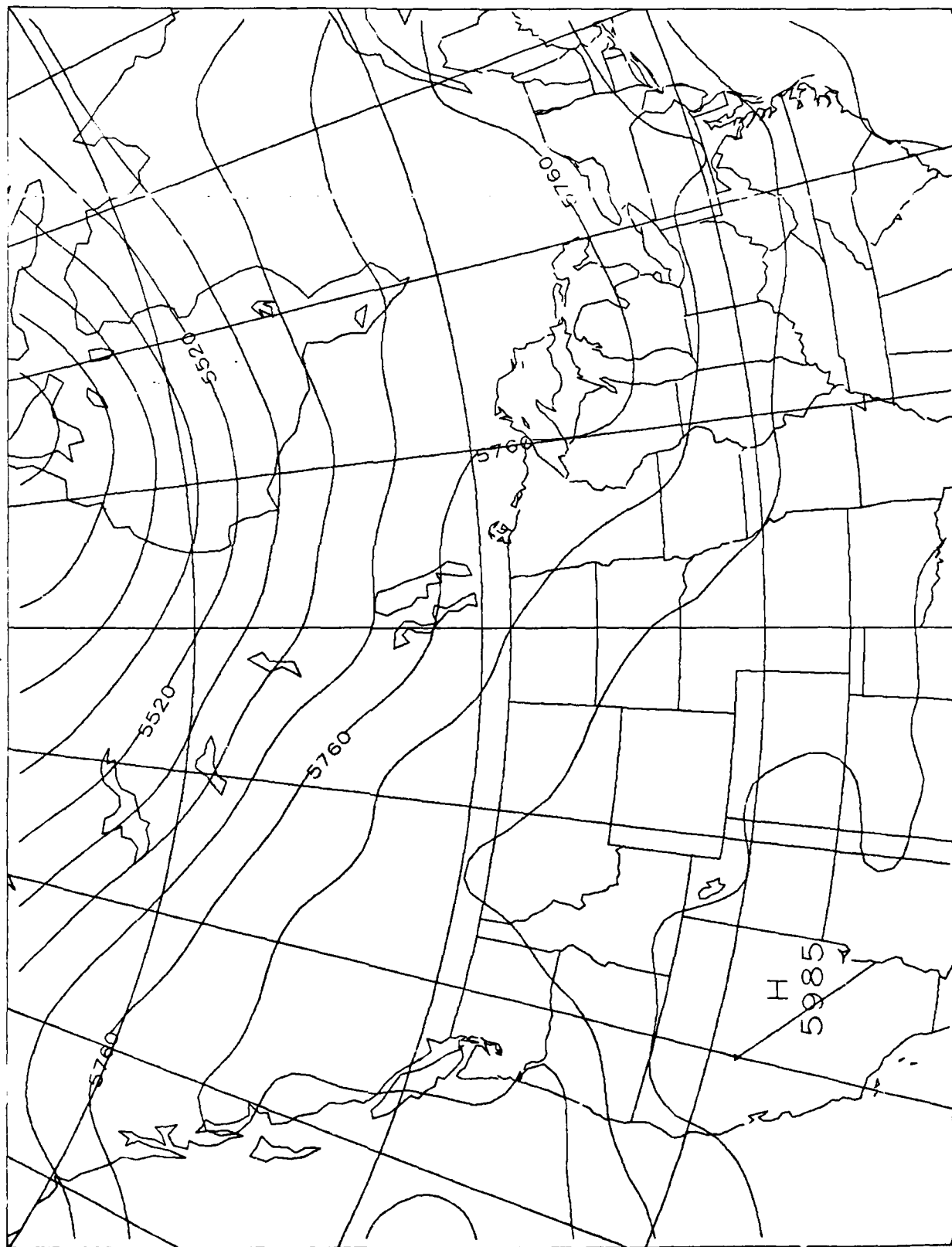


Fig. 3 Observed 500 mb height (gpm) at 4 pm (PST) 2 August, 1982

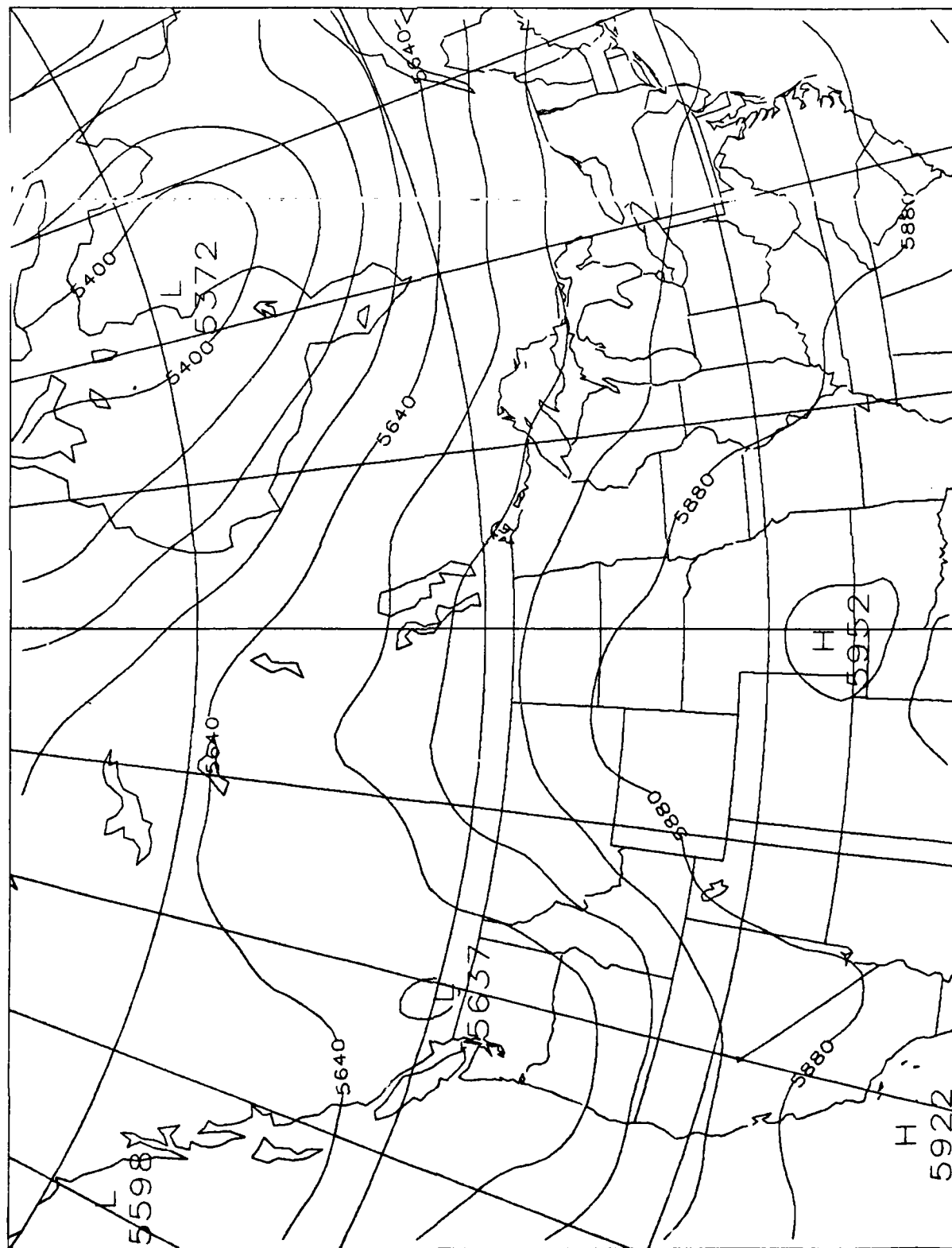


Fig. 4 Predicted 500 mb height (gpm) at 4 pm (PST) 2 August, 1982

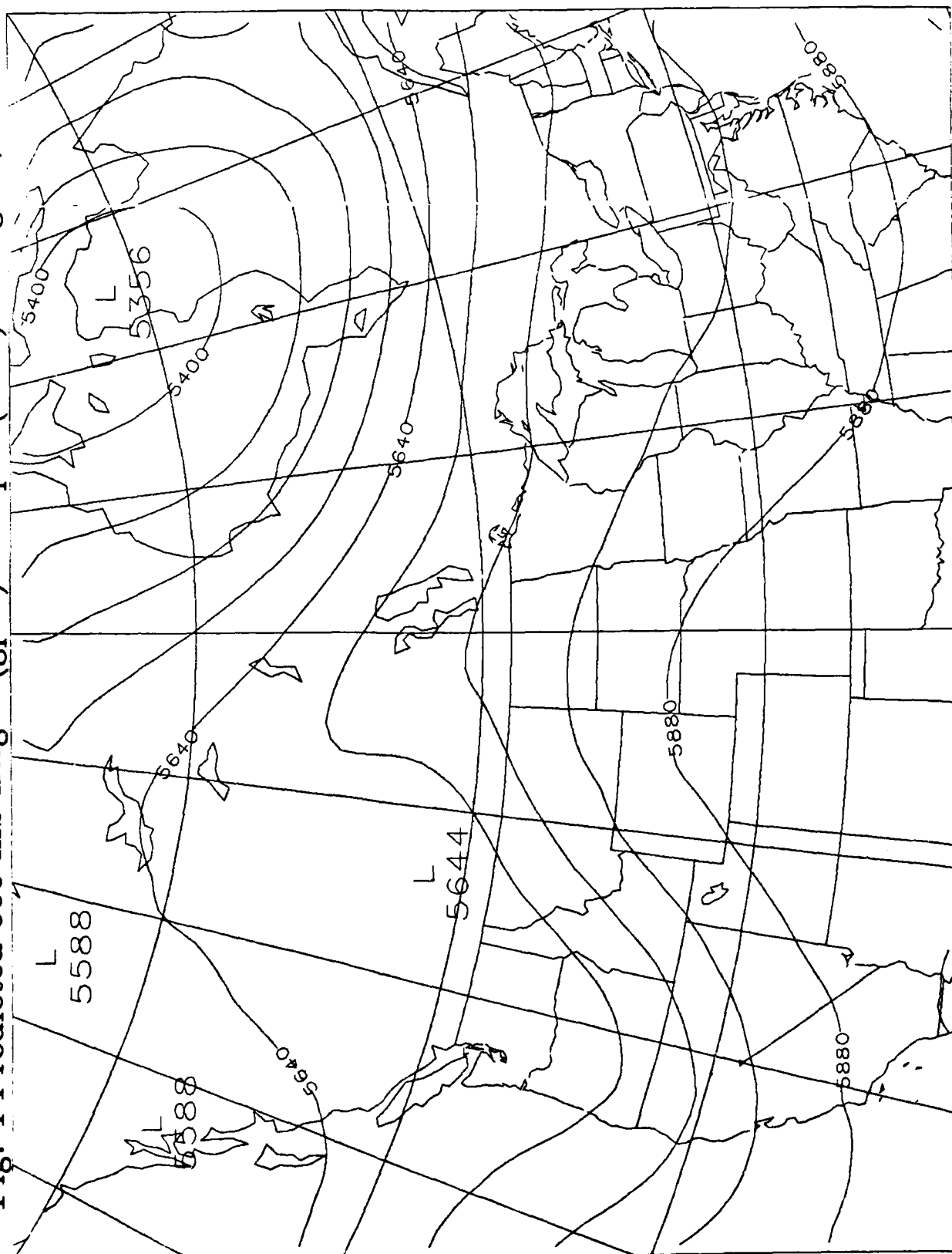


Fig. 5 Observed surface temperature ($^{\circ}\text{C}$) at 4 pm (PST) 2 August, 1982

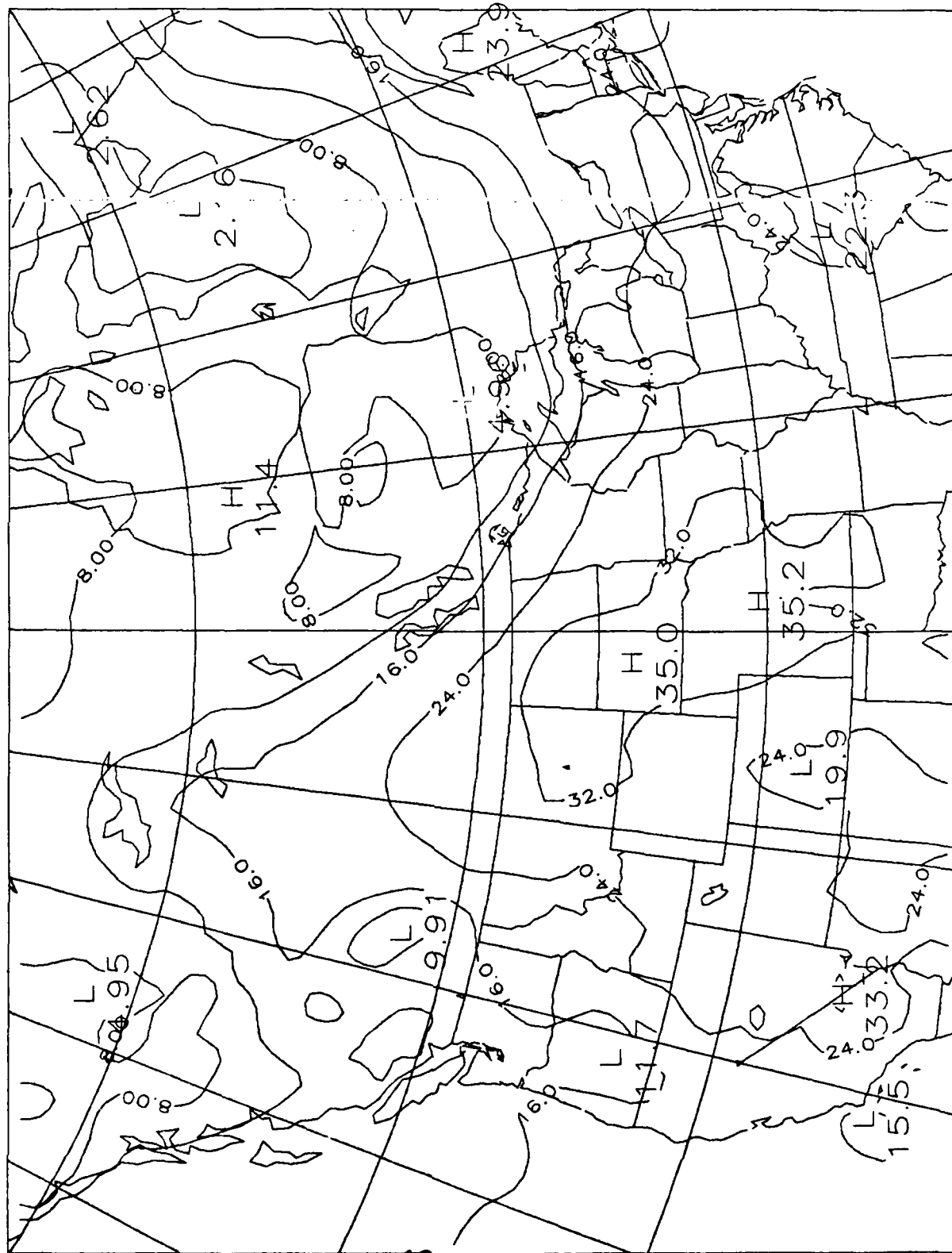
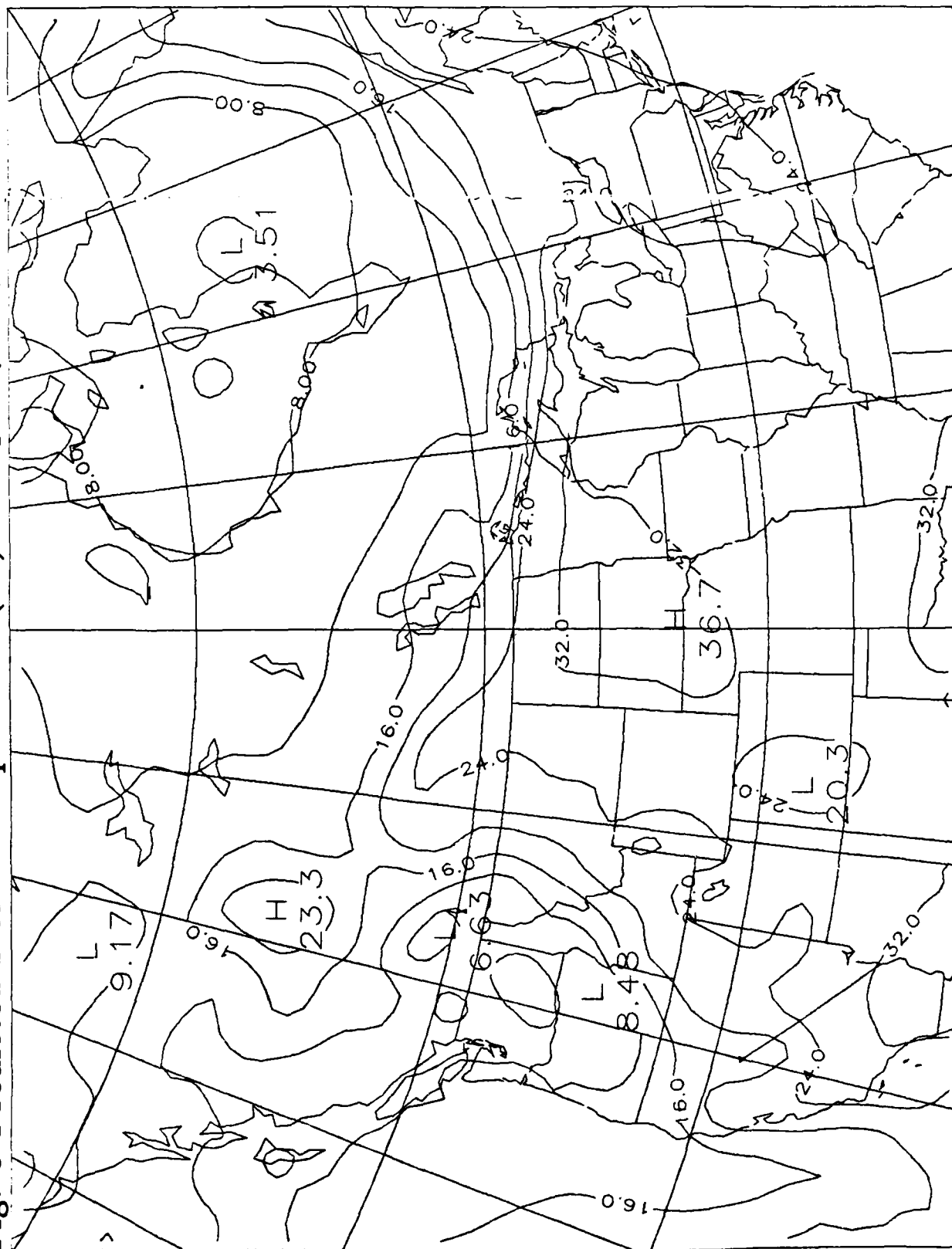


Fig. 6 Predicted surface temperature ($^{\circ}\text{C}$) at 4 pm (PST) 2 August, 1982



Microphysical and Radiative Simulations of Optically Thick Smoke Clouds on the Continental Scale

Owen B. Toon¹, Douglas Westphal^{1,2}, Krishnamurthy Santhanam³

¹ NASA Ames Research Center Moffett Field Ca 94035

² Pennsylvania State University, University Park, Pa. 16802

³ Sterling Software, Palo Alto Ca. 94303

We are using the Penn State/NCAR regional scale dynamical model in conjunction with radiative transfer and aerosol microphysical models developed at Ames Research Center in order to simulate optically thick smoke clouds as they evolve over several day time periods. Our eventual goal is to study the interactions of the plumes from many large, separate fires representing the results of a nuclear conflict. However, we first wish to establish the ability of the model to simulate the plume from a single large fire. We have therefore chosen to model the July-August 1982 smoke plume which originated over British Columbia and spread over the East Coast of the United States. The particle size, optical depth, single scattering albedo, horizontal extent of the cloud and effect of the cloud on the surface radiation budget and surface temperature have all been determined by a variety of researchers from ground based, satellite and aircraft observations. We are presently assembling a comprehensive set of data on this smoke cloud. Here we present two dimensional simulations of the cloud. We use a wind profile and water vapor concentration observed at one station as a representative. We then advect smoke over a several day time period. Our goals are: to determine the relative importance of vertical wind shear and duration of the fire for the geographic area covered by smoke at any one time; to determine the importance of coagulation to smoke particle size; and to estimate the radiative heating rates in the cloud and the effects of the cloud on the surface energy budget. These preliminary calculations will be used to guide more sophisticated three dimensional interactive calculations.

REGIONAL SCALE SIMULATIONS OF OPTICALLY THICK SMOKE CLOUDS

GOAL: Perform interactive simulations of dense smoke clouds including dynamics, radiative transfer, aerosol physics and water vapor condensation.

Steps:

- 1. Identify natural test case and gather data.**
- 2. Perform 3-d non-interactive simulations of meteorology.**
- 3. Perform 2-d simulations of aerosol physics and radiative heating to determine which processes are important.**
- 4. Perform 3-d non-interactive simulations of aerosol physics and radiative transfer.**
- 5. Perform 3-d interactive simulations.**
- 6. Perform simulations of alternative fire possibilities (multiple fires, shorter duration fires, more intense fires).**

Questions addressed by 2-d aerosol and radiative simulations

- 1. Does coagulation affect the optical properties of the cloud?**
- 2. Are the heating rates within the cloud significant?**
- 3. What are the properties of the initial cloud that are needed to explain the observed properties downwind (particle size, refractive indices)?**
- 4. Is dry deposition significant in the few day time period?**

Initial conditions

- 1. Cloud originally located over 12° of longitude at altitudes of 1 to 3 km.**
- 2. Initial size distribution chosen to reproduce Lodi spectral optical depth data. (Log normal with number mean size of $0.06\mu\text{m}$, $\sigma = 1.6$).**
- 3. Wind speed increases in proportion to the inverse pressure with a value of 10m/sec in the middle of the cloud.**
- 4. Vertical diffusion is constant at $10^4 \text{ cm}^2 \text{ s}^{-1}$.**
- 5. Coagulation and sedimentation assume unit density spheres.**

Sensitivity tests

- 1. No coagulation**
- 2. No vertical wind shear**
- 3. High diffusion ($10^6 \text{ cm}^2 \text{ s}^{-1}$) in lowest km**

Figure Captions

Fig. 1 Panels a-d illustrate the evolution of the optical depth, mass concentration, number concentration, and extinction coefficient for three days of cloud dispersal. The particle concentration decreases by a factor of about 20 due to coagulation and the optical depth first increases, due to the particle size increases, and then decreases due to spreading of the cloud. Optical depths of about 2 were observed in the July 82 smoke plume over the East coast of the United States.

Fig.2 Illustrates the size distribution initially and the size distribution after 72 hours. Coagulation leads to an increase of size into the range observed.

Fig. 3 Illustrates the properties of the cloud after 72 hours if coagulation is not included. Comparison with Fig. 1d shows that coagulation leads to an increase in optical depth.

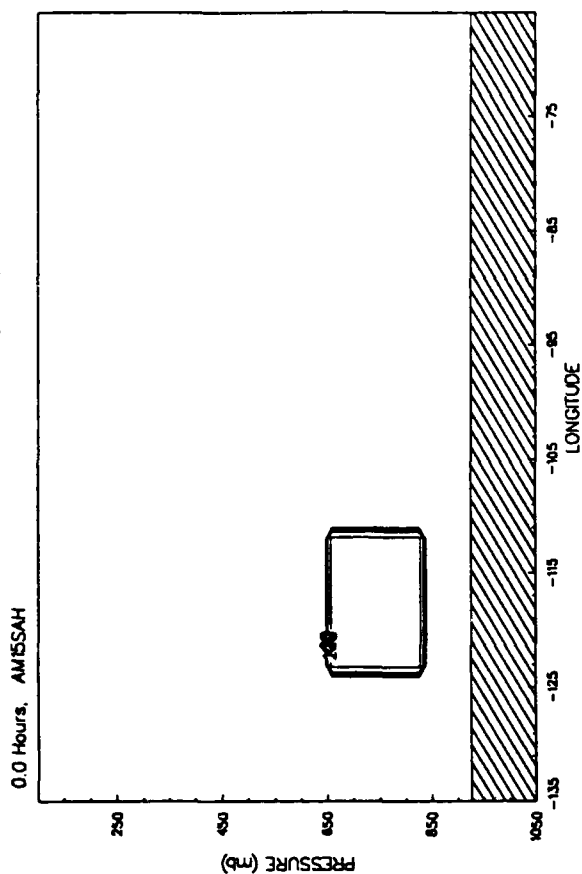
Fig. 4 Illustrates the cloud properties after 72 hours without vertical wind shear. In this case the optical depth is about the same as after 24 hours (Fig. 1b) indicating that shear is reducing the optical depth by dispersing the cloud. However further coagulation beyond 24 hours is not affecting the optical depth.

Fig. 5 Illustrates the cloud properties after 72 hours with a boundary layer having high diffusion coefficients. The optical depth is somewhat reduced, indicating that dry deposition may be important.

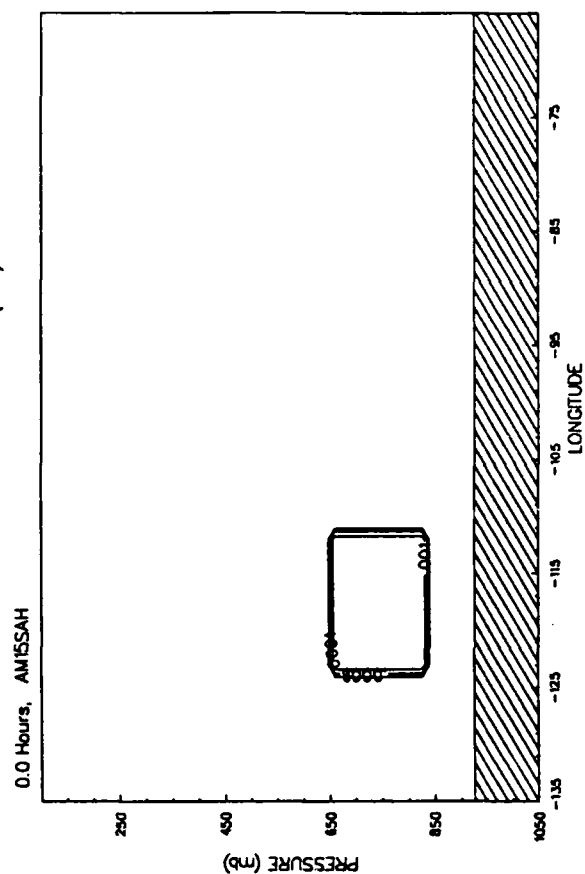
Fig. 6 Illustrates the additional heating rate when the cloud is present. At noon (72 hours) significant heating rates occur in the smoke cloud. At night the cloud has almost no effect on the heating rate.

Fig. 7 Part a Illustrates the surface net radiation budget with no cloud while Part b illustrates the radiation with a cloud. At noon the cloud reduces the solar energy reaching the ground by almost 50% and the total energy by about 25%.

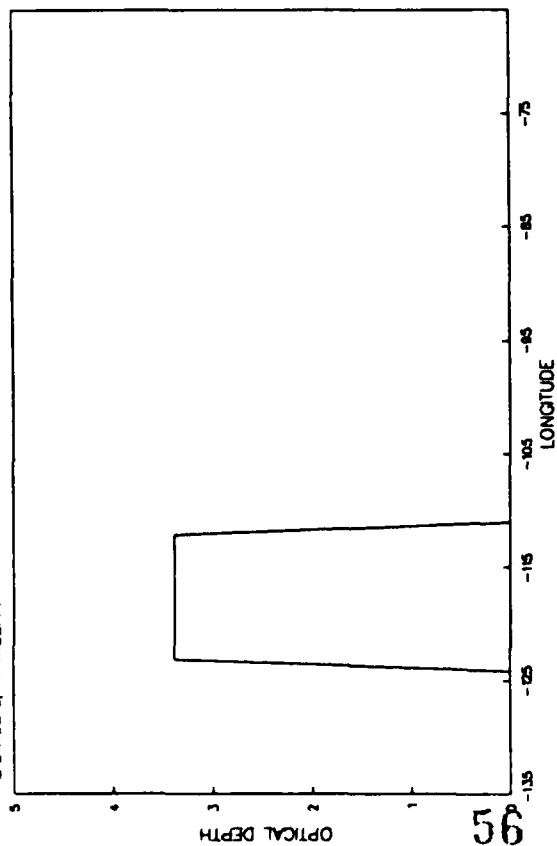
50.0°N MASS ($\mu\text{g m}^{-3}$)



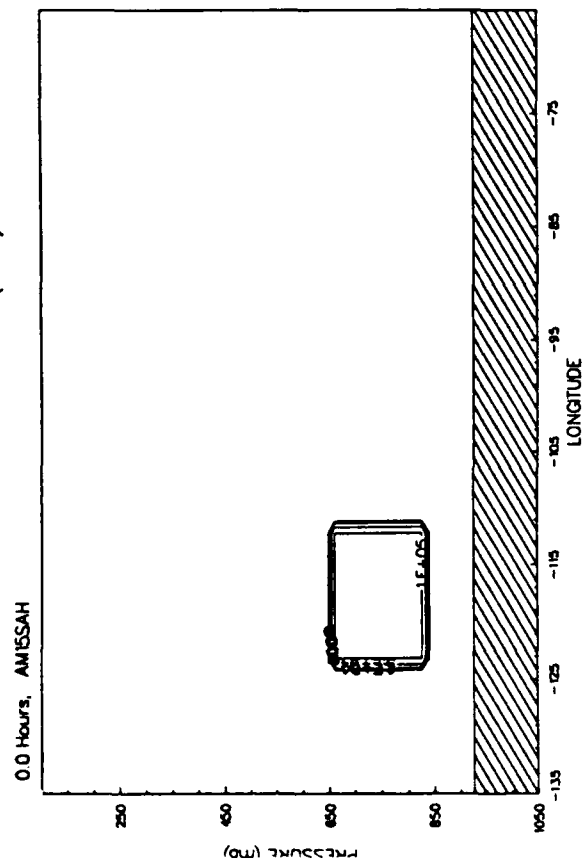
50.0°N EXTINCTION (m^{-1})



0.0 Hours, AMISSAH

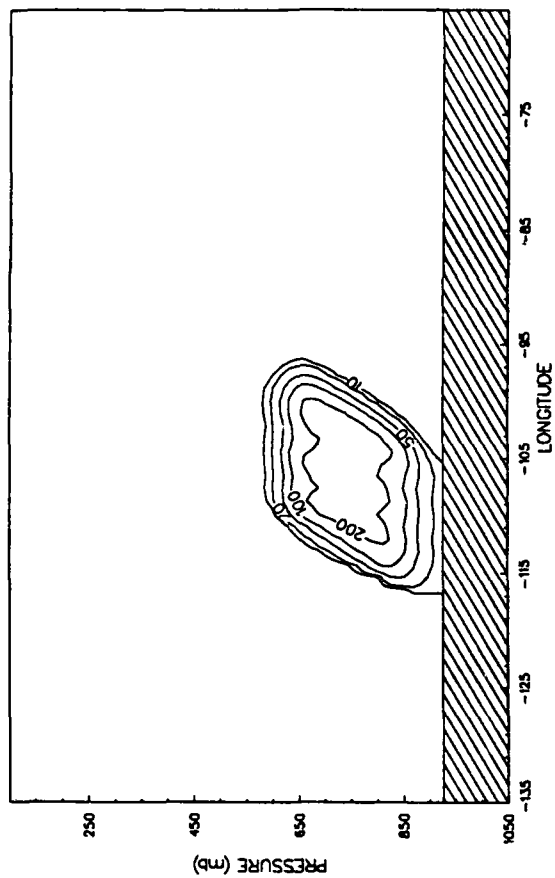


50.0°N TOTAL NUMBER (cm^{-3})



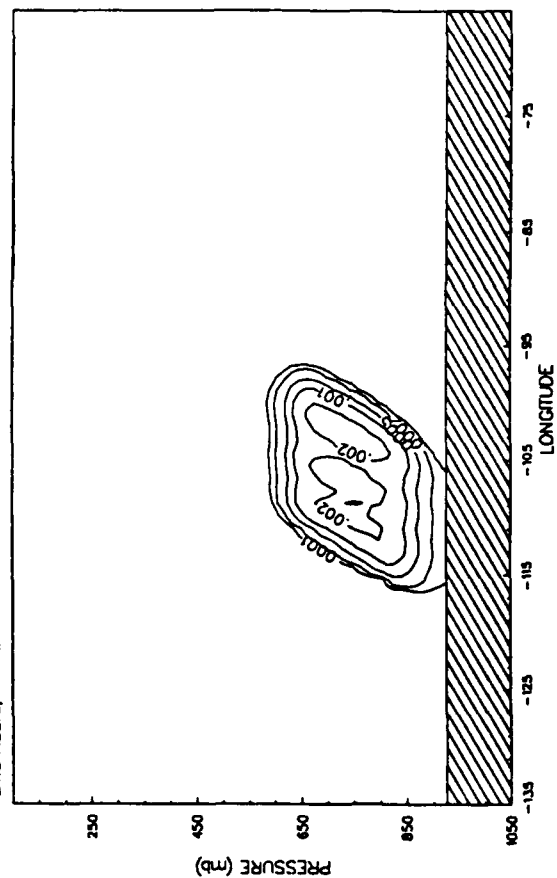
50.0°N MASS ($\mu\text{g m}^{-3}$)

24.0 Hours, AMISSAH

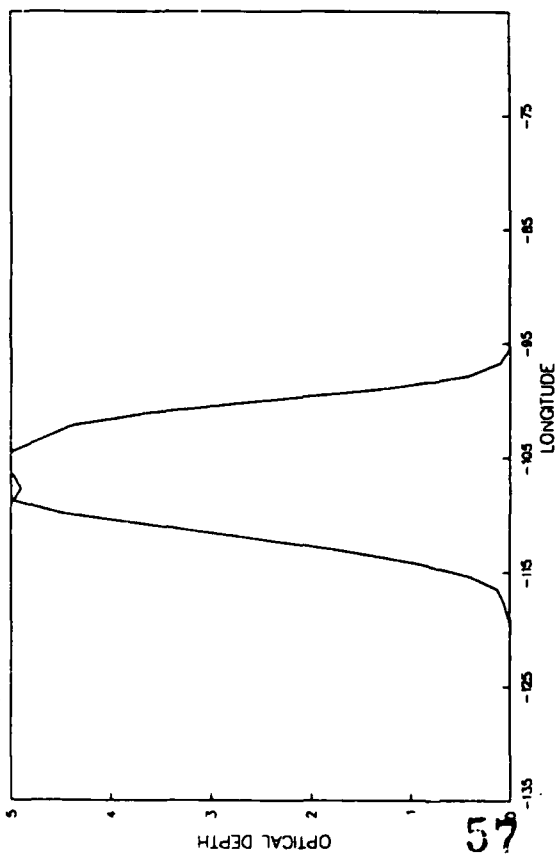


50.0°N EXTINCTION (m^{-1})

24.0 Hours, AMISSAH

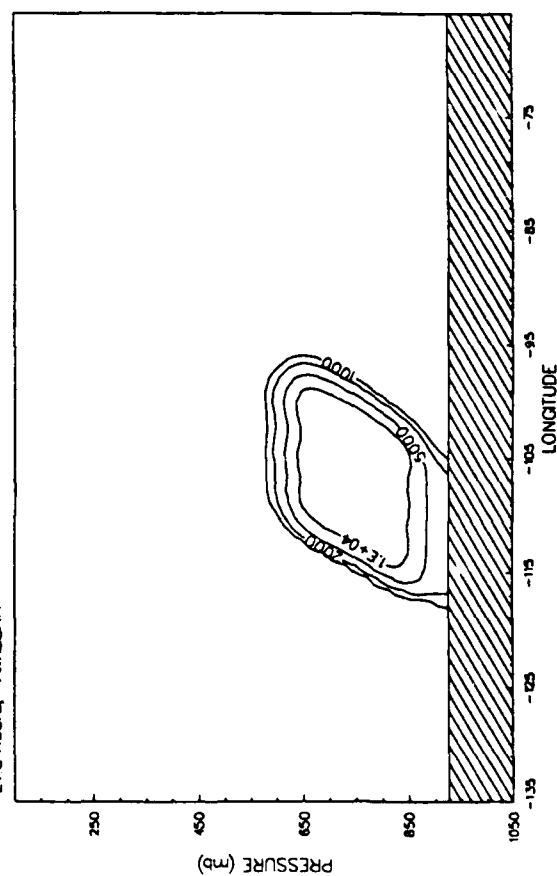


24.0 Hours, AMISSAH

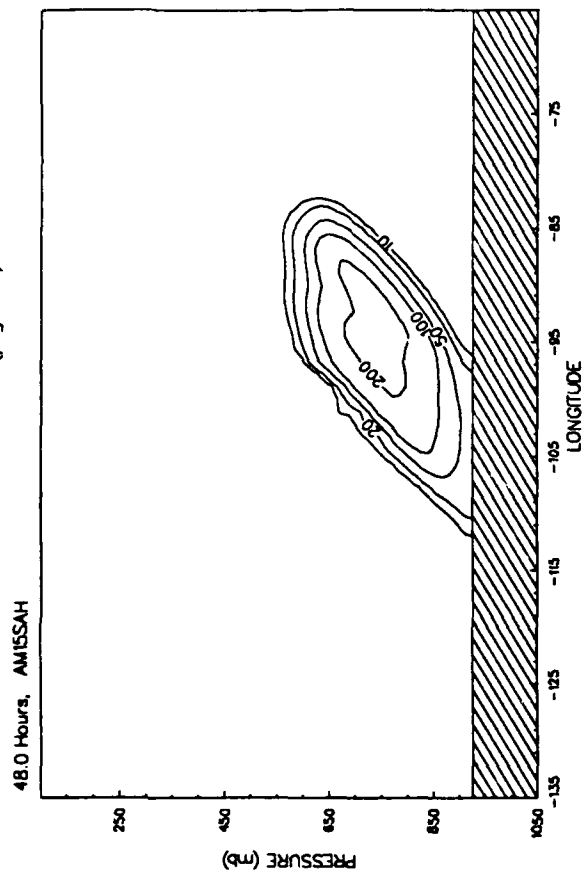


50.0°N TOTAL NUMBER (cm^{-3})

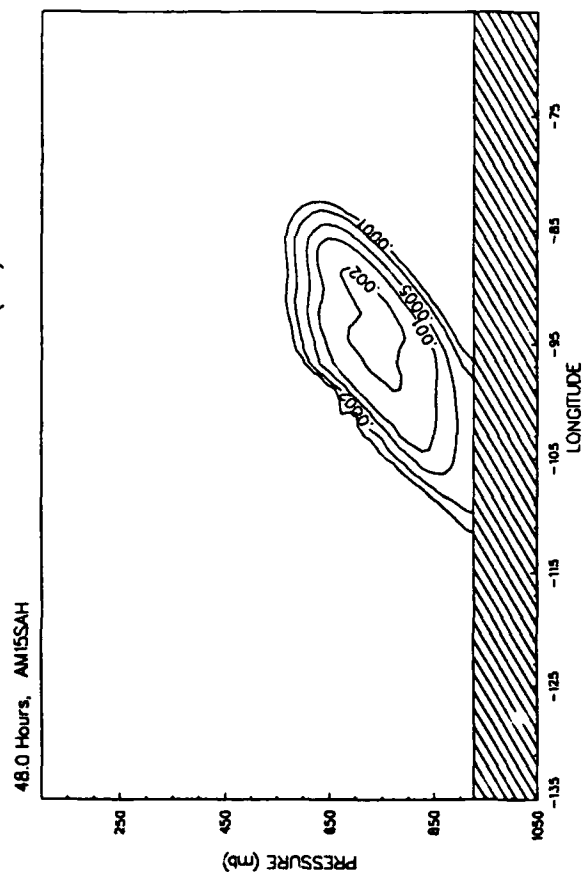
24.0 Hours, AMISSAH



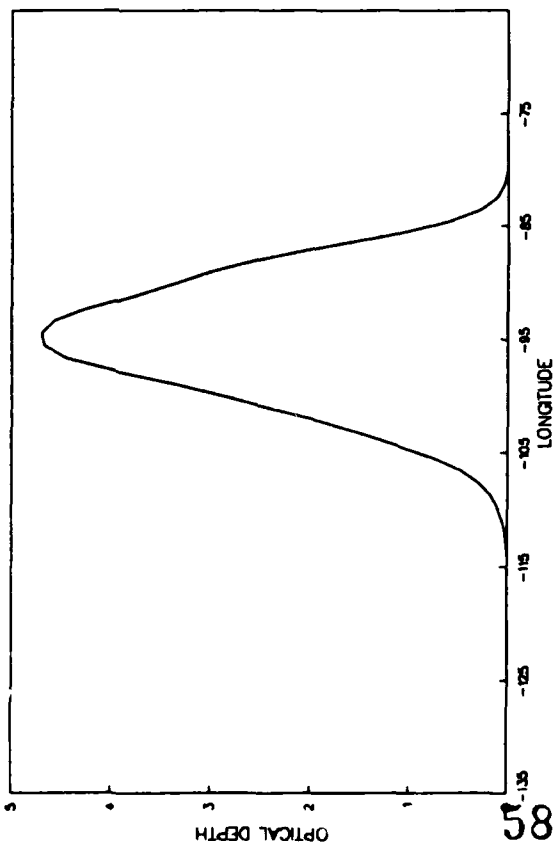
50.0°N MASS ($\mu\text{g m}^{-3}$)



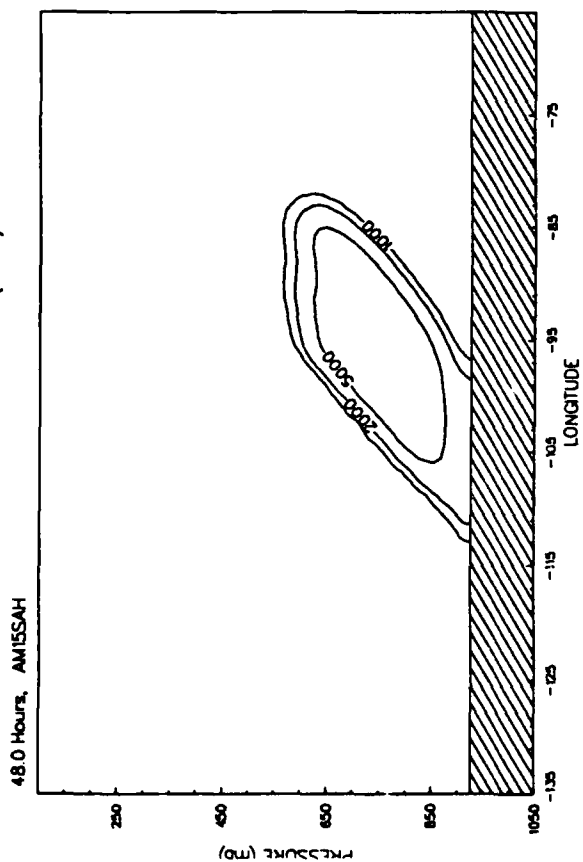
50.0°N EXTINCTION (m^{-1})



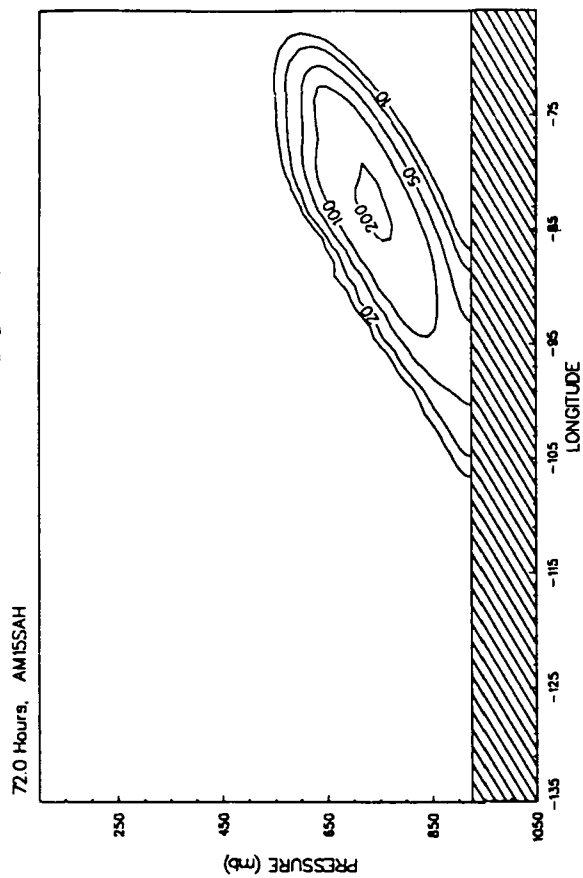
48.0 Hours, AMISSAH



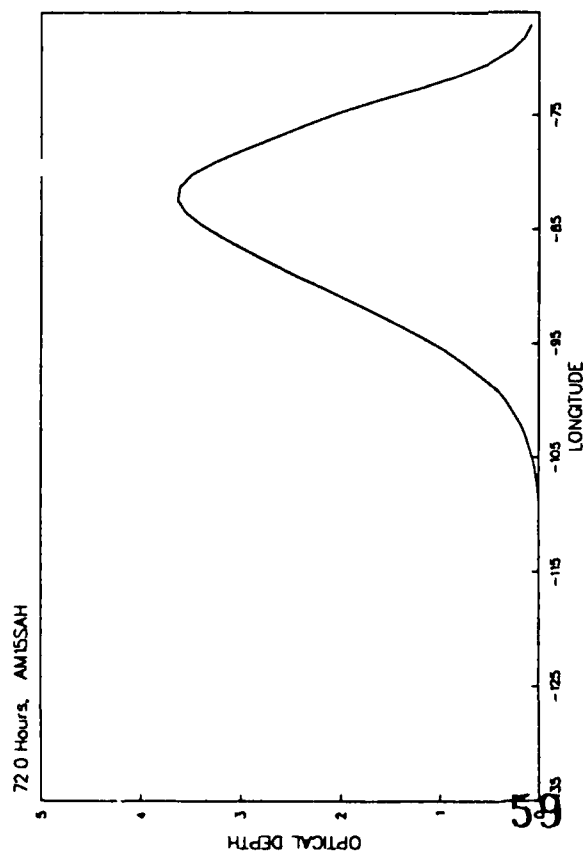
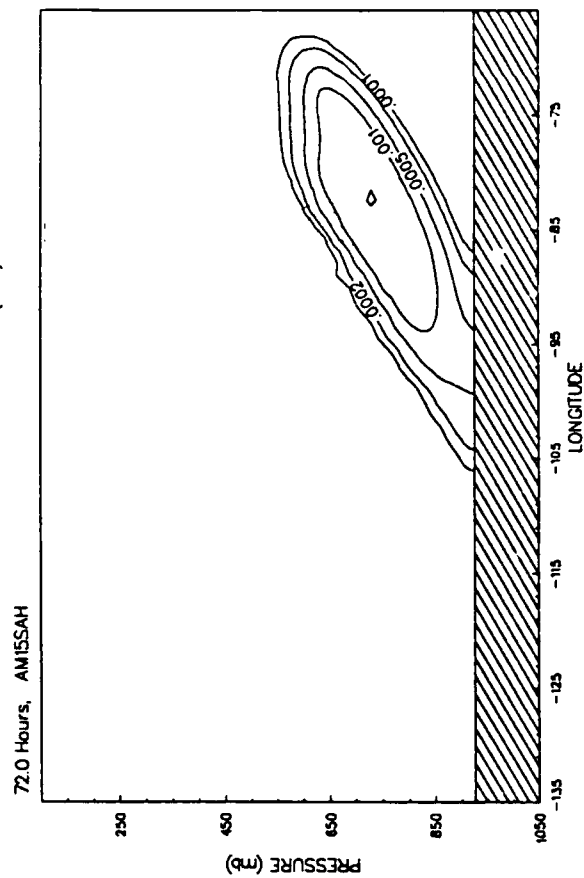
50.0°N TOTAL NUMBER (cm^{-3})



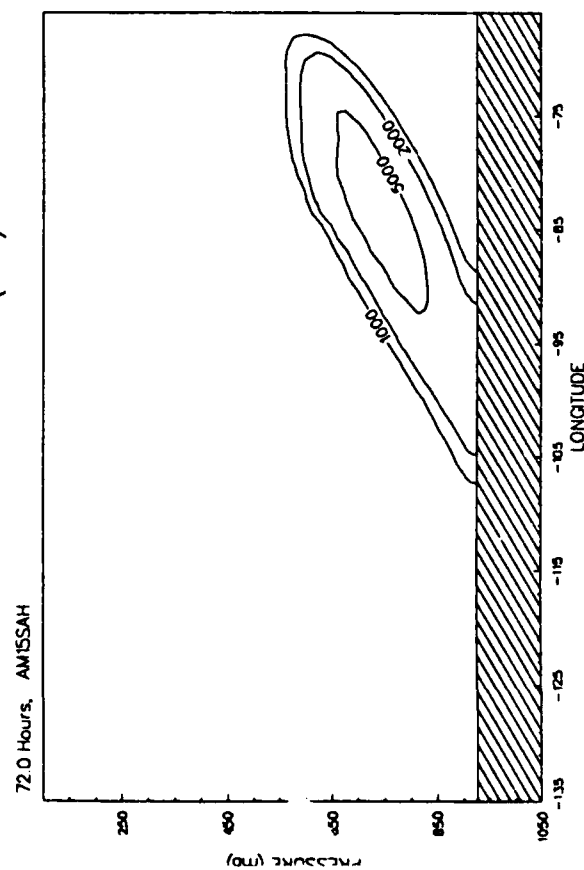
50.0°N MASS ($\mu\text{g m}^{-3}$)

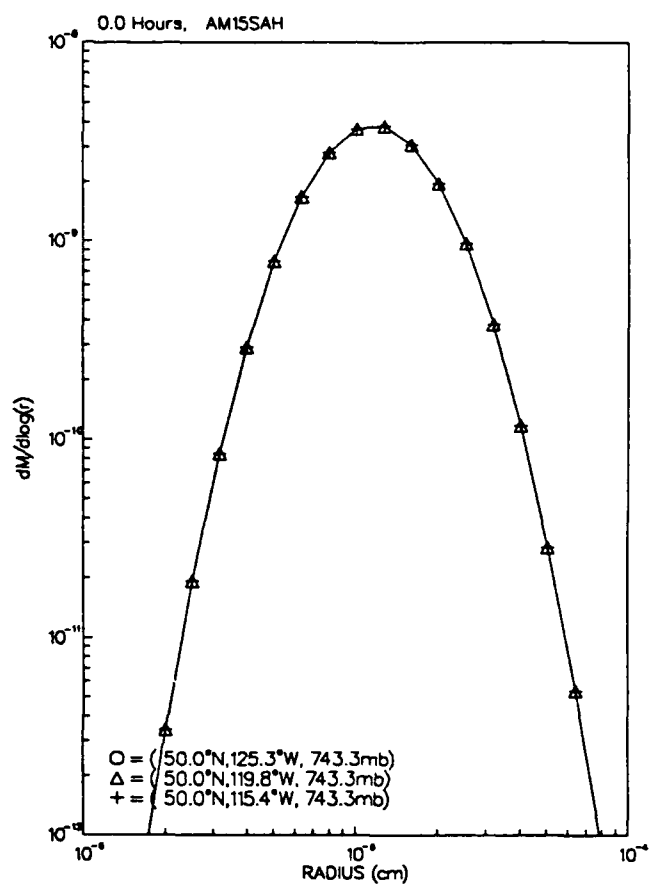
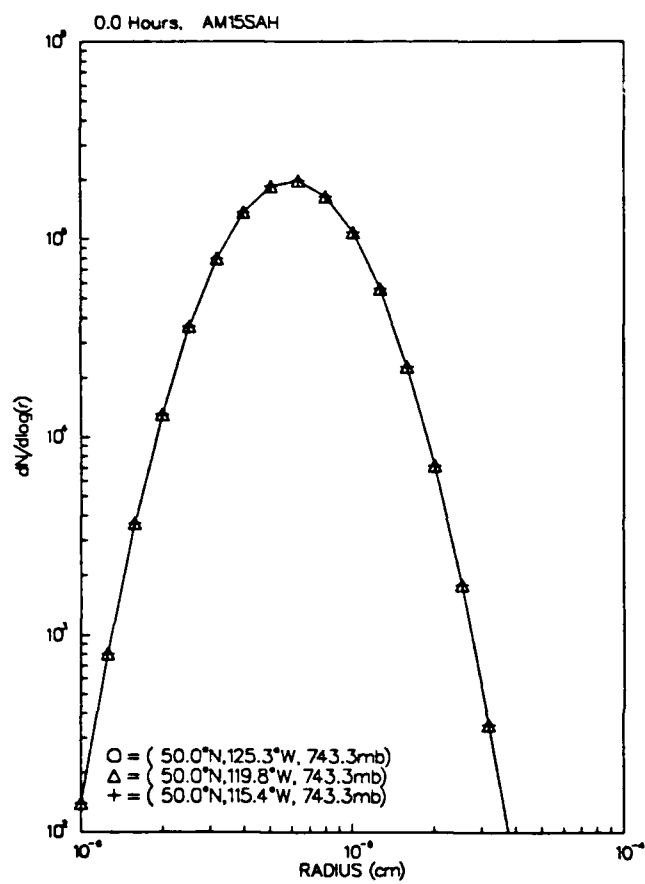


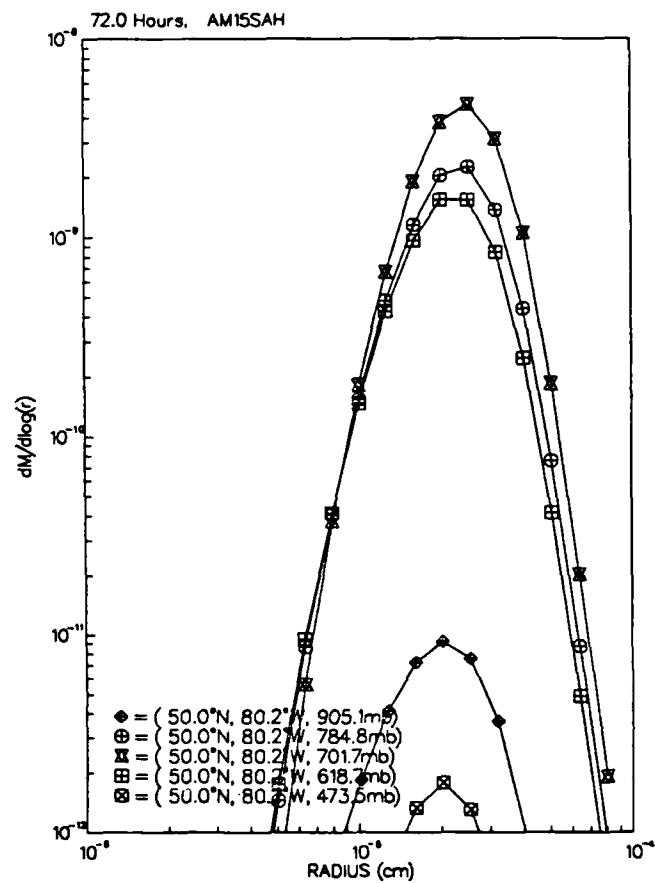
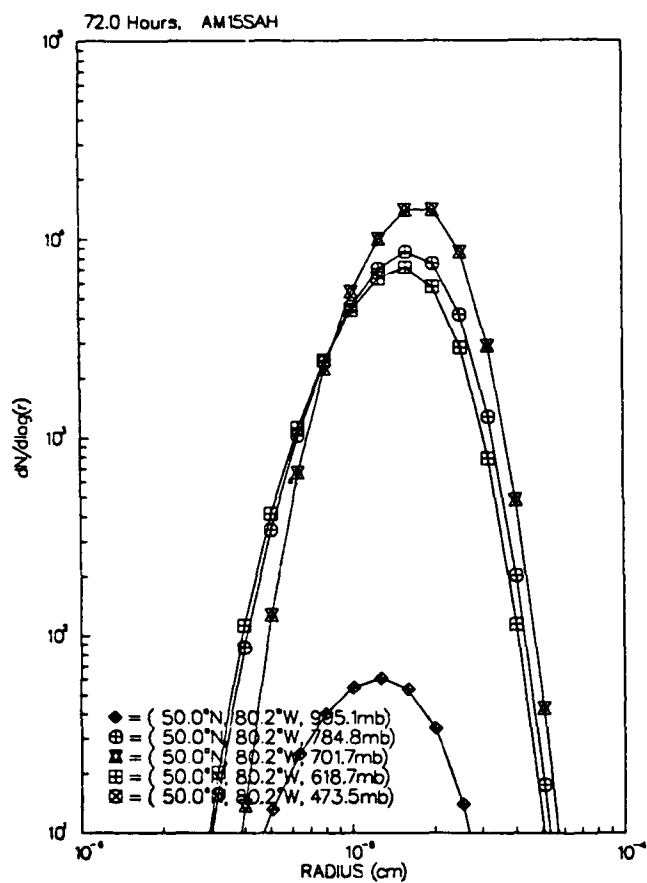
50.0°N EXTINCTION (m^{-1})



50.0°N TOTAL NUMBER (cm^{-3})

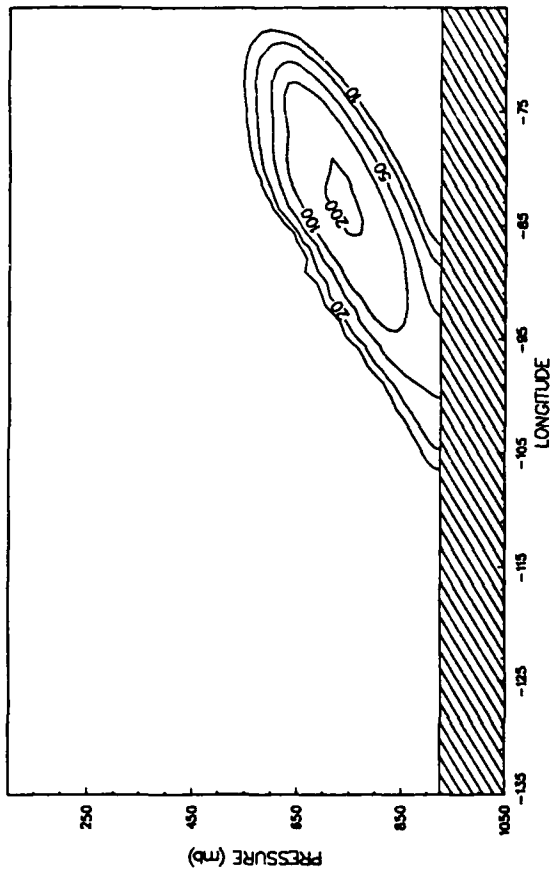






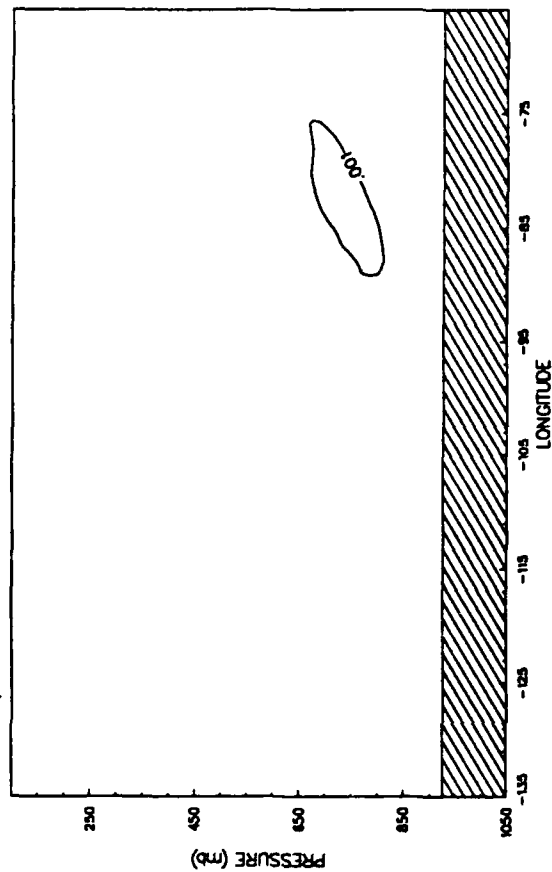
50.0°N MASS ($\mu\text{g m}^{-3}$)

72.0 Hours, AMISSAH

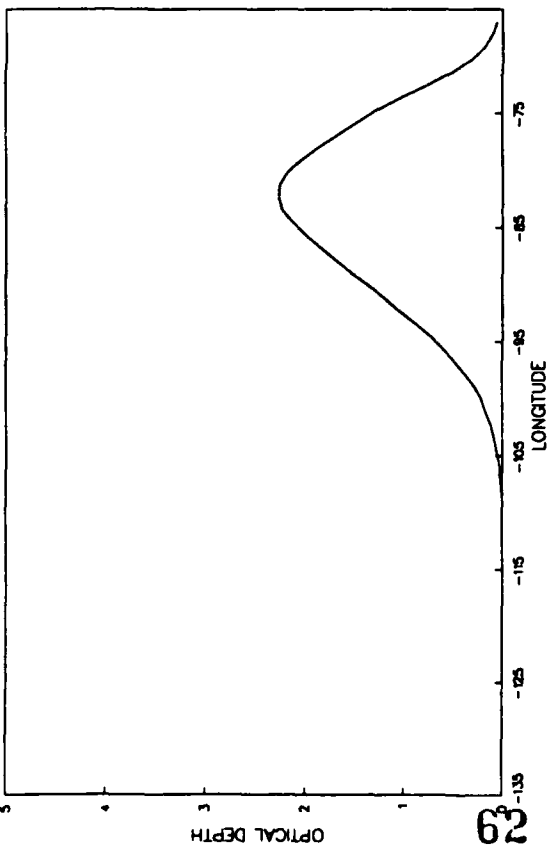


50.0°N EXTINCTION (m^{-1})

72.0 Hours, AMISSAH

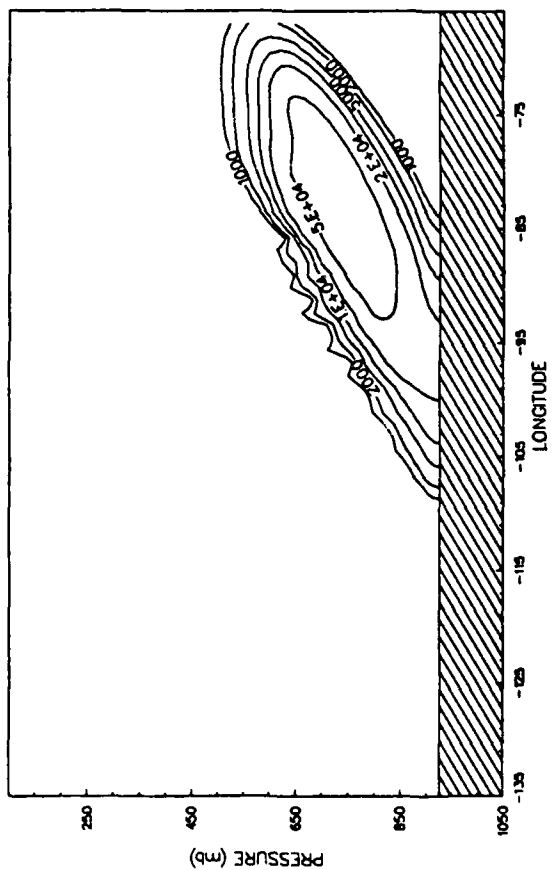


72.0 Hours, AMISSAH



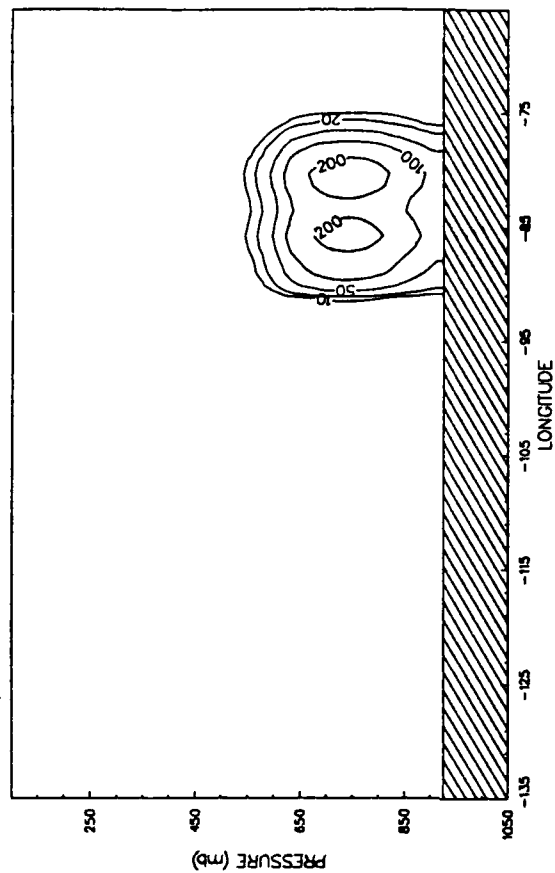
50.0°N TOTAL NUMBER (cm^{-3})

72.0 Hours, AMISSAH



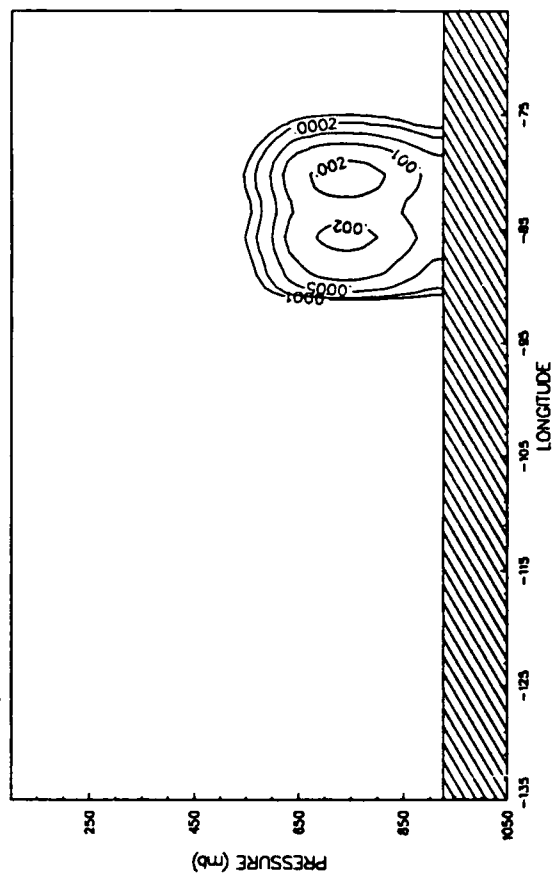
50.0°N MASS ($\mu\text{g m}^{-3}$)

72.0 Hours, AMISSAH

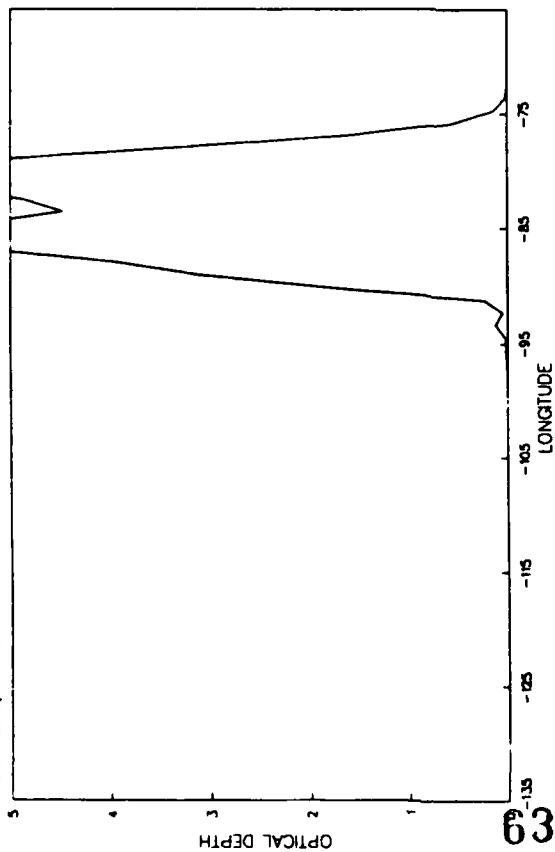


50.0°N EXTINCTION (m^{-1})

72.0 Hours, AMISSAH

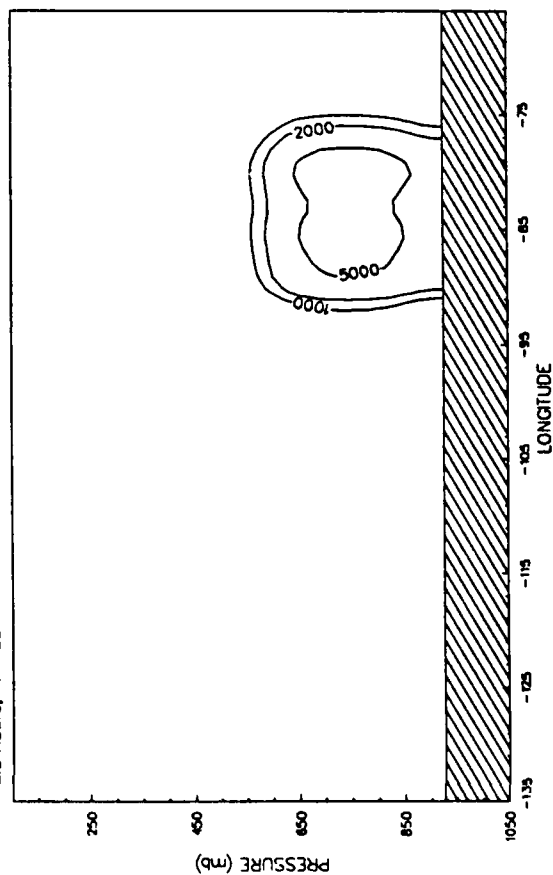


72.0 Hours, AMISSAH



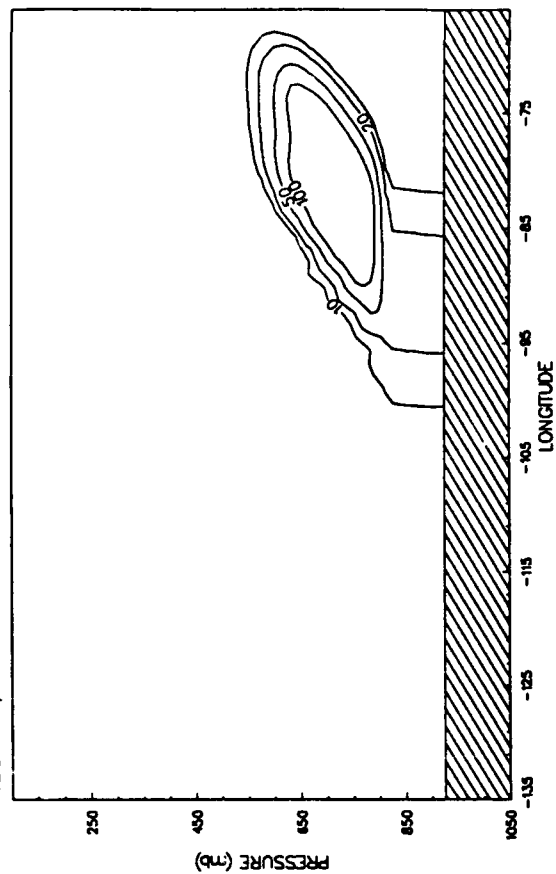
50.0°N TOTAL NUMBER (cm^{-3})

72.0 Hours, AMISSAH



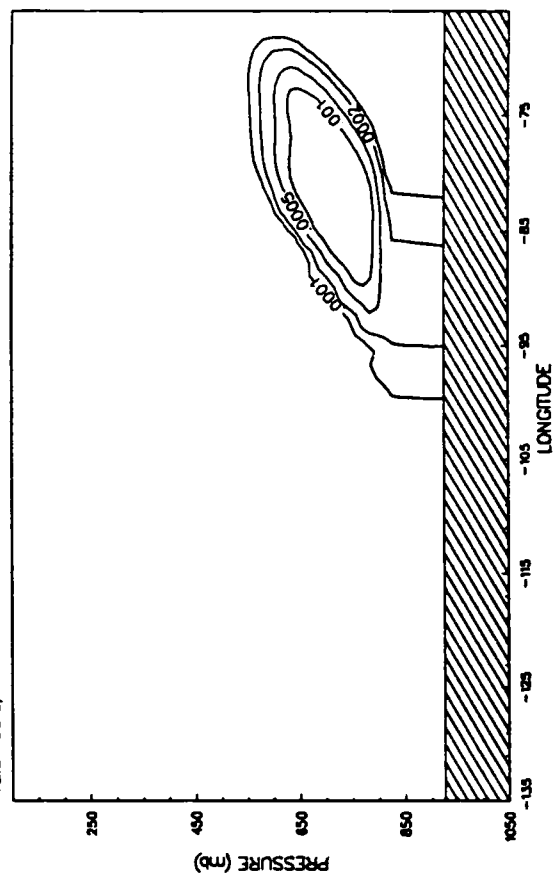
50.0°N MASS ($\mu\text{g m}^{-3}$)

72.0 Hours, AMISSAH

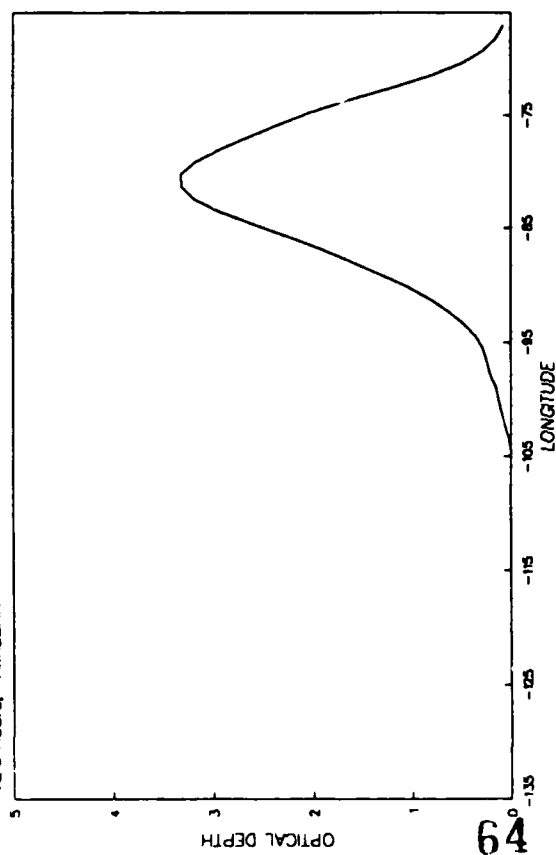


50.0°N EXTINCTION (m^{-1})

72.0 Hours, AMISSAH

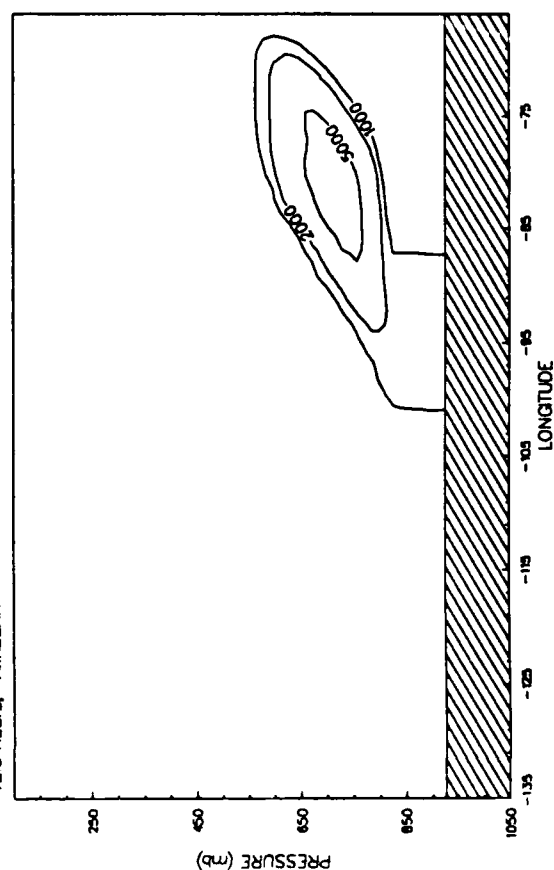


72.0 Hours, AMISSAH

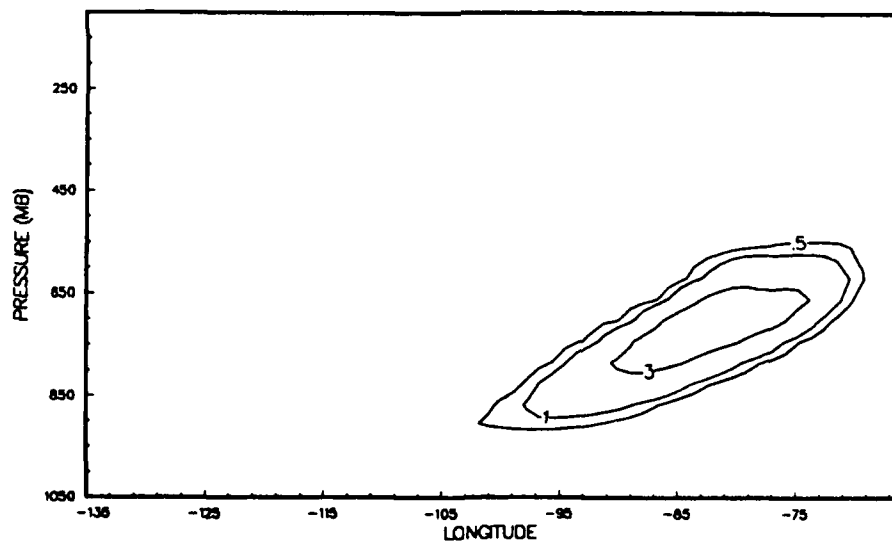


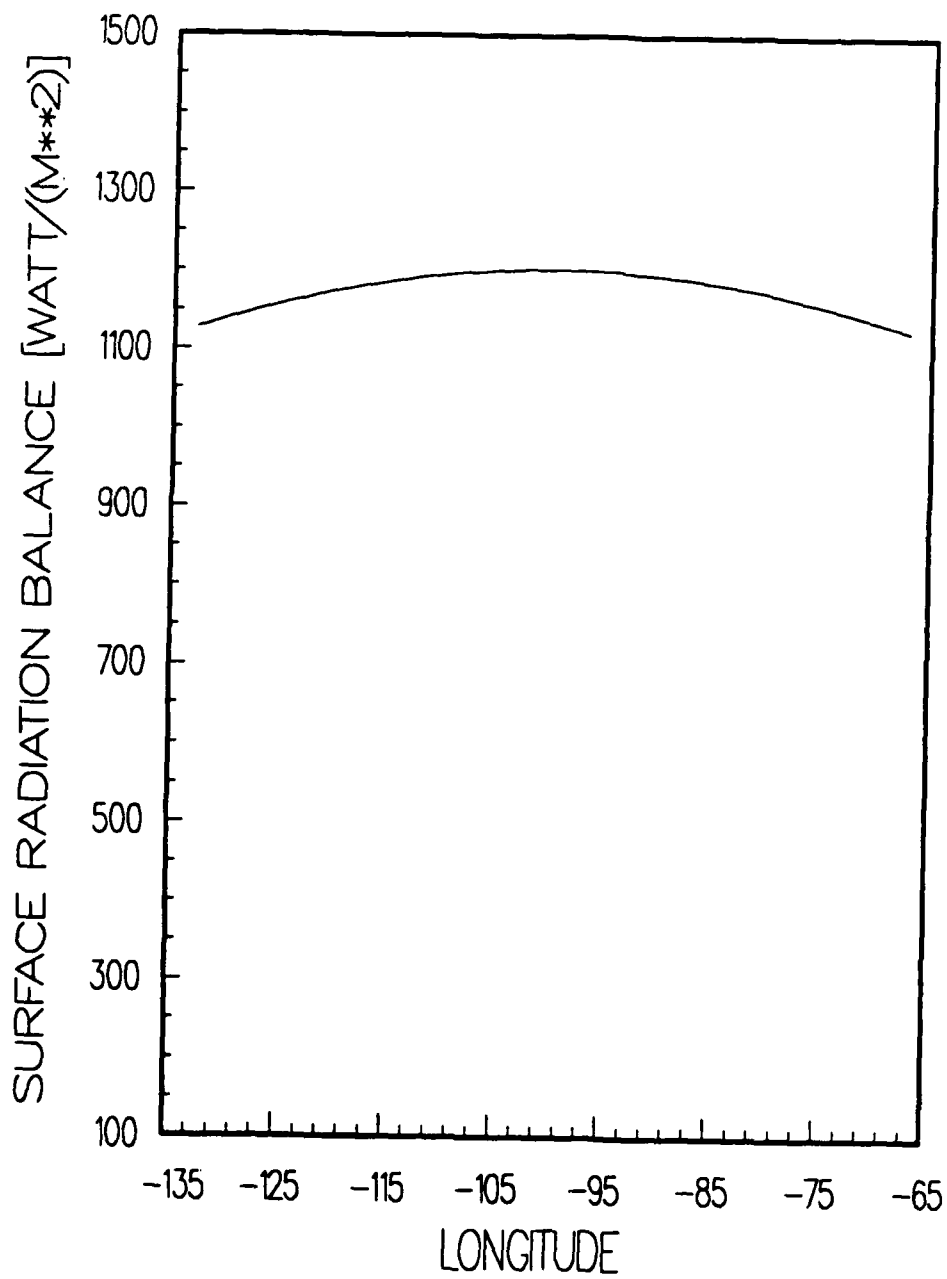
50.0°N TOTAL NUMBER (cm^{-3})

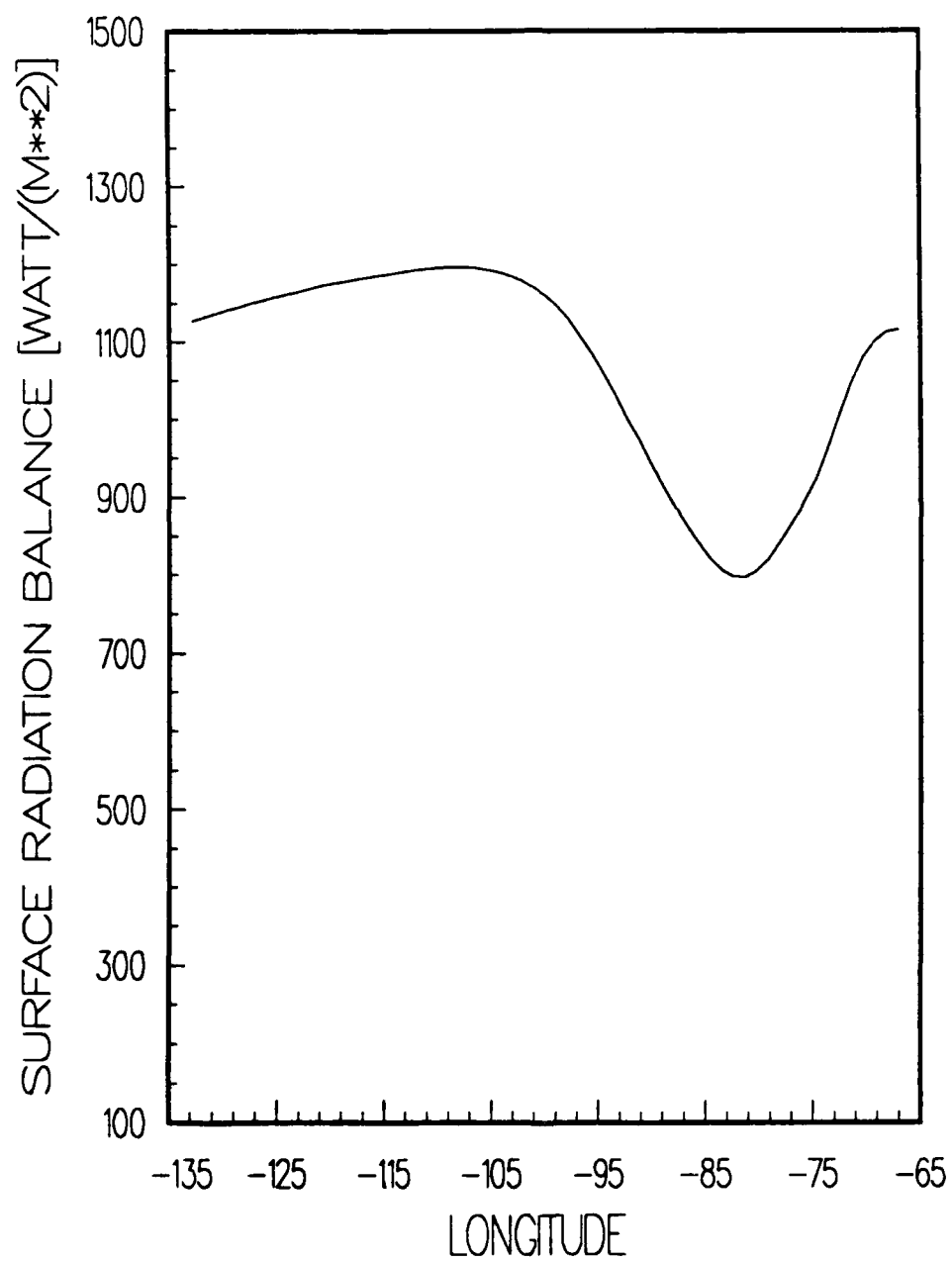
72.0 Hours, AMISSAH



NET HEATING RATE (DEG/DAY)







CONCLUSIONS

1. Coagulation leads to an increase in cloud optical depth over the first few days.
2. Dry deposition is an important loss process.
3. An imaginary refractive index in the range of 0.01 to 0.02 and an initial particle size distribution similar to those observed at Lodi lead to sizes and single scattering albedos after a few days which are close to those observed.
4. Significant heating rates occur in the cloud and a substantial light loss occurs at the surface.

SURFACE TEMPERATURE EFFECTS OF FOREST FIRE SMOKE PLUMES

Alan Robock
Department of Meteorology
University of Maryland
College Park, Maryland 20742

Paper presented at DNA Global Effects Program
Technical Meeting, Santa Barbara, CA, 7-9 April 1987

ABSTRACT

The location of smoke clouds from extensive Canadian forest fires is determined from satellite imagery for cases in the summers of 1981 and 1982. As these smoke clouds pass over the Midwestern United States, surface air temperature effects are determined by comparing actual surface air temperatures with those forecast using Model Output Statistics (MOS) by the United States National Weather Service. A cooling of 1.5 to 4°C is found in the daytime under the smoke plumes. No effect is found at night. This corresponds to theoretical estimates of the effects of an elevated smoke plume. It serves as observational confirmation of portions of the nuclear winter theory.

1. Introduction

Crutzen and Birks (1982) suggested that smoke from forest fires ignited by nuclear weapons would be extensive enough to block out significant amounts of sunlight. Subsequent work, such as Crutzen et al. (1984), Turco et al. (1984), National Academy of Sciences (1985), and SCOPE (1986), has pointed out that the smoke from urban and industrial fires would be much

more effective at preventing solar radiation from reaching the earth's surface than forest fire smoke after a large-scale nuclear war. With both urban and rural targets, not only would more urban smoke be generated, but its optical properties would make it more effective at blocking sunlight.

The effects of forest fire smoke are still interesting, however, for two reasons. First of all, a lot of forest fire smoke would still be generated in many nuclear war scenarios, especially those that include only non-urban military targets. The optical properties and surface temperature effects of this smoke is an important part of the study of nuclear winter.

Secondly, in order to understand nuclear winter, it would be nice to have some actual observations of the effects of smoke to compare to the theoretical models. Extensive contemporary urban and industrial smoke plumes are not available for study. Each year, however, forest fires are generated by lightning, and in some cases can produce extensive smoke plumes. Ginsburg and Golitsyn (1986) presented observations of daytime surface cooling from extensive Siberian forest fires in 1915. Wexler (1950) presented anecdotal evidence of daytime cooling at the surface of 2-5°C from "The Great Smoke Pall" caused by extensive Canadian forest fires. In this paper, two such cases, in which smoke from western Canadian forest fires drifted across the midwestern United States are investigated to attempt to measure their surface temperature effects. It is believed that "The Great Smoke Pall" and the Siberian fires of 1915 were more optically thick cloud than the ones investigated here.

2. Data Analysis

The location of smoke clouds from extensive Canadian forest fires was determined from satellite imagery for cases in the summers of 1981 and 1982. The smoke clouds are easy to detect with visible wavelength imagery (Figs. 2-7, 9), but are invisible in infrared imagery (Fig. 8, which can be compared with the visible image in Fig. 3), implying a much greater optical depth in the visible as compared to the infrared. Within 2-3 days after being produced, the smoke plumes in the 1982 case grew into an extensive shield covering about 10^6 km². There was some patchiness evident (Figs. 2-7), but the smoke veil maintained a coherent structure for several days. In the 1981 case, the smoke appeared to be in streaks, with patches of less dense smoke in between (Fig. 9). The total area covered was about the same as the 1982 case.

As these smoke clouds passed over the midwestern United States, surface air temperature effects were determined by comparing actual surface air temperatures with those forecast using Model Output Statistics (MOS) by the United States National Weather Service (Glahn and Lowry, 1972). This MOS error technique has been used successfully before to determine surface air temperature effects of the Mount St. Helens volcanic eruption of 1980 (Robock and Mass, 1982). The analysis was done in regions of high pressure where synoptic disturbances were not affecting the temperature. The errors are attributed to the presence of aerosols in the atmosphere, since the aerosol content is not a MOS predictor. The locations of all the MOS stations used in this analysis are shown in Fig. 1.

Intense forest fires burned in British Columbia, Canada, on 29 and 30 July 1982 (Ferrare, personal communication). Smoke from these fires was transported by the prevailing winds, and crossed the U.S. border in North Dakota on 31 July. It proceeded across the Midwest and then east over the Mid-Atlantic states. Smoke from these fires was reported over Western Europe on 5 and 6 August. Such was also the case for The Great Smoke Pall (Wexler, 1950) and demonstrates the ability of the atmosphere to transport smoke over long distances before it is removed.

Figures 2-7 show both visible wavelength GOES satellite images and MOS surface temperature forecast errors for 31 July and 1 August 1982 at 1500, 1800 and 2100 GMT (10 am, 1 pm and 4 pm CDT - local time in the Midwest) each day. Smoke plumes appear gray in these images, and can easily be detected over the Midwest. On the original images, the smoke plume which was headed for Europe can easily be seen on 1 August over the Atlantic Ocean.

Forecast errors of -2 to -4°C are evident under the smoke plumes. Forecast errors are not evident under the smoke plumes at other times of the day. Since the errors are only evident at times of maximum daily insolation, their predominant effect on shortwave radiation is demonstrated.

Forecast errors of the same or greater amplitude are also evident in other locations in the Figures. Upon close inspection, each can be attributed to the presence or absence of water clouds or mesoscale features which were not well forecast by the LFM numerical forecasting model, which provides the

predictors for the MOS forecasts. In clear areas, however, the only large errors are under the smoke cloud. For example, in Fig. 2, for 1500 GMT on 31 July, the negative area in eastern Michigan can be attributed to an unforecast mesoscale region of cloudiness. The positive error region in western Tennessee and Kentucky is associated with a mesoscale clear area in an otherwise overcast region.

In Fig. 3, for 1800 GMT, 31 July, the same error regions are present as in Fig. 2, except that an additional negative area appears in Virginia under a heavy water cloud bank, and small negative areas appear east and west of Lake Ontario. These latter areas become more extensive and of higher amplitude three hours later in Fig. 4. They are associated with strong cold advection behind a rapidly developing mesoscale Low, the center of which is located on the Vermont-Canadian border. This is easily seen on the synoptic weather maps (not presented here) and presumably was not well forecast by the LFM, which does not handle weather systems of this small scale well. In Figs. 3 and 4 the moderating effects of Lakes Erie and Ontario are evident, as the maximum cooling associated with this cold advection is over the land areas between the lakes. The only other negative error area, and by far the largest one, is under the forest fire smoke veil. Areas of fair weather cumulus over Illinois, Indiana and Ohio do not produce large MOS errors.

On 1 August (Figs. 5-7) the only large error regions (both negative) are associated with a small region of water clouds over Wisconsin and the forest fire smoke veil. The region around the Great Lakes under the smoke veil has errors between

-1°C and -2°C, evidence again of a moderating effect of the lakes. The thickest patch of smoke appears over Baltimore, Maryland, in Fig. 7 at 2100 GMT, and has an error of -4.1°C associated with it.

The results presented here are from forecasts made from LFM runs 12 to 24 hours before the forecast time. Comparisons were made with forecasts made with earlier and later model runs, and the results were virtually the same. The errors (cooling) found were much larger than the run to run differences.

Attempts were made to estimate the height of the smoke as it passed over the Midwest. Winds were examined at different levels during this time and compared to the motion of the smoke. The winds corresponding most closely to the motion were at 700 mb (3.2 km). The jet of smoke headed to Europe on 1 August corresponded to winds between the 700 mb and 500 mb levels (3 - 5.5 km).

Eloranta (personal communication) happened to be conducting a vertical profile study of lower level haze on the next day over the eastern shore of Chesapeake Bay, due east of Baltimore at 1700 GMT. The portion of the smoke veil that was over Kentucky on 1 August appears from satellite images to have been over Maryland at that time. He flew up into the base of the forest fire smoke plume at an altitude of approximately 3.5 km and at 4.5 km (the highest altitude reached) he was still in the smoke.

A preliminary analysis of the 12 August 1981 case (Fig. 9) also shows daytime cooling under the smoke. In this case, the smoke is not as uniform, but appears in streaks. The cooling in

this case is -1.5 to -3°C . A preliminary examination of the satellite images from this case shows shorter shadows at sunrise and cumuliform clouds casting shadows on the smoke later in the day. These both suggest that the smoke was at a lower elevation on these days.

3. Discussion

A cooling of 1.5 to 4°C is found in the daytime under forest fire smoke plumes in two cases in 1981 and 1982. No effect is found at night. This corresponds to theoretical estimates of the effects of an elevated smoke plume (Ginsburg and Golitsyn, 1986) with optical depth of approximately 2. Ferrare (personal communication) reports theoretical estimates of the optical depth of this smoke cloud, based on multi-spectral satellite measurements, of 2 to 3.

This result serves as observational confirmation of portions of the nuclear winter theory. Smoke from burning cities, which could result from a large scale nuclear war, would be a better absorber of shortwave radiation than forest fire smoke, and would therefore produce even larger surface temperature drops. The relative amounts of forest fire and city fire smoke resulting from a nuclear war would be scenario-dependent.

4. Plans for further work

Several more aspects of this research are planned. These include:

- complete study of 11-13 August 1981 case. Satellite images and MOS forecasts have already been obtained.

- search for other cases to study that can use the same research technique. They would have to have extensive smoke veils over clear areas of the U.S. One possibility is 10 September 1981 (Fig. 6, Chung and Lee, 1984).
- use a radiative-convective model to calculate the theoretical surface cooling that would result from the cases studied here. This would require knowledge of the height of the smoke cloud and the radiative parameters of the smoke particles. Ferrare (personal communication), in collaboration with Kaufman and Fraser at NASA/GLA will complete within the next month a study of the 1982 case presented here, in which they use a multi-spectral satellite technique to obtain the optical depth, single-scatter albedo and mean mass radius of the smoke particles at a number of locations on several days. I intend to obtain the data from them and do these calculations.
- I have obtained data from the U.S. network of surface radiation stations for the 1982 case, and will search them for information which may be useful to compare to the Ferrare data.
- work with Toon and Westphal (personal communication) who are using a mesoscale dynamic and radiative model to study the 1982 case. I will compare the location of the smoke plume and the surface temperatures that I have obtained to those that they calculate. This will help to verify their model and suggest other observational studies of this case.

ACKNOWLEDGMENTS

I thank Rich Ferrare for valuable discussions of the 1982 case and for providing preliminary satellite photos, Ed Eloranta for providing in situ smoke cloud data taken 2 August 1982 over Maryland, Mike Matson and Will Gould for information on availability of satellite images of smoke, Paul Dallavalle for MOS forecasts and surface temperature observations, Sunny Bae for plotting the maps, Marco Rodriguez for drafting the figures and Sherri West for proofreading the manuscript. This work was supported by NOAA grant NA87AA-D-CP003 from the National Climate Program Office, which was funded by the Defense Nuclear Agency.

REFERENCES

- Chung, Y.-S. and H. V. Lee, 1984: Detection of forest-fire smoke plumes by satellite imagery. Atmospheric Environment, 18, 2143-2151.
- Crutzen, P. J., and J. W. Birks, 1982: The atmosphere after a nuclear war: twilight at noon. Ambio, 11, 115-125.
- Ginsburg, A. S. and G. S. Golitsyn, 1986: Comparative analysis of mass forest and "nuclear" fires. Paper presented at the Second All-Union Conference of Soviet Scientists for Peace and Against Nuclear Threat, Moscow, 27-29 May 1986.
- Glahn, H. R. and D. A. Lowry, 1972: The use of model output statistics (MOS) in objective weather forecasting. J. Appl. Meteor., 11, 1203-1211.
- National Academy of Sciences, 1985: The Effects on the Atmosphere of a Major Nuclear Exchange. NAS Press,

Washington, D.C., 193 pp.

Robock, A. and C. Mass, 1982: The Mount St. Helens volcanic eruption of 18 May 1980: large short-term surface temperature effects. Science, 216, 628-630.

SCOPE, 1986: Environmental Consequences of Nuclear War. SCOPE 28. Volume I. Physical and Atmospheric Effects, Eds. Pittock, A. B., Ackerman, T. P., Crutzen, P. J., MacCracken, M. C., Shapiro, C. S. and R. P. Turco; Volume II. Ecological and Agricultural Effects, Eds., Harwell, M. A. and T. C. Hutchinson, John Wiley & Sons, New York, 1080 pp.

Turco, R. P., Toon, O. B., Ackerman, T. P., Pollack, J. B. and C. Sagan, 1983: Nuclear winter: global consequences of multiple nuclear explosions. Science, 222, 1283-1292.

Wexler, H., 1950: The great smoke pall -- September 24-30, 1950. Weatherwise, December, 129-142.

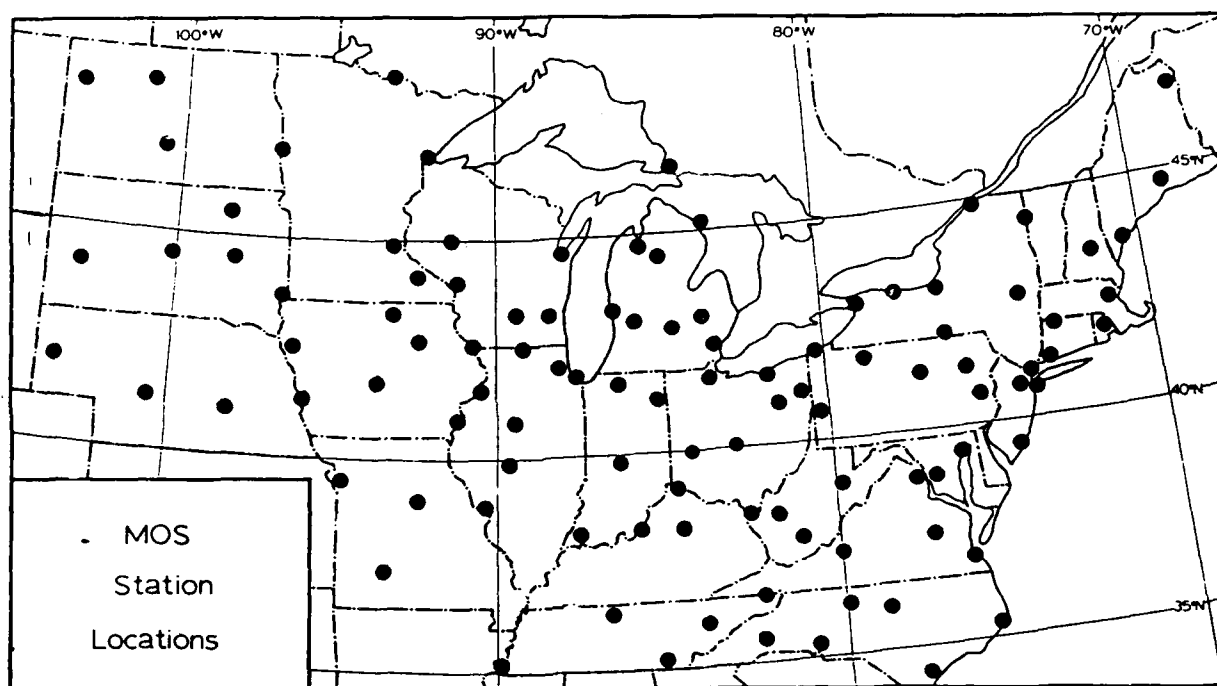


Fig. 1

1501 31JUL82 17A-2 01163 14662 WB1

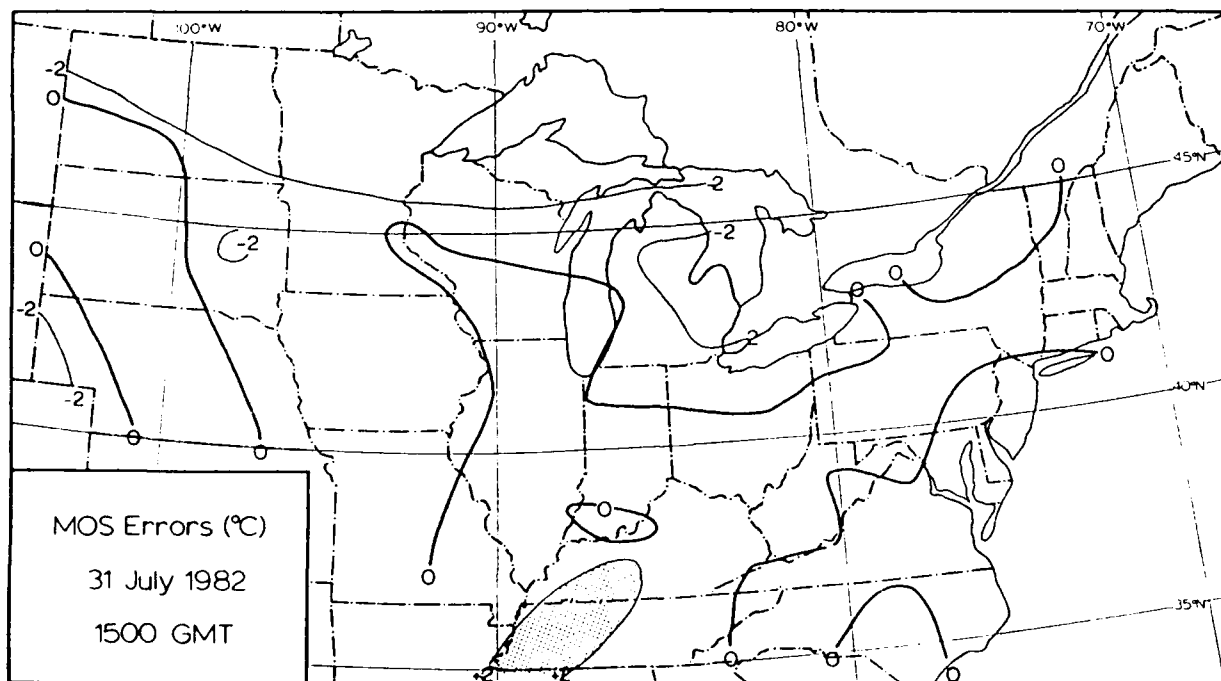
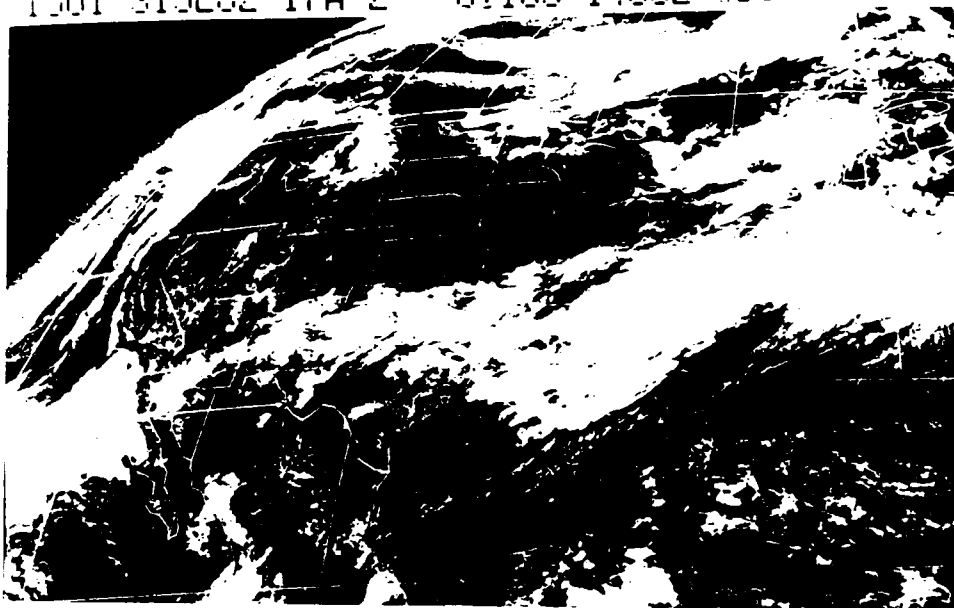


Fig. 2

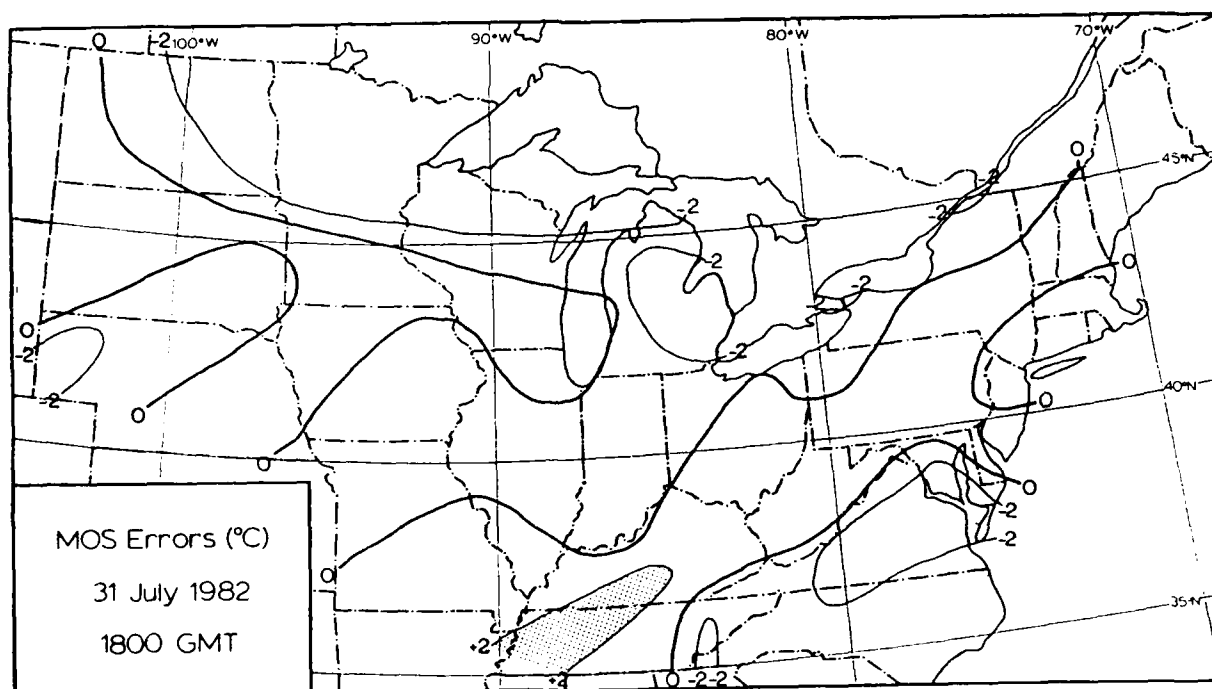
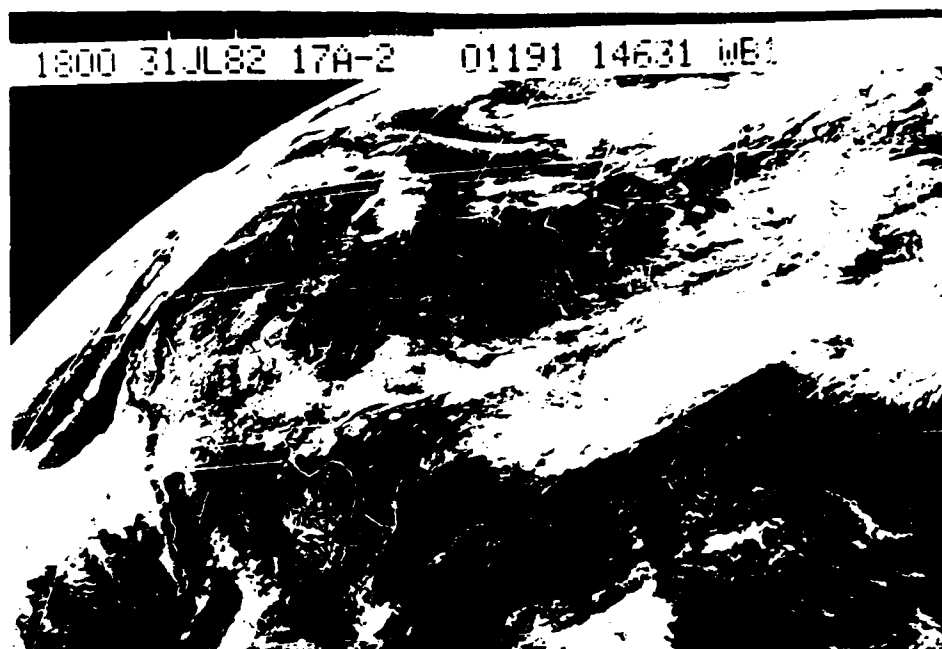


Fig. 3

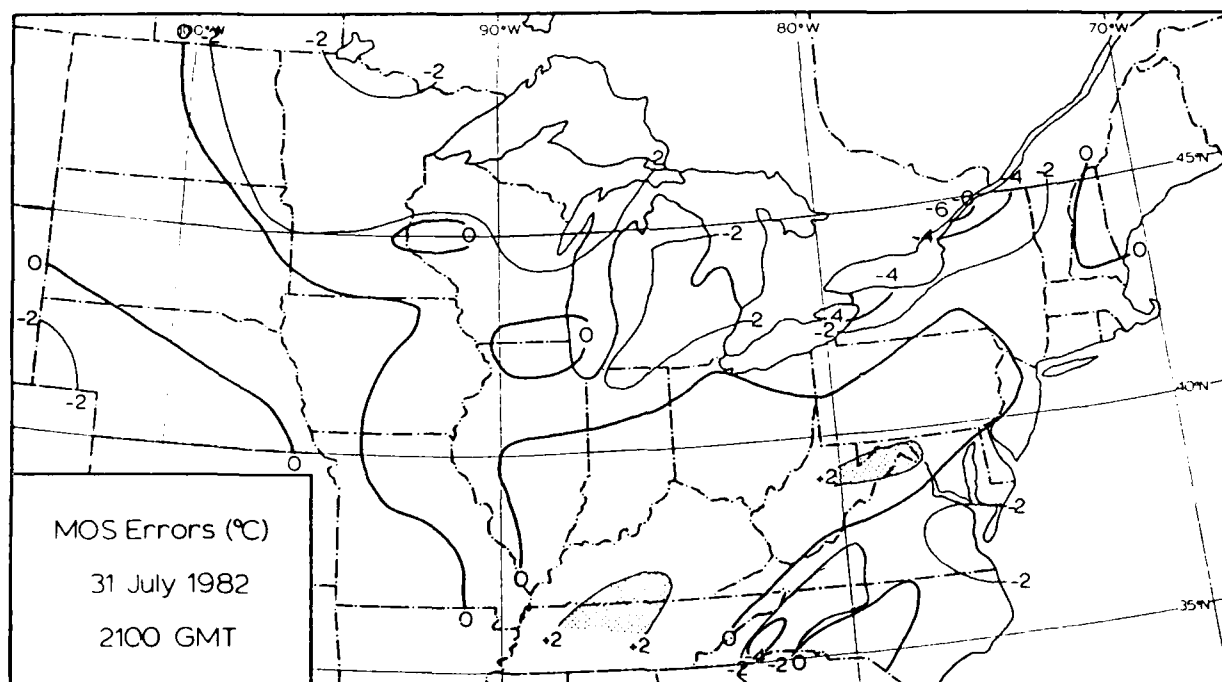
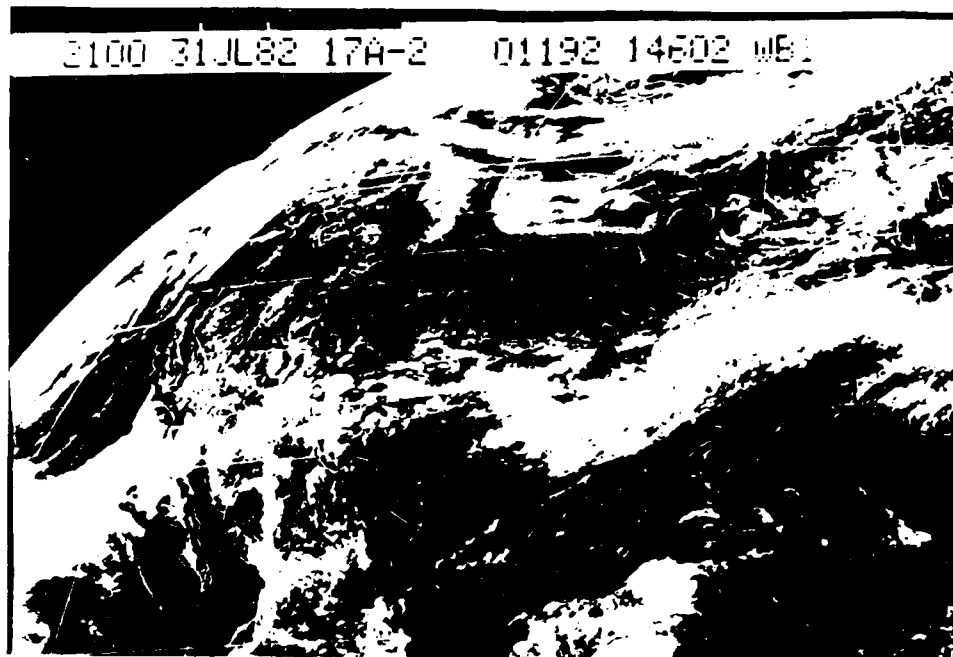


Fig. 4

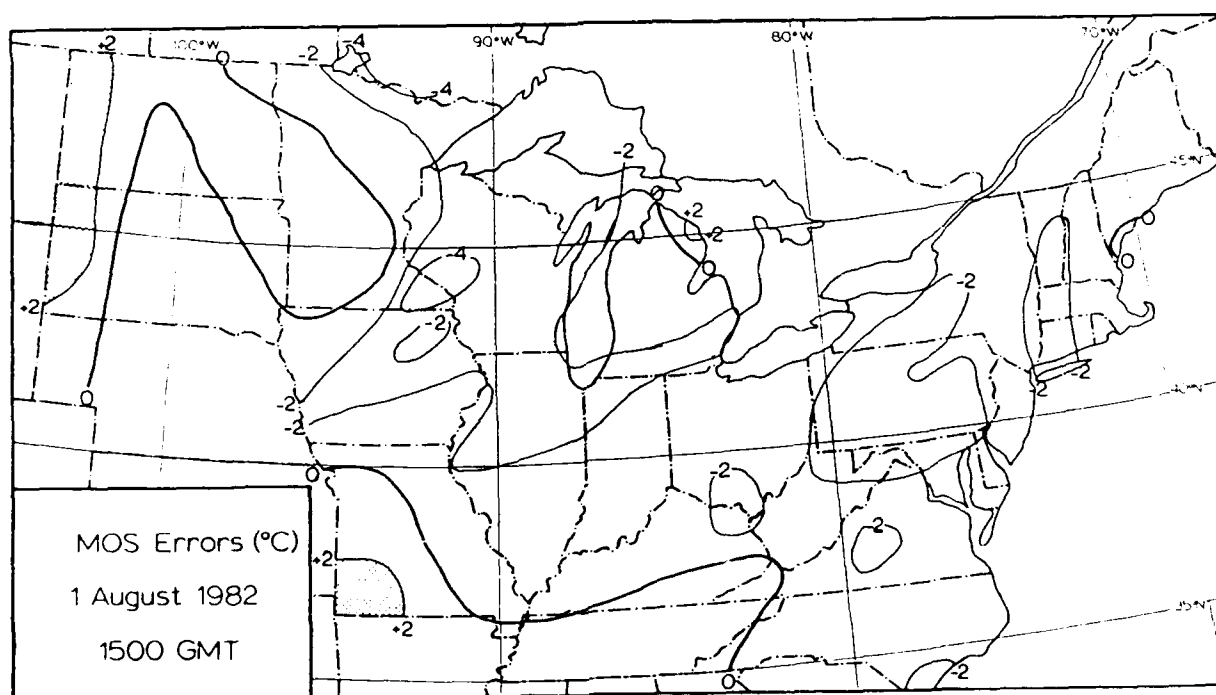
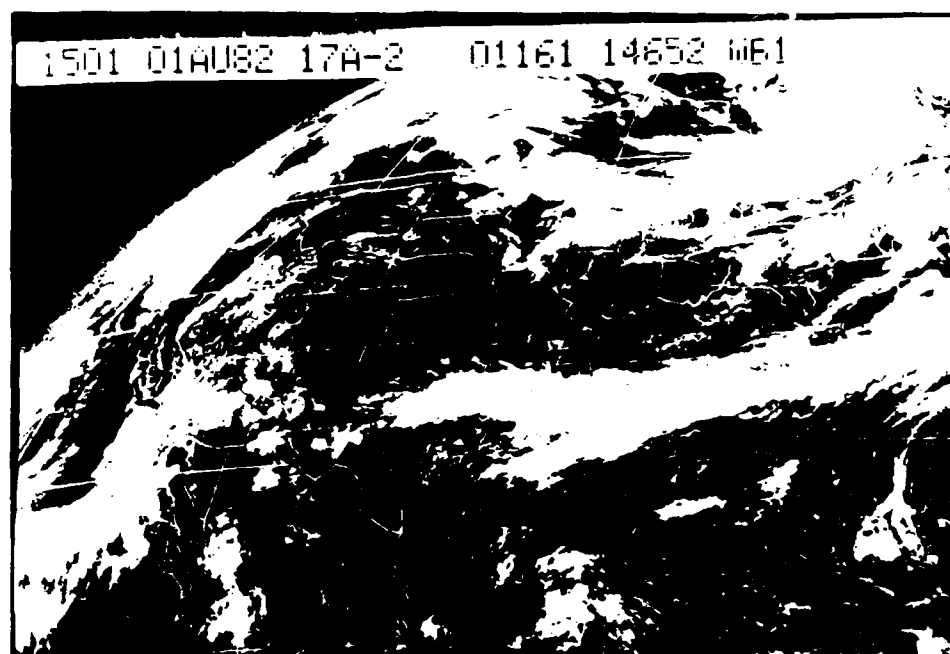


Fig. 5

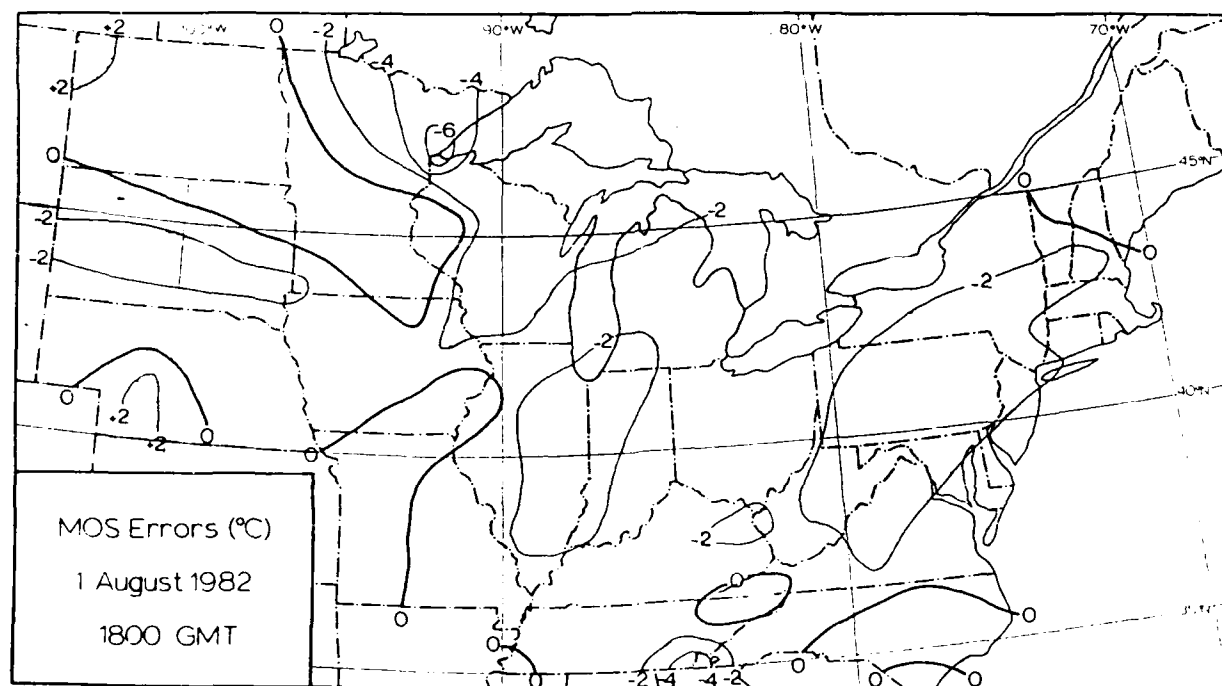
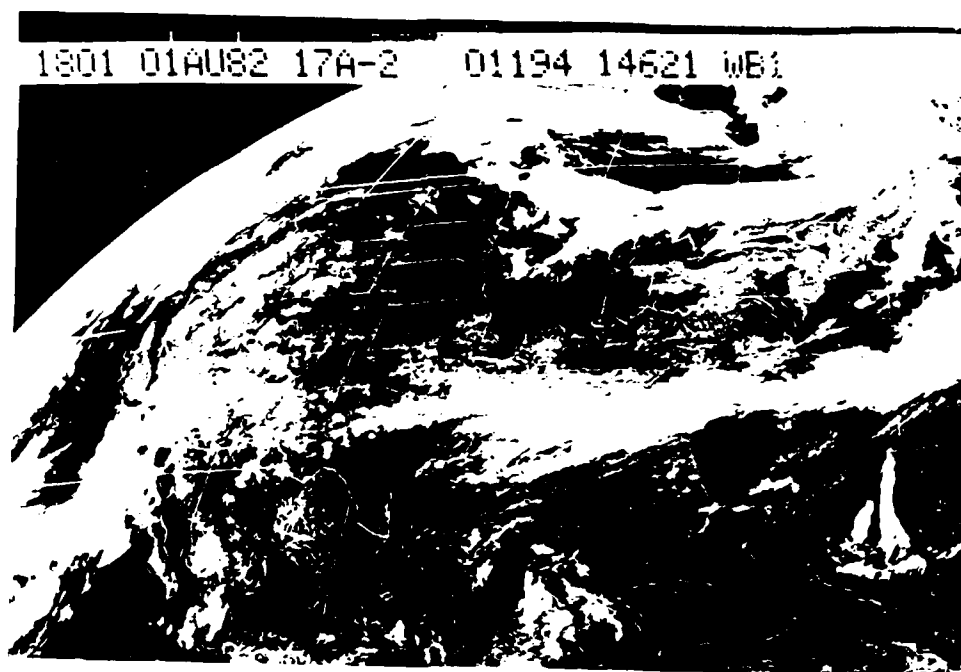


Fig. 6

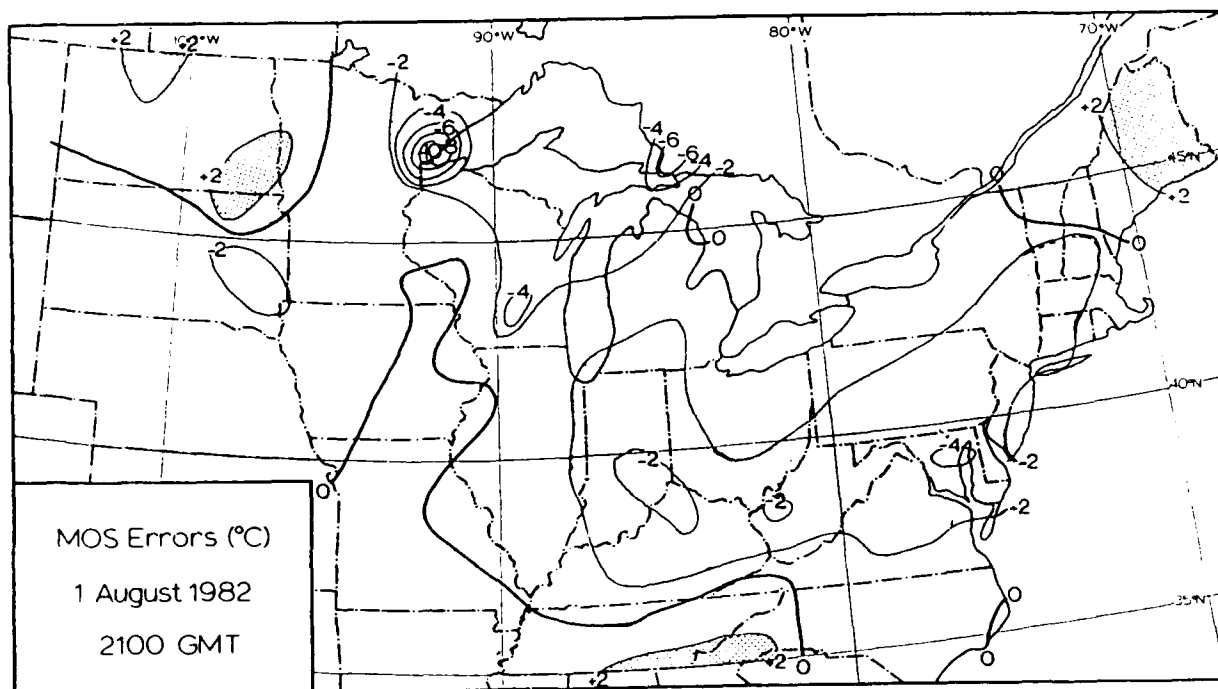
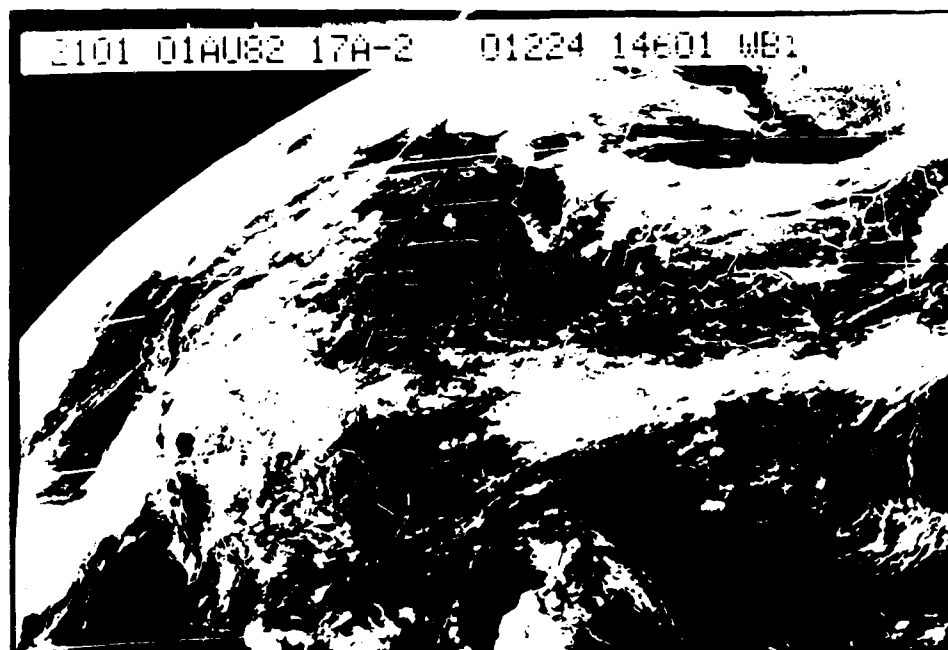


Fig. 7

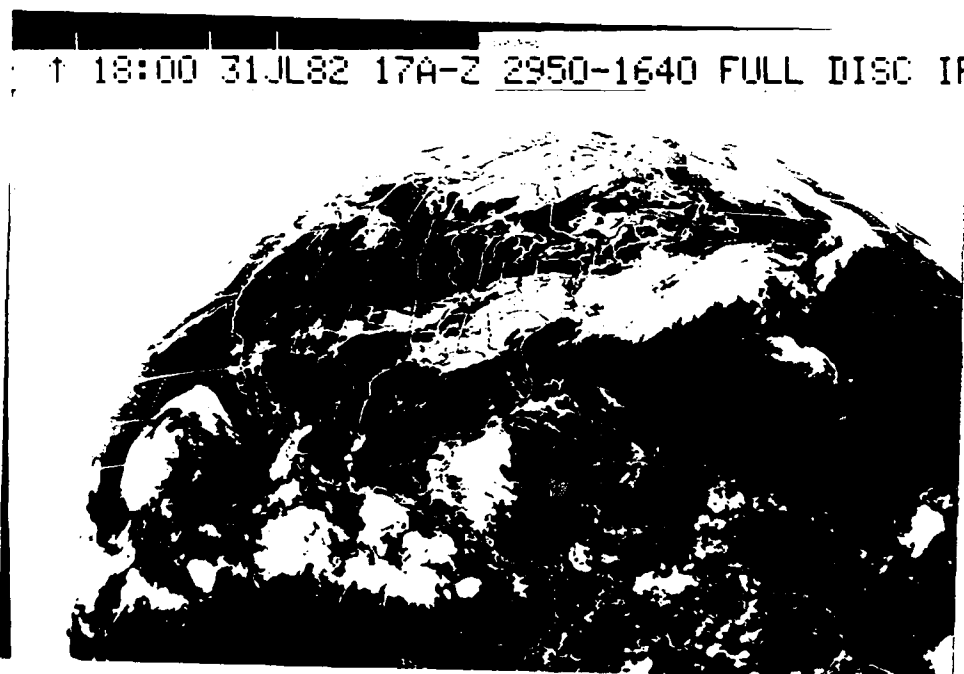


Fig. 8. IR image.

(Compare to Fig. 3)

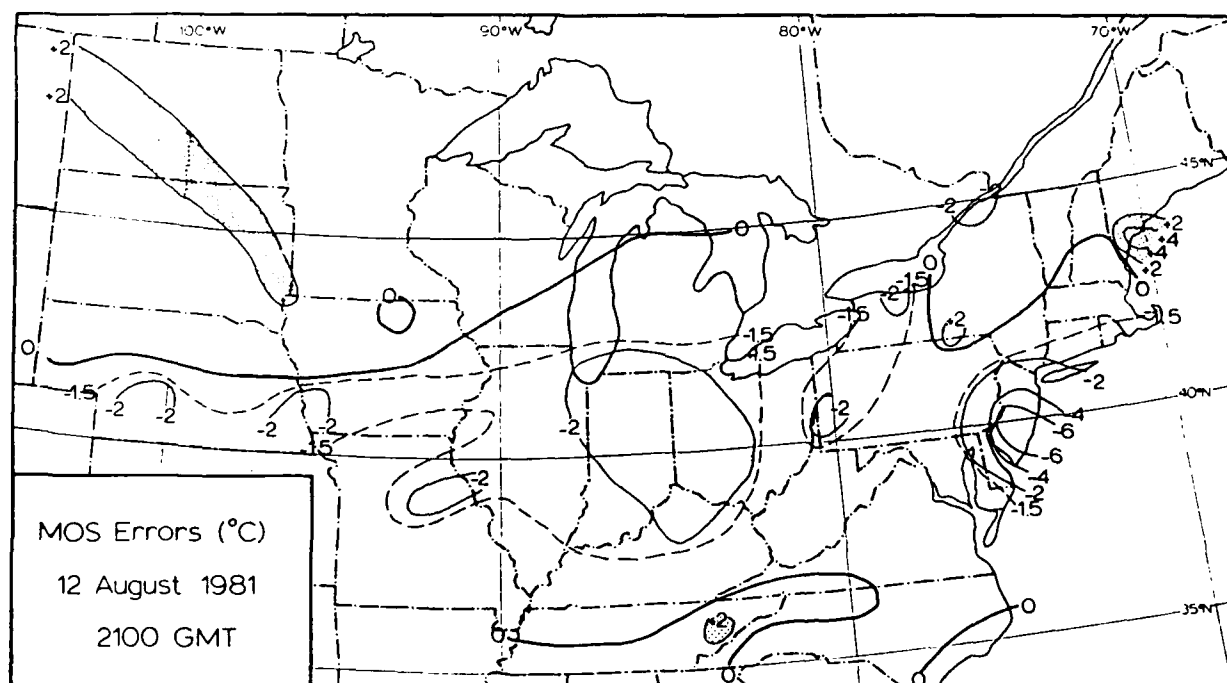
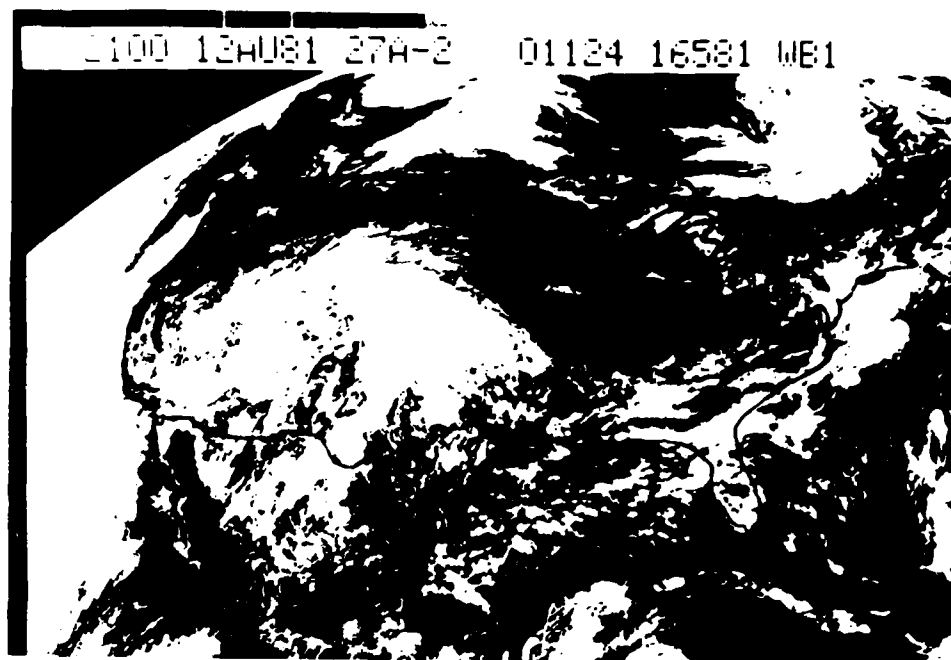


Fig. 9

Radioactivity; A Survey*

Charles S. Shapiro
Lawrence Livermore National Laboratory
and San Francisco State University

and

Ted F. Harvey
Lawrence Livermore National Laboratory

ABSTRACT

1. Sources of Radioactivity; fission, fusion, neutron activation -- weapons, fuel cycle facilities.
2. Global Fallout; injection and deposition parameters -- scenarios, models, meteorology; intermediate time scale (tropospheric) and long time scale (stratospheric), "nuclear winter" climate effects.
3. Local Fallout; injection and deposition parameters -- scenarios, models, meteorology.
4. Dose Assessments and Biological Effects; acute vs. chronic, high dose and low dose, protection factors (humans) and unshielded dose (other biota), biological repair, external dose and internal dose.
5. Nuclear Fuel Cycle Sources; reactors, spent fuel storage, reprocessing plants, waste storage facilities, Chernobyl -- a case study.
6. Future Work.

Presented at the Defense Nuclear Agency
"Global Effects Program Technical Meeting,"
Santa Barbara, California, April 7-9, 1987.

*This work was performed under the auspices of the U.S. Department of Energy by Lawrence Livermore National Laboratory under Contract W-7405-Eng-48.

IMPORTANT ASSUMPTIONS IN ESTIMATING RADIONUCLIDE EFFECTS



Scenario (total yield, yield mix, number of warheads, etc.)

Fission/fusion fraction

Height of burst

Stabilization height of debris cloud

Meteorological conditions

Scavenging and deposition rates

Time of year

Table 1. Sources of radioactivity in nuclear explosions

SOURCE	ISOTOPES OF INTEREST	STRENGTH OF SOURCE
1. Fission Fragments	Atomic weights 70 to 160	2.9×10^{23} Fragments per Kiloton of fission activity at 1 hour = 4×10^8 Ci activity at 1 year = 10^4 Ci
2. Fusion Reaction Products	Principally tritium (${}^3_1\text{H}$) from reaction ${}^2_1\text{H} + {}^3_1\text{H} \rightarrow {}^4_2\text{He} + {}^1_0\text{n}$	Depends on weapon design. Magnitude 10^4 Ci/Kiloton 10^{23} to 10^{24} atoms ${}^3_1\text{H}$ /kiloton Fusion Energy release can vary from 0 to 99% of total
3. Neutron Activation	Depends on explosion location and bomb case material. A principle isotope is carbon 14 from atmospheric nitrogen ${}^{14}_7\text{N} + {}^1_0\text{n} \rightarrow {}^{14}_6\text{C} + {}^1_1\text{H}$	2×10^{23} neutrons liberated in fission and in fusion per kiloton
4. Fissile Materials	Plutonium 239	Depends on weapon design. Comes from nonfissioned weapon material plus neutron activation of uranium

a) "Distribution & Evolution of Radioelements After Nuclear Explosion", M. Dupuis UCRL-transl-10617-\$ translated from Bull. Inform. Science & Technology : 149 (June 1970), pp. 41-52.

b) E. Eriksson, TELLUS 17: pp. 118-130 (1965).

Fission Product Spectrum

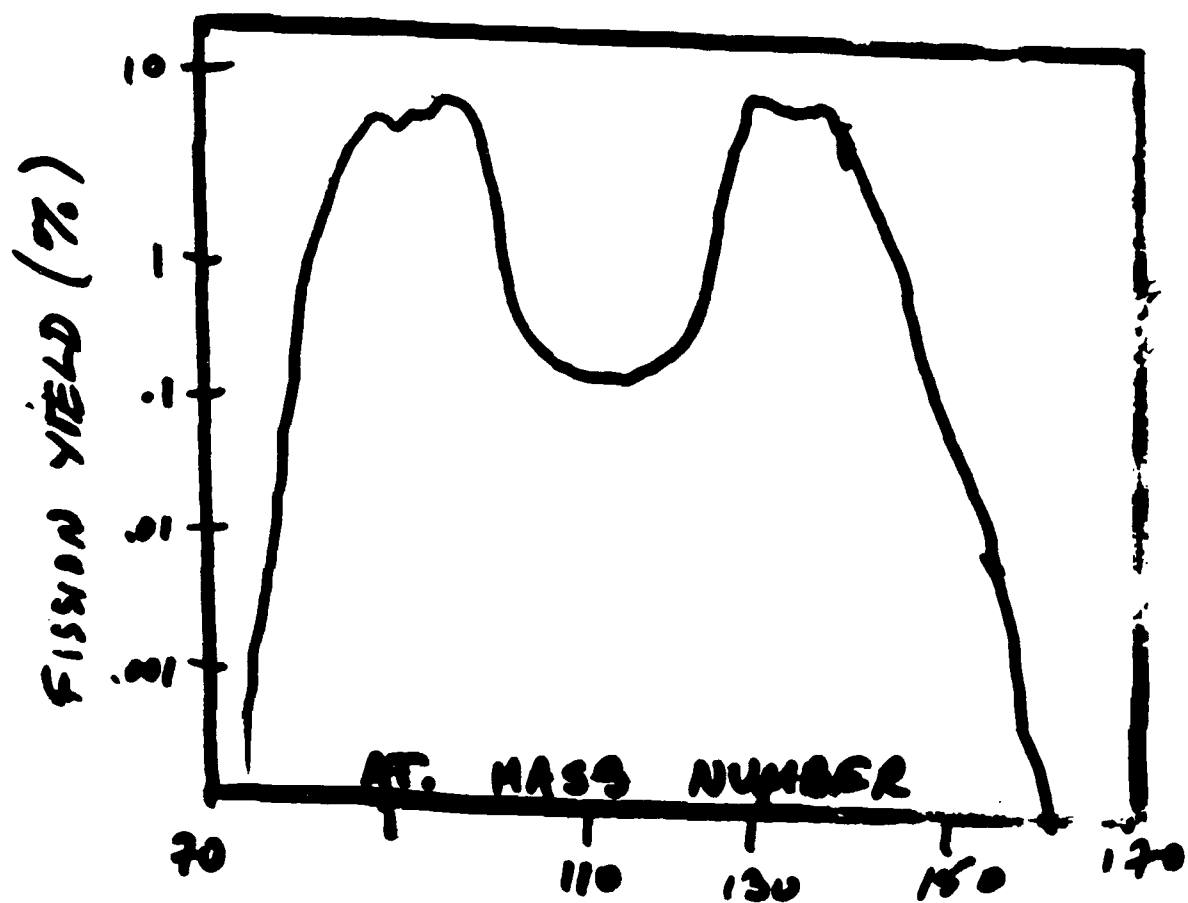
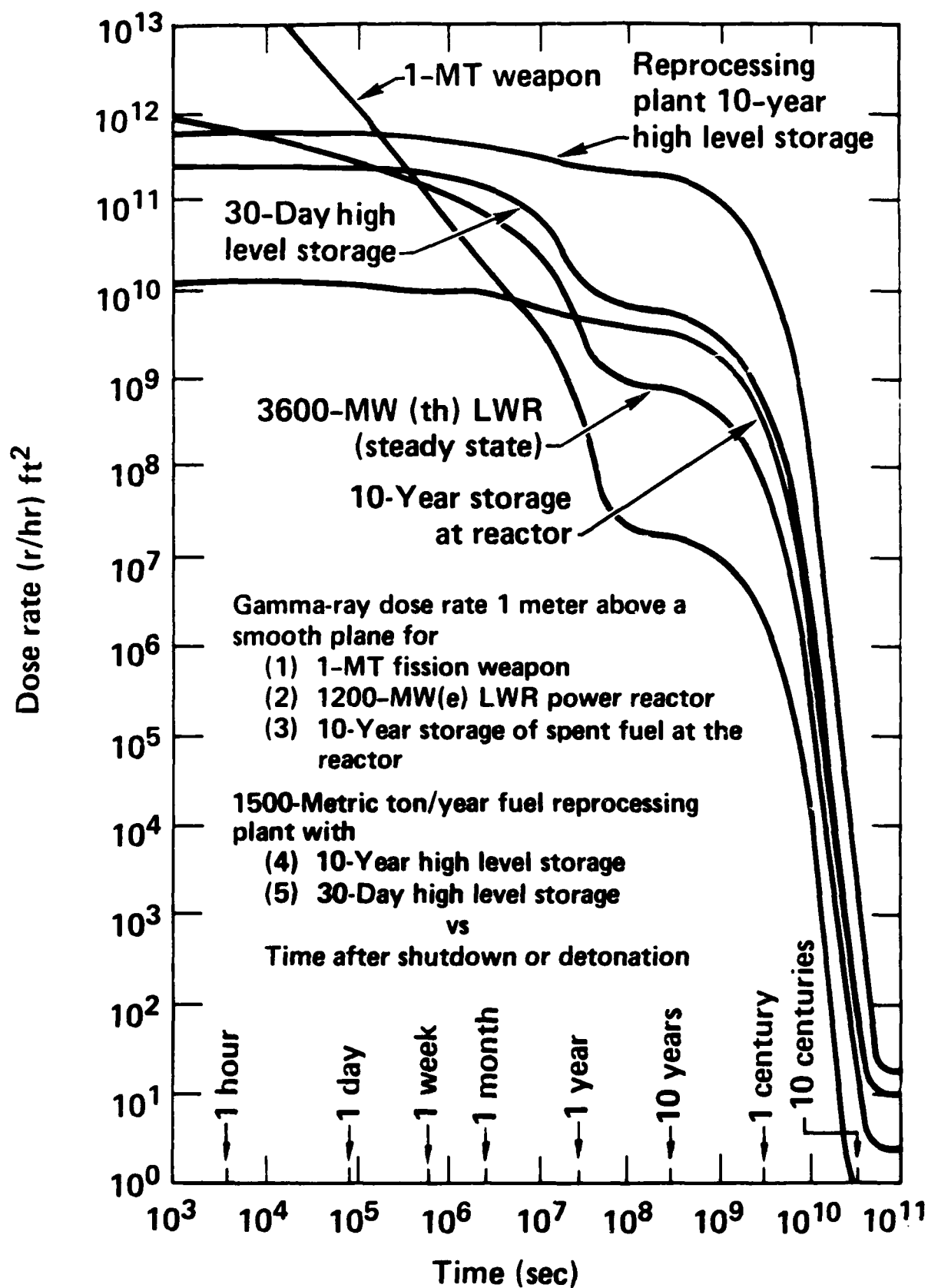
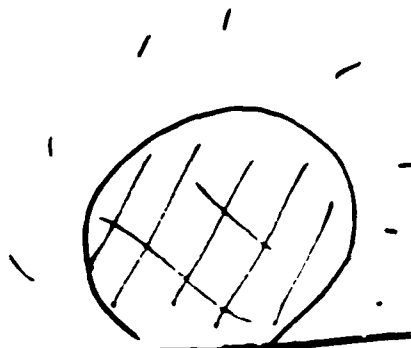


Figure 9.8. Gamma-ray dose rate area integral versus time after shutdown or detonation (Chester and Chester, 1976).

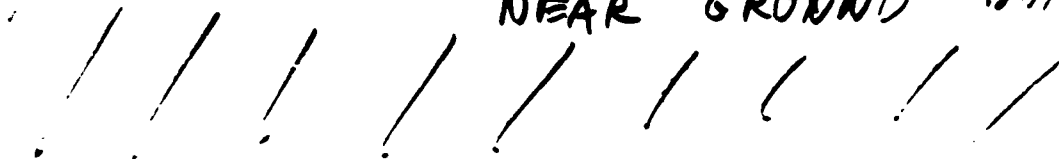




AIR BURST



NEAR GROUND BURST

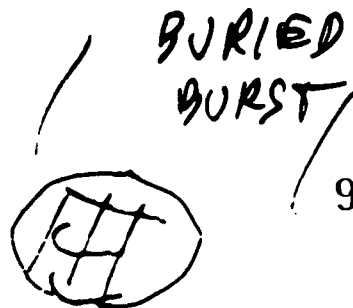


GROUND BURST



PARTIALLY
SUBMERGED
BURST

Local Fallout is produced by ground or near-ground bursts



BURIED
BURST

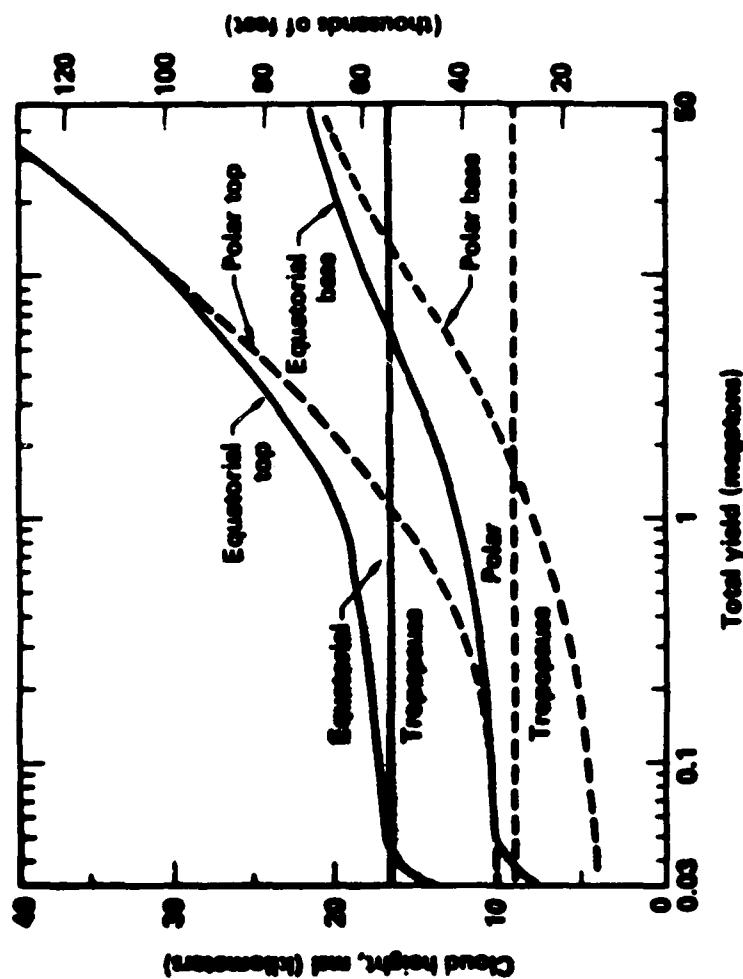


Figure 2. "Mushroom cap" cloud top and base as a function of total yield of device. "Equatorial" refers to 0-30 degrees latitude; "polar" refers to 30-90 degrees (Peterson, 1970).

The subsequent behaviour of the radioactivity depends on the height distribution of injection.

GLOBAL FALLOUT

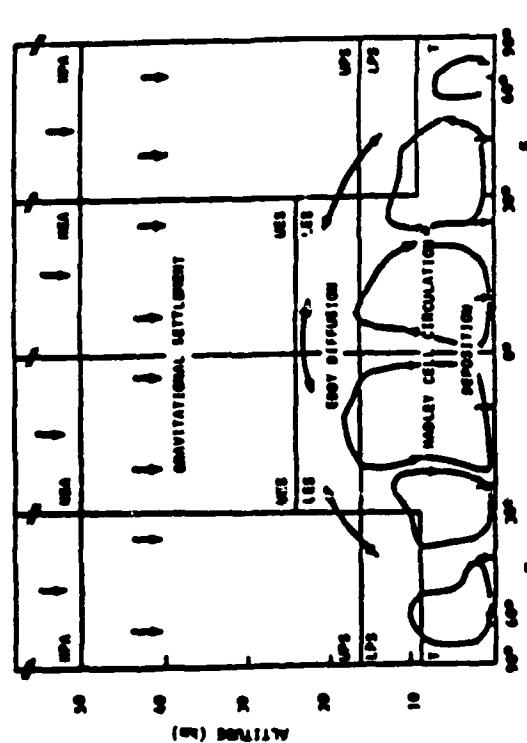


Figure 11. Atmospheric regions and the predominant atmospheric transport processes

MODELS

GLODEP2: Estimates gamma ray dose from global fallout.

Authors: L. Edwards, T. Harvey, K. Peterson

Reference: UCID-20033 (1984)

*Global
Falloff
(unperturbed
atmosphere)*

GRANTOUR: Calculates the 3-D transport, diffusion, and wet and dry deposition and dose from tropospheric global fallout.

*Global Fallout
Unperturbed plus
"nuclear winter"
atm.*

Authors: J. Walton and M. MacCracken

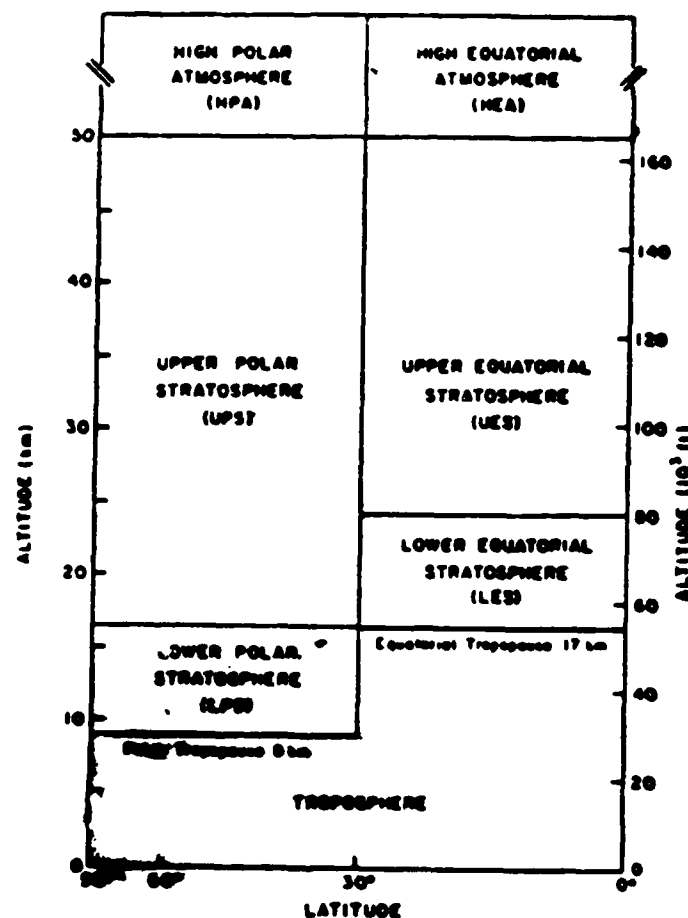
Reference: UCID-19985 (1984)

KDFOC2: Calculates local fallout.

Authors: T. Harvey and F. Serduke

Reference: UCRL-52858 (1979)

OUR ATMOSPHERIC MODEL CONSISTS OF FOUR VERTICAL COMPARTMENTS



BECAUSE INJECTIONS OCCUR IN POLAR OR EQUATORIAL ATMOSPHERES,
THERE ARE EIGHT COMPARTMENTS

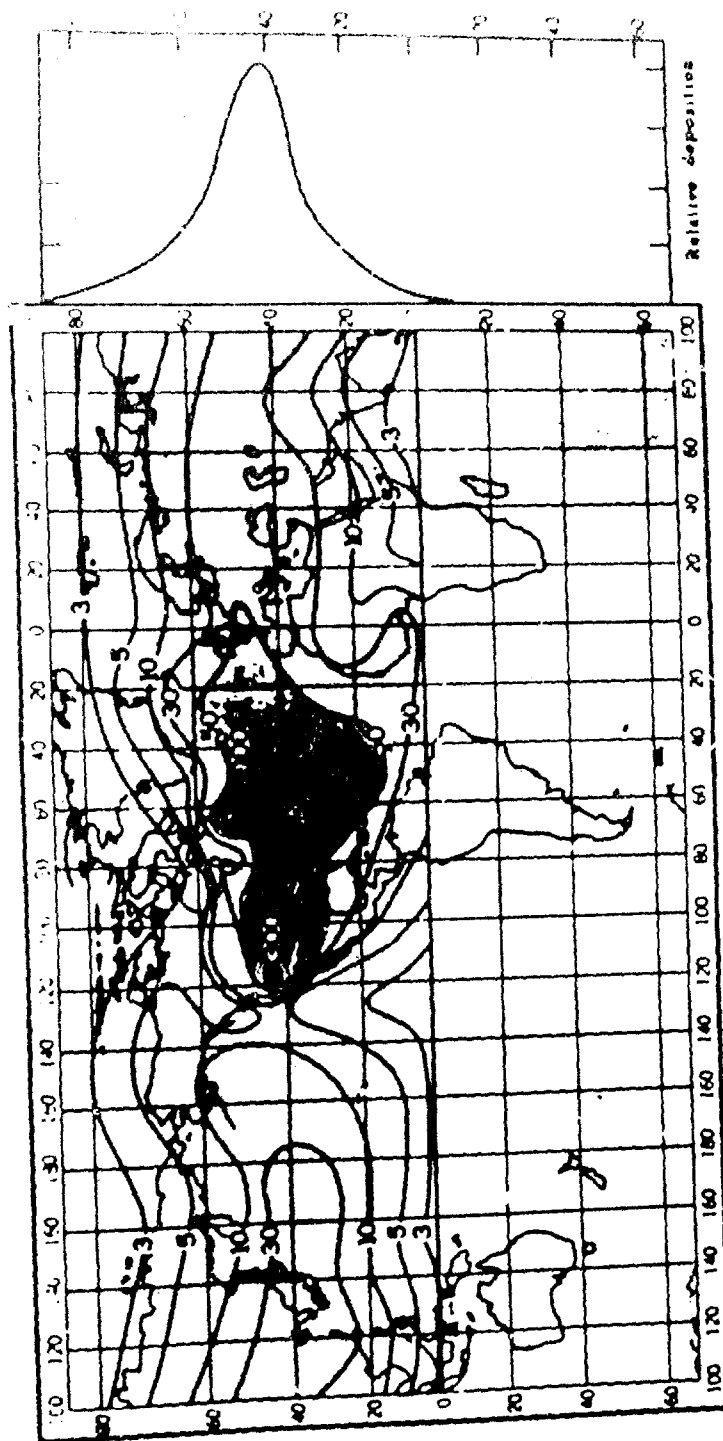


Figure 5. Worldwide fallout of radioactivity from nuclear weapons tests in Nevada in 1953. The explosions were in the kiloton range of yields, and debris was confined to the troposphere. The intensity of fallout is shown in relative units (L. Machta).

*Troposphere injection model was
a Gaussian in latitude.*

Nuclear War Scenario

Knox (1983) 5300 Mt baseline nuclear war		SCOPE (1986) 6000 Mt baseline nuclear war	
Total yield/warhead (Mt)	Total fission yield injected (Mt)	Total yield/warhead (Mt)	Total fission yield injected (Mt)
20.0	305	5.0	308.7
9.0	235	1.0	1100.0
1.0-2.0	355	.5	522.1
0.9	675	.3	234.3
0.75	15	.2	87.3
0.55	220	.1	89.6
0.3-0.4	115	.05	33.1
0.1-0.2	110		
<0.1	1		

Mt of fission products injected into atmosphere	Knox	SCOPE
polar troposphere	226	473
lower polar stratosphere	1234	1652
upper polar stratosphere	571	250
Total	2031	2375

Fraction of yield in surface bursts	0.47	0.42
Fission fraction	0.5	0.5
Total number of explosions	6,235	12,641
Average yield per explosion (Mt)	.85	.47

**Global Fallout Dose Assessments (Rads) for an
Unperturbed Atmosphere With No Smoke**

Knox (1983) 5300 Mt baseline nuclear war

Latitude band	A	B	C	D
70-90N	2.9	6.6	4.5	8.01
50-70N	21.7	22.1	27.3	21.3
30-50N	27.4	27.2	32.9	26.4
10-30N	5.6	9.0	6.9	8.6
10S-10N	0.5	1.1	0.8	1.2
10-30S	0.4	0.6	0.6	0.6
30-50S	0.6	0.8	0.8	0.8
50-70S	0.5	0.5	0.5	0.5
70-90S	0.2	0.1	0.1	0.1
Area averaged--N.H.	13.1	14.6	16.2	14.3
Area averaged--S.H.	0.5	0.6	0.6	0.6
Area averaged--Global	6.8	7.6	8.4	7.5
Global population dose ($\times 10^{10}$) person-rads	5.5	6.3	6.7	6.1

A = Summer injection using GLODEP2

B = Summer injection using GRANTOUR (run for 30 days) with stratospheric contributions from GLODEP2

C = Winter injection using GLODEP2

D = Winter injection using GRANTOUR (run for 30 days) with stratospheric contributions from GLODEP2

Global Fallout Dose Assessments (Rads) using GRANTOUR;
Comparing Perturbed Atmosphere (Smoke) and
Unperturbed Atmosphere (No Smoke);
Land Areas Only

Latitude band	K1 (No Smoke)	K2 (Smoke)	S1 (No Smoke)	S2 (Smoke)	K3 (No Smoke)	K4 (Smoke)
90-70N	8.4	6.5	13.5	9.6	8.0	8.1
70-50N	26.4	17.2	45.9	26.6	22.4	22.1
50-30N	32.6	23.2	55.8	36.0	28.0	26.9
30-10N	10.1	7.1	16.4	10.1	8.7	8.0
10S-10N	1.1	1.2	1.5	1.7	1.2	1.2
10-30S	0.6	0.7	0.6	0.8	0.6	0.6
30-50S	0.7	0.9	0.6	0.9	0.7	0.7
50-70S	0.3	0.4	0.2	0.3	0.3	0.3
70-90S	0.1	0.1	0.1	0.1	0.1	0.1
Area averaged--N.H.	20.7	14.4	35.3	22.0	17.8	17.2
Area averaged--S.H.	0.5	0.6	0.5	0.7	0.5	0.5
Area averaged--Global	14.3	10.0	24.3	15.2	12.32	11.9
Global population dose ($\times 10^{10}$) person-rads	7.4	5.2	12.4	7.9	6.3	6.0

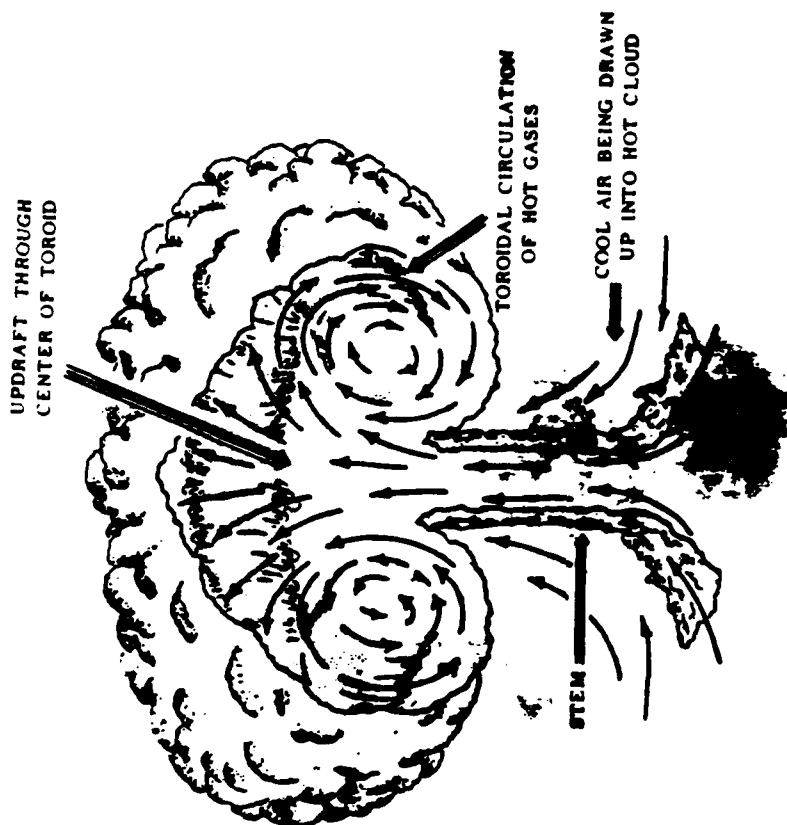
K1 & K2 = Knox 5300 Mt (1983) Summer injection

S1 & S2 = SCOPE 6000 Mt (1986) Summer injection

K3 & K4 = Knox 5300 Mt (1983) Winter injection

The doses here include the stratospheric contributions as calculated by
GLODEP2 and GRANTOUR (run for 30 days)

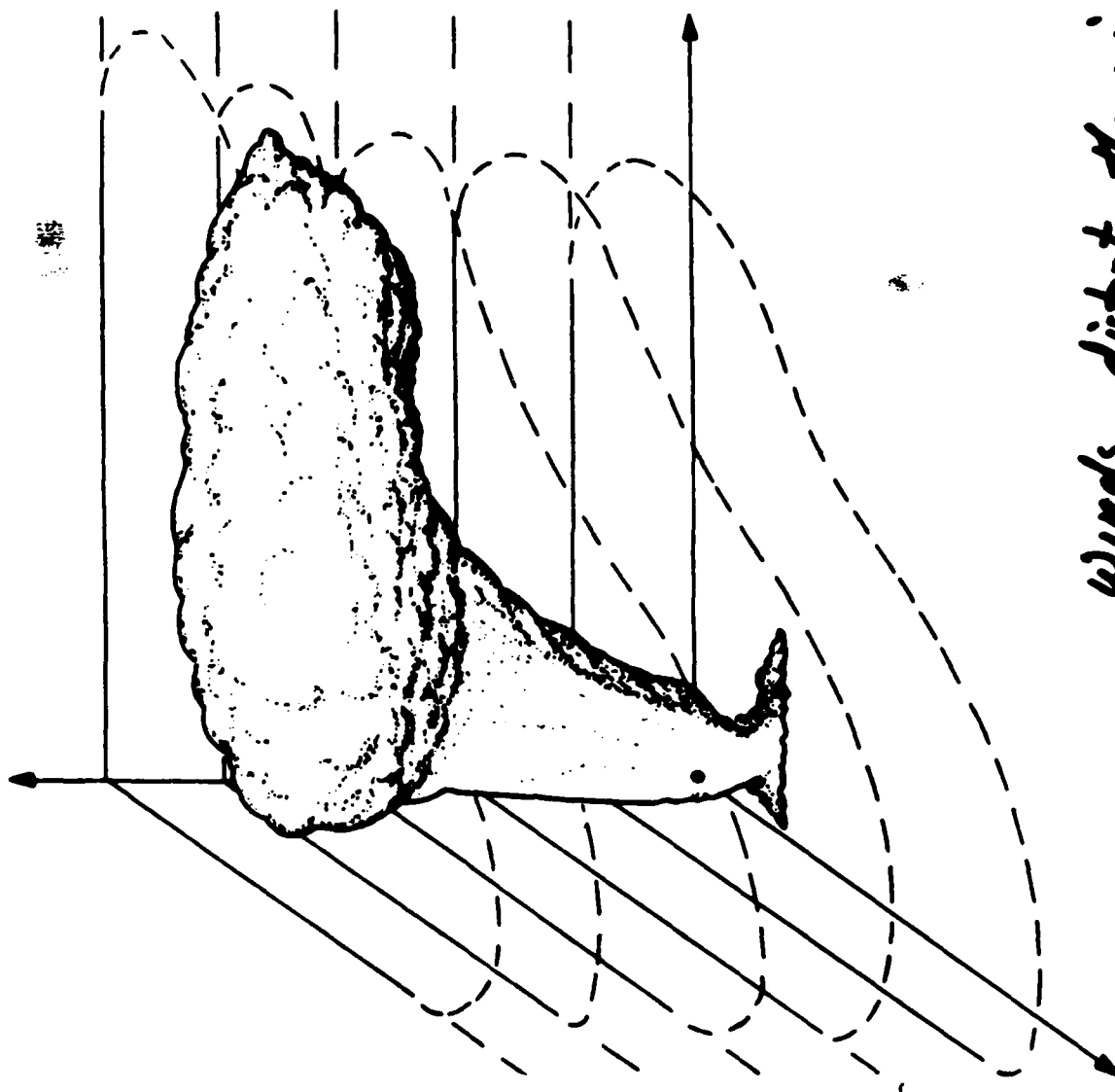
LOCAL FALLOUT



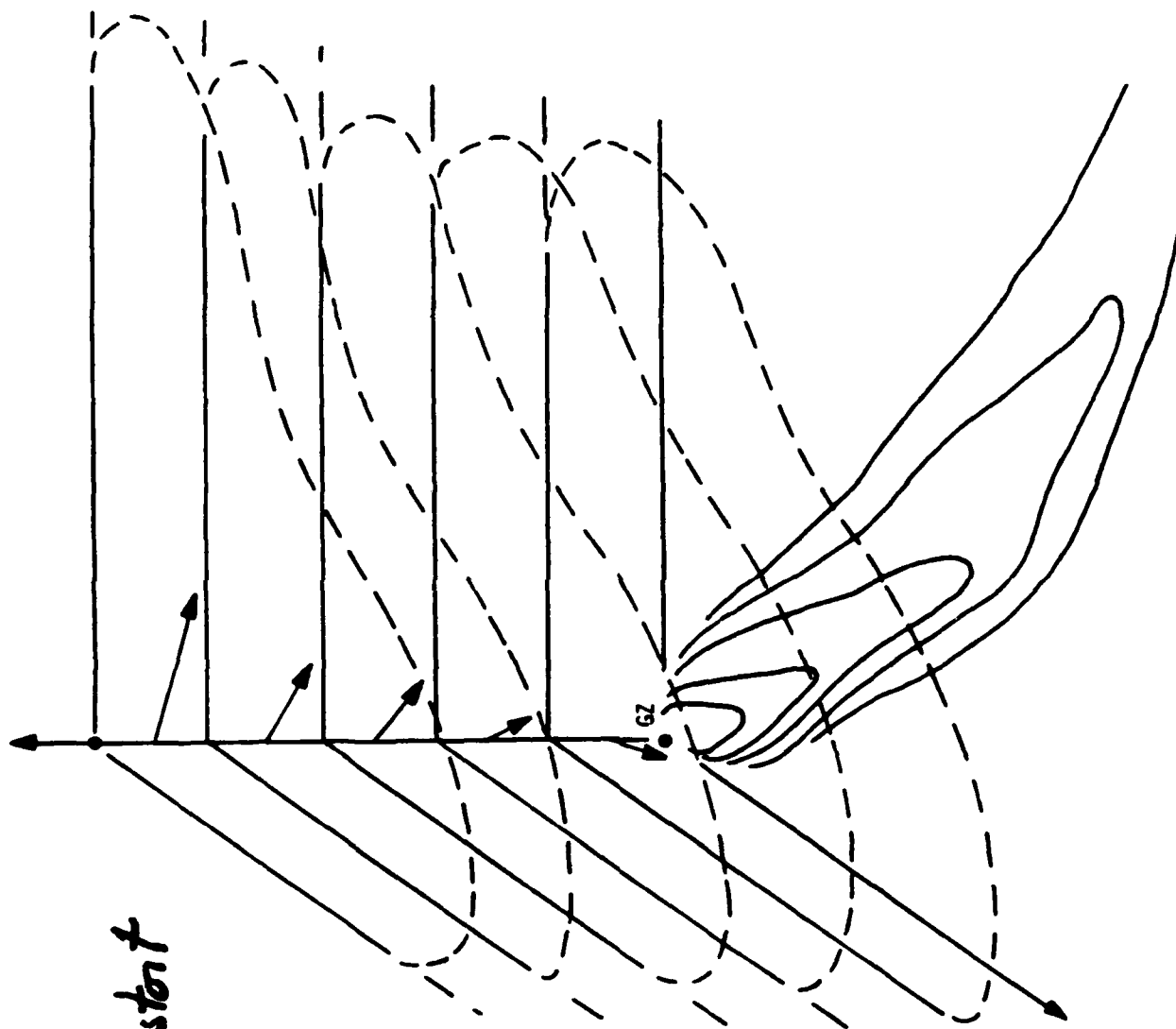
FORECASTING EARLY F10
DEPENDS ON COMPLEX
INITIAL CONDITIONS



SMALL YIELD LOW
AIRBURST



*Winds distort the rising
nuclear cloud*



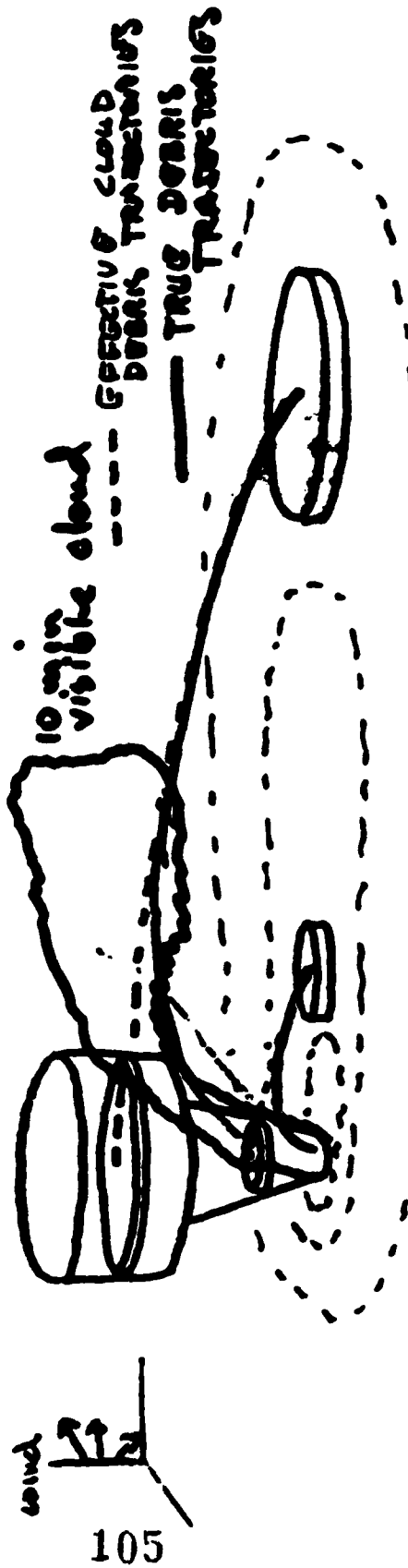
*They also distort
the fallout
pattern*

*We want to
predict the
pattern*

KDFOC2 - MODEL

● THE EFFECTIVE CLOUD

● That "stabilized" debris cloud which when transported to the surface yields the observed fallout pattern



EFFECTIVE CLOUD IS CALIBRATED VS. DATA

→ ACTIVITY-SIZE DISTRIBUTION

→ ACTIVITY - HEIGHT DISTRIBUTIONS

● SURFACE-BURST EFFECTIVE CLOUD

PARTICLE SIZES - SMALL BOY $\bar{r} = 15\mu$
 10^6

80% OF ACTIVITY ON SMALL PARTICLES

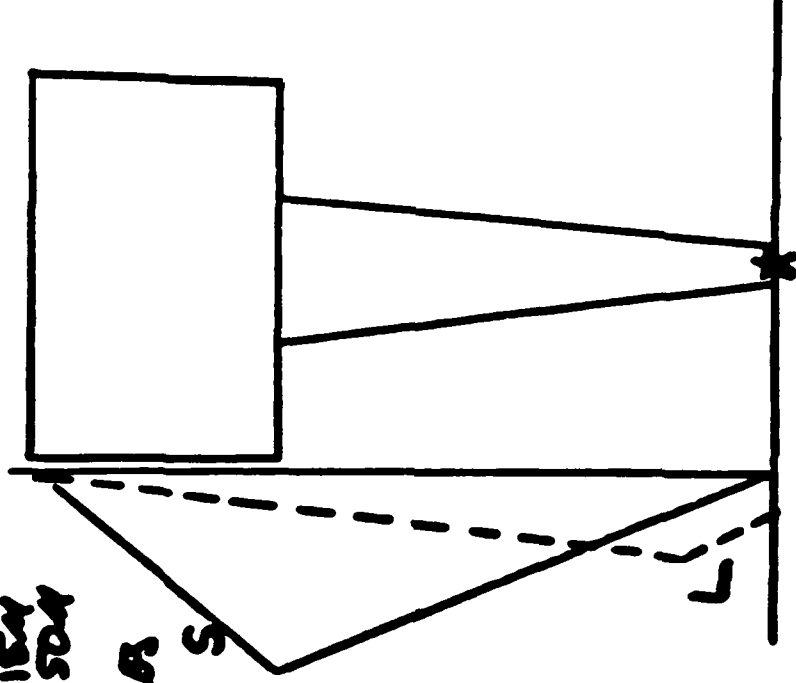
20% OF ACTIVITY ON LARGE " S

STEM IS TAPERED TO
 3 FOOTBALL RADII $R_p = 30W^{1/3}$

AVERAGE EMPIRICAL SIZES FOR CLOUD

NOTE: SHORT RANGE, HI LEVEL
 F/O FROM STEM ONLY

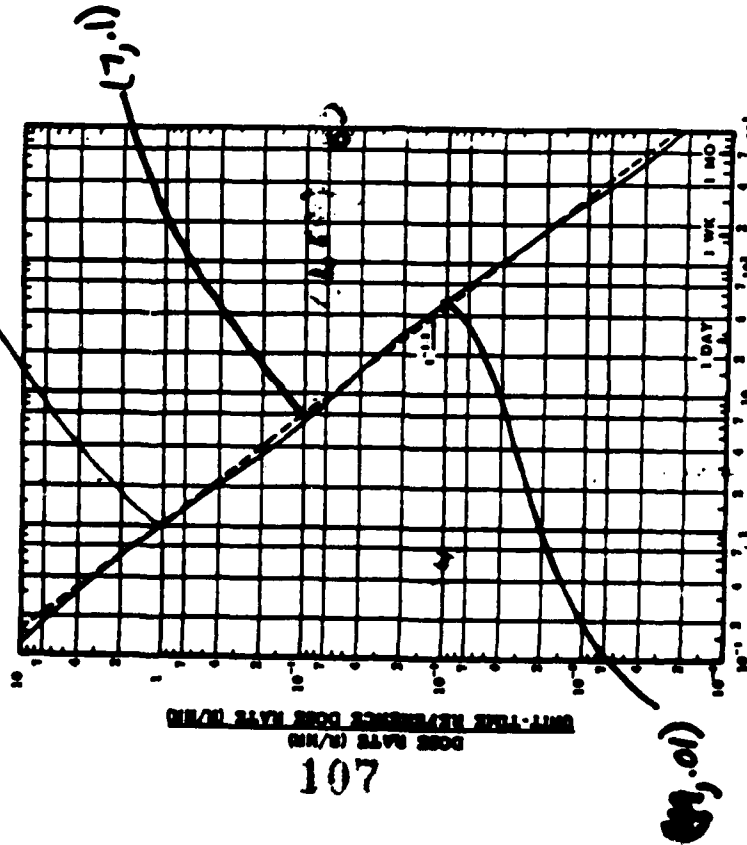
INSIDE A FEW KM FOR 1 KT
 MAIN CAN'T FALL, FAST ENOUGH



The Dose - Area Integral measures Blastoid Toxicity

Time Dependence

Figure 2.3
(1 hr, 100 R/hr)



Dependence of dose rate from early fallout upon time after explosion

Amount of Hazard (K-factor)

Reference time = 1 hr. after burst (H=1)

$$K = \int I(a) da$$

= ~ 3500 R/hr Theory

= 1000 R/hr measured

over 1 mi² per det

= 1000 $\frac{R \cdot mi^2}{hr \cdot det}$ @ H=1 hr

At 7 hrs K = 100 R/hr

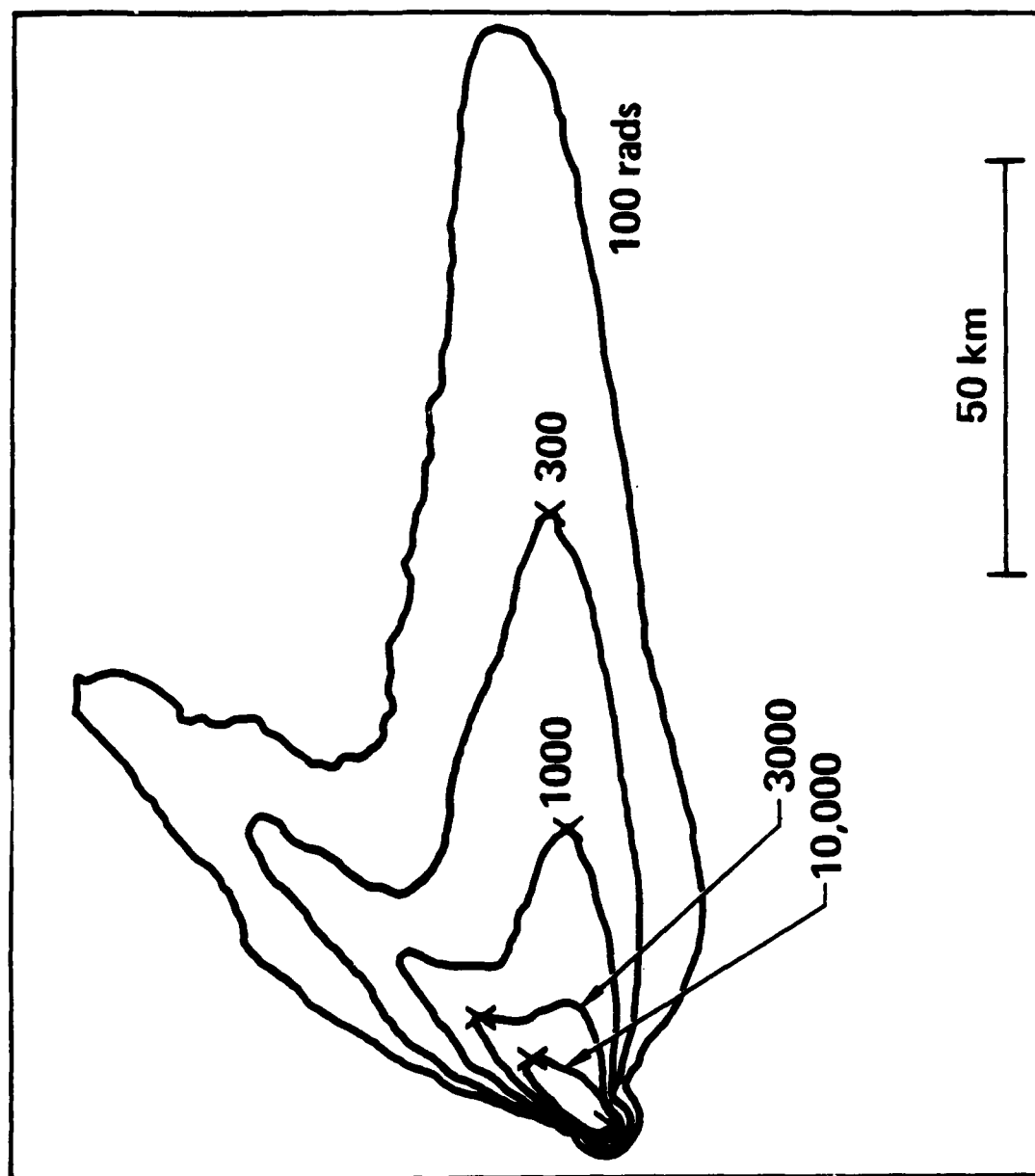
2 days K = 10 R/hr

2 weeks K = 1 R/hr

3 months K = 0.1 R/hr

If spread over 10 mi², then dose rate at 1 hr would be ~ 100 R/hr

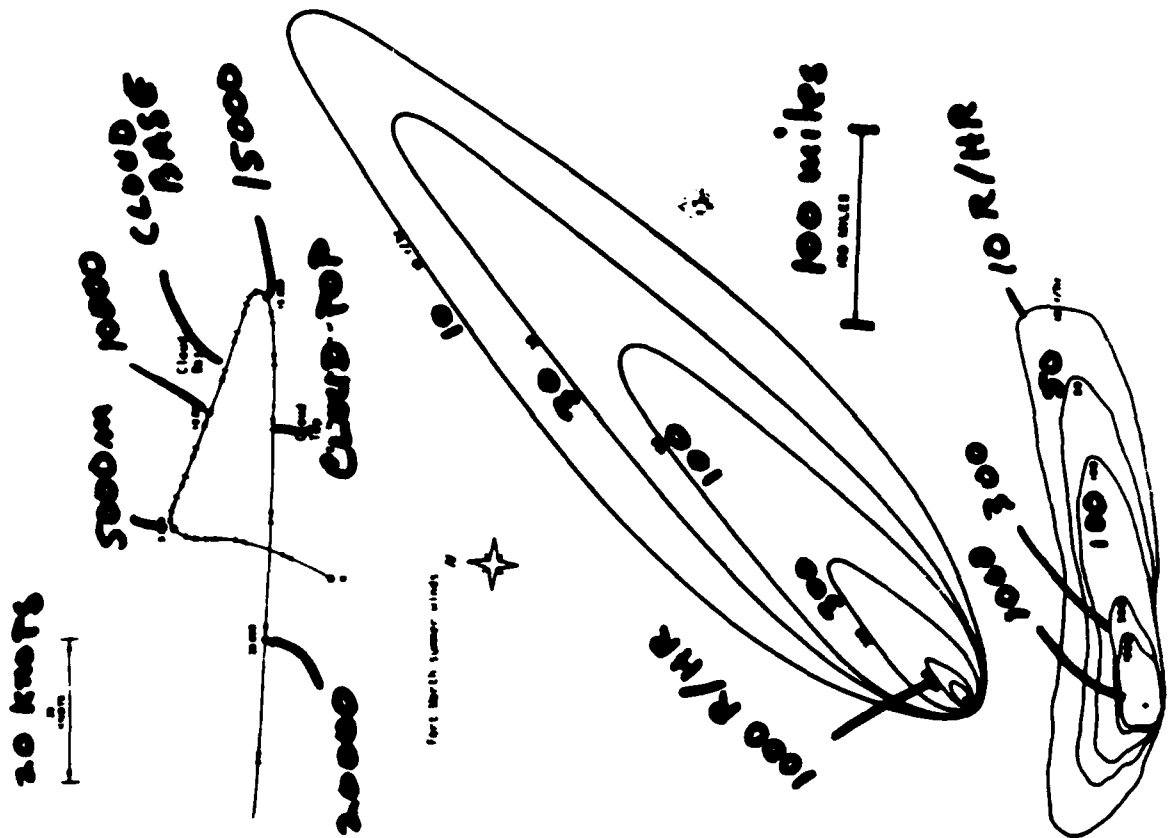
Figure 1 48-hour dose predictions for a 1-Mt all-fusion weapon detonated at surface. A mid-continental Northern Hemisphere summer wind profile was used. The double-lobed pattern is due to a strong directional wind shear that is typical during this season. For a 1-Mt weapon, the lofting of radioactivity is so high that topographic features are not expected to play a large role in pattern development; thus, a flat surface has been used. The protection factor is 1. The local terrain is assumed to be a rolling grassy plain.

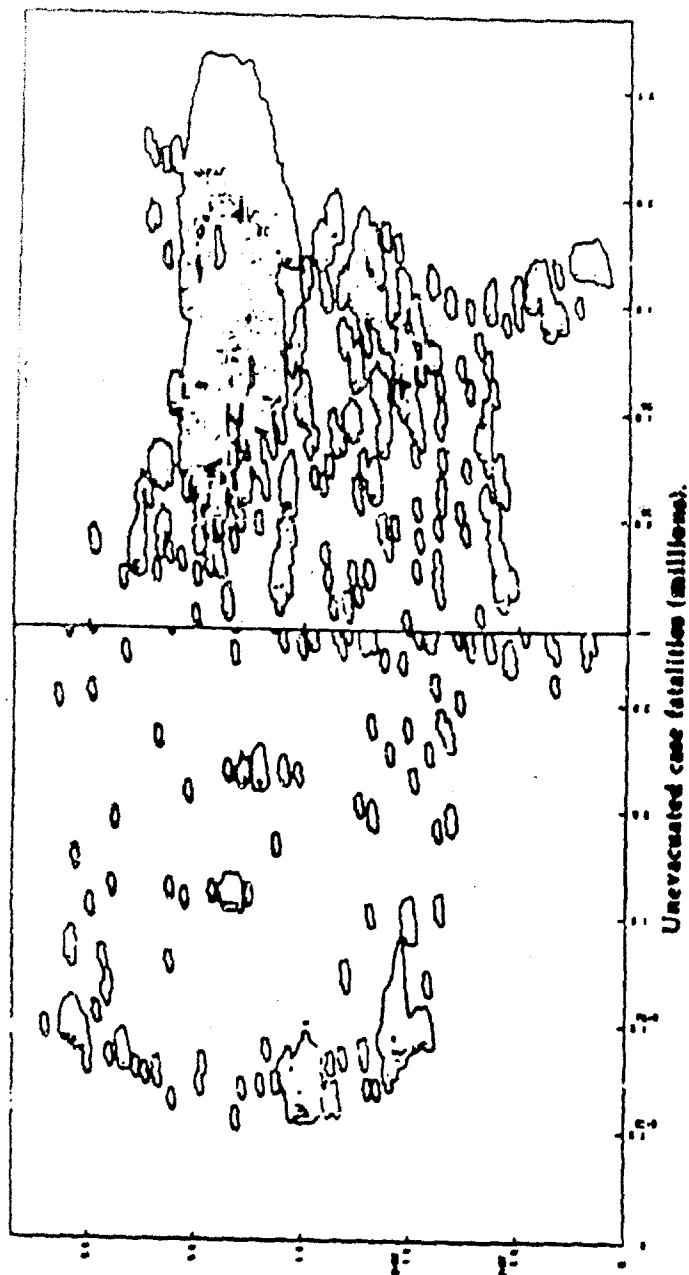


DOWN AND DISTANCES AND AREAS
WERE WITHIN FACTOR OF 2
WITH FEW EXCEPTIONS



IDENTIFIED MODELS CAN BE WAY OFF





Unevacuated case fatalities (millions).

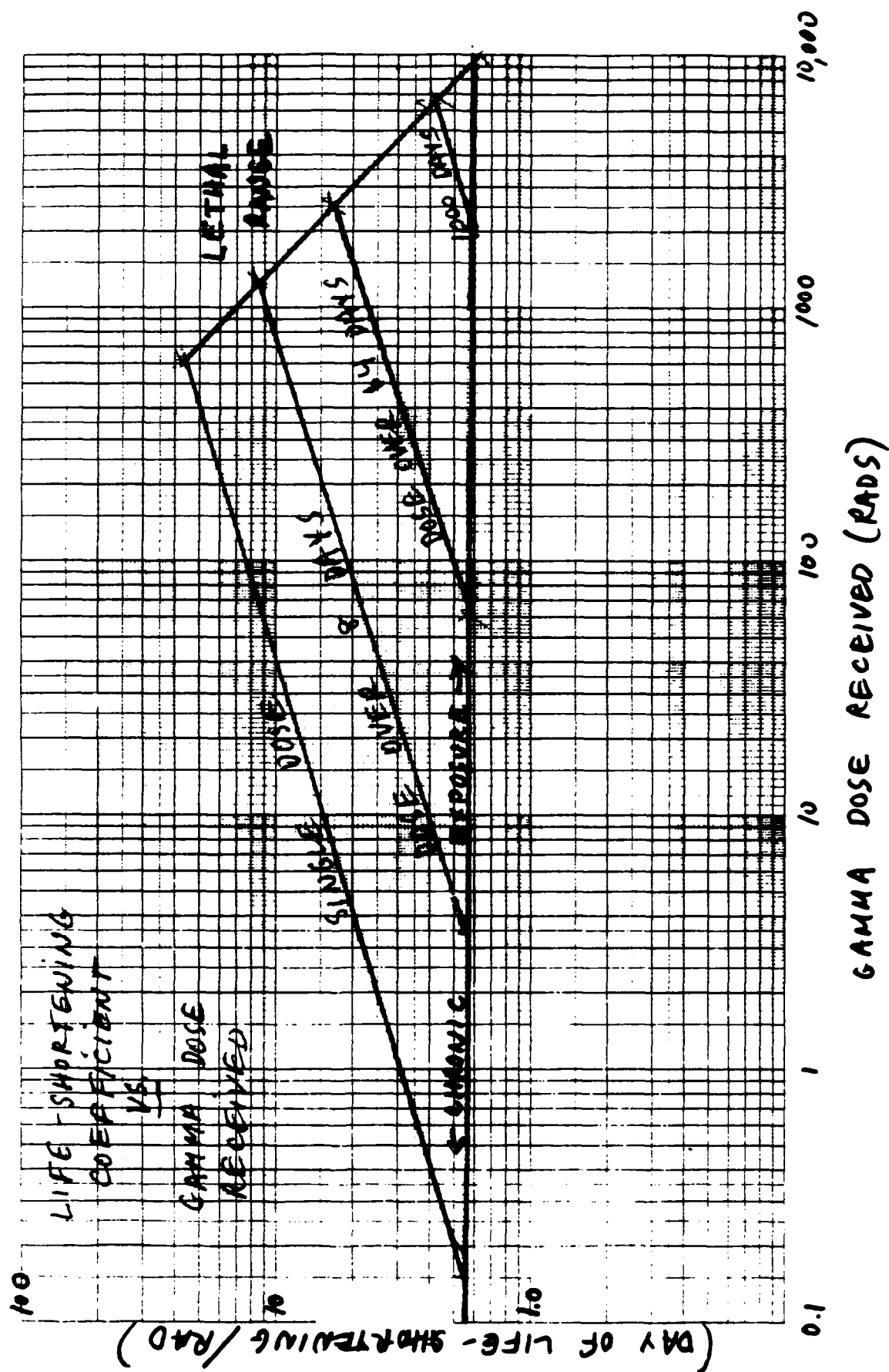
Approx. number of 1-Mt. 10% fusion weapons	Fallout shelter system			
	FS1	FS2	FS3	FS4
1000	140	145	144	144
3000	165	190	148	144
6000	175	140	100	150

Evacuated case fatalities (millions).

Approx. number of 1-Mt. 90% fusion weapons	Fallout shelter system			
	FS1	FS2	FS3	FS4
1000	45	10	4	4
3000	70	25	10	5
6000	100	45	15	10

**EVACUATION + SHELTERING ARE
SIGNIFICANT**

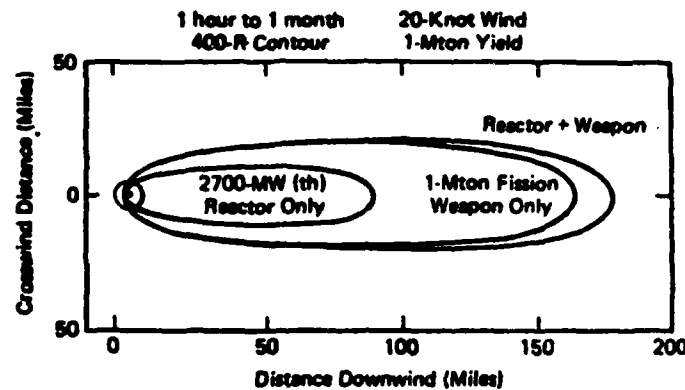
Radiation Effects Depend on Time Dependence of Dose



Radiation From Nuclear Fuel Cycle Facilities

Local Fallout

Early times are dominated by weapons fallout.



The 400-R leadose contours for one hour to one week for fallout from a 1000-MW(e) reactor, 1-Mton fission weapon, and combination.

Figure 1 1,000 MW(e) LMFBR and 1-Mton Fission Weapon Contours. From Chester and Chester (Ref. 15)

Local Fallout
 Longer Times are Dominated By Reactor
 Radioactivity (Dose Rates as much
 lower)

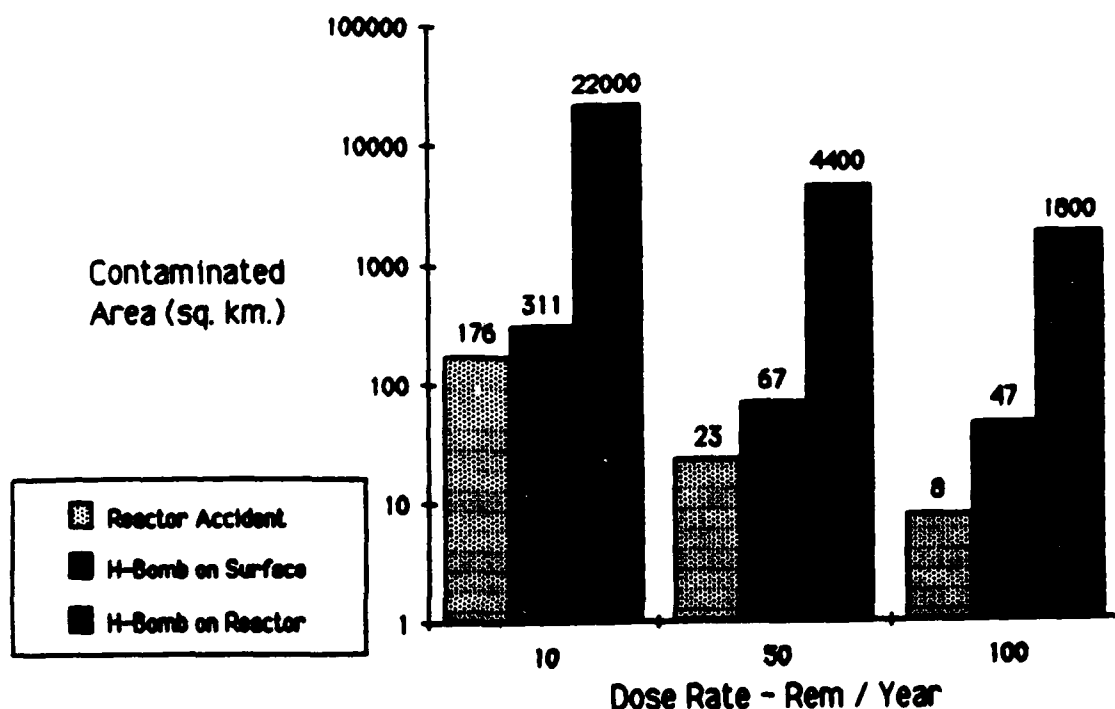


Figure 2 From Fetter and Telpie, (Ref. 14) DENIAL OF LAND to the survivors of a release of radioactivity depends on the dose of radiation the survivors would be willing (or compelled) to absorb. Presumably a dose rate of even a few rem per year would be intolerable after a peacetime accident, whereas the survivors of a nuclear attack might attempt to endure far more. The bars show the amount of land that must remain uninhabited for a year if the maximum acceptable dose rate is 10 rem per year (left), 50 rem per year (middle) or 100 rem per year (right). Again three possible sources of radioactive contamination are considered: a grave reactor accident (light color), the ground-level detonation of a thermonuclear weapon (medium color) and the detonation of a thermonuclear weapon on a reactor (dark color). If more than 10 rem per year is unacceptable, the amount of land that must remain uninhabited for a year after the attack on the reactor is 22,000 square kilometers.

Global Fallout

TABLE 8.11. Uniform 50-year gamma-ray dose in rads as a function of the 9 latitude bands for the weapons and a 100 Gw(c) of nuclear power industry. These values do not take into account any weathering, sheltering or rainfall factors.

Source	Latitude bands								
	90-70N	70-50N	50-30N	30-10N	10N-10S	10-30S	30-50S	50-70S	70-90S
Weapons	4.5	27.3	32.9	6.9	0.8	0.6	0.8	0.5	0.09
LWR	1.8	6.3	9.1	3.0	0.6	0.3	0.3	0.1	0.01
SFS	6.7	23.8	32.7	11.3	2.3	1.0	1.0	0.4	0.03
FRP	4.1	14.6	20.1	7.0	1.4	0.6	0.6	0.2	0.02
TOTAL	17.1	72.0	94.8	28.2	5.1	2.5	2.7	1.2	0.15

Internal Dose Calculations

- Forage-cow-milk,
- Pasture- meat (including steer, lamb, and hog meat),
- Leafy vegetable,
- Grains and other non-leafy crops,
- Fresh and salt water fish, and other edible aquatic animals.

- Surface air concentration of the radionuclide,
- Deposition of Cs-137 on the grass or dry feed,
- Fraction of the nuclide that remains on the forage,
- Residence time of the nuclide on the forage,
- Intake rates of both wet (grass) and dry (hay) feed consumed by the cow,
- Concentration in milk,
- Dose per unit activity ingested,
- Infant's milk consumption rate.

- (a) little or no effect,
- (b) slight to moderate effect,
- (c) moderate to large effect.
- (d) large effect.

Dose Conversion Factors (DCF)

$$DCF = TIC * DT * DF$$

$[Sv/(Bq/m^2)]$

$TIC =$ Time Integrated Concentration
in food per unit deposition

$[(Bq/kgm) / (Bq/m^2-day)]$

$DT =$ dietary intake

$[kg/day]$

$DF =$ dose factor

$[Sv/Bq]$

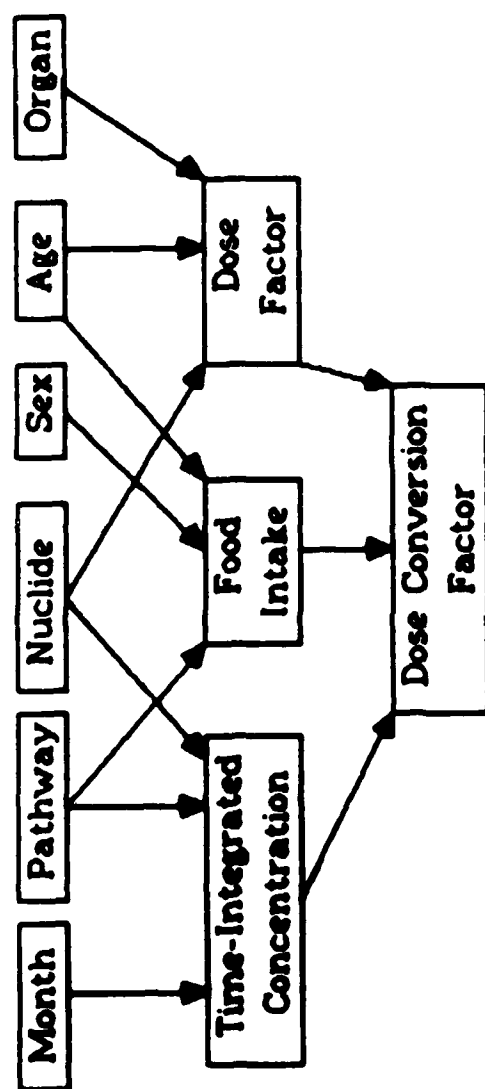


Figure 3. A simple flow chart illustrating the relationship between variables that contribute to a dose conversion factor.

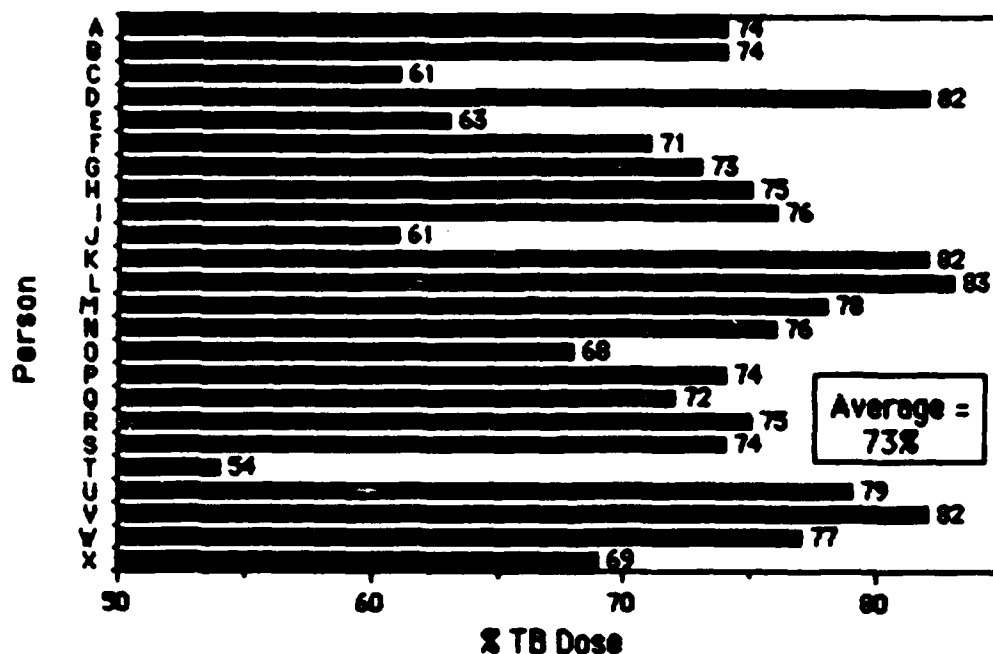


Fig. 1 Reconstructed Total Body doses to offsite residents of NTS during the 1950's.

Most of the dose from Nevada atmospheric Tests were from four radionuclides
 $(Cs^{137}, I^{131}, Sr^{90}, Sr^{89})$.

POSSIBLE FUTURE TRENDS

(1.) Changing Nature of Stockpile and Scenarios

- (a) increased accuracy**
- (b) decreased field per device**
- (c) decreased total yield**
- (d) earth penetrating warheads**
- (e) changing targets**

(2.) S.D.I.

- (a) targeting of warheads in flight and dispersal of fissile fuel**
- (b) targeting of nuclear power plants dedicated to ground based laser stations**

Overview of

Radioactivity

1. Local Fallout from Weapons

~ 7% of protagonist's Land - 450 Rad-48 hr.
Dose (external gammas, 50 years)

UNCERTAINTIES: SCENARIO, MODEL, PARAMETERS
Re

2. Global Fallout (Weapons)

N.H. avg. \rightarrow 10 to 20 Rads ; S.H. $\times \frac{1}{20} \times$
30-50° N Lat. \rightarrow 20-60 "

"Hot spots" \rightarrow 100 "

Size of weapons \rightarrow important

Nuclear winter \rightarrow lower doses N.H. (15%)
higher " S.H. (100% but still small)

UNCERTAINTIES: SCENARIO, MODEL, PARAMETERS

3. Nuclear Fuel Cycle Facilities

Global \rightarrow 200 in 3X, $\left. \begin{matrix} \text{storage} \\ \text{reprocessing} \\ \text{waste} \end{matrix} \right\}$ important

Local \rightarrow In 1st weeks weapons dominates
Longer term - fuel cycle "

4. Internal Dose Contribution ... in progress.

**SYMPTOMATOLOGY OF ACUTE RADIATION EFFECTS IN HUMANS AFTER
EXPOSURE TO DOSES OF 50 TO 3000 RADS (cGy)**

**George H. Anno
Pacific-Sierra Research Corporation
Los Angeles, California**

**Siegmund J. Baum
Bethesda Physiological Studies
Bethesda, Maryland**

**Robert W. Young
Defense Nuclear Agency
Washington, D.C.**

**H. Rodney Withers
UCLA Center for Health Sciences
Department of Radiation Oncology
Los Angeles, California**

**Paper Presented At
GLOBAL EFFECTS PROGRAM TECHNICAL MEETING
Santa Barbara, California**

7-9 April 1987

INTRODUCTION

[Slide 1] Because of continuing interest in acute radiobiological effects of ionizing radiation, we reviewed the available literature to develop a symptomatology basis for assessing early functional impairment of individuals who may be involved in civil defense, medical care, and various military activities in the event of nuclear attack.

This paper will summarize our information sources and describe how we distilled from them descriptions of human signs and symptoms* for prompt ionizing dose in the range 50 to 3000 rads (cGy) midline body tissue.

Before I get started, let me first mention that the authors would like to acknowledge the Radiation Policy Directorate of the Defense Nuclear Agency, in particular Drs. David Auton and Robert Young, for supporting our effort.

This review was undertaken as a group effort where varying individual interpretation of frequently imprecise or

*"Symptoms" is used to mean both subjective evidence and objective signs of radiation sickness.

lacking information was resolved by arriving at a consensus in constructing our representations of acute radiation sequelae. Rather than restating the well known variability in acute human response to radiation, specifically, our objective was to analyze the available data and correlate radiation sickness symptoms with dose levels and time in order to develop a consensus about typical symptomatology for incidence, onset time, severity, and duration.

**SYMPTOMATOLOGY OF ACUTE RADIATION EFFECTS
IN HUMANS AFTER DOSE OF 50 TO 3000 RAD (cGy)**

GEORGE H. ANNO

**PACIFIC-SIERRA EATON RESEARCH
LOS ANGELES, CALIFORNIA**

SIEGMUND J. BAUM

**BETHESDA PHYSIOLOGICAL STUDIES
BETHESDA, MARYLAND**

ROBERT W. YOUNG

**DEFENSE NUCLEAR AGENCY
WASHINGTON, D.C.**

H. RODNEY WITHERS

**UCLA DEPT. OF RADIATION ONCOLOGY
CENTER FOR HEALTH SCIENCES
LOS ANGELES, CALIFORNIA**

SOURCES OF INFORMATION

[Slide 2] Data on human radiation sickness signs and symptoms (for convenience we simply refer to symptoms) are both diverse and sparse. Our information, representing a review of well over 100 references, fall into four general categories: (1) case studies of nuclear accident victims, (2) records of total-body radiation therapy patients, (3) "composite" analyses based on data from a variety of sources, and (4) expert opinion, sometimes elicited in private communication. Additional information comes from survivors of the atomic bombings in Japan and those accidentally irradiated in nuclear tests in the South Pacific.

No one source category provides a comprehensive picture of the incidence, severity, and duration of radiation sickness in humans. For example, the data on atomic bomb survivors are usable for delayed hematological effects (1 week postexposure) but are more uncertain for early acute effects; records of symptoms during the first few postexposure days were constructed some time after the fact. To refine a plausible description of acute symptoms, we evaluated the data from a variety of sources. The handouts contain a list of our references.

With the next few slides, I will point out what aspects we focused on to construct our typical sequelae representations.

HUMAN DATA/100+ REFERENCES

- **Accident victims**
- **Therapy patients**
- **Composite sources**
- **Expert opinion**
- **(Atomic bomb survivors)**

ANALYTICAL CONSIDERATIONS

[Slide 3] The period of acute illness is conventionally divided into the prodromal or initial phase (1 to 3 days after exposure) and manifest illness phase (1 to 6 weeks after exposure); these times, of course, depend upon dose level.

The main prodromal symptoms relevant to functional impairment are nausea, vomiting, anorexia, diarrhea, fluid loss, and electrolyte imbalance. Concomitant effects, either a direct result of radiation or secondary to fluid loss, are headaches, fainting, and prostration. Other early effects with a different pathophysiological base are fatigue (more specifically fatigability) and weakness.

The manifest-illness phase is dominated by bleeding, fever, infection, and ulceration due to injury of the hemopoietic system. Higher doses can produce hypotension, dizziness, and disorientation. Fluid loss, electrolyte imbalance, and delayed diarrhea recur after relatively high doses because of damage to the intestines.

Symptoms were also grouped according to physiological relationship designated by the double capital letters in

parentheses, i.e., upper gastrointestinal distress (UG), lower gastrointestinal distress (LG), fatigability and weakness (FW), etc.

[Slide 4] To express symptom severity, we use the terms "mild," "moderate," and "severe"--common clinical distinctions--but we are unable to quantify the terms for most of the symptoms. For example, by what measure could one distinguish moderate from severe nausea or headaches? Some quantitative links are possible but we mainly rely on qualitative understanding of the distinctions.

Mild vomiting or diarrhea may mean a single to a few episodes; moderate, several episodes; and severe, many and profuse episodes. Fatigue and weakness are potentially quantifiable since exertion, necessary to reveal those symptoms, is measurable; however, few data have been collected. With regard to hypotension, "mild" may refer to a 10 percent drop in blood pressure; and "severe," a drop of 30 percent or more. We quantify hemopoietic injury by drops in lymphocyte, granulocyte, and platelet counts. Net continued fluid losses of up to 2 liters are considered mild to moderate; more than 2 liters can be severe.

ACUTE RADIATION SYMPTOMS

- Nausea } Upper Gastrointestinal Distress (UG)
Vomiting }
- Diarrhea – Lower Gastrointestinal Distress (LG)
- Fatigability } (FW)
Weakness }
- Hypotension } (HY)
Dizziness }
Disorientation }
- Infection } (IB)
Bleeding }
Fever }
Ulceration }
- Fluid loss } (FL)
Electrolyte imbalance }
Headache }
Fainting }
Prostration }

Also, our correlations of severity level with time are gross representations; even though severity may vary considerably over time, we did not attempt to develop detailed time-intensity profiles because of the lack of appropriate quantitative data.

[Slide 5] For symptom incidence we largely utilized results from probit analysis of data from the accounts of accident victims and over 2000 therapy patients. However, the probit data are not specifically correlated with postexposure time, but we were able to infer the time dependence of symptom incidence from various portions of the body of literature reviewed.

Results of probit analysis relating symptom incidence to radiation dose are shown on lognormal probability paper; the straight-line curves assume a lognormal distribution and the concave curves, a normal distribution. The lognormal form generally fits the data better. Exceptions are the incidence of diarrhea at doses above 250 rads and the incidence of fatigue at doses above 300 rads, for which we use the normal curve estimates.

SYMPTOM SEVERITY QUALITATIVE REPRESENTATION

- **Mild**
- **Mild to moderate**
- **Moderate**
- **Moderate to severe**
- **Severe**

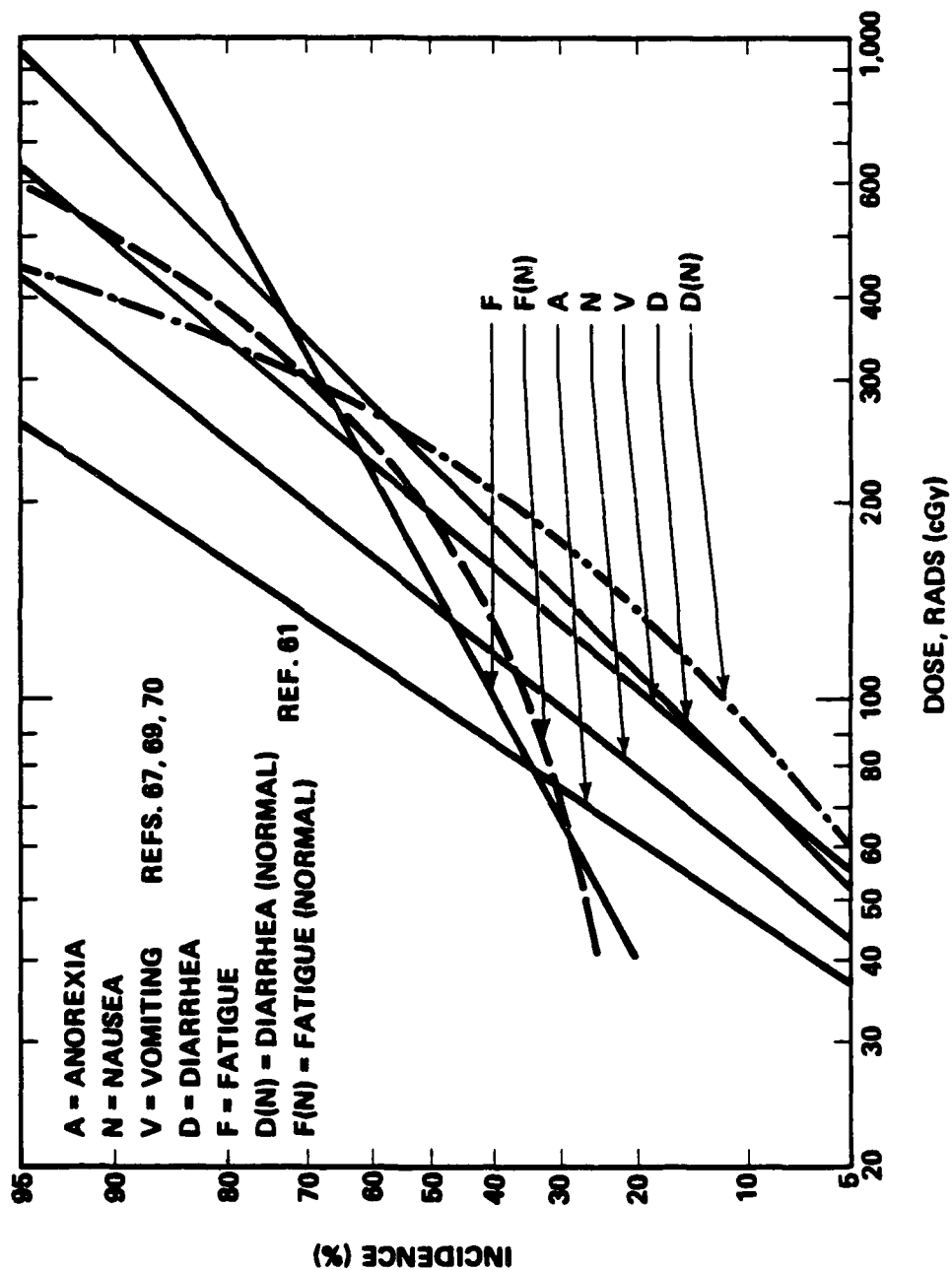
The probit curves for diarrhea reflect data gathered over a six-week period following exposure. Since the data are not time-resolved, the curves include later as well as early occurrences. However, clinical experience indicates that delayed diarrhea occurs a few days to a week after exposure. Early diarrhea most likely doesn't occur unless the dose is at least 300 rads where about 10 percent would experience one or two episodes 3 to 6 hours after exposure; at 2000 to 3000 rads, 30 percent could have early diarrhea.

[Slide 6] Because of the sparseness and quality of human data, quantification of incidence of death due to radiation is uncertain. The three curves shown here illustrate the uncertainty: the LD_{50} ranges from 256 to 325 rads. We use the right-hand curve estimated for healthy adult humans based on an LD_{50} of 450 rads (cGy) air dose; the slope is from experiments with large animals, since lethality dose curves tend to be parallel for dogs, swine, sheep, goats, etc.

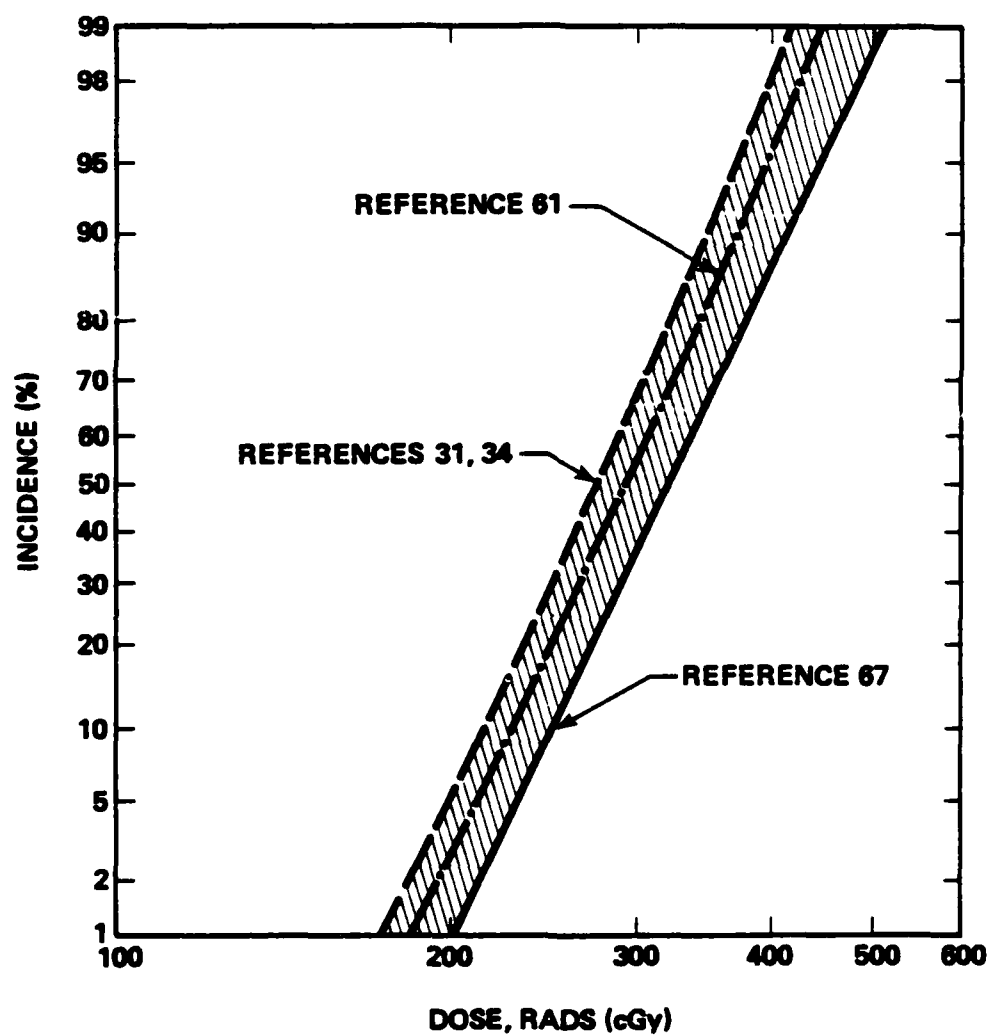
[Slide 7] For mean time of death, we use the ranges given by the heavily outlined boxes to indicate the period over which fatalities are likely to occur for a given dose

SYMPTOM INCIDENCE RELATED TO DOSE

(PROBIT ANALYSIS—ACCIDENT VICTIMS AND THERAPY PATIENTS)



LETHALITY RELATED TO DOSE

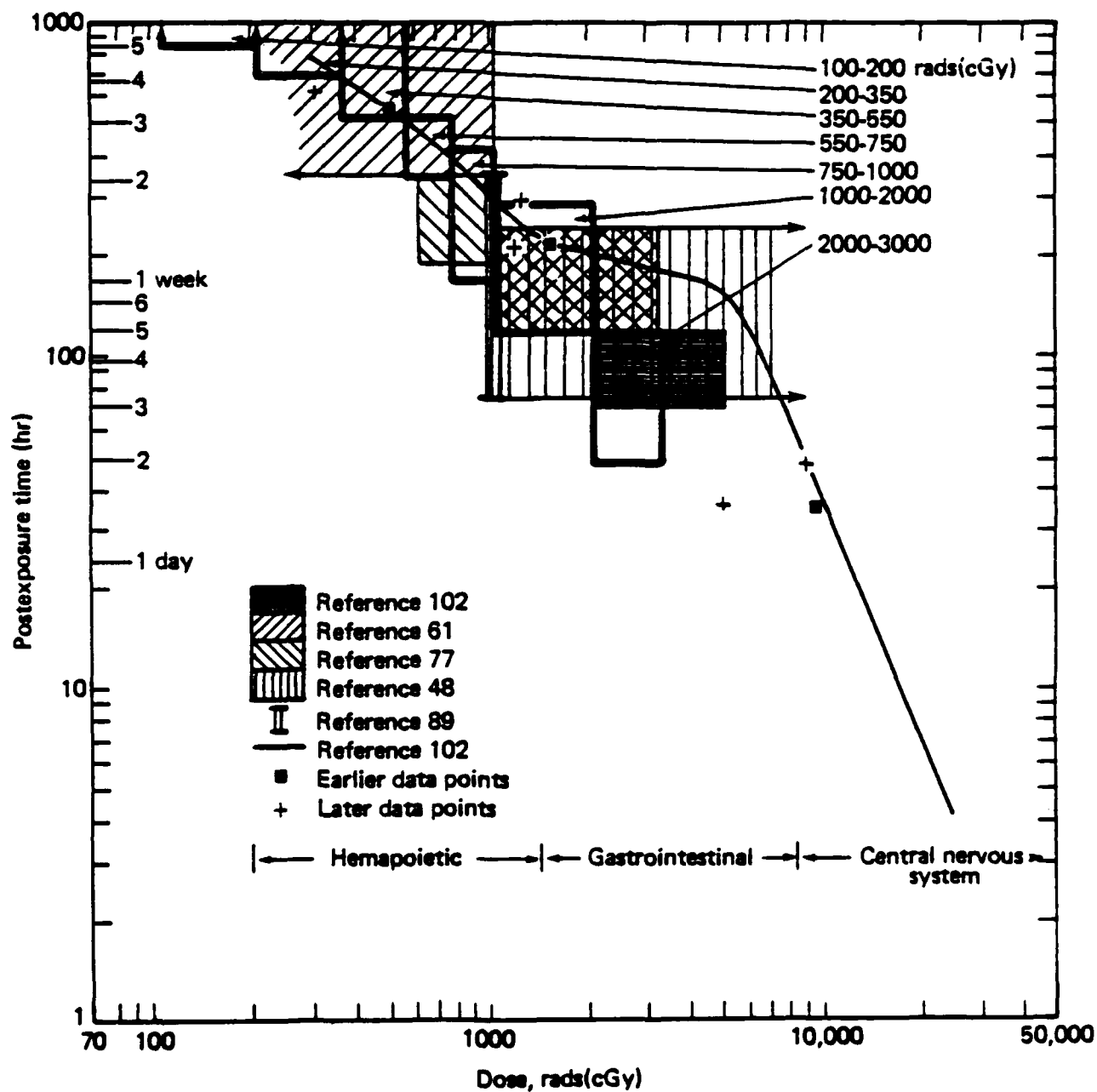


level. Data are insufficient to specify a time distribution of mortality. These ranges are consistent with a consensus of fairly recent opinion and some more recent data points for human fatalities. For comparison a curve previously drawn through three earlier human data points is shown; the curve's shape is inferred from animal data. Relative to the curve, a trend toward earlier death with doses above around 1300 rads is suggested.

[Slide 8] Estimates of the onset of prodromal symptoms are based on the data points logarithmically plotted here against dose indicated by symbols representing the four categories. Accident, therapy, and expert opinion symbols indicate firm information; lines connecting the composite symbols indicate fairly wide ranges of uncertainty; arrows indicate open-ended values and thus reflect an even larger measure of uncertainty.

Because the data vary greatly in density and precision, numerical curve fitting techniques (such as regression analysis) were not applied. Instead, we drew a curve through the data points to represent "typical" individuals favoring accident and therapy data over the other two categories, which shows onset time inversely proportional to dose.

TIME OF DEATH RELATED TO DOSE



(The exact trend at the high end of the dose range is uncertain because of the lack of empirical data. However, the curve is supported by the accident data point at 8800 rads, and expert opinion suggesting that persons exposed to several thousand rads will probably show the entire range of prodromal symptoms within 5 to 15 minutes.)

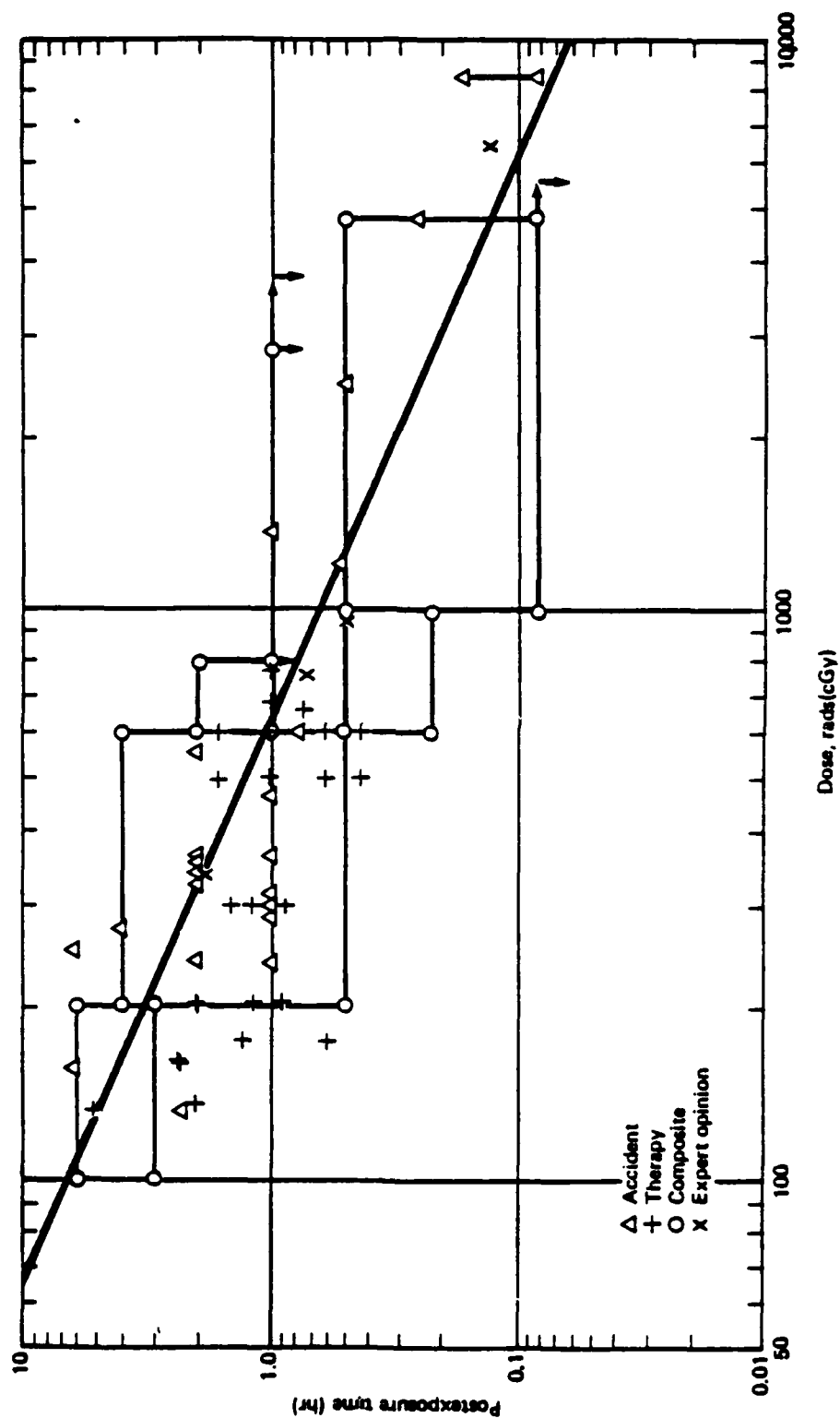
Prodromal symptom duration, manifest illness phase onset and duration were related to dose plotting appropriate data in a similar manner. I should like to point out that our estimates of duration account for symptom occurrence in three ways: continuously at one level of severity (e.g., anorexia); continuously with varying severity (e.g., fatigue); and intermittently (e.g., vomiting and diarrhea).

Let me briefly comment on the variety of dose rate contained in the data. Accident victims were exposed to from hundreds to thousands of rads in a fraction of a second as compared to therapy patients undergoing total-body irradiation exposed to from a few to 30 rads/min given over periods of minutes to hours.

Given the great differences in dose rate between accident victims and therapy patients, we might expect their prodromal symptoms to begin at different times. However,

correlation of onset time with dose level shows no marked difference between the two groups suggesting that onset depends more on total dose rather than dose rate in the therapy range. We, therefore, believe data from therapy patients are applicable for deriving typical acute response patterns for symptoms such as nausea, vomiting, and fatigability.

ONSET OF PRODROMAL SYMPTOMS RELATED TO DOSE



SYMPTOMATOLOGY DESCRIPTIONS

[Slide 9] We subdivided the dose range of 50 to 3000 rads into eight subranges reflecting important pathophysical events. Doses in the lowest range, 50 to 100 rads, cause minor acute damage to the hemopoietic system and mild prodromal effects (nausea, vomiting, anorexia) in a small number of irradiated persons.

In the dose range 100 to 200 rads, prodromal effects and injury to the hemopoietic system (primarily the bone marrow stem and precursor cells) increase significantly. However, victims will probably survive, except for the 2 to 5 percent who will die after doses of about 200 rads. The probability of death increases if victims are already weakened by other conditions, such as infection.

Although survival is possible from 200 to 350 rads, prodromal effects become pronounced. Victims also suffer moderate to severe bone marrow damage. As the dose reaches about 325 rads, 50 percent who do not receive appropriate medical care may die within 60 days.

From 350 to 550 rads, symptoms are more severe affecting nearly all exposed. If untreated, 50 to 99 percent may

die, primarily because of extensive injury to the hemopoietic system, manifested by overwhelming infections and bleeding.

Between 550 and 750 rads, responses begin to reflect the combined effects of gastrointestinal and hemopoietic damage. Survival is almost impossible short of a compatible bone marrow transplant and extensive medical care. Nearly everyone irradiated at this level suffers severe prodromal effects during the first day after exposure.

Between 750 and 1000 rads, injuries are much more severe due to greater depletion of bone marrow stem cells, increased gastrointestinal damage, and systemic complications from bacterial endotoxins entering the blood stream.

At 1000 to 2000 rads, death results in less than two weeks from septicemia due to severe gastrointestinal injury, complicated by complete bone marrow damage and the cessation of granulocyte production. Above about 1300 rads, death may occur sooner from electrolyte imbalance and dehydration due to vomiting and diarrhea, especially in hot or humid conditions. Extremely severe gastrointestinal and cardiovascular damage causes death within 2 to 5 days after doses of 2000 to 3000 rads.

DOSE RANGES AND ASSOCIATED PATHOPHYSIOLOGICAL EVENTS

Dose Range rads(cGy)	Pathophysiological Events		
	Prodromal Effects	Manifest-Illness Effects	Survival
50-100	Mild	Slight decrease in blood cell count	Virtually certain
100-200	Mild to moderate	Beginning symptoms of bone marrow damage	Probable (> 90 percent)
200-350	Moderate	Moderate to severe bone marrow damage	Possible-- Bottom third of range: LD _{5/60} Middle third: LD _{10/60} Top third: LD _{50/60}
350-550	Severe	Severe bone marrow damage	Death within 3½-6 weeks-- Bottom half: LD _{90/60} Top half: LD _{99/60}
550-750	Severe	Bone marrow pancytopenia and moderate intestinal damage	Death within 2-3 weeks
750-1000	Severe	Combined gastrointestinal and bone marrow damage; hypotension	Death within 1-2½ weeks
1000-2000	Severe gastrointestinal damage Upper half of range; early transient incapacitation; gastrointestinal death		Death within 5-12 days
2000-3000	Gastrointestinal and cardiovascular damage		Death within 2-5 days

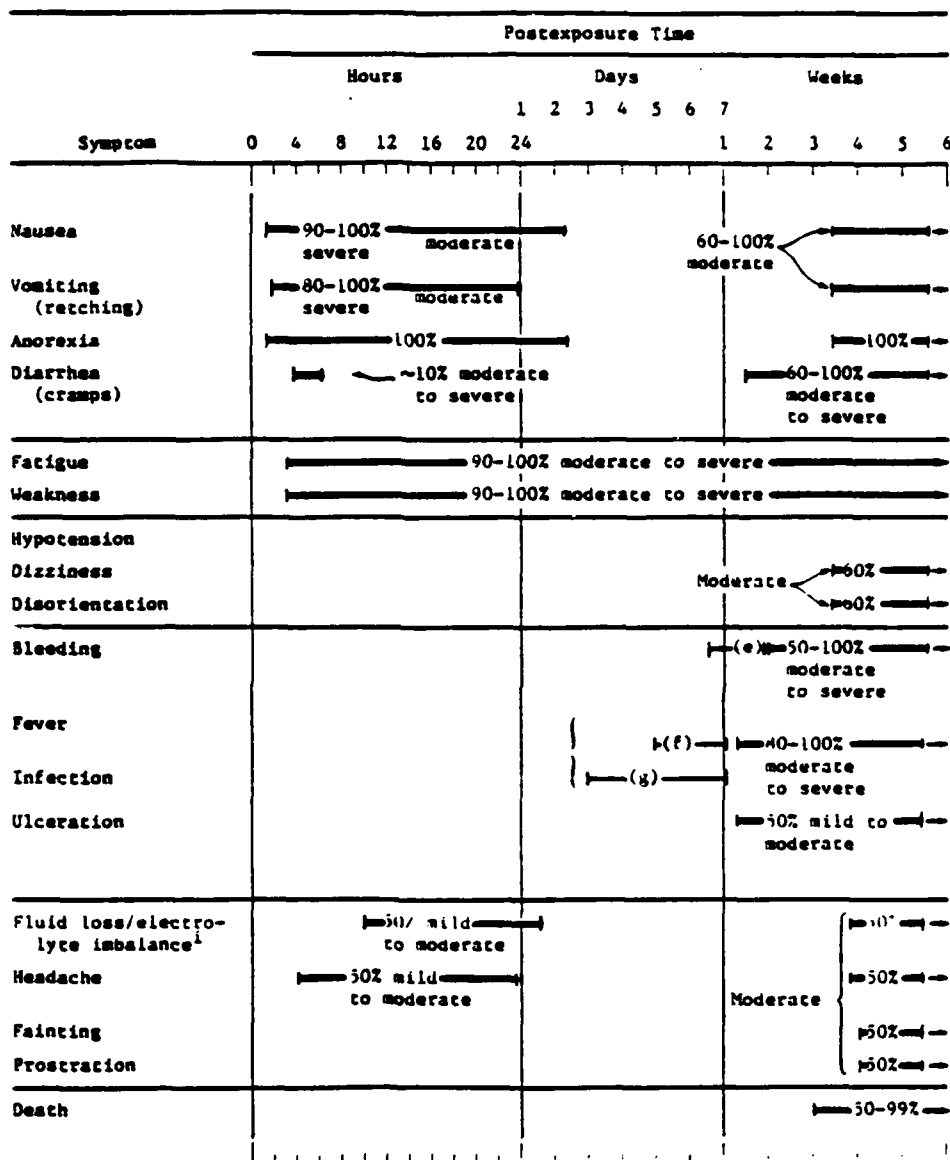
[Slide 10] Here is an example of the symptom charts we developed for the 350 to 500 rads dose range. Symptom charts for all eight dose ranges are included in the handouts.

The charts portray symptom onset severity, duration, and incidence. Symptom incidence is expressed as percentage affected. Both symptom incidence and severity are expressed broadly with time because of the lack of specific time-resolved data.

(Essentially, this chart shows nearly all persons exposed experience moderate to severe symptoms the first day postexposure, moderating within a day or so. Fluid loss without replacement from severe or prolonged vomiting can affect electrolyte balance. With the exception of fatigability and weakness, there is a period of symptom remission from about 2 days to a week following exposure.)

[Slide 11] Next, I will present some summary slides which illustrate the overall picture we formed for acute radiation sickness symptomatology; these illustrations are in the handouts so I won't spend much time discussing them.

SYMPTOMS FOR DOSE RANGE 350 TO 550 RADS (cGy)



^aSevere drop in platelets: from $3 \times 10^3/\text{mm}^3$ to $0.1 \times 10^3-0/\text{mm}^3$.

^bSevere drop in granulocytes: from $6 \times 10^3/\text{mm}^3$ to $0.5 \times 10^3-0/\text{mm}^3$.

^cSevere drop in lymphocytes: from $3 \times 10^3/\text{mm}^3$ to $0.4-0.1 \times 10^3/\text{mm}^3$.

This is a summary chart of the six symptom groups for all eight dose ranges for times up to six weeks following exposure. Each of the six groups include symptoms indicated in Slide 3; symptom incidence is also indicated along with severity, denoted by shading.

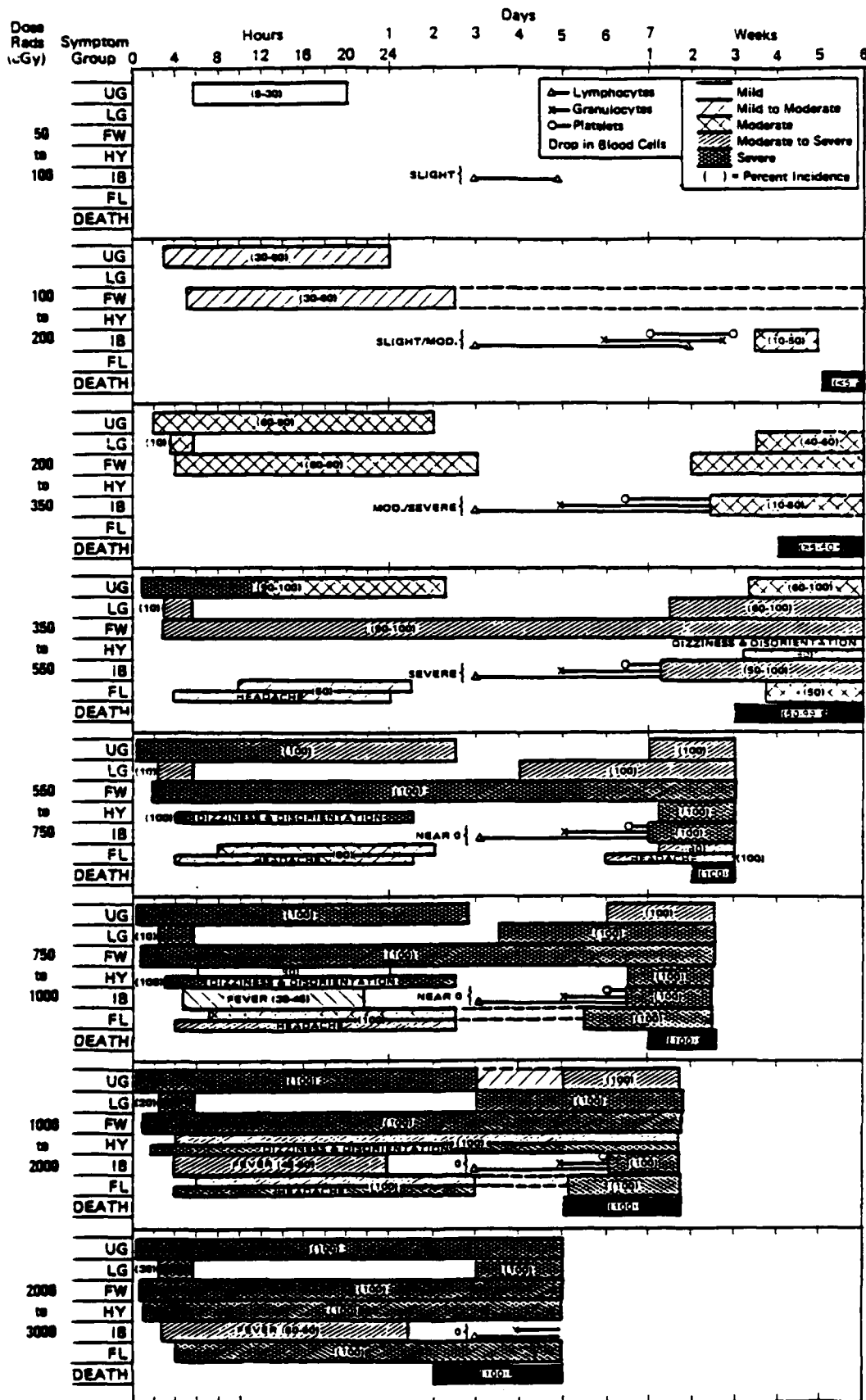
[Slide 12] This chart shows the combined symptom course of acute radiation sickness for the eight dose ranges. Notice that beginning with the 350 to 550 rads dose range, fatigability and weakness (FW) continues with no remission period.

[Slide 13] Here are some surface plots which illustrate symptom severity related to dose level and postexposure time. Because dose and time are expressed logarithmically (to include the full range of dose and time) visual distortion is introduced where the slope of the surface for small doses and/or early times appears much more pronounced than that of large doses and/or times.

[Slide 14] These are additional surface plots of symptom severity plus a composite representation of all the

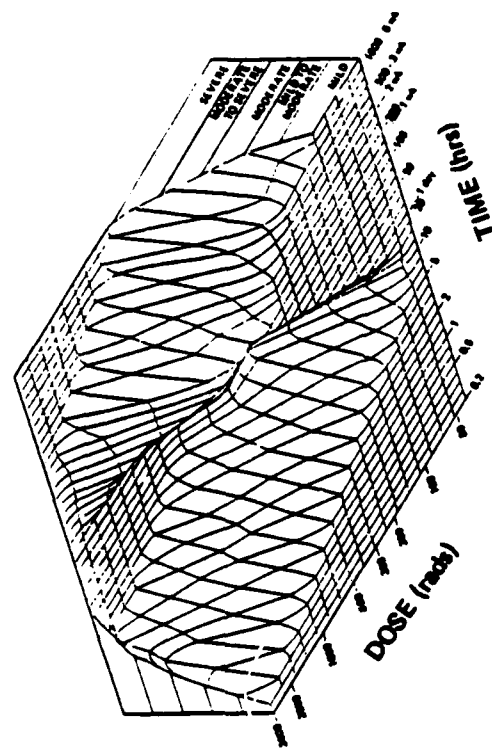
ACUTE RADIATION SYMPTOMS

Postexposure Time

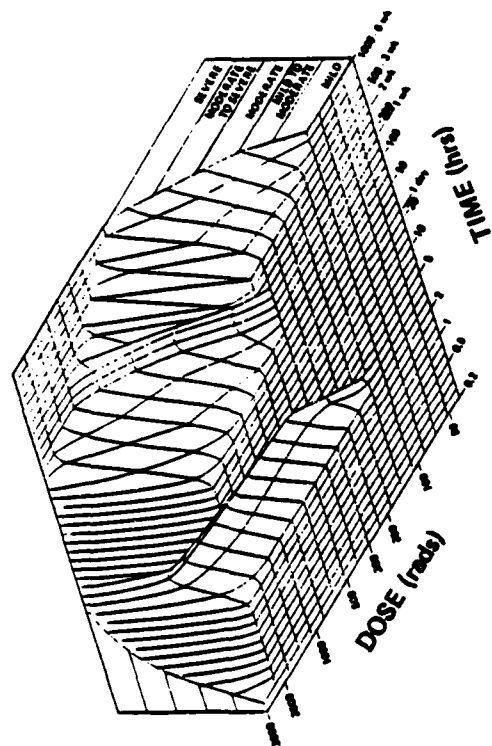


ACUTE RADIATION SICKNESS DOSE-TIME SYMPTOM SEVERITY

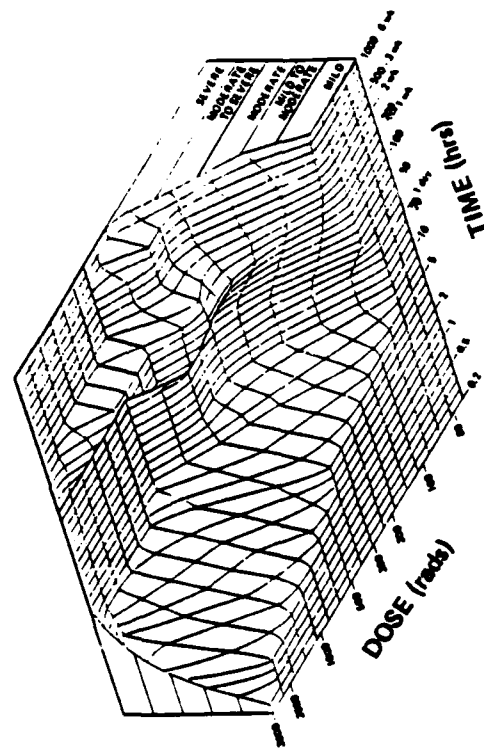
UPPER GASTROINTESTINAL DISTRESS



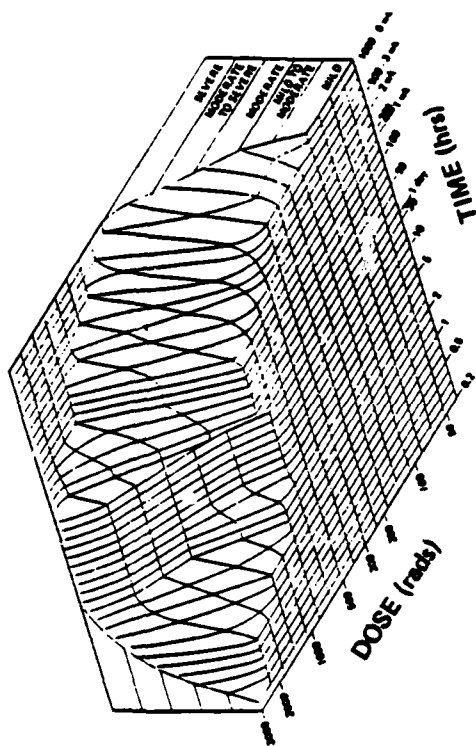
LOWER GASTROINTESTINAL DISTRESS



FATIGABILITY AND WEAKNESS



HYPOTENSION

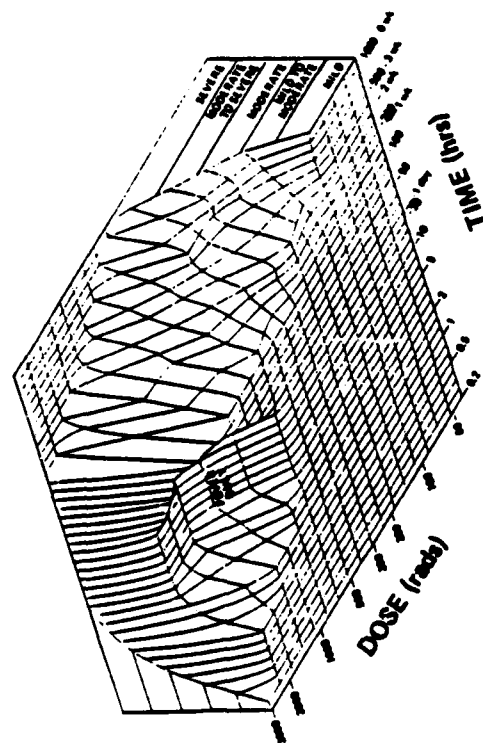


symptom groups referred to as "Acute Radiation Sickness."

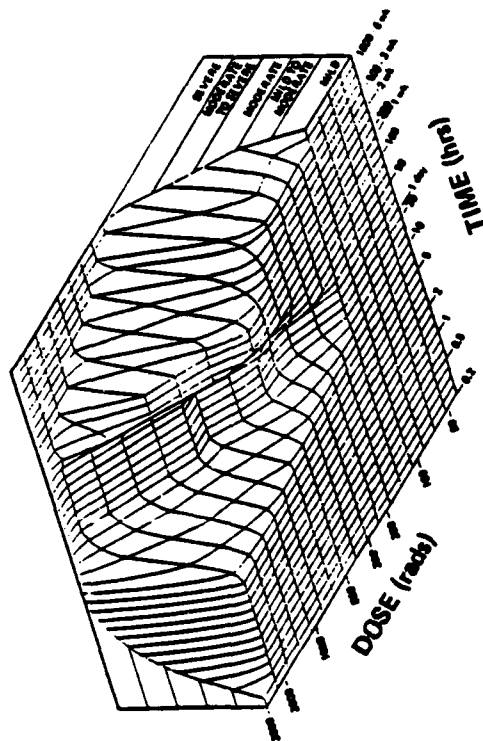
In conclusion, we point out that general application of these descriptions carries some reservations because of differences in population characteristics, environmental conditions, and medical attention. Accident victims and therapy patients had the benefit of medical care, which may not be available. On the other hand, factors such as youth, vigor, and motivation may to some extent counter the effects of radiation injury on functional capability. The data do not permit a quantitative assessment of the tradeoffs between postexposure medical care and preexposure robustness. Although both are important, we believe that preexposure health condition may be relatively less important in resisting the debilitating effects of radiation than postexposure medical care, barring prior infection (bacterial or viral) or serious disease. The medical care (environmental control, broad spectrum antibiotics, antifungal, antiviral, fresh platelets, total parenteral feeding, electrolyte replacement) given to the Chernobyl accident victims seems to bear this out based on larger LD₅₀ estimates (400 to 600 rads) made by some. However, complications from secondary injury (thermal and beta radiation skin burns) as well as dose protraction (few to several hours) compounds such an assessment.

ACUTE RADIATION SICKNESS DOSE-TIME SYMPTOM SEVERITY

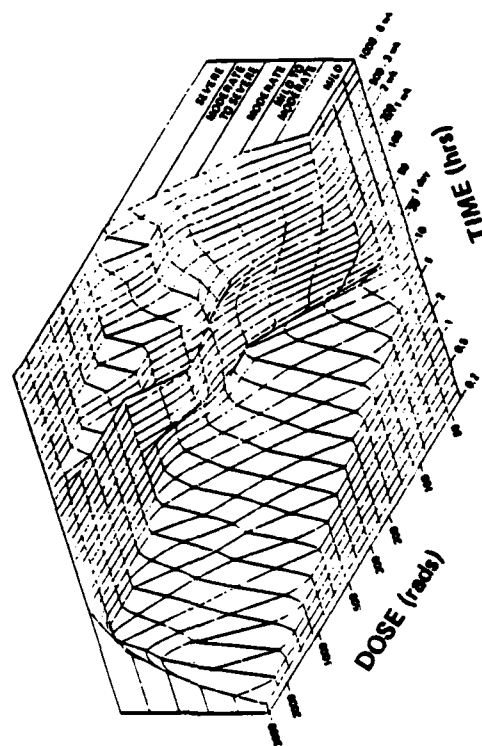
INFECTION AND BLEEDING



FLUID LOSS AND ELECTROLYTE IMBALANCE



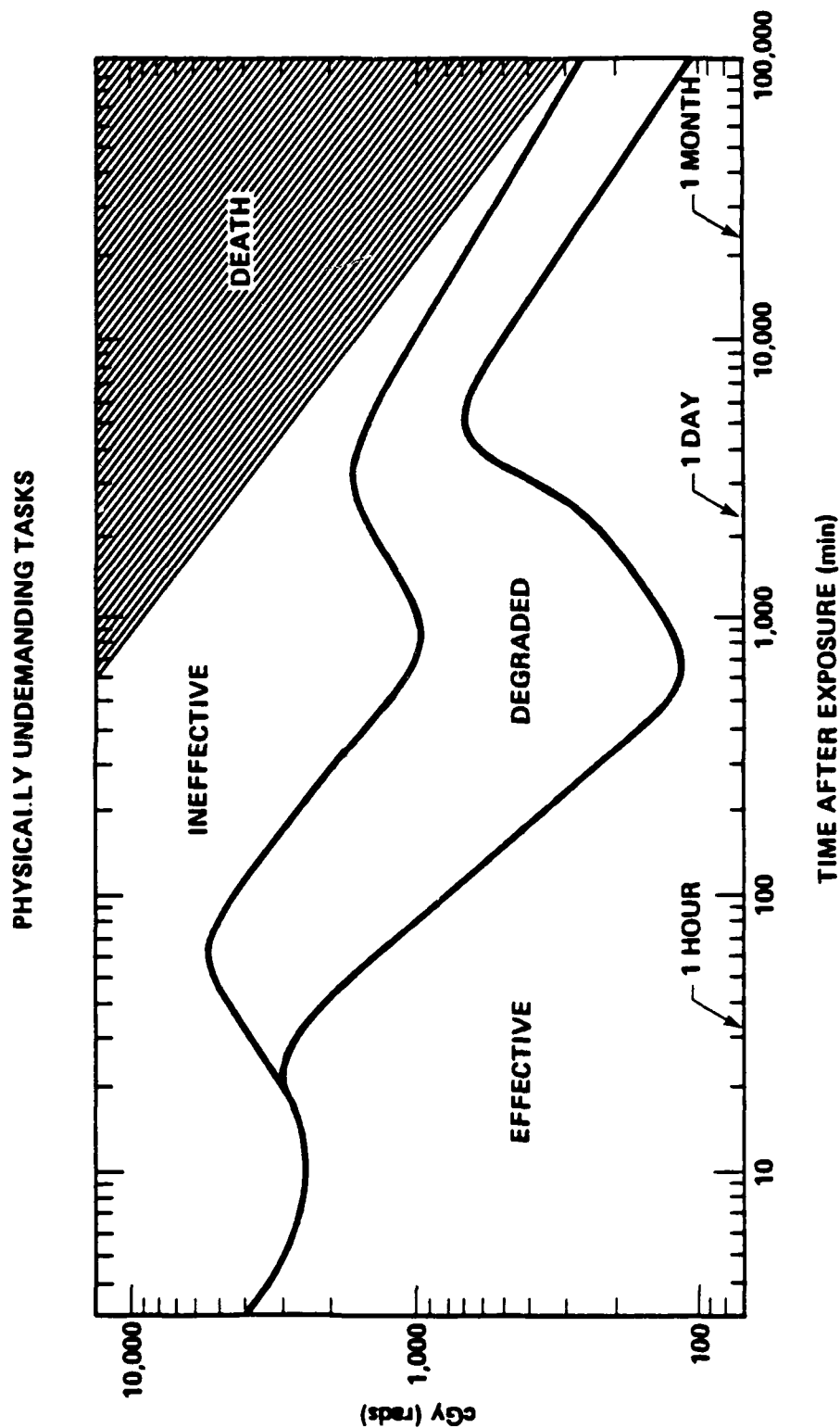
ACUTE RADIATION SICKNESS



[Slide 15] Our study of acute radiation sickness provides the basis for estimating the expected functional capability of individuals after a brief exposure to ionizing radiation. Here we can get an idea of the gross functional impairment of individuals who may be involved in emergency civil defense activities. Physically undemanding tasks are those that require cognitive capability such as communication, navigation and plotting, counting, fine motor coordination, etc. "Effective" may correspond to from normal to 75% capability; "degraded", from 25 to 75% capability; and "ineffective", less than 25% capability. The low portion of the curves from 10-15 hrs postexposure corresponds to the maximum expression of initial symptoms of acute radiation sickness. The high portion of the curves from 2 to 4 days represents a transient period of remission of symptoms followed by a second onset due to the latent expression of symptoms caused by radiation damage to the blood-forming organs.

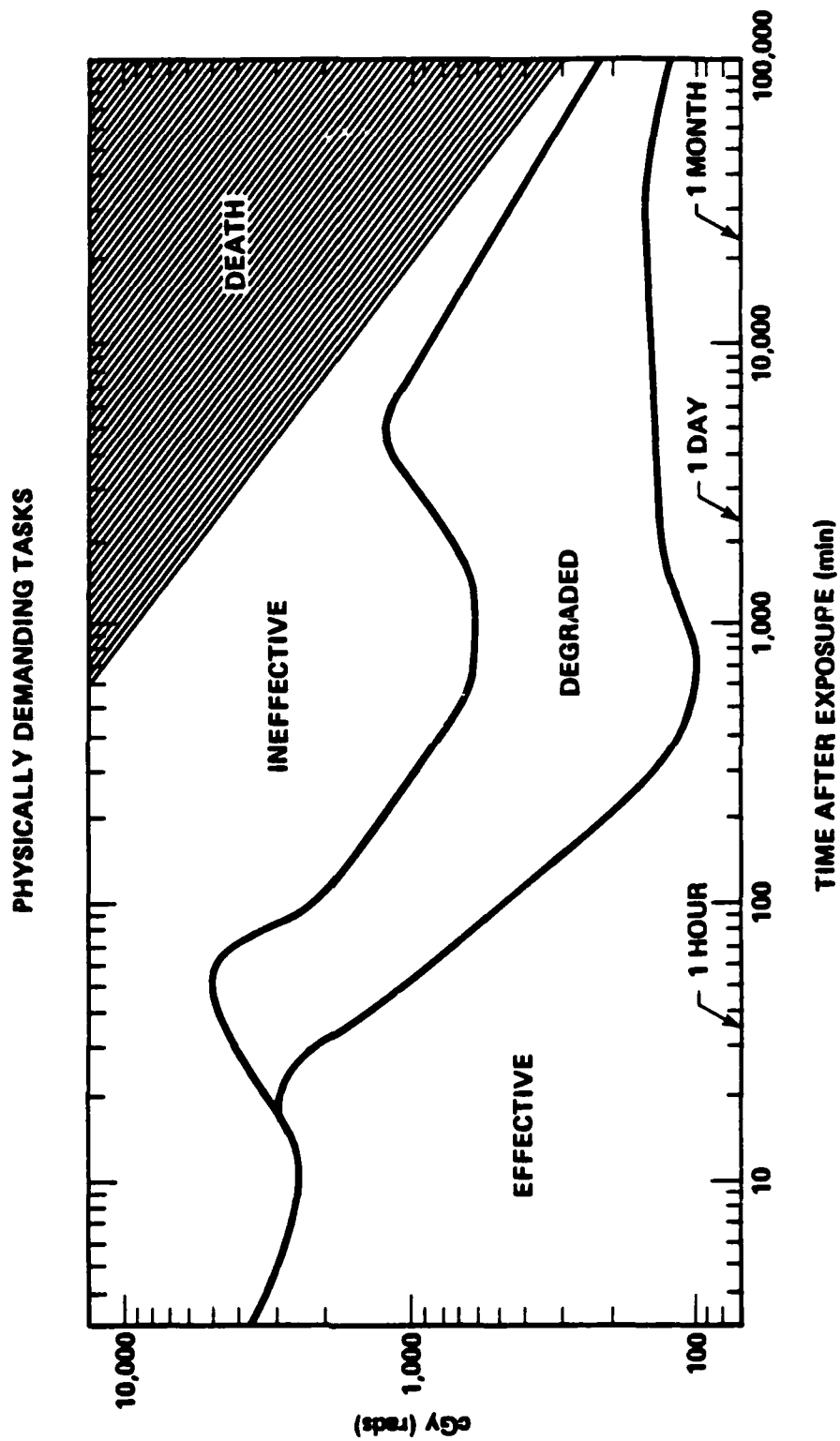
[Slide 16] Physically demanding tasks, for example, lifting and moving heavy objects, climbing flights of stairs, running or walking appreciable distances, etc., are more adversely affected by radiation than undemanding ones. For example, functional capability for performing physically

EXPECTED HUMAN FUNCTIONAL CAPABILITY



demanding tasks would continue to be affected after several hours postexposure for doses as low as 150 rads (cGy).

EXPECTED HUMAN FUNCTIONAL CAPABILITY



ACUTE RADIATION SYMPTOM CHARTS
50 TO 3000 RADS (cGy) MIDLINE BODY TISSUE

DISCUSSION

Doses of 50 to 100 Rads (cGy)

Acute radiation effects at this level are mild and occur only during the first day after exposure. Blood cell counts may drop slightly, but typical victims will surely survive.

Doses of 100 to 200 Rads (cGy)

Between 20 and 70 percent of exposed persons develop nausea and vomiting. About 30 to 60 percent complain of fatigue and weakness. Significant destruction of bone marrow stem cells may lead to a 25 to 35 percent drop in blood cell production. As a result, mild bleeding, fever, and infection may occur during the fourth and fifth postexposure weeks. Up to 5 percent may die 5 to 6 weeks after exposure to 200 rads (cGy).

Doses of 200 to 350 Rads (cGy)

Commencing in this dose range, about 10 percent may experience one or two episodes of moderate diarrhea 4 to 6 hours postexposure. Most victims tire easily and experience mild to moderate weakness intermittently over the 6 weeks. Under normal conditions, vomiting and diarrhea are not

enough to cause serious fluid loss and electrolyte imbalance. In hot or humid conditions, however, combined fluid loss and electrolyte imbalance could become serious.

Injury to the hemopoietic system is indicated by moderate bleeding, fever, infection, and ulceration 3 to 5 weeks postexposure; more than 50 percent of those exposed are affected. During the fourth and fifth weeks, moderate diarrhea may complicate their condition. Five to 50 percent of nontreated persons may die during the fifth week; death comes earlier to those with preexisting infections, for example, of the upper respiratory tract.

Doses of 350 to 550 Rads (cGy)

In this next higher dose range, symptoms are more severe affecting nearly all exposed persons. Severe and prolonged vomiting can take a toll on electrolyte balance which may be accelerated by perspiration through heat, humidity, or activity.

Nearly all show moderate to severe fatigue and weakness for many weeks. If untreated, 50 to 99 percent may die, primarily because of extensive injury to the hemopoietic system, manifested in overwhelming infections and bleeding during the third to sixth weeks. Nausea, vomiting, and anorexia may recur at that time. Diarrhea, electrolyte imbalance, and headaches affect at least half. The condition

of the lethally irradiated during their last days may be complicated by dizziness, disorientation, fainting, prostration, and symptoms of infection and bleeding.

Doses of 550 to 750 Rads (cGy)

Virtually all exposed persons experience severe nausea and vomiting the first postexposure day, moderating over the next day or two. During that time they also experience dizziness and disorientation.

With the near-maximum destruction of bone marrow stem cells and absence of granulocytes, untreated persons lose their defense against infection. By the end of the first postexposure week, infection is rampant from endogenous bacteria that have escaped from the injured gastrointestinal tract.

The combination of hemopoietic damage and gastrointestinal lesions reduces the survival of all untreated persons to 2 to 3 weeks. During the entire time they suffer from severe fatigue and weakness. Toward the end of the first week, nausea, vomiting, and anorexia recur. Moderate to severe diarrhea may begin as early as the fourth day. Severe bleeding, headaches, hypotension, dehydration, electrolyte imbalance, and fainting complicate the condition of all prior to death.

Doses of 750 to 1000 Rads (cGy)

The survival time for untreated persons diminishes to 2 to 2 1/2 weeks. Symptoms resemble those experienced at the preceding dose range, with the following notable differences:

- o Severe nausea and vomiting may continue into the third day before moderating.
- o During the first day, hypotension affects about 80 percent; moderate fever, 30 to 45 percent.
- o Electrolyte imbalance is a persistent problem from the sixth hour on.
- o All have moderate to severe headaches during the first day.
- o Nearly three-quarters are prostrate before the end of the first week.

Much of our description of symptoms at this dose range derives from postexposure observations of patients treated with total-body irradiation for leukemia. There are undeniable difficulties in extrapolating from sick people under close medical attention to otherwise healthy individuals. Nevertheless, therapy patients constitute the only substantial number of irradiated persons whose reactions have been

thoroughly documented, so their experience is relevant to this inquiry.

Doses of 1000 to 2000 Rads (cGy)

Severe nausea and vomiting affect all within 30 minutes of exposure and continue intermittently, along with anorexia, until death the second week. Severe headaches begin after about 4 hours and continue for 2 to 3 days. Symptom severity may diminish somewhat during days 3 to 5. Gastrointestinal injury predominates, manifested 4 to 6 days after exposure by the abrupt return of severe nausea, vomiting, anorexia, and diarrhea, along with high fever, abdominal distension, and undetectable peristalsis (ileus). During the second week, severe dehydration, hemoconcentration, and circulatory collapse, compounded by septicemia, lead to coma and death.

Doses of 2000 to 3000 Rads (cGy)

Symptoms are more severe versions of those described for the preceding dose range. Gastrointestinal injury predominates, complicated by cardiovascular lesions. Prodromal effects, including severe headache and drowsiness, appear almost immediately after exposure and may persist as the gastrointestinal syndrome develops. Severe dehydration and electrolyte imbalance are manifested several hours after

exposure: but in time the greater loss is from severe diarrhea. The increased permeability of capillaries in the intestines and elsewhere in the body releases fluids into the interstitial spaces.

Symptoms for dose range 50 to 100 rads (cGy)

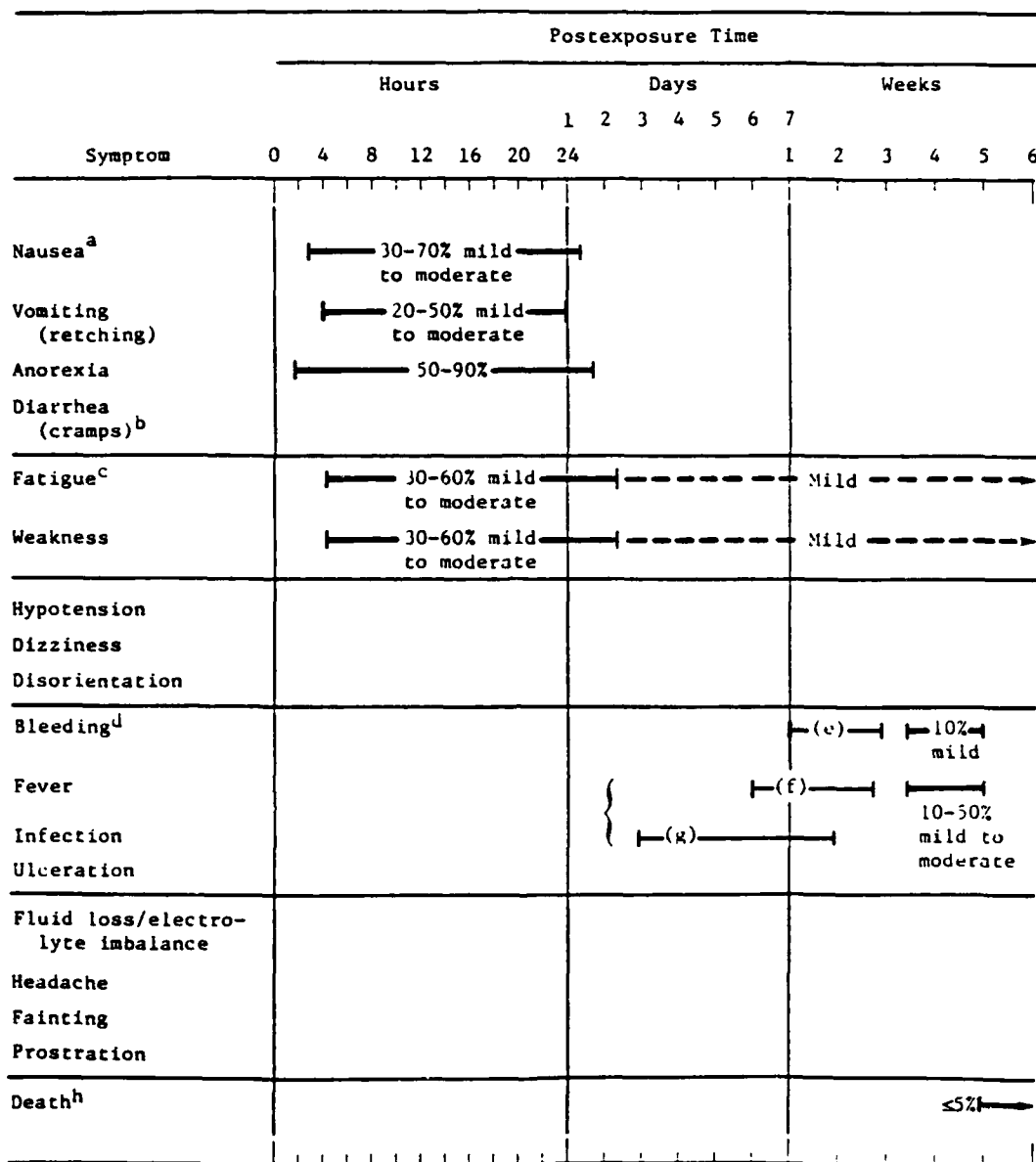
Symptom	Postexposure Time																							
	Hours								Days							Weeks								
	0	4	8	12	16	20	24	1	2	3	4	5	6	7	1	2	3	4	5	6				
Nausea ^a																								
Vomiting (retching)																								
Anorexia																								
Diarrhea (cramps)																								
Fatigue																								
Weakness																								
Hypotension																								
Dizziness																								
Disorientation																								
Bleeding ^b																								
Fever																								
Infection																								
Ulceration																								
Fluid loss/electro- lyte imbalance																								
Headache																								
Fainting																								
Prostration																								
Death																								

^aReferences for this group of symptoms: 1, 7, 15, 22, 26-30, 33, 37, 42, 50, 62, 66, 71, 72, 76, 78, 80, 85, 92, 96, 97, 105-107, 110, 111. These symptoms not observed in American servicemen exposed to approximately 78 rads (cGy) of fallout radiation, according to Refs. 26-29.

^bReferences for this group of symptoms: 1, 7, 14, 15, 26-30, 33, 50, 64, 72, 101, 105, 106, 108.

^cSlight drop in lymphocyte, platelet, and granulocyte counts; no overt symptoms.

Symptoms for dose range 100 to 200 rads (cGy)



^aReferences for this group of symptoms: 4, 6, 7, 15, 17, 21, 22, 26-29, 33, 37, 42, 44, 45, 50, 51, 56, 62, 65, 66, 74, 76, 78-82, 85-87, 90-92, 95, 96, 104, 105, 107, 111.

^bTen percent of the Marshallese victims exposed to 175 rads (cGy) experienced diarrhea during the first postexposure day, according to Ref. 4.

^cReferences for this group of symptoms: 7, 50, 60, 65, 81, 85, 86, 90, 101, 102.

^dReferences for this group of symptoms: 6, 7, 14, 18, 21, 25, 26-29, 33, 35, 60, 62, 64, 65, 75, 76, 78, 79, 81, 82, 85, 89, 101, 104, 105, 107, 110.

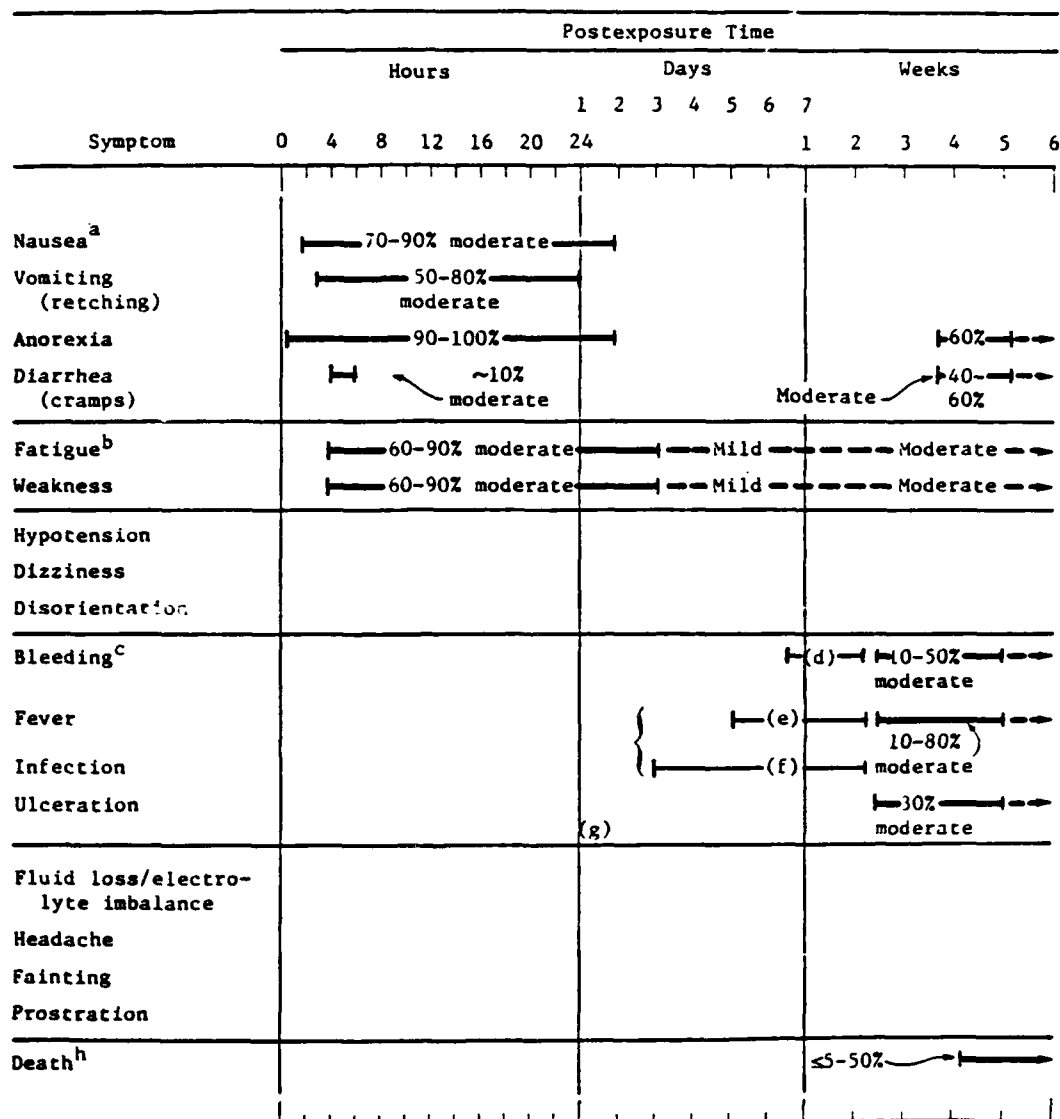
^eSlight to moderate drop in platelets: from $3 \times 10^5/\text{mm}^3$ to $1.8-0.8 \times 10^5/\text{mm}^3$.

^fSlight to moderate drop in granulocytes: from $6 \times 10^3/\text{mm}^3$ to $4.5-2.0 \times 10^3/\text{mm}^3$.

^gSlight to moderate drop in lymphocytes: from $3 \times 10^3/\text{mm}^3$ to $2.0-1.0 \times 10^3/\text{mm}^3$.

^hReferences for this event: 4, 14, 61, 81.

Symptoms for dose range 200 to 350 rads (cGy)



^aReferences for this group of symptoms: 4, 6, 7, 12, 15, 18, 21, 22, 32, 33, 35, 37, 41-44, 47, 50, 51, 53, 56, 60, 62, 65, 75, 76, 80-82, 85-88, 90, 92, 95-97, 105-111.

^bReferences for this group of symptoms: 1, 7, 14, 43, 65, 71, 76, 81, 101, 104, 109, 110.

^cReferences for this group of symptoms: 2, 6, 7, 14, 15, 33, 35, 39, 54, 56, 60, 62, 64, 65, 71, 75, 76, 79, 81, 82, 85, 88, 95, 97, 101, 105, 106, 110.

^dModerate drop in platelets: from $3 \times 10^5/\text{mm}^3$ to $0.8-0.1 \times 10^5/\text{mm}^3$.

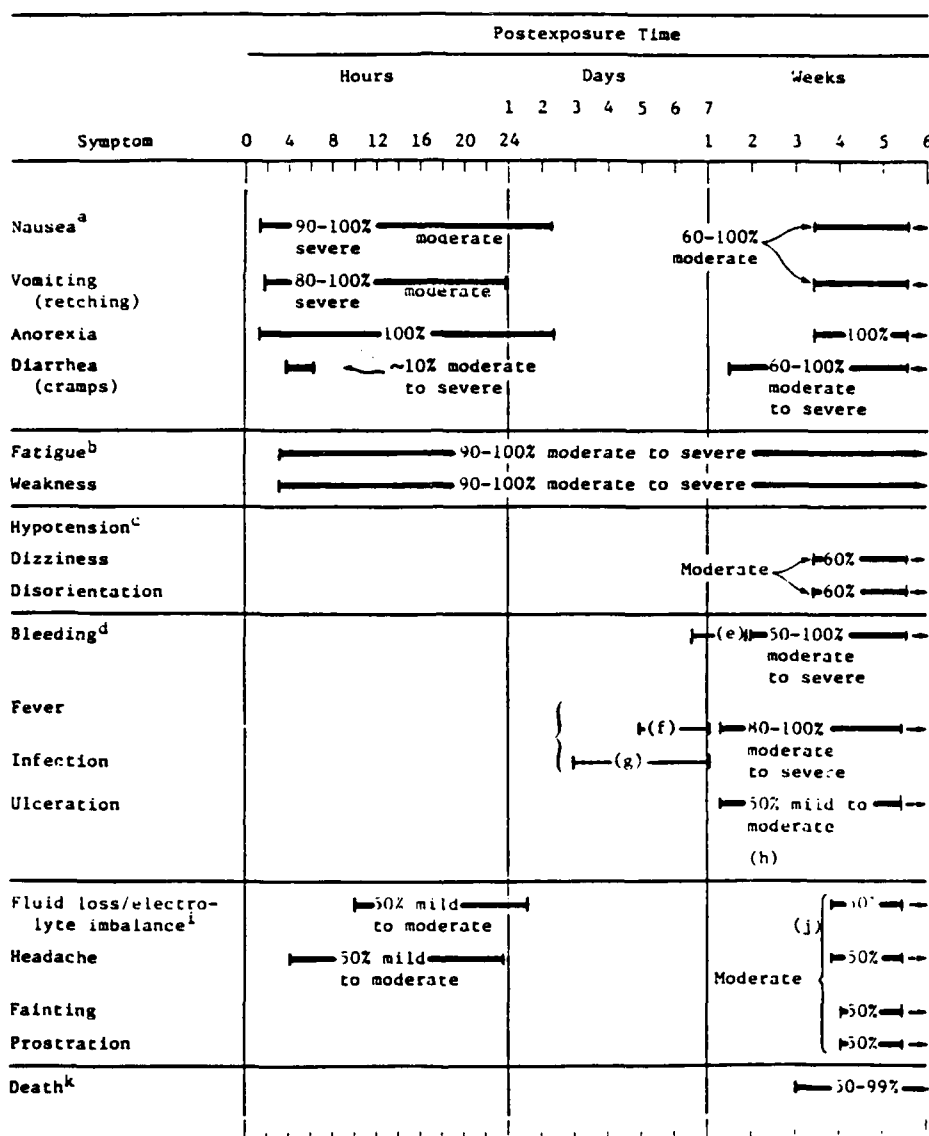
^eModerate drop in granulocytes: from $6 \times 10^3/\text{mm}^3$ to $2.0-0.5 \times 10^3/\text{mm}^3$.

^fModerate to severe drop in lymphocytes: from $3 \times 10^3/\text{mm}^3$ to $1.0-0.4 \times 10^3/\text{mm}^3$.

^gEpilation.

^hReferences for this event: 4, 7, 14, 61, 81.

Symptoms for dose range 350 to 550 rads (cGy)



^aReferences for this group of symptoms: 1, 4, 6, 7, 14, 15, 21, 22, 32, 33, 37, 41, 42, 50, 51, 53, 56, 58, 62, 76, 77, 79-82, 85, 87, 89, 90, 95-97, 101, 105, 106, 110, 111.

^bReferences for this group of symptoms: 1, 6, 7, 14, 47, 51, 53, 65, 78, 81, 85, 90, 101.

^cReferences for this group of symptoms: 77, 89.

^dReferences for this group of symptoms: 1, 6, 7, 14, 15, 18, 31, 33, 35, 54, 58, 62, 64, 65, 67, 71, 75, 76, 77, 81, 85, 90, 95, 101, 105-107, 110, 111.

^eSevere drop in platelets: from $3 \times 10^5/\text{mm}^3$ to $0.1 \times 10^5-0/\text{mm}^3$.

^fSevere drop in granulocytes: from $6 \times 10^3/\text{mm}^3$ to $0.5 \times 10^3-0/\text{mm}^3$.

^gSevere drop in lymphocytes: from $3 \times 10^3/\text{mm}^3$ to $0.4-0.1 \times 10^3/\text{mm}^3$.

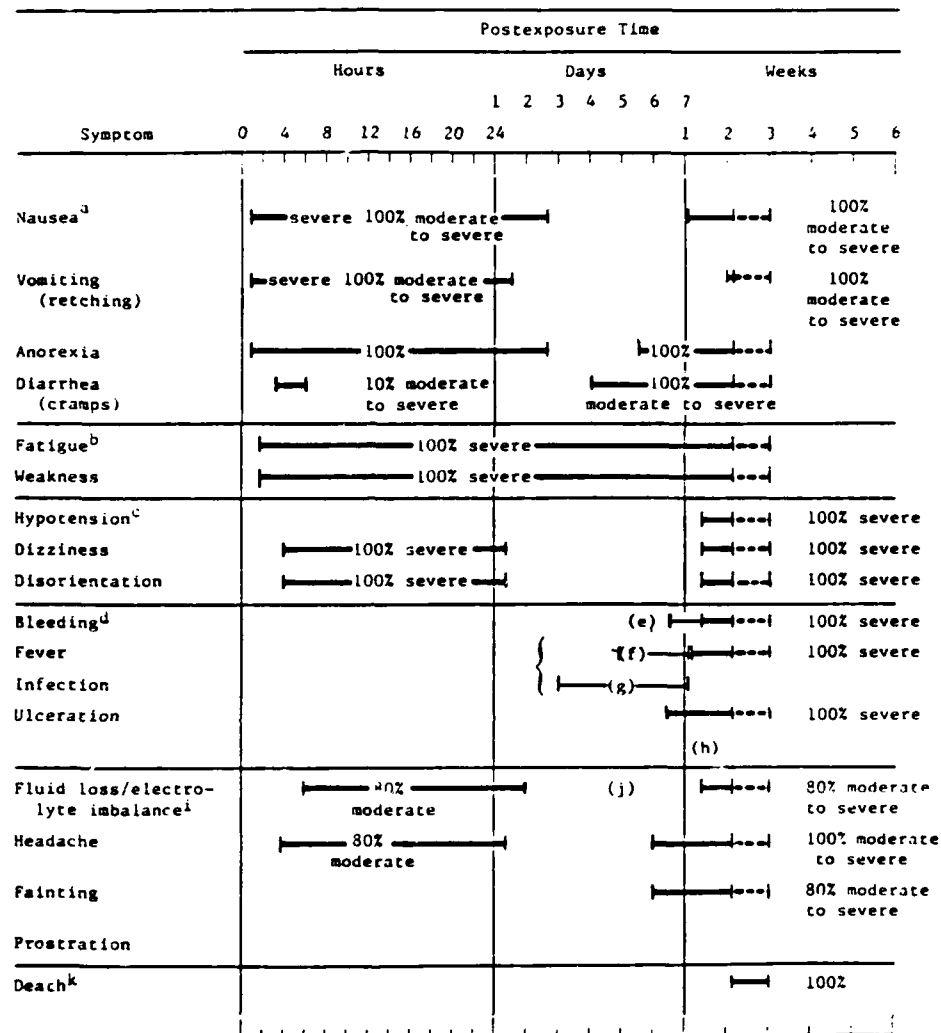
^hEpilation.

ⁱReferences for this group of symptoms: 7, 14, 71, 81, 89, 101.

^jMild intestinal damage.

^kReferences for this event: 4, 14, 61, 81.

Symptoms for dose range 550 to 750 rads (cGy)



^aReferences for this group of symptoms: 1, 4, 6, 7, 14, 15, 21, 22, 31, 32, 33, 41, 42, 44, 45, 47, 50, 51, 53, 57, 62, 65, 71, 76, 79-82, 85, 87, 90, 95-98, 101, 105, 106, 111.

^bReferences for this group of symptoms: 1, 6, 7, 14, 31, 47, 51, 53, 78, 81, 84, 90, 101.

^cReferences for this group of symptoms: 6, 7, 14, 15, 32, 33, 50, 61, 62, 65, 67, 71, 76, 85, 90, 95, 97, 101, 105, 106, 108.

^dReferences for this group of symptoms: 1, 6, 7, 12, 14, 15, 33, 35, 45, 58, 62, 64, 65, 67, 71, 75, 76, 79, 81, 85, 87, 90, 101, 105, 106.

^ePlatelet count drops nearly to zero.

^fGranulocyte count drops nearly to zero.

^gLymphocyte count drops nearly to zero.

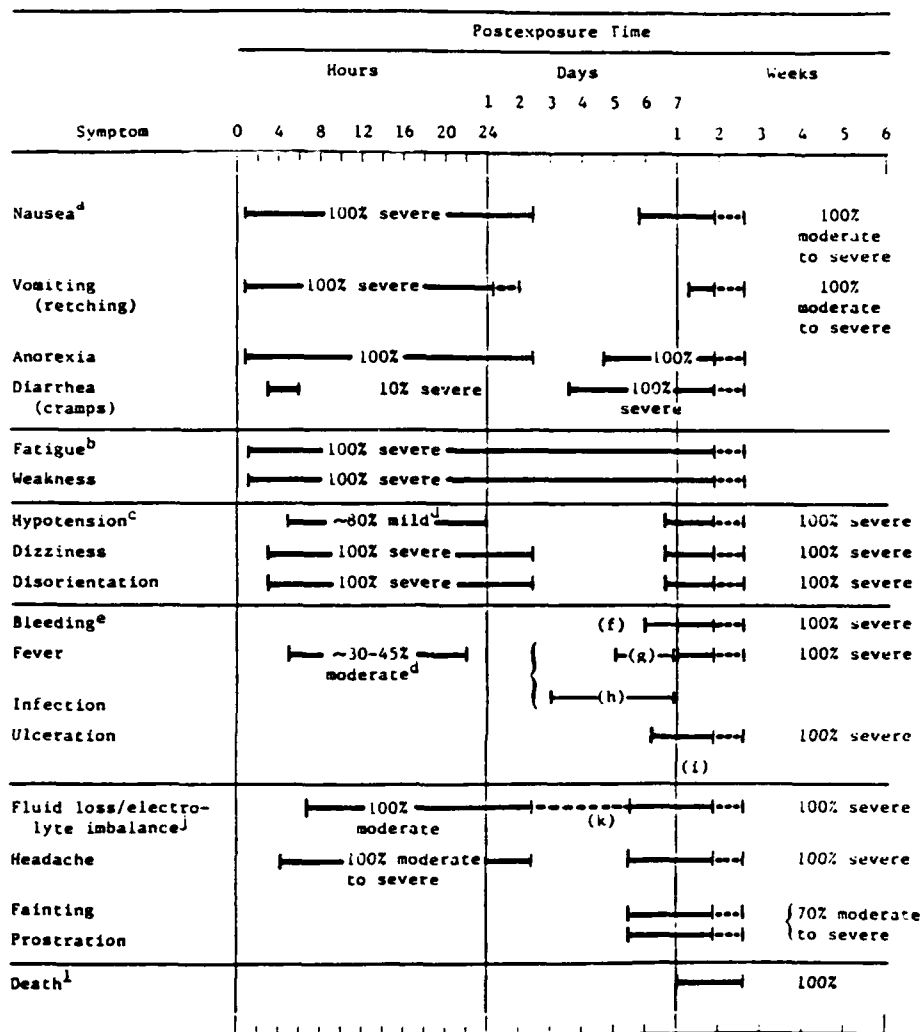
^hEpilepsy.

ⁱReferences for this group of symptoms: 1, 6, 7, 12, 13, 14, 15, 33, 35, 62, 64, 65, 71, 75, 76, 79, 81, 85, 87, 90, 101, 105, 106.

^jModerate intestinal damage.

^kReferences for this event: 4, 14, 31, 61, 77, 81.

Symptoms for dose range 750 to 1000¹ rads (cGy)



^aReferences for this group of symptoms: 6, 7, 14, 15, 21, 22, 33, 41, 44, 47, 50, 51, 53, 57, 62, 65, 71, 76, 79-82, 85, 87, 90, 93, 95, 96, 101, 106.

^bReferences for this group of symptoms: 1, 6, 7, 14, 32, 47, 51, 53, 65, 67, 78, 85, 101.

^cReferences for this group of symptoms: 6, 7, 14, 15, 33, 50, 61, 62, 65, 71, 76, 79, 80, 82, 85, 87, 89, 93, 101, 105, 106.

^dBlood pressure drops 25 percent; temperature increases to 102°F, according to Ref. 33.

^eReferences for this group of symptoms: 6, 7, 14, 15, 21, 30, 31, 33, 51, 53, 61, 62, 65, 71, 72, 79-82, 85, 87, 89, 90, 93, 95, 101, 106.

^fPlatelet count drops to zero.

^gGranulocyte count drops to zero.

^hLymphocyte count drops to zero.

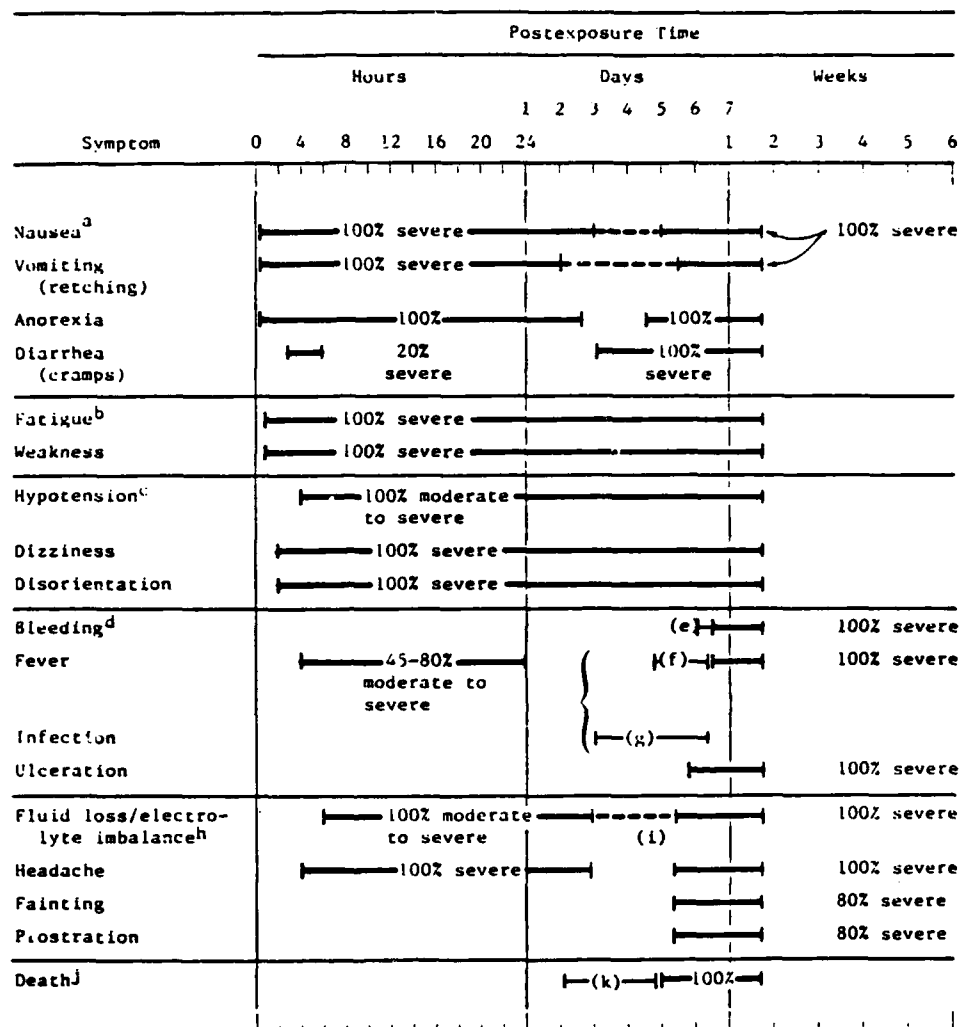
ⁱEpilation.

^jReferences for this group of symptoms: 6, 7, 14, 15, 33, 50, 61, 62, 65, 71, 72, 76, 79-82, 85, 89, 101, 106.

^kModerate to severe intestinal damage.

^lReferences for this event: 4, 14, 61, 77, 81.

Symptoms for dose range 1000 to 2000 rads (cGy)



^aReferences for this group of symptoms: 6, 7, 14, 15, 21, 22, 31, 33, 47, 50, 62, 65, 67, 71, 76, 79-82, 85, 87, 90, 95, 101, 105, 106.

^bReferences for this group of symptoms: 6, 7, 14, 47, 53, 65, 71, 78, 85, 90, 101.

^cReferences for this group of symptoms: 6, 7, 14, 15, 33, 50, 61, 62, 65, 71, 76, 79-82, 85, 87, 89, 101, 105, 106.

^dReferences for this group of symptoms: 6, 7, 14, 15, 21, 22, 33, 47, 50, 62, 65, 67, 71, 76, 79-82, 85, 87, 90, 95, 101, 105, 106.

^ePlatelet count drops to zero.

^fGranulocyte count drops to zero.

^gLymphocyte count drops to zero.

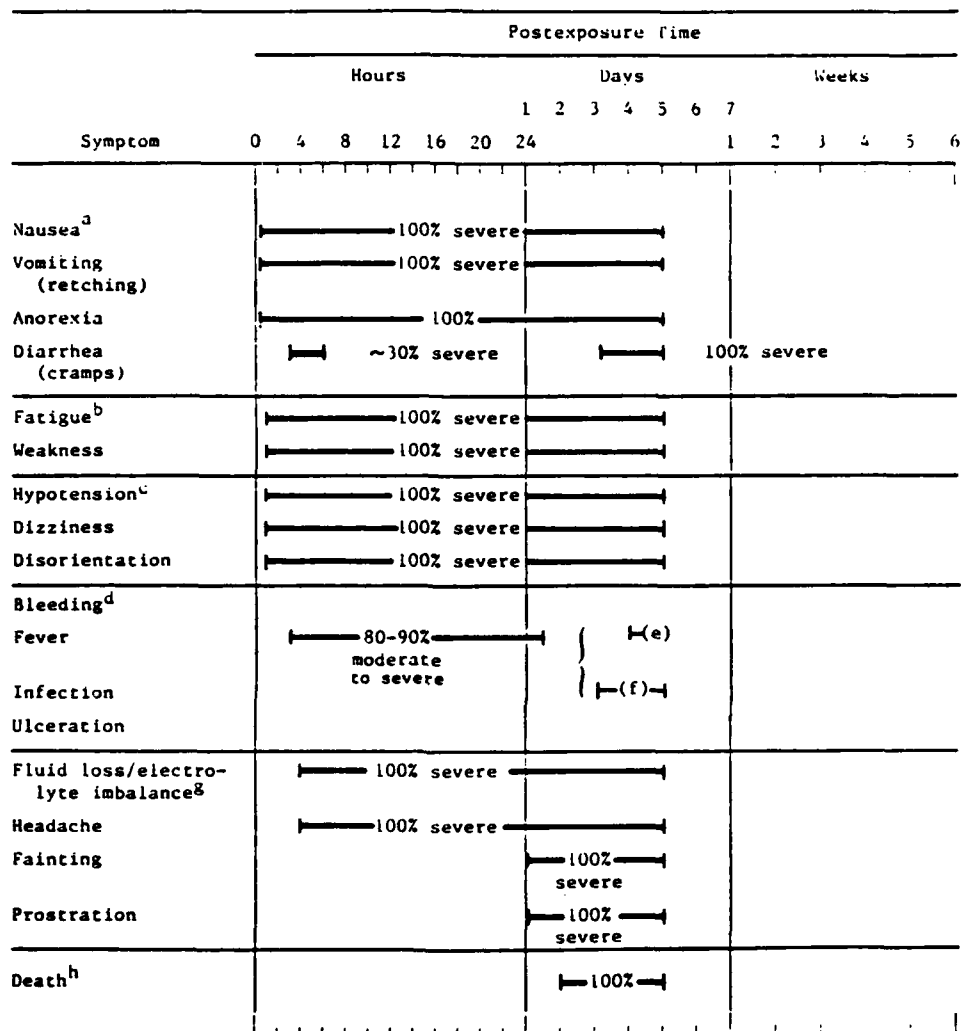
^hReferences for this group of symptoms: 7, 14, 15, 33, 50, 61, 65, 68, 75, 76, 79-82, 85, 95, 101, 105, 106, 108.

ⁱSevere intestinal damage.

^jReferences for this event: 4, 14, 61, 81, 98.

^kRenal failure, according to Ref. 98.

Symptoms for dose range 2000 to 3000 rads (cGy)



^aReferences for this group of symptoms: 6, 7, 14, 15, 21, 22, 42, 44, 50, 62, 65, 71, 76, 79-82, 85, 87, 90, 95, 101, 106, 108.

^bReferences for this group of symptoms: 6, 7, 14, 15, 21, 22, 50, 62, 65, 71, 76, 79-82, 85, 87, 90, 94, 95, 101, 105, 106, 108.

^cReferences for this group of symptoms: 14, 50, 61, 71, 76, 79, 80, 82, 85, 87, 94, 95, 101, 105, 108.

^dReferences for this group of symptoms: 7, 14, 50, 61, 71, 75, 76, 79-82, 85, 87, 94, 95, 101, 105, 106, 108.

^eGranulocyte count drops to zero.

^fLymphocyte count drops to zero.

^gReferences for this group of symptoms: 14, 15, 33, 50, 61, 62, 71, 75, 76, 77, 80, 82, 85, 87, 95, 101, 105, 108.

^hReferences for this event: 4, 14, 61, 77, 81.

REFERENCES

1. Adams, R., and S. Cullen, The Final Epidemic: Physicians and Scientists on Nuclear War, Educational Foundation for Nuclear Science, Chicago, Illinois, 1981.
2. Adelstein, S. J., and J. B. Dealy, Jr., "Hematologic Responses to Human Whole-Body Irradiation," Am. J. Roentgenol., Radium Ther. and Nucl. Med., Vol. 93, 1965, pp. 927-934.
3. Ainsworth, E. J., G. F. Leong, K. Kendall, and E. L. Alpen, "Cooperative Lethality Response of Neutron- and X-Irradiated Dogs," Radiat. Res., Vol. 26, 1965, pp. 33-34.
4. Alpen, E. L., Radiological Hazard Evaluation: A Critical Review of Present Concepts and a New Approach Thereto, U.S. Naval Radiological Defense Laboratory, San Francisco, California, Report USNRDL-TR-186, 1957.
5. Anderson, A. C., and L. S. Rosenblatt, "The Effect of Whole Body X-Irradiation on the Median Life Span of Female Dogs (Beagles)," Radiat. Res., Vol. 39, 1969, pp. 177-200.
6. Andrews, G. A., "Total-Body Irradiation in the Human Being," Excerpta Medica, International Congress Series 105, 1965, pp. 1583-1589.
7. Andrews, G. A., and R. J. Cloutier, "Accidental Acute Radiation Injury," Arch. Environ. Health, Vol. 10, 1965, pp. 498-507.
8. Anno, G. H., Acute Radiation Response in Humans: Informal Comments by Physicians and Radiobiologists, Pacific-Sierra Research Corporation, Note 492 (rev.), June 1983.
9. Anno, G. H., H. L. Brode, and R. Washton-Brown, Initial Human Response to Nuclear Radiation, Pacific-Sierra Research Corporation, Note 477, April 1982.
10. Barret, A., "Total Body Irradiation (TBI) before Bone Marrow Transplantation in Leukemia: A Cooperative Study from the European Group for Bone Marrow Transplantation," Br. J. Radiol., Vol. 55, 1982, pp. 562-567.
11. Baum, S. J., "Erythrocyte Stem Cell Kinetics in the Post-irradiation Rat," Radiat. Res., Vol. 30, 1967, pp. 316-324.

12. Blakely, J., The Care of Radiation Casualties, Charles C. Thomas Co., Springfield, Illinois, 1968.
13. Bond, V. P., "Radiation Mortality in Different Mammalian Species," in V. P. Bond and T. Sugahara (eds.), Comparative Cellular and Species Radiosensitivity, Igaku Shoin, Tokyo, 1969.
14. Bond, V. P., T. M. Fliedner, and J. O. Archambeau, Mammalian Radiation Lethality: A Disturbance in Cellular Kinetics, Academic Press, New York, 1965.
15. Bond, V. P., T. M. Fliedner, and E. P. Cronkite, "Evaluation and Management of Heavily Irradiated Individuals," J. Nucl. Med., Vol. 1, 1960, pp. 221-238.
16. Borison, H., and S. C. Wang, "Physiology and Pharmacology of Vomiting," Pharmacol. Rev., Vol. 5, 1953, pp. 193-230.
17. Brown, W. M. Court, "Symptomatic Disturbance after Single-Therapeutic Dose of X-Rays," Br. Med. J., 11 April 1953, pp. 802-805.
18. Brown, W. M. Court, and J. D. Abbatt, "The Effect of a Single Dose of X-Rays on the Peripheral Blood Count of Man," Br. J. Haematol., Vol. 1, 1955, pp. 75-85.
19. Brown, W. M. Court, and R. Doll, Leukemia and Aplastic Anemia in Patients Irradiated for Ankylosing Spondylitis, British Medical Research Council, special report series 1-50, Her Majesty's Stationery Office, London, 1957.
20. -----, "Mortality from Cancer and Other Causes after Radiotherapy for Ankylosing Spondylitis," Br. Med. J., Vol. 2, 1965, pp. 1327-1332.
21. Brucer, M. B. (comp.), The Acute Radiation Syndrome: A Medical Report on the Y-12 Accident, June 16, 1958, U.S. Atomic Energy Commission, Report ORINS-25, April 1959.
22. Cairnie, A. B., and H. A. Robitaille, Arguments for the Greater Importance of the Prodromal Syndrome Than Incapacitation (Involving Early Transient Incapacitation) the Consideration of Radiation Effects in Irradiated Military Personnel, Together with a Proposal to Simulate the Prodromal Effects Using Lithium Carbonate, [Canadian] Defense Research Establishment, Ottawa, Report 836, December 1980.

23. Carpenter, D. O., Early Transient Incapacitation: A Review with Consideration of Underlying Mechanisms, Armed Forces Radiobiological Research Institute, Bethesda, Maryland, Scientific report SR-79-1, 1979.
24. Chin H., and S. C. Wang, "Locus of Emetic Action Following Irradiation," Proc. Soc. Exp. Biol. Med., Vol. 85, 1954, pp. 472-474.
25. Conard, R. A., "Acute Myelogenous Leukemias Following Fallout Radiation Exposure," J. Am. Med. Assn., Vol. 232, 1975, pp. 1356-1357.
26. -----, A Twenty-Year Review of Medical Findings in a Marshallese Population Accidentally Exposed to Radioactive Fallout, Brookhaven National Laboratory, Long Island, New York, Report BNL 50424 (TLD-4500), 1975.
27. Conard, R. A., et al., Medical Survey of Rongelap People Eight Years after Exposure to Fallout, Brookhaven National Laboratory, Long Island, New York, Report BNL 780 (T-296), 1963.
28. Conard, R. A., et al., Review of Medical Findings in a Marshallese Population Twenty-six Years after Accidental Exposure to Radioactive Fallout, Brookhaven National Laboratory, Long Island, New York, Report BNL 51261 (TLD-4500), 1980.
29. Cronkite, E. P., et al., "Response of Human Beings Accidentally Exposed to Significant Fallout Radiation," J. Am. Med. Assn., Vol. 159, 1955, pp. 430-434.
30. Cronkite, E. P., V. P. Bond, and C. L. Dunham, Some Effects of Ionizing Radiation on Human Beings, Atomic Energy Commission Report TID 5358, 1956.
31. Cronkite, E. P., and V. P. Bond, "Acute Radiation Syndrome in Man," U.S. Armed Forces Med. J., Vol. 9, 1958, pp. 313-324.
32. Cronkite, E. P., et al., "Diagnosis and Therapy of Acute Radiation Injury," Ch. 2 of Atomic Medicine, 3d ed., The Williams & Williams Co., Baltimore, Maryland, 1959.
33. Cronkite, E. P., and V. P. Bond, Radiation Injury in Man, Charles C. Thomas Co., Springfield, Illinois, 1960.

34. Cronkite, E. P., "The Effects of Dose, Dose Rate and Depth Dose upon Radiation Mortality," Proceedings of a Symposium on the Control of Exposures of the Public to Ionizing Radiation in the Event of Accident or Attack, National Council on Radiation Protection and Measurement, Bethesda, Maryland, May 1982, pp. 21-27.
35. Dienstbier, Z., M. Arient, and J. Pospisil, "Hamatologische Veranderung bei der Strahlenkrankheit-IV; Hamokoagulationsveranderungen," Atompraxis, Vol. 9, 1963, pp. 189-194.
36. Edsall, D. L., and R. Pemberton, "The Nature of the General Toxic Reaction Following Exposure to X-Rays," Am. J. Med. Sc., Vol. 133, 1970, pp. 426-431.
37. Ellinger, F., et al., "A Clinical Study of Radiation Sickness," Am. J. Roentgenol., Radium Ther. and Nucl. Med., Vol. 68, 1952, pp. 275-280.
38. Fanger, H., and C. C. Lushbaugh, "Radiation Death from Cardiovascular Shock Following a Criticality Accident," Arch. Path., Vol. 83, May 1967, pp. 446-460.
39. Finch, S. C., "Recognition of Radiation-Induced Late Bone Marrow Changes," Ann. N. Y. Acad. Sci., Vol. 145, 1967, pp. 748-754.
40. Fliedner, T. M., and D. van Beckum, private communication, July 1983.
41. Gerstner, H. B., "Acute Clinical Effects of Penetrating Nuclear Radiation," J. Am. Med. Assn., Vol. 168, 27 September 1958, pp. 381-388.
42. -----, "Acute Radiation Syndrome in Man," U.S. Armed Forces Med. J., Vol. 9, 1958, p. 313.
43. -----, "Reaction to Short Term Radiation in Man," Annual Rev. Med., Vol. 11, 1960, pp. 289-302.
44. -----, "Practical Implication of the Initial Reaction to Penetrating Ionizing Radiation," unpublished manuscript, U.S. Air Force School of Aerospace Medicine, Brooks Air Force Base, Texas, 1970.
45. Gilberti, M. V., "The 1967 Radiation Accident near Pittsburgh, Pennsylvania, and a Follow-Up Report," in K. F. Hubner and S. A. Fry (eds.), The Medical Basis for Radiation Accident Preparedness, Elsevier North Holland, Inc., New York, 1980.

46. Glasstone, S., and P. J. Dolan, The Effects of Nuclear Weapons, 3d ed., U.S. Departments of Defense and Energy, 1977.
47. Grant, G. A., et al., A Predictive Study of the Incidence of Vomiting in Irradiated Military Personnel, [Canadian] Defense Research Establishment, Ottawa, Report 817, 1979.
48. Hall, E. J., Radiobiology for the Radiobiologist, Harper & Row, Hagerstown, Maryland, 1978.
49. Hemplemann, L. H., C. C. Lushbaugh, and G. L. Voetz, "What Happened to the Survivors of the Early Los Alamos Nuclear Accidents?" in K. F. Hubner and S. A. Fry (eds.), The Medical Basis for Radiation Accident Preparedness, Elsevier North Holland, Inc., New York, 1980.
50. Howland, J. W., "Injury and Recovery from Ionizing Radiation Exposure," Annual Rev. Med., Vol. 7, 1956, pp. 225-244.
51. Howland, J. W., M. Ingram, H. Mermagen, and C. L. Hansen, Jr., "The Lockport Incident: Accidental Partial Body Exposure of Humans to Large Doses of X-Irradiation," Diagnosis and Treatment of Acute Radiation Injury, International Atomic Energy Agency and World Health Organization, International Documents Service, New York, 1961, pp. 11-26.
52. Hubner, K. F., and S. A. Fry (eds.), The Medical Basis for Radiation Accident Preparedness, Elsevier North Holland, Inc., New York, 1980.
53. Ingram, M., J. W. Howland, and C. L. Hansen, "Sequential Manifestation of Acute Radiation Injury vs. 'Acute Radiation Syndrome' Stereotype," Ann. N Y Acad. Sci., Vol. 114, 1964, pp. 356-367.
54. Ishida, M., and I. Matsubayashi, An Analysis of Early Mortality Rates Following the Atomic Bomb in Hiroshima, Atomic Bomb Casualty Committee, Hiroshima, Technical report 20-61, 1948.
55. Ishimaru, T., et al., "Leukemia in Atomic Bomb Survivors, Hiroshima and Nagasaki, 1 October, 1950-30 September, 1966," Radiat. Res., Vol. 45, 1971, pp. 216-233.

56. Jammet, H. P., "Treatment of Victims of the Zero-Energy Reactor Accident at Vinca," Diagnosis and Treatment of Acute Radiation Injury, International Atomic Energy Agency and World Health Organization, International Documents Service, New York, 1961.
57. Jammet, H. P., et al., "Etude de Six Cas d'Irradiation Totale Aigue Accidentale," Rev. Franc. Etud. Clin. Biol., Vol. 4, 1959, pp. 210-225.
58. Jammet, H. P., R. Gongora, R. Le Go, and M. J. Doley, "Clinical and Biological Comparison of Two Acute Accidental Irradiations: Mol (1965) and Brescia (1975)," in K. F. Hubner and S. A. Fry (eds.), The Medical Basis for Radiation Accident Preparedness, Elsevier North Holland, Inc., New York, 1980.
59. Karas, J. S. and J. B. Stanbury, "Fatal Radiation Syndromes from an Accidental Nuclear Excursion," New Eng. J. Med., Vol. 272, No. 15, 1965, pp. 755-761.
60. Kumatori, T., "Hematological Effects on Heavily Irradiated Japanese Fishermen," in T. Sugahara and O. Hug (eds.), Biological Aspects of Radiation Protection, Igaku Shoin, Tokyo, 1971.
61. Langham, W. H. (ed.), Radiobiological Factors in Manned Space Flight, National Academy of Sciences, National Research Council Publication 1487, 1967.
62. Laumets, E., Time History of Biological Response to Ionizing Radiation, U.S. Naval Radiobiological Defense Laboratory, San Francisco, California, Report USNRDL-TR-905, November 1965.
63. Levin, S., et al., Early Biological Effects from Initial Nuclear Radiation in Hiroshima and Nagasaki, Armed Forces Radiobiological Research Institute, Bethesda, Maryland, 1983 (forthcoming).
64. Liebow, A. A., S. Warren, and E. De Coursey, "Pathology of Atomic Bomb Casualties," Am. J. Path., Vol. 25, 1949, p. 853.
65. Lushbaugh, C. C., "What Can We Expect to Happen?" Rocky Mount. Med. J., January 1962.

66. -----, Recent Progress in Assessment of Human Resistance to Total-Body Irradiation, National Academy of Sciences, National Research Council conference paper 671135, April 1968.
67. -----, "Reflections on Some Recent Progress in Human Radiobiology," Advances in Radiation Biology, Vol. 3, Academic Press, New York, 1969, pp. 277-315.
68. -----, "Theoretical and Practical Aspects of Models Explaining 'Gastrointestinal Death' and other Lethal Radiation Syndromes," in V. P. Bond and T. Sugahara (eds.), Comparative Cellular and Species Radiosensitivity, Igaku Shoin, Tokyo, 1969, pp. 288-297.
69. -----, "Human Radiation Tolerance," Ch. 10 in J. Parker, Jr., and V. R. West (eds.), Bioastronautics Data Book, National Aeronautics and Space Administration, report NASA-S-30006, 1973.
70. -----, "The Impact of Estimates of Human Radiation Tolerance upon Radiation Emergency Management," Proceedings of a Symposium on the Control of Exposure of the Public to Ionizing Radiation in the Event of Accident or Attack, National Council on Radiation Protection and Measurement, Bethesda, Maryland, May 1982, pp. 46-57.
71. Lushbaugh, C. C., et al., "Clinical Studies of Radiation Effects in Man," Radiat. Res. Suppl., Vol. 1, 1967, pp. 398-412.
72. Martin, E. J., and R. H. Rowland, Castle Series, 1954, Defense Nuclear Agency, Report DNA 6035F, April 1982.
73. Martinez, R. G., et al., "Observations on the Accidental Exposure of a Family to a Source of Cobalt-60," Rev. Med. Inst. Mex., Seguro Social, Vol. 3, 1964, pp. 14-68 (translated by F. V. Comas).
74. McCandless, J. B., "Accidental Acute Whole-Body Gamma Irradiation of Seven Clinically Well Persons," J. Am. Med. Assn., Vol. 192, 1965, pp. 85-88.
75. McFarland, W., and H. A. Pearson, "Hematological Events as Dosimeters in Human Total-Body Irradiation," Radiol., Vol. 80, 1963, pp. 850-855.
76. McLean, A. S., "Early Adverse Effects of Radiation," Br. Med. Bull., Vol. 29, 1973, pp. 69-73.

77. Messerschmidt, O., Medical Procedures in a Nuclear Disaster, Verlag Karl Thieming, Munich, 1979.
78. Miller, L. S., G. H. Fletcher, and H. B. Gerstner, "Radiobiologic Observations on Cancer Patients Treated with Whole-Body X-Radiation," Radiat. Res., Vol. 8, 1958, pp. 150-165.
79. NATO Handbook on the Medical Aspects of NBC Defensive Operations, U.S. Departments of the Army, Navy, and Air Force, Report AMED P-6, August 1973.
80. Nuclear Weapons Employment Doctrine and Procedures, U.S. Army, FM 101-31-1, 1977.
81. Ohkita, T. II, "A Review of Thirty Years Study of Hiroshima and Nagasaki ATOMIC Bomb Survivors," Jpn. J. Radiat. Res., supplement 16, 1975, pp. 49-66.
82. Oughterson, A. W., and S. Warren, Medical Effects of the Atomic Bomb in Japan, McGraw-Hill Book Company, New York, 1956.
83. Pendic, B., "The Zero-Energy Reactor Accident at Vinca," Diagnosis and Treatment of Acute Radiation Injury, International Atomic Energy Agency and World Health Organization, International Documents Service, New York, 1961.
84. Porvaznik, M., "Tight Junction Disruption and Recovery after Sublethal Gamma Irradiation," Radiat. Res., Vol. 78, 1979, pp. 233-259.
85. Prasad, K. N., Human Radiation Biology, Harper & Row, Hagerstown, Maryland, 1974.
86. Radiological Factors Affecting Decision-Making in a Nuclear Attack, National Council on Radiation Protection and Measurement, Bethesda, Maryland, Report 42, November 1974.
87. R & D Associates, "Collateral Damage Implications of Low Radiation Dose Criteria for Battlefield Nuclear Operations," unpublished manuscript, January 1980.

88. Rider, W. D., and R. Hasselback, "The Symptomatic and Hematological Disturbance Following Total Body Radiation at 300-rad Gamma-Ray Irradiation," lectures presented at McGill University, Montreal, August 1967, in Guidelines to Radiological Health, U.S. Public Health Service, Washington, D.C., 1968, pp. 139-144.
89. Rubin, P., and G. W. Casarett, Clinical Radiation Pathology, W. B. Saunders Company, Philadelphia, 1968.
90. Saenger, E. L. (ed.), Medical Aspects of Radiation Accidents, U.S. Atomic Energy Commission, 1963.
91. Saenger, E. L., et al., Metabolic Changes in Humans Following Total Body Irradiation, Defense Atomic Support Agency, Washington, D.C., Report 1633, 1964.
92. Saenger, E. L., et al., Radiation Effects in Man: Manifestations and Therapeutic Efforts, Defense Nuclear Agency, Report 2751, October 1971.
93. Salazar, O. M., et al., "Systemic (Half-Body) Radiation Therapy: Response and Toxicity," J. Radiat. Oncol. Biol. Phys., Vol. 4, 1978, pp. 937-950.
94. Shipman, T. L., "Acute Radiation Death Resulting from an Accidental Nuclear Critical Excursion," J. Occup. Med., Vol. 3, No. 3, 1961, pp. 145-192.
95. Storb, R., "Total-Body Irradiation and Marrow Transplantation," Transplant. Proc., Vol. 9, 1977, pp. 1113-1119.
96. Thoma, George E., Jr., and N. Wald, "The Diagnosis and Management of Accidental Radiation Injury," J. Occup. Med., Vol. 1, August 1959, pp. 421-447.
97. -----, "The Acute Radiation Syndrome in Man," in Epidemiology of Radiation Injury, postgraduate course syllabus, St. Louis University, School of Medicine, August 1961.
98. Thomas, E. D., et al., "Allogeneic Marrow Grafting for Hematologic Malignancy Using HL-A Matched Donor-Recipient Sibling Pairs," Blood, Vol. 38, No. 3, September 1971, pp. 267-287.
99. Thomas, E. D. K. Dicke, and G. Santos, private communication, July 1983.

100. Thomson, J. F., et al., "Studies on the Effects of Continuous Exposure of Animals to Gamma Radiation from Cobalt-60 Plane Sources," Am. J. Roentgenol., Vol. 69, 1953, pp. 830-838.
101. Upton, A. C., "Effects of Radiation on Man," Annual Rev. Nucl. Sci., Vol. 18, 1968, pp. 495-528.
102. ----, Radiation Injury: Effects, Principles, and Perspectives, The University of Chicago Press, Chicago, 1969.
103. Vodopick, H., and G. A. Andrews, The Clinical Effects of an Accidental Radiation Exposure, Oak Ridge Associated Universities Publications, Oak Ridge, Tennessee, July 1973.
104. ----, "The University of Tennessee Comparative Animal Research Laboratory Accident in 1971," in K. F. Hubner and S. A. Fry (eds.), The Medical Basis for Radiation Accident Preparedness, Elsevier North Holland, Inc., New York, 1980.
105. Wald, N., and G. E. Thoma, Jr., Radiation Accidents: Medical Aspects of Neutron and Gamma-Ray Exposures, Oak Ridge National Laboratory, Report ONRL-2748, Part B, March 1961.
106. Wald, N., G. E. Thoma, and G. Broun, "Hematologic Manifestations of Radiation Exposure in Man," Prog. Hematol., Vol. 3, 1962, pp. 1-5.
107. Warren, S., "The Early Changes Caused by Radiation," J. Mt. Sinai Hospital, Vol. 19, 1952, pp. 443-455.
108. ----, "You, Your Patient, and Radioactive Fallout," New Eng. J. Med., Vol. 266, 1962, pp. 1123-1125.
109. Yochmowitz, M. G., and G. C. Brown, "Performance in a 12-Hour, 300-Rad Profile," Aviat. Space Environ. Med., 1977, pp. 241-247.
110. Zellmer, R. W., "Human Ability to Perform after Acute Sublethal Radiation," Mil. Med., Vol. 126, September 1961, pp. 681-687.
111. Zellmer, R. W., and J. E. Pickering, Biological Effects of Nuclear Radiation in Primates, U.S. Air Force School of Aviation Medicine, Brooks Air Force Base, Texas, Technical Report 60-77, 1960.

SECTION 2

GLOBAL CLIMATE SIMULATIONS

**A COMPARISON OF
EULERIAN AND LAGRANGIAN METHODS
FOR TRACER TRANSPORT IN A GCM**

**Bob Malone, Gary Glatzmaier,
and David Langley**

***Earth and Space Sciences Division
Los Alamos National Laboratory***

A Comparison of Eulerian and Lagrangian Methods
for Tracer Transport in a GCM

Robert C. Malone and Gary A. Glatzmaier
Los Alamos National Laboratory

Recent studies of "nuclear winter" with three-dimensional models have highlighted the need for numerical algorithms for the interactive transport of smoke that have high spatial resolution but do not suffer from excessive numerical diffusion. Two issues of importance for nuclear winter are (1) the residence time of smoke in a high-altitude, stably stratified layer heated by sunlight and (2) the degree of nonuniformity ("patchiness") of areal coverage by smoke. Numerical diffusion, which particularly afflicts coarse resolution Eulerian transport methods, may lead to significant errors in simulation studies of these effects.

Although no observations exist to compare with nuclear winter simulations in which the atmospheric circulation and structure are modified by solar heating of smoke, analogues in the normal atmosphere do exist that can be used as benchmarks for large-scale transport simulations with a GCM. Two for which good data are available are (1) the residence time in the stratosphere of radioactive particulates and gases from high-yield atmospheric nuclear weapon tests and (2) the dispersal in the troposphere of deuterated-methane tracer. Simulations of both phenomena with Eulerian and Lagrangian transport models will be presented and compared with observational data to illustrate the relative merits of the methods.

Simulations of interactive smoke transport with solar heating of smoke will also be presented using both methods.

What's New in the Model

- **Absorption of infrared radiation by smoke**
- **Stability-dependent vertical mixing in the planetary boundary layer and free atmosphere**
- **Subsurface storage and vertical diffusion of heat and water in soil**
- **Annual cycle of solar declination**
- **Diurnal cycle of solar zenith angle**
- **High-resolution, non-diffusive Lagrangian tracer transport**

EULERIAN TRANSPORT MODEL

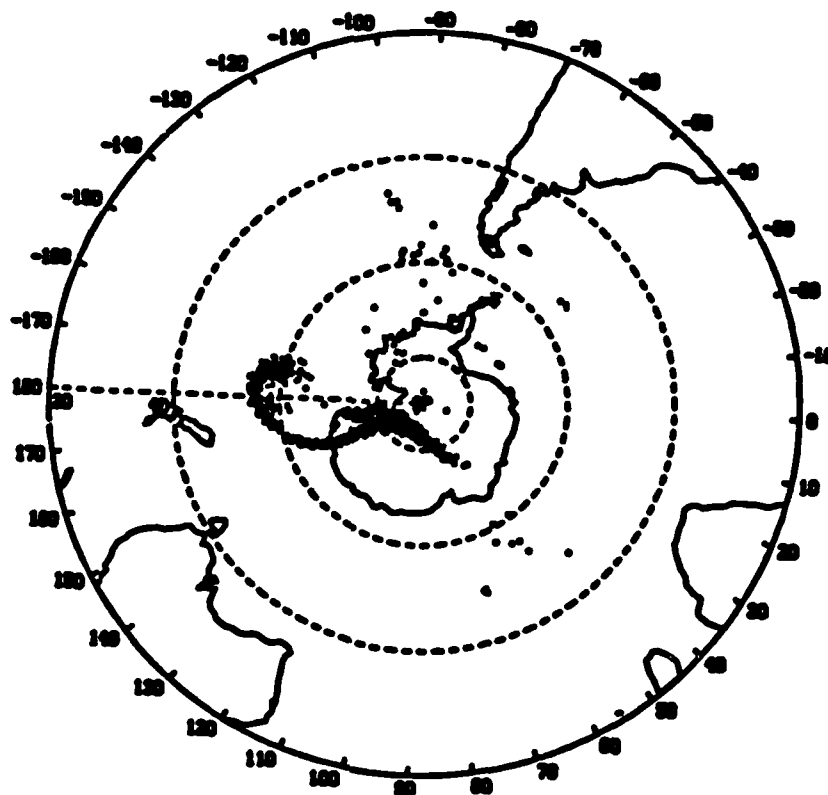
- **Calculates tracer concentration at discrete grid points**
- **Has same resolution as underlying GCM**
- **Limitation: number of grid points affordable in GCM**

LAGRANGIAN TRACER MODEL

- **Tracer is represented by a large number of discrete particles**
- **Particle coordinates not restricted to GCM grid points**
- **Limitation: large number of particles needed to adequately represent local concentrations on grid**

HEAVY METHANE EXPERIMENTS

- Three releases of 1 kg CD₄ in midtroposphere near 55S, 165E (January, June, October 1984)
- Precisely characterized source: time, place, altitude, amount. Inert tracer.
- Samples collected
 - on airplane flights between Antarctic stations, and to/from New Zealand (1 hour averages)
 - at surface stations (3 day averages)
 - for 60 days after release
- Detection limit $\sim 10^{-17}$ g CD₄ / g air
- Samples above limit found out to 20 days
(longest data series for a tropospheric tracer?)
- Principal shortcoming: limited sampling precludes complete picture of large-scale distribution.



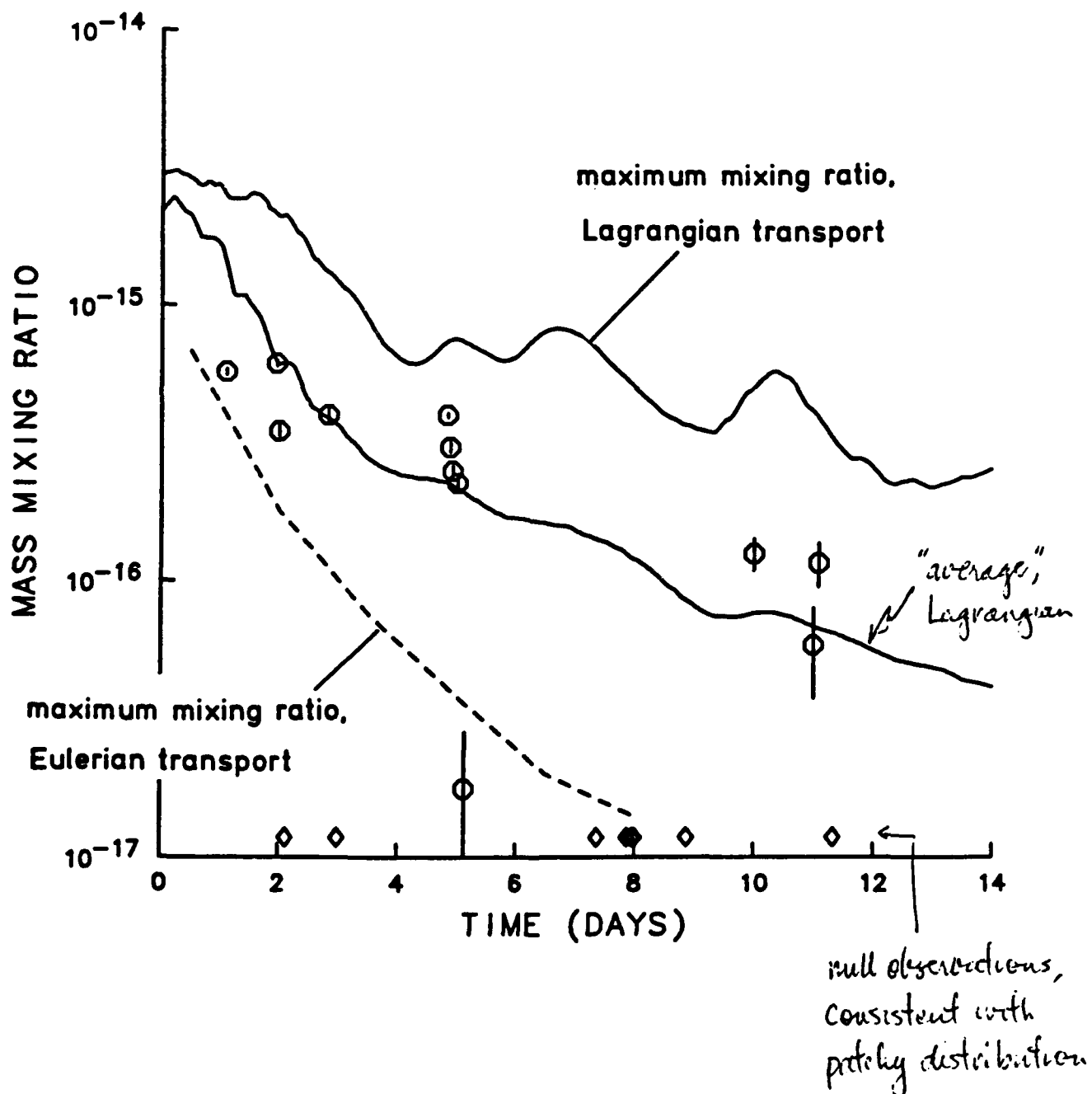
Simulated
distributions
at day 10

Lagrangian
transport



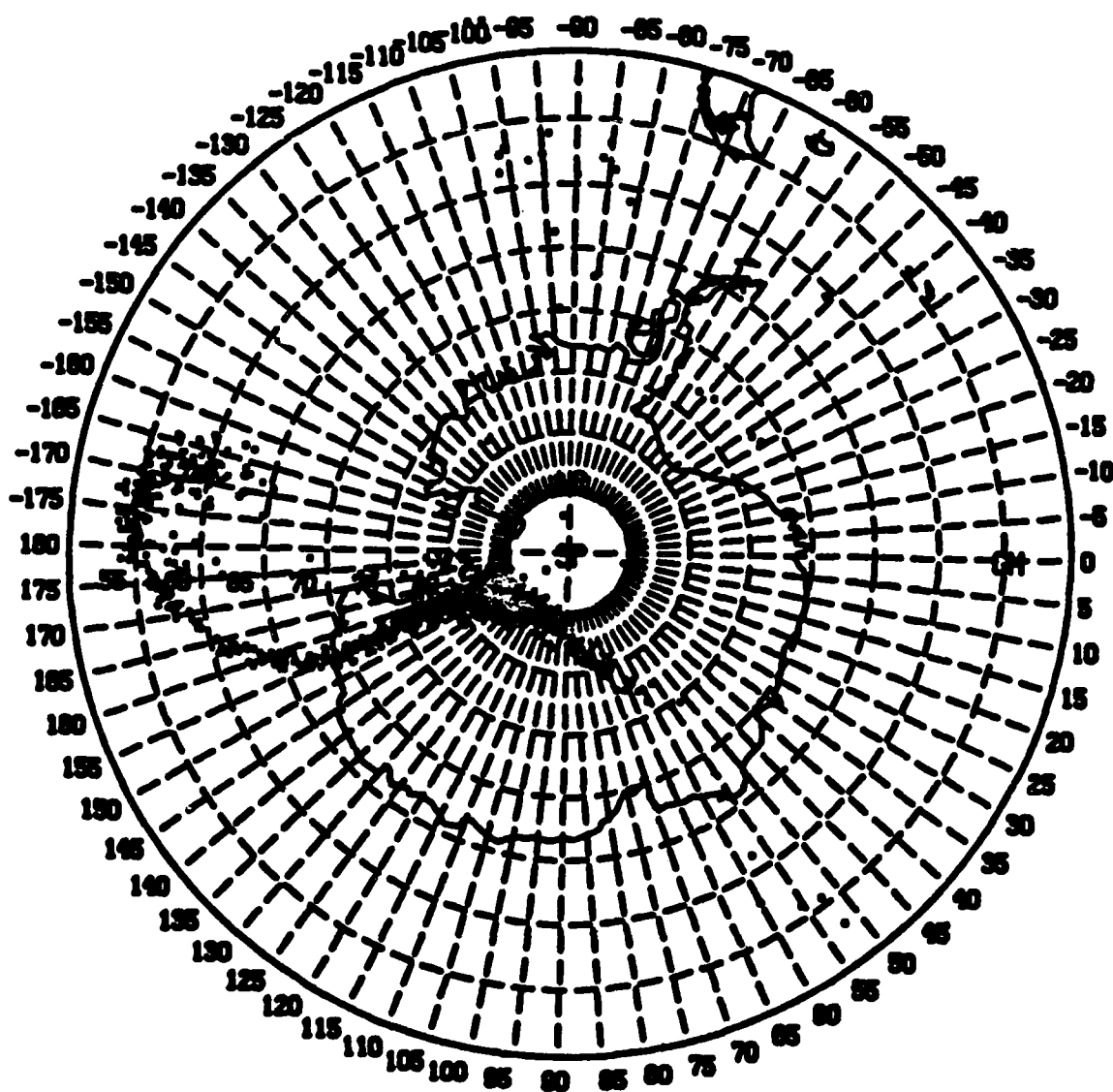
Eulerian
transport

COMPARISON OF OBSERVATIONS WITH LAGRANGIAN AND EULERIAN TRANSPORT MODELS



Simulated distribution compared with resolution of
typical GCM grid ($5^{\circ} \times 5^{\circ}$)

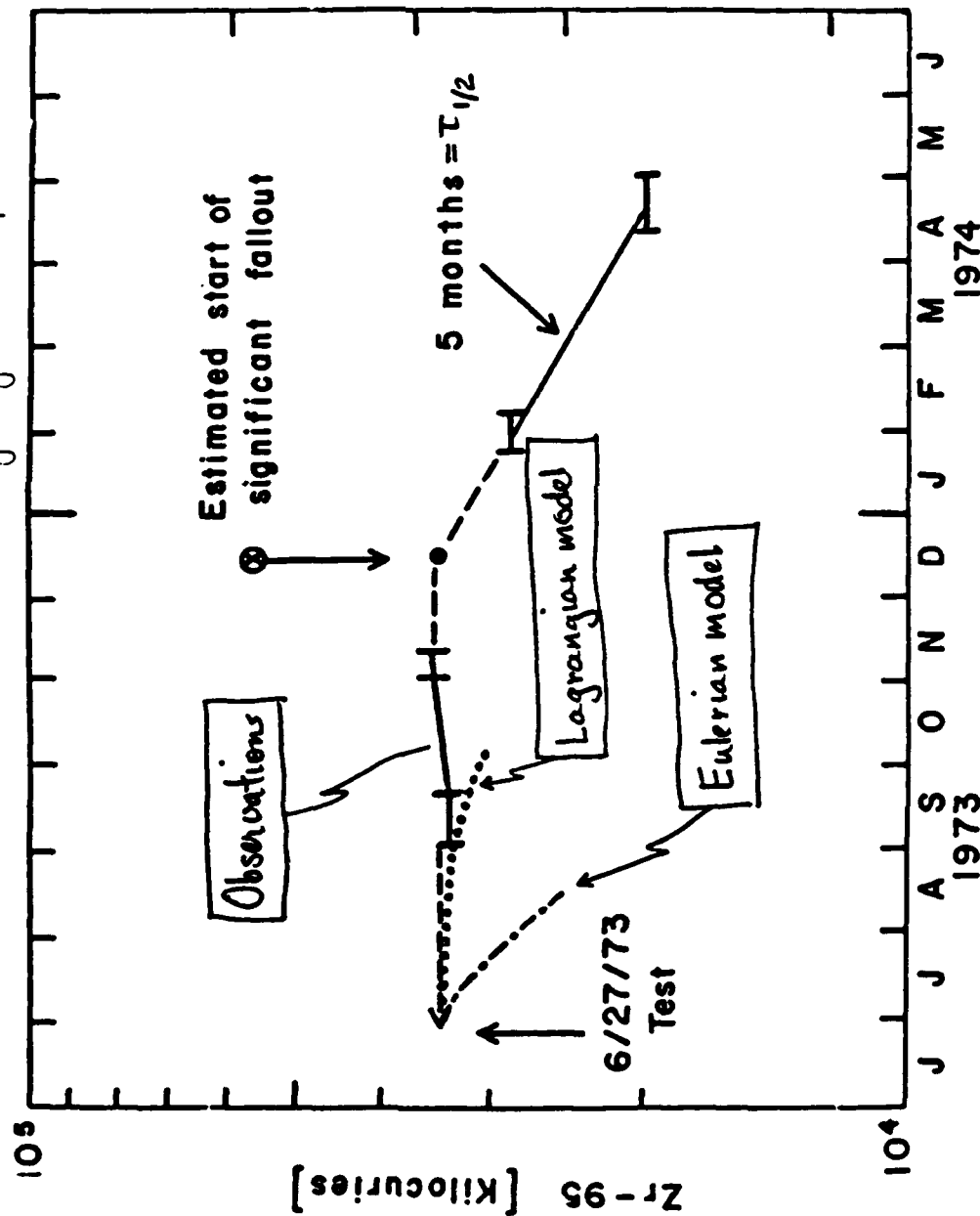
DAY=10.0



STRATOSPHERIC RESIDENCE TIME

- Some disagreement among observations, but recent data indicates 1/e-times of 1 year in lower stratosphere
- Observations show comparable residence times in stratosphere for gases (HTO), radionuclides, and volcanic sulfates
- Radionuclide data suggests no removal for a long period (3-6 months) following lower stratospheric injections
- Eulerian transport model gives immediate fallout with 1/e-times in lower stratosphere of 2-3 months
- Lagrangian transport model gives negligible removal for 2-3 months and slow removal thereafter (longer run with annual cycle needed to determine residence time)

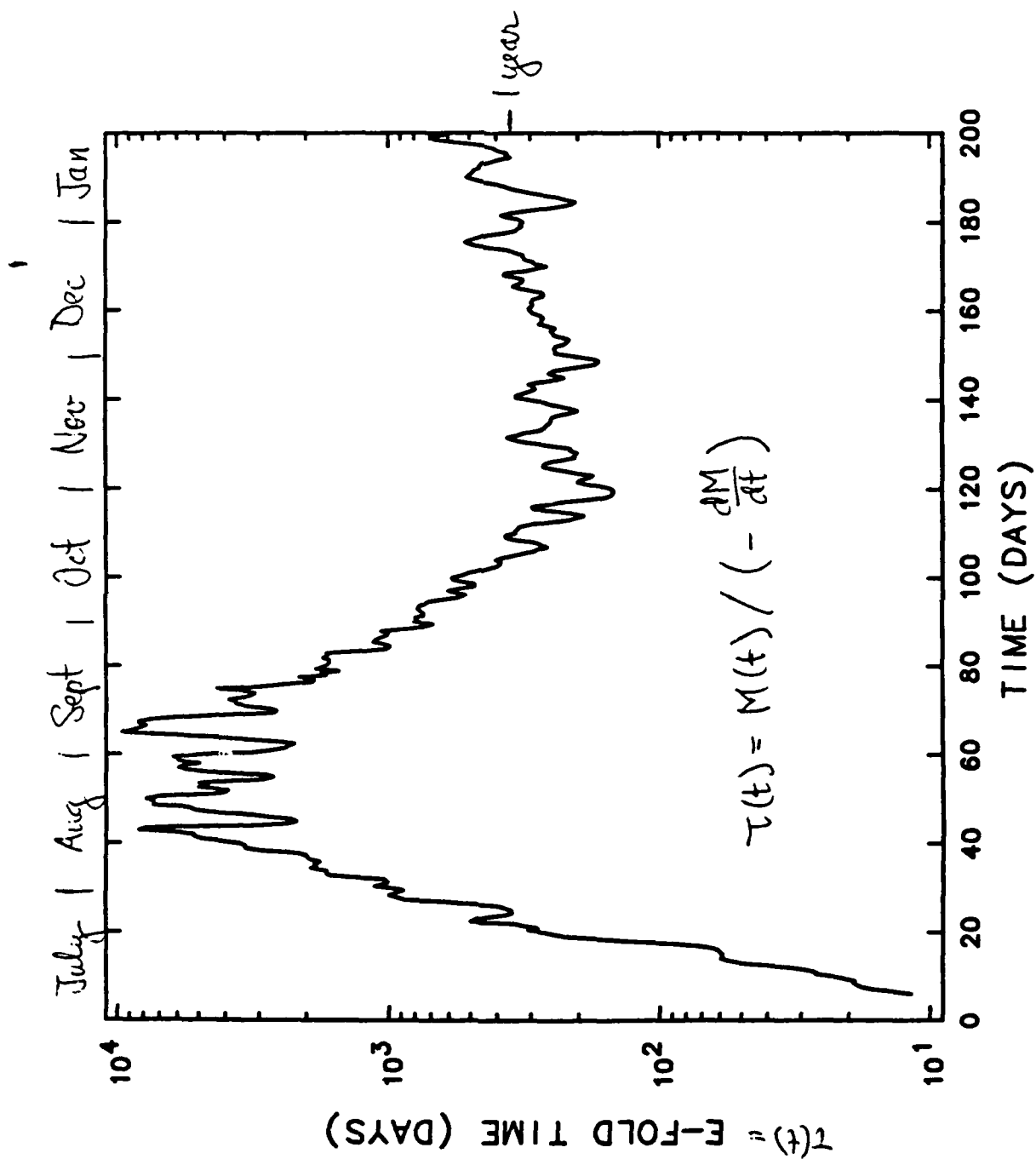
Stratospheric aerosol depletion: Comparison of Observations with Eulerian and Lagrangian Transport Models



Obs: Telegadas

Changes in Smoke Transport

- **Smoke lofting faster in new model than in old model**
 - **buoyancy greater in hot spots (stability-dependent vertical mixing of heat less efficient than DCA)**
 - **more inhomogeneous smoke distribution (Lagrangian model) drives smaller-scale circulations than does old (Eulerian) model**
 - **diurnal cycle: greater heating in daytime, followed by dilution due to dispersion; then subsidence at night?**
- **Less perturbation of tropical troposphere (less numerical diffusion horizontally and vertically)**
- **Longer residence times (≈ 1 yr) than before ($\approx 1/2$ yr), evolving plausibly with changing solar declination**



Smoke Mass Fraction Remaining

180 Tg injections, NAS profile

Lagrangian transport of smoke

Annual cycle

Precipitation scavenging

Gravitational sedimentation (1μ)

No coagulation

No reactions with ozone

<u>Injected in</u>	<u>Smoke mass fraction after 20 days</u>	
	<u>Lagrangian model</u>	<u>Eulerian model</u>
late June	47%	42%
mid-April	42%	
mid-August	42%	
mid-October	32%	
late December	27%	25%

<u>Injected in</u>	<u>Smoke mass fraction after 200 days</u>	
	<u>Lagrangian model</u>	
late June	31%	(annual cycle to January)

Chemical Reaction of Smoke with Ozone

(*Conjectures* about likely interactions with transport)

- **If reaction time is short (< few days)**
 - **thermal perturbations by smoke reduced**
 - **smoke lofting and spreading reduced**
 - **ozone depletion concentrated in northern midlatitudes**

- **If reaction time is long (> 1 month)**
 - **thermal perturbation and smoke distribution similar to present model**
 - **ozone depletion will occur in both hemispheres**
 - **solar heating of smoke further reduces ozone through temperature-dependence of ozone reactions (Vupputuri)**

**Improvements in the
Los Alamos Global Climate Model
and their Effects on
Nuclear Winter Simulations**

**Gary Glatzmaier, Bob Malone,
and David Langley**

**Earth and Space Sciences Division
Los Alamos National Laboratory**

IMPROVEMENTS IN THE LOS ALAMOS GLOBAL CLIMATE MODEL AND THEIR EFFECTS ON NUCLEAR WINTER SIMULATIONS

**Gary A. Glatzmaier and Robert C. Malone
Los Alamos National Laboratory**

We have improved the Los Alamos global climate model in several ways in order to obtain more realistic nuclear winter simulations. Our new model has absorption of infrared radiation by smoke, stability-dependent vertical diffusion in the atmosphere, heat and moisture storage in the soil, Lagrangian transport of smoke, and diurnal and annual cycles.

The absorption of infrared radiation by smoke moderates surface cooling by about 15-25%, in agreement with previous investigations.

The fixed, linear, stability-independent vertical diffusion coefficients for momentum, heat, and water vapor and the infinitely efficient "dry-convective-adjustment" algorithm of the old model have been replaced with time-varying nonlinear vertical diffusion coefficients that depend on the local atmospheric stability and wind shear. For the simulated normal atmosphere, this nonlinear diffusion is significant only in the lower one to two kilometers, the planetary boundary layer, where the atmosphere can become unstable to small-scale turbulence. However, for a simulated nuclear winter, solar-heating of lofted smoke produces a stable inversion in the troposphere which severely reduces the vertical diffusion coefficients during the first week.

For the calculation of surface temperatures, we replaced the diagnostic "heat-balance" algorithm of the old model with prognostic equations describing heat storage and thermal diffusion in six soil layers down to five meters below the surface. In addition, the time-independent saturated soil moisture condition of the old model was replaced with prognostic equations describing surface and subsurface storage of moisture.

With the nonlinear, time and spatially dependent, vertical diffusion in the atmosphere and the heat storage in the soil, we are now able to run with a diurnal cycle.

The Eulerian transport of smoke in our old model has been replaced by a Lagrangian transport scheme (described by R. Malone) which allows us to make longer nuclear winter simulations with an annual cycle.

The influences of all these model improvements on surface cooling and smoke lofting and residence time will be described.

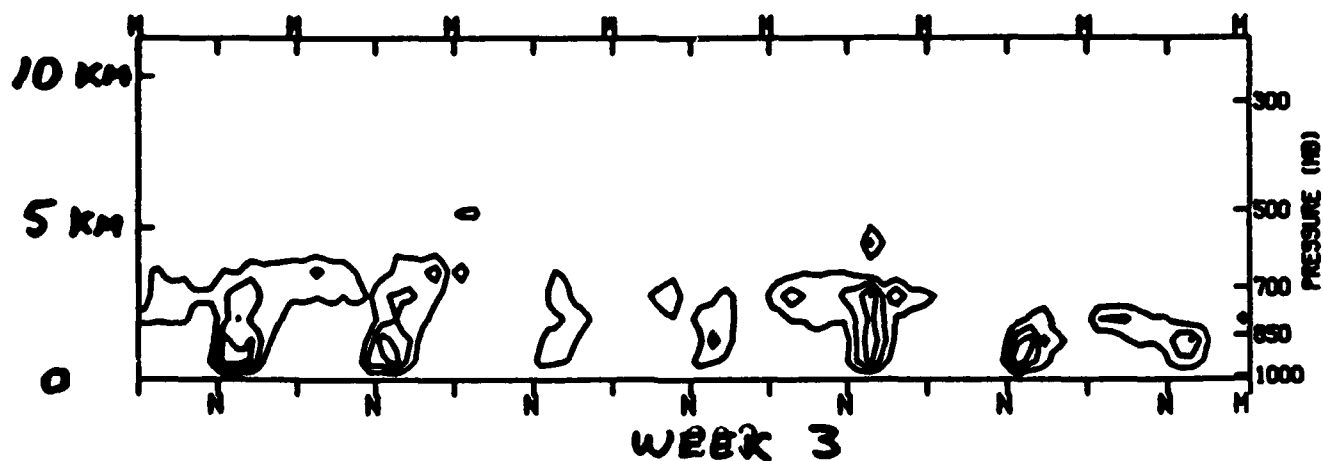
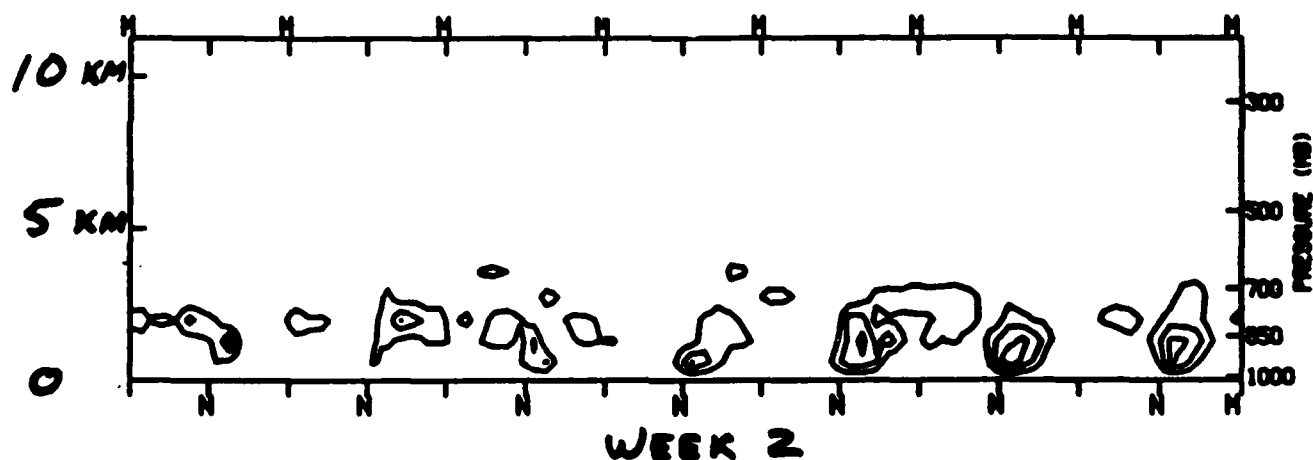
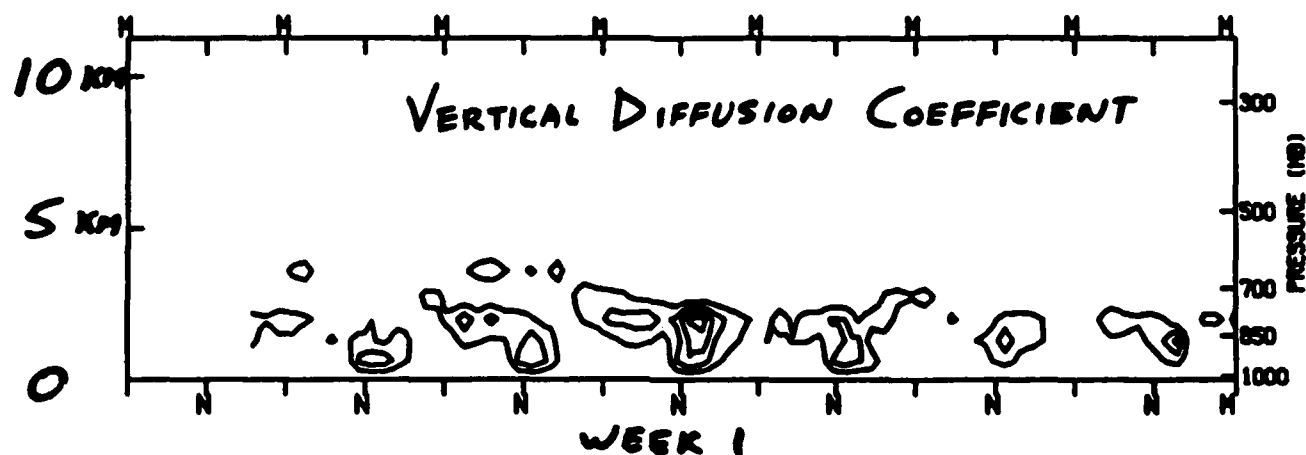
Improvements in the Los Alamos Global Climate Model

- **Subsurface storage and vertical diffusion of moisture in a 2-level soil model (10cm, 50cm).**
- **Subsurface storage and vertical diffusion of heat in a 6-level soil model (5cm - 5m).**
- **Stability-dependent vertical diffusion in the 20-level atmospheric model (30m - 30km).**
- **Absorption of infrared radiation by smoke.**
- **High-resolution, non-diffusive Lagrangian transport of smoke.**
- **Annual cycle of solar declination.**
- **Diurnal cycle of solar zenith angle.**

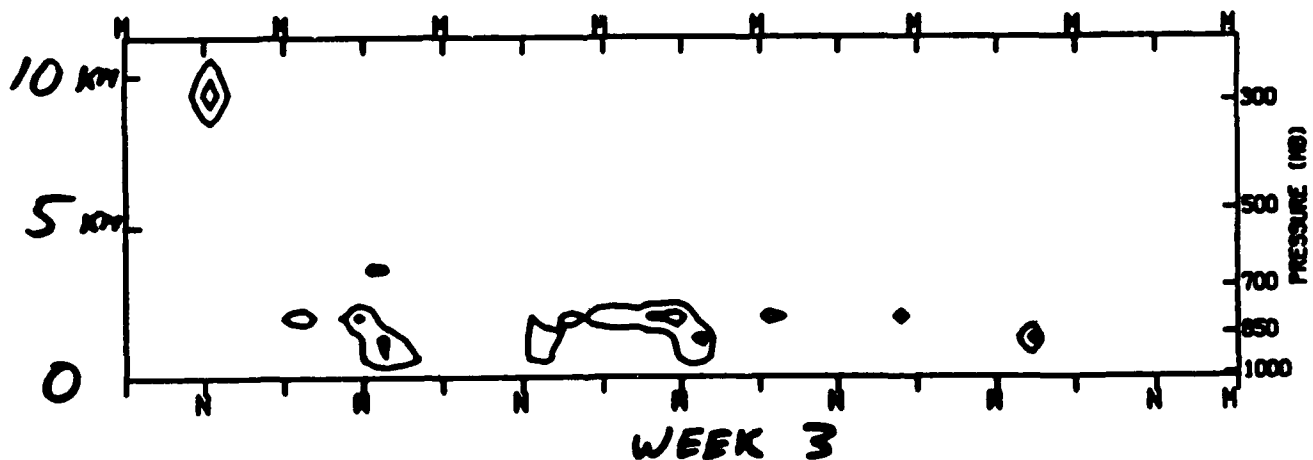
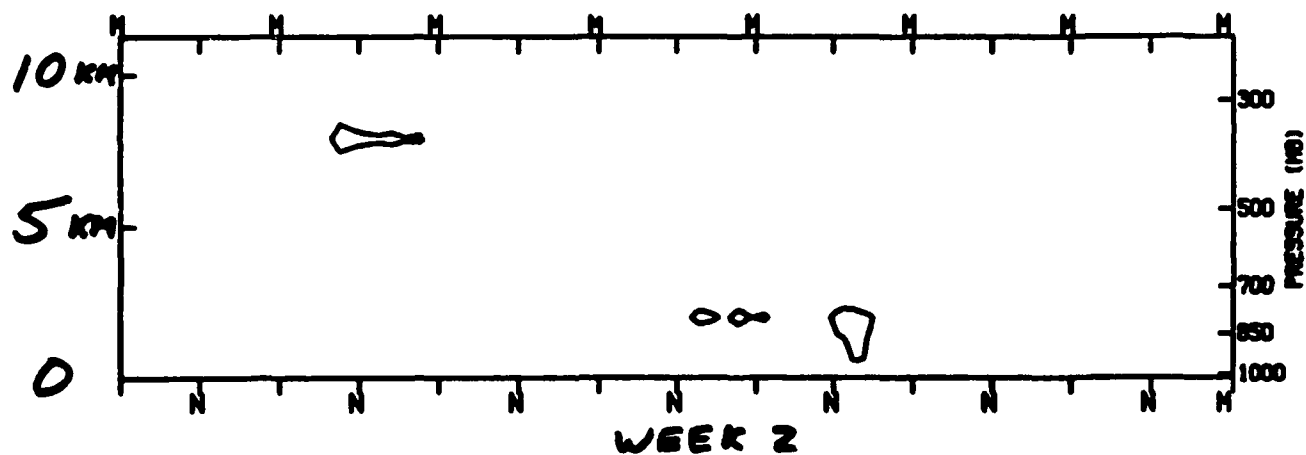
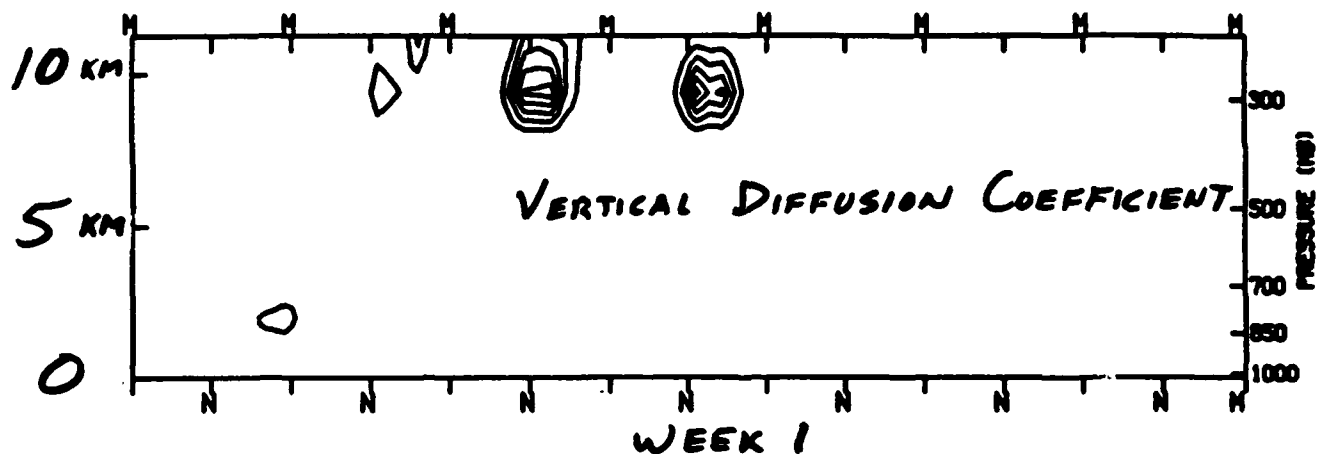
Stability-Dependent Vertical Mixing

- **Richardson number-dependent vertical diffusion coefficient computed locally**
- **Replaces "dry convective adjustment" and neutral-stability linear vertical diffusion**
- **In normal atmosphere, active only in PBL**
- **During nuclear winter, active in PBL and in free atmosphere above smoke clouds**
- **Vertical mixing in PBL ceases over land during first week of nuclear winter due to stable inversion.**
- **Because new method mixes less efficiently than DCA, hot spots in the atmosphere are more buoyant. Smoke lofting is faster than in old model with DCA.**

UNPERTURBED
(JUN 29 - JUL 19)



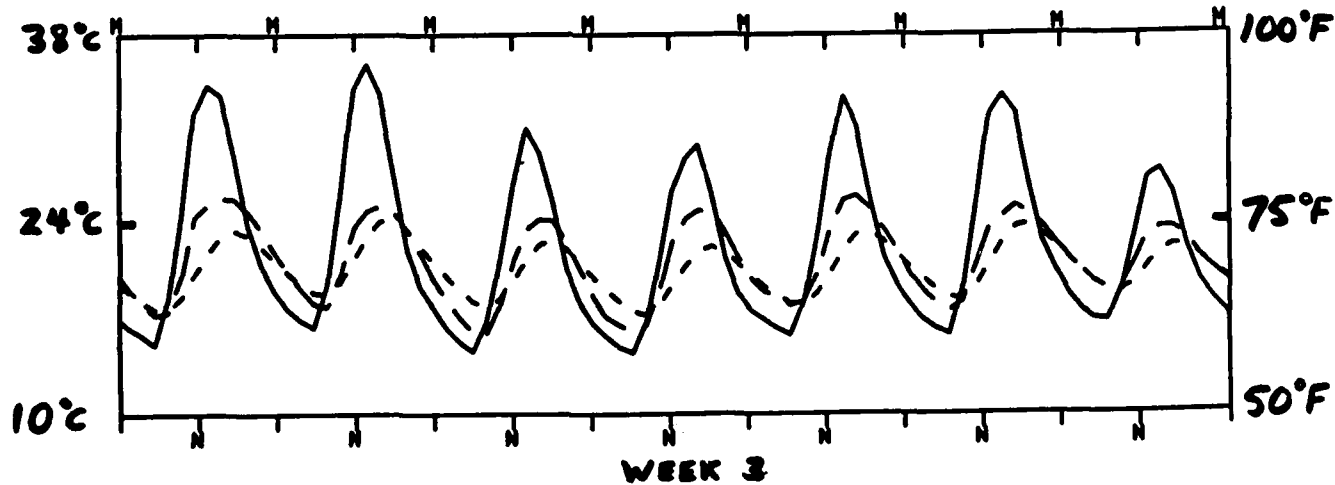
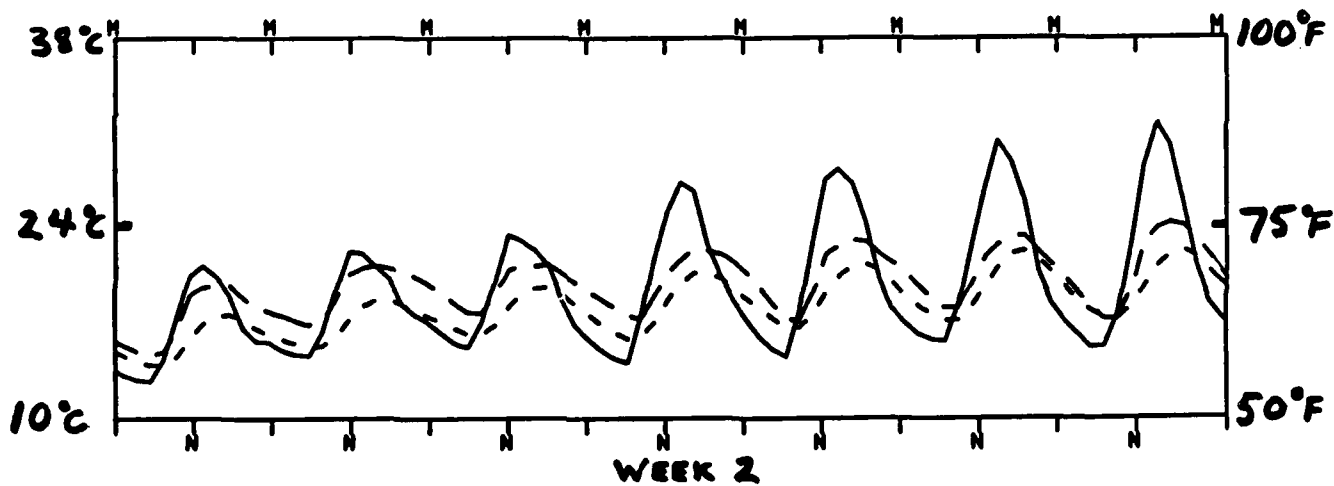
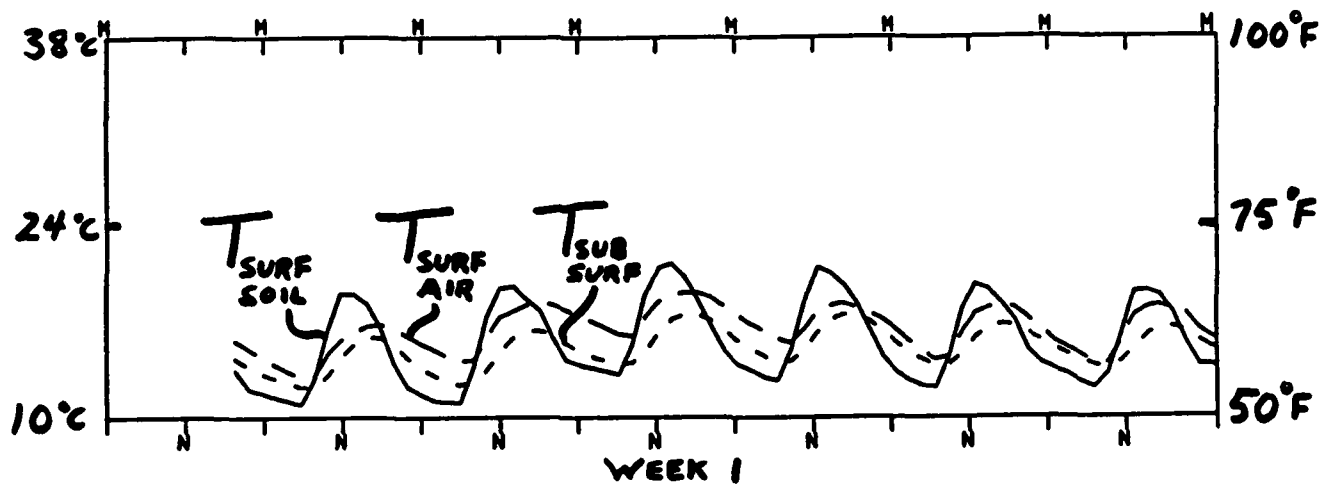
NUCLEAR WINTER (JUN 29 - JUL 19)



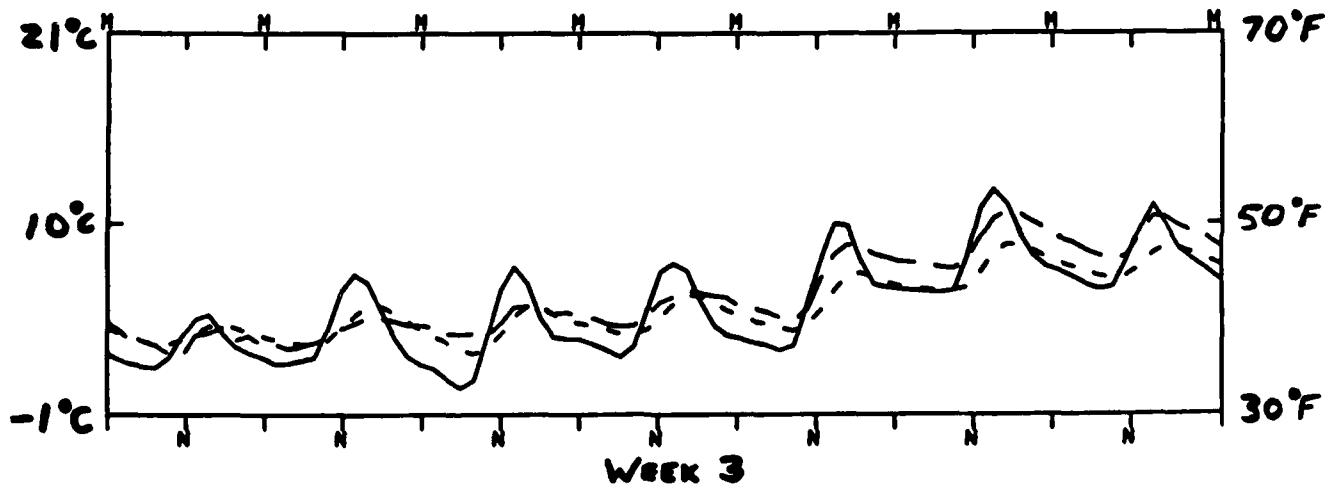
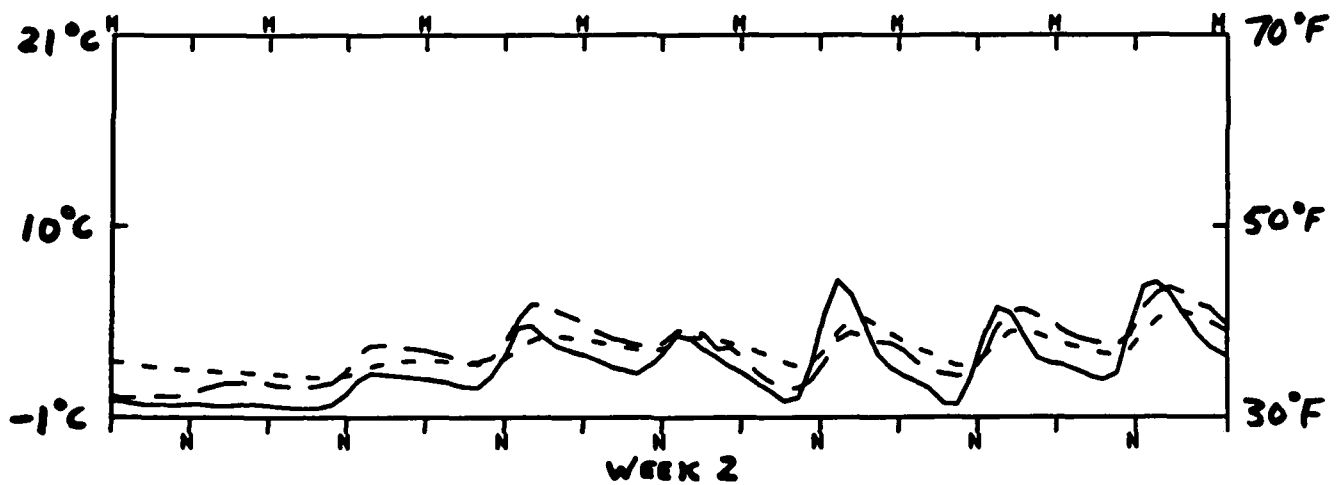
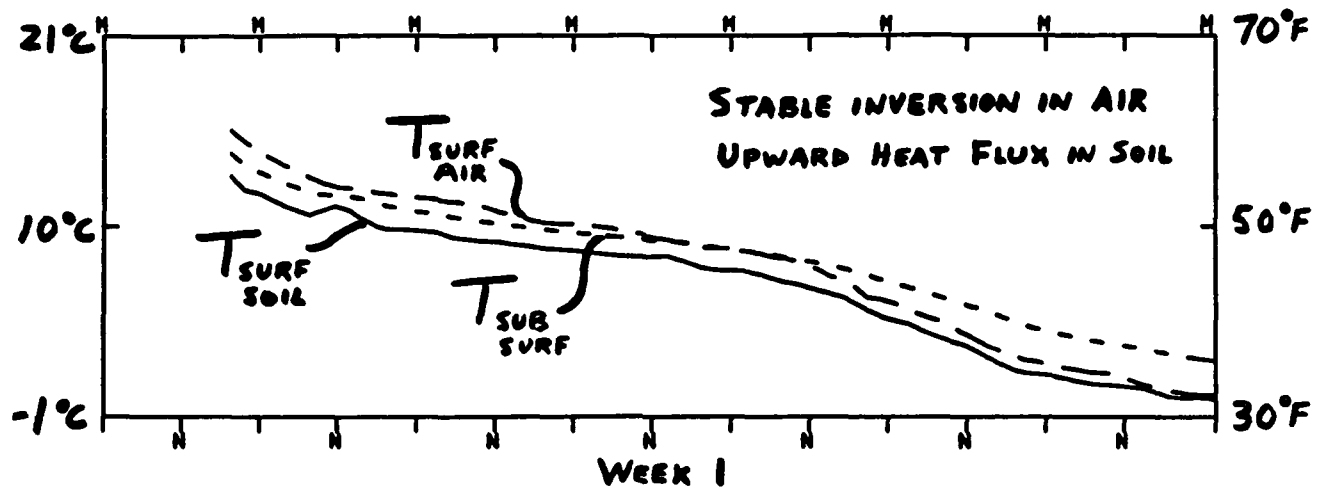
Subsurface Heat and Water Storage and Diffusion

- **For temperature, 6 nonuniform levels to 5m**
- **For water, 2-layer "bucket model"**
- **Replaces simple energy balance assumption (no soil heat capacity) and fixed wetness**
- **Thermal inertia needed for diurnal cycle**
- **Upward diffusion supplies heat to surface when radiation deficit occurs (polar night and nuclear winter)**
- **When atmosphere is stable, upward diffusion of heat approximately compensates for absence of erroneous heat flux supplied in old model by "neutral-stability linear vertical diffusion".**

UNPERTURBED (JUN 29 - JUL 19)



NUCLEAR WINTER (JUN 29 - JUL 19)



Modification of predicted surface cooling by model improvements

ΔT = change in surface air temperature
relative to an unperturbed July,
averaged over the USA,
averaged over days 5-15.

	$\Delta T(^{\circ}\text{C})$	$\delta(\Delta T)$
"Old Model"	-15	
+ heat and moisture storage in soil	-10	+5
+ stability-dependent vertical diffusion	-11	-1
+ absorption of IR by smoke	-8	+3
+ Lagrangian transport of smoke	-8	0
+ diurnal cycle	-8	0

Seasonal dependence of predicted surface cooling

ΔT = change in surface air temperature
relative to an unperturbed season,
averaged over the USA,
averaged over days 5-15.

	$\Delta T(^{\circ}\text{C})$
July	-8
October	-6
April	-5
January	-4

200 day evolution of predicted surface cooling (Jun 29 - Jan 15)

**ΔT = change in surface air temperature
relative to an unperturbed season,
averaged over the USA,
averaged over a ten-day period.**

**τ = optical depth,
averaged over the USA,
averaged over the ten-day period.**

Days	$\Delta T(^{\circ}\text{C})$	τ
5-15 (Jul 4 - Jul 14)	-8	2.0
30-40 (Jul 29 - Aug 8)	-1	0.6
190-200 (Jan 5 - Jan 15)	-4	0.4

A Theory of Radiative-Dynamical Instability*

STEVEN J. GHAN

**Lawrence Livermore National Laboratory
Livermore, CA 94550**

ABSTRACT

Numerical simulations of the global scale response to summertime injections of absorptive smoke into the atmosphere exhibit a self-lofting mechanism, in which radiative heating and the dynamical circulation interact to loft the smoke to ever higher altitudes. After making several plausible approximations, I shall demonstrate that for small perturbations this mechanism is an unstable interaction.

Linearized equations governing the conservation of vorticity, enthalpy, and aerosol concentration are solved analytically under certain assumptions, producing an expression for the exponential growth rate of internal waves propagating in a stratified fluid with a strong vertical gradient in the distribution of solar-absorbing aerosols. Comparison of the analytical growth rate with smoke lofting rates simulated by GCMs yields reasonable agreement, thus providing theoretical support for the numerical results.

*This work was performed under the auspices of the U.S. Department of Energy by the Lawrence Livermore National Laboratory under Contract W-7405-Eng-48.

July Day = 0.5



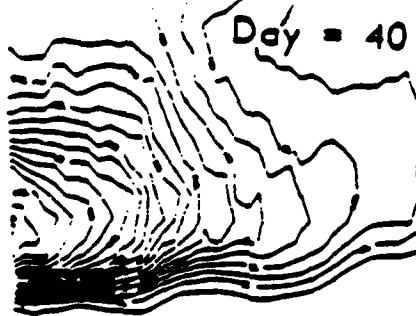
Day = 5



Day = 10



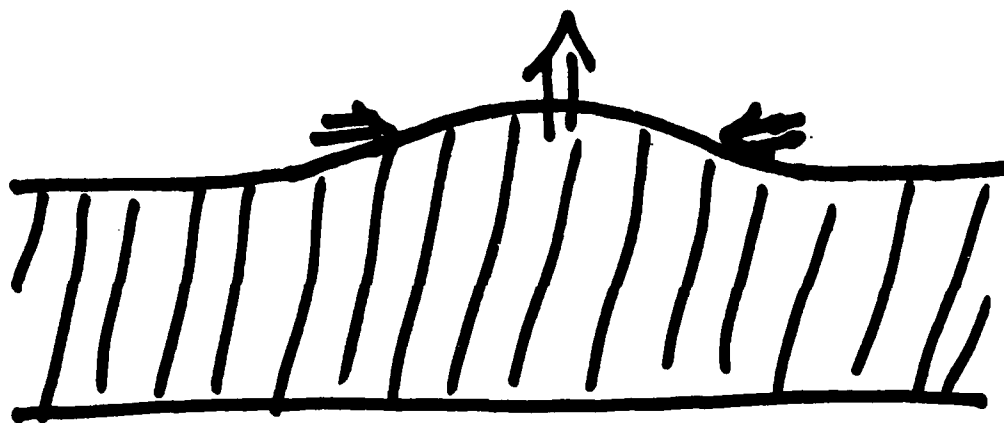
Day = 40



Why a theory?

- Deepens understanding
- Reveals parametric dependence
- Applies to some scales not resolved by GCMs
- Independent of numerical treatment

Physical Mechanism



General Procedure

- Express heating in terms of absorber mixing ratio
- Linearize equations for mass, momentum, heat, absorber
- Reduce system to single PDE
- Assume solution form $e^{i(kx+ly+mz-\sigma t)}$
- Solve resulting algebraic equation for σ
- Solutions unstable for $\text{Im}(\sigma) > 0$

Radiative Heating

- Neglect scattering
- Grey approximation

$$Q(z) = -\frac{\partial E}{\partial z} = -\mu S_0 \frac{\partial T}{\partial z}$$

$$= S_0 \alpha \rho_0 g(z) T(z)$$

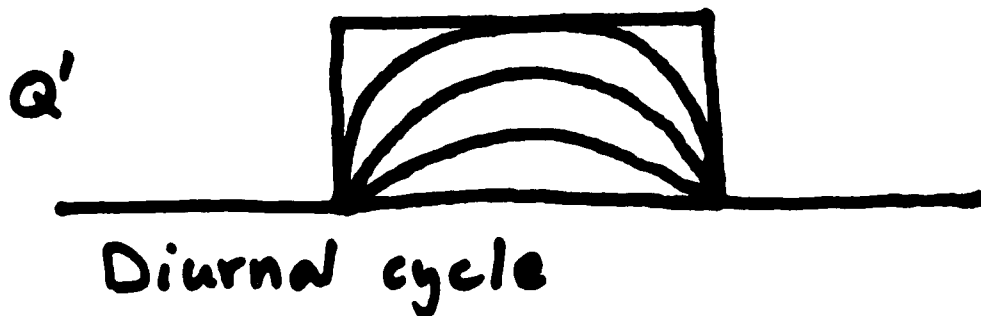
where

$$T(z) = \exp\left(-\frac{1}{\mu} \int_z^{\infty} \alpha \rho_0 g dz'\right)$$

For small perturbations

$$Q' \approx \begin{cases} S_0 \alpha \rho_0 \bar{T} g' & \mu \geq 0 \\ 0 & \mu < 0 \end{cases}$$

Note: Q' independent of μ for $\bar{T} \neq 1$



Quasi-Geostrophic Flow

$$D \nabla^2 \psi + \beta \frac{\partial \psi}{\partial x} = f \frac{\partial w}{\partial z} \quad \text{vorticity}$$

$$f D \frac{\partial \psi}{\partial z} = -N^2 w + \frac{RQ}{c_p \rho_0 H} \quad \text{heat}$$

where

$$D \equiv \frac{\partial}{\partial t} + u_0 \frac{\partial}{\partial x} + \frac{\partial}{\partial t}$$

Eliminate ψ

$$f^2 D \frac{\partial^2 w}{\partial z^2} + (D \nabla^2 + \beta \frac{\partial}{\partial x}) (N^2 w - \frac{RQ}{c_p \rho_0 H}) = 0$$

Combine with

$$Q = S_0 \rho_0 \bar{T} q$$

$$Dq = -\frac{\partial \bar{q}}{\partial z} w$$

Yields

$$f^2 D^2 \frac{\partial^2 w}{\partial z^2} + N^2 (D \nabla^2 + \beta \frac{\partial}{\partial x}) (D - \alpha) w = 0$$

where

$$\alpha = - \frac{R S_0 \rho_0 \bar{T}}{c_p N^2 H} \frac{\partial \bar{q}}{\partial z}$$

Assume constant N^2, α

Solution form

$$w(x, y, z, t) = w_0 e^{i(kx + ly + mz - \sigma t)}$$

Then $D = -i\sigma + u_0 ik + z^{-1}$

unstable for $\text{Re}(D) > z^{-1}$

Substitute into wave equation

$$\Rightarrow f_0^2 m^2 D^2 + N^2 (k^2 D - ik\beta)(D - \alpha) = 0$$

quadratic in D

Two solutions:

- Rossby mode unstable for $\alpha < 0$
- Advective mode unstable for $\alpha > 0$

Primitive Equations

$$\frac{\partial u}{\partial x} + \frac{\partial v}{\partial y} + \frac{\partial w}{\partial z} = 0$$

$$Du - fv = -\frac{\partial \phi}{\partial x}$$

$$Dv + fu = -\frac{\partial \phi}{\partial y}$$

$$D\frac{\partial \phi}{\partial z} = -N^2 w + \frac{RQ}{c_p \rho_0 H}$$

$$Q = S_0 \alpha \rho_0 \bar{T} q$$

$$Dq = -\frac{\partial \bar{q}}{\partial z} w$$

Reduce to single equation for v

$$(D^2 + f^2) D^2 \frac{\partial^2 v}{\partial z^2} + N^2 (D D^2 + \beta \frac{\partial}{\partial x}) (D - \alpha) v = 0$$

Quartic in D

Four solutions:

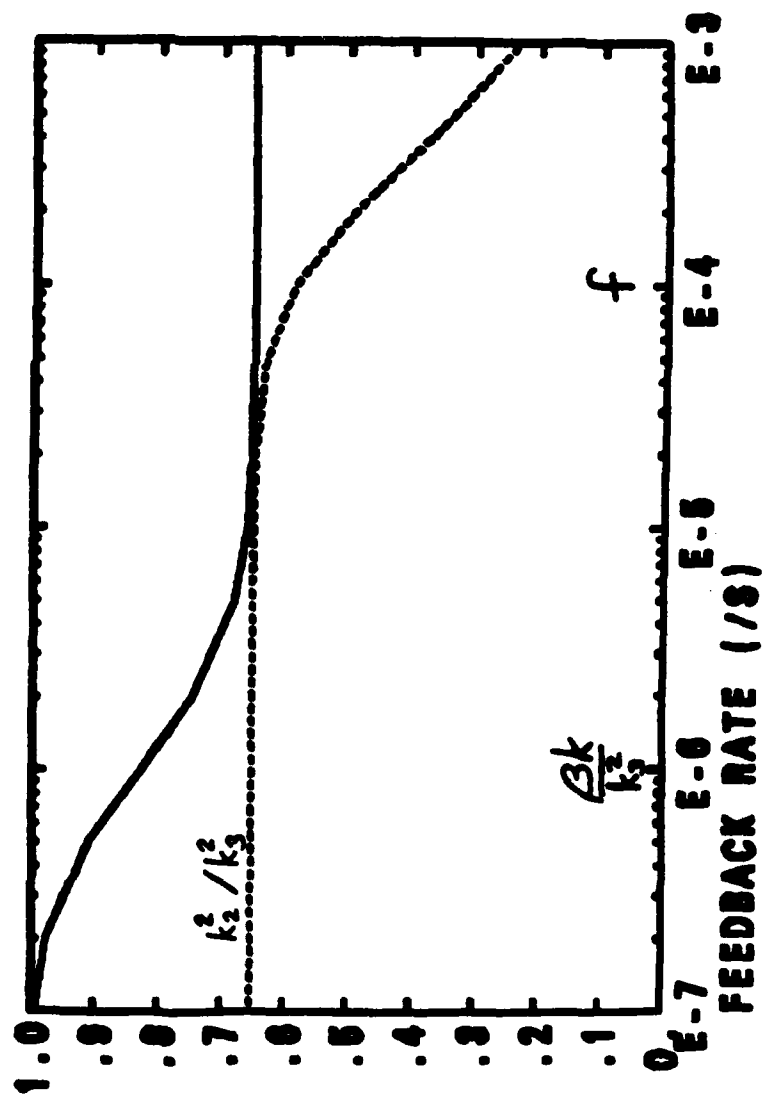
- Rossby, both gravity modes unstable for $\alpha < 0$
- Advective mode unstable for $\alpha > 0$

Additional modes with $v = 0$

GROWTH RATE / FEEDBACK RATE

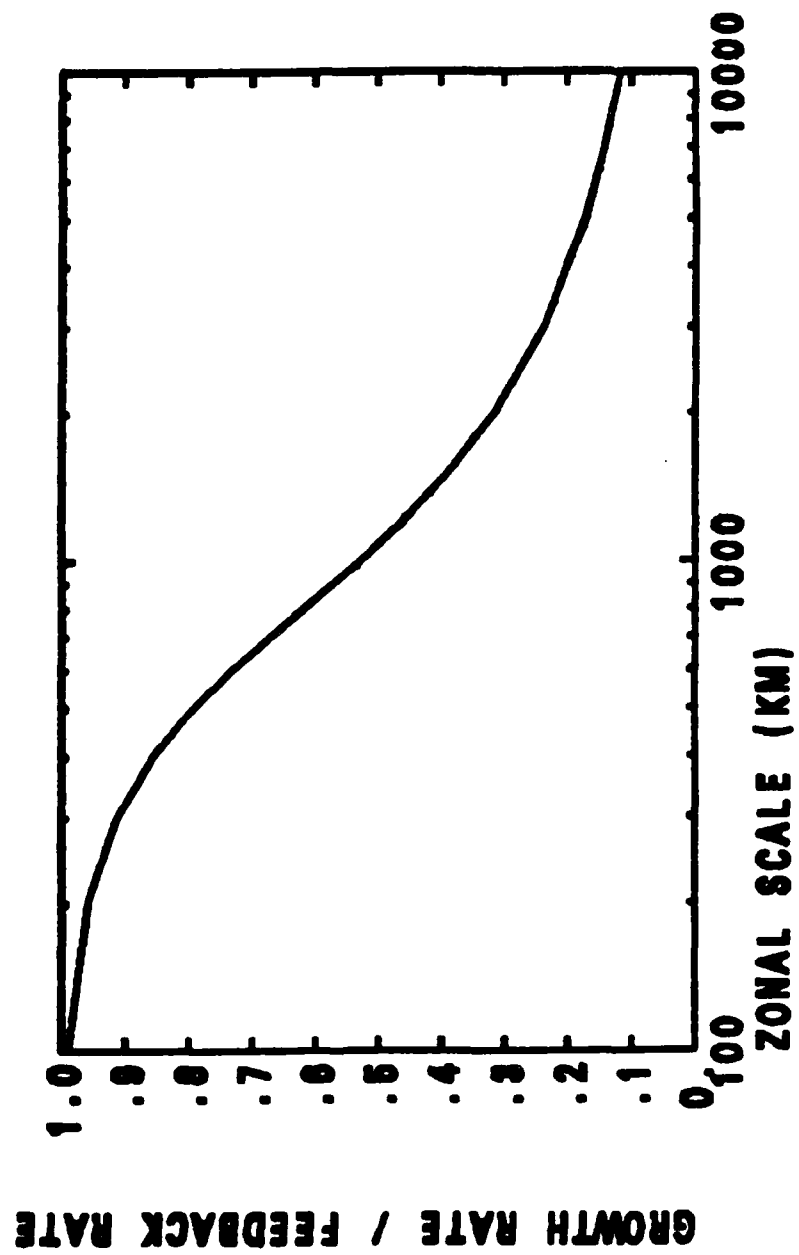
----- PRIMITIVE EQUATIONS F-PLANE
 ——— QUASI-GEOSTROPHIC BETA-PLANE

XL- 1000 KM YL- 1000 KM ZL- 10 KM



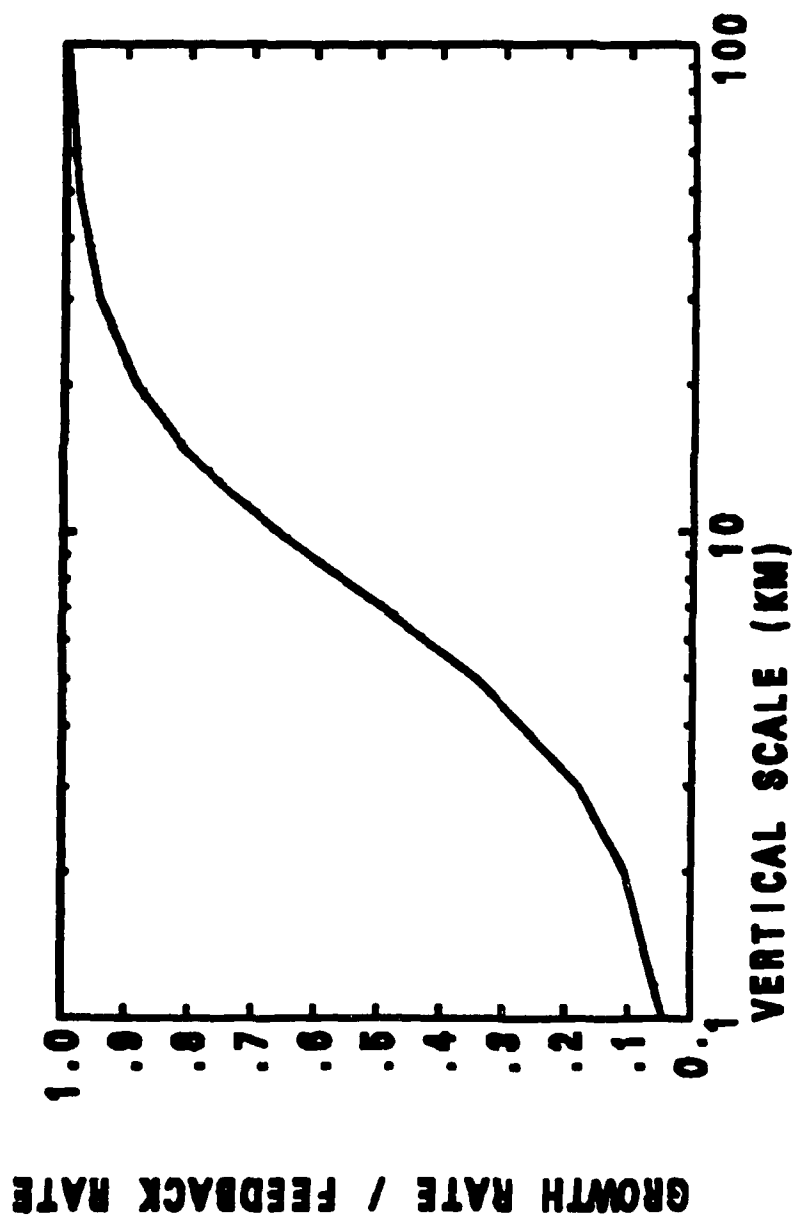
QUASI-GEOSTROPHIC BETA-PLANE

YL-10000 KM ZL- 10 KM ALPHA- 1.E-08



QUASI-GEOSTROPHIC BETA-PLANE

XL- 1000 KM YL- 1000 KM ALPHA- $1.E-05$



The radiative-dynamical feedback

- renders the advective mode unstable for $\alpha > 0$
- for a given α , the growth rate is largest for short, deep perturbations
- the growth rate never exceeds the feedback rate α

Radiative-Dynamical Feedback Rate

$$\alpha = - \frac{R S_0 a \bar{T}}{c_p N^2 H} \frac{\partial \bar{\theta}}{\partial z}$$

Assume $\bar{\theta}(z)$ decreases exponentially with scale height h . Then

$$a \frac{\partial \bar{\theta}}{\partial z} = - \frac{a \bar{\theta}}{h} = - \frac{\tau_a}{\rho_0} \frac{H+h}{H h^2}$$

For typical terrestrial values,

$$\alpha \sim 400 \tau_a \exp(-\frac{\tau_a}{\mu}) \frac{H+h}{H h^2}$$

Maximum: $\frac{\partial \alpha}{\partial \tau_a} = 0$ for $\tau_a = \mu$

$$\alpha_{\max} \sim 150 \mu \frac{H+h}{H h^2}$$

For $\mu=1$, $\alpha_{\max} \sim (3.4 \text{ days})^{-1}$ for $h=10^4 \text{ m}$
 $\sim (1.6 \text{ hours})^{-1}$ for $h=10^3 \text{ m}$

Necessary Assumptions

- Hydrostatic
- Small perturbations
- Basic state :
 - horizontally uniform
 - no vertical shear
 - constant N^2
 - constant α
- No scattering
- No infrared effects

Unstable Radiative-Dynamical Interactions

Steven J. Ghan

Lawrence Livermore National Laboratory

An outstanding feature of the terrestrial and Martian atmospheres is their near-transparency with respect to solar radiation. Although terrestrial water clouds scatter a significant fraction of the incoming solar radiation, and ozone absorbs much of the ultraviolet radiation, most absorption of visible radiation normally occurs at the surface. Radiative heating rates throughout most of the troposphere are dominated by infrared radiative cooling.

In the Martian atmosphere this situation is occasionally disrupted by global-scale dust storms, which increase the solar opacity of the atmosphere, leading to substantial tropospheric warming. Although such global storms fortunately do not develop in the terrestrial atmosphere, recent numerical simulations (Malone et al., 1986) involving the terrestrial atmospheric response to massive injections of absorptive smoke produced by hypothetical post-nuclear war fires have exhibited a similar phenomenon. Substantial lofting of the smoke is found to occur in these simulations, suggesting that the feedback between short-wave radiative heating and the dynamical response to the heating can be important.

Although the interaction between the aerosol distribution, the shortwave radiative heating, and the dynamical circulation in Martian dust storms and in hypothetical terrestrial smoke storms is appreciated in the literature, the unstable nature of the interaction has not been rigorously demonstrated. Gierasch et al. (1973) discuss a radiative instability mechanism involving clouds, but it is driven by longwave radiation. Gierasch and Goody

(1973) define a growth phase for Martian dust storms, but treat the dynamical circulation diagnostically rather than prognostically. Leovy et al. (1973) treat the dynamical circulation prognostically, but simply prescribe the aerosol distribution. Aside from these early analytical attempts to explain extraterrestrial cloud bands and Martian dust storms, most subsequent work on the radiative-dynamical interaction has been numerical (Haberle et al., 1982; Haberle et al., 1985; Malone et al., 1986). Thus, a rigorous theoretical demonstration of the shortwave radiative-dynamical instability, and an analysis of the conditions under which it is important, does not presently exist. Given the current interest in Martian dust storms, hypothetical terrestrial smoke storms, and radiative-dynamical interactions in general, such a theory is desirable. Here I shall summarize the progress I have made in developing just such a theory.

The theory is based on a variety of simplifying approximations. Necessary assumptions are that the atmosphere is hydrostatic, that perturbations to an assumed basic state are small, that short-wave scattering and infrared emission by the absorber are unimportant, and that the basic state is horizontally uniform with no vertical variations in the basic state flow, the Brunt-Vaisala frequency N , or in the radiative-dynamical feedback rate

$$\alpha = -\frac{RS_0a\bar{T}}{c_p N^2 H} \frac{\partial \bar{q}}{\partial z}$$

where R is the gas constant, S_0 is the solar constant, a is the absorption cross-section of the absorber, \bar{T} is the basic state short-wave transmissivity, c_p is the specific heat at constant pressure, H is the density scale height, z is altitude, and \bar{q} is the basic state absorber mixing ratio. Additional simplifying assumptions, which can be relaxed for a more general, but complicated analysis, are that solar absorption is "grey", that damping of perturbations is equally rapid for momentum, heat, and absorber mixing ratio, that density is constant (the Boussinesq approximation), and that motions are quasi-geostrophic and localized enough to neglect the sphericity of the earth and latitudinal variations in the Coriolis parameter f .

The general solution procedure is to first express the solar heating in terms of perturbations in the distribution of absorber q . The equations governing conservation of mass, momentum, heat and absorber mixing ratio are then linearized about the basic state. The linear system of equations is then reduced to a single partial differential equation (PDE). By expressing solutions in terms of orthogonal basis functions with a time dependence given by $\exp(-i\sigma t)$, the PDE reduces to an algebraic equation for σ . In the absence of dissipation, solutions are unstable if $\text{Im}(\sigma) > 0$.

In the absence of radiative-dynamical feedback ($\alpha=0$), solutions correspond to the Rossby mode, the advective mode, and (for the primitive equations) two inertia-gravity modes. The Rossby and inertia-gravity modes propagate with respect to the basic state flow, while the advective mode does not. All of these modes are neutrally stable.

In the presence of radiative-dynamical feedback, the advective mode becomes unstable for positive α (ie., basic state absorber decreasing with altitude). For a given feedback rate, the growth rate of disturbances is found to be greatest for short, deep perturbations, but never exceeds the feedback rate. For feedback rates less than the Coriolis parameter f , the quasi-geostrophic theory is accurate, while for feedback rates greater than the Rossby wave frequency the assumption of constant f is adequate. For feedback rates greater than f but less than the Rossby wave frequency, the growth rate is proportional to the feedback rate.

For negative α (absorber concentration decreasing with altitude), the advective mode is damped, but the Rossby and inertia-gravity modes are unstable. However, the net vertical transport of absorber mixing ratio for these circulation modes is downward rather than upward, so they cannot be responsible for the smoke lofting.

The feedback rate, because it characterizes the growth rate of perturbations, is the most important parameter of the problem. If one assumes that the absorber mixing ratio decreases exponentially with altitude, the feedback rate is found to be largest when the absorption optical depth equals the cosine of the solar zenith angle. Above this level,

the vertical gradient of absorber mixing ratio becomes small, while below this level, the transmission of solar radiation becomes small. For typical terrestrial values for R , S_0 , a , c_p , N , and H , the maximum feedback rate (ie., when the zenith angle is zero and the absorption optical depth is unity) is found to be $3.4 \times 10^{-6} \text{ s}^{-1}$ for an absorber scale height of 10 km, and $1.7 \times 10^{-4} \text{ s}^{-1}$ for an absorber scale height of 1 km, corresponding to time scales of 3.4 days and 1.6 hours, respectively. These feedback rates are consistent with the time scales of smoke lofting exhibited in the GCM simulations of Malone et al. (1986).

References

Gierasch, P. J., and R. M. Goody, 1973: A model of a Martian Great Dust Storm. *J. Atmos. Sci.*, 30, 169–179.

Gierasch, P. J., A. P. Ingersoll, and R. T. Williams, 1973: Radiative instability of a cloudy planetary atmosphere. *Icarus*, 19, 473–481.

Haberle, R. M., C. B. Leovy, and J. B. Pollack, 1982: Some effects of global dust storms on the atmospheric circulation of Mars. *Icarus*, 50, 322–367.

Haberle, R. M., T. P. Ackerman, O. B. Toon, and J. L. Hollingsworth, 1985: Global transport of atmospheric smoke following a major nuclear exchange. *Geophys. Res. Lett.*, 12, 405–408.

Leovy, C. B., R. W. Zurek, and J. B. Pollack, 1973: Mechanisms for Mars dust storms. *J. Atmos. Sci.*, 30, 749–762.

Malone, R. C., L. H. Auer, G. A. Glatzmaier, M. C. Wood, and O. B. Toon, 1986: Nuclear winter: Three-dimensional simulations including interactive transport, scavenging, and solar heating of smoke. *J. Geophys. Res.*, 91, 1039–1054.

CHRONIC EFFECTS OF LARGE ATMOSPHERIC SMOKE INJECTIONS: INTERACTIONS WITH THE OCEAN MIXED LAYER, SEA ICE, AND GROUND HYDROLOGY

Steven J. Ghan, Michael C. MacCracken, John J. Walton (all at: Lawrence Livermore National Laboratory, L-262, P.O. Box 808, Livermore, CA 94550).

A set of extended integrations is performed using a general circulation model of the troposphere and ocean mixed layer initialized with a large summertime injection of absorptive smoke over North America and Eurasia. The smoke is subject to coagulation and removal as well as advective and convective transport.

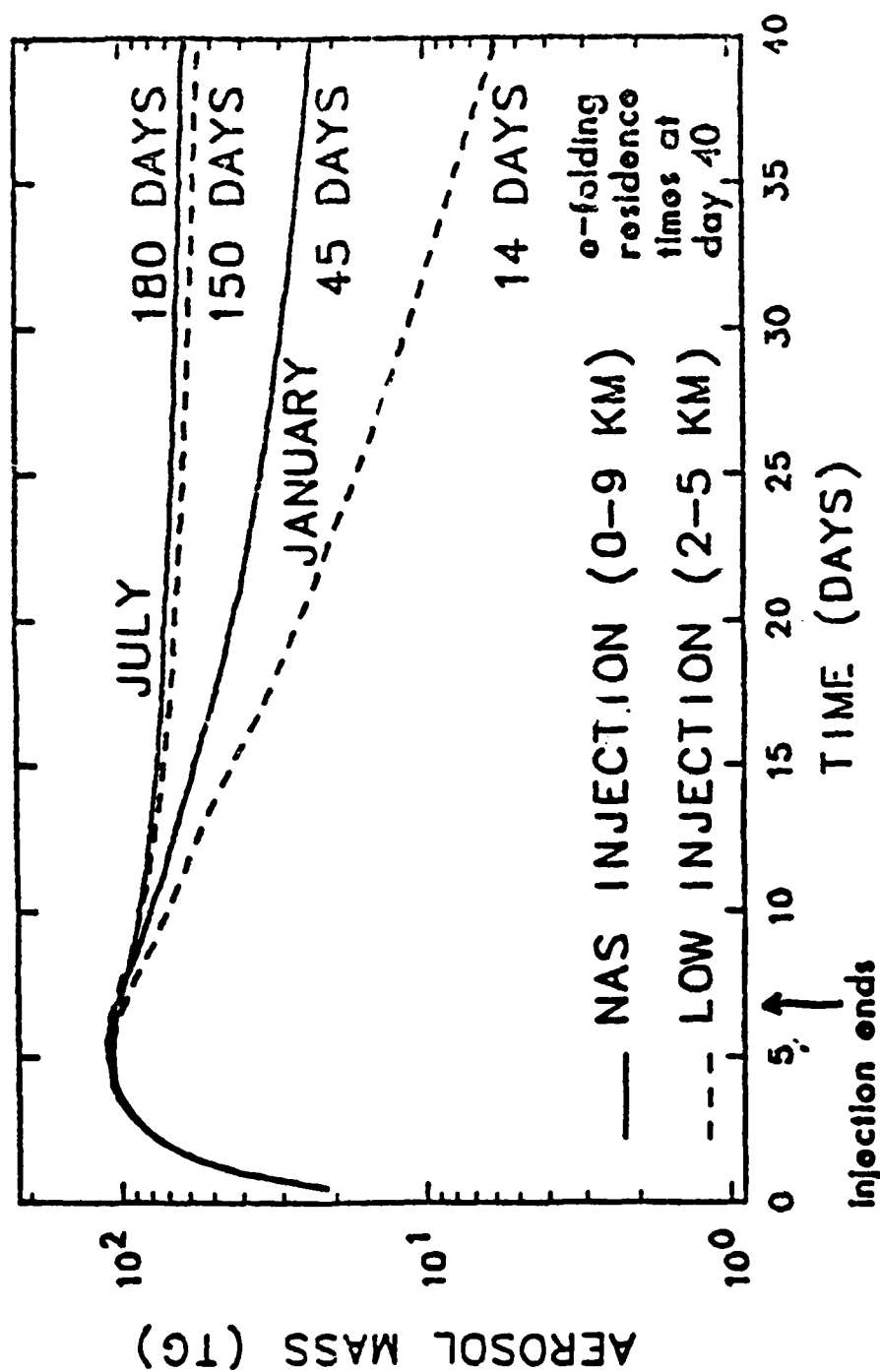
Several aspects of the climatic response support the conclusions of Robock using an energy balance climate model. The ocean mixed layer in northern midlatitudes cools 5-10 K relative to the control climate within three months. During the northern winter following the injection, this cooling decreases as a result of the reduction in smoke and the smaller wintertime insolation. During the following northern summer, enhanced sea ice coverage insulates the ocean mixed layer from the atmosphere, hence reducing summertime warming at the normal ice margin. During the subsequent winter, the enhanced sea ice coverage reduces the surface heat capacity, hence increasing wintertime cooling of the ocean surface, but reducing the cooling of the ocean mixed layer.

Other aspects of the response are quite different, however. Due to a smoke-induced reduction in land precipitation, substantial surface warming and drying occurs in the tropics during the first months following the injection. In addition, the ocean mixed layer deepens considerably as a result of entrainment induced by both greater surface cooling and enhanced mechanical stirring.

This work was performed under the auspices of the U.S. Department of energy by the Lawrence Livermore National Laboratory under Contract W-405-Eng-48.

INFLUENCE OF SOLAR HEATING ON SCAVENGING

Interactive Tracer: "Low" and "NAS" Injections. 170 Tg



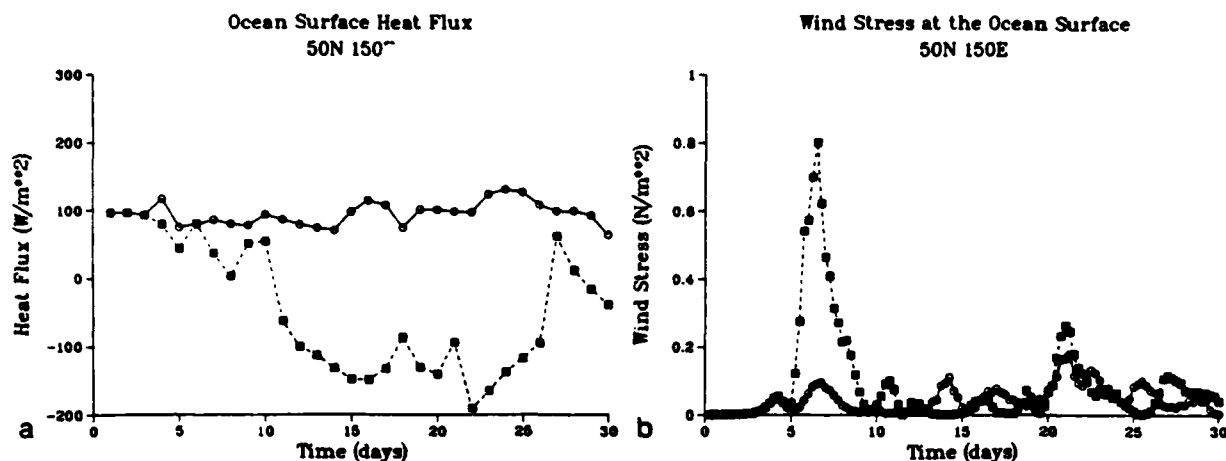


Fig. 4. Time evolution of the calibrated (a) net surface heat flux Q_s and (b) surface wind stress τ at 50°N , 150°E used in the control experiment (solid lines) and the nuclear winter experiment (dashed).

By examining Table 2 and Figures 2 and 3, it is possible to determine for each geographical location whether the model-simulated SST decrease during the nuclear winter experiment was due to enhanced air-sea cooling or entrainment. For example, at the first location (50°N , 150°W), the net heat flux into the ocean was 55 W m^{-2} less during the nuclear winter experiment than during the control experiment (Table 2). If the average MLD at this location during nuclear winter is taken to be 50 m (Figure 3), this decrease in surface heat flux cannot account for more than a 1°C difference in SST at the end of the month. This implies that well over half of the 2.8°C decrease in SST in the nuclear winter experiment (Figure 2) was caused by entrainment. This interpretation is also consistent with the much greater wind stress, an important factor in producing entrainment, experienced during nuclear winter at this location (Table 2). In the same way, we find that more than half of the decrease in SST at the second geographical location (50°N , 150°E) is due to a decrease in the net surface heat flux, with the rest due to enhanced entrainment (see Figure 5b, and additional discussion below). At the third location (50°N , 50°W), where there was little change in the wind stress and MLD due to nuclear winter, all of the SST decrease is attributed to the rather large decrease (126 W m^{-2}) in the net surface heat flux. The only other location where the SST response was significant is the East China Sea point (30°N , 125°E), and there most of the SST decrease is accounted for simply by the very large change in the net surface heat flux caused by the extraordinary sensible and latent heat fluxes noted above.

We now examine the response of the upper ocean to nuclear winter in greater detail by describing the time evolution of the vertical thermal structure and its relation to the atmospheric forcing at one of the experimental ocean locations. The point at 50°N , 150°E is chosen for this purpose because the atmospheric forcing during the control and nuclear winter experiments at this location is fairly representative of the other locations as well. This point, located approximately 500 km west of the southern tip of the Kamchatka peninsula in the sea of Okhotsk, experiences a doubling of the average wind stress and a 139 W m^{-2} decrease in the net surface heat flux due to the smoke injection (Table 2). The results for this point are shown in Figures 4a-d 5.

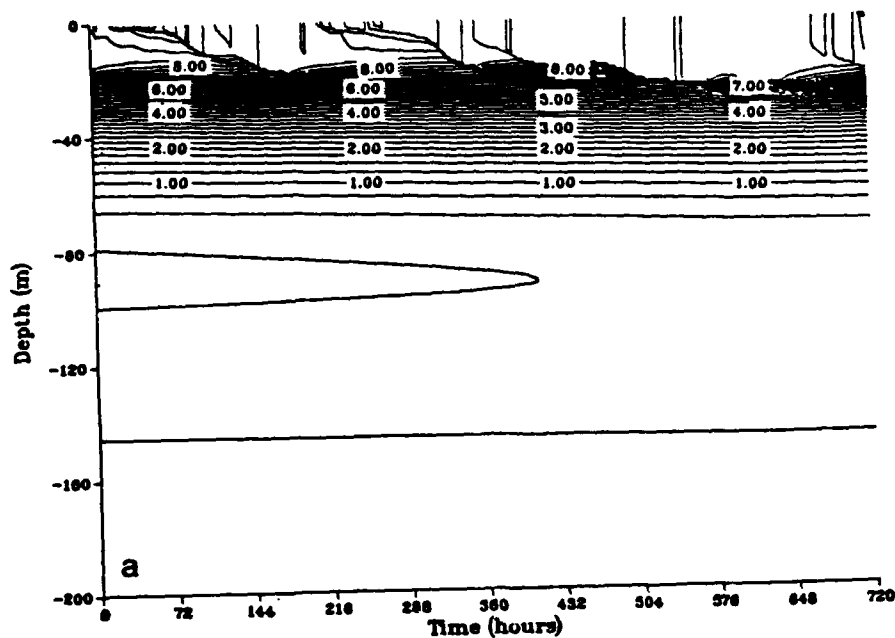
Looking first at the atmospheric forcing (Figure 4), we see that the net heat flux is affected by the smoke as early as July 3, and that an exceptionally strong wind event lasting several days occurs shortly thereafter. For 16 consecutive days during the nuclear winter experiment, from July 11 to 26, the solar radiation is reduced essentially to zero by the thick smoke cloud originating over nearby Siberia, and this produces a net heat loss ($Q_s < 0$) which lasts almost to the end of the month. By the end of the month, the net heat flux has partially returned to normal. Except for the enormous wind storm during the first week, the wind stress is quite similar in the two experiments. This characteristic of a strong wind event early in the month, followed by severe reductions in solar radiation and subsequent partial recovery, is typical of the atmospheric forcing during nuclear winter at other locations as well.

The response of the upper ocean thermal structure (Figure 5) is easily understood in terms of the above forcing. During the control experiment, the upper ocean responds to a cycle of typical summer wind events on July 6, 13, 16, 21, and 25. The ocean's response to these wind events is seen in the deepening and coalescence of the isotherms representing an enhanced vertical temperature gradient at the base of the mixed layer caused by the wind-generated downward mixing of warm surface layer water. In between these characteristically gentle wind events, the isotherms tend to spread out in the vertical as the mixed layer shallows and warms owing to the net surface heating. The evolution during the nuclear winter experiment is very different. The wind storm on July 5 deepens and cools the mixed layer, and the subsequent negative (upward) heat flux and relatively normal winds produce a gradual cooling and slow deepening of the mixed layer during the remainder of the month. In spite of the drastic changes in the atmospheric forcing during the nuclear winter experiment, the response of the ocean is confined to the upper 60 m.

DISCUSSION

In this study we have examined the short-term response of the upper ocean to the simulated forcing of a hypothetical atmospheric nuclear winter. The atmospheric forcing was derived from fields produced by a two-level atmospheric general circulation model in both a control and a nuclear winter simulation. The ocean was represented by a one-dimensional

50N 150E



50N 150E

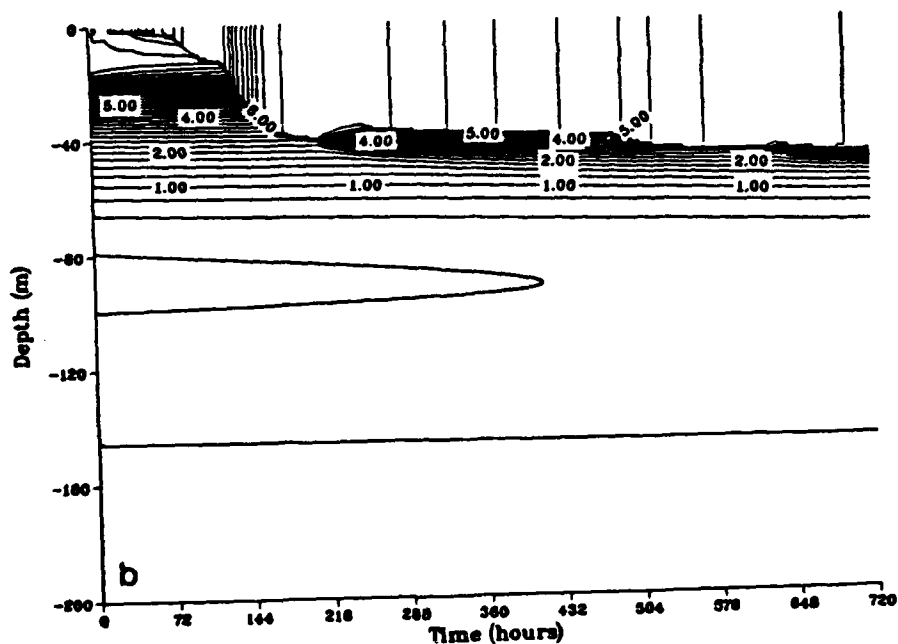
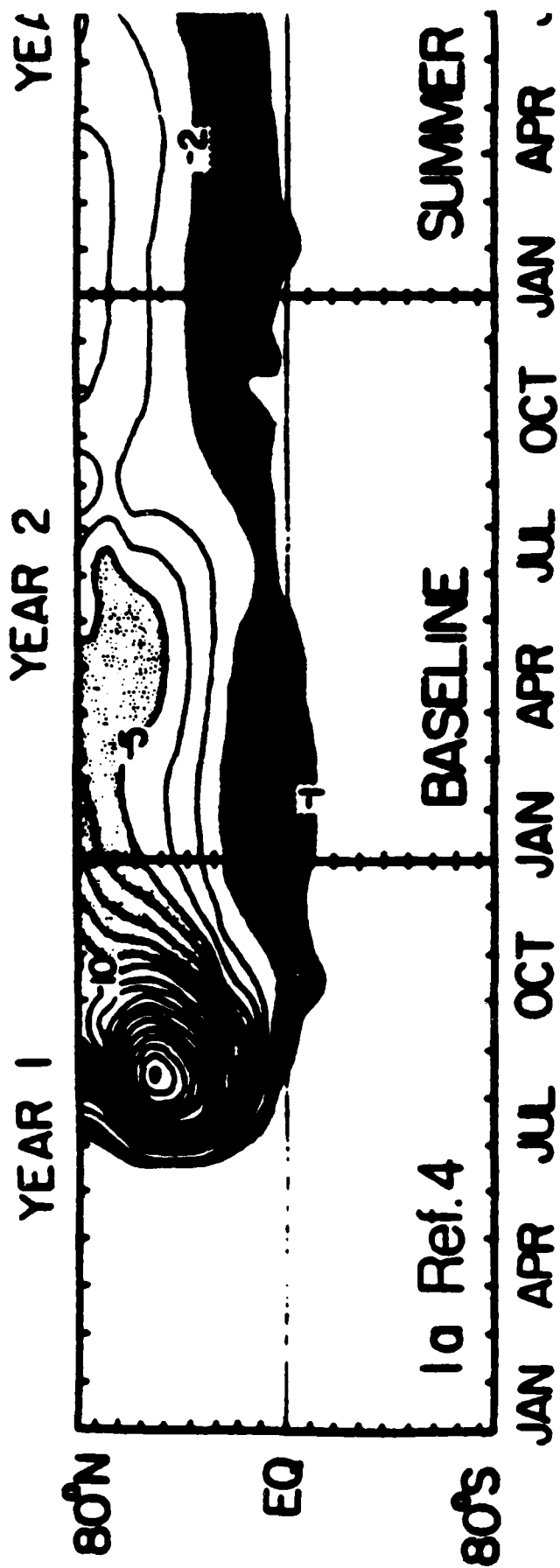


Fig. 5. Temperature (in degrees Celsius) as a function of time (0–30 days) and depth (0–200 m) at 50°N, 150°E in the (a) control and (b) nuclear winter experiments.

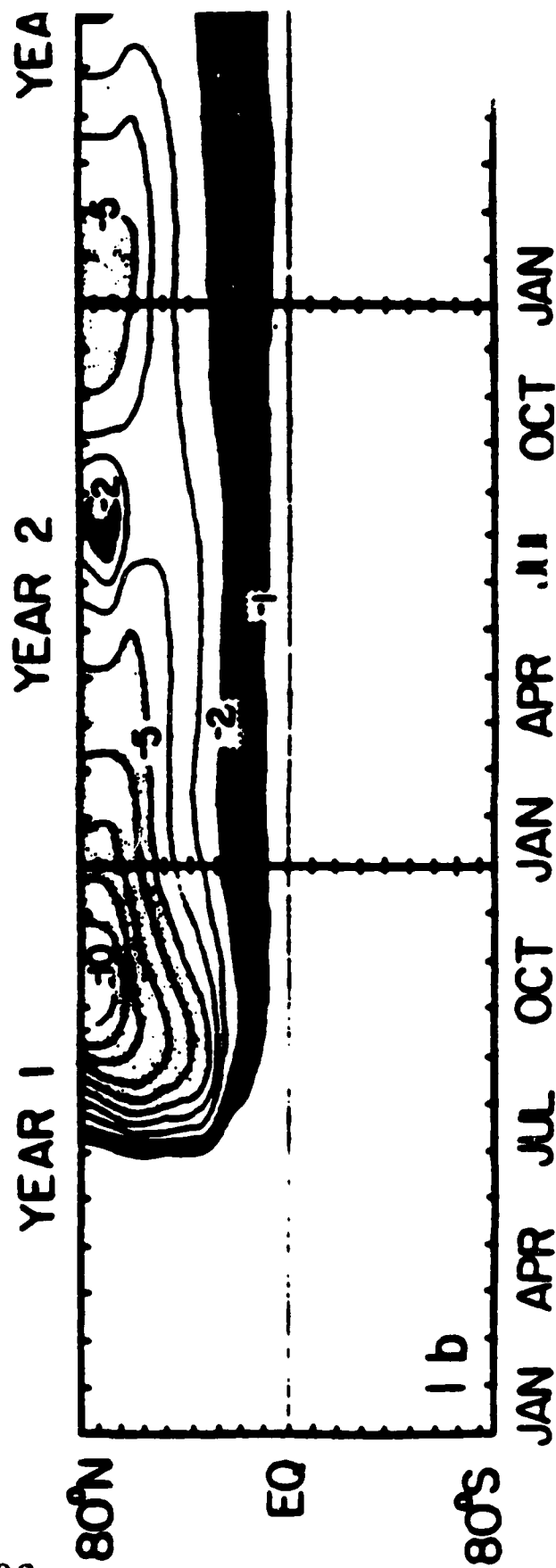
mixed layer model applied at six different locations in the North Atlantic and North Pacific oceans. Since there was no negative feedback with regard to the heat exchange between the ocean and atmosphere, the intensity of the modeled ocean response may be regarded as an upper bound (i.e., the actual response may be weaker). This is a useful thing to know,

particularly for estimating the size of the feedback from the ocean and its potential effect on the atmosphere.

Our results indicate that at some of the locations, depending on the distance upwind from the point in question to the nearest source of smoke, the upper ocean experiences a significant cooling in response to a large scale nuclear exchange.



233



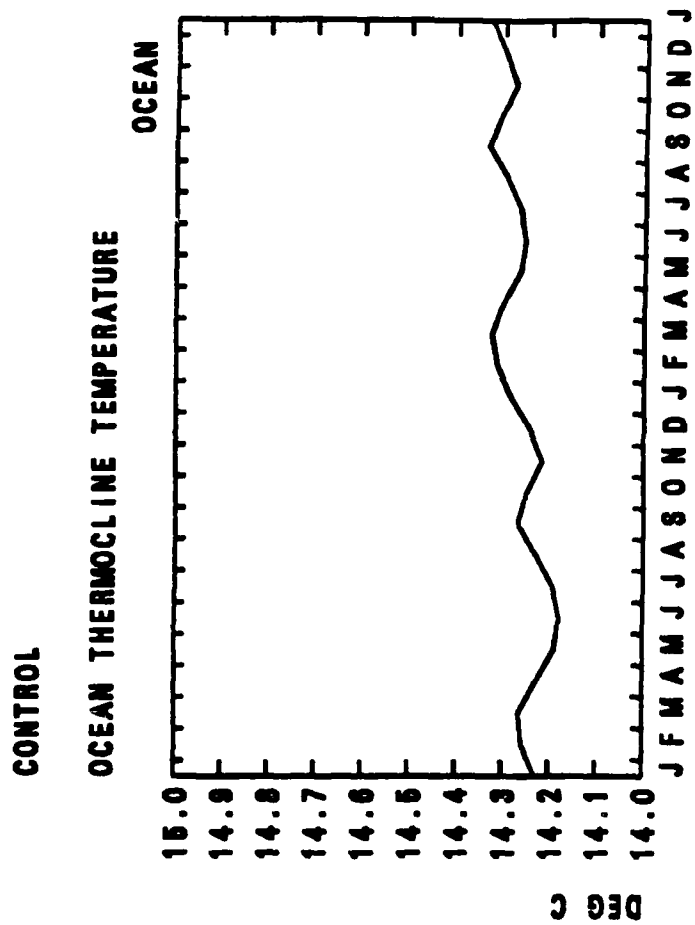
Issues

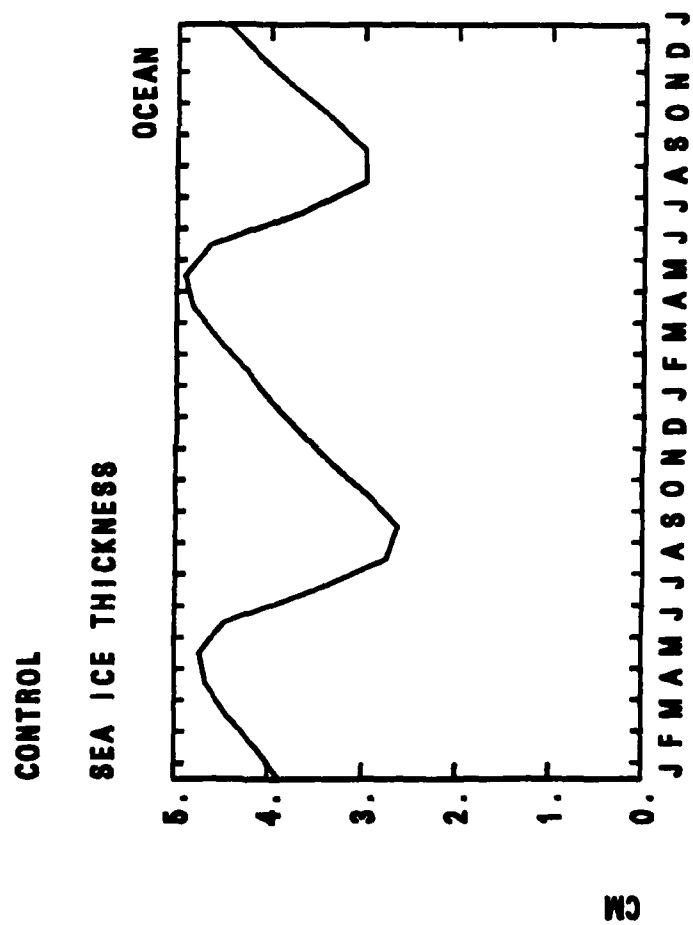
- Are dynamical aspects of the ocean mixed layer response important?
- What are the roles of sea ice formation and the hydrological cycle in the chronic response?

OSU/LLNL TROPOSPHERIC GCM
LAGRANGIAN TRACE SPECIES
TRANSPORT

POLLARD 2-LAYER OCEAN

- MIXED LAYER
- THERMOCLINE
- DYNAMICAL
- PARAMETERIZED ENTRAINMENT
- THERMODYNAMIC SEA ICE

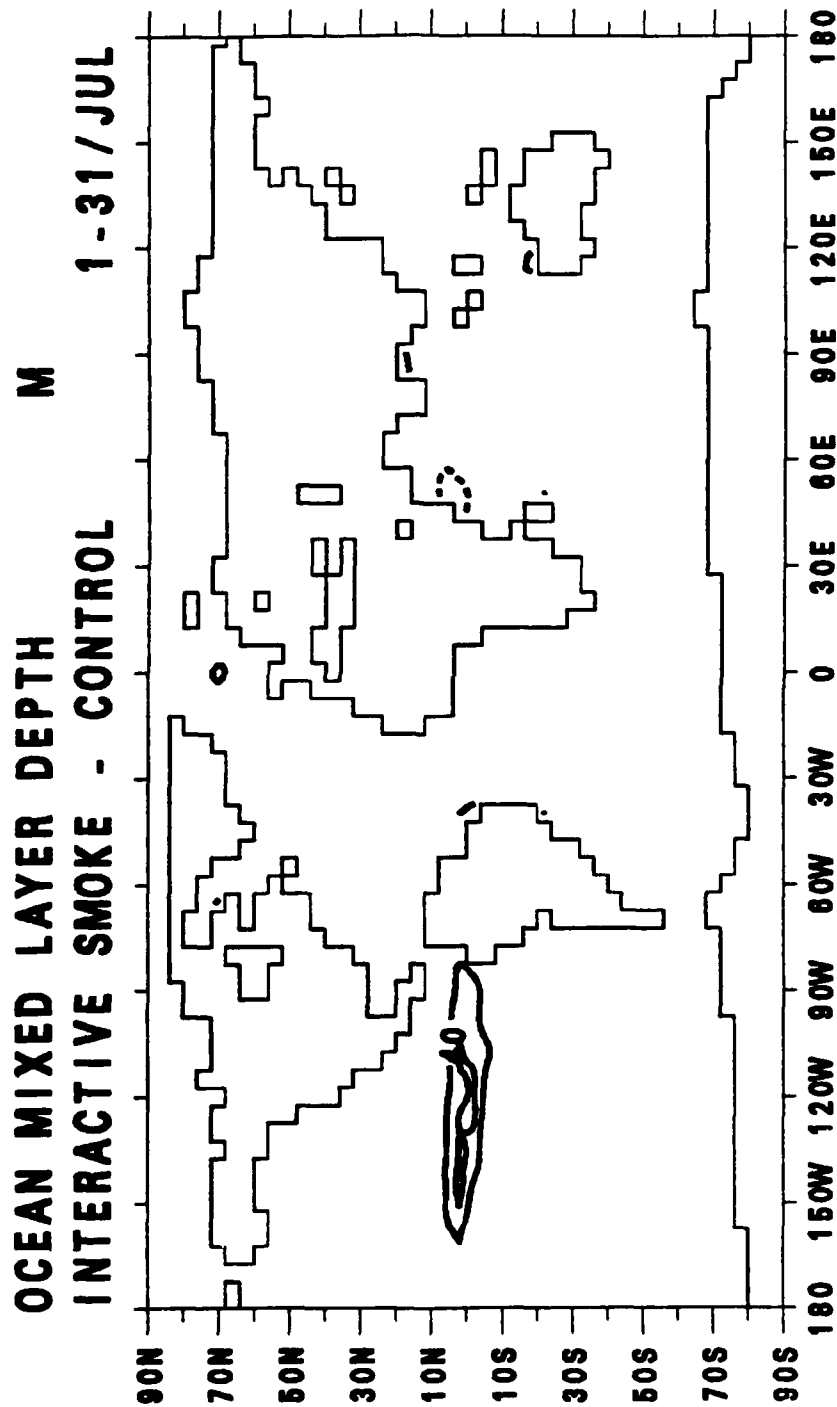


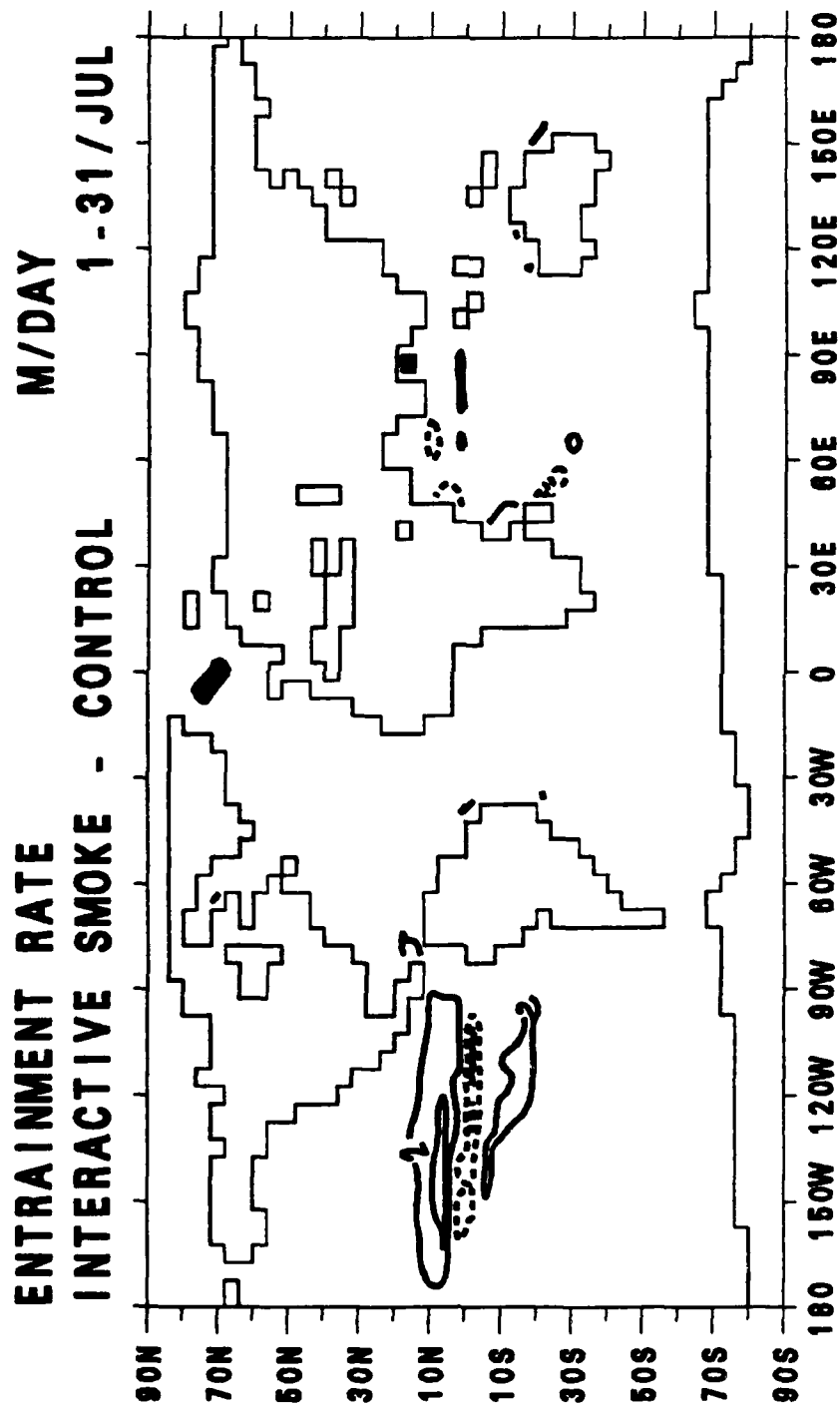


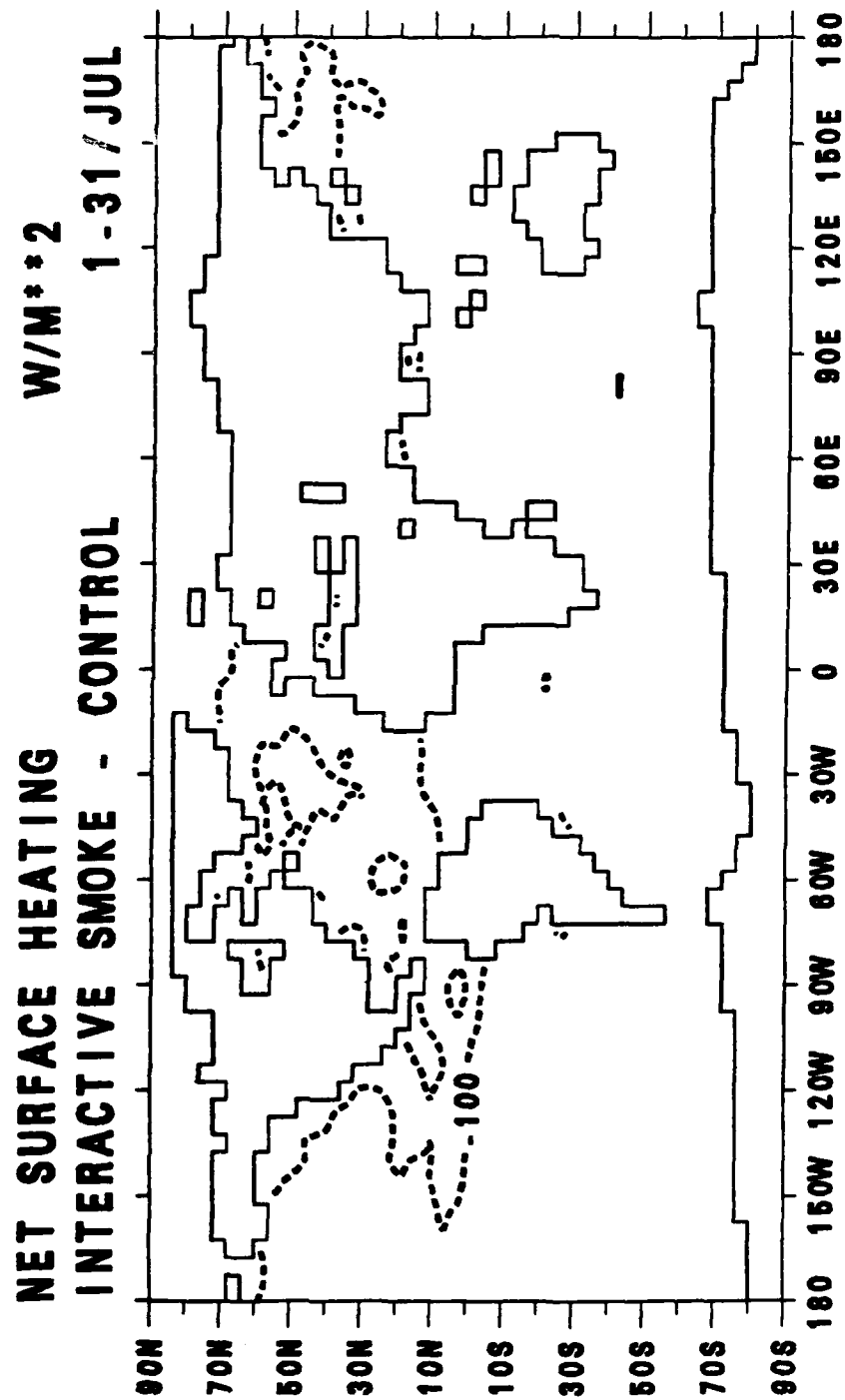
Experiment

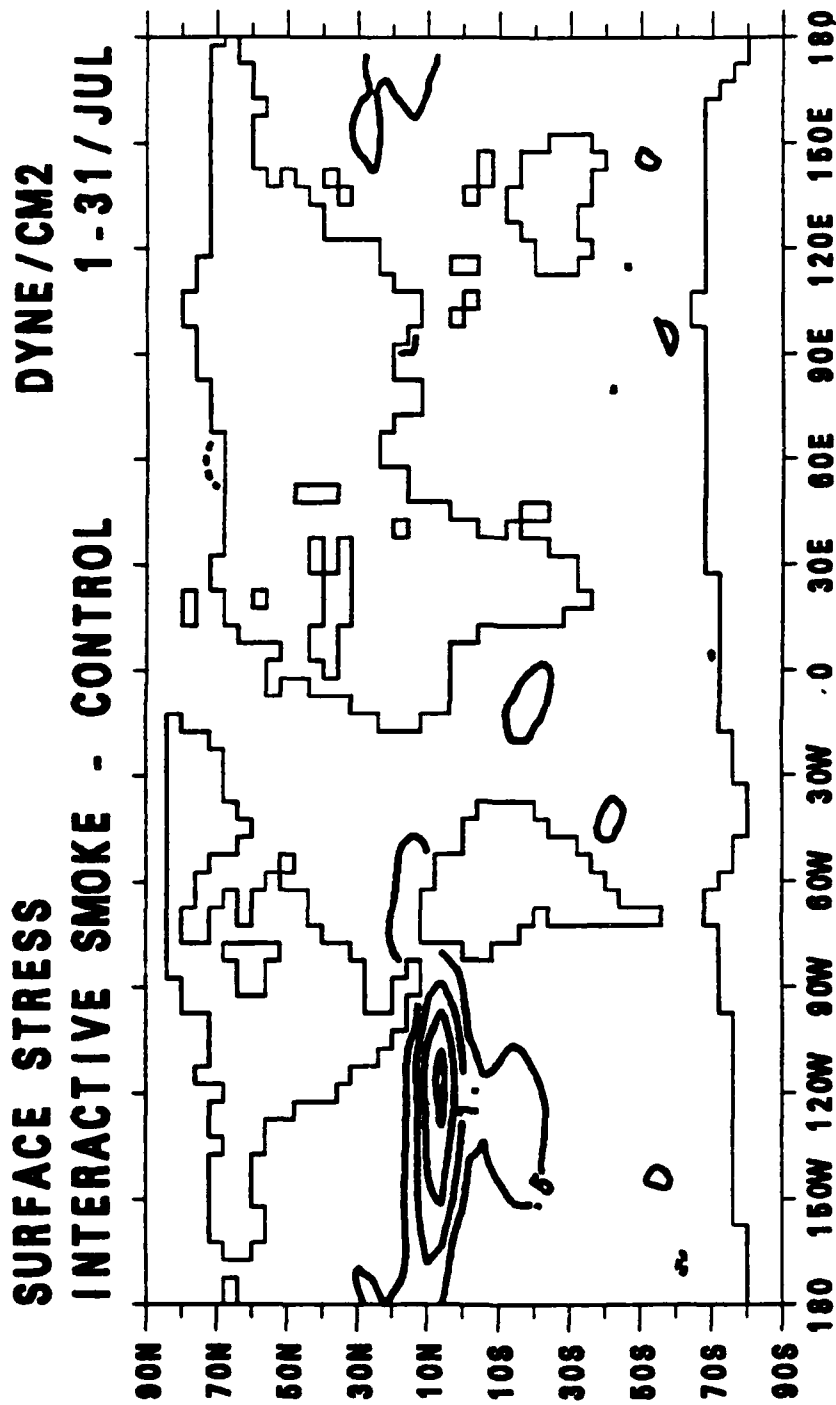
Bangkok 50 T_g ($\bar{\epsilon}_a = 1$)

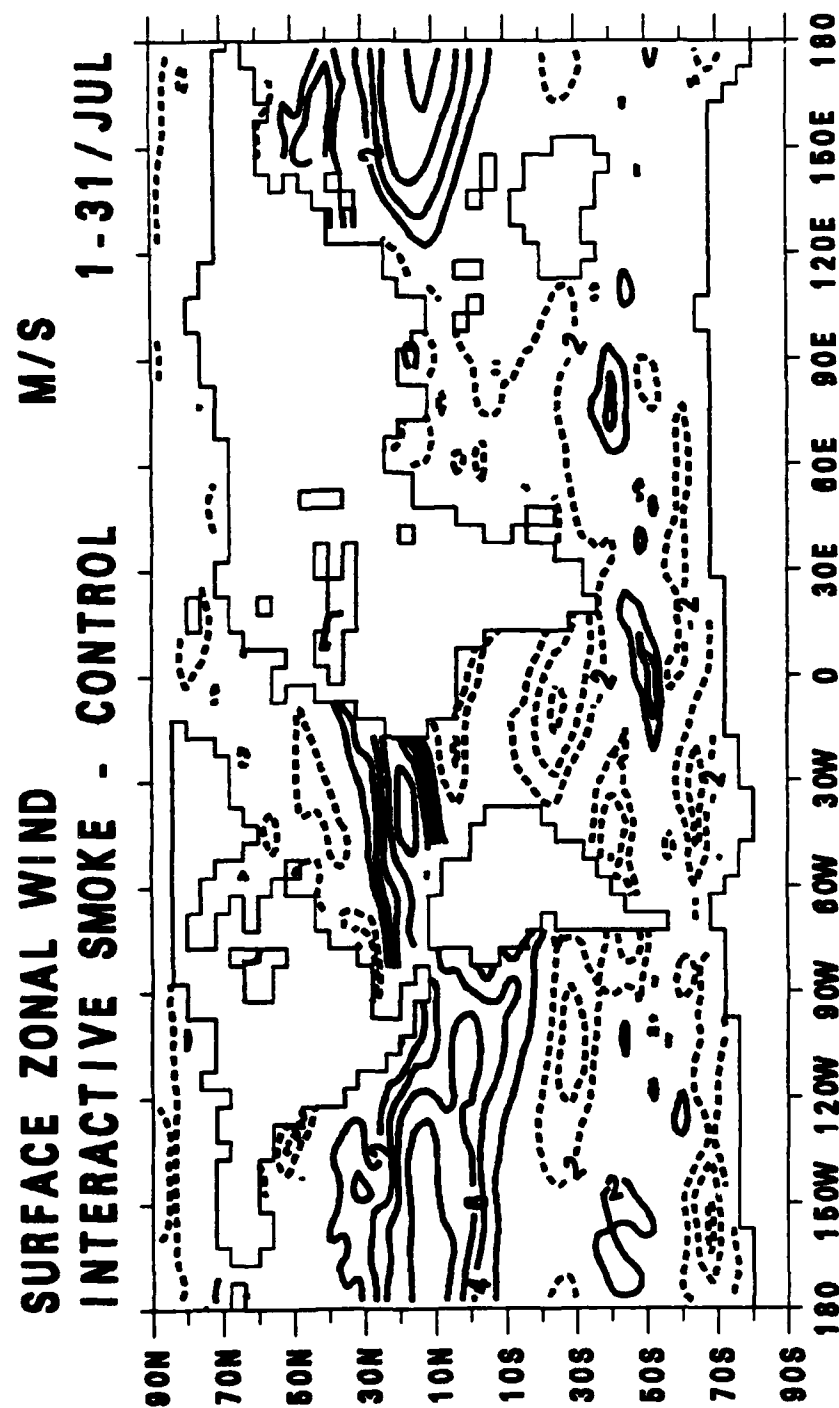
1-3 July injection

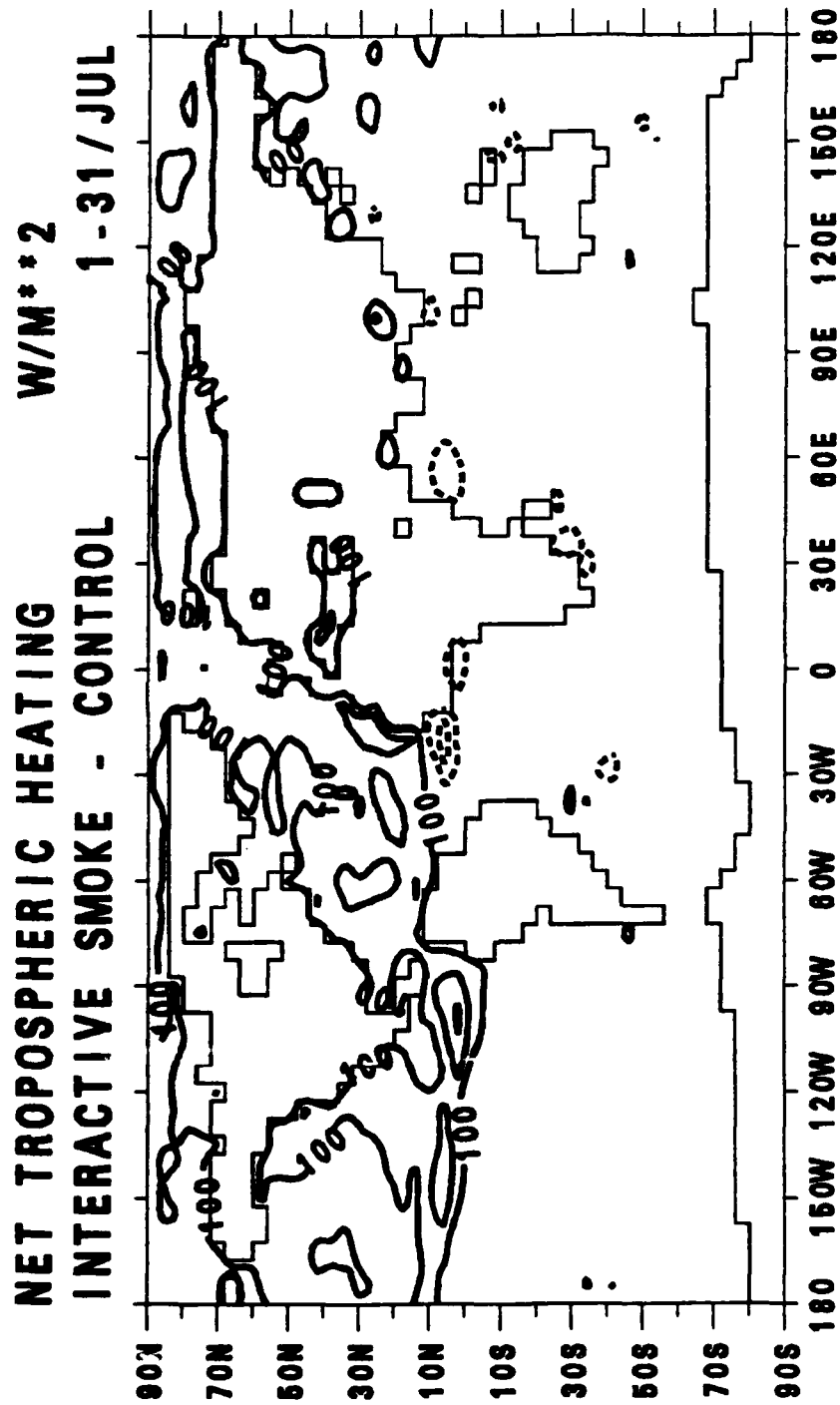




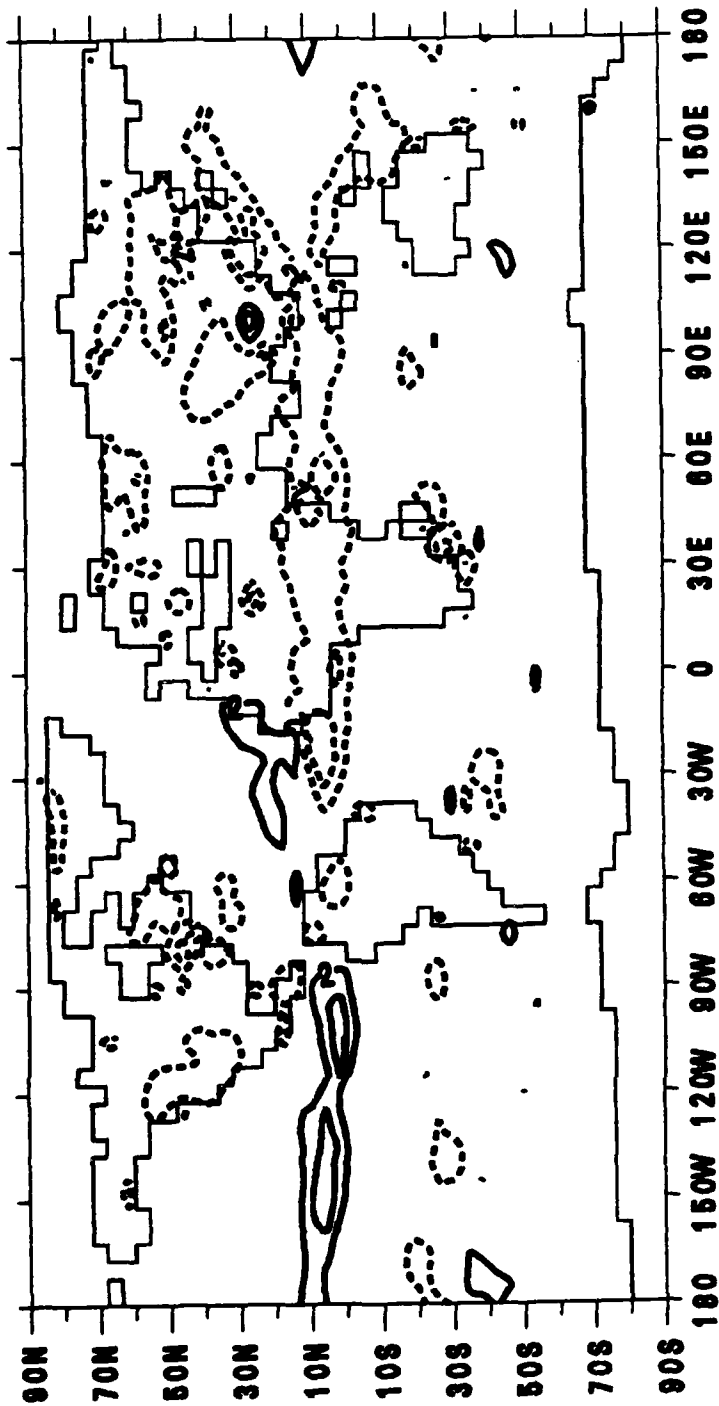


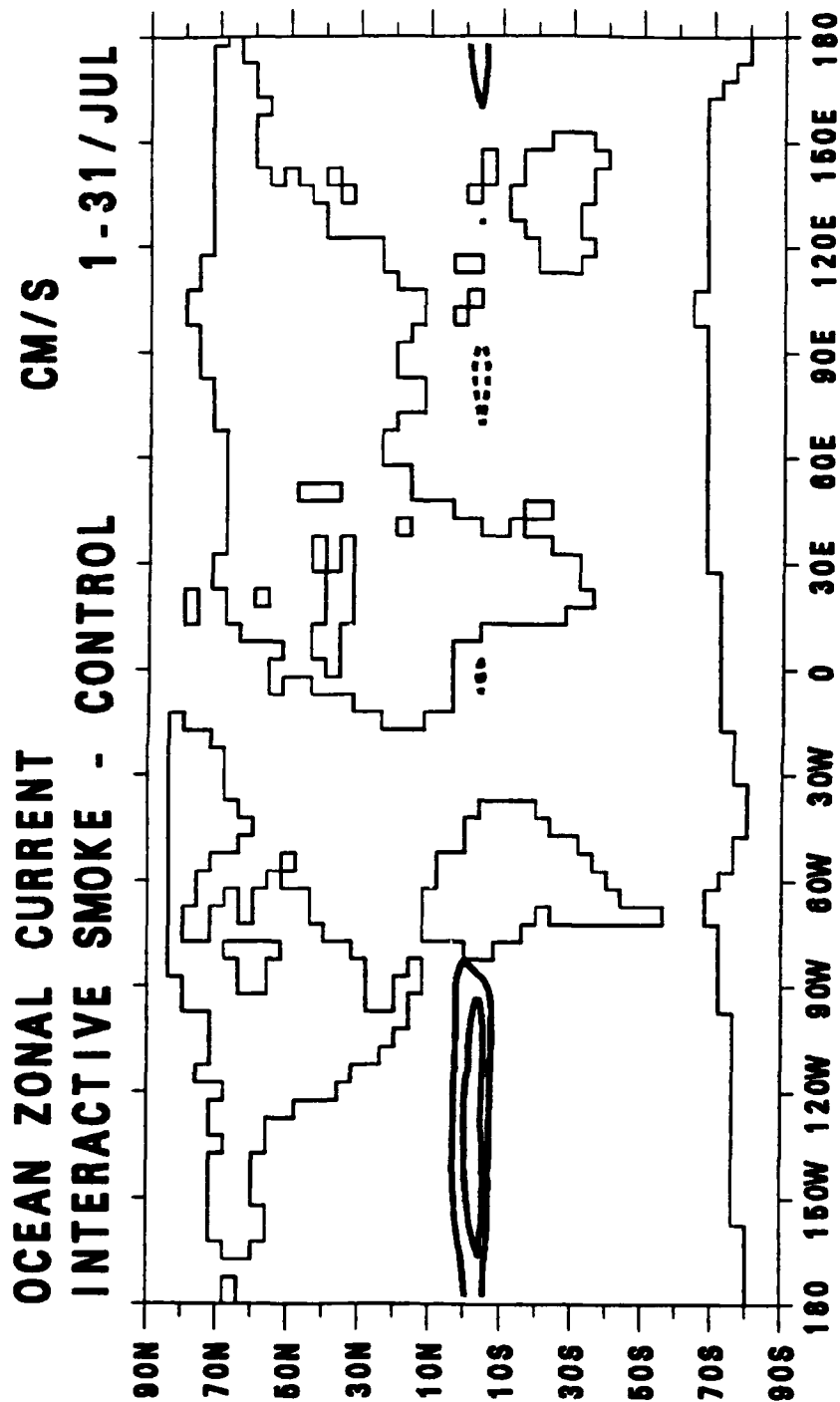




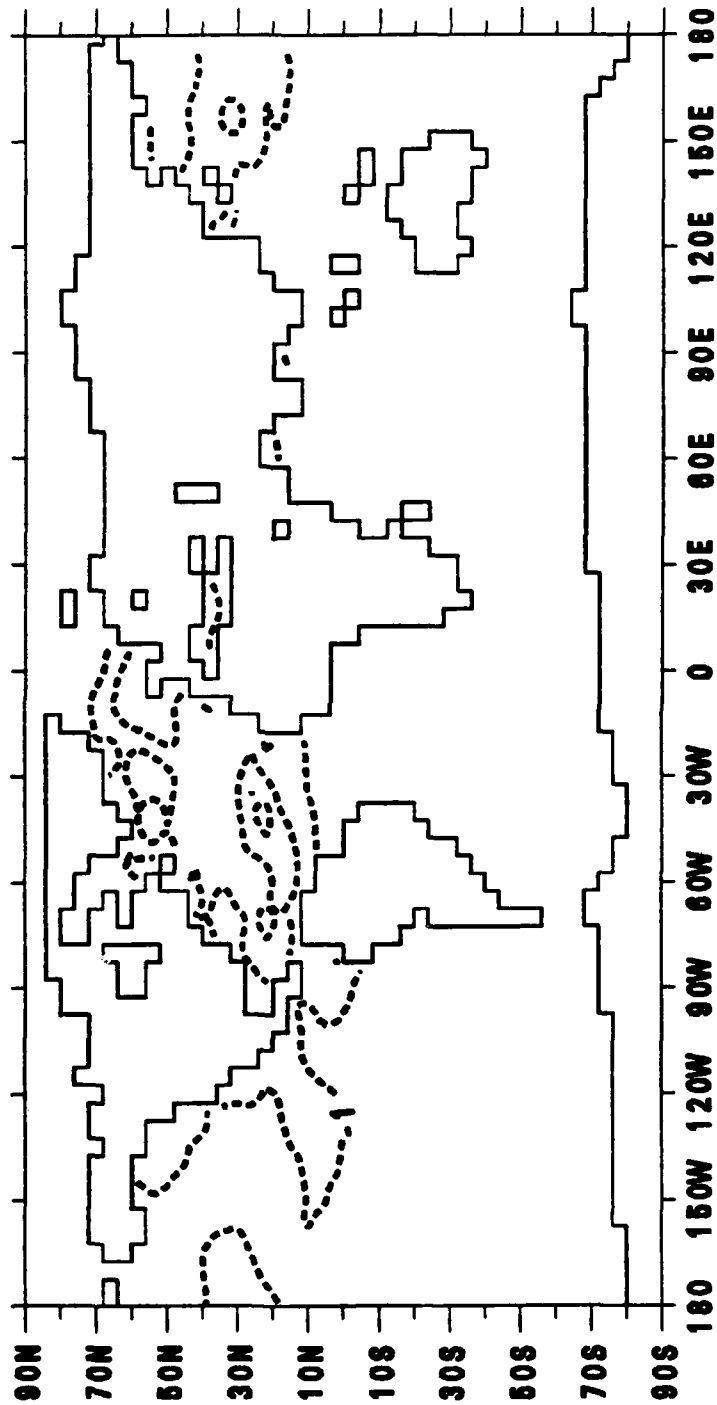


TOTAL PRECIPITATION AT SURFACE MM/DAY
INTERACTIVE SMOKE - CONTROL **1-31/JUL**

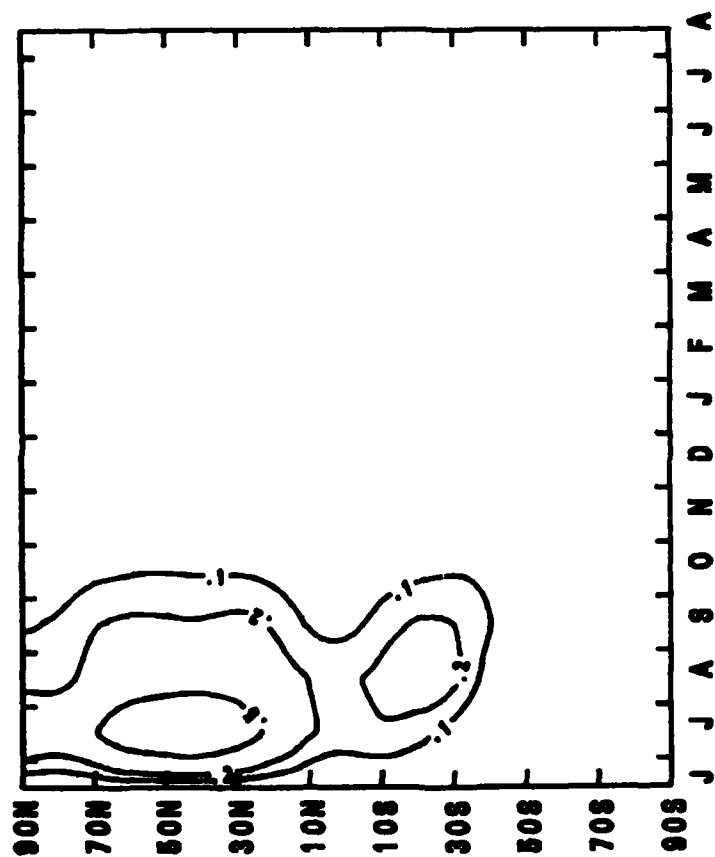


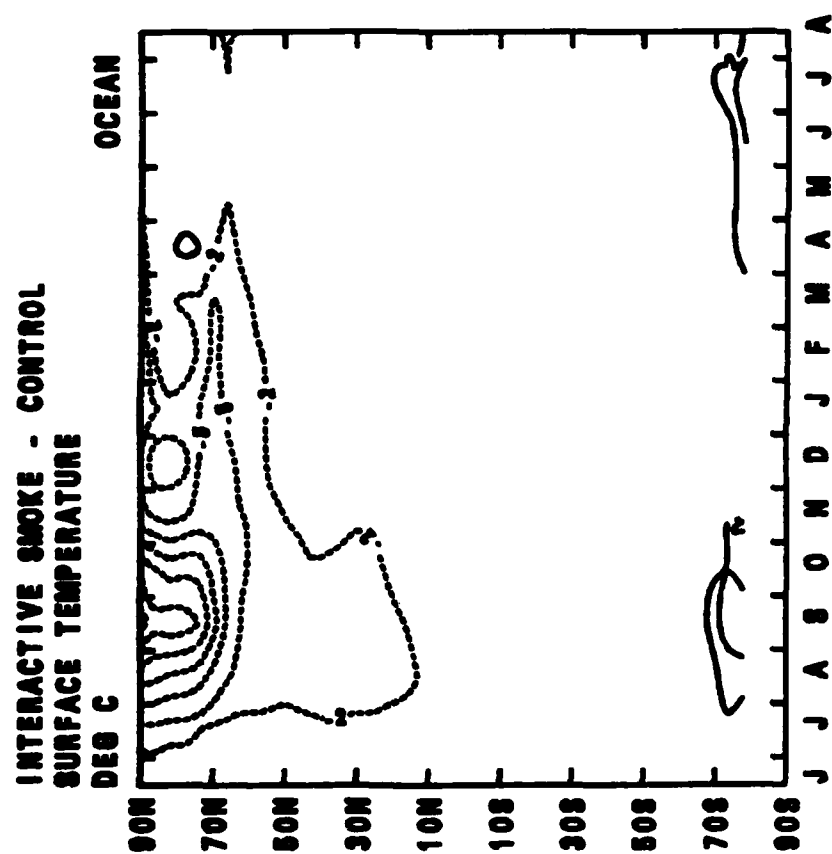


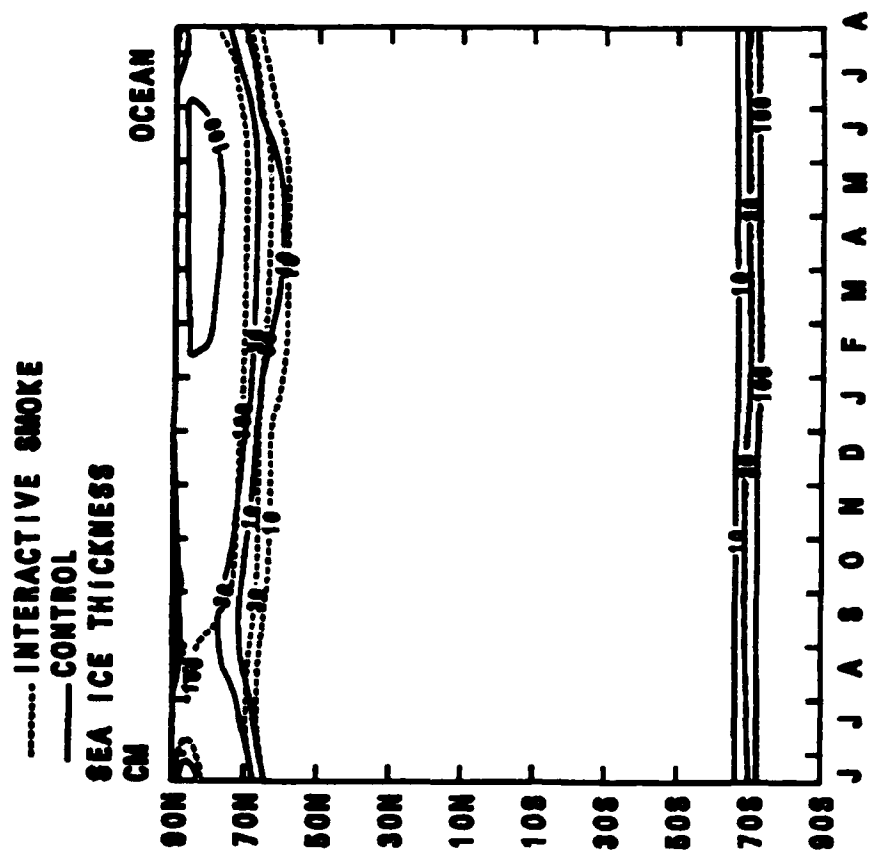
OCEAN MIXED LAYER TEMPERATURE DEG C
INTERACTIVE SMOKE - CONTROL 1-31/JUL

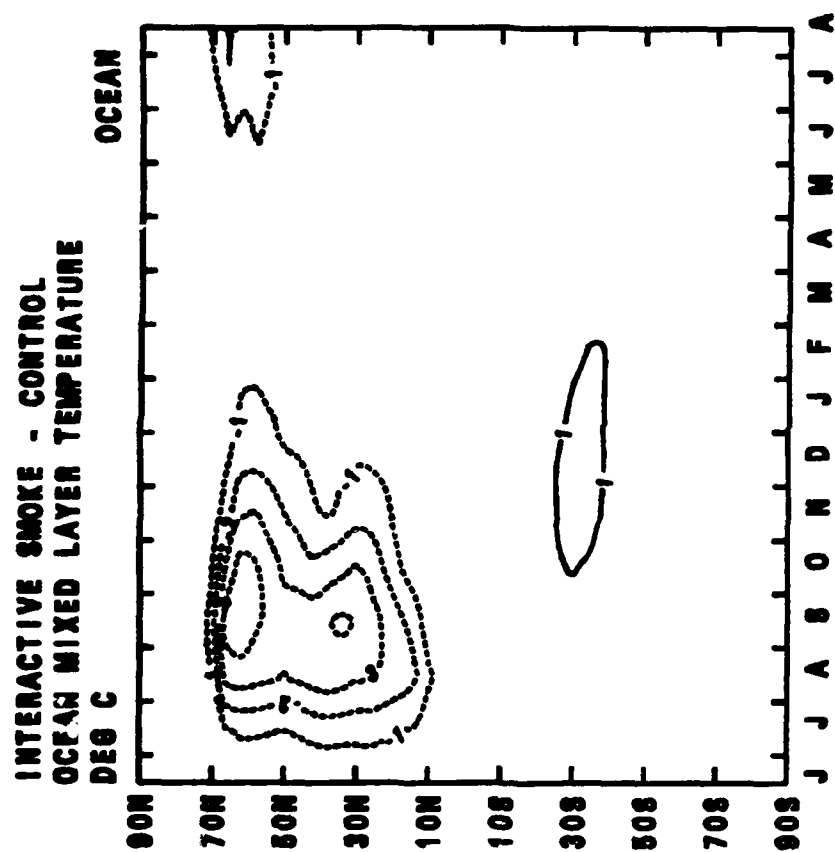


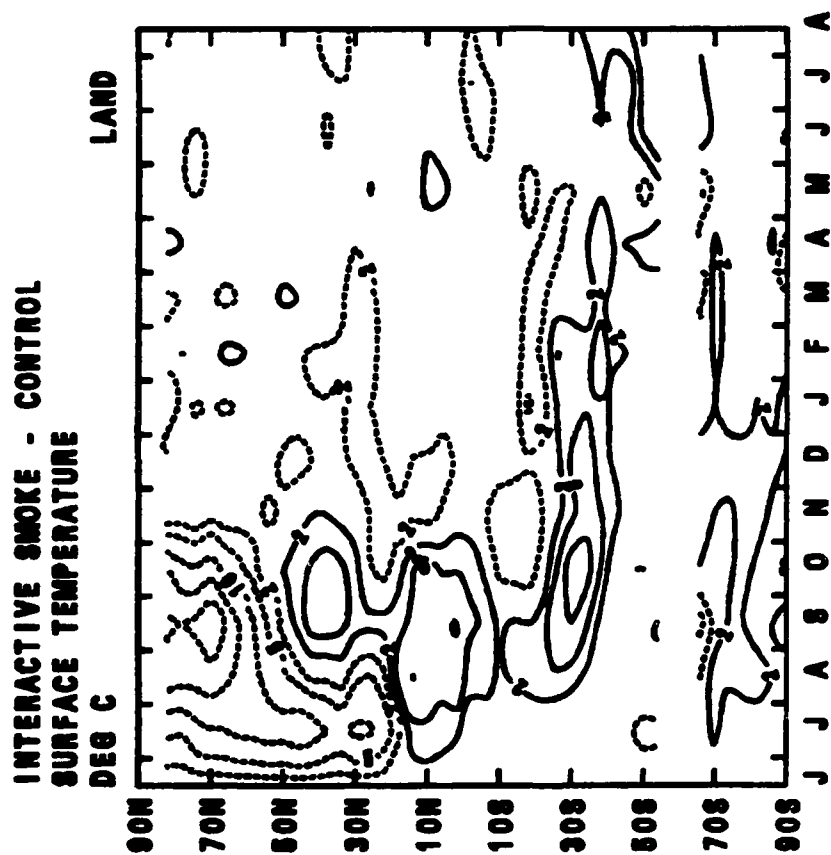
INTERACTIVE SMOKE
SMOKE ABSORPTION OPTICAL DEPTH



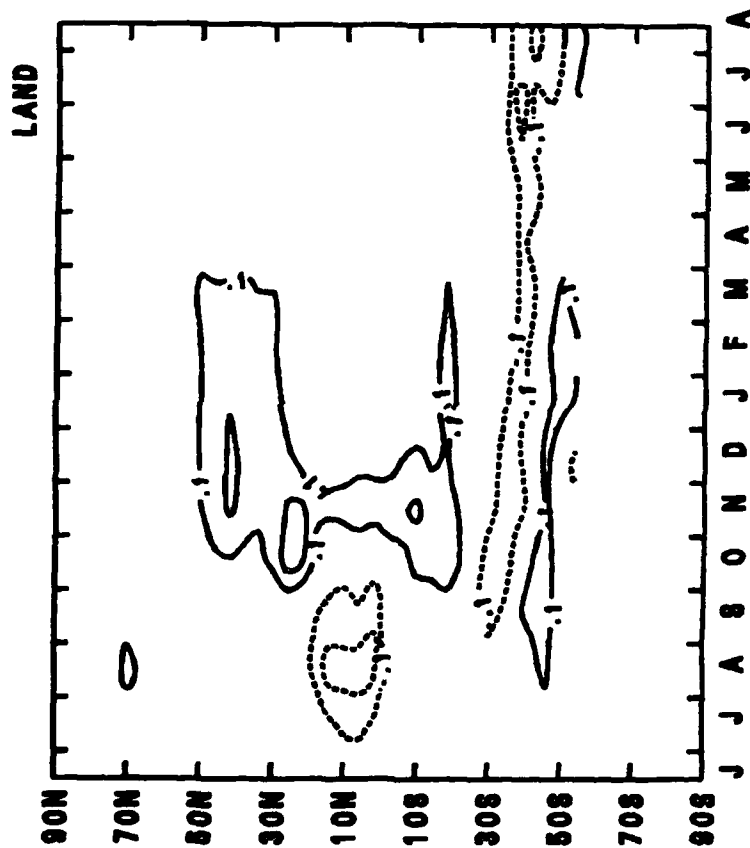


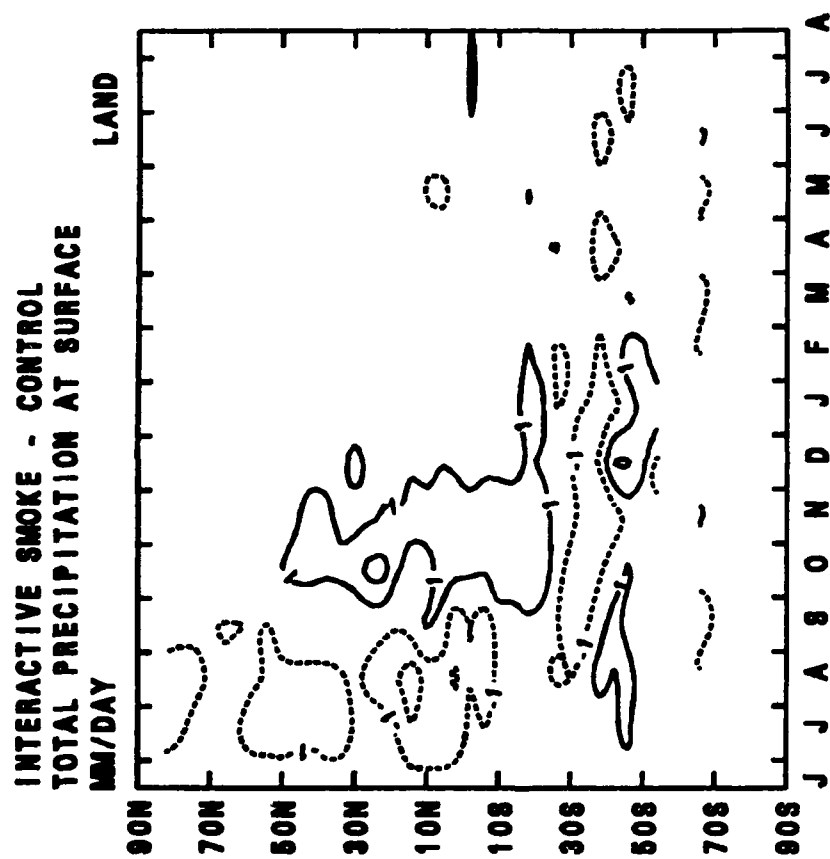


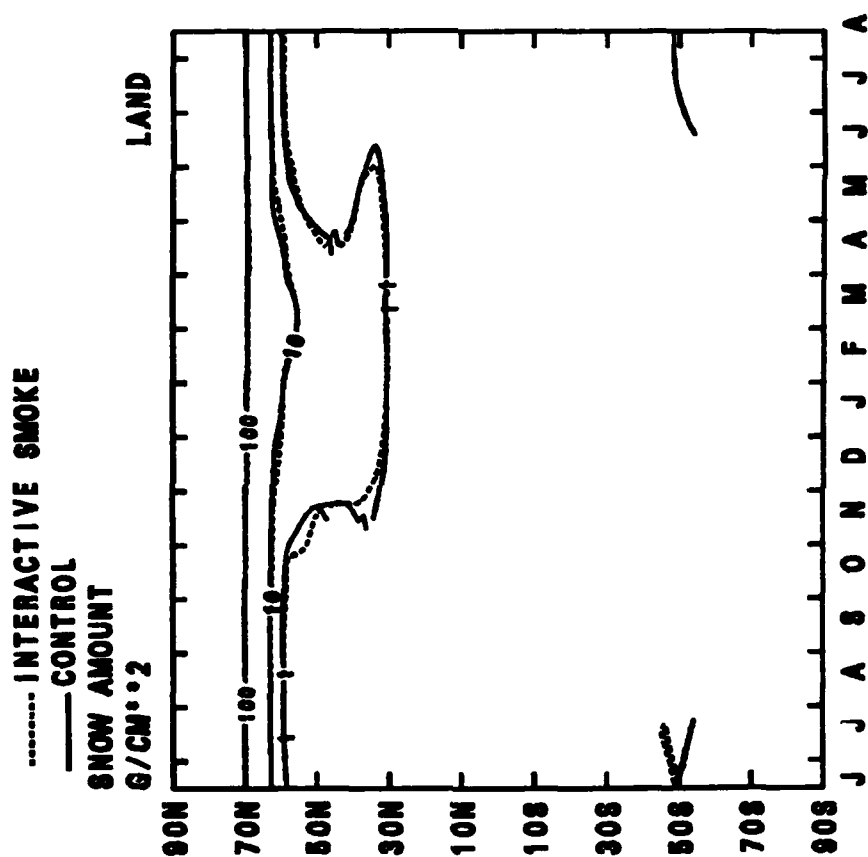




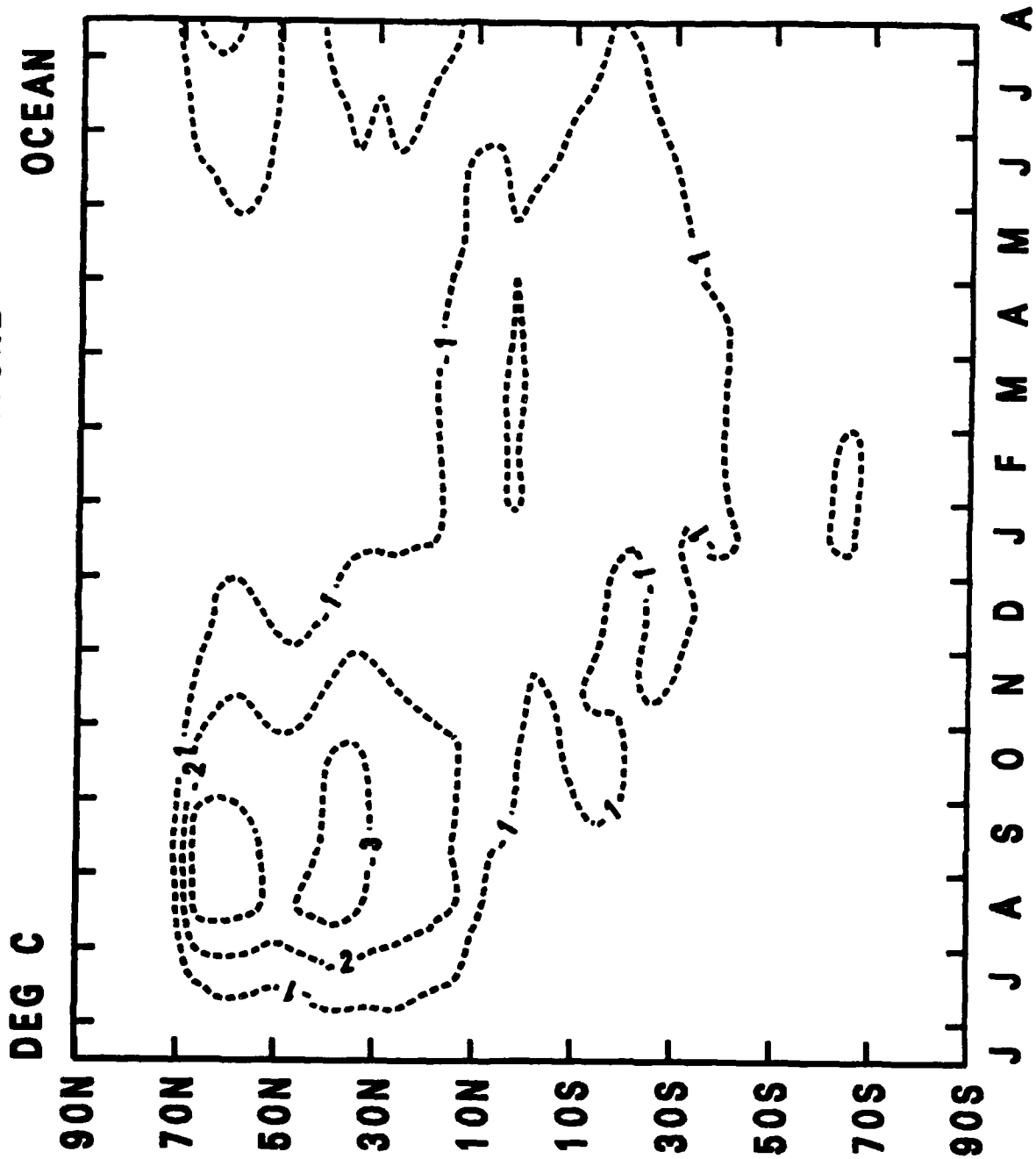
INTERACTIVE SMOKE - CONTROL
GROUND WETNESS



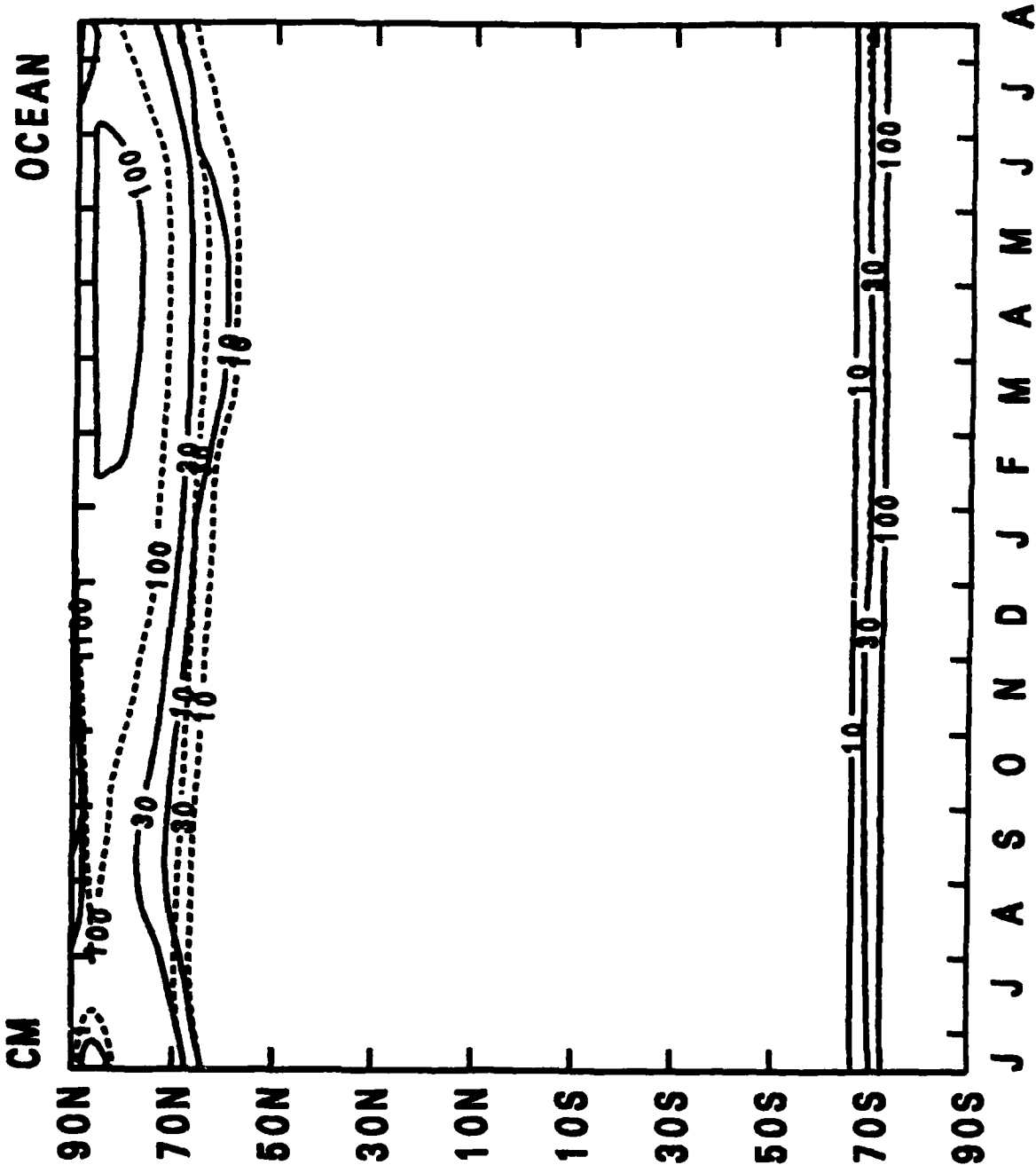




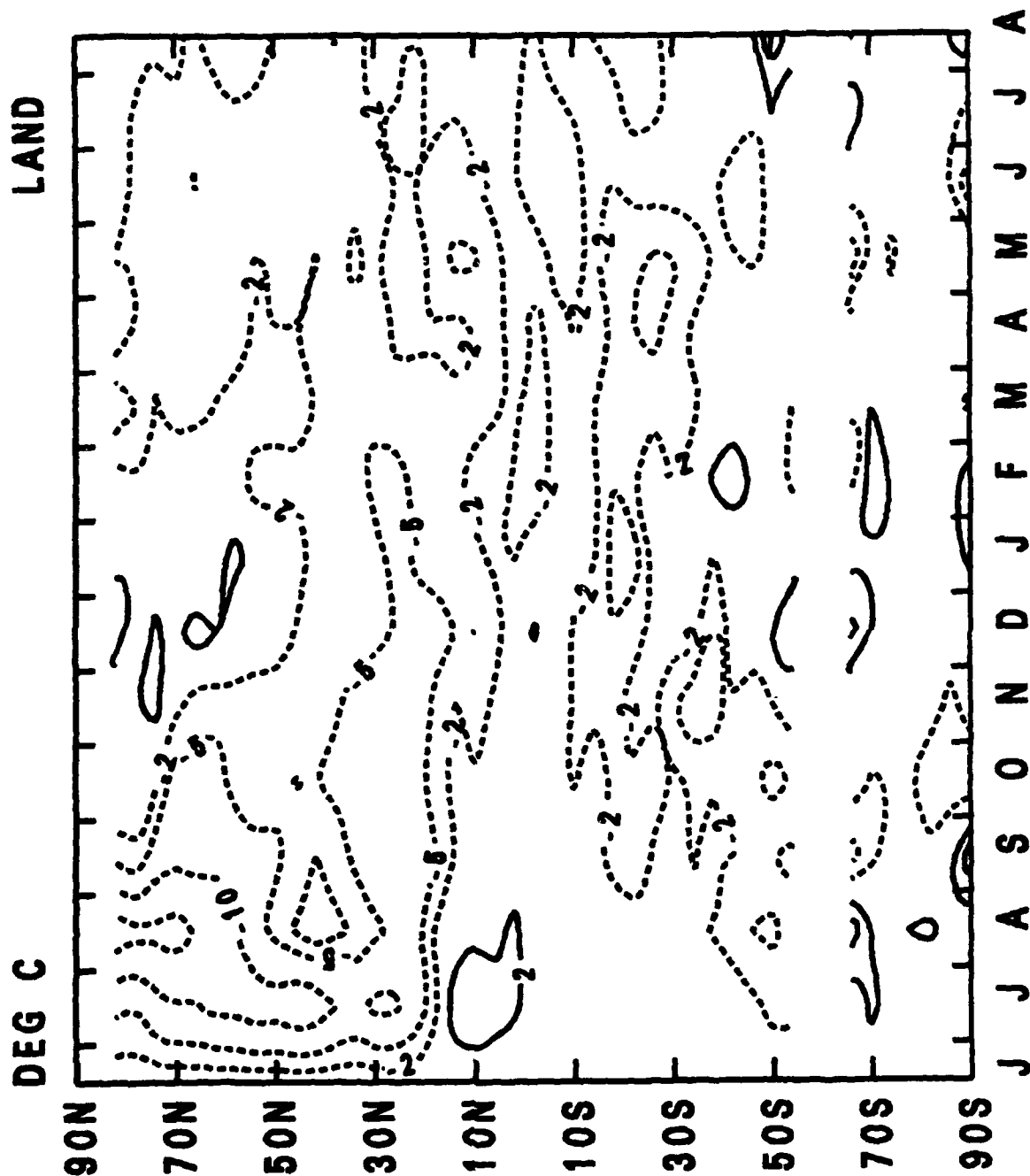
UNIFORM SMOKE - CONTROL OCEAN MIXED LAYER TEMPERATURE



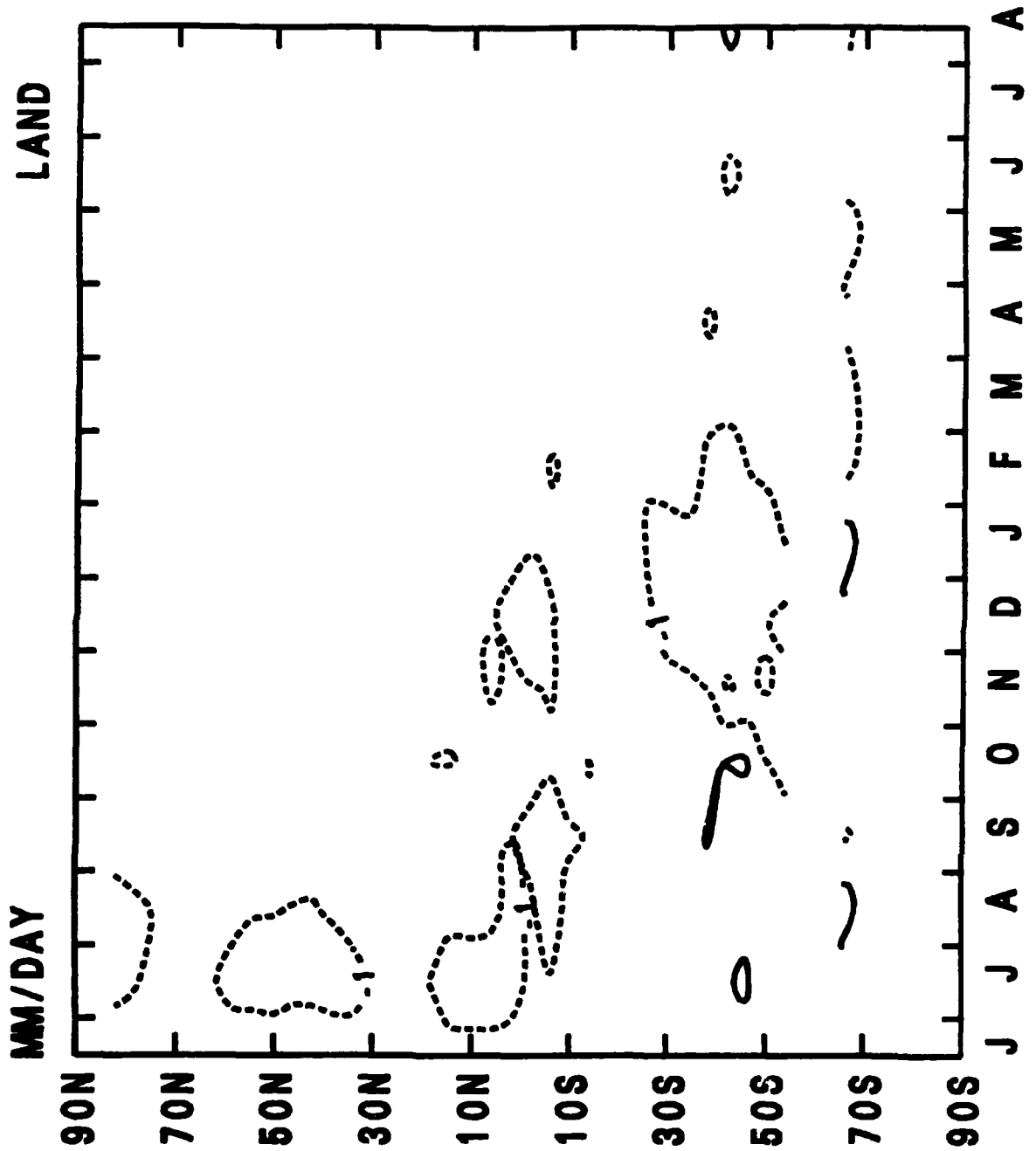
..... UNIFORM SMOKE
 ——— CONTROL
 SEA ICE THICKNESS
 CM



UNIFORM SMOKE - CONTROL SURFACE TEMPERATURE



UNIFORM SMOKE - CONTROL
TOTAL PRECIPITATION AT SURFACE



The Climatic Response to Large Atmospheric Smoke Injections

- 1) Process Sensitivities
- 2) SCORF Bangkok scenarios

M. MacCracken

S. Ghan

J. Walton

LLNL SMOKE/CLIMATE MODEL

Smoke model: LLNL/GRANTOUR

Handles smoke transport, coagulation, scavenging, settling, . . .

Lagrangian sampler parcels (10000)

- Equal air mass ($400 \text{ km} \times 400 \text{ km} \times 200 \text{ mb}$)
- Variable smoke mass in each parcel
- Scavenging, coagulation (and chemistry) done on each parcel
- Advection is Lagrangian (no numerical diffusion)
 - done by parcel, not species
 - longer time step, no gravity waves
- Interparcel mixing (local), subgrid scale diffusion, convective mixing, settling done on $4^\circ \times 5^\circ$ grid; changes interpolated to parcels (some numerical smoothing)

Two particle sizes

- < $1 \mu\text{m}$: inefficient removal, large radiative effect
- > $1 \mu\text{m}$: efficient removal, smaller radiative effect

Scavenging

Convective: fractional time and grid area

Large-scale: fractional time

LLNL SMOKE/CLIMATE MODEL

Climate model: OSU/GCM

**Troposphere (2 layers, sfc to 200 mb)
Fixed sea surface temperatures
Perpetual July (low soil moisture → land being warm)
Diurnal radiation (includes absorption and scattering by smoke)
Smoke has effect on IR radiation
Cloudiness is calculated
Stability dependent boundary layer**

Coupling: Synchronous, 24 hours

In progress:

**Adaptation/modification of NCAR/CCM
Coupling to GRANTOUR (10⁶ parcels)
— may need special stratospheric parcels**

OSU/GRANTOUR Sensitivity Experiments

<u>Property</u>	<u>Nominal</u>	<u>Variations</u>
Smoke Amount	150 Tg	15, 50, 450 Tg
Mode Radius	0.4 μm ($\sigma = 1.5$)	0.1 μm ($\sigma = 2.$)
Extinction coeff.	2.98 m^2/g	4.97 m^2/g
Optical Characteristics	1.75 - 0.3i	1.5 - 0.1i
Absorption coeff.	1.59 m^2/g	1.34 m^2/g
Vertical distribution	Uniform	High, Low
Solar Radiation	Diurnal	Daily Avg.
IR Effects (ext. coeff)	0.3 m^2/g	0
Season	July	Jan, April
Ground wetness	Interactive	Fixed
Removal (wet and dry)	Interactive	Doubled, off
Initial meteorology	July 1	July 10
Surface vertical diffusivity	Variable	Neutral
Atmospheric Average Absorp Optical Depth	0.91	0.09, 0.3, 2.7

SMOKE INJECTION SENSITIVITY STUDIES

Case Studied	% Mass Remaining at 30 Days	Residence Time at 30 Days	Temperature Change Land 28-72°N 1-10 days	21-30 days	Precipitation Change (%) Land 28-72°N 1-10 days	Land-Tropics 21-30d.
150 Tg Jan.	11%	17 days	-1.8°C	-1.1°C	-7%	-1%
April	35	108	-4.0	-5.2	-40	-64
July	49	108	-8.2	-3.3	-51	-79
264 July						
15 Tg	25	25	-1.1	1.7	-43	-38
50 Tg	43	79	-4.4	2.4	-53	-77
150 Tg	49	108	-8.2	-3.3	-51	-79
450 Tg	52	174	-9.8	-10.0	-52	-66

150 Tg $\approx \tau_A(NH)$ of 0.91

Factors Capable of Amplifying Temperature Response

Factor	Effect on land temp. 28°-72°N		Factor treated in LNL model baseline	Factor treated in NCAR model baseline
	Days 1-10	Days 21-30		
Ground vs sfc air temp.	4.1	~0		✓
Uncoagulated injection (or more absorbing smoke)	2.4	6.6		some
Interactive sfc. stability	2.3	0.6	✓	
Perturbation to scavenging rate	1.5	4.5	✓	✓
Higher altitude injection	0.3	1.0		
Prolonged injection	0.2	0.1		✓

LLNL Baseline Case $\Delta T = -8.2$ $\Delta T = -3.3$

Factors Capable of Moderating Temperature Response

Factor	Effect on land temp 28°-72°N Days 1-10	Days 21-30	Factor treated in LLNL model baseline	Factor treated in NCAR model baseline
Particle IR effects	2.5	2.1	✓	✓
Lower altitude injection	0.9	0.2		(in 7 km case)
Removal processes	0.7	2.7	✓	✓
Diurnal cycle of solar radiation	0.5	2.5	✓	
Scattering by aerosols	0.5	2.3	✓	✓
More dust-like smoke	0.5	~0		
Interactive soil moisture	0.2	0.9	✓	
Coagulation of particles	0.1	1.8	✓	✓
<hr/>				
		LLNL	NCAR	
NCAR model vs. LLNL model		13.7	11.9	Days 6-15
(similar case with removal and coagulation off)		18.7	15.6	

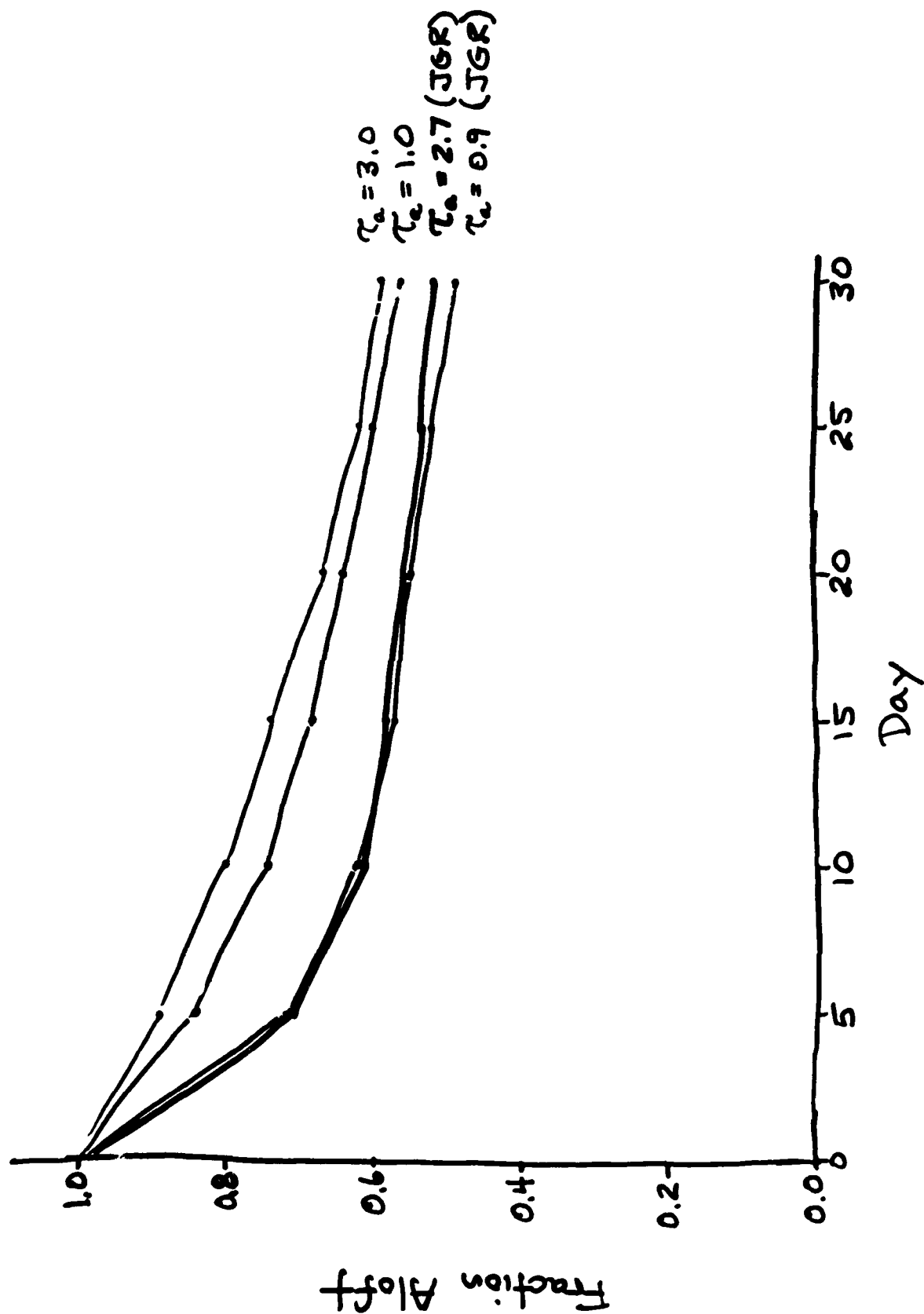
SCOPE, ENUNWAK Proposed Scenarios

	N.H. Avg. Absorption Optical Depth	Smoke Mass (Tg)	Height of Injection	Vertical Distribution
Case 1	0.3	15	0-7	const. mix. ratio
Case 2	1.0	50	0-tropopause	const. mix. ratio
Case 3	3.0	150	{ 0-tropopause trop to (trop + 3 km)	const. mass density linear decr. to zero

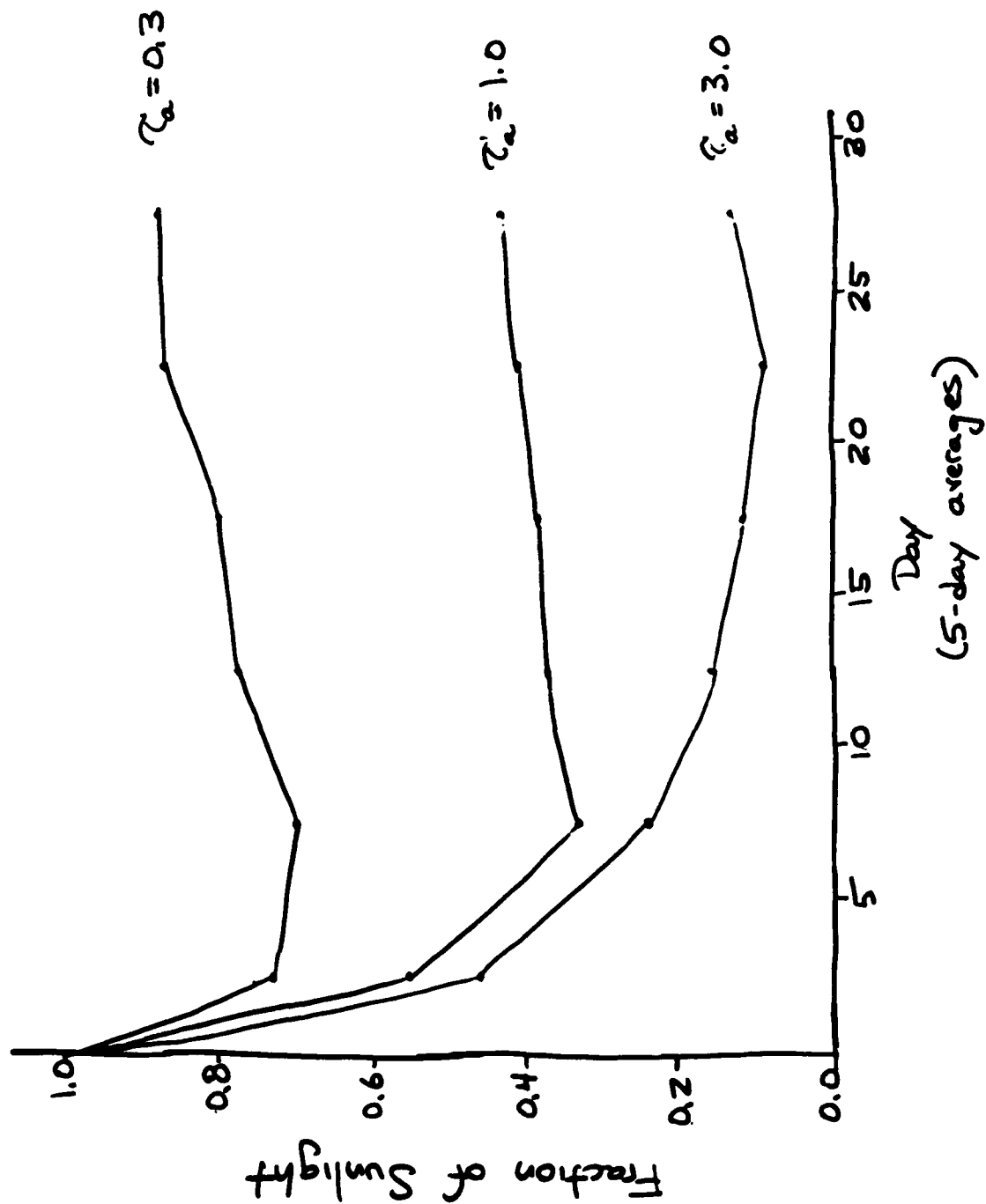
Other assumptions:

1. Specific absorption $5 \text{ m}^2/\text{g}$ at $0.51 \mu\text{m}$ for all particle sizes
2. Single scatter albedo in visible 0.5
3. Specific extinction at $10 \mu\text{m}$ of $1 \text{ m}^2/\text{g}$
4. Mean mode radius $0.3 \mu\text{m}$ for coag. and scav.
5. Three-day injection period

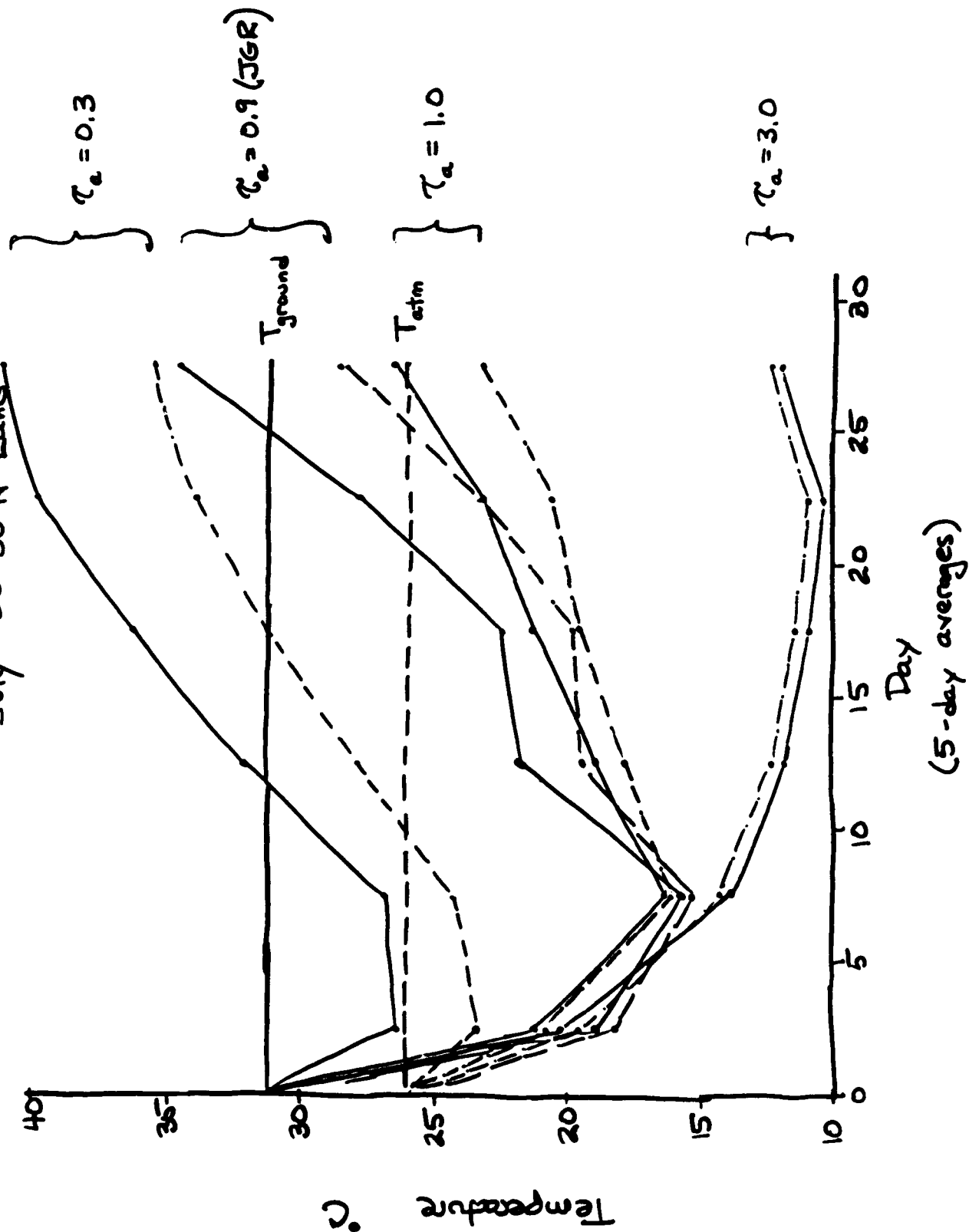
Fraction of Mass Remaining Aloft July



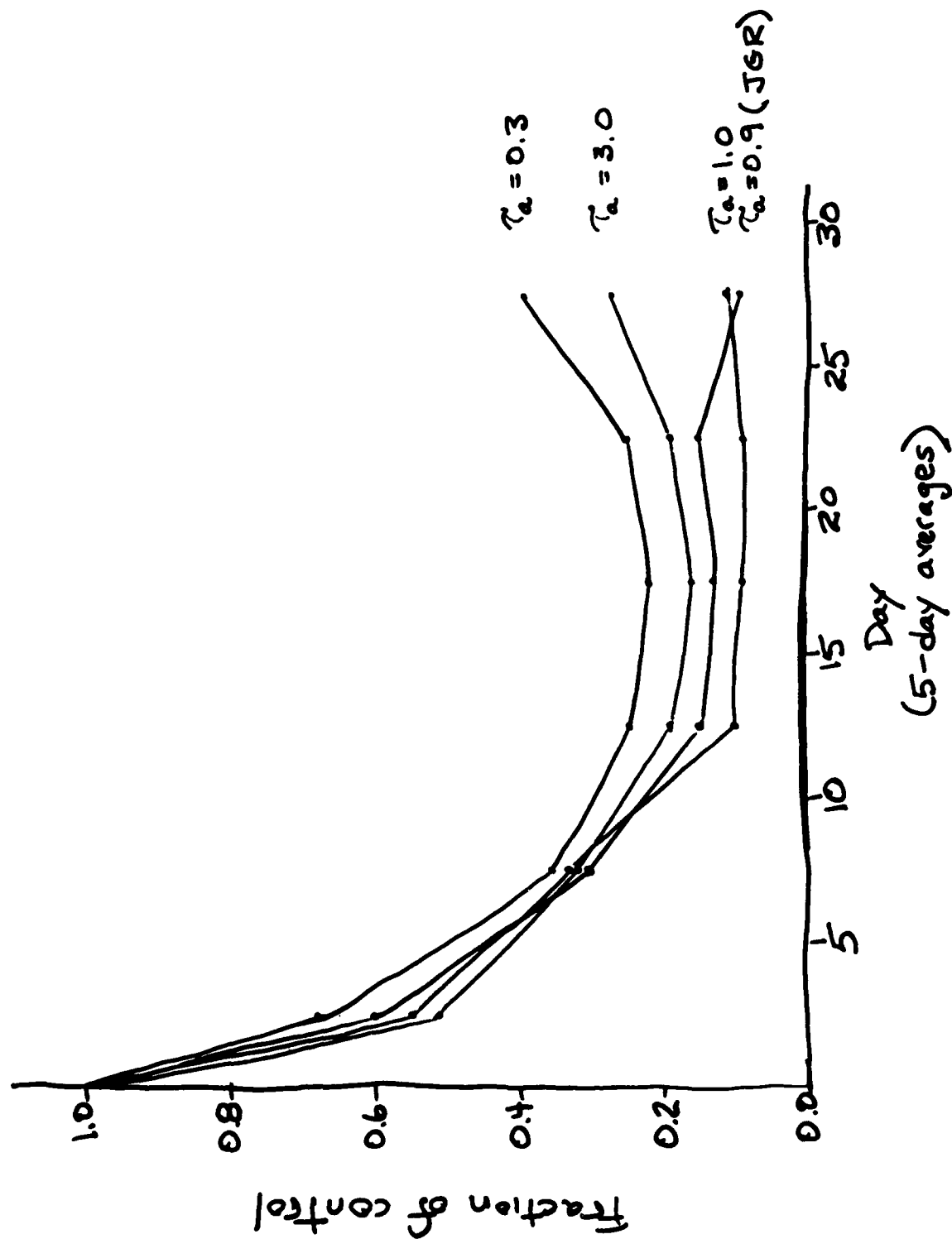
Fraction of Sunlight
July land 30-50°N



Surface Air and Ground Temperatures July 30-50°N Land

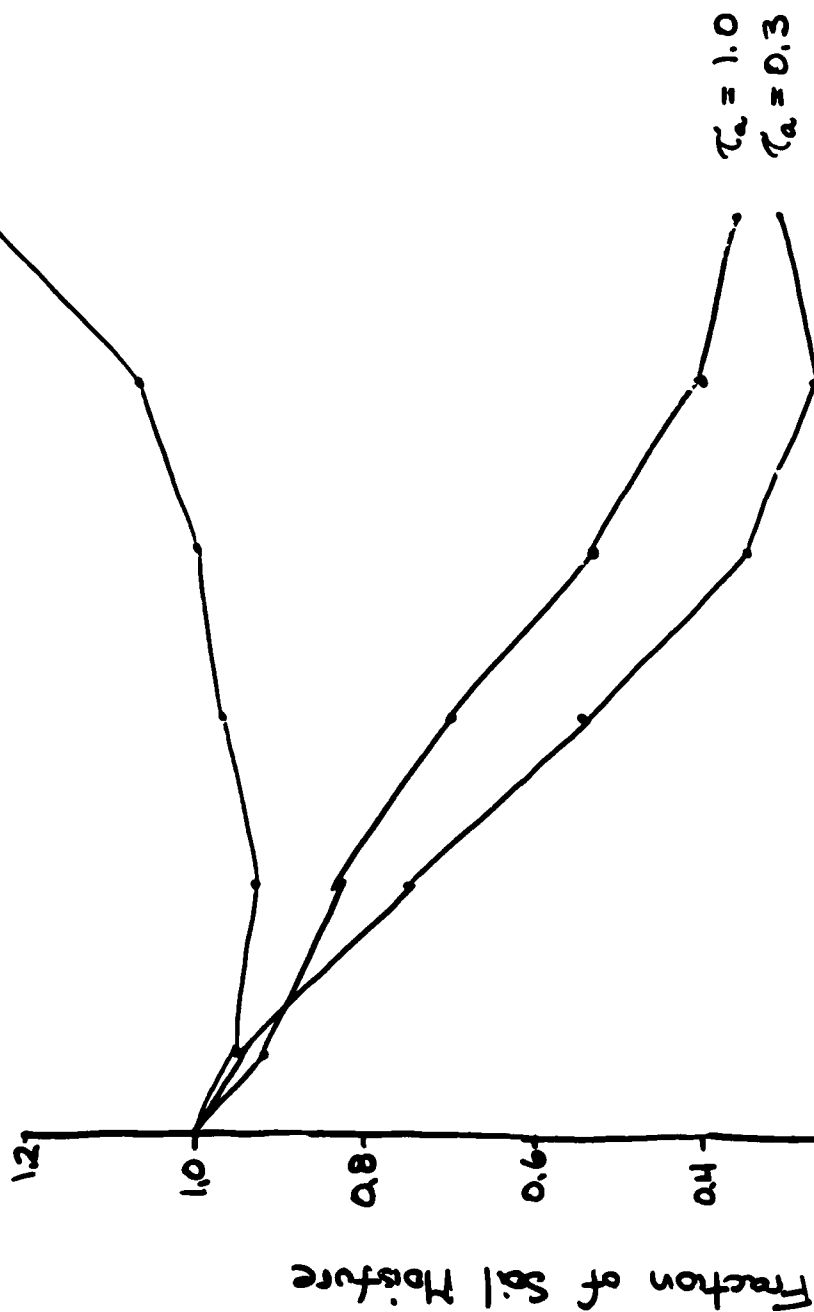


Precipitation on land 30-50°N July



Fraction of Soil Moisture
JULY 30-50°N

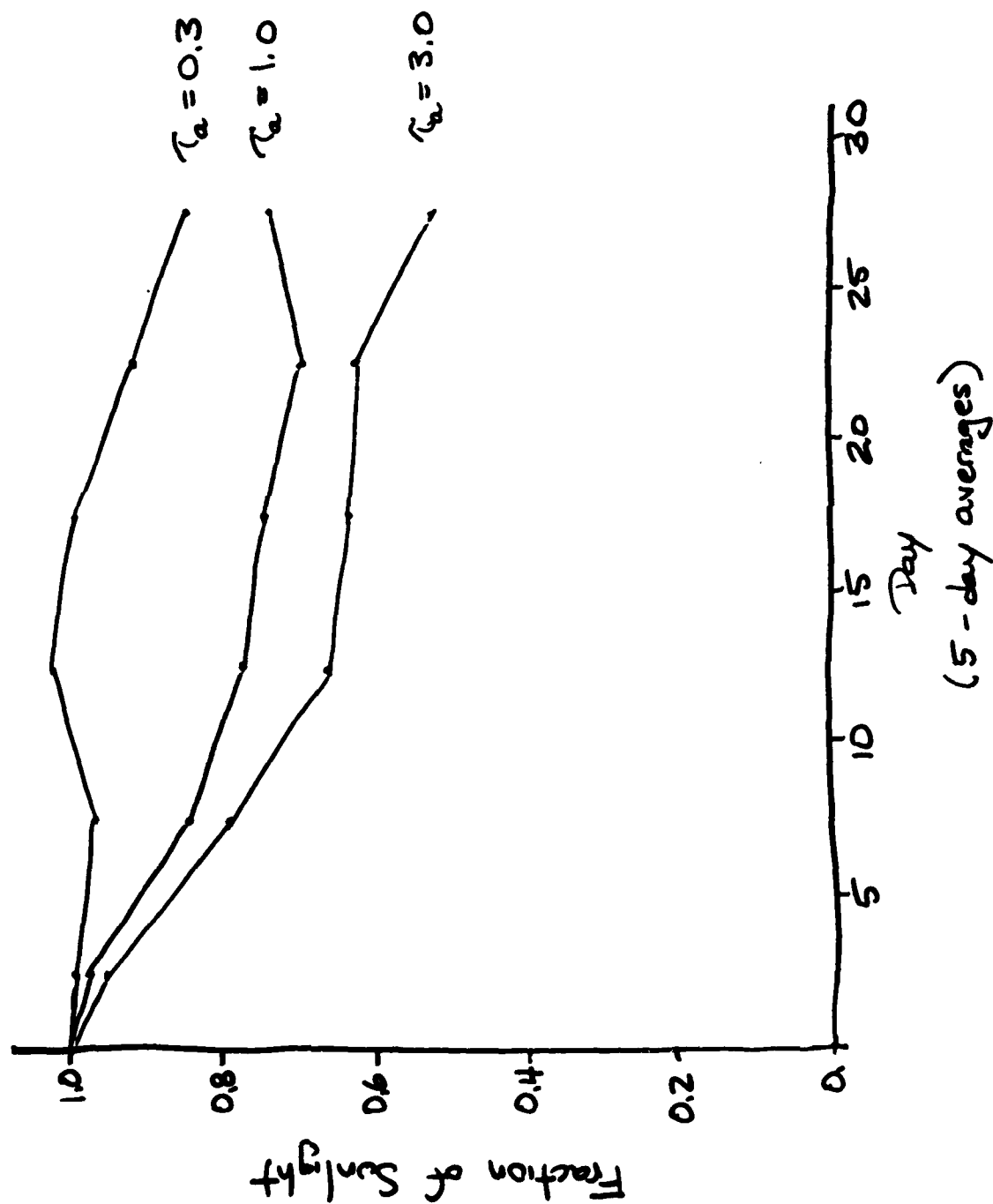
$\tau_a = 3.0$



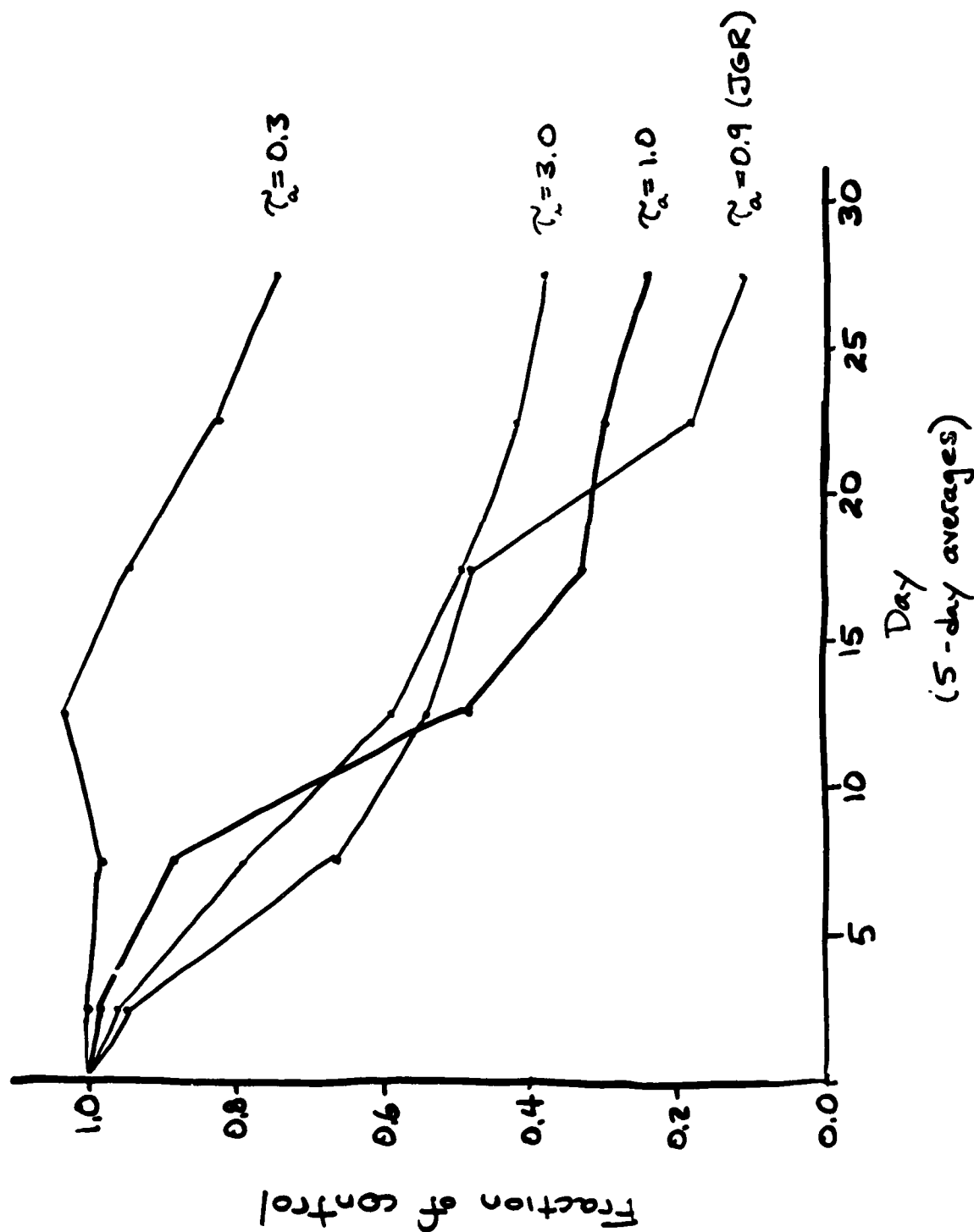
$\tau_a = 1.0$
 $\tau_a = 0.3$

Day
(5 day averages)

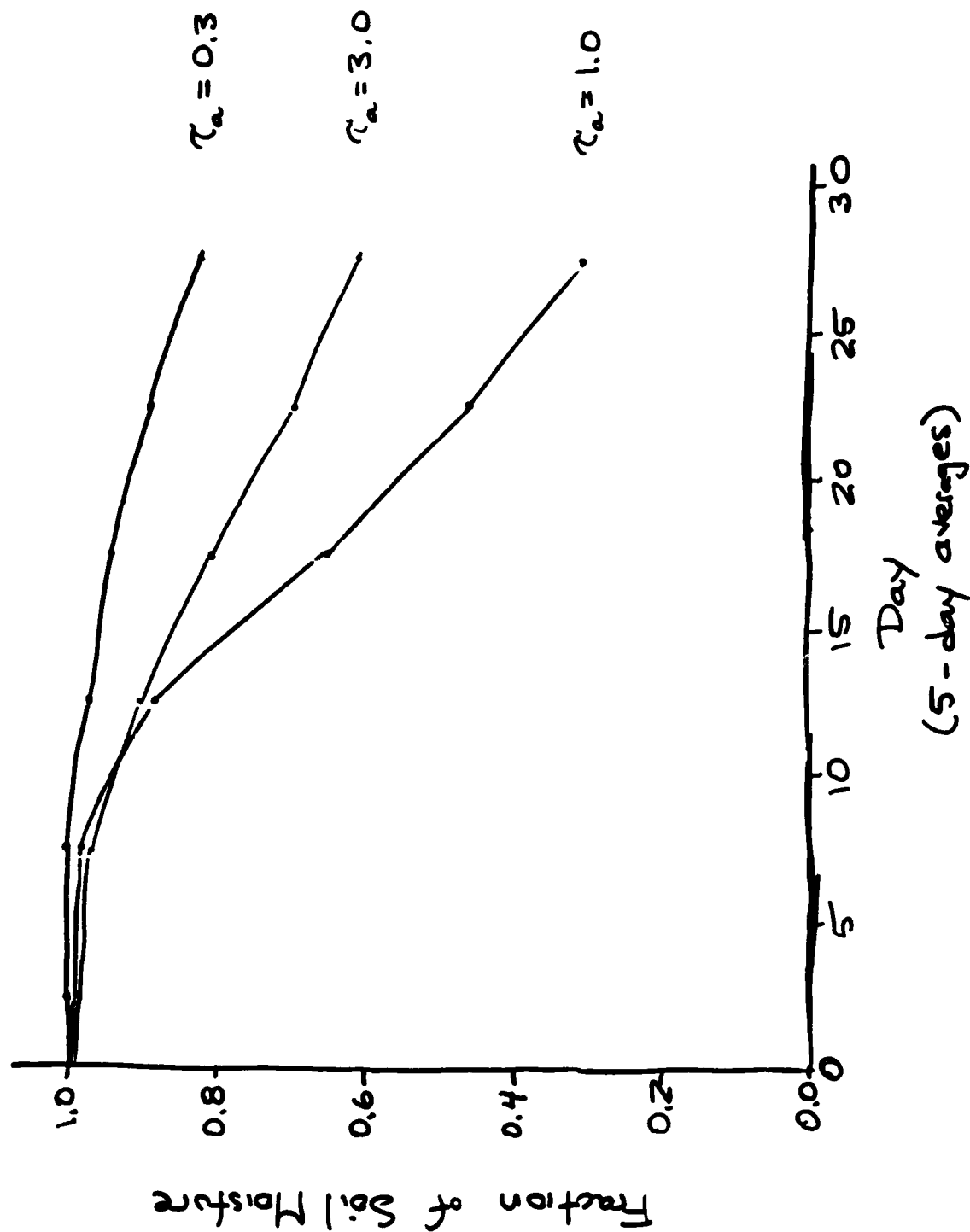
Fraction of Sunlight
July land 0-30°N



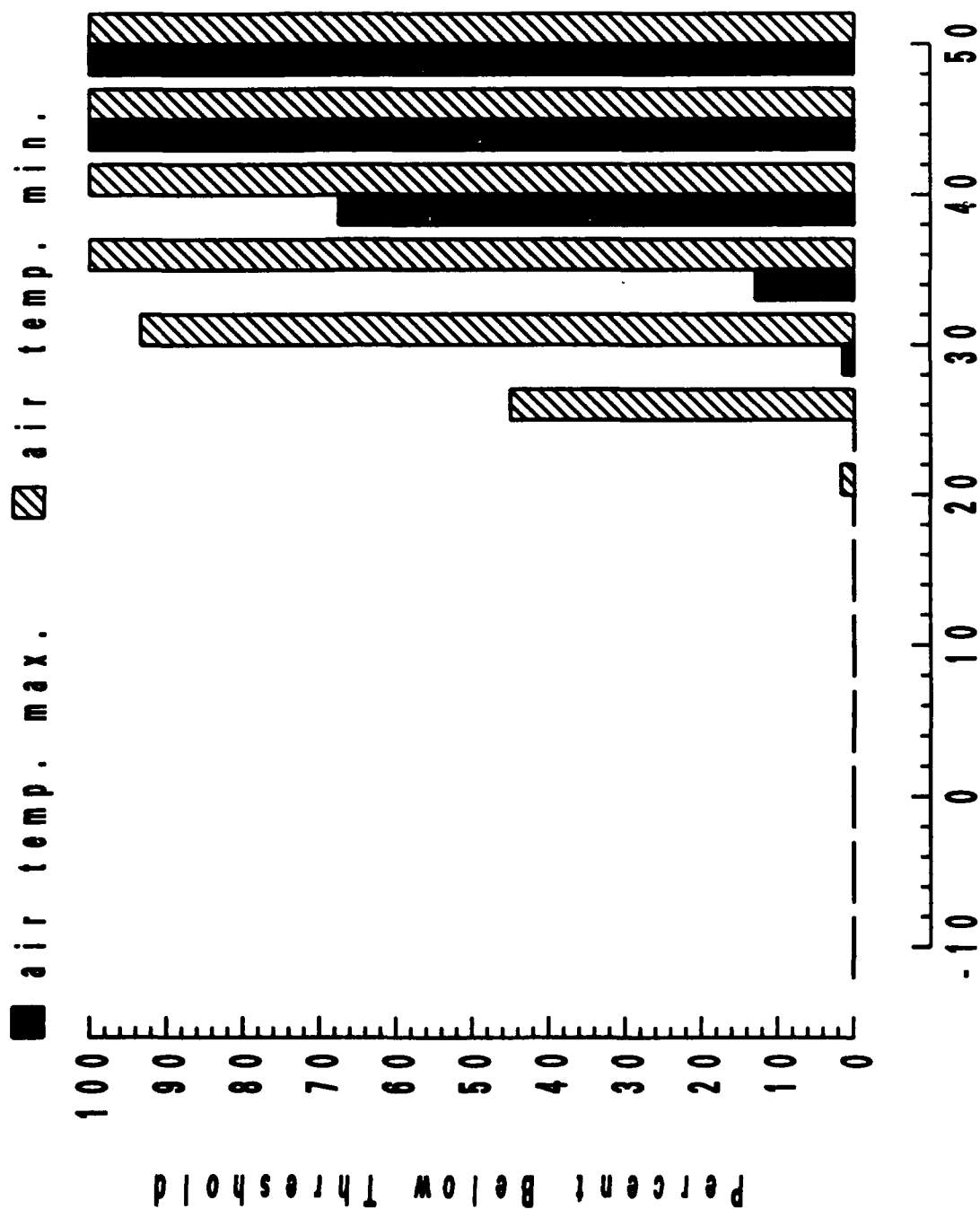
Precipitation on land 0-30°N July



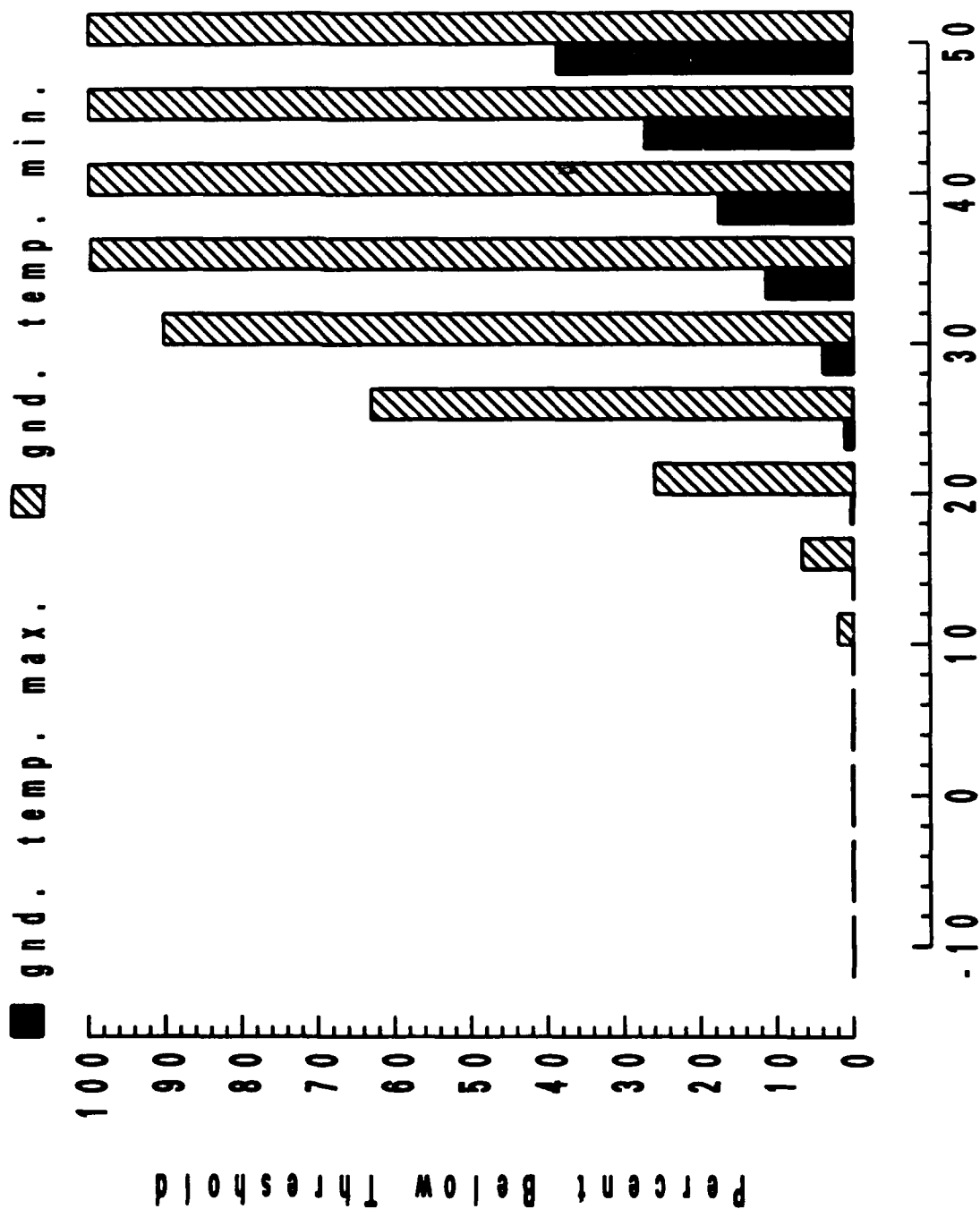
Fraction of Soil Moisture
July Land 0-30°N



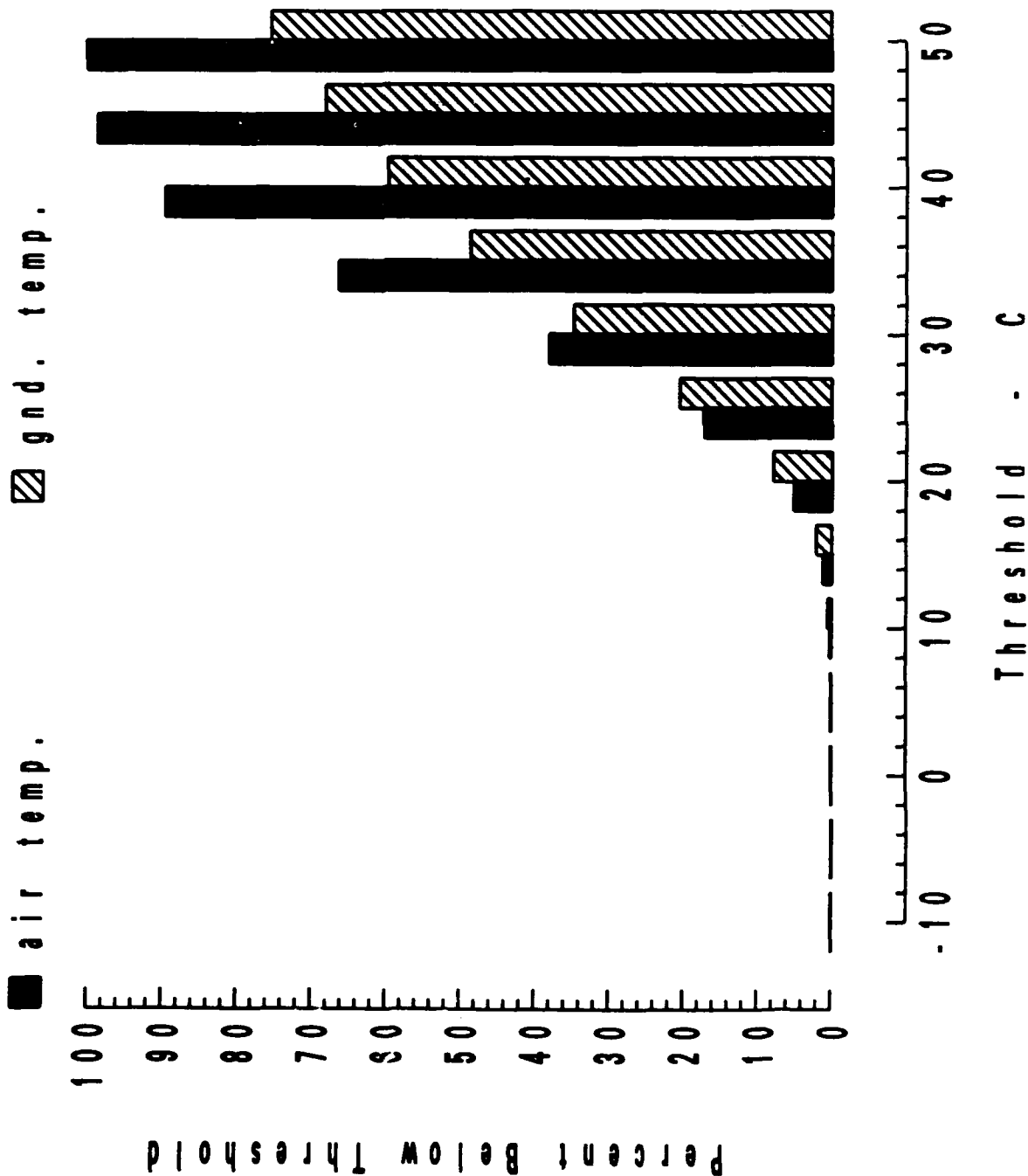
lat (-12, 0), lon (-60, -45)
 Amazon
 control run



lat (32, 44), lon (-105, -85)
 Central USA
 control run

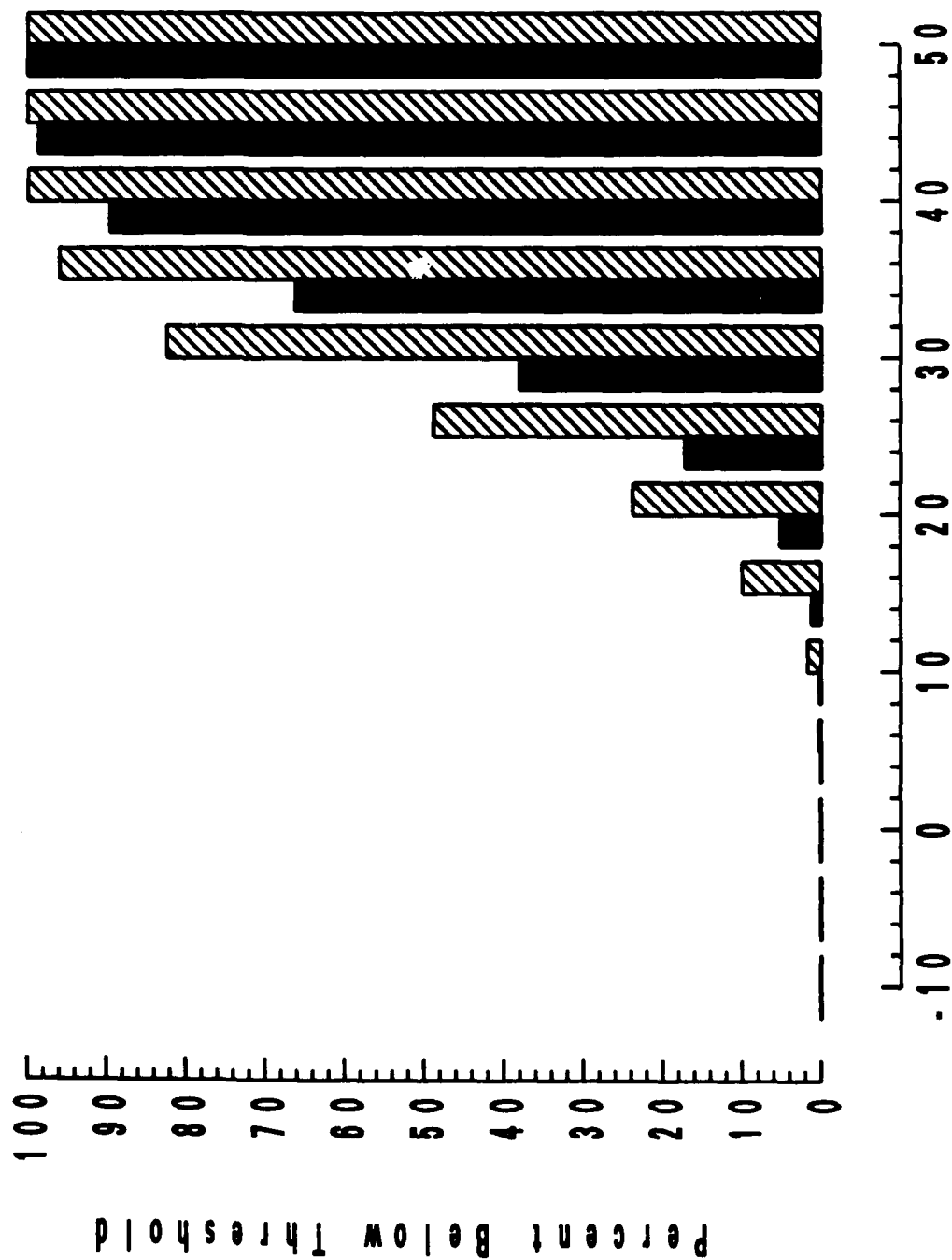


lat (32, 44), lon (-105, -85)
 Central USA
 control run

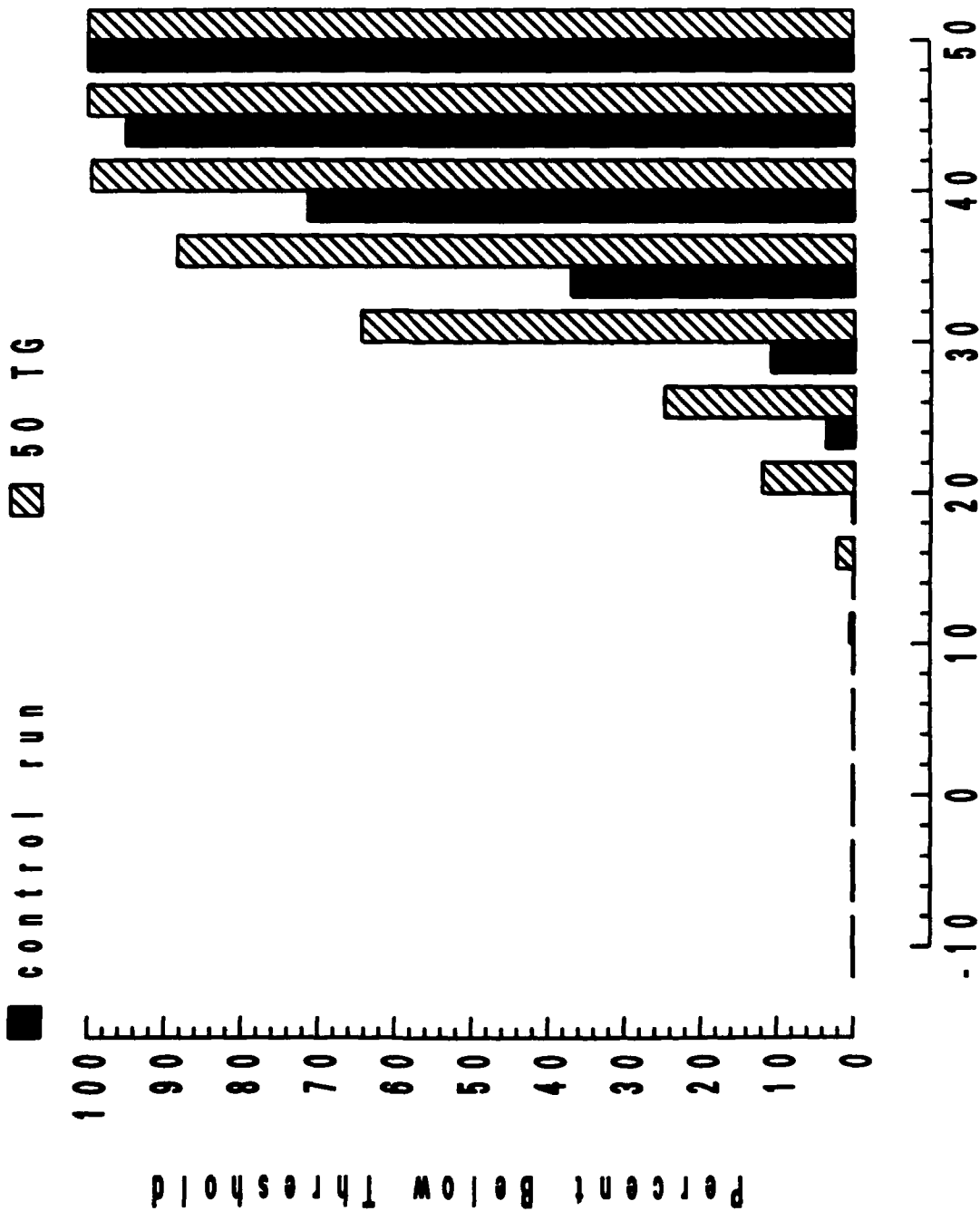


lat (32, 44), lon (-105, -85)
 Central USA
 surface air temperature

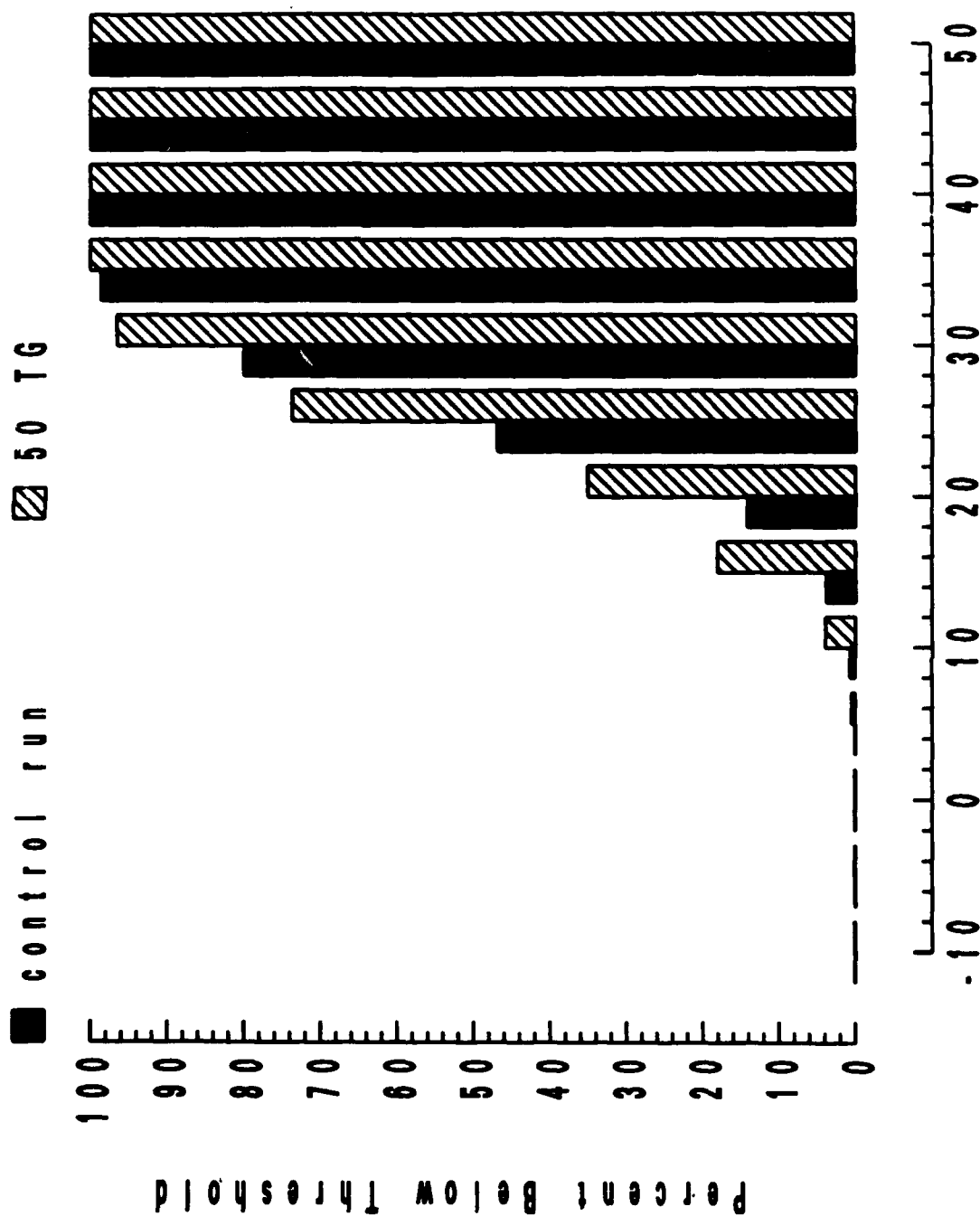
■ control run ▨ 50 TG



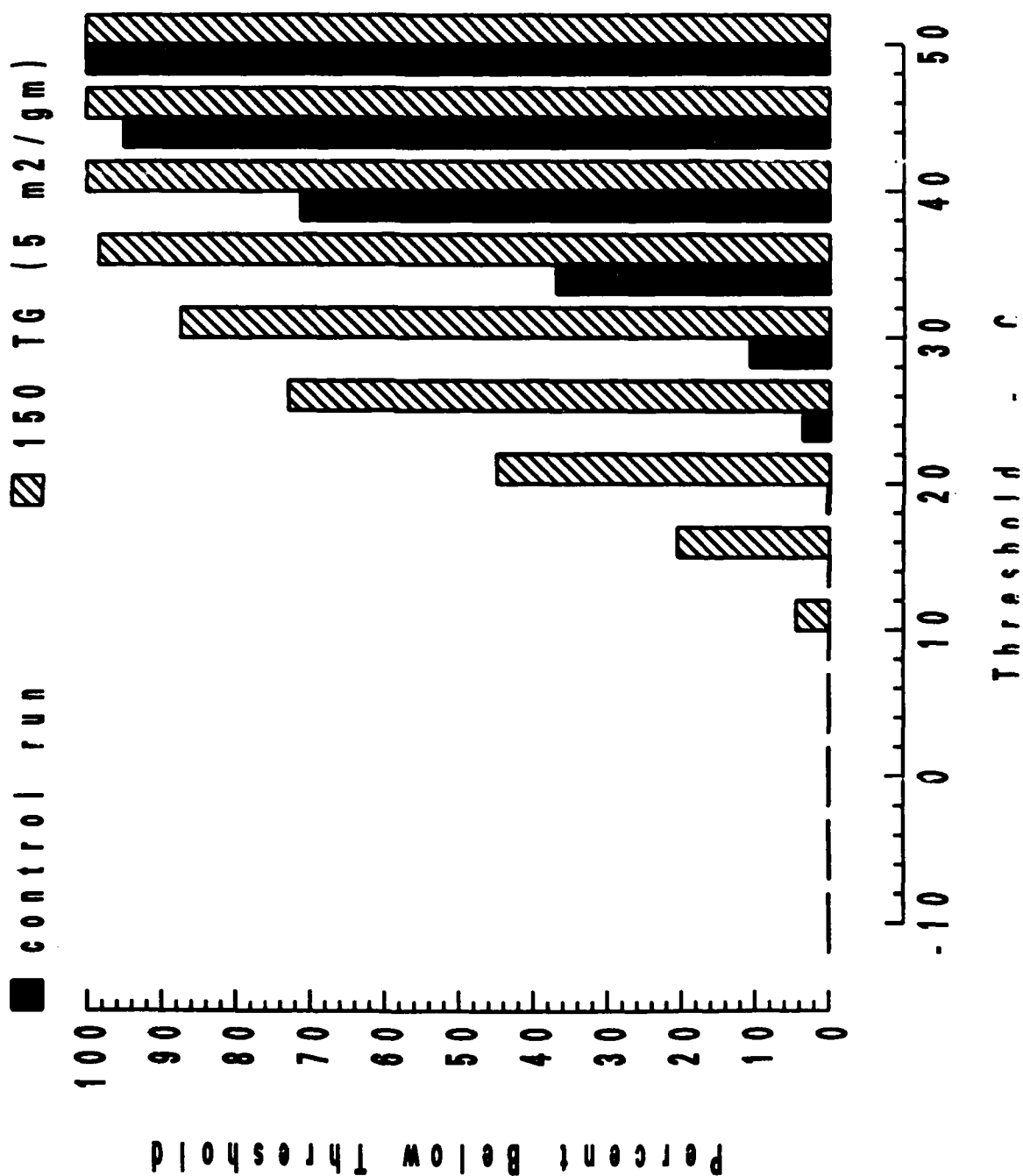
lat (32, 44), lon (-105, -85)
 Central USA
 surface air temperature maximum



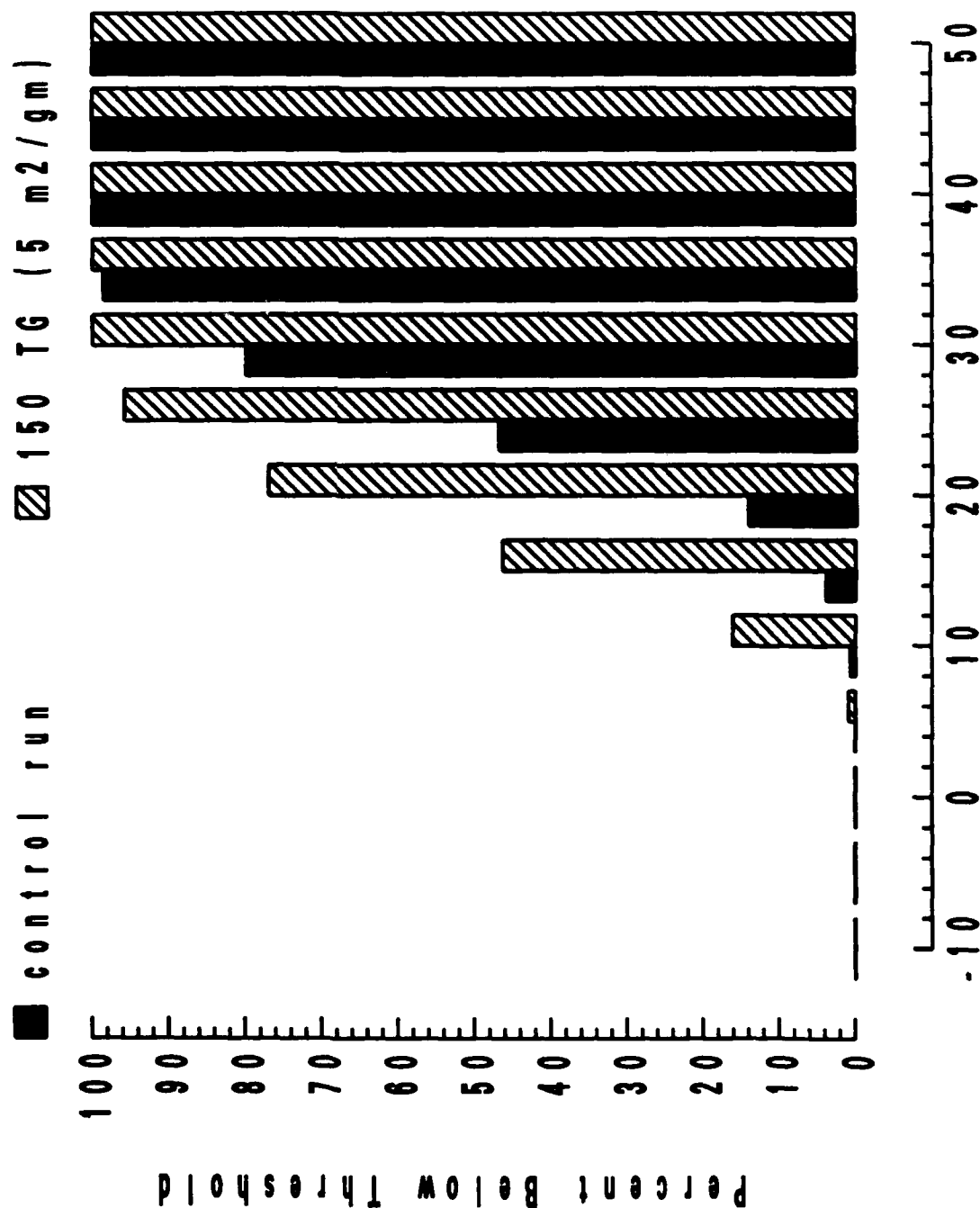
lat (32, 44), lon (-105, -85)
 Central USA
 surface air temperature minimum



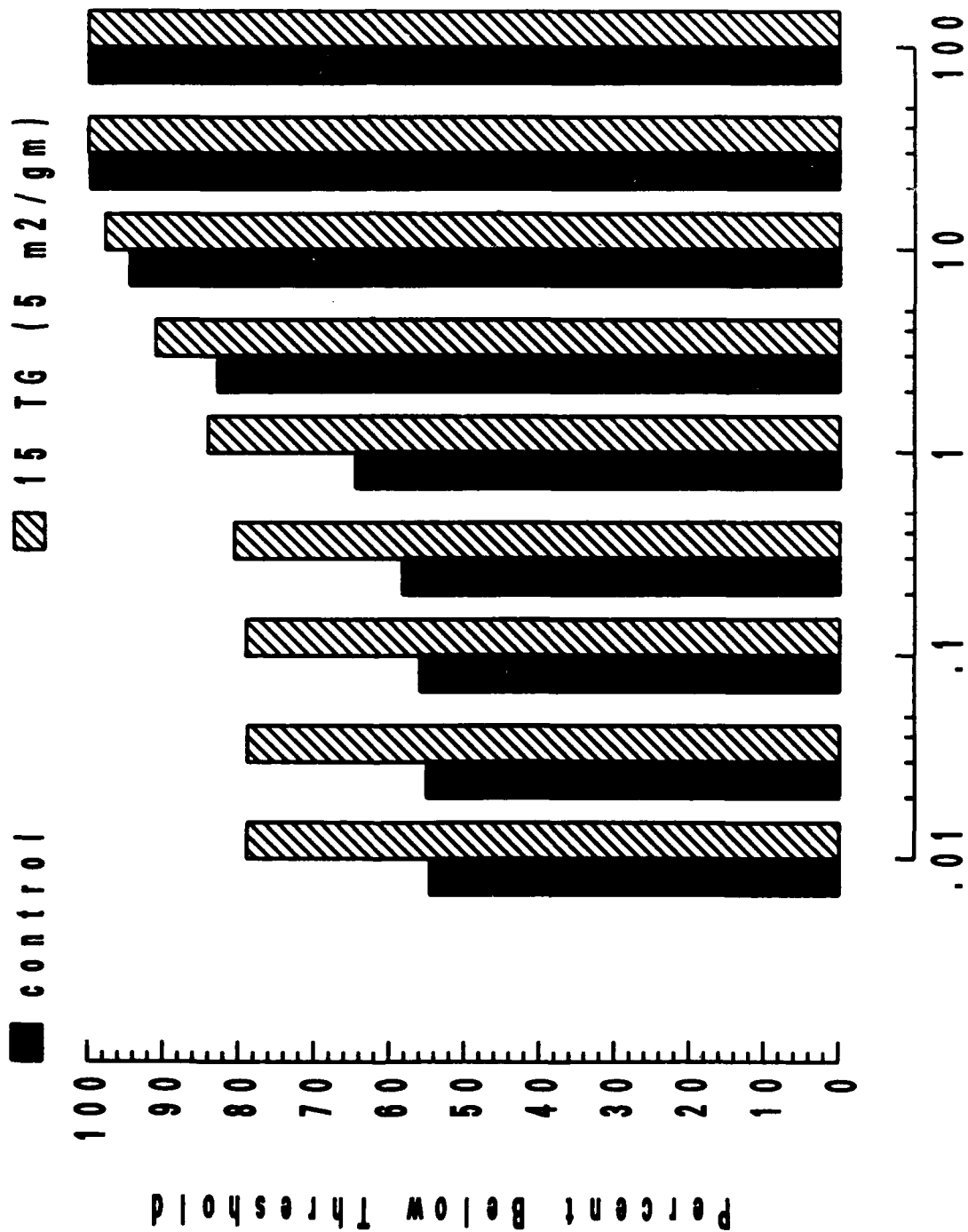
lat (32, 44), lon (-105, -85)
 Central USA
 surface air temperature maximum



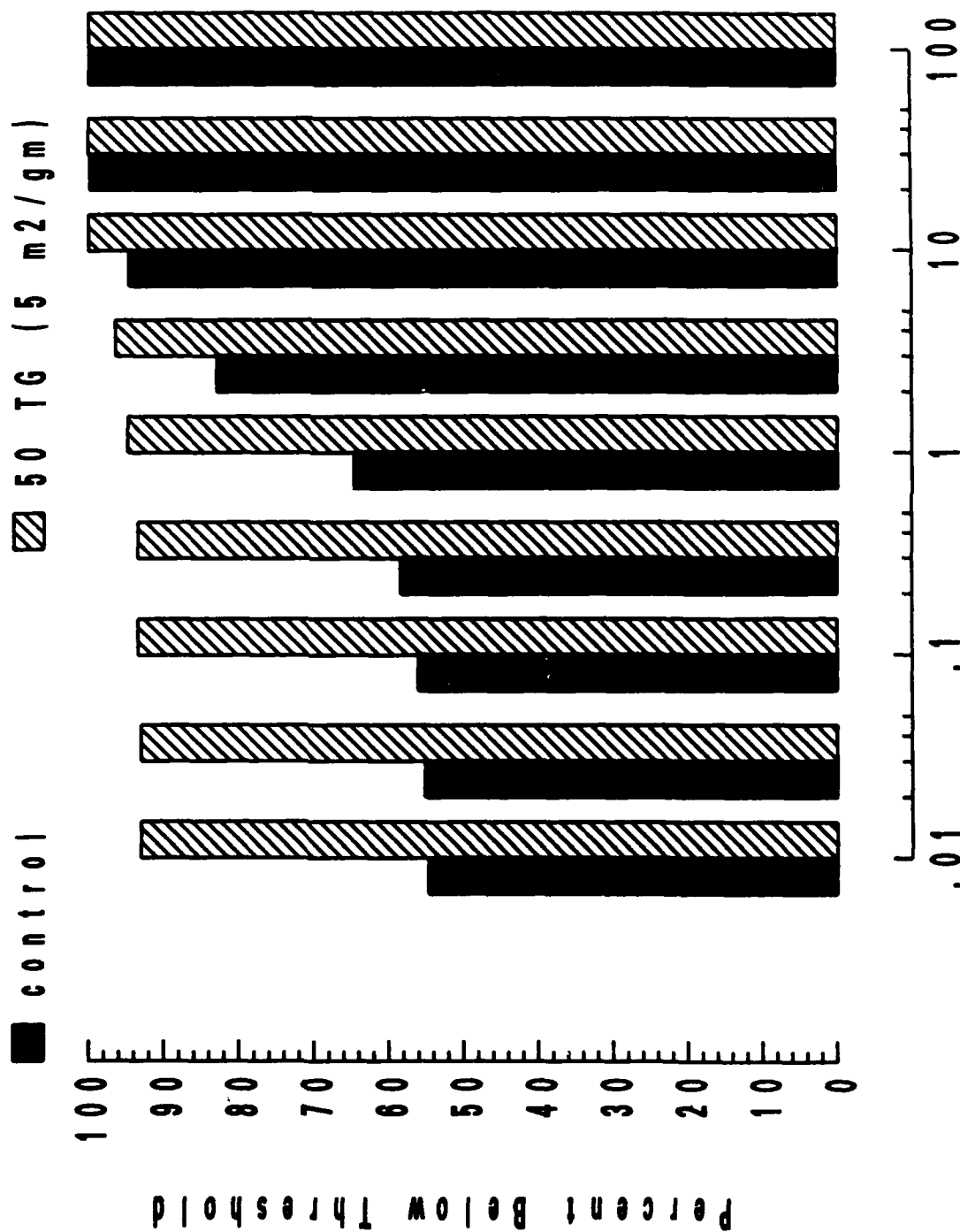
lat (32, 44), lon (-105, -85)
 Central USA
 surface air temperature minimum



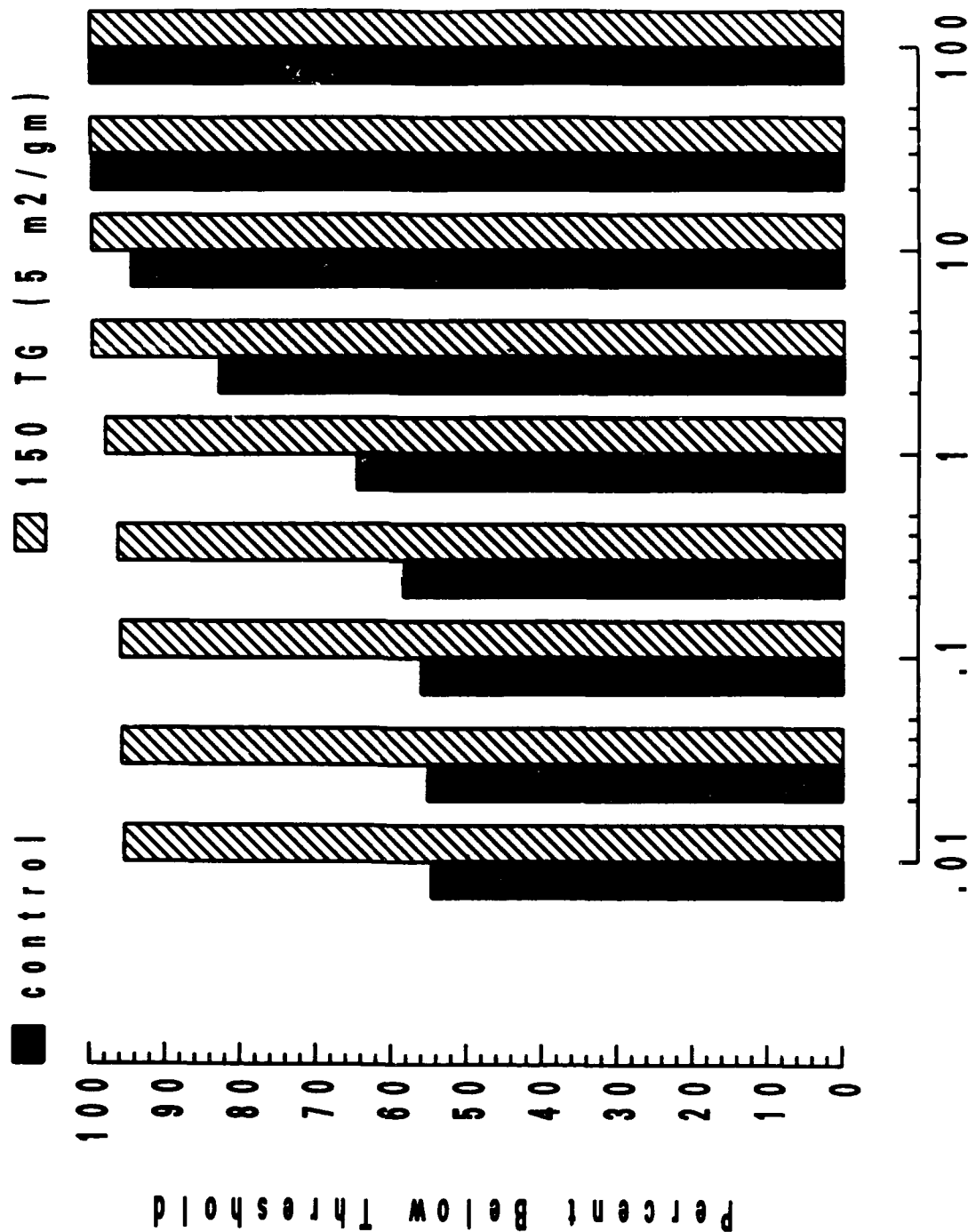
lat (32, 44), lon (-105, -85)
 Central USA
 total precipitation



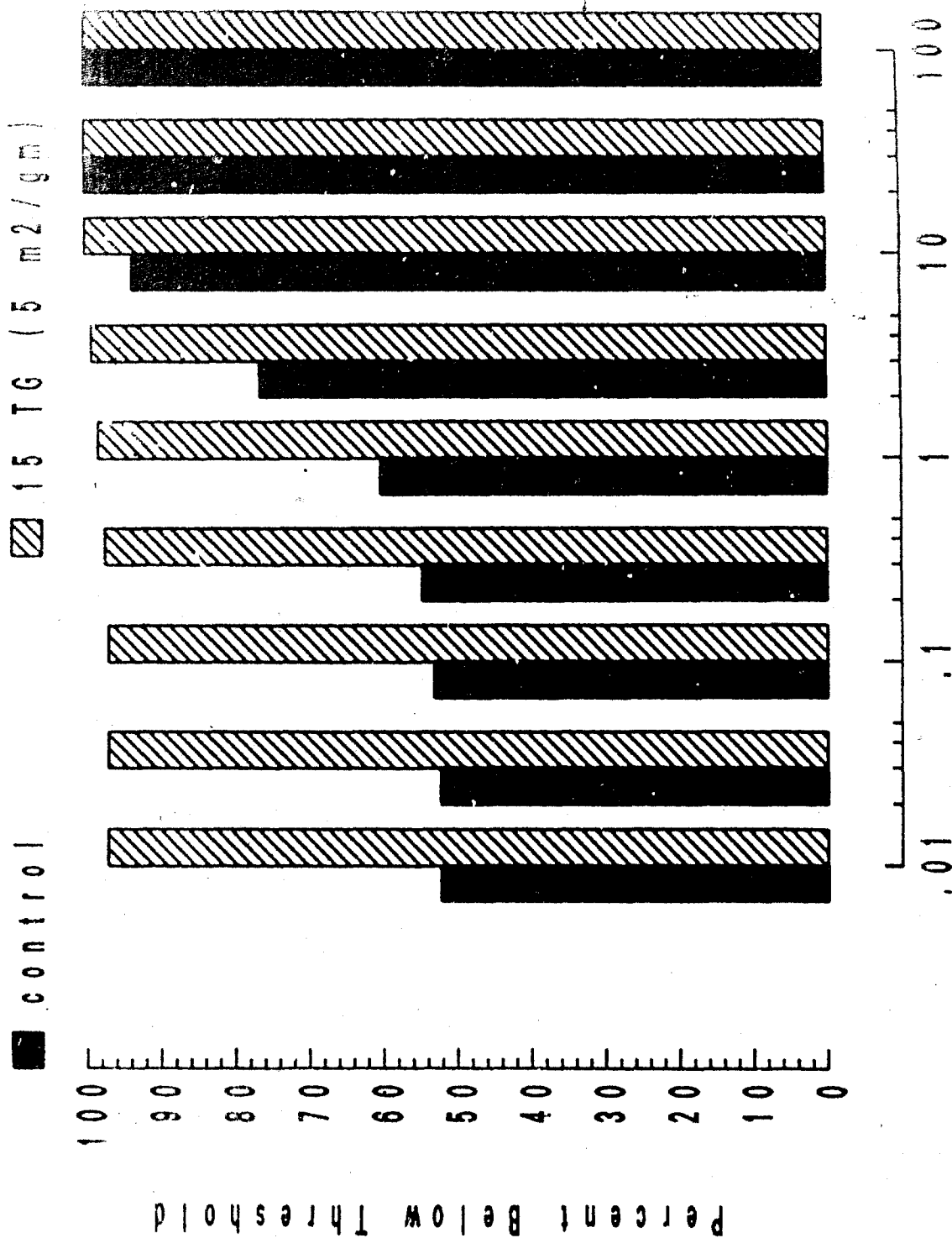
lat (32, 44), lon (-105, -85)
 Central USA
 total precipitation



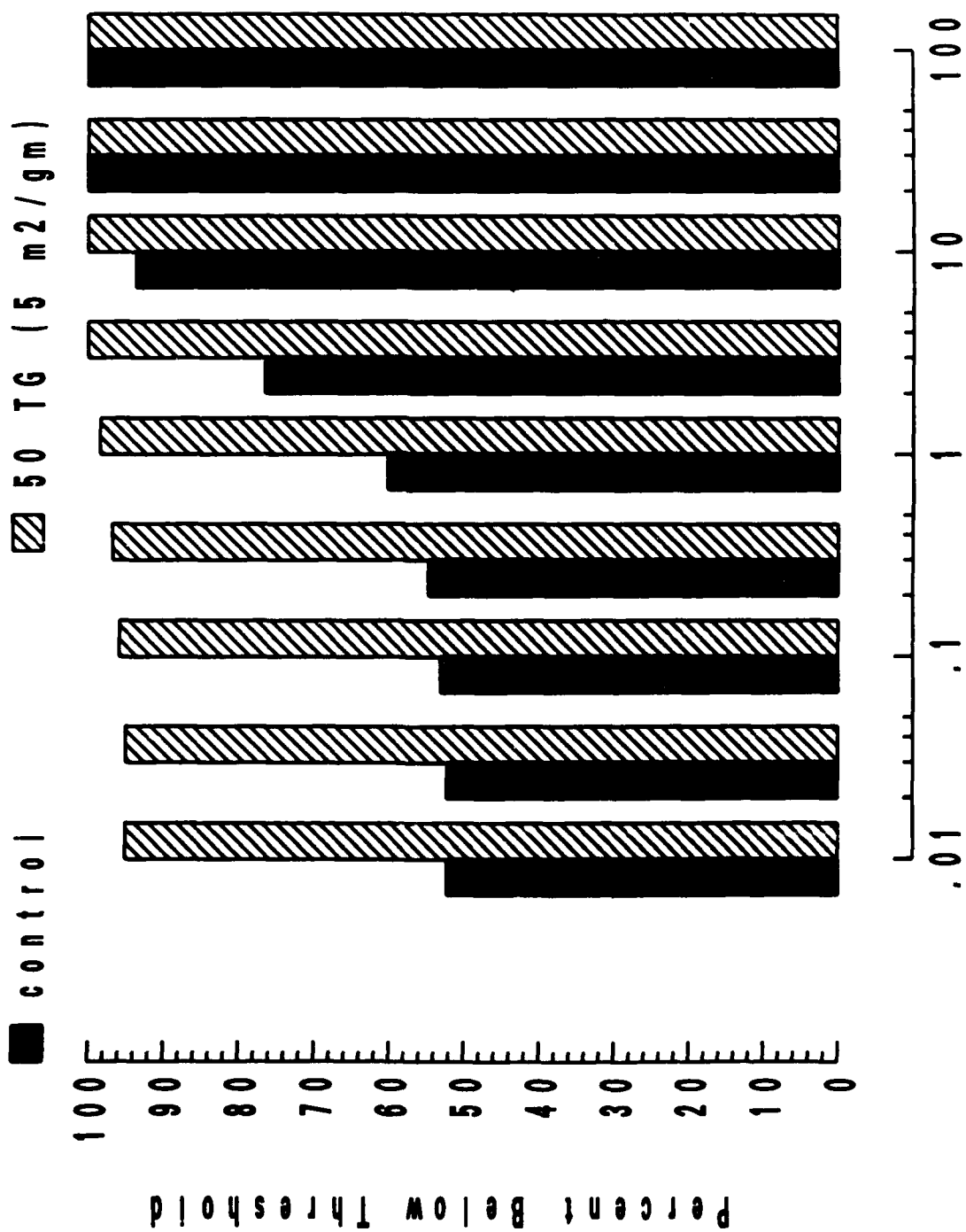
lat (32, 44), lon (-105, -85)
 Central USA
 total precipitation



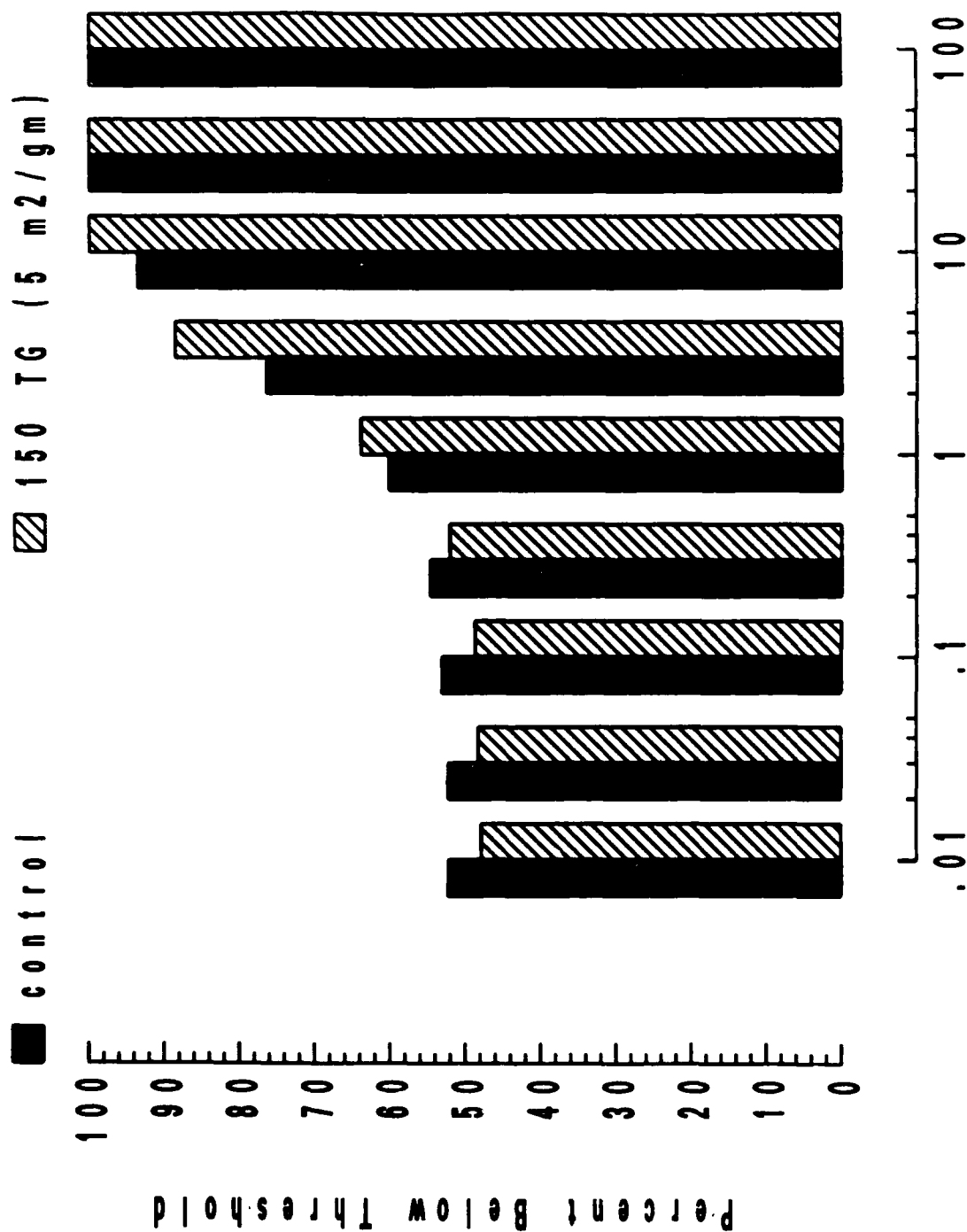
lat (44, 52), lon (25 40)
 Ukraine
 total precipitation



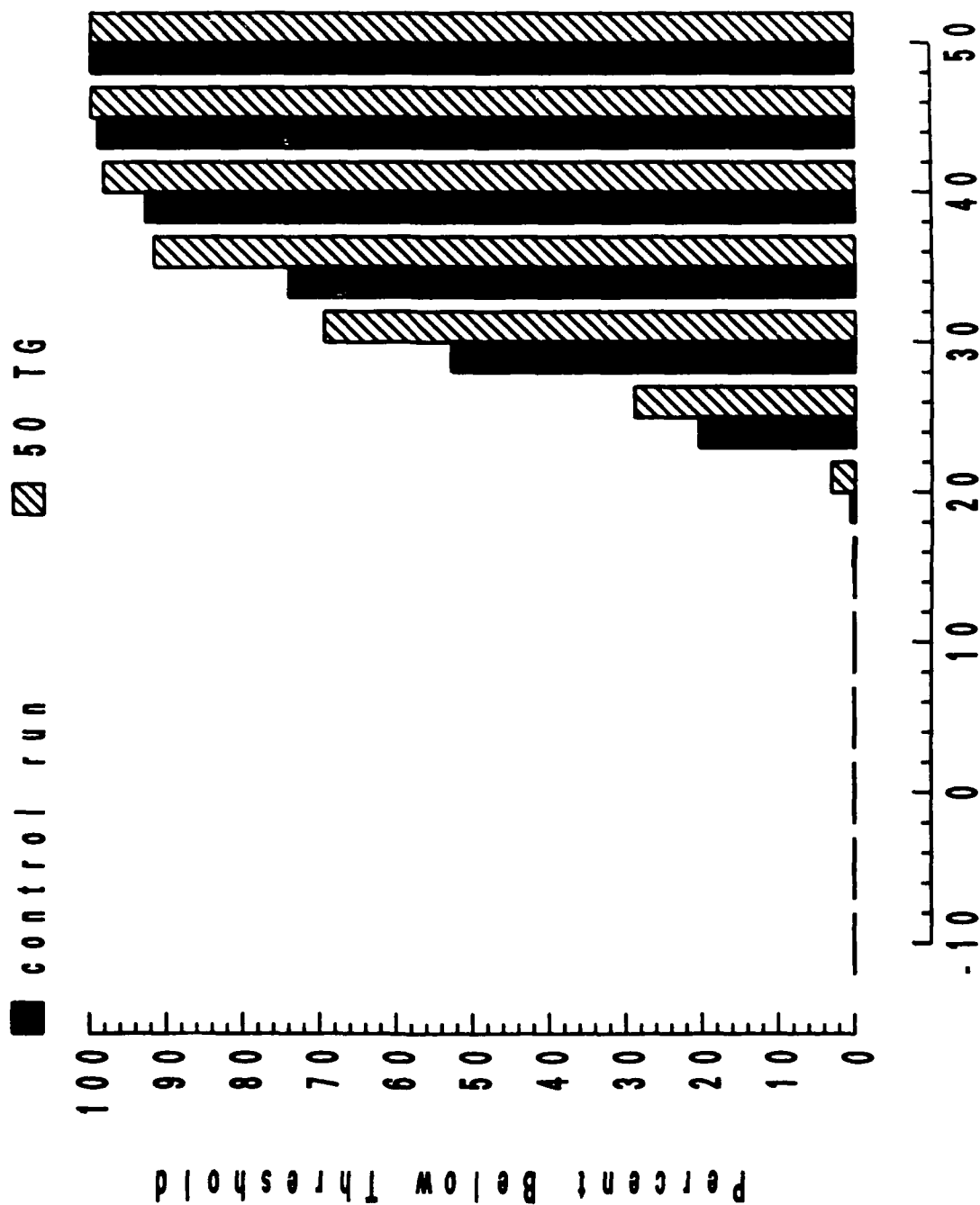
lat (44, 52), lon (25, 40)
 Ukraine
 total precipitation



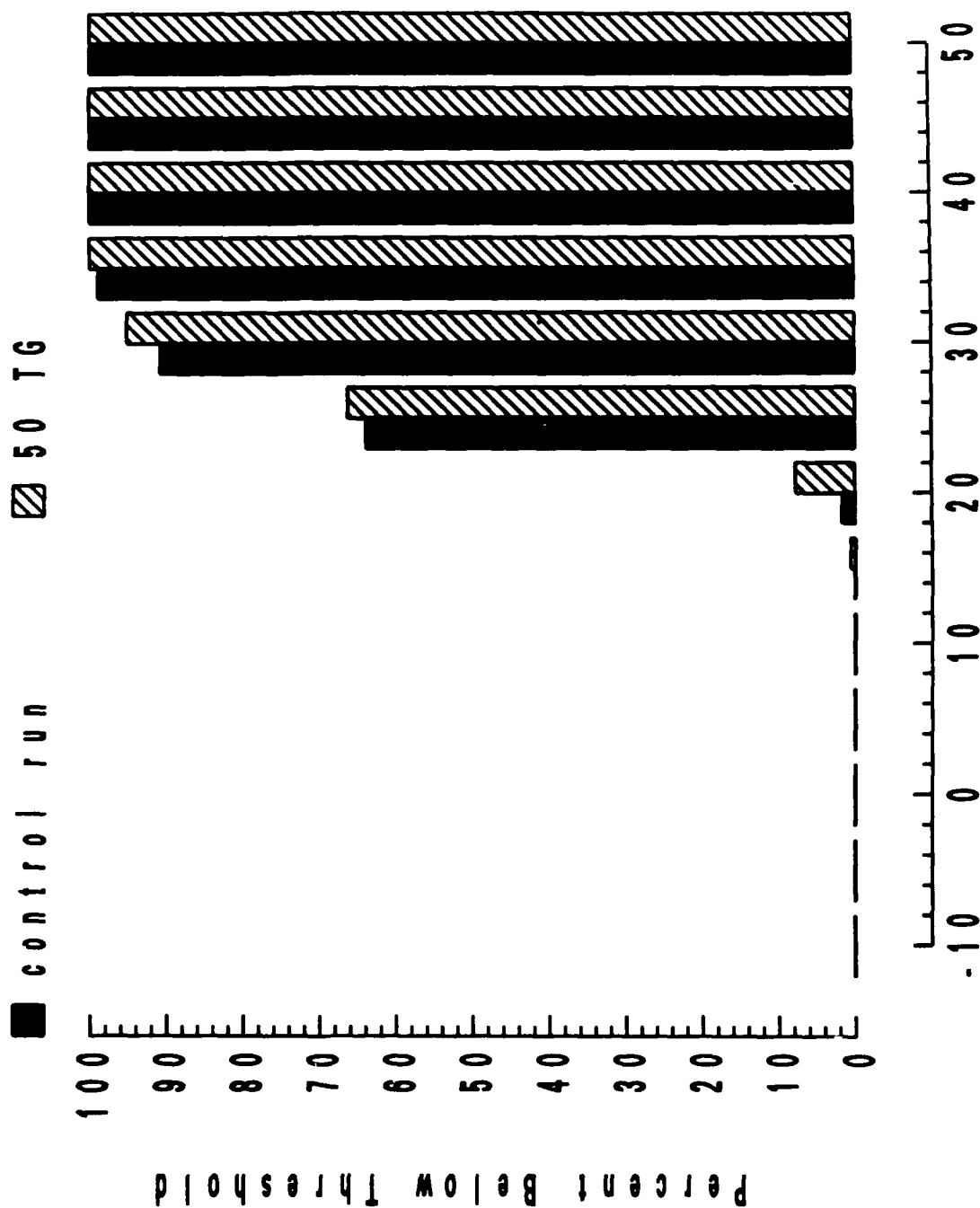
lat (44, 52), lon (25, 40)
 Ukraine
 total precipitation



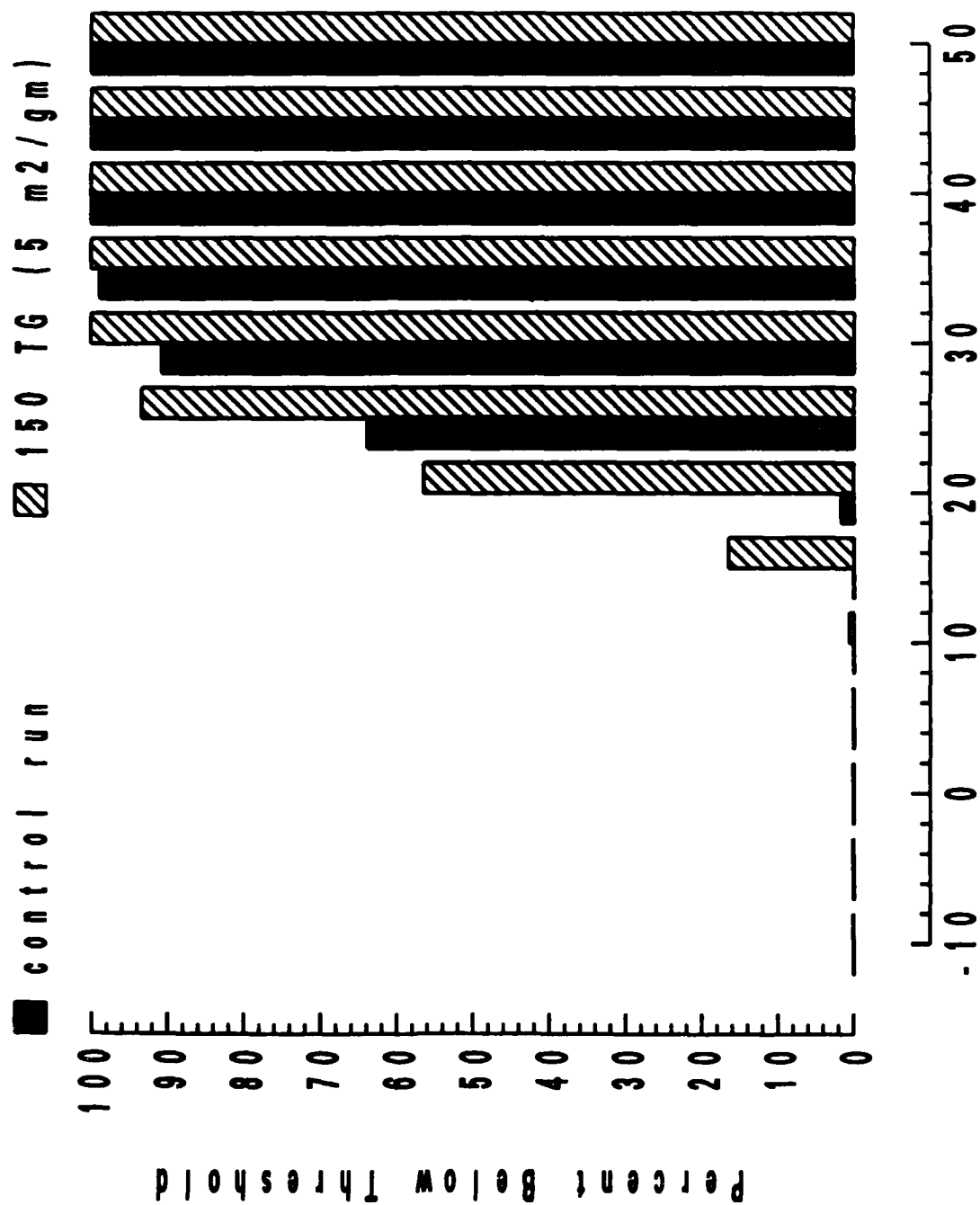
lat (24, 32), lon (110, 120)
 Southern China
 surface air temperature



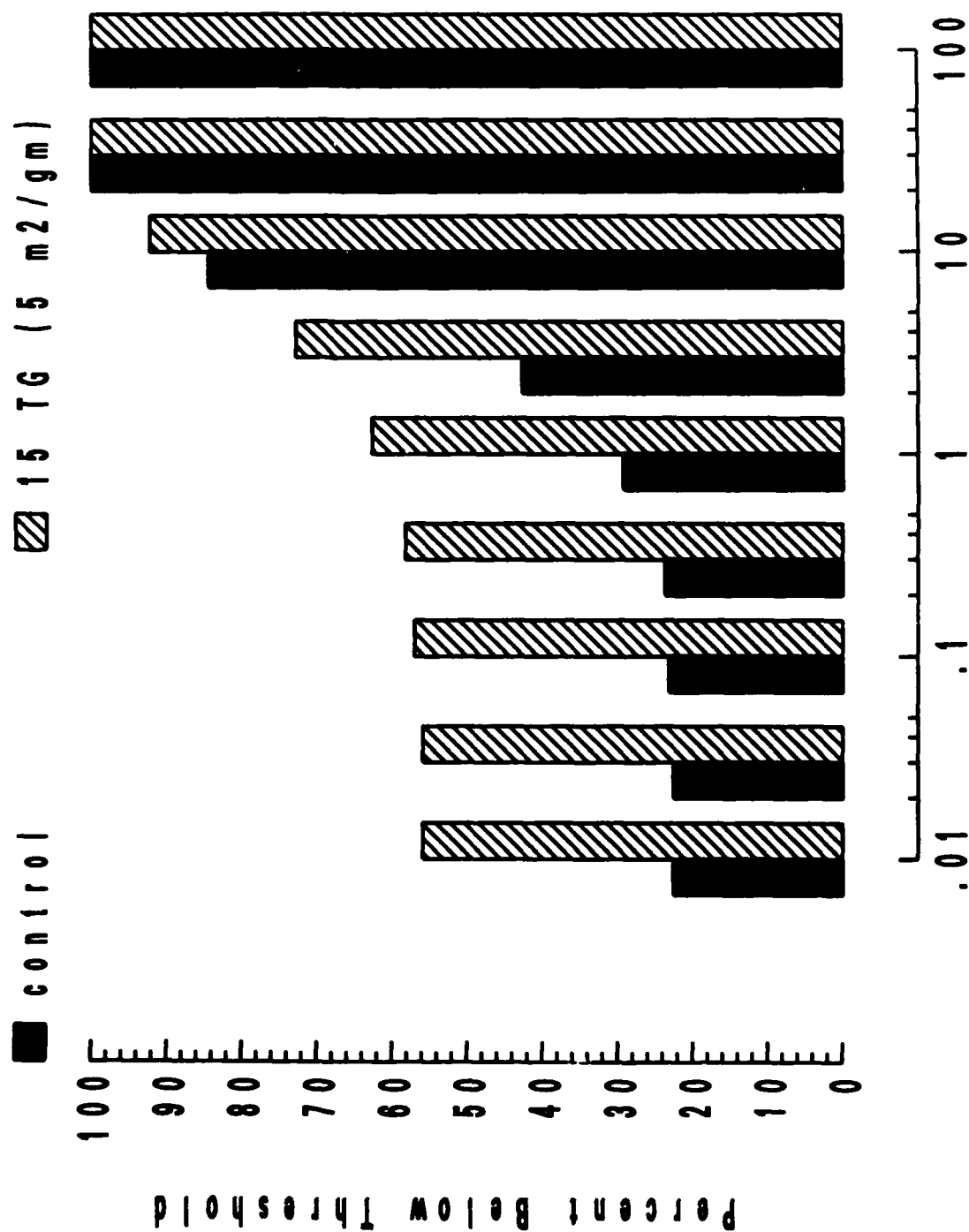
lat (24, 32), lon (110, 120)
 Southern China
 surface air temperature minimum



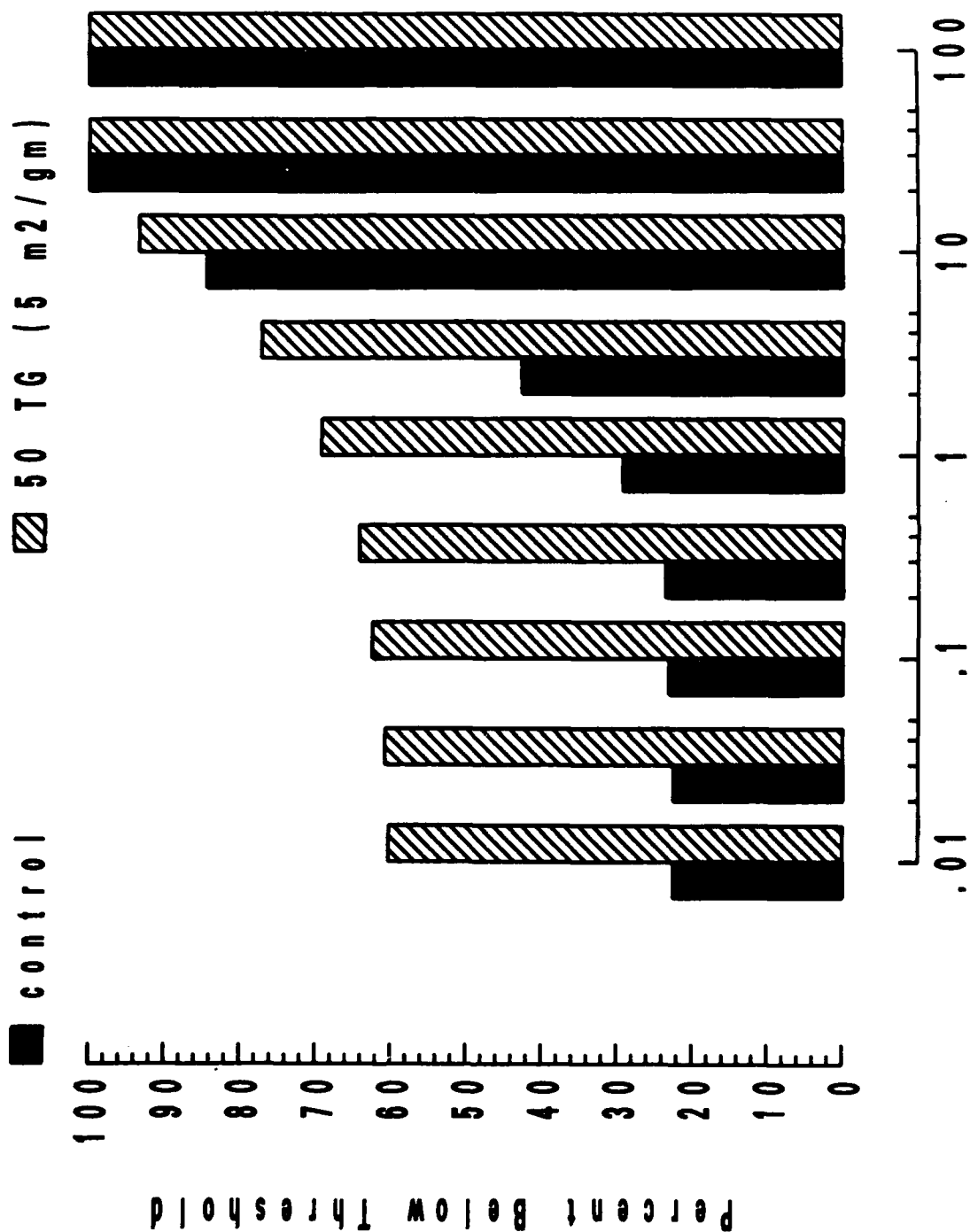
lat (24, 32), lon (110, 120)
 Southern China
 surface air temperature minimum



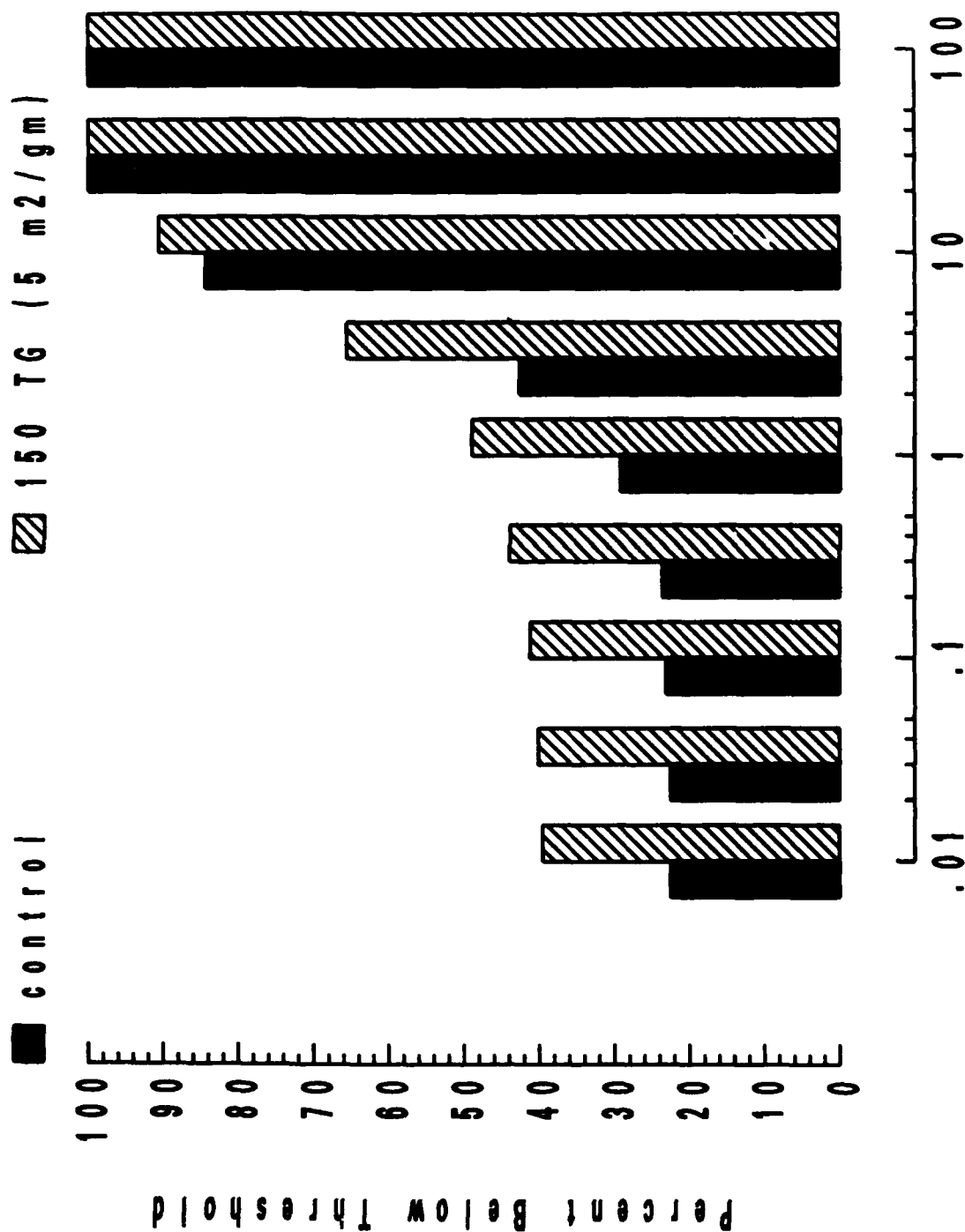
lat (24, 32), lon (110, 120)
 Southern China
 total precipitation



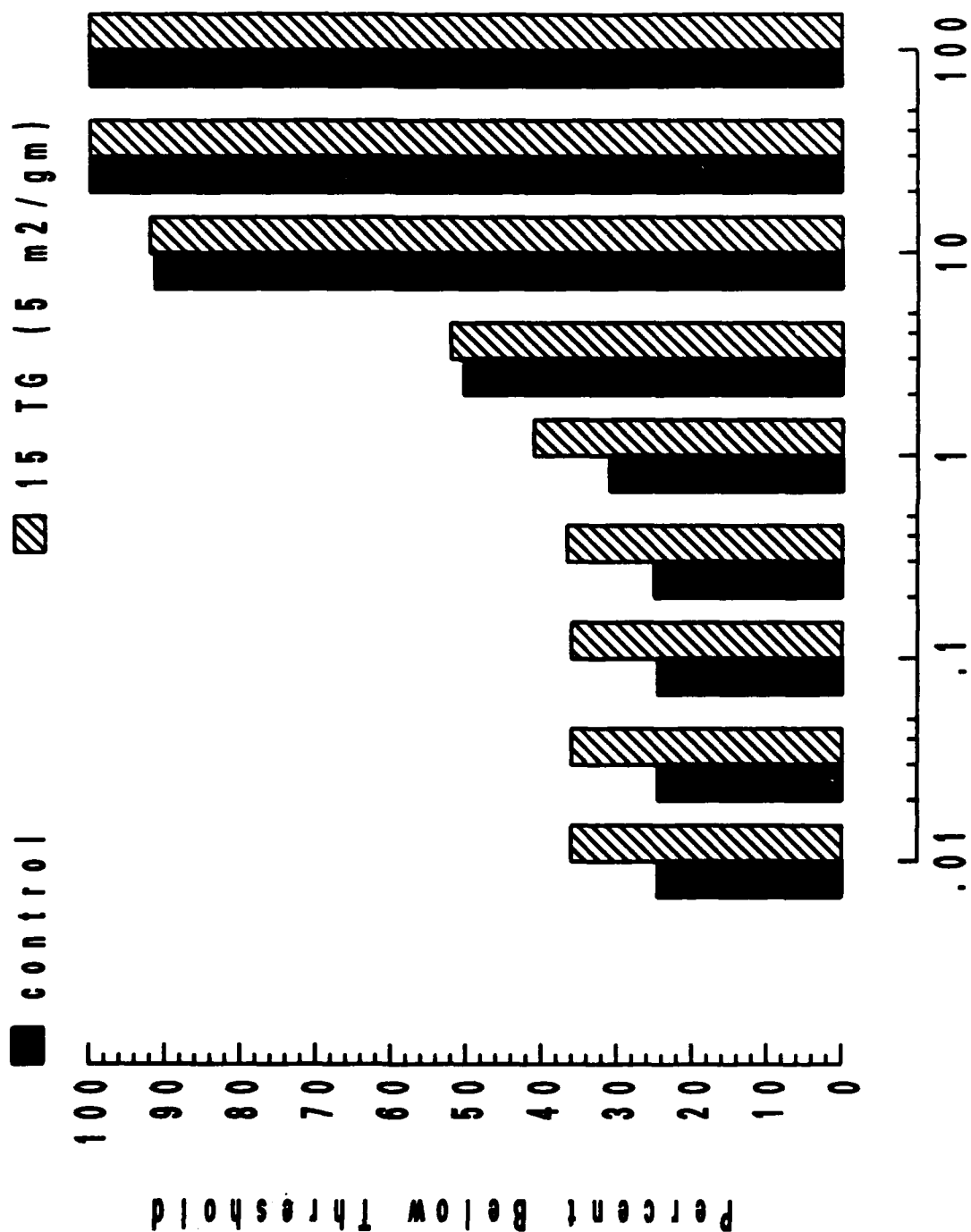
lat (24, 32), lon (110, 120)
 Southern China
 total precipitation



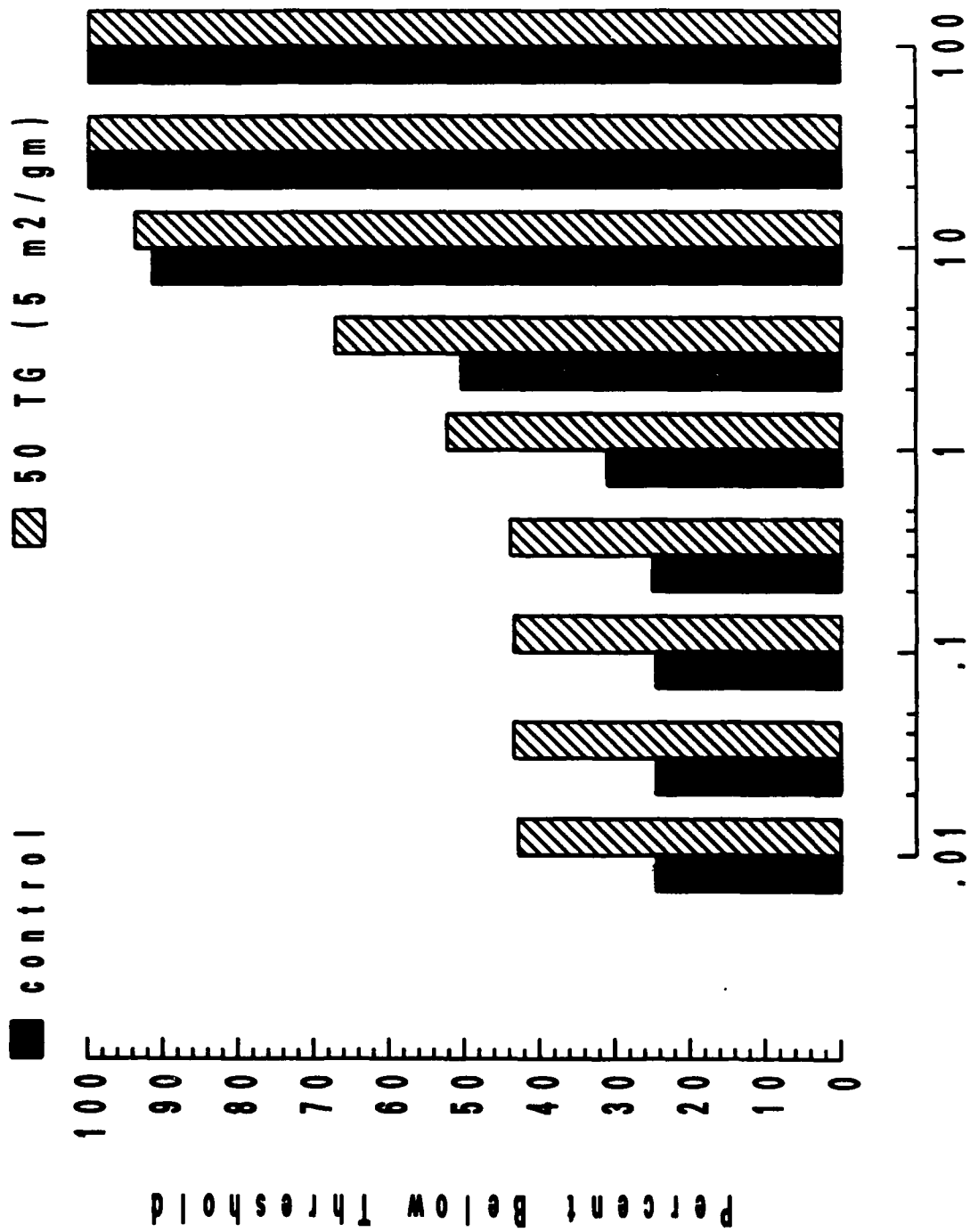
lat (24, 32), lon (110, 120)
 Southern China
 total precipitation



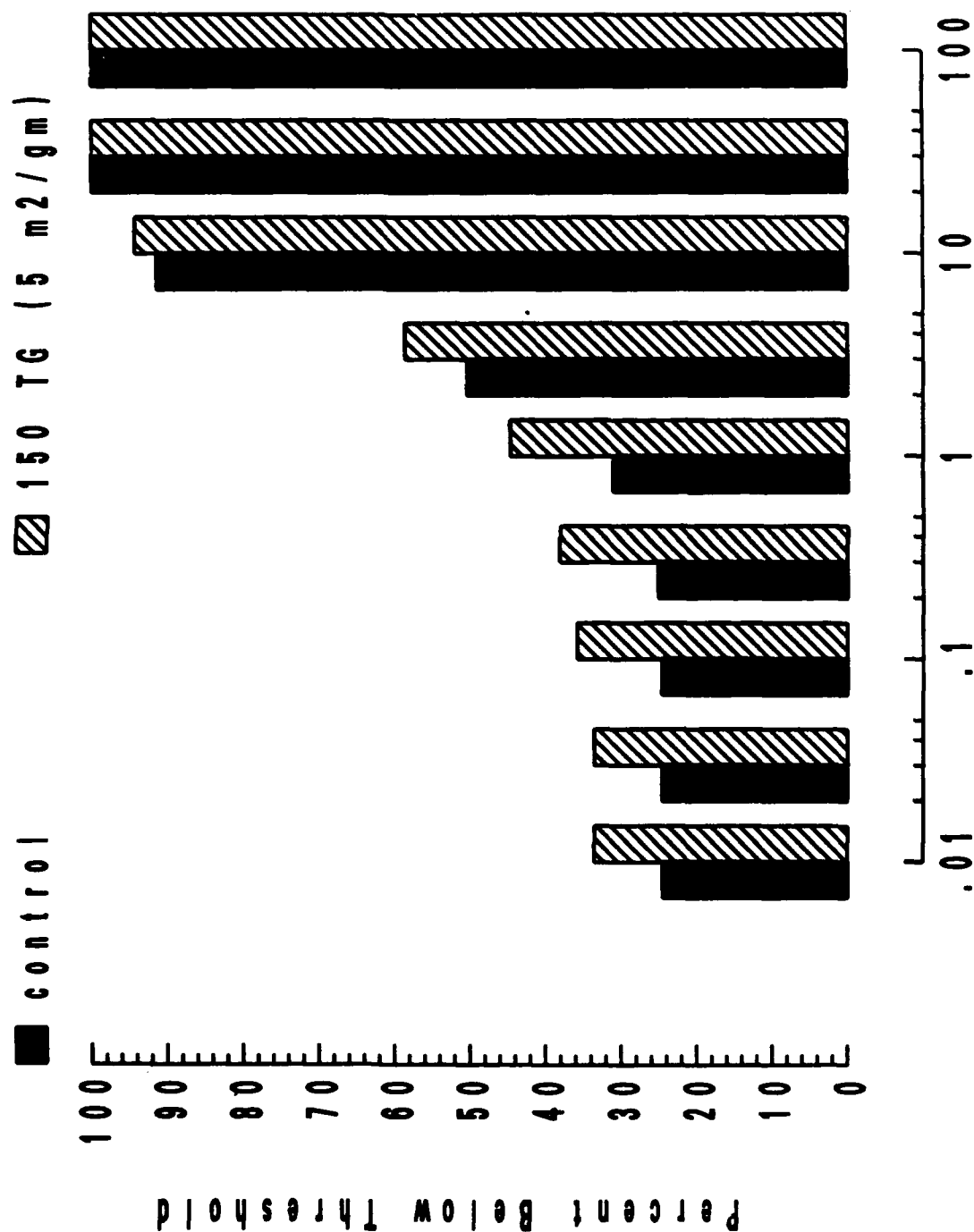
lat (12, 24), lon (75, 80)
 India
 total precipitation



lat (12, 24), lon (75, 80)
 India
 total precipitation



lat (12, 24), lon (75, 80)
 India
 total precipitation



Protracted climatic effects of massive smoke injection into the atmosphere

Curt Covey

Meteorology and Physical Oceanography Division,
Rosenstiel School of Marine and Atmospheric Science,
University of Miami, Miami, Florida 33149, USA

Climate perturbations caused by sudden injections of aerosols into the atmosphere have received increased attention with the realization that fires started by a nuclear war might release sufficient quantities of smoke to block sunlight from the Earth's surface and dramatically reduce temperatures over land¹⁻³. Three-dimensional atmospheric general circulation models which include aerosol transport indicate that much of the smoke could survive in the atmosphere for months or more⁴⁻⁶, implying significant climatic effects on such timescales, but these models generally assume fixed sea surface temperature and sea ice, and therefore cannot properly simulate cooling for more than a few weeks. This report describes a general circulation model run in which the foregoing assumptions are relaxed and the climate impact of massive smoke loading is assessed for four months of simulated time. Two competing long-term effects are apparent: positive feedback on surface cooling due to enhanced sea ice formation, and surface warming at some latitudes due in part to heat transport from the upper troposphere, where smoke aerosols absorb sunlight.

It is instructive to compare results from the general circulation model (GCM) to those obtained by Robock⁷ using a one-dimensional (in latitude) energy balance model (EBM) in multi-year simulations of nuclear war climate effects. In the present study, total column absorption optical depth of smoke τ is prescribed as a function of time to be twice the value normally assumed by Robock except that we restrict $\tau \leq 3$, that is, underneath the smoke $\tau = 3$ for the first 30 days and thereafter τ decreases with a half life of 30 days. This prescription ensures that GCM results of interest are obviously significant compared to model-generated variability (that is, weather fluctuations) and also that during the first 20 days after aerosol injection the smoke concentrations assumed for this study are identical to those used in our earlier GCM experiments with prescribed sea surface temperature (SST)^{8,9}. In all studies discussed here, including Robock's, smoke is assumed to exist in a uniform band of latitudes between 30° and 70° N and is injected into the atmosphere at approximately the Northern Hemisphere spring equinox. In the GCM runs smoke is assumed to be distributed between 1 and 10 km altitude at constant mixing ratio.

The assumed initial condition $\tau = 3$ in the Northern Hemisphere mid-latitudes is equivalent to 34×10^{12} g of amorphous elemental carbon with absorption cross section $10 \text{ m}^2 \text{ g}^{-1}$ and corresponds to 'baseline' estimates of nuclear war smoke production published by the US National Academy of Sciences² and the International Council of Scientific Unions³. However, longer term optical depths, $\tau = 2.4$ at 40 days and 0.5 at 110 days, greatly exceed values implied by GCMs which compute smoke removal^{5-6,10}, and of course the assumption that smoke is fixed in space is unrealistic. Thus, the present study is an intercomparison of climate model responses to hypothetical perturbations, with application to nuclear war climate effects; it is not an attempt to directly simulate 'nuclear winter'. The use of extreme smoke amounts and the assumption that smoke does not spread beyond the Northern Hemisphere mid-latitudes mean that long-term temperature effects are probably overestimated by the present study. Indeed, in reporting a long-term 'nuclear winter' simulation including smoke spreading by a two-level GCM, Stenchikov¹¹ does not elucidate the surface temperature feedback processes discussed below, perhaps because these processes are less obvious with more realistic (smaller) smoke concentrations.

The GCM used in this study is the NCAR (National Center

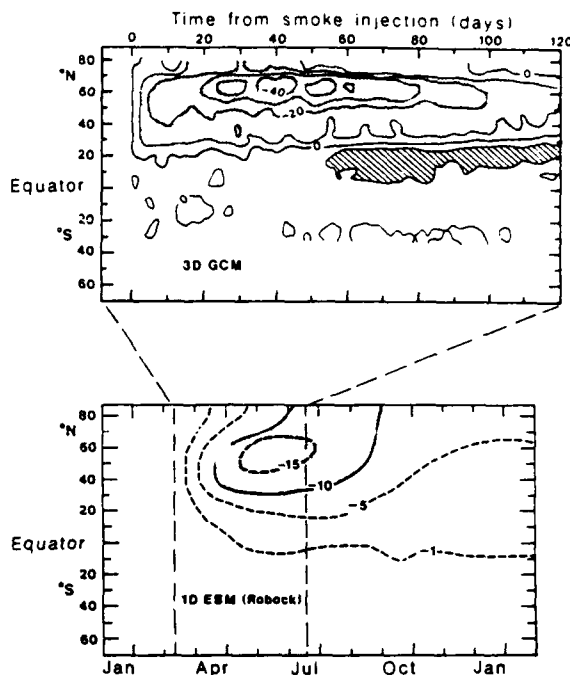


Fig. 1 Zonally averaged land surface temperature difference in °C between prescribed smoke experiments and controls. The upper panel shows results obtained in the present study; the lower panel is redrawn from ref. 7 and shows results from a one-dimensional energy balance climate model. In both cases solid line contours are drawn at 10 °C intervals, and shaded areas indicate temperatures more than 10 °C cooler than control runs while hatched areas indicate temperatures more than 10 °C warmer than control runs. GCM results are shown for 130 days and the thin dashed lines indicate the corresponding time period in Robock's simulation. Results from the GCM are not plotted at latitudes which are more than 90% ocean.

for Atmospheric Research) Community Climate Model (CCM)¹². Results presented here were obtained with a research version of the CCM developed by Washington and Meehl^{13,14} for studies of the CO₂ greenhouse effect. In this model SSTs are computed assuming a static mixed layer of constant heat capacity, and sea ice is computed with a simple thermodynamic model. This GCM, hereafter referred to as the CCM/mixed layer model, was modified as described by Covey *et al.*^{8,9} to include absorption of sunlight by smoke. Similar representations of mixed layer heat capacity and sea ice are used in Robock's EBM. (The earlier studies of Covey *et al.*^{8,9} made use of a version of the CCM in which SST and sea ice are prescribed at seasonally varying climatological values¹⁵; this model will be referred to as the prescribed SST version.)

Figure 1 shows the smoke-induced land surface cooling (that is, the temperature difference in °C between prescribed smoke experiments and controls) averaged over longitude and plotted as a function of latitude and time. The upper panel shows results from the CCM/mixed layer model and the lower panel shows results from Robock's EBM ('Run 4' of ref. 7). During the first half of the 120 day simulation with the CCM/mixed layer model, land surface cooling underneath the assumed smoke cloud is about twice that exhibited by Robock's model. Maximum cooling in the GCM is 47 °C at day 37 and 60° N latitude (poleward of the sea ice margin, slightly to the north of maximum cooling in Robock's model). During this time period smoke optical depths assumed in both the CCM/mixed layer model and Robock's simulation are > 1 , so the discrepancy in the amount of cooling between the two models is difficult to explain by the difference in smoke loading. The CCM/mixed layer model may

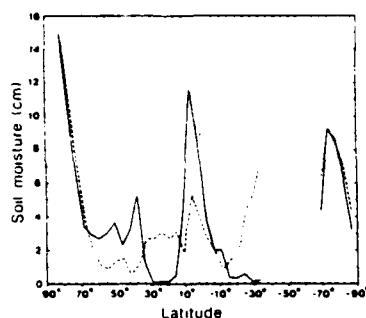


Fig. 2 Soil moisture content averaged over longitude and over days 110 to 120 after smoke injection (that is, the final 10 days of the GCM simulation) for the smoke-perturbed case (solid line) and the control case (dashed line). Results are not plotted at latitudes which are more than 90% ocean.

exaggerate the amount of cooling because it overpredicts the unperturbed amount of sea ice, possibly due to neglect of poleward heat transport by the oceans^{13,14}; the maximum temperature drop exhibited by the CCM/mixed layer model is almost twice that of the prescribed SST version during the time that smoke loadings in the two GCMs are identical. On the other hand, Robock's model may well underpredict the maximum degree of land surface cooling because its limited resolution—10° latitude, no longitude resolutions within land and ocean sectors, no height resolution—requires the cooling to be spread out over a large volume of space. The latter consideration may also explain in part the rapid cooling exhibited by the CCM during the first few days after aerosol injection⁵; the EBM, in contrast, takes several weeks to obtain land surface cooling >10°C. Another factor contributing to rapid initial cooling in the GCM is atmospheric dynamics, not included in the EBM. An examination of the lower tropospheric wind and temperature fields (not shown) indicates that ocean-to-land temperature advection takes about two weeks to increase to its maximum value as the circulation in the perturbed case evolves to a more zonally symmetric state. Two weeks is approximately the thermal relaxation time of the lower troposphere, that is, the quantity $C_p T g^{-1} \Delta P / (\sigma T^4)$ where C_p is the heat capacity of air at constant pressure, T is the air temperature, g is the acceleration of gravity, ΔP is the pressure difference between the surface and the 85 kPa pressure level, and σ is the Stefan-Boltzmann constant.

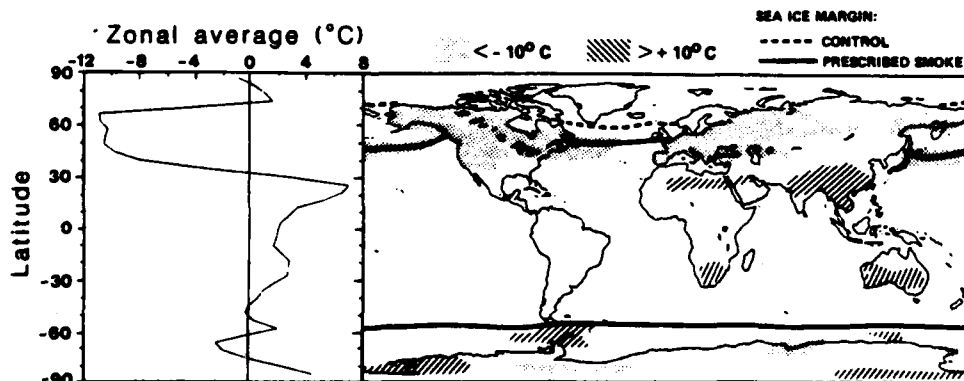
Unlike the situation early on, from about 100 to 120 days after smoke injection the amount of cooling in the CCM/mixed layer model is about as small or smaller than that in Robock's EBM, despite doubled smoke loading. Furthermore, throughout the second half of the CCM simulation land surface tem-

peratures immediately south of the assumed smoke cloud are significantly warmer than control values (see the hatched areas in Fig. 1). The EBM's surface temperatures are everywhere colder when smoke is injected into the model, for the following reason. Since the EBM has no height resolution the method of assuming smoke is to simply decrease the solar constant by the amount corresponding to absorption by the appropriate optical depth. This situation is quite different from that expected in the real atmosphere, in which smoke warmed by absorption of sunlight should overlie a cool surface (see Fig. 1a in ref. 8). It is possible that in the CCM simulation some of the heat from the upper troposphere is eventually transported (presumably via infrared radiation¹⁶) down to the surface, reversing long-term surface cooling in those areas which are not covered by smoke. This effect would no doubt be smaller in a more realistic treatment of protracted nuclear war-generated smoke, which would be more widespread, thinner, less black, and higher than the idealized fixed smoke considered here; nevertheless it is possible that the effect could moderate long-term surface cooling.

Partial support for the foregoing hypothesis comes from an analysis of the GCM's land surface energy budget averaged over the final 10 days of the model run. At 20° N latitude infrared flux from the atmosphere to land surface is 92 W m⁻² greater in the smoke-perturbed case than in the control case. A smaller warming effect (28 W m⁻²) is produced by loss of upward latent heat flux due to a drying out of soil moisture in the 15–30° N latitude zone (Fig. 2). The latter type of warming mechanism has been observed in a previous GCM simulation of nuclear war-generated smoke effects¹⁷. However, underneath the smoke (47° N) the dominant change in surface energy balance is between decreased absorption of solar radiation and decreased upward infrared and sensible heat fluxes; within this latitude band, the infrared flux received by the surface from the atmosphere is not significantly greater in the smoke-perturbed case than in the control case.

The differences in soil moisture between the control and perturbed cases (Fig. 2) are for the most part as expected from previous experiments with the CCM⁹. In general, the CCM responds to fixed upper tropospheric smoke loadings by decreasing cloudiness where the smoke is heated by sunlight while increasing cloudiness at lower levels, resulting in only small changes in precipitation underneath the smoke. (This result is not consistent with results from the Oregon State University two-layer model¹⁷ and may be due to the CCM's assumptions of 100% relative humidity immediately above the surface together with boundary layer condensation at only 80% relative humidity.) Accordingly, soil moisture is greater underneath the smoke in the perturbed case, where surface cooling inhibits evaporation. As pointed out above, soil moisture essentially disappears from latitudes 15–30° N, where surface warming from enhanced downward infrared radiation increases evaporation

Fig. 3 Surface temperature difference (prescribed smoke case minus control case) averaged over days 110 to 120 after smoke injection. On the left side the zonal average is shown as a function of latitude. On the right side the geographical distribution is shown, with shaded areas indicating greater than 10°C cooling and hatched areas indicating greater than 10°C warming; also the control case (thick dashed line) and perturbed case (thick solid line) sea ice margins are indicated (the two coincide in the Southern Hemisphere).



during the first half of the smoke-perturbed model integration. For latitudes 15–30° S, the expected location of the downward branch of an enhanced cross-equatorial Hadley circulation in the perturbed case (see Fig. 4b in ref. 8), a decrease in precipitation leads to the drying out of soil moisture apparent in Fig. 2. Finally, soil moisture more than doubles in the perturbed case in a narrow latitude band centered on 8° N due to a burst of precipitation during the last 10 days of the model integration, which occurs for unknown reasons.

The geographical distribution of surface cooling and sea ice averaged over the final 10 days of the CCM/mixed layer model simulation is depicted in Fig. 3. As expected from Robock's EBM results⁷ the extent of sea ice is significantly greater in the smoke-perturbed case. The GCM obtains greatest cooling in the western parts of the North American and Eurasian land masses, downwind of the sea ice, in contrast to early times when maximum cooling occurs in the eastern parts⁸. Cooling of Europe due to enhanced North Atlantic sea ice has a palaeoclimatic analogue: the Younger Dryas period, 10,000–11,000 years ago, exhibited this phenomenon according to both observational¹⁸ and model¹⁹ studies.

In summary, the three-dimensional GCM simulation, while qualitatively confirming a positive feedback due to sea ice that enhances long-term cooling due to nuclear war-generated smoke, reveals additional effects that can moderate or perhaps even reverse long-term cooling. The latter appear to dominate by the end of the GCM run, when the extent of land area that is cooled in excess of 10° C is much smaller than it is in the analogous EBM experiment ('Run 4' in Fig. 1 of ref. 7) despite the fact that the GCM experiment assumed more smoke. However, both classes of effects are probably exaggerated by the assumption of very large quantities of smoke that is fixed in space, and by other model simplifications such as lack of ocean heat transport (leading to overprediction of sea ice). It is therefore necessary to perform more realistic GCM experiments, particularly including model-computed smoke transport and removal, in order to quantitatively assess the relative importance of the positive and negative feedbacks discussed here.

I thank Warren Washington and Gerald Meehl for providing both the model and valuable advice on its use, and Lynda Verplank for expert assistance with programming. This work was supported by the NSF (grant ATM-8504807).

Received 2 October; accepted 15 December 1986.

1. Turco, R. P., Toon, O. B., Ackerman, T., Pollack, J. B. & Sagan, C. *Science* **222**, 1283–1291 (1983).
2. US National Research Council *The Effects on the Atmosphere of a Major Nuclear Exchange* (National Academy Press, Washington, DC, 1985).
3. Pittock, A. B. et al. *Environmental Consequences of Nuclear War. Volume I. Physical and Atmospheric Effects* (Wiley, New York, 1986).
4. Thompson, S. L. *Nature* **317**, 35–39 (1985).
5. Malone, R. C., Auer, L. H., Glatzmaier, G. A., Wood, M. C. & Toon, O. B. *Science* **230**, 317–319 (1985).
6. Malone, R. C., Auer, L. H., Glatzmaier, G. A., Wood, M. C. & Toon, O. B. *J. geophys. Res.* **91**, 1039–1053 (1986).
7. Robock, A. *Nature* **310**, 667–670 (1984).
8. Covey, C., Schneider, S. H. & Thompson, S. L. *Nature* **308**, 21–25 (1984).
9. Covey, C., Thompson, S. L. & Schneider, S. H. *J. geophys. Res.* **90**, 5615–5628 (1985).
10. Thompson, S. L. & Giorgi, F. *J. geophys. Res.* (in the press).
11. Stenchikov, G. L. in *The Night After ... Climatic and Biological Consequences of Nuclear War* (ed. Veikov, Y.) 53–82 (Mir, Moscow, 1985).
12. Pitcher, E. J. et al. *J. Atmos. Sci.* **40**, 580–604 (1983).
13. Washington, W. M. & Meehl, G. A. *J. geophys. Res.* **89**, 9475–9503 (1984).
14. Meehl, G. A. & Washington, W. M. *J. phys. Oceanogr.* **15**, 92–104 (1985).
15. Chervin, R. M. *J. Atmos. Sci.* **43**, 233–251 (1986).
16. Cess, R. D., Potter, G. L., Ghan, S. J. & Gates, W. L. *J. geophys. Res.* **90**, 12937–12950 (1985).
17. Ghan, S. J., MacCracken, M. C. & Walton, J. J. *Lawrence Livermore natn. Laboratory tech. Not.* UCRL-92324 (1985).
18. Broecker, W. S., Peteet, D. M. & Rind, D. *Nature* **315**, 21–26 (1985).
19. Schneider, S. H., Peteet, D. M., & North, G. R. in *Abrupt Climate Changes* (eds Berger, W. H. & Labeyrie, L.) (Reidel, Dordrecht, in the press).

Model for study of prolonged
(10 month) climate impact of
atmospheric smoke injections

Climate model (Washington & Meehl 1984)

3D atmospheric GCM (NCAR CCM)
snowcover / soil moisture (Manabe)
thermodynamic sea ice model (Semtner)
mixed layer heat capacity = "ocean model"

Assumptions about smoke (Covey et al. 1984)

Fixed in space: 1-10 km, 30°N - 70°N

Variable in time

Constant for first 30 days

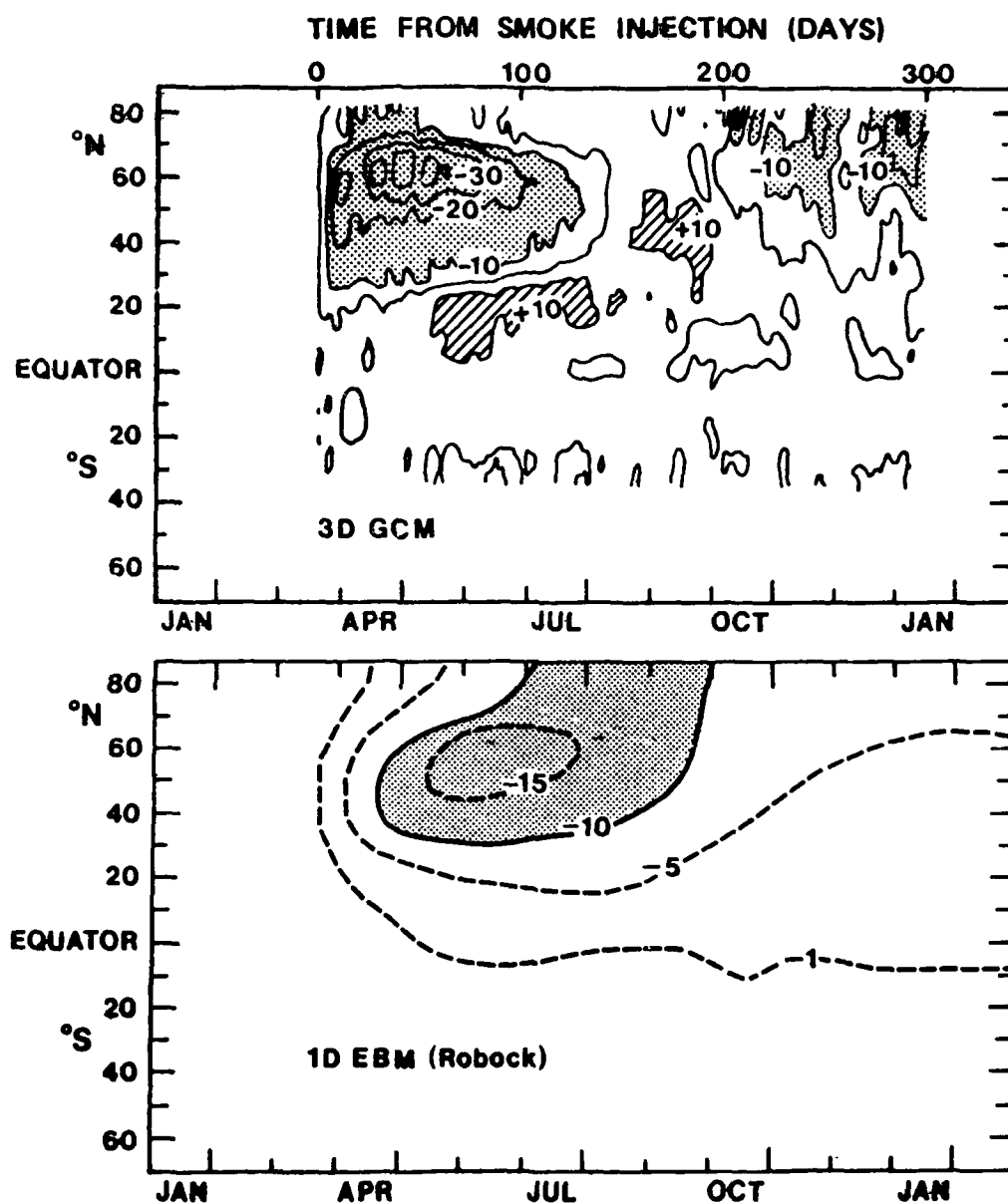
Then half-life of 30 days

Very large smoke amounts

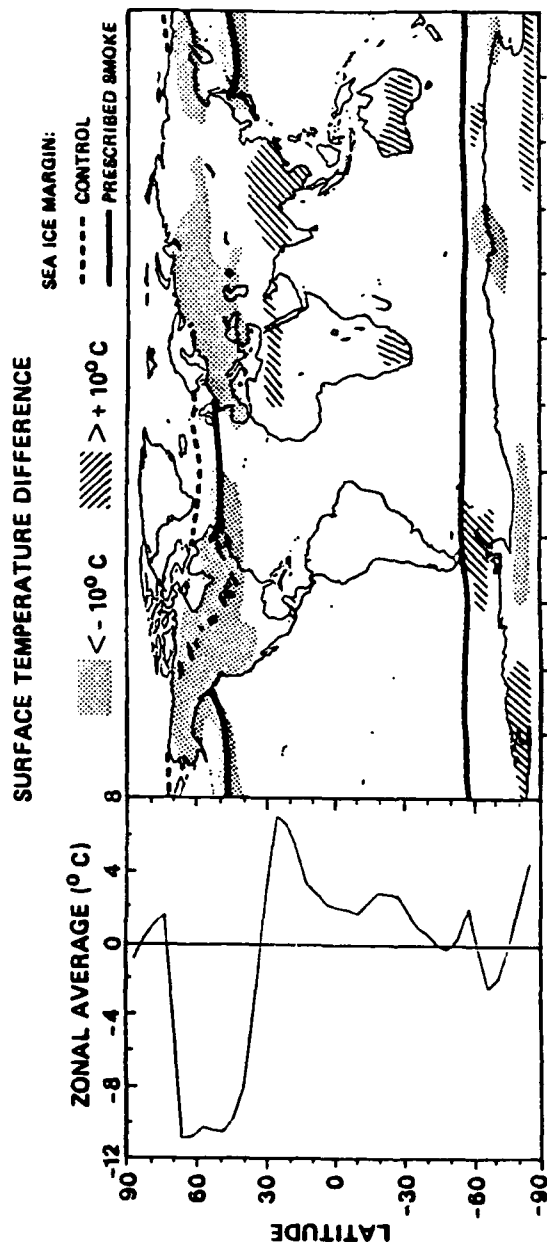
Absorption optical depth = 3 for 30 days

Thereafter, smoke $\sim 2 \times$ TTAPS baseline

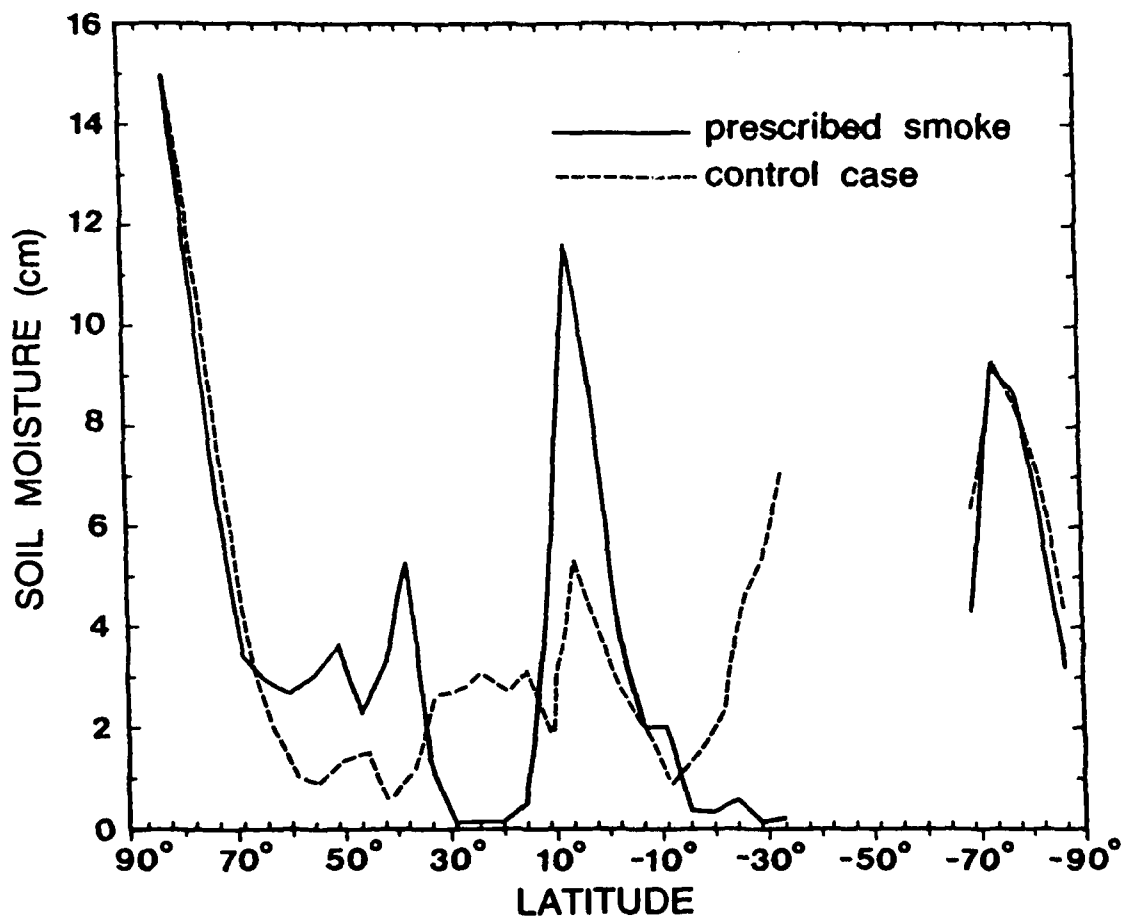
CHANGE IN LAND SURFACE TEMPERATURE (Perturbed Case) - (Control Case)



*Time average for Days 110-120
(July 7-17)*



Time average for Days 110-120



CONCLUSIONS

1. Long-term feedbacks

a. Sea ice feedback enhances cooling*

b. Upper tropospheric heat diminishes cooling

Both effects are exaggerated by the idealized assumptions about smoke.

2. Changes in hydrology budget

* cf. Robock, 1984

Effects of Vertical Injection Profile and Infrared Opacity in GCM Simulations of Nuclear War Smoke

Stephen H. Schneider

*National Center for Atmospheric Research
P.O. Box 3000, Boulder, Colorado 80307*

A global general circulation model (GCM) that allows for the transport, removal and radiative effects of smoke aerosols has been used to examine the effects of initial smoke vertical injection profile and smoke thermal infrared opacity on the subsequent evolution of land surface temperatures. Two vertical injection profiles are considered: constant mass mixing ratio (CMR) from 0–7 km altitude, and constant density (CD) concentration from 0–10 km altitude. Both profiles prescribe the same column loading. A variety of simulations have been done with both profiles. In general, the CD cases produce midlatitude land temperature decreases roughly 3°C larger than the CMR cases in the first two weeks of the simulations. The CD cases also show a substantially slower overall rate of smoke removal from the atmosphere as compared to removal rates in the CMR cases. This has a much greater relative impact on subtropical acute temperature responses than on mid to high latitude temperature declines. 1-D radiative/convective modeling and 3-D GCM modeling show the ameliorative effect of smoke infrared opacity generally becomes larger with increasing height of smoke injection for smoke injection cloud tops in the low to middle troposphere. Variation of smoke injection cloud tops in the middle to upper troposphere produces little variation in the surface temperature effect of smoke infrared opacity. Increasing the solar "blackness" of smoke by increasing the fractional carbon content while holding the total carbon mass fixed is shown to reduce the ameliorative effect of smoke infrared opacity.

Analysis of Surface Temperature Variability and Extremes in GCM Simulations of Large Smoke Injections

Starley L. Thompson

*National Center for Atmospheric Research
P.O. Box 3000, Boulder, Colorado 80307*

Simulations of massive nuclear war smoke injections performed with a global general circulation model (GCM) have been analyzed to determine some statistics of surface temperature variability and extremes. In the context of environmental effects, such analyses may be more meaningful than the traditional reliance on temporal or spatial means because biological processes are particularly susceptible to environmental variability. Global maps of coldest temperature reached at any time during an integration imply a more severe, but more realistic, picture of potential environmental effects than either daily "snapshots" or time averages. Probability distributions of temperatures for selected geographic regions highlight regional differences as well as providing probability estimates for temperatures below arbitrary threshold values. The enhanced information content in the probability distributions, as compared to simple means, could make a substantial difference in environmental inferences drawn from the data. For example, some regions whose time mean temperatures are well above freezing nonetheless show a substantial probability of near or sub-freezing events. While the particular analyses currently available cannot be considered quantitatively reliable due to current model limitations, the analysis methodology appears promising and should be applied to future GCM simulations.

Effects of Smoke IR and Injection Profile

Simulation Description		Temperature Change (°C)			
Height	Profile	Smoke IR	50-70°N	30-50°N	10-30°N
7 km	CMR	Yes	-12.9	-10.0	-3.9
7 km	CMR	No	-17.7	-13.9	-5.0
10 km	CD	Yes	-14.2	-13.2	-8.5
10 km	CD	No	-19.9	-17.2	-9.8

Smoke IR Warming Effect (°C)

Vertical Profile	1-D Clear	1-D Partly Cloudy	3-D GCM
0-10 km CD	7.5	5.0	4.0
0-7 km CMR	5.6	4.9	3.9
3 km scale height	4.8	3.9	—
1 km scale height	2.9	2.8	—

“Sooty” Vs. “Medium” Smoke

Simulation Description			Temperature Change (°C)		
Height	Profile	Smoke	50-70°N	30-50°N	10-30°N
7 km	CMR	180 Tg Medium	-13.9	-12.9	-5.9
7 km	CMR	50 Tg Sooty	-16.4	-14.3	-6.5
10 km	CD	180 Tg Medium	-14.0	-15.3	-10.6
10 km	CD	50 Tg Sooty	-17.8	-17.0	-10.1

Model Intercomparison

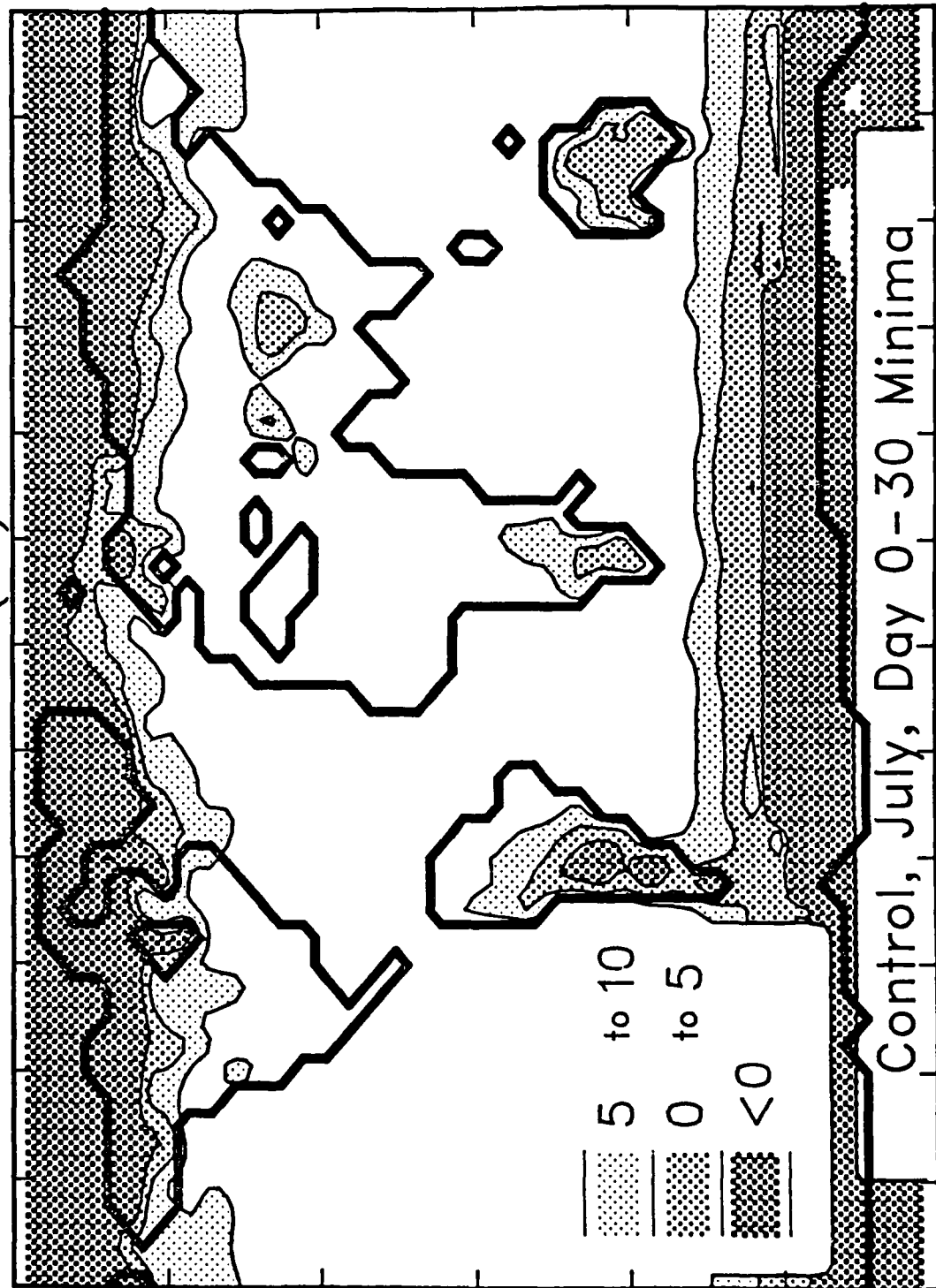
Change in day 5–15 land surface and land surface air temperatures over the latitude band 30–70°N for two general circulation models having nearly equivalent smoke scenarios. (LLNL results from S.J. Ghan, personal communication.)

Temperature Change (°C)

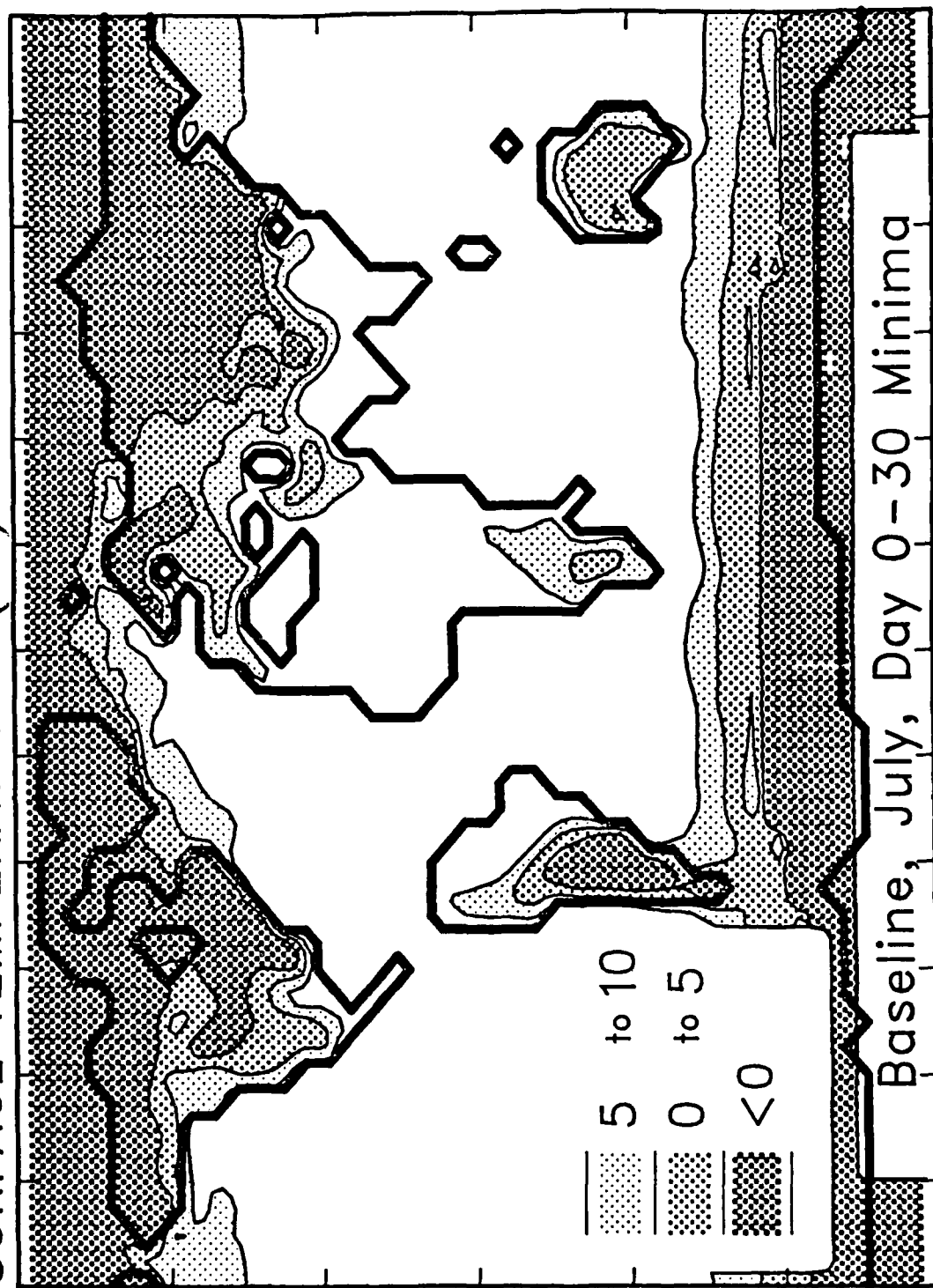
312

	Surface Air	Surface
NCAR	-11.9	-15.6
LLNL	-13.7	-18.7

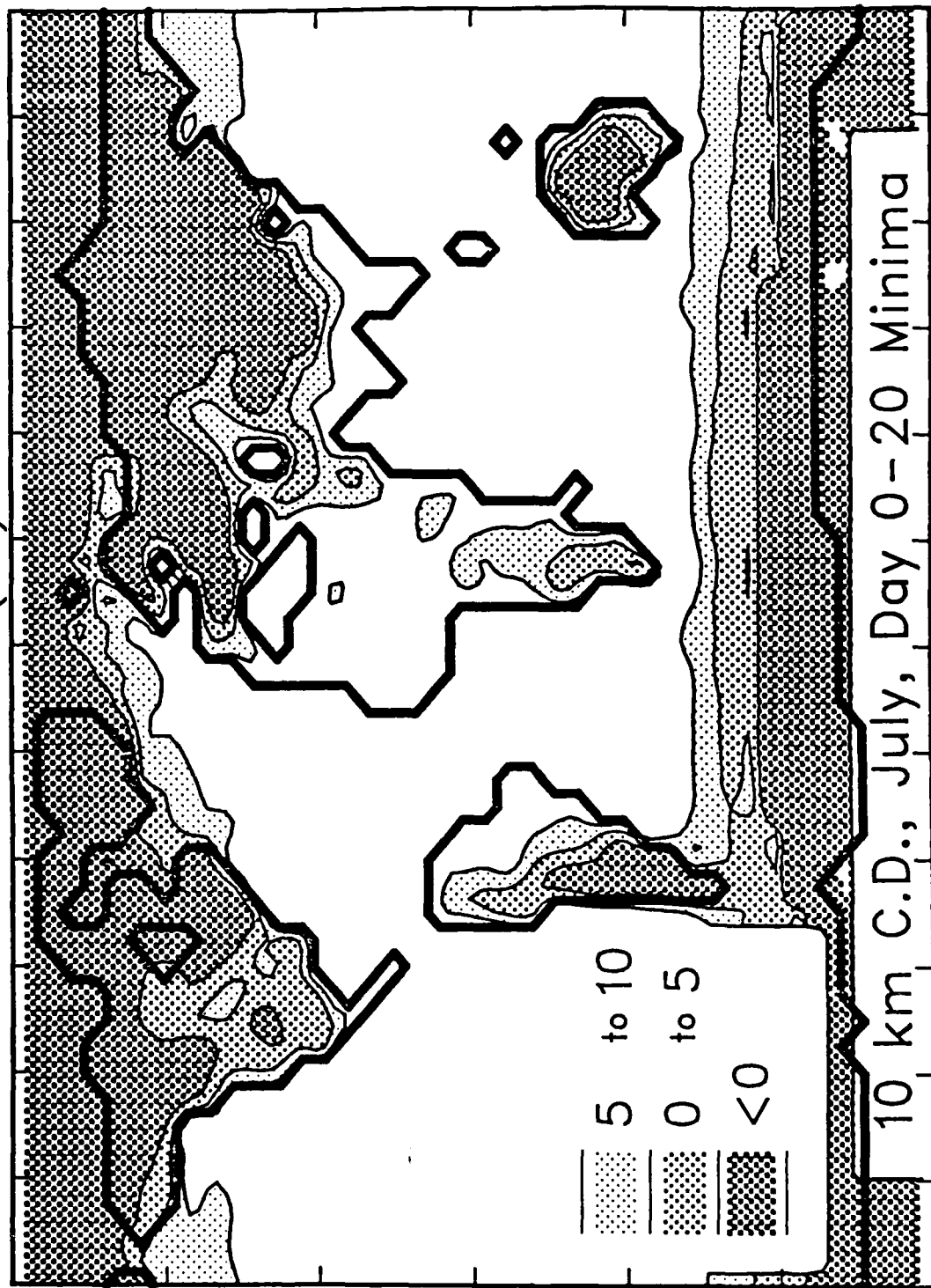
SURFACE TEMPERATURE (°C)



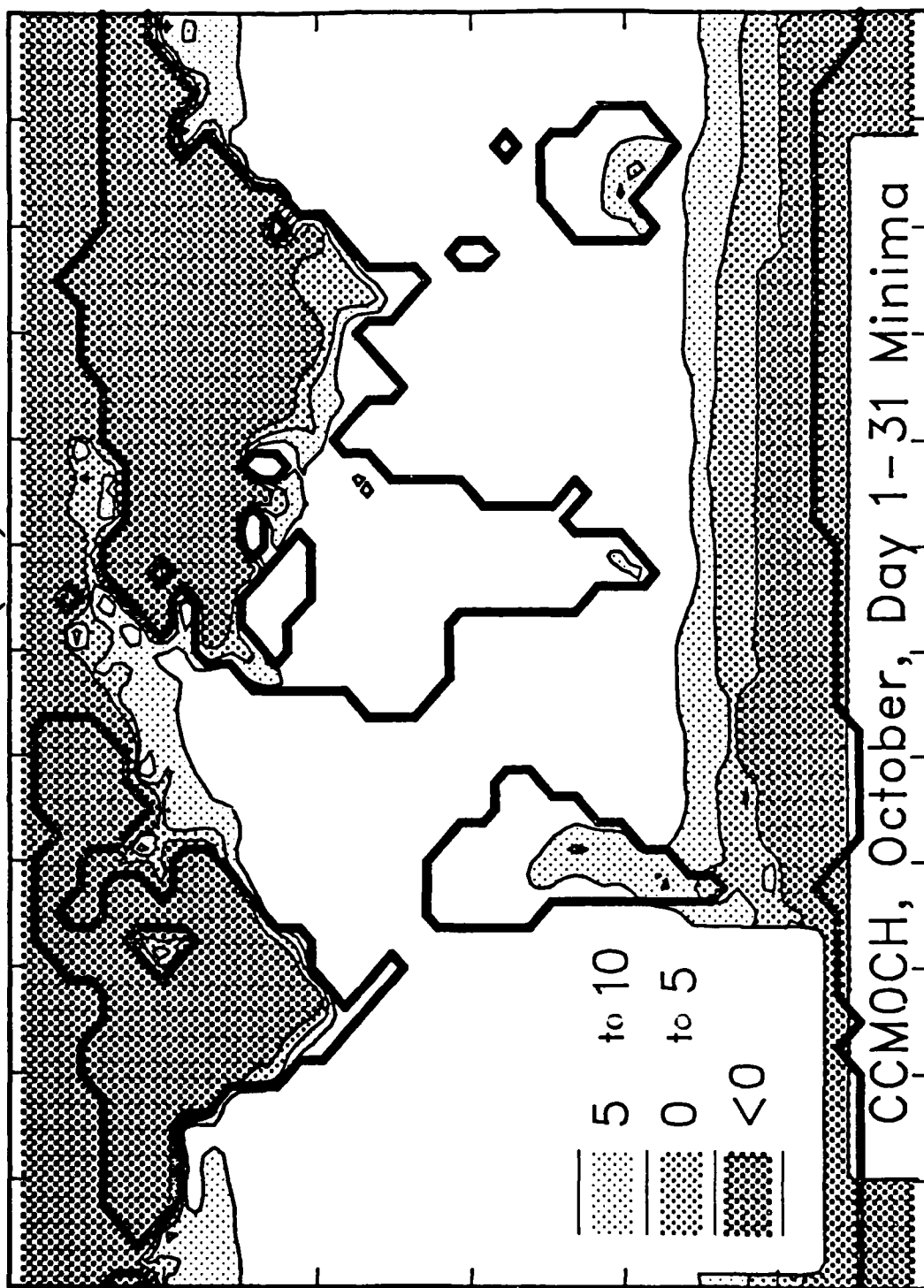
SURFACE TEMPERATURE (°C)

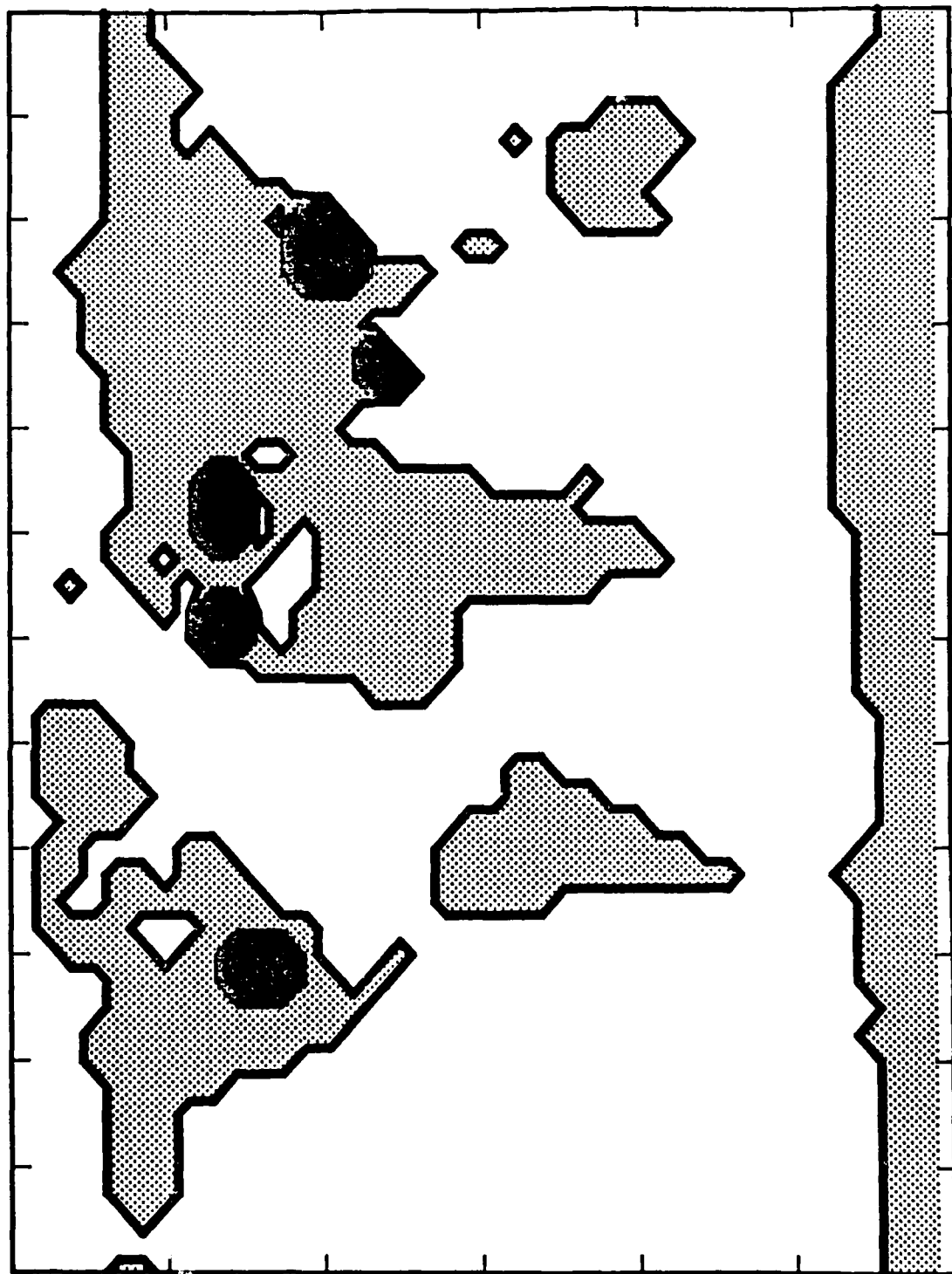


SURFACE TEMPERATURE (°C)

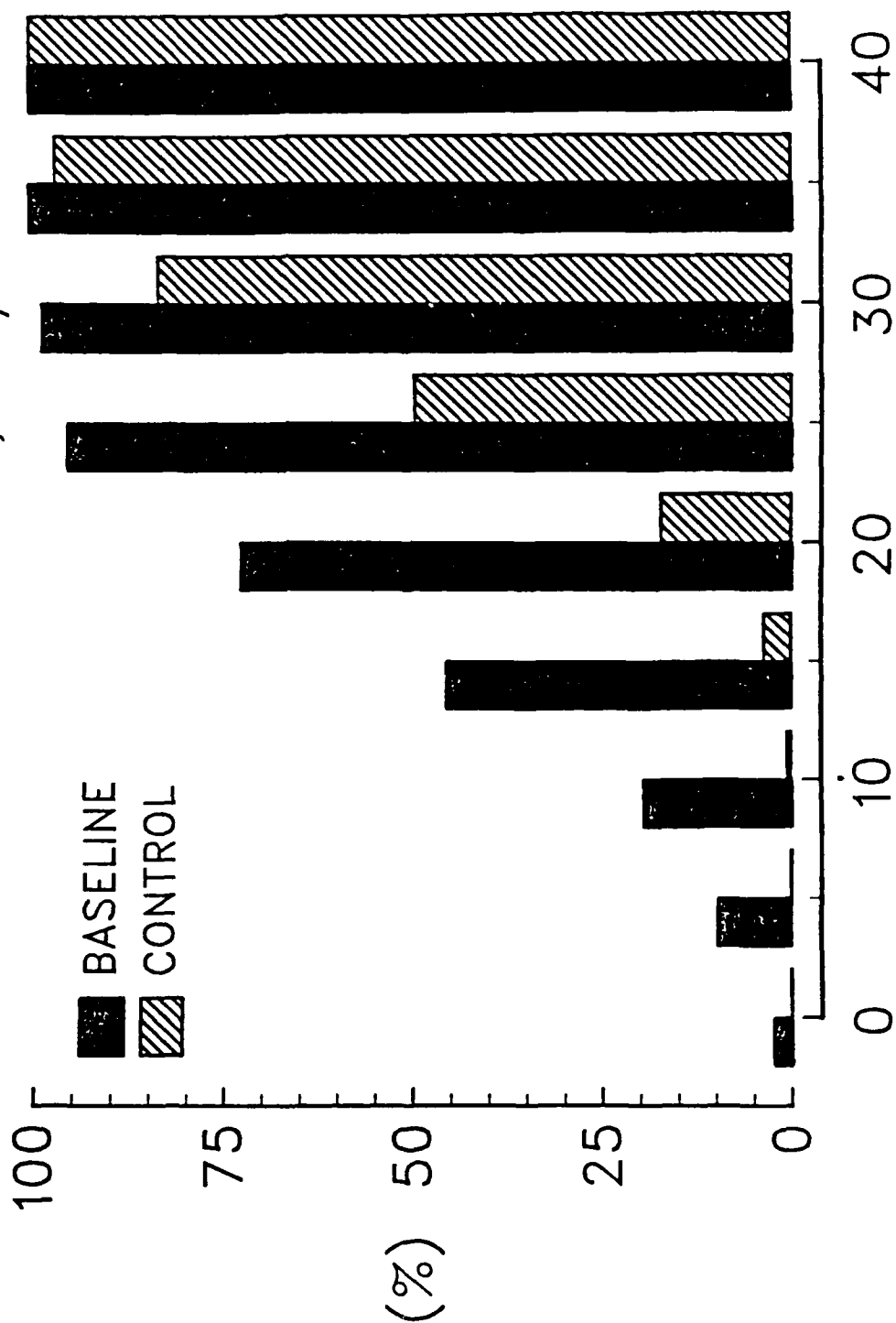


SURFACE TEMPERATURE (°C)

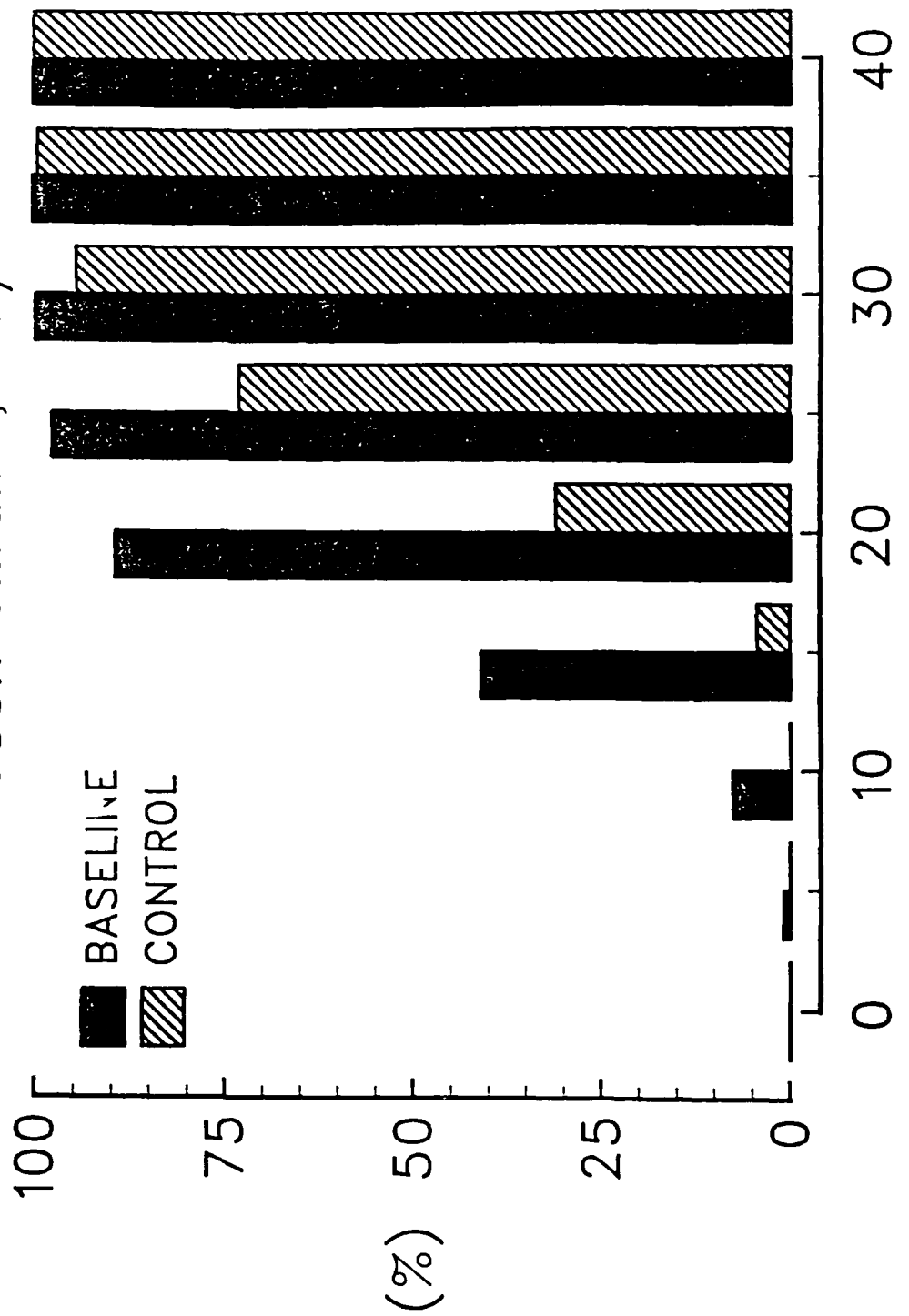




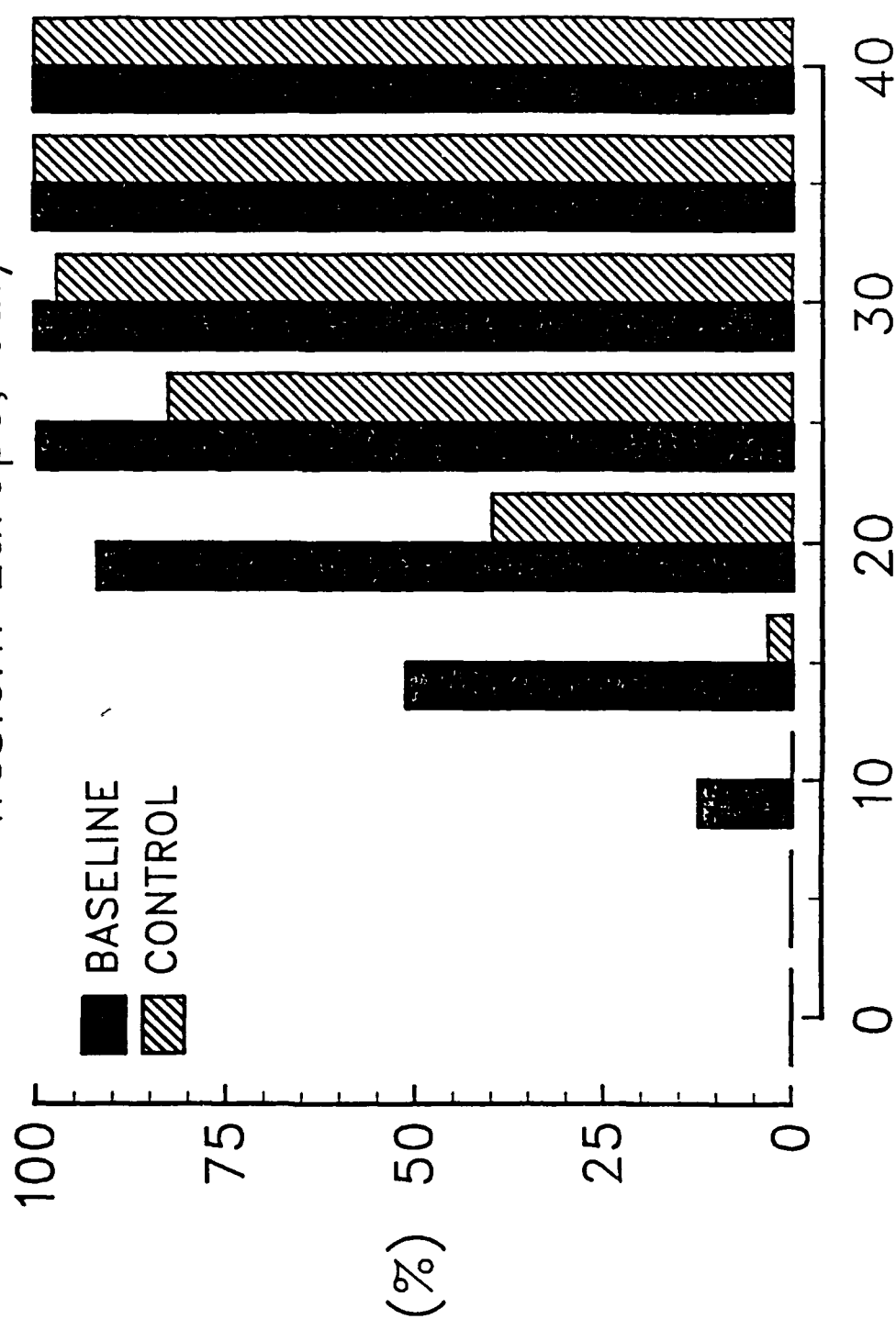
Sub-Threshold Temperature Probability U.S. Midwest, July



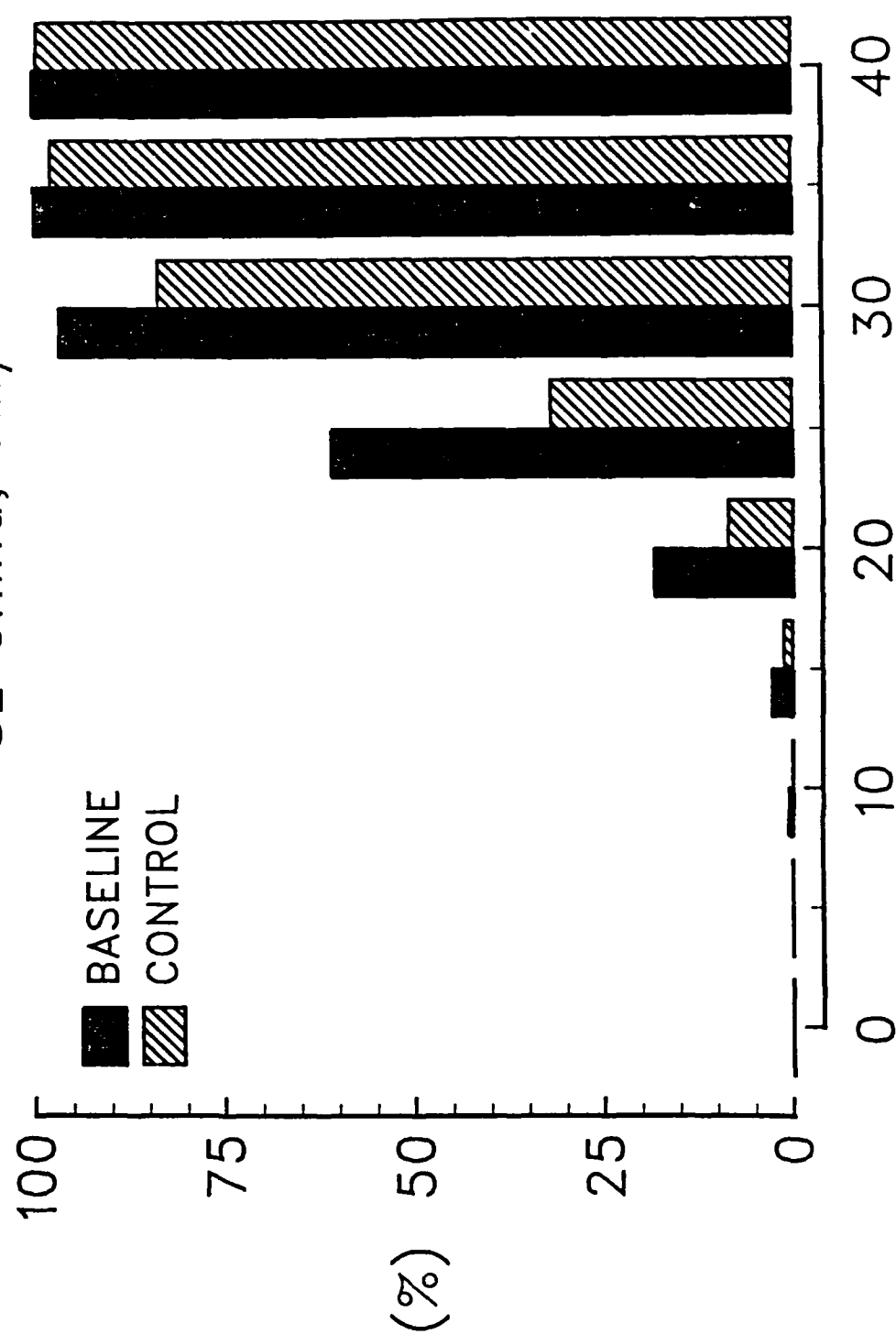
Sub-Threshold Temperature Probability USSR Ukraine, July



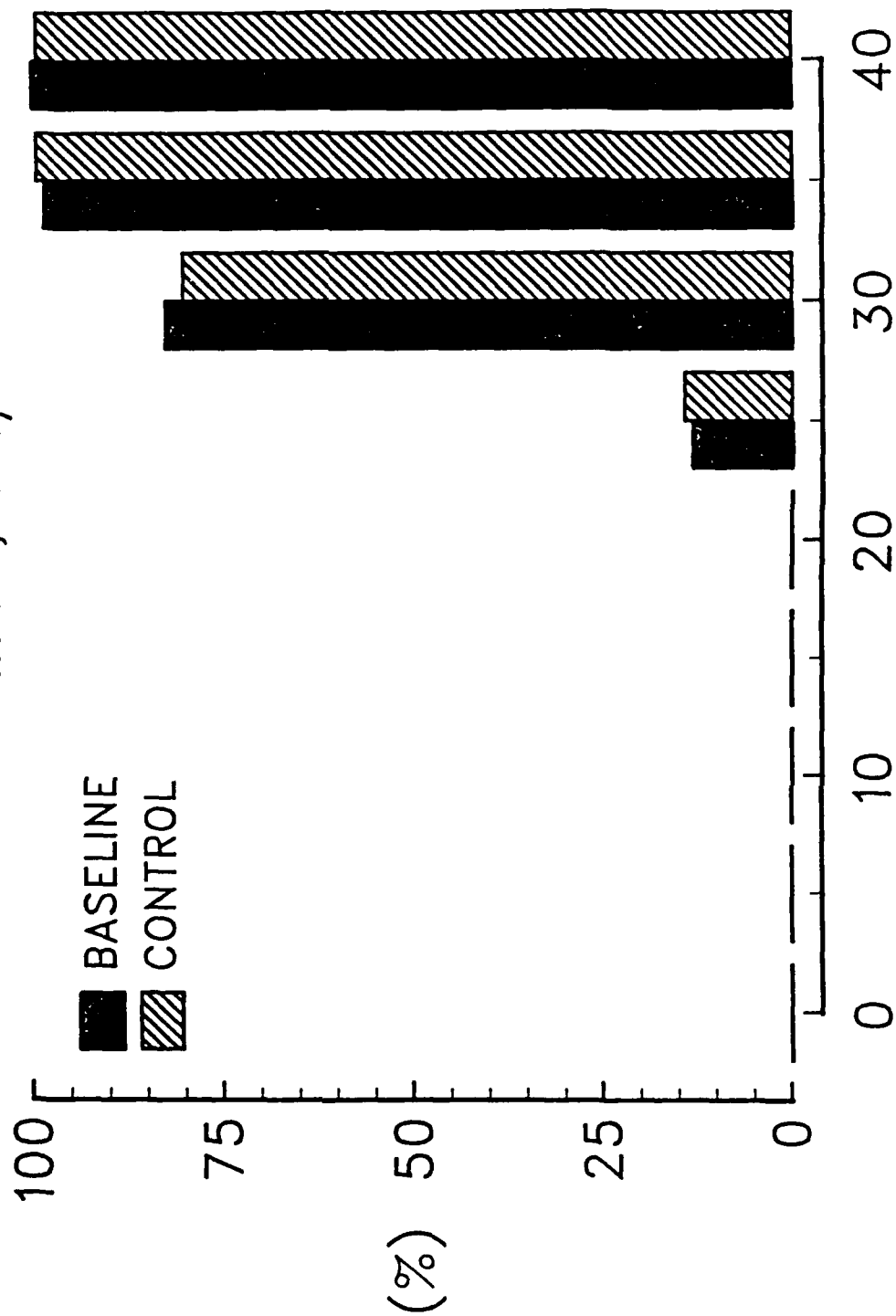
Sub-Threshold Temperature Probability
Western Europe, July



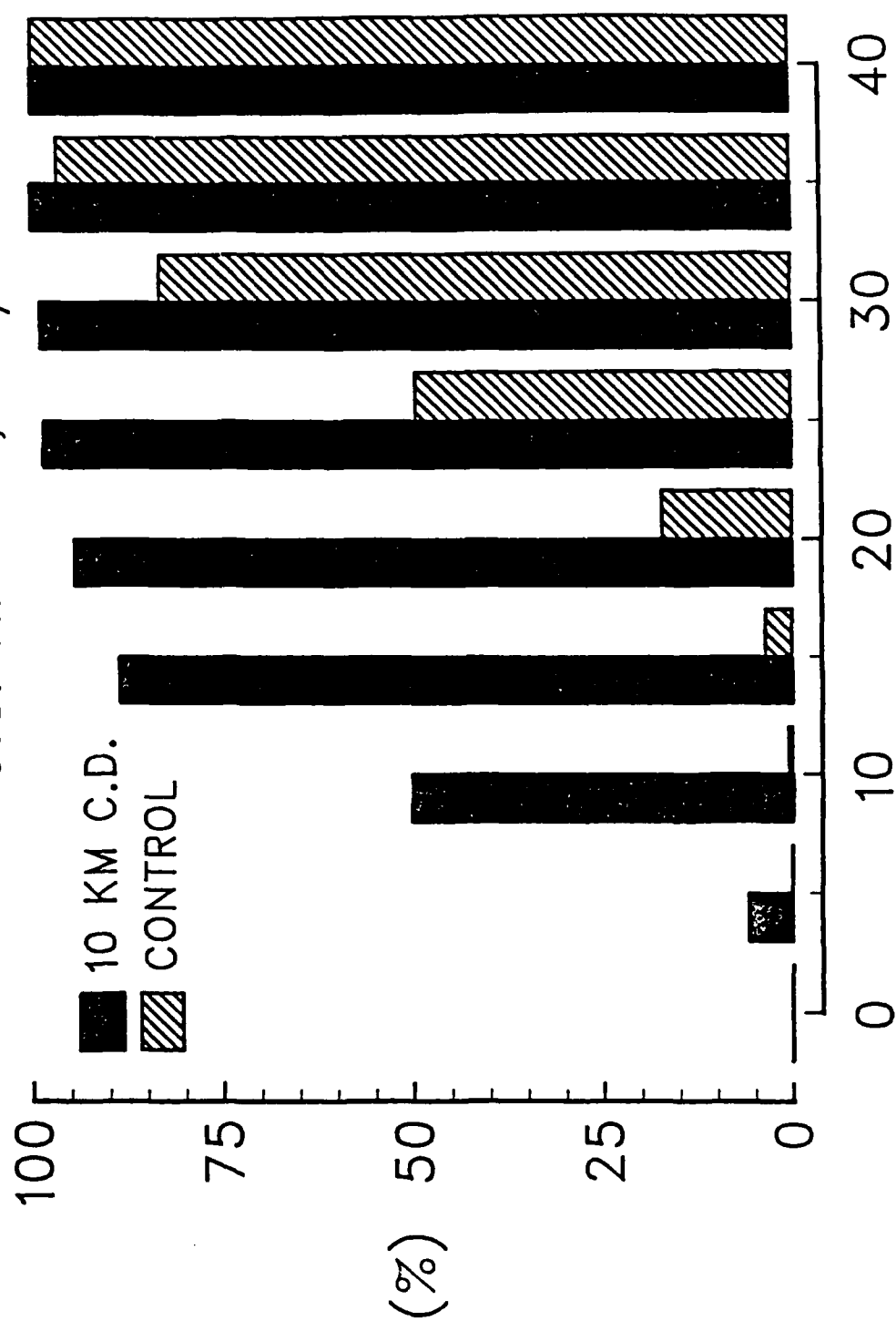
Sub-Threshold Temperature Probability SE China, July



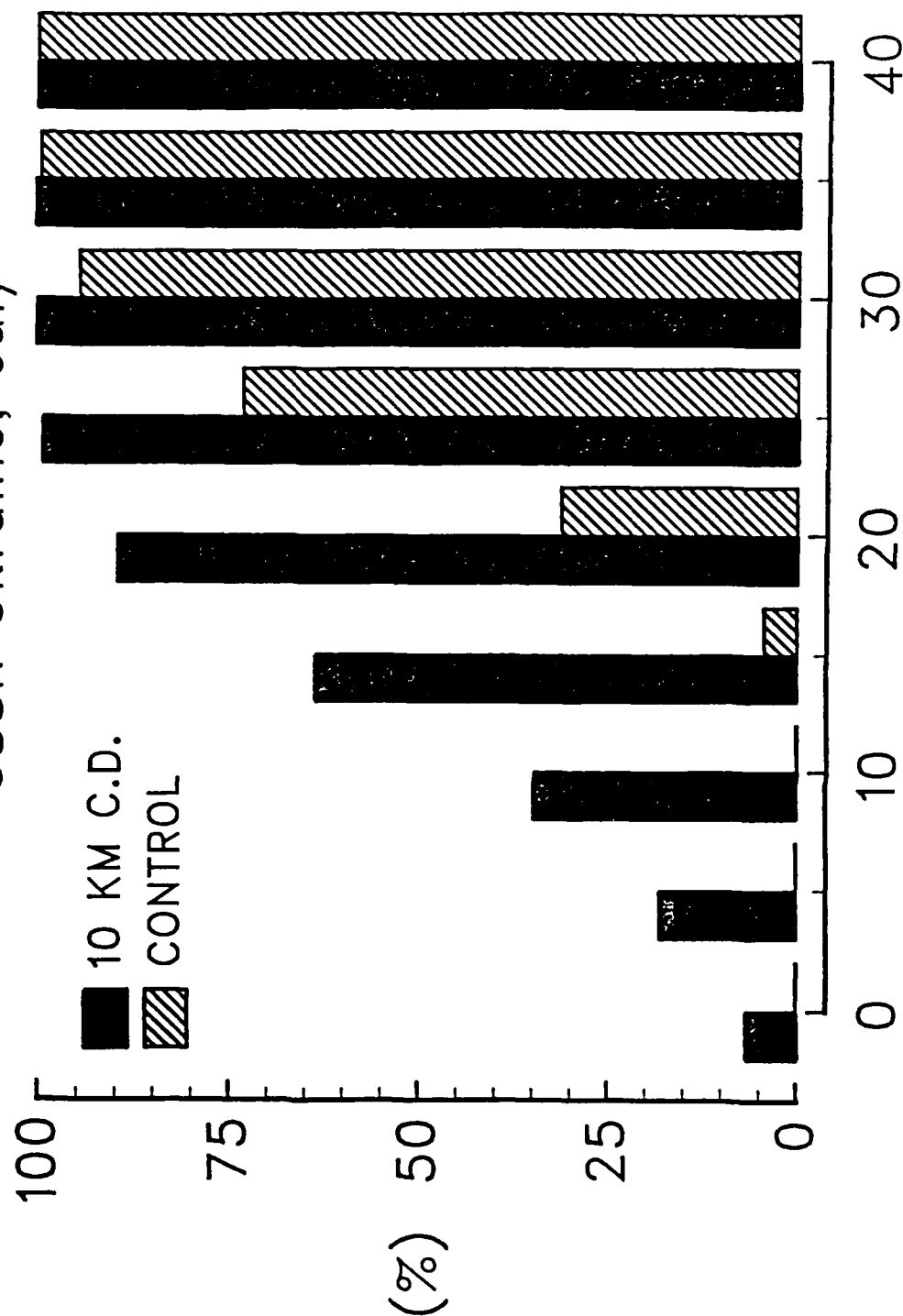
Sub-Threshold Temperature Probability
India, July



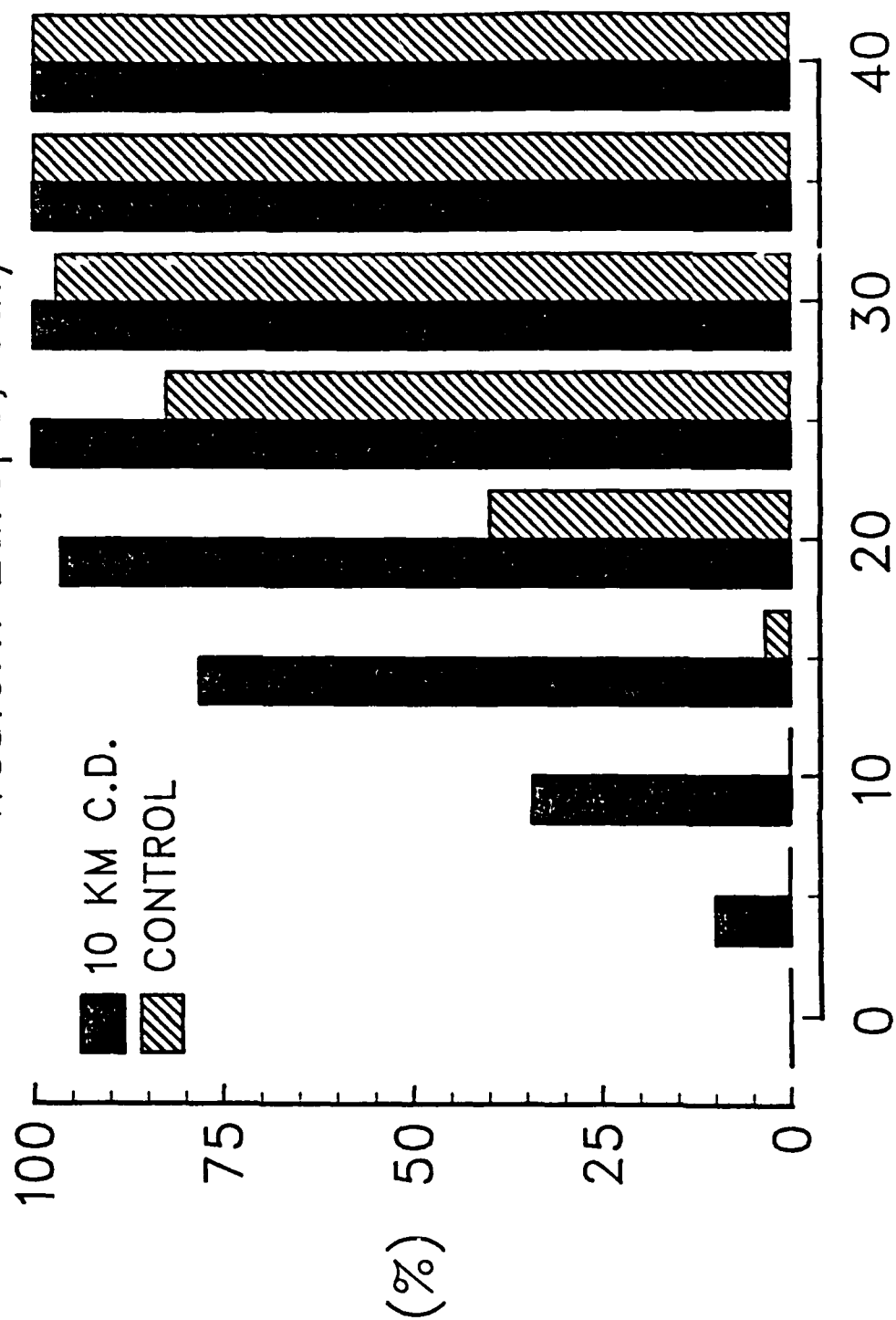
Sub-Threshold Temperature Probability U.S. Midwest, July



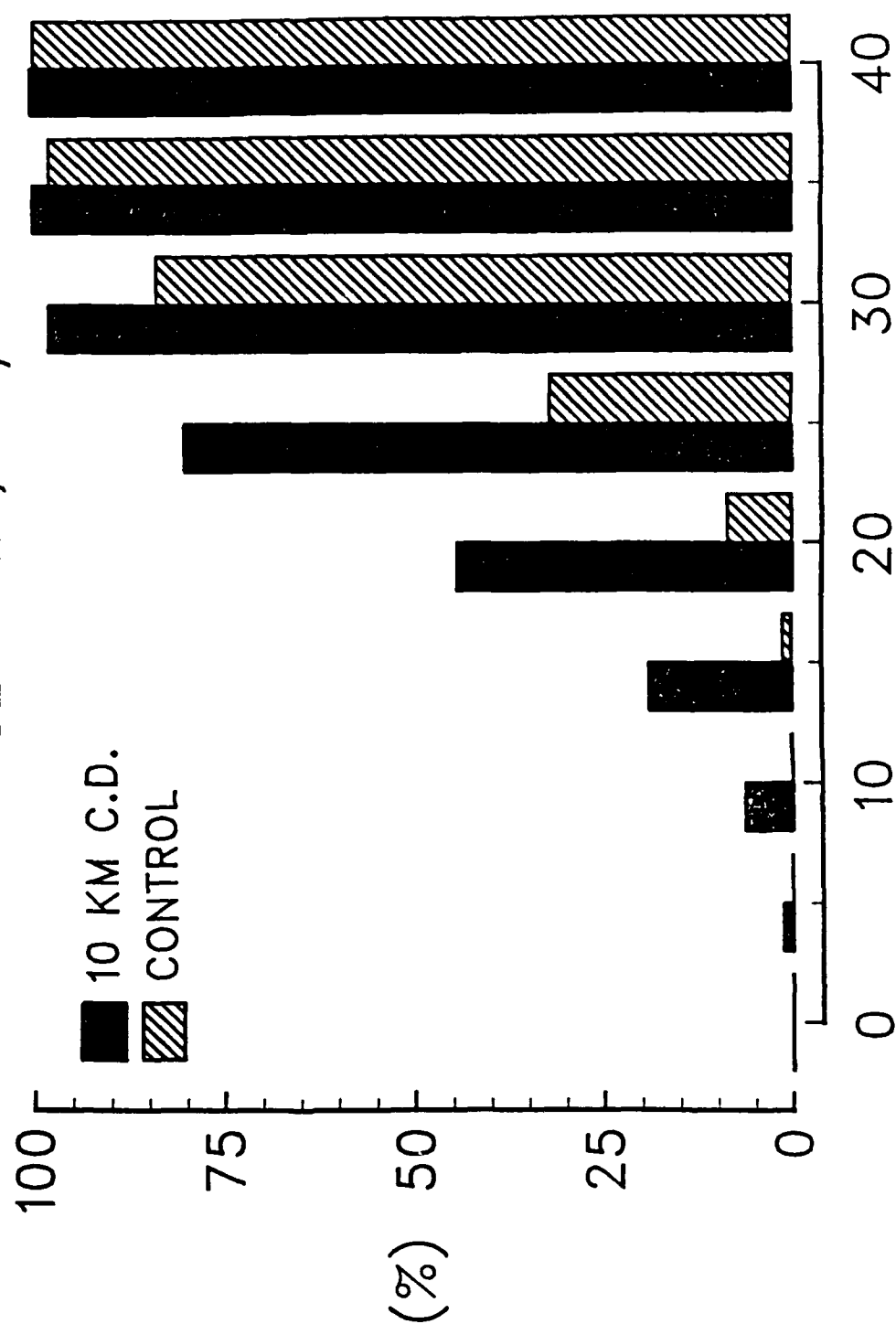
Sub-Threshold Temperature Probability USSR Ukraine, July



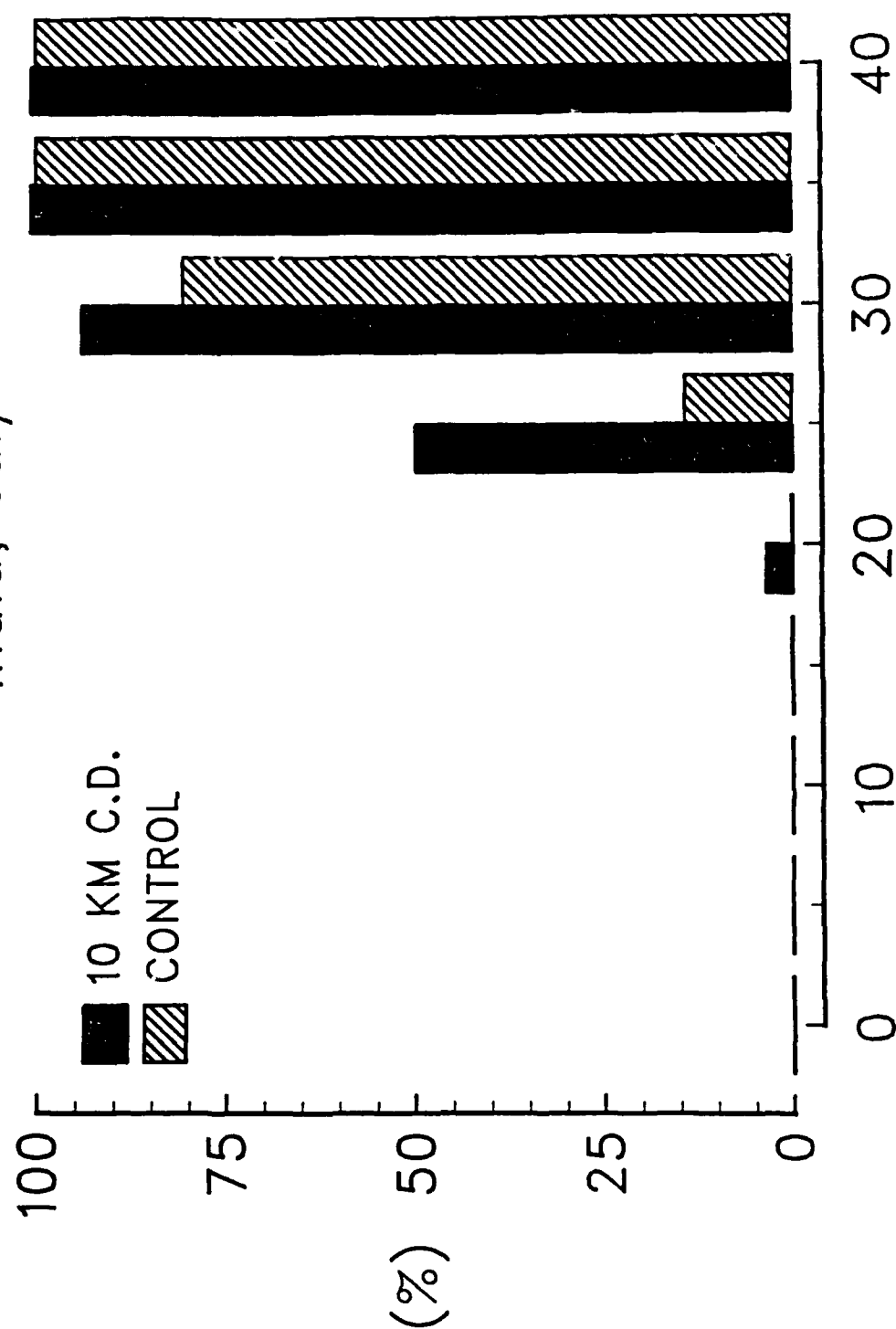
Sub-Threshold Temperature Probability Western Europe, July



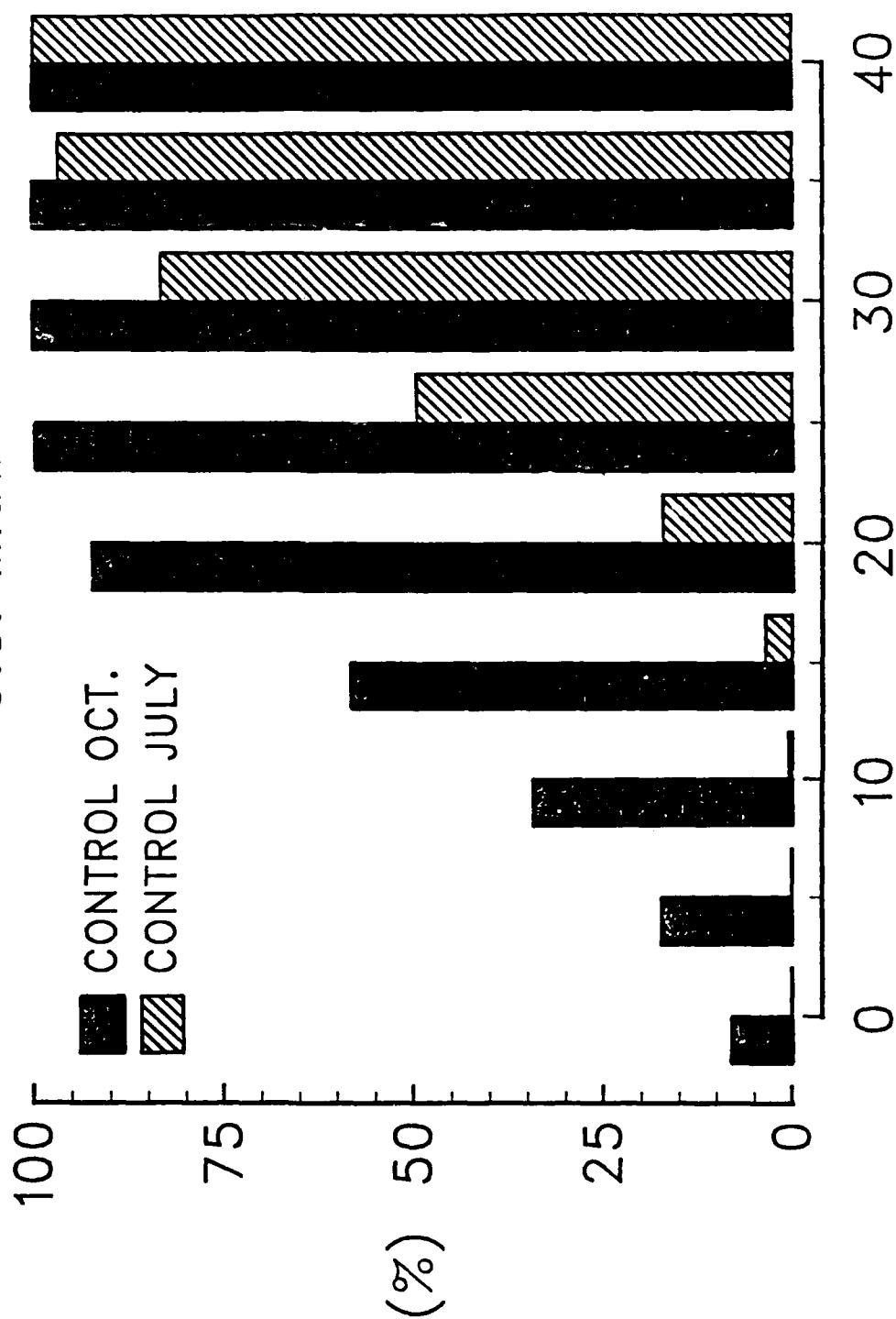
Sub-Threshold Temperature Probability SE China, July



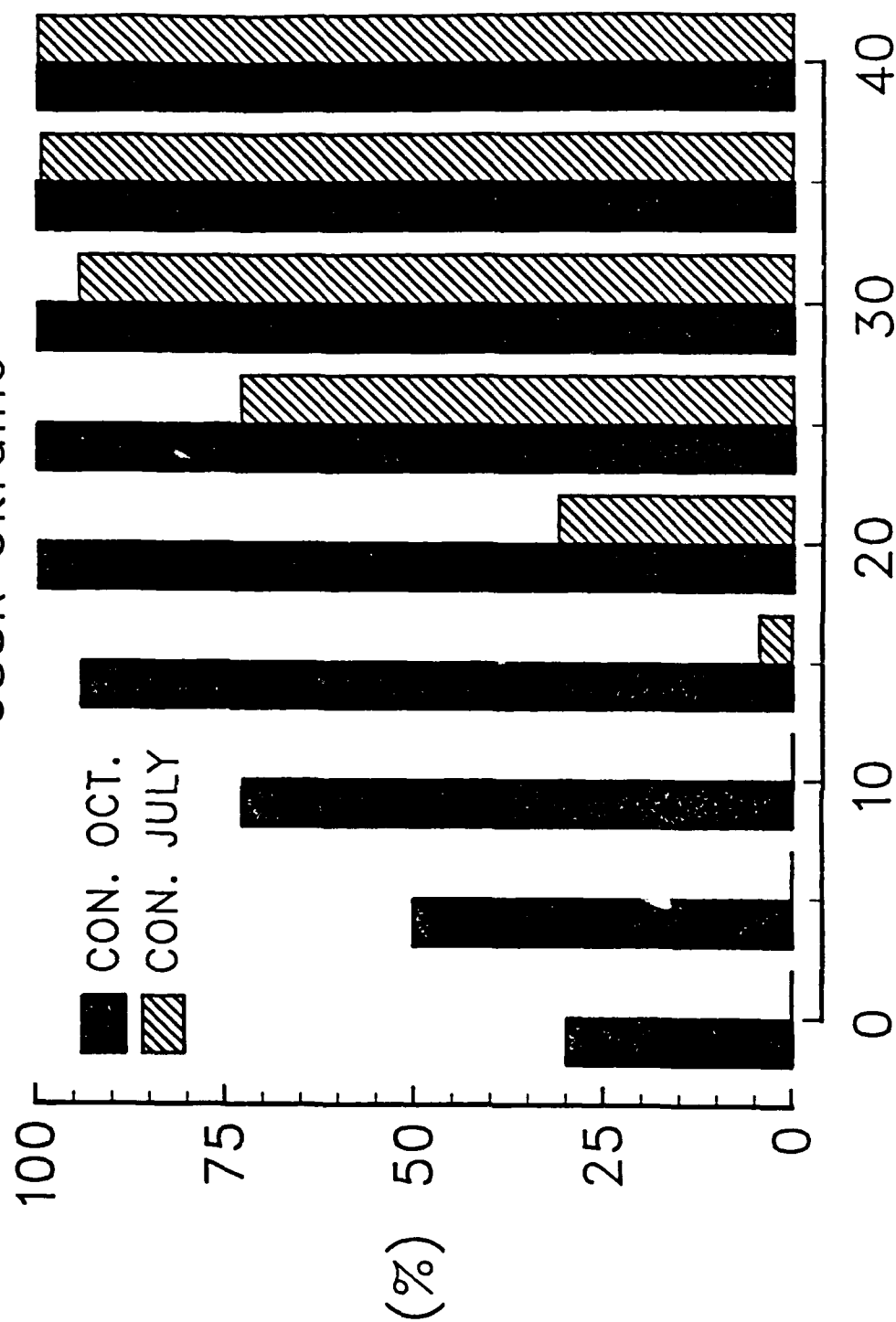
Sub-Threshold Temperature Probability India, July



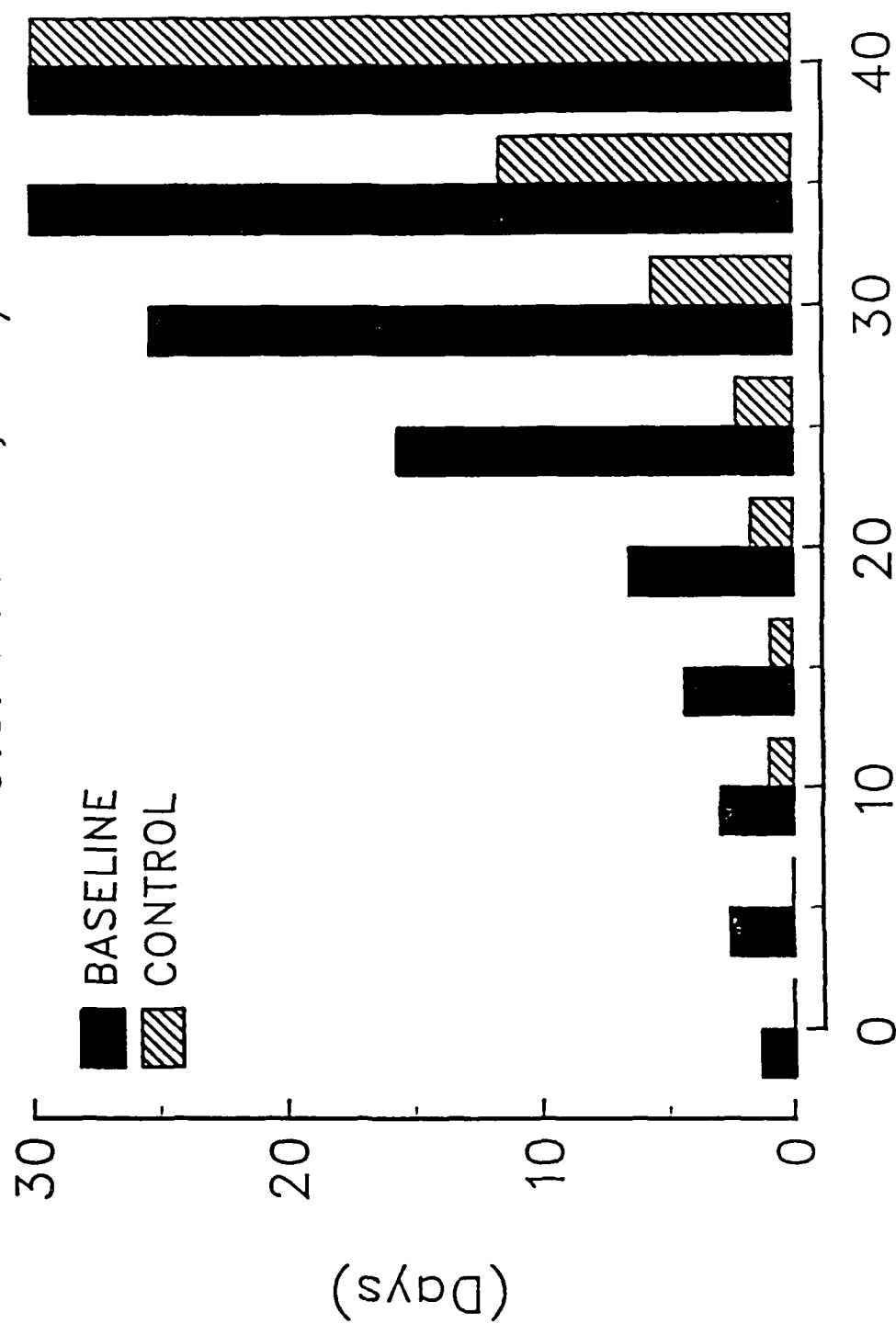
Sub-Threshold Temperature Probability U.S. Midwest



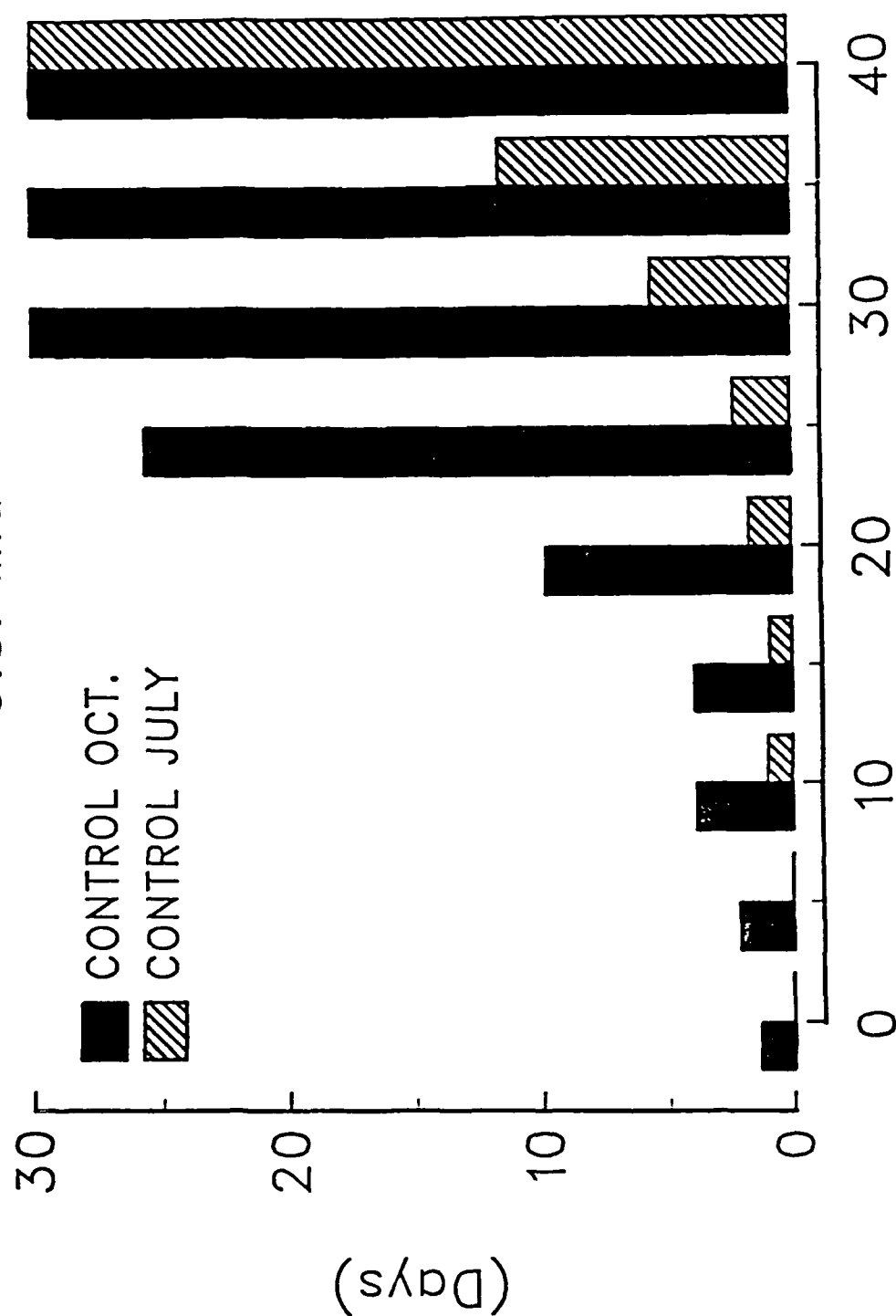
Sub-Threshold Temperature Probability USSR Ukraine



Sub-Threshold Mean Run Duration U.S. Midwest, July



Sub-Threshold Mean Run Duration U.S. Midwest



SECTION 3

LODI CANYON EXPERIMENT

Emission factor measurements for Lodi test fires
using surface based emissions sampling equipment

by

Darold E. Ward and Colin C. Hardy
Fire and Air Resource Management Project
USDA--Forest Service
4043 Roosevelt Way NE
Seattle, WA 98105

ABSTRACT

Surface systems of towers and cables were used for supporting sample packages over small fires of about 0.5 hectares in size preliminary to the large LODI fire of December 1986. The purpose of the experiment was to measure emissions of particulate matter and gases and compare emission factors for these materials to the measurements acquired through using airborne sampling techniques. The subplots were located to represent a diversity of fuel conditions of the larger LODI area: chamise, standing chaparral, and felled chaparral. Burning of the test fires was accomplished by lighting the fire along the top of the subunit and allowing the fire to back downhill for approximately 30 meters and then lighting the fire along the bottom of the plot to get maximum fire intensity as the fire headed uphill toward the location of the sampling equipment. Samples were collected for different periods of the flaming and smoldering combustion processes to obtain samples representing as early as possible emissions produced by each of these processes. In addition, real time measurements of temperature at the location of the sample packages and the verticle velocity were measured in real time. The concentration of CO and CO₂ were measured in real time.

Results from these tests are compared with tests of emissions from logging slash fires in the Pacific Northwest states of Oregon and Washington. Some of the results for the LODI subplot emissions study are summarized in the table below:

Emission Factors

PM2.5	8.3 g/kg
CO	61.5 g/kg
CH ₃ Cl	.036 g/kg

Percent composition of PM2.5

Cl	3.630%
Pb	0.339%
K	8.419%
Organic carbon	51.4%
Elemental carbon	8.9% maximum of 16.9%

Absorption Measurements from Preliminary
Site Burns in Lodi Canyon

E. M. Patterson

Georgia Institute of Technology
Atlanta, Georgia

D. A. Ward

USDA Forest Service
Seattle, Washington

We have measured the absorption properties of smoke samples collected during preliminary burns in the Lodi Canyon. These absorption properties are expressed in terms of the specific absorption of the material. These measurements show a range of values of specific absorption.

We will present these data and will discuss these results in terms of the range of variation of the data, the relation of the absorption data to the elemental carbon concentrations, and the comparison of these results with earlier, similar measurements.

Vertical Plume Velocities in a Controlled Burn.

John Hallett
Desert Research Institute
Reno, Nevada 89506

Time lapse photography from a fixed point on the ground were made for the smoke plumes rising from the Lodi Canyon controlled burn and a controlled JP-4 burn in Sandia Albuquerque, New Mexico. The plume ascent rate was measured at the visual periphery of a rising plume top, and of individual elements following puffing oscillatory motion from the source ($1/2 - 1$ Hz). In the case of the Lodi burn, the slant angle was $3 \text{ km}/15 \text{ km} \sim 10^\circ$, in the oil fire $\sim 15^\circ$, so error of order $\cos 15^\circ$, $\sim 5\%$ are inherent in these measurements. If we assume a simple plume or thermal model, then the central velocities are approximately twice the cap velocity.

Results

Lodi Canyon: A sequence of photographs shows a plume rising with top velocity 3.0 m s^{-1} below the main inversion at $\sim 7000 \text{ ft}$. As the plume passes through the inversion level the rise velocity falls to 1 m s^{-1} , Fig. 1 decelerates until the maximum rise is \sim plume width (1 km) and then sinks back with a velocity of order of the rise velocity to a level somewhat above the visual (aerosol) inversion. The smoke subsequently moves laterally and is on occasion diluted by mixing in a Kelvin-Helmholtz instability wave system in the prevailing shear.

Sandia Oil: The plume rose to a height of ~ 1500 ft. above the fire site, and was carried away in the shear towards the west. The cap in velocity (Fig. 4) showed a maximum about halfway up the plume ($\sim 7 \text{ m s}^{-1}$) being $\sim 4 \text{ m s}^{-1}$ near the base decelerating to 4 m s^{-1} near 1000 ft. and falling to zero at 1500 ft. Lower level winds are a few m s^{-1} increasing to $10\text{-}12 \text{ m s}^{-1}$ above ~ 1000 ft. (Fig. 3).

Visually, the strong turbulence visible in the plume above the fire and in the cap as it rose into the environment died out quickly as the plume bent over and was carried downstream in the higher velocity aloft. The "statistical" plume had a half angle expansion of $20 \pm 2^\circ$ during its initial rise stage, and gave a smoke layer carried downstream, ~ 400 ft. deep with top at 1500 ft. Above the burn site, it was estimated that overall dilution was:

$$\frac{\text{vertical volume flux at } 200 \text{ m}}{\text{horizontal volume flux at } 500 \text{ m}} = \frac{20 \times 20 \times 5 \text{ m}^3}{100 \times 100 \times 10 \text{ m}} \sim 50$$

The turned over cloud was everywhere optically thin as the sun's disc could always be seen; it appeared white, indicating a large particle size for the soot, $\sim 1 \mu\text{m}$.



Fig. 1: Lodi Canyon burn - plume cap shape.



Fig. 2: Sandia Oil pool fire - cap rise ΔT , 5 s.

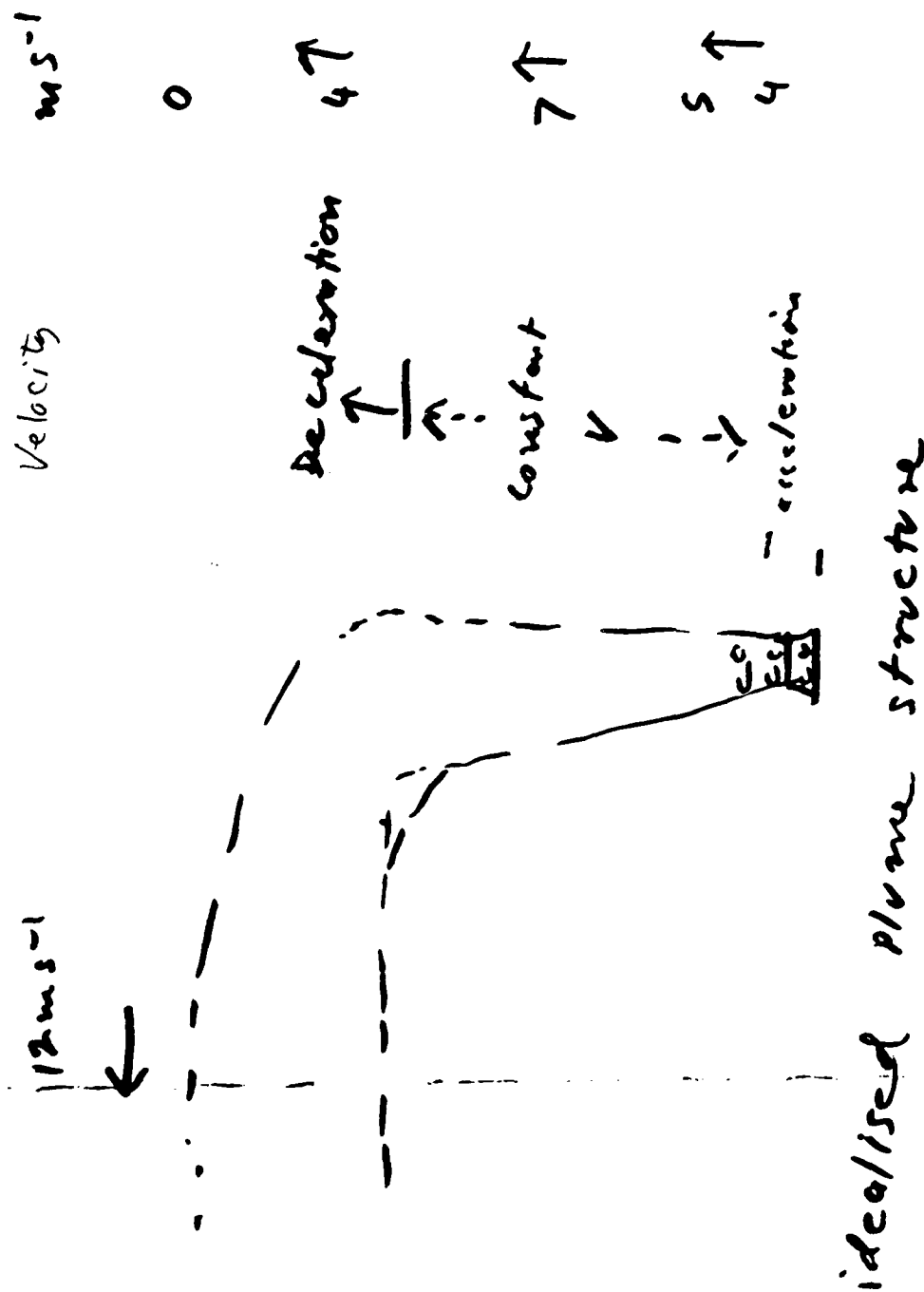


Fig. 3: Sandia Oil pool fire velocity variation with height.
Note the necking in of the plume just above the fire.

Paper Submitted for Presentation at The "Global Effects Program"
Technical Meeting Santa Barbara, 7 - 9 April 1987

Anomalous Production of Sulfur and Nitrogen Species in the Lodi Fire

Dean A. Hegg, Lawrence F. Radke, Peter V. Hobbs and Charles A. Brock
Department of Atmospheric Sciences, University of Washington
Seattle WA, 98195
and
Philip J. Riggan
U. S. Forest Service, Riverside, CA 92507

ABSTRACT

The Lodi burn near Los Angeles on 12 December 1986 produced unexpectedly large emissions of NO_x , SO_2 , and NO_3^- . NO_x to CO_2 molar ratios of 0.6 were observed, compared to the value of 2×10^{-3} adopted by SCOPE and measured by us in prescribed burns of forest products in rural areas of Washington State.

It is postulated that the high emissions of NO_x , SO_2 and NO_3^- in the Lodi burn were due to the resuspension of previously deposited air pollutants onto the vegetation. As such, the emissions measured in the Lodi burn may be more relevant to the burning of biomass near urban areas that have been used in modeling the nuclear winter scenario.

PLUME CHARACTERIZATION STUDIES ON THE LODI CANYON
PRESCRIBED BURN* - W. Einfeld, B. D. Zak, B. V. Mokler and
D. J. Morrison, Sandia National Laboratories,**PO BOX 5800,
Albuquerque, New Mexico, 87185

The prescribed chaparral forest burn conducted at Lodi Canyon, CA in December, 1986 provided an opportunity for several agencies to collaborate in a major plume characterization effort. The Sandia Twin Otter research aircraft was used to make an extensive set of measurements on plume characteristics both at the head of the fire zone and 5 - 10 kilometers downwind. Instruments flown on the aircraft included a mobility analyzer with a measurement range of 0.01 - 0.8 μm and optical particle counters with measurement ranges of 0.1 - 16 μm . Plume aerosol samples were collected using a 1 cubic meter grab bag sampler and associated filter collection, gas sampling and pumping system. Other instruments on the aircraft for this fire included a NASA sun photometer and a Desert Research Institute cloud condensation nuclei counter.

Results to be reported will include particle size distributions, aerosol emission factors as determined by the carbon balance technique, and smoke optical properties.

*This work performed at Sandia National Laboratories, Albuquerque, New Mexico, supported by the United States Department of Energy under Contract DE-AC04-76DP00789

**A United States Department of Energy Facility

SANDIA TWIN OTTER AIRCRAFT - LODI FIRE SAMPLING CONFIGURATION

Particle Size/Count

PMS ASASP-100-X.....0.1 - 3 μ M

PMS FSSP-100-X.....0.5 - 16 μ M

TSI DMPS.....0.01 - 0.8 μ M

TSI Condensation Nuclei Counter

DRI Cloud Condensation Nuclei Counter

DRI Formvar replicator

Aerosol Chemistry - 1 cubic meter grab sampling system

Aerosol mass, aerosol carbon, gaseous carbon

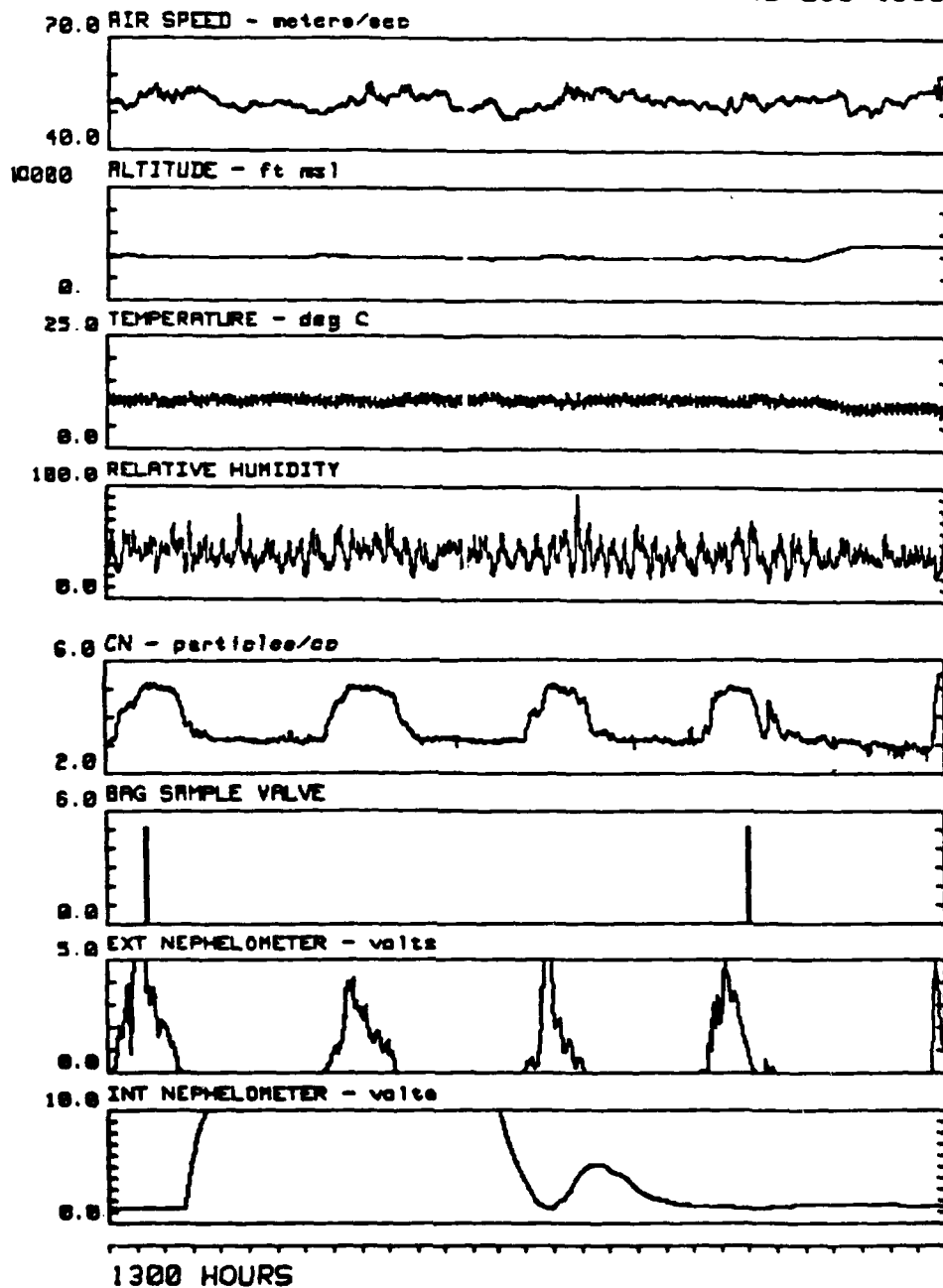
Optical Measurements

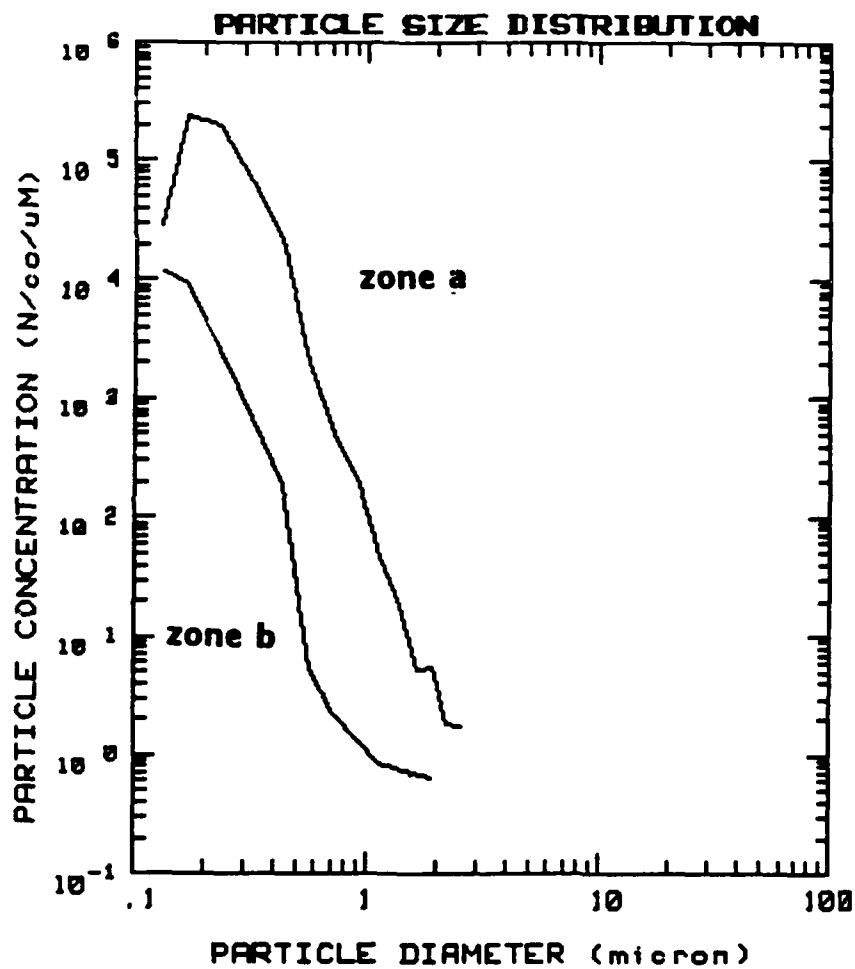
MRI NEPHELOMETERS (bag and probe)

NASA SUN TRACKING PHOTOMETER

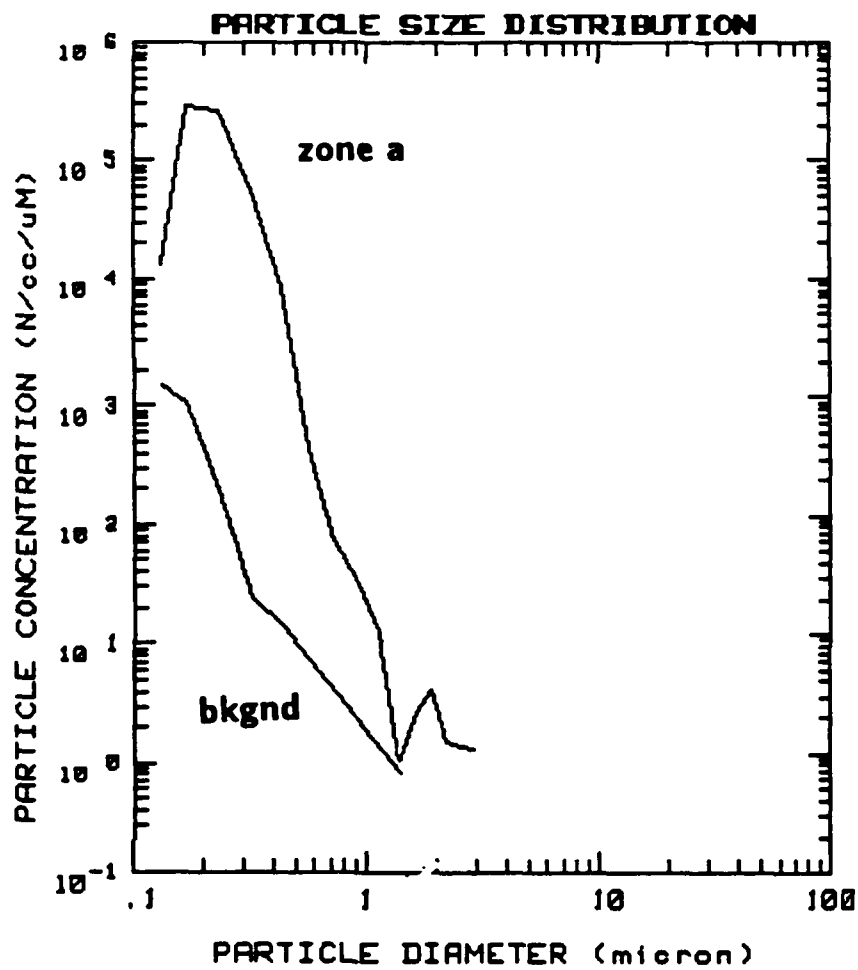
LODI FIRE

12 Dec 1986

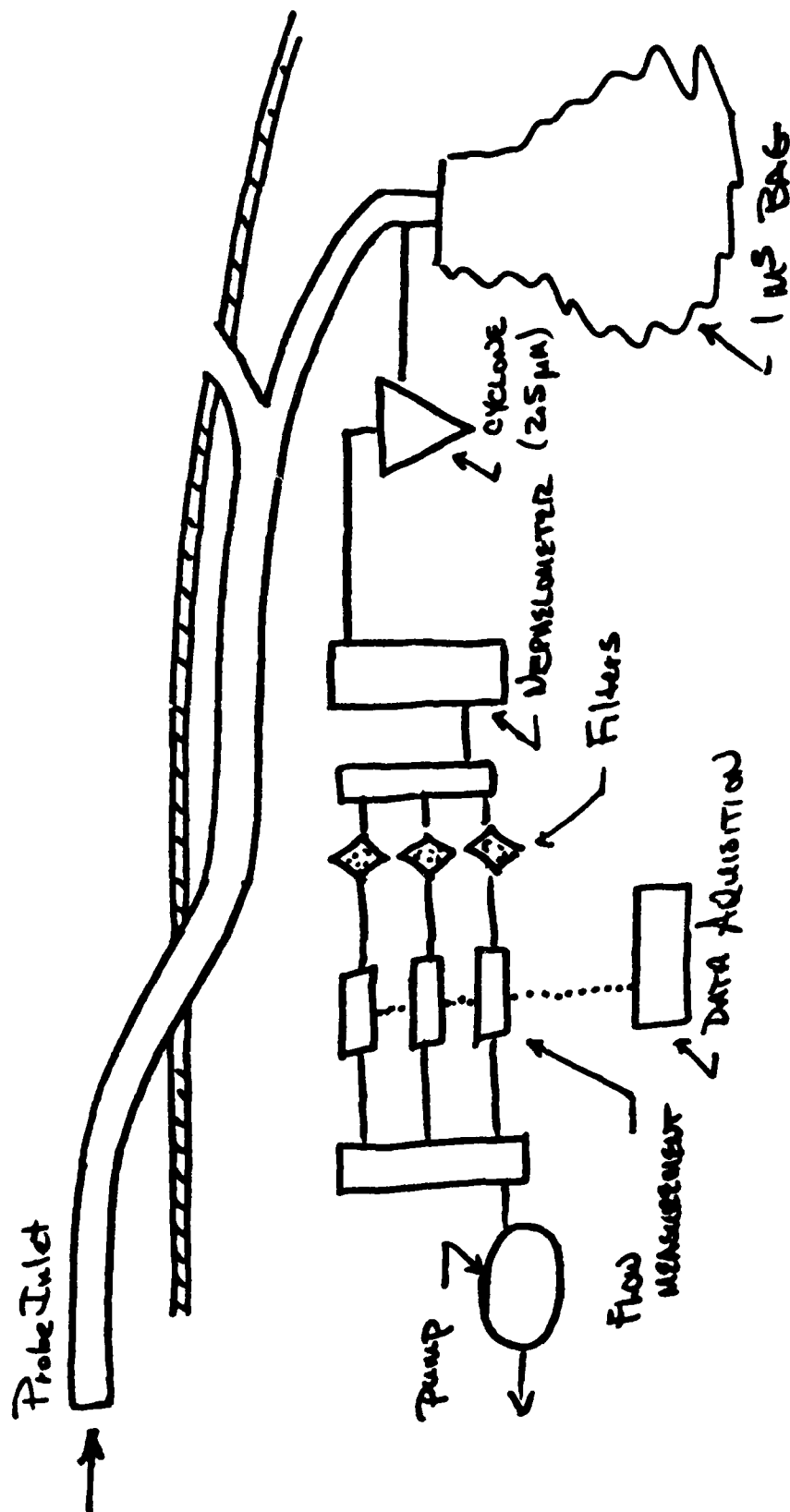




Head of fire and downwind comparison



Head of fire and background comparison



TWIN OTTER AEROSOL SAMPLING SYSTEM

ANALYTICAL METHODS

Aerosol carbon - Sunset Labs

furnace combustion / reduction / FID detection

Gaseous carbon - Sandia Labs

2 liter grab sample / GC analysis / sonic detector

Aerosol elemental composition - Lawrence Berkely Lab

X-ray fluorescence on teflon filters

SAMPLE TIME LOCATION	LODI FINE 12-DEC-86						LODI FINE 03-DEC-86		EROLE DUPN 03-DEC-86	
	BAG 1 1242 ZONE A	UHG 2 1301 ZONE A	BAG 3 1323 ZONE A	BAG 4 1416 ZONE B	BAG 5 1459 ZONE A	BAG 6 1558 ZONE H	UHG 1 1031 ZONE H	UHG 1 1031 ZONE H	BAG 1 1229 ZONE A	
PM-2.5 UUNC (mg/m3)	0.480	1.026	0.281	0.452	1.832	0.352	1.171	1.171	0.933	
XRF CONC (mg/m3)	0.027	0.041	0.014	0.047	0.255	0.014	0.000	0.000	0.037	
OC CONC (mg/m3)	0.392	0.482	0.153	0.338	0.967	0.379	0.502	0.502	0.330	
EC CONC (mg/m3)	0.058	0.002	0.018	0.040	0.180	0.063	0.166	0.166	0.059	
AC CONC (mg/m3)	0.450	0.564	0.171	0.387	1.146	0.441	0.698	0.698	0.397	
GC CONC (mg/m3)	29.960	30.495	6.955	19.795	90.975	25.145	39.590	39.590	27.285	
TC CONC (mg/m3)	30.410	31.059	7.126	20.182	100.121	25.506	40.288	40.288	27.682	
OC/PM-2.5	0.82	0.47	0.54	0.75	0.53	1.08	0.45	0.45	0.36	
EC/PM-2.5	0.12	0.08	0.07	0.11	0.10	0.18	0.14	0.14	0.06	
HC/PM-2.5	0.94	0.55	0.61	0.85	0.63	1.25	0.60	0.60	0.47	
AC+XRF/PM-2.5	0.99	0.59	0.66	0.96	0.77	1.35	0.60	0.60	0.47	
TC/PM-2.5	63.42	30.27	25.32	44.60	54.65	72.76	34.40	34.40	29.65	
F/PM-2.5	0.021	0.020	0.016	0.047	0.071	0.035	0.105	0.105	0.016	
Fuel C fraction	0.5	0.5	0.5	0.5	0.5	0.5	0.5	0.5	0.5	
Emission factor (PM-2.5) (%)	0.79	1.65	1.97	1.12	0.91	0.69	1.45	1.45	1.69	
Emission factor (PM-2.5 EC) (%)	0.10	0.13	0.13	0.12	0.09	0.12	0.21	0.21	0.11	

LOOT FIRE
12 DEC 1986

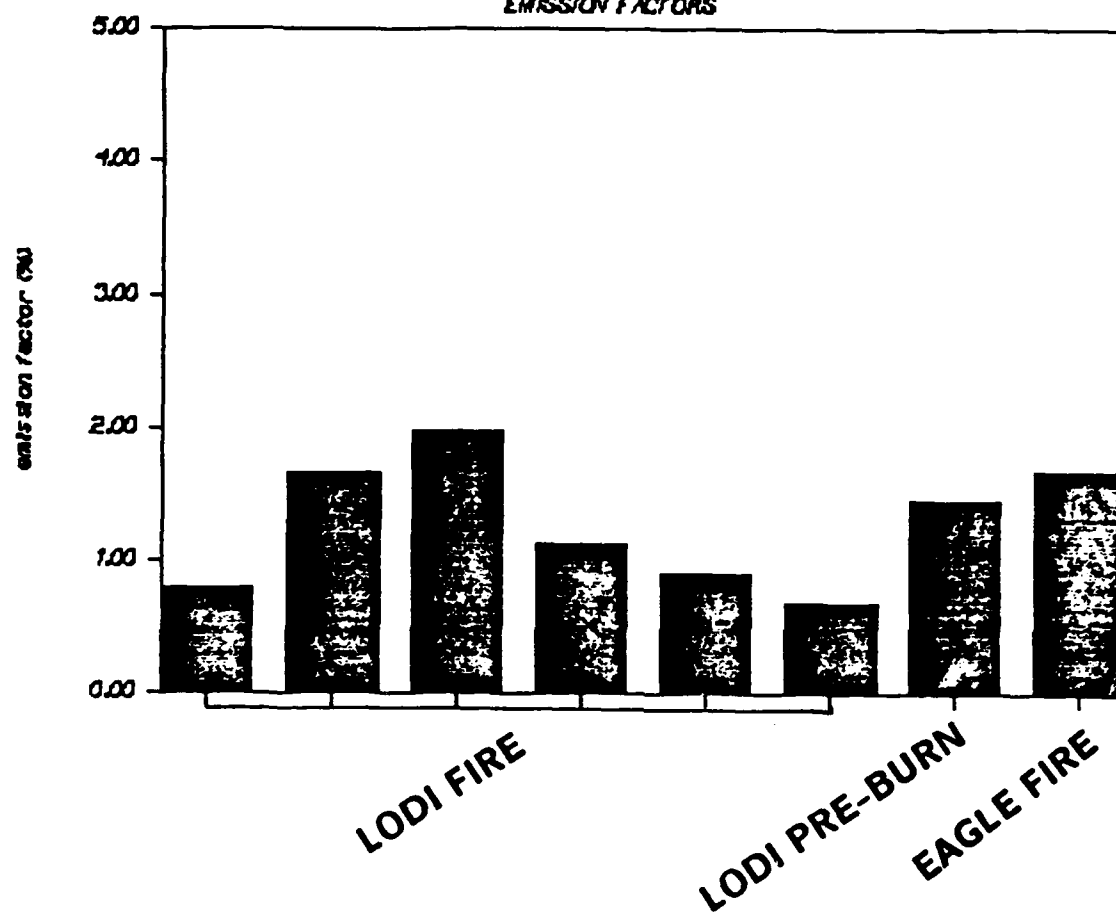
SAMPLE TIME LOCATION	BAG 1 1242 ZONE A	BAG 2 1301 ZONE A	BAG 3 1323 ZONE A	BAG 4 1436 ZONE B	BAG 5 1459 ZONE A	BAG 6 1558 ZONE A
----------------------------	-------------------------	-------------------------	-------------------------	-------------------------	-------------------------	-------------------------

XRF DATA

S (ng/cm2)	41	82	39	79	493	45
K (ng/cm2)	173	392	117	402	2630	243
Fe (ng/cm2)	34	15	18	22	121	25
Pb (ng/cm2)	10	17	8	17	105	12
XRF total (ng/cm2)	466	787	359	891	5149	673
S conc (ug/m3)	1.91	3.49	1.21	3.41	20.25	1.87
K conc (ug/m3)	8.05	16.68	3.63	17.36	106.70	10.11
Fe conc (ug/m3)	1.58	0.64	0.56	0.95	4.91	1.04
Pb conc (ug/m3)	0.47	0.72	0.25	0.73	4.26	0.50
XRF total conc (ug/m3)	21.70	33.48	11.14	38.49	208.90	28.00
K/MR55	0.017	0.016	0.013	0.038	0.058	0.029

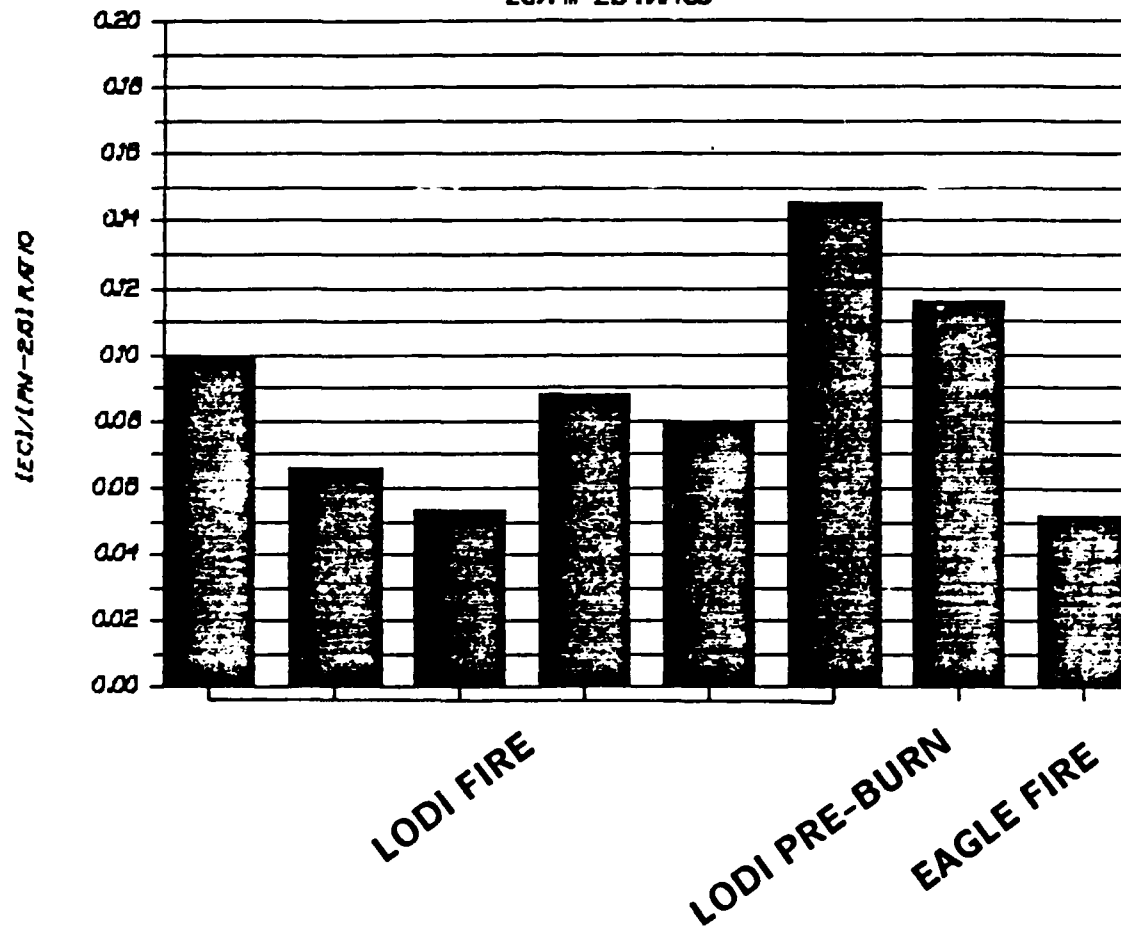
LODI FIRES

EMISSION FACTORS

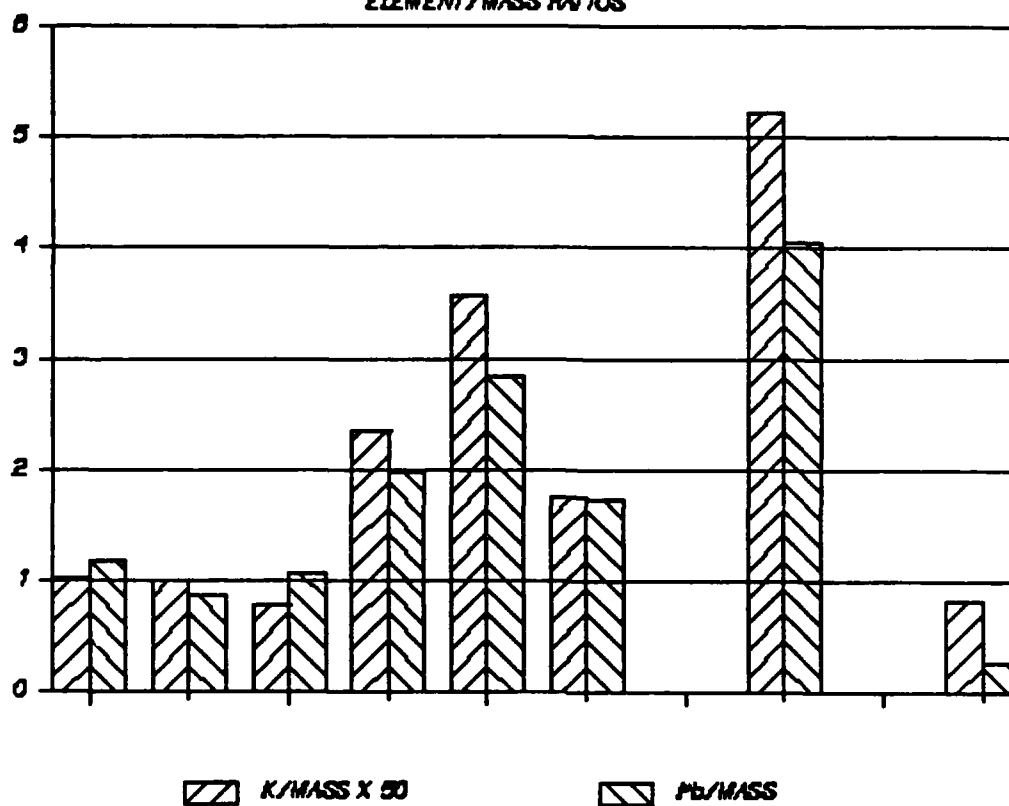


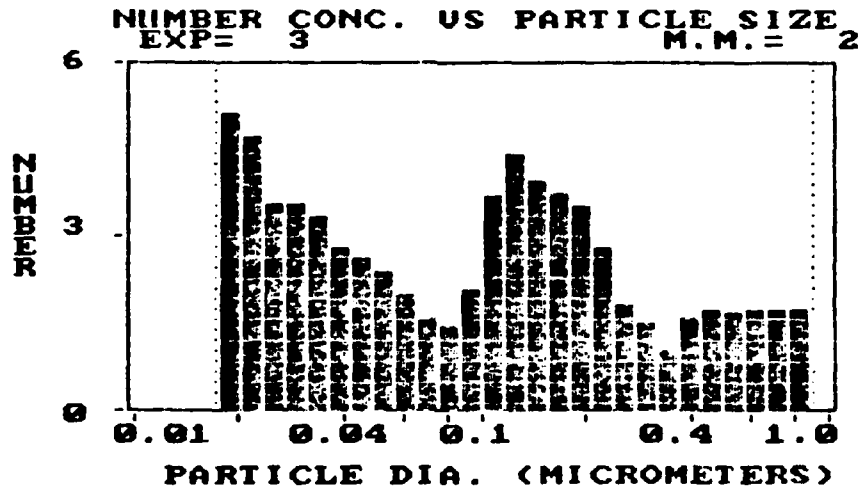
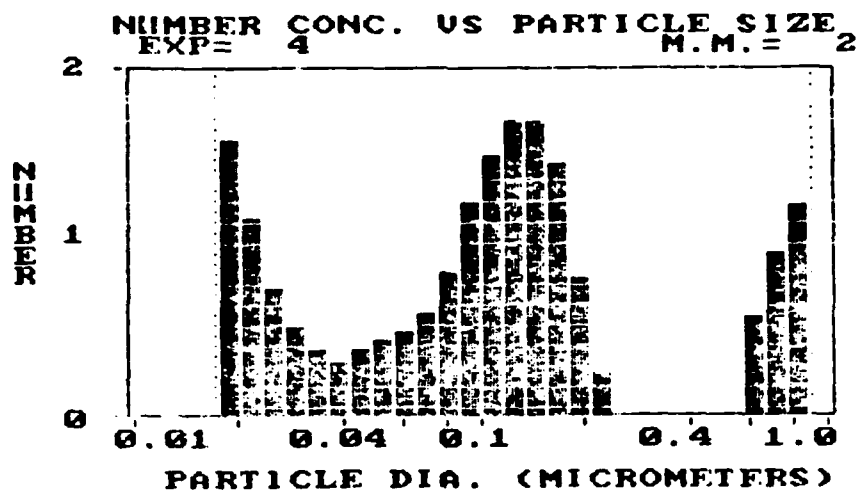
LODI FIRES

EC/PM-25 RATIOS



LODI FIRES ELEMENT/MASS RATIOS





Head of fire and downwind DMPS comparison

LO01 FIRE
12-DEC-1986

SMOKE OPTICAL PROPERTIES

SAMPLE>>> TIME LOCATION	BAG 1 1242 ZONE A	BAG 2 1301 ZONE A	BAG 3 1323 ZONE A	BAG 4 1436 ZONE A	BAG 5 1459 ZONE B	BAG 6 1558 ZONE A
B-sp (Mm-1)	2064	ERR	544	1795	ERR	1462
mass (ug/m3)	480	1026	281	452	1832	352
sp scattering coeff (m2/g)	4.30	ERR	1.94	3.97	ERR	4.15
elemental carbon (ug/m3)	47	67	15	40	147	51
B-sp (Mm-1)	423	603	135	360	1323	459
B-ext (Mm-1)	2487	ERR	679	2155	ERR	1921
ss albedo	0.83	ERR	0.80	0.83	ERR	0.76

LODI FIRE - MEASUREMENT SUMMARY

Emission factor 0.012 / 0.005

EC/MASS ratio 0.089 / 0.032

Sp Mass Scatt Coeff 3.6 / 1.1
(m²/g)

Single scatt albedo 0.79 / 0.04

Measurements of Cloud Active Aerosol in Large Scale Fires.

James G. Hudson
Desert Research Institute
Reno, Nevada 89506

CN and CCN concentration vs. time plots are shown in the following 10 figures. These measurements were made in the Lodi Canyon brush fire of 12 December 1986, and the Sandia Oil fire of 13 March 1987.

It is noted that the changes in the CCN concentrations lag the similar changes in the CN concentrations by nearly a minute. This is approximately the time required for the sample to pass through the cloud chamber where droplet growth occurs before entry to the optical counter where recording takes place. When this explanation is taken into account it is apparent that the two instruments are observing the same features of the plumes. Greater resolution is observed with the *CN counter simply because the data is recorded at 1 second intervals instead of 8 second intervals.* Nevertheless, the time widths of the plumes as observed by the two instruments are similar. They are generally within the difference in time resolution (7 seconds). Therefore the CCN instrument does not appear to be smearing the concentration in time. The particles are being recorded with the same time separation which they had in the sample tube when they went into the instrument. Hence, the CCN spectrometer is capable of better time resolution if the software can be changed to allow shorter recording intervals. This is now currently under development. This would be quite valuable because this is the only instrument with multiple channel data which can be resolved on such a time scale.

Figures 1-7 for the Lodi brush fire show rather high CN and CCN concentrations. The most surprising aspect of these measurements is the very high ratio of CCN to CN. The majority of the plume penetrations show a ratio of nearly one. That is nearly all of the particles appear to be CCN active at 1% supersaturation. This ratio is quite variable as some of the penetrations display a much lower ratio. Differences among the plume penetrations will be examined to see if there is a reason for these variations in the CCN/CN ratio. Nevertheless, it appears that the smoke from brushfires is perhaps more hygroscopic than previously thought.

The CCN concentrations which are presented here are unprecedented. These are by far the highest CCN concentrations ever measured. CCN instruments are usually limited to a few thousand per cubic centimeter because of depletion of water vapor in the cloud chamber. The main reason this chamber can measure such high concentrations is that it is possible to reduce the sample flow rate to very low values ($<5 \text{ cm}^3/\text{min.}$) and still measure and record this rate. Apparently, this technique works correctly because the CN measurements indicate that the CCN concentrations could not possibly be any higher. Therefore, vapor depletion and other problems associated with high count rates seem to have been overcome. There are a number of errors such as these which could reduce the measured CCN concentrations but the only known error which would raise the measured concentration is a leak.

The last possibility was checked during one of the plume penetrations. The fifth penetration of Figure 1 and the first penetration of Figure 4 display a zero CCN concentration. This is as it should be because a filter was placed on the CCN sample inlet during this penetration. Therefore, no particles were getting into the instrument except those which were measured to enter through the sample tube.

The last penetrations of Figures 5 and 7 seem to display CCN concentrations higher than the CN concentrations. However, the CCN sample flow rates in these cases slipped to such low values ($<1 \text{ cm}^3/\text{min.}$) that they were probably not accurate.

Figures 8-10 show CN and CCN data from the oil pool fire. The most obvious difference from the brush fires is the much lower particle concentrations. The next important contrast with the brush fires is the fact that the CCN concentrations in the oil fire show very small increases over the background concentrations. The ratio of CCN to CN is much smaller for the oil fire. There the oil smoke is much less hygroscopic than the brushfire smoke. Those results are consistent with laboratory work presented in another paper in these proceedings.

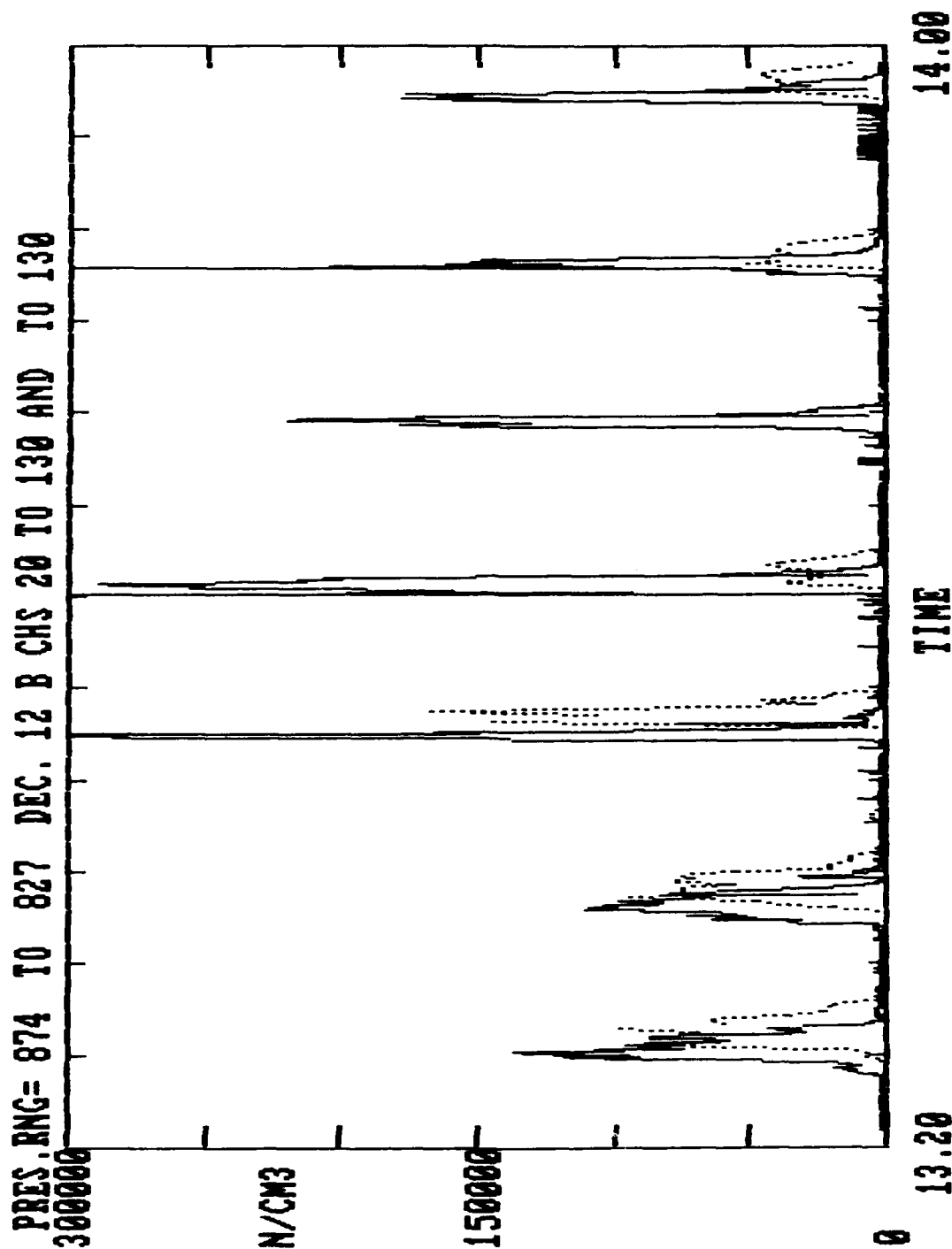


Fig. 1 CN and CCN concentrations vs. time during a flight in the Lodi fire of 12 December. Concentration is given in number per cubic cm while time is shown in fractions of an hour. The solid line is the CN concentration while the dashed line is the CCN concentration at approximately 1% supersaturation. The CN data is recorded every second while the CCN data was recorded at about 8 second intervals. This figure shows seven penetrations of the smoke plumes.

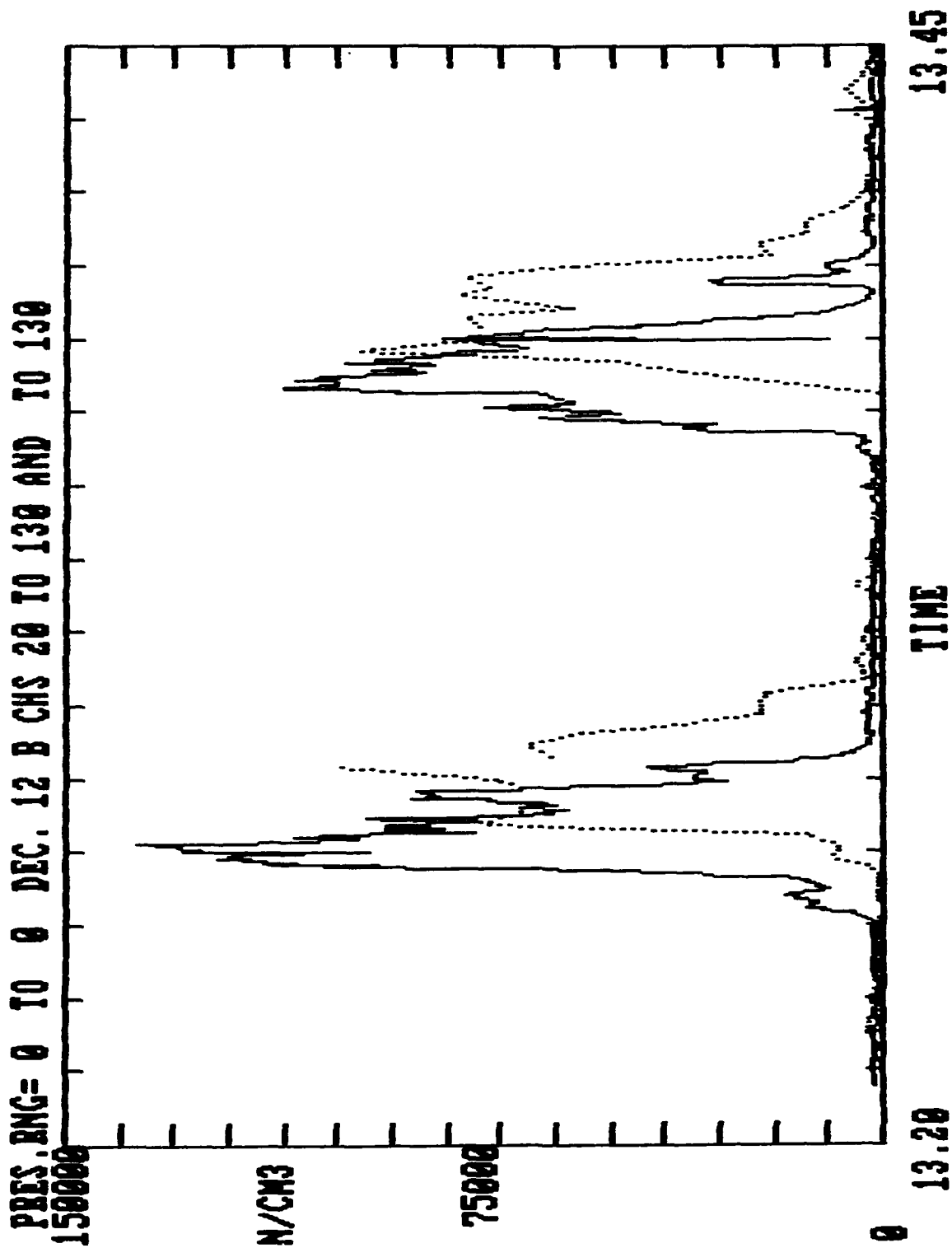


Fig. 2 As Fig. 1. Expansion of the first two penetrations shown in Figure 1.

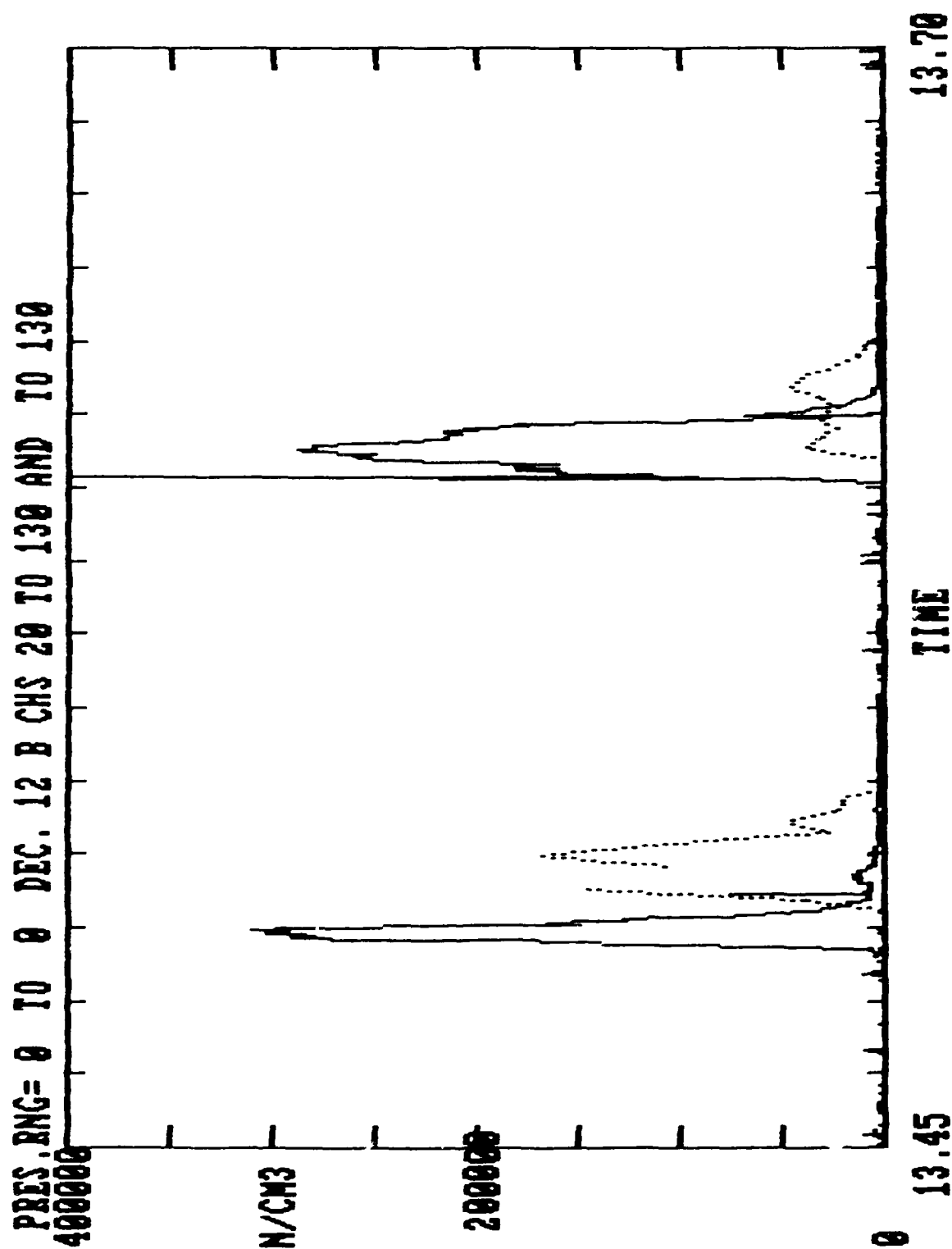


Fig. 2 As Fig. 1. Expansion of the third and fourth penetrations shown in Figure 1.

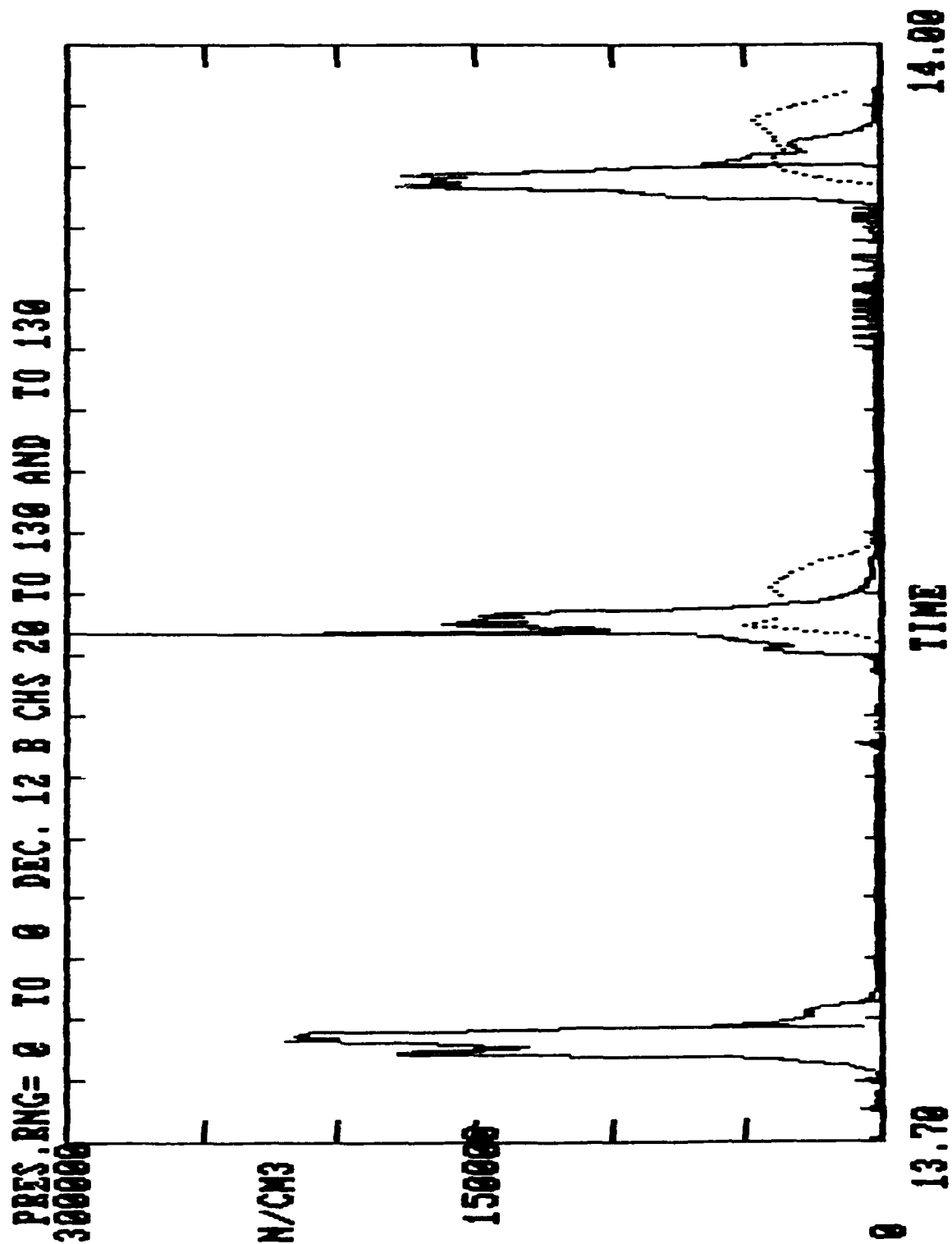


Fig. 4 As Fig. 2. Expansion of the last three penetrations shown in Figure 1.

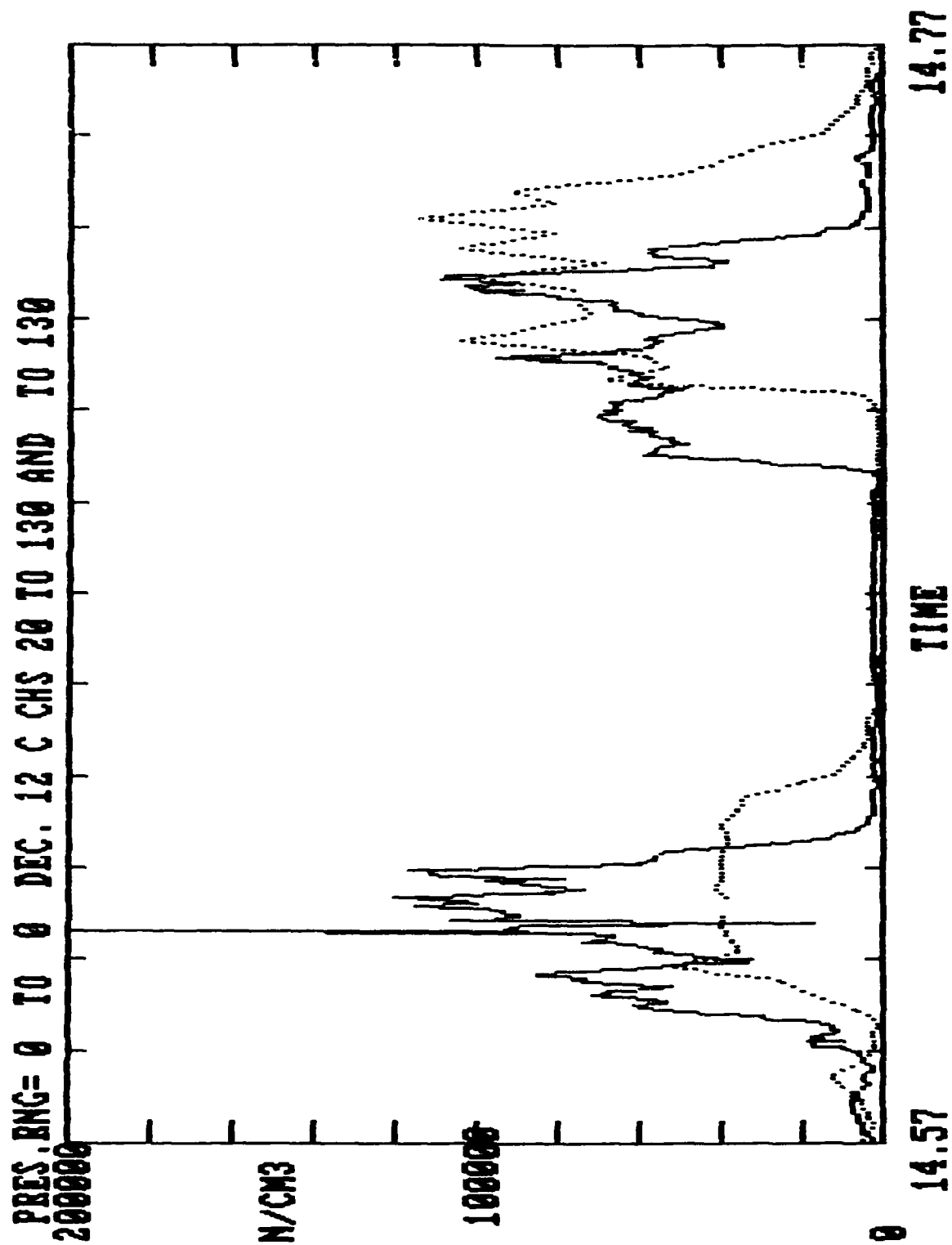


Fig. 5 As Fig. 1. Another set of plume penetrations.

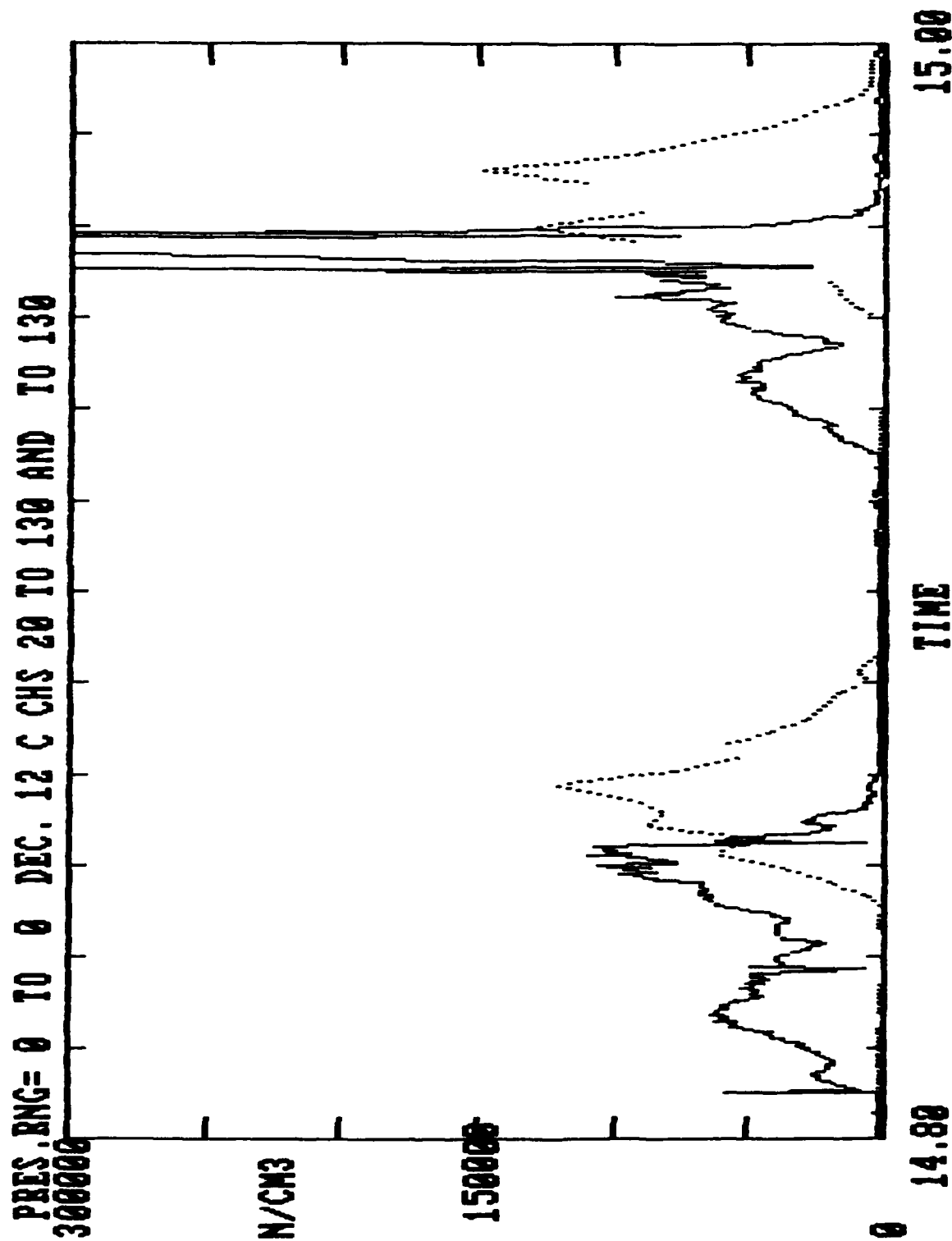


Fig. 6 As Fig. 5 for later penetrations. The last penetration shown here has an especially strong updraft which caused some minor cabin damage and interruption of the instruments.

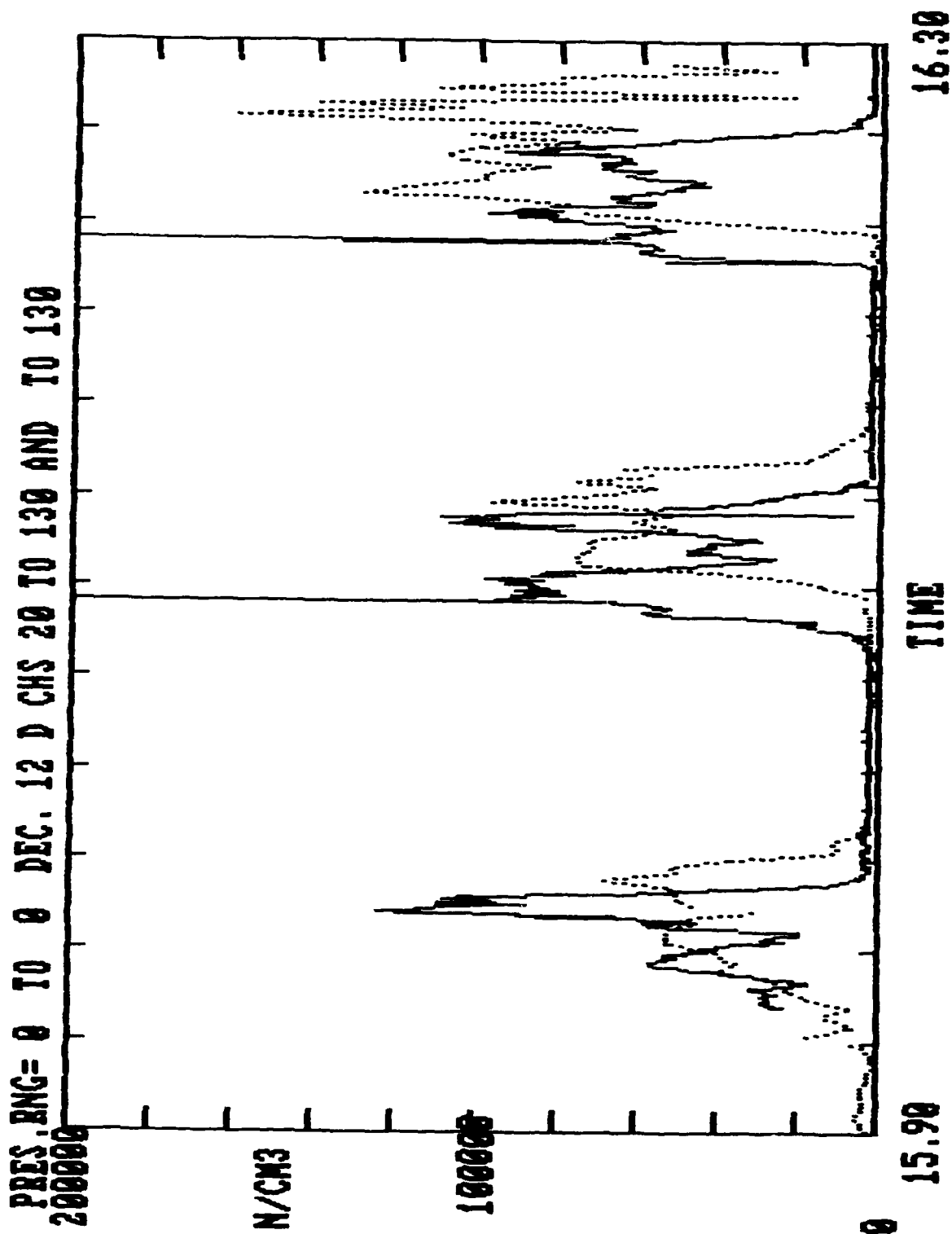


Fig. 7 AB Fig. 5.

PRES. ENG= 749 TO 725 MAR 13 CHS 20 TO 130 AND TO 130

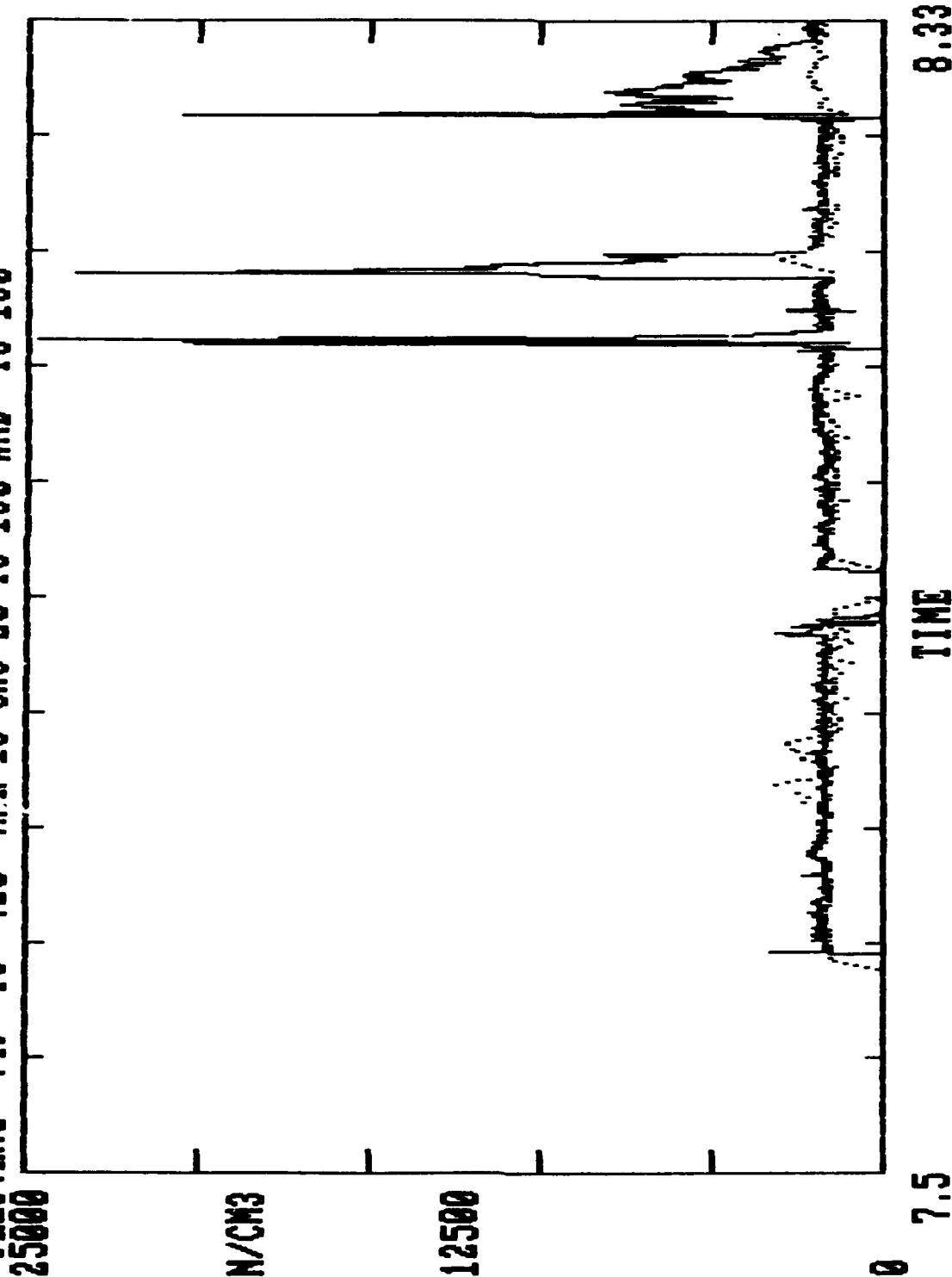


Fig. 8 As Fig. 1 except that this is for the oil pool fire of 13 March. Shown here are background concentrations before the fire, a filter on the sample inlet to monitor the instrument noise, and three penetrations of the plume.

PRES. RNG= 763 TO 715 MAR 13 CHS 20 TO 130 AND TO 130

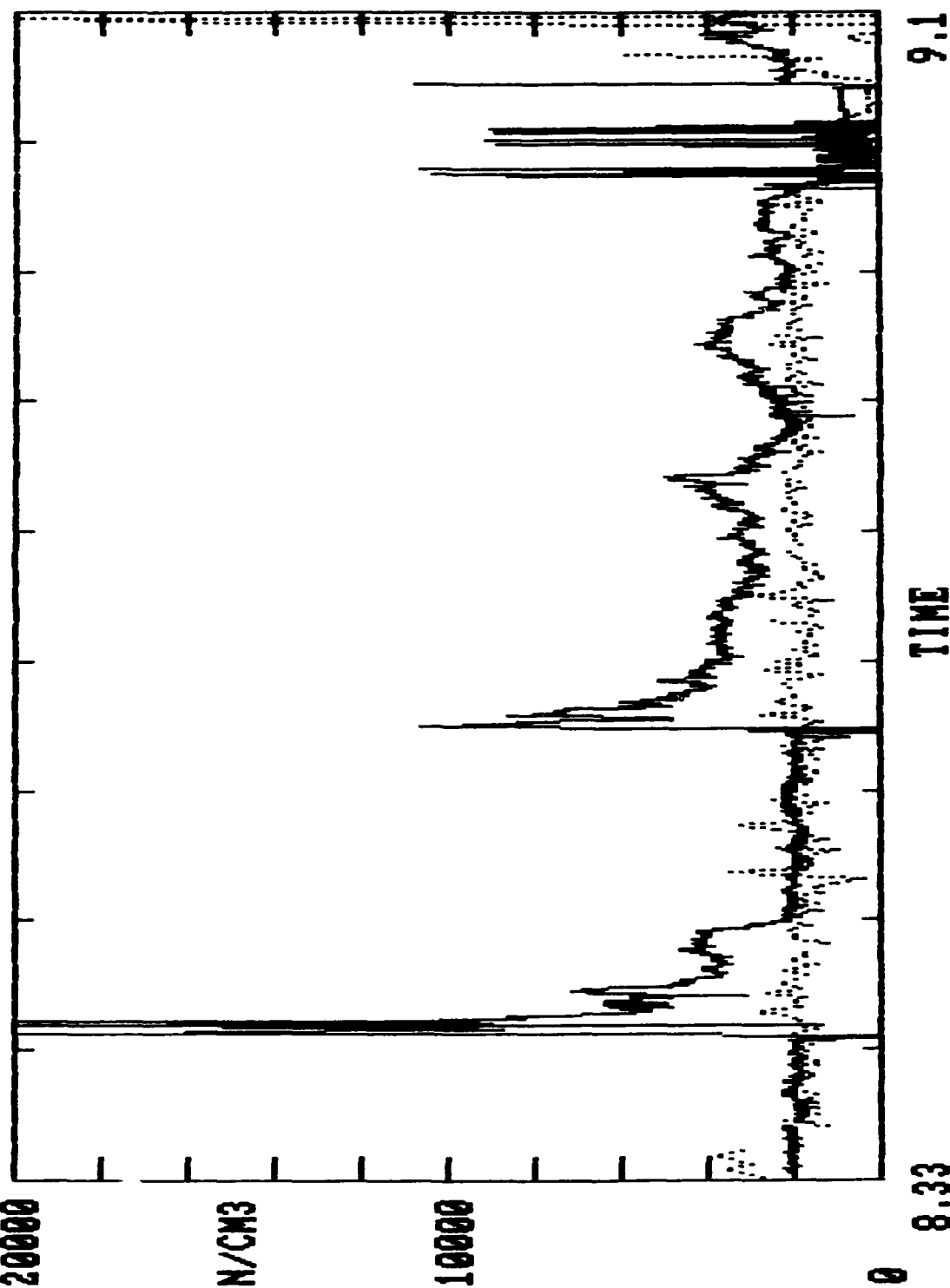


Fig. 9 As Fig. 8.

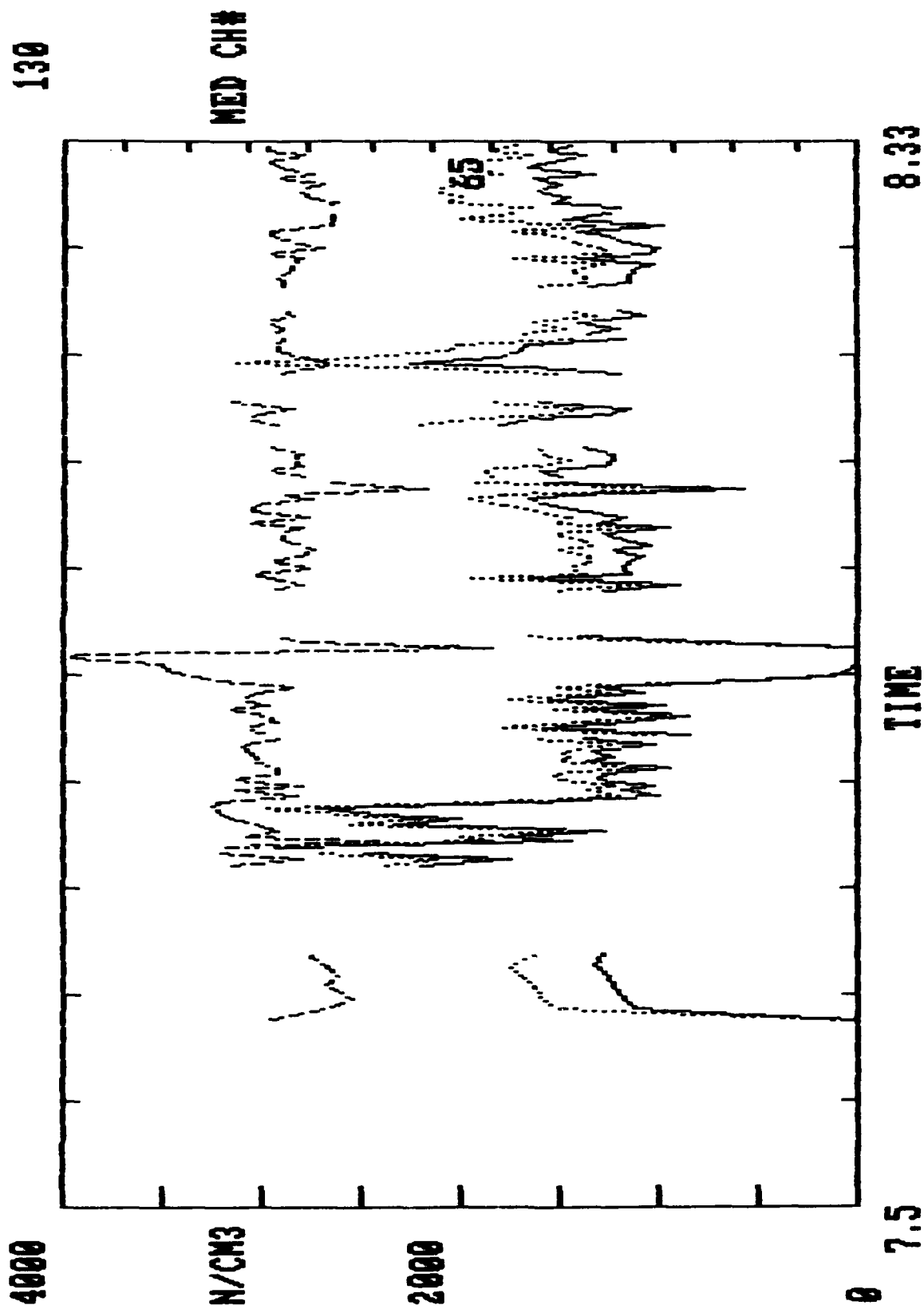


Fig.10 Expansion of Fig. 8 showing only the CCN concentrations at two super-saturations, 1% and 0.5% (approx.), and the median channel number of the CCN spectrum (~95).

OPTICAL DEPTH MEASUREMENTS OF FOREST FIRE SMOKES: TWO CASE STUDIES.

R.F.Pueschel, P.B.Russell, T.P.Ackerman, D.A.Allen and D.S.Colburn. NASA Ames Research Center, Moffett Field, CA 94035.

B.D.Zak and W.Einfeld. SANDIA National Laboratories, Albuquerque, NM 87185.

Since installing the Ames Tracking Airborne Sunphotometer on the Sandia Laboratories' Twin Otter research aircraft, we had opportunities to measure optical depths between 380 and 1020 nm in smokes from a fire of opportunity near Fresno, CA on 11 Sep 1986, and from the Lodi Canyon controlled burn on 12 December 1986.

The optical depths of both smokes are similar in magnitude and wavelength dependence. At short wavelengths, the optical depths of the smokes are increased by up to one order of magnitude over those of background air. The increase at 1020 nm wavelengths is up to 2 orders of magnitude for the Lodi Canyon fire, but less than one order in the smoke of the Fresno fire over the respective background optical depths.

The optical depth in background air in the vicinity of Los Angeles differs markedly from that of the Central Valley. A strong wavelength dependence suggests the prevalence in the Los Angeles atmosphere of very small particles and fewer large aerosols than are found in central California.

Aging of the Lodi Canyon controlled burn smoke indicates a decrease of optical depths due to dilution, and a wavelength dependence that suggests an alteration of the smoke particle size distribution; the aged smoke aerosol contains fewer small particles and has a larger modal particle size than does the fresh smoke.

DISTRIBUTION LIST

DEPARTMENT OF DEFENSE

ARMED FORCES RADIOBIOLOGY RSCH INST
ATTN: COL G IRVING

ASSISTANT TO THE SECRETARY OF DEFENSE
ATOMIC ENERGY
ATTN: LTCOL L MILLS

DEFENSE INTELLIGENCE AGENCY
ATTN: N BARON
ATTN: RTS-2B

DEFENSE NUCLEAR AGENCY
ATTN: DFRA
ATTN: G ULLRICH
ATTN: K SCHWARTZ
ATTN: L WITTWER
ATTN: G BAKER
ATTN: R WEBB
ATTN: D AUTON
ATTN: LT COL E WERZ
ATTN: M FRANKEL
ATTN: M FLOHR
ATTN: COL T HAWKINS

4 CYS ATTN: TITL

DEFENSE TECH INFO CENTER
12CYS ATTN: DD

DIRECTOR
ATTN: LTCOL G BETOURNE
ATTN: R RUFFIN

NATIONAL DEFENSE UNIVERSITY
ATTN: COL S GARDINER
ATTN: G FOSTER
ATTN: H ALMOND

DEPARTMENT OF THE ARMY

U S ARMY ATMOSPHERIC SCIENCES LAB
ATTN: R SUTHERLAND
ATTN: MR RUBIO

U S ARMY CORPS OF ENGINEERS
ATTN: R GOMEZ
ATTN: DR CHOROMOKOS

U S ARMY CORPS OF ENGINEERS
ATTN: L ZIEGLER
ATTN: R BECKER

U S ARMY ENGR WATERWAYS EXPR STA
ATTN: DR V E LAGARDE

U S ARMY MISSILE INTELL AGENCY
ATTN: J GAMBLE

U S ARMY NATICK RSCH DEV & ENGRG CTR
ATTN: H M EL-BISI

U S ARMY STRATEGIC DEFENSE COMMAND
ATTN: DR J LILLY
ATTN: G EDLIN
ATTN: J VEENEMAN

ATTN: M CAPPS
ATTN: R BRADSHAW

DEPARTMENT OF THE NAVY

CNO EXECUTIVE PANEL
ATTN: CAP L BROOKS

NAVAL RESEARCH LABORATORY
ATTN: R JEK

NAVAL SURFACE WARFARE CENTER
ATTN: S MASTERS

DEPARTMENT OF THE AIR FORCE

AF/INYXC
ATTN: LTCOL N BARRY

AIR FORCE GEOPHYSICS LABORATORY
ATTN: D CHISHOLM
ATTN: R MURPHY
ATTN: H GARDINER
ATTN: R BANTA
ATTN: H S MUENCH

AIR FORCE INSTITUTE OF TECH/EN
ATTN: MAJ S R BERGGREN
ATTN: DR C BRIDGEMAN

AIR FORCE OFFICE OF SCI RSCH
ATTN: D BALL

AIR FORCE SPACE DIVISION
ATTN: CAPT K O'BRYAN

AIR FORCE TECH APPLICATIONS CTR
ATTN: J MARSHALL

AIR FORCE WEAPONS LABORATORY
ATTN: CAPT LEONG
ATTN: J JANNI
ATTN: J W AUBREY

BALLISTIC MISSILE OFFICE
ATTN: LT ROTHCHILD
ATTN: TOMASZEWSKI

DEPUTY CHIEF OF STAFF
ATTN: AFXOX

STRATEGIC AIR COMMAND
3 CYS ATTN: CAPT W NICHOLS
ATTN: LT COL W GIFFORD
ATTN: T BAZZOLI

DEPARTMENT OF ENERGY

ARGONNE NATIONAL LABORATORY
ATTN: H DRUCKER
ATTN: M WESLEY

BROOKHAVEN NATIONAL LABORATORY
ATTN: B MANOWITZ
ATTN: E WEINSTOCK

DASIAC-TN-87-35-V2 (DL CONTINUED)

DEPARTMENT OF ENERGY
ATTN: I NEDDOW
ATTN: T HARRIS

DESERT RESEARCH INSTITUTE
ATTN: J HALLETT
ATTN: J HUDSON

LAWRENCE BERKELEY NATIONAL LAB
ATTN: H ROSEN

LAWRENCE LIVERMORE NATIONAL LAB
ATTN: C R MOLENKAMP
ATTN: C SHAPIRO
ATTN: F LUTHER
ATTN: G BING
ATTN: G SIMONSON
ATTN: J PENNER
ATTN: A GROSSMAN
ATTN: J KNOX
ATTN: L ANSPAUGH
ATTN: R PERRETT
ATTN: M MACCRACKEN
ATTN: S GHAN

LOS ALAMOS NATIONAL LABORATORY
ATTN: D SAPPENFIELD
ATTN: E J CHAPYAK
ATTN: E JONES
ATTN: E SYMBALISTY
ATTN: G GLATZMAIER
ATTN: G M SMITH
ATTN: L H AUER
ATTN: M GILLESPIE
ATTN: L CLOUTMAN
ATTN: R MALONE
ATTN: T YAMATTA

OAK RIDGE NATIONAL LABORATORY
ATTN: D FIELDS

SANDIA NATIONAL LABORATORIES
ATTN: B ZAK
ATTN: R BACKSTROM
ATTN: D DAHLGREN
ATTN: D FORDHAM
ATTN: D WILLIAMS
ATTN: K D BERGERON
ATTN: L TROST
ATTN: M D BENNETT

OTHER GOVERNMENT

CENTRAL INTELLIGENCE AGENCY
ATTN: R NELSON

DEPARTMENT OF AGRICULTURE
ATTN: D HAINES

DEPARTMENT OF TRANSPORTATION
ATTN: COL M ROESCH

ENVIRONMENTAL PROTECTION AGENCY
ATTN: R COTHERN
ATTN: W E FALLON

FEDERAL EMERGENCY MGT AGENCY
ATTN: B W BLANCHARD
ATTN: J KELLETT
ATTN: J LABARRE
ATTN: J POWERS

GENERAL ACCOUNTING OFFICE
ATTN: P BOLLEA
ATTN: V BIELECKI

NASA
ATTN: N CRAYBILL
ATTN: W R COFER

NASA
ATTN: D WESTPHAL
ATTN: R HABERLE
ATTN: O TOON
ATTN: R PUESCHEL
ATTN: R YOUNG
ATTN: T ACKERMAN

NATIONAL BUREAU OF STANDARDS
ATTN: G MULHOLLAND
ATTN: R LEVINE
ATTN: R REHM
ATTN: R SCHRACK

NATIONAL BUREAU OF STANDARDS
ATTN: H BAUM

NATIONAL CENTER ATMOSPHERIC RSCH
ATTN: J KIEHL
ATTN: S SCHNEIDER
ATTN: S THOMPSON

NATIONAL CLIMATE PROGRAM OFFICE
ATTN: A HECHT
ATTN: M YERG

NATIONAL OCEANIC & ATMOSPHERIC ADMIN
ATTN: F FEHSENFELD
ATTN: J DELUISI
ATTN: V DERR

NATIONAL OCEANIC & ATMOSPHERIC ADMIN.
ATTN: B HICKS

NATIONAL RESEARCH COUNCIL
ATTN: R DEFRIES

NATIONAL SCIENCE FOUNDATION
ATTN: E BIERLY
ATTN: H VIRJI
ATTN: L HAMATY
ATTN: R SINCLAIR
ATTN: R TAYLOR

NUCLEAR REGULATORY COMMISSION
ATTN: R ALEXANDER

OFFICE OF SCIENCE AND TECH POLICY
ATTN: B HEALY
ATTN: MAJ HARRISON
ATTN: T RONA

OFFICE OF TECHNOLOGY ASSESSMENT
ATTN: R WILLIAMSON

U S ARMS CONTROL & DISARMAMENT AGCY
ATTN: B DOENGES
ATTN: G PITMAN
ATTN: H SCHAEFFER
ATTN: R GODESKY

U S DEPARTMENT OF STATE
ATTN: C CLEMENT
ATTN: S CLEARY
ATTN: T VREBALOVICH

U S GEOLOGICAL SURVEY
ATTN: R DECKER

U S GEOLOGICAL SURVEY
ATTN: E SHOEMAKER

U S HOUSE OF REPRESENTATIVES
ATTN: C BAYER
ATTN: J DUGAN

U S HOUSE OF REPRESENTATIVES
ATTN: J FREIWALD
ATTN: M HERBST

US DEPARTMENT AGRICULTURE
ATTN: D WARD

DEPARTMENT OF DEFENSE CONTRACTORS

AEROSPACE CORP
ATTN: C RICE
ATTN: G LIGHT
ATTN: L R MARTIN

AMERICAN ASSN ADV OF SCIENCE
ATTN: D M BURNS

ANALYTIC SERVICES, INC (ANSER)
ATTN: R BROFFT

APPLIED RESEARCH CORP
ATTN: A ENDAL

AT&T DEFENSIVE SYSTEMS STUDIES
ATTN: R JANOW

ATMOSPHERIC AND ENVIRONMENTAL RES
ATTN: N SZE

AUDIO INTELLIGENCE DEVICES INC
ATTN: H BAUM

AVCO CORPORATION
ATTN: G GRANT

BALL AEROSPACE SYSTEMS DIVISION
ATTN: B CUMMINGS
ATTN: C BRADFORD

BDM CORP
ATTN: J LEECH

BERKELEY RSCH ASSOCIATES, INC
ATTN: S BRECHT

BOEING TECH & MANAGEMENT SVCS, INC
ATTN: G HALL

C. L. CONSULTING SERVICES
ATTN: F FEER

CALIF RESEARCH & TECHNOLOGY, INC
ATTN: M ROSENBLATT
ATTN: R GAJ
ATTN: S KRUEGER

CALSPAN CORP
ATTN: R MAMBRETTI
ATTN: R MISSERT

CARNEGIE CORPORATION OF NEW YORK
ATTN: D ARSENIAN

CHARLES STARK DRAPER LAB, INC
ATTN: A TETEWski

COLORADO STATE UNIVERSITY
ATTN: D KRUEGER
ATTN: W COTTON

COMPUTER SCIENCES CORP
ATTN: G CABLE

DARTSIDE CONSULTING
ATTN: A FORESTER

DELTA RESEARCH, INC
ATTN: L WEINER
ATTN: M RADKE

DYNAMICS TECHNOLOGY, INC
ATTN: D HOVE

ENW INTERNATIONAL, LTD
ATTN: J CANE

EOS TECHNOLOGIES, INC
ATTN: B GABBARD
ATTN: N JENSEN
ATTN: W LELEVIER

FACTORY MUTUAL RESEARCH CORP
ATTN: M A DELICHATSIOS

FEDERATION OF AMERICAN SCIENTISTS
ATTN: J STONE

GENERAL ELECTRIC CO
ATTN: R E SCHMIDT

GENERAL RESEARCH CORP
ATTN: B BENNETT
ATTN: J BALTES

HORIZONS TECHNOLOGY INC
ATTN: J AMBROSE

DASIAC-TN-87-35-V2 (DL CONTINUED)

HORIZONS TECHNOLOGY, INC ATTN: R W LOWEN ATTN: W T KREISS	ATTN: S JAEGER ATTN: W YUCKER
HUGHES AIRCRAFT CO ATTN: E DIVITA	MERIDIAN CORP ATTN: E DANIELS ATTN: F BAITMAN
INFORMATION SCIENCE, INC ATTN: W DUDZIAK	MIDWEST RESEARCH INSTITUTE ATTN: J S KINSEY
INSTITUTE FOR DEFENSE ANALYSES ATTN: E BAUER ATTN: F ALBINI	MISSION RESEARCH CORP ATTN: R ARMSTRONG
JOHNS HOPKINS UNIVERSITY ATTN: M LENEVSKY ATTN: R FRISTROM ATTN: W BERL	MISSION RESEARCH CORP ATTN: C LAUER ATTN: C LONGMIRE ATTN: D SOWLE ATTN: G MCCRATOR ATTN: R BIGONI ATTN: T OLD
KAMAN SCIENCES CORP ATTN: J RUSH ATTN: J SCRUGGS	MITRE CORPORATION ATTN: J SAWYER
KAMAN SCIENCES CORP ATTN: P GRIFFIN ATTN: P TRACY	MRJ INC ATTN: D FREIWALD
KAMAN SCIENCES CORPORATION ATTN: D ADERSON ATTN: DASIAC	NATIONAL ADVISORY COMMITTEE ATTN: J ALMAZAN ATTN: J BISHOP
KAMAN TEMPO ATTN: B GAMBILL ATTN: D FOXWELL ATTN: DASIAC ATTN: E MARTIN ATTN: R RUTHERFORD ATTN: R YOUNG ATTN: S FIFER ATTN: W KNAPP	NATIONAL INST. FOR PUBLIC POLICY ATTN: K PAYNE
LOCKHEED MISSILES & SPACE CO, INC ATTN: J HENLEY ATTN: J PEREZ	NICHOLS RESEARCH CORP, INC ATTN: H SMITH ATTN: J SMITH ATTN: M FRASER ATTN: R BYRN
LOCKHEED MISSILES & SPACE CO, INC ATTN: P DOLAN ATTN: W MORAN	NORTHROP SERVICES INC ATTN: T OVERTON
M I T LINCOLN LAB ATTN: S WEINER	ORLANDO TECHNOLOGY INC ATTN: R SZCZEPANSKI
MARTIN MARIETTA DENVER AEROSPACE ATTN: D HAMPTON	PACIFIC-SIERRA RESEARCH CORP ATTN: G ANNO ATTN: H BRODE ATTN: M DORE ATTN: R SMALL
MCDONNELL DOUGLAS CORP ATTN: T CRANOR ATTN: T TRANER	PHOTOMETRICS, INC ATTN: I L KOFSKY
MCDONNELL DOUGLAS CORP ATTN: A MONA ATTN: F SAGE ATTN: G BATUREVICH ATTN: J GROSSMAN ATTN: R HALPRIN	PHOTON RESEARCH ASSOCIATES ATTN: J MYER
	PHYSICAL RESEARCH INC ATTN: H FITZ
	PHYSICAL RESEARCH INC ATTN: D MATUSKA
	PHYSICAL RESEARCH INC ATTN: J WANG

PHYSICAL RESEARCH, INC
ATTN: D WESTPHAL
ATTN: D WHITENER
ATTN: H WHEELER
ATTN: R BUFF
ATTN: R DELIBERIS
ATTN: T STEPHENS
ATTN: W C BLACKWELL

PHYSICAL RESEARCH, INC
ATTN: G HARNEY
ATTN: J DEVORE
ATTN: J THOMPSON
ATTN: R STOECKLY
ATTN: W SCHLUETER

PHYSICAL RESEARCH, INC
ATTN: H SUGIUCHI

POLYTECHNIC OF NEW YORK
ATTN: B J BULKIN
ATTN: G TESORO

PRINCETON UNIVERSITY
ATTN: J MAHLMAN

QUADRI CORP
ATTN: H BURNSWORTH

R & D ASSOCIATES
ATTN: A KUHL
ATTN: F GILMORE
ATTN: G JONES
ATTN: J SANBORN
ATTN: R TURCO

R & D ASSOCIATES
ATTN: B YOOIN
ATTN: C KNOWLES

R J EDWARDS INC
ATTN: R SEITZ

RADIATION RESEARCH ASSOCIATES, INC
ATTN: B CAMPBELL
ATTN: M WELLS

RAND CORP
ATTN: P ROMERO

ROCKWELL INTERNATIONAL CORP
ATTN: J KELLEY

S-CUBED
ATTN: B FREEMAN
ATTN: K D PYATT, JR
ATTN: R LAFRENZ

SCIENCE APPLICATIONS INC
ATTN: R EDELMAN

SCIENCE APPLICATIONS INTL CORP
ATTN: C HILL

SCIENCE APPLICATIONS INTL CORP
ATTN: B MORTON

ATTN: B SCOTT
ATTN: D SACHS
ATTN: G T PHILLIPS
ATTN: J BENGSTOM
ATTN: D HAMLIN

SCIENCE APPLICATIONS INTL CORP
ATTN: D BACON
ATTN: DR L GOURE
ATTN: F GIESSLER
ATTN: J COCKAYNE
ATTN: J GAHAN
ATTN: J SHANNON
ATTN: J STUART
ATTN: M SHARFF
ATTN: W LAYSON

SCIENCE APPLICATIONS INTL CORP
ATTN: J SONTOWSKI

SCIENCE APPLICATIONS INTL CORP
ATTN: T HARRIS

SCIENTIFIC RESEARCH ASSOC, INC
ATTN: B WEINBERG

SRI INTERNATIONAL
ATTN: C WITHAM
ATTN: D GOLDEN
ATTN: D MACDONALD
ATTN: D ROBERTS
ATTN: E UTHE
ATTN: G ABRAHAMSON
ATTN: J BACKOVSKY
ATTN: W CHESNUT

STAN MARTIN AND ASSOCIATES
ATTN: S B MARTIN

STANTON CONSULTING
ATTN: M STANTON

SWETL, INC
ATTN: T Y PALMER

SYSTEM PLANNING CORP
ATTN: B GARRETT
ATTN: C FELDBAUM
ATTN: J SCOURAS
ATTN: M BIENVENU
ATTN: R SCHEERBAUM

SYSTEMS AND APPLIED SCIENCES CORP
ATTN: M KAPLAN

TELEDYNE BROWN ENGINEERING
ATTN: A ORTELL
ATTN: F LEOPARD
ATTN: J FORD

TELEDYNE BROWN ENGINEERING
ATTN: D GUICE

TEXAS ENGR EXPERIMENT STATION
ATTN: W H MARLOW

DASIAC-TN-87-35-V2 (DL CONTINUED)

TOYON RESEARCH CORP

ATTN: C TRUAX
ATTN: J GARBARINO
ATTN: J ISE

TRW INC

ATTN: H BURNSWORTH
ATTN: J BELING

TRW INC

ATTN: F FENDELL
ATTN: G KIRCHNER
ATTN: H CROWDER
ATTN: J FEDELE
ATTN: M BRONSTEIN
ATTN: R BACHARACH
ATTN: S FINK
ATTN: T NGUYEN

TRW SPACE & DEFENSE, DEFENSE SYSTEMS

ATTN: M HAAS

VISIDYNE, INC

ATTN: H SMITH
ATTN: J CARPENTER

WASHINGTON, UNIVERSITY OF

ATTN: J I KATZ

FOREIGN

AERE ENVIRONMENTAL AND MEDICAL SC

ATTN: S PENKETT

ATOMIC WEAPONS RSCH ESTABLISHMENT

ATTN: P F A RICHARDS

ATOMIC WEAPONS RSCH ESTABLISHMENT

ATTN: D L JONES
ATTN: D M MOODY

AUSTRALIA EMBASSY

ATTN: A TEBBS
ATTN: AIR VICE MARSHAL B GRATION
ATTN: DR A J BEDFORD

BRITISH DEFENCE STAFF

ATTN: J EDMONDS

CANADIAN FORESTRY SERVICE

ATTN: B STOCKS
ATTN: T LYNHAM

CSIRO

ATTN: I GALBALLY

CSIRO: ATMOSPHERIC RESEARCH

ATTN: A PITTOCK

EMBASSY OF BELGIUM

ATTN: L ARNOULD

ISRAEL EMBASSY

ATTN: N BELKIND

MAX-PLANCK INSTITUTE FOR CHEMISTRY

ATTN: P J CRUTZEN

MINISTRY OF DEFENCE

ATTN: R RIDLEY

NATIONAL DEFENCE HEADQUARTERS

ATTN: H A ROBITALLE

TRINITY COLLEGE

ATTN: F HARE

DIRECTORY OF OTHER

ATMOS. SCIENCES

ATTN: G SISCOE

BUCKNELL UNIVERSITY

ATTN: O ANDERSON

CALIFORNIA, UNIVERSITY

ATTN: R WILLIAMSON

CALIFORNIA, UNIVERSITY OF

ATTN: L BADASH

COLORADO, UNIVERSITY LIBRARIES

ATTN: J BIRKS
ATTN: R SCHNELL

DREXEL UNUNIVERSITY

ATTN: J FRIEND

GEORGE MASON UNIVERSITY

ATTN: PROF S SINGER
ATTN: R EHRlich

GEORGE WASHINGTON UNIVERSITY

ATTN: R GOULARD

GEORGIA INST OF TECH

ATTN: E PATTERSON

HARVARD COLLEGE LIBRARY

ATTN: W PRESS

HARVARD UNIVERSITY

ATTN: G CARRIER

HARVARD UNIVERSITY

ATTN: D EARDLEY

IOWA, UNIVERSITY OF

ATTN: S PYNE

MARYLAND UNIVERSITY OF

ATTN: A ROBOCK
ATTN: A VOGELMANN
ATTN: R ELLINGSON

MIAMI LIBRARY UNIVERSITY OF

ATTN: C CONVEY

MIAMI UNIV LIBRARY

ATTN: J PROSPERO

NEW YORK STATE UNIVERSITY OF
ATTN: R CESS

OAK RIDGE ASSOCIATED UNIVERSITIES
ATTN: C WHITTLE

SOUTH DAKOTA SCH OF MINES & TECH LIB
ATTN: H ORVILLE

TENNESSEE, UNIVERSITY OF
ATTN: K FOX

UNIVERSITY OF SOUTH FLORIDA
ATTN: S YING

UNIVERSITY OF WASHINGTON
ATTN: C LEOVY
ATTN: L RAOKE
ATTN: P HOBBS

VIRGINIA POLYTECHNIC INST LIB
ATTN: M NADLER

WISCONSIN UNIVERSITY OF
ATTN: P WANG